Effect of Fluid Rheology, Electrokinetics, and Particle-deformation on Creeping Flow and Heat Transfer Through a Swarm of Cylindrical Particles

THESIS

Submitted in partial fulfilment of the requirements for the degree of

DOCTOR OF PHILOSOPHY

by

AMIT KUMAR SAINI
2019PHXF0422P

Under the Supervision of

DR. ASHISH TIWARI

BIRLA INSTITUTE OF TECHNOLOGY AND SCIENCE, PILANI
2024

Dedicated to My Parents

Mr. Ghisa Ram Saini

and

Smt. Mohini Devi

BIRLA INSTITUTE OF TECHNOLOGY & SCIENCE, PILANI

CERTIFICATE

This is to certify that the thesis titled **"Effect of Fluid Rheology, Electrokinetics, and Particle-deformation on Creeping Flow and Heat Transfer Through a Swarm of Cylindrical Particles"** submitted by **Mr. Amit Kumar Saini**, ID No. **2019PHXF0422P** for the award of Ph.D. of the institute embodies original work done by him under my supervision.

_____

Signature of the Supervisor
Name: **DR. ASHISH TIWARI**
Designation: **Associate Professor**

Date: —

Acknowledgements

I am profoundly grateful for reaching this milestone of completing my Ph.D. thesis, made possible by the grace of the Almighty and the unwavering support of my mentors, family, and friends. From the beginning to this point, their belief in me and generous guidance have been instrumental in shaping this work. This journey, both challenging and rewarding, would not have been possible without their encouragement and commitment to my success.

I am deeply honored to extend my heartfelt gratitude to my esteemed supervisor, Prof. Ashish Tiwari, whose invaluable guidance, profound wisdom, and steadfast support have been instrumental in the completion of this thesis. Being assigned Prof. Tiwari as my supervisor turned out to be the best part of my Ph.D. journey. He gave me the freedom to explore my research while stepping in with insightful guidance exactly when needed. He challenged my thinking, respected my perspective, and helped me build confidence in my own instincts. Our shared passion for interdisciplinary research strengthened our connection, inspiring me to pursue meaningful problems over trends. I am truly thankful for his mentorship and hope to carry his advice forward into the future.

I would like to express my heartfelt thanks to the members of my Doctoral Advisory Committee (DAC), Prof. Bhupendra kumar Sharma and Prof. Anirudh Singh Rana, for their willingness to lend their expertise and knowledge to this research. Their thoughtful and constructive feedback has helped refine my ideas, sharpen my focus, and develop my analytical skills.

I'm truly grateful to Prof. B. K. Sharma, Prof. Devendra Kumar (former HoDs), and Prof. Ashish Tiwari, our current HoD, for their kind guidance and support. I also want to thank all the faculty members and fellow research scholars for their encouragement and camaraderie throughout my research journey. The friendships and memories we've made mean so much to me, and I'll carry them forward always. Thank you all for being such an important part of this journey!

I am immensely appreciative of the support from the Vice-Chancellor, Director, Dean of Academics (AGSRD), and Registrar of BITS Pilani, who provided me with the opportunity to pursue a role that aligns with my qualifications, allowing me to apply and develop my skills. I am also deeply grateful to the Council of Scientific & Industrial Research (CSIR), India, for their fellowship support throughout my Ph.D. journey.

I want to extend my heartfelt thanks to my seniors, Dr. Satyendra Singh Chauhan and Dr. Pallav Shah, for their invaluable guidance and support. Their insights and experiences have

greatly enriched my journey, and I truly appreciate the time and effort they have invested in my development. Their willingness to share knowledge has been a constant source of inspiration for me. At the same time, my junior colleagues—Yogesh Kuntal, Neelima Ghiya, Komal Verma, and Ansal—have infused our research discussions with fresh energy and perspectives, motivating me to push the boundaries of my work. I feel incredibly fortunate to have collaborated with such talented and dedicated individuals, and I am grateful for their encouragement along the way.

I feel incredibly lucky to have formed friendships with an amazing crew: Anurag, Rahul, Digvijay, Jasrat, Uttam, Sampuran, Pradeep, Pramod, Shreebhagwan, Wasim, Vikas, and Pankaj. I truly see these friends as my hard-earned gems, each one shining brightly with the unforgettable memories we've crafted together! I can't forget to give a special shout-out to my Ph.D. buddies—Gourav, Umesh, Sanjiv, Shipra, Anshu, Ashwini, Mahendra, Sonu, Satpal, Yogesh, Ankit, Vijaypal, Saddam, Himanshu, Parveen, Chandan, Sajan, Pallav, Deepak, Kapil, Sugandha, Komal, Barkha, Mohit, Ranjan, Prabin, Rohit, Ajay, Anand—and the list just keeps growing! They say the Ph.D. journey can feel like a rollercoaster ride, complete with its ups and downs, but having such a fantastic company turns every twist and turn into an adventure. I already find myself nostalgic, missing those days of laughter, late-night brainstorming sessions, and the wild debates over who had the best study snacks.

I want to express my heartfelt gratitude to my parents, Ghisa Ram Saini and Mohini Devi, whose unconditional love and unwavering support have been the invisible core strength of my career. Their out-of-league efforts to provide me with every opportunity for education have shaped me into the person I am today. I am also thankful for my siblings, Vikas and Aayushi, and my sister-in-law, Krishana, whose encouragement and belief in me have been invaluable throughout this journey. Together, they have fostered an environment filled with love and inspiration, empowering me to pursue my dreams and overcome challenges. I am forever indebted to them for their sacrifices and dedication to my educational journey.

I am indebted to the many individuals who have contributed to this work in various ways. I extend my sincere gratitude to all those who have supported and accompanied me throughout this remarkable endeavor.

Place: BITS Pilani
Date: November 2024

Amit Kumar Saini
(Department of Mathematics)

Abstract

Fluid dynamics of liquids past a membrane is an important fundamental aspect of various natural and engineered systems, influencing phenomena from sediment transport in rivers to particle-laden flows in industrial processes. In this phenomenon, the membrane can be conceptualized as consisting of a swarm of regularly distributed solid particles, with the flow past the membrane analogous to the fluid flow around these particles within the swarm. The topic of flow past a swarm of particles has been a topic of immense interest for researchers to get an insight into the flow of fluid through porous media owing to its prominent applications in diverse areas like physical and biological science such as flow through smooth muscle cells, petroleum reservoir rocks, wastewater treatment filtration processes, blood flow via the lungs, digestive system design and the sand beds. While analyzing fluid flow through a swarm of porous particles, it is not easy to simultaneously discuss the role and contributions of every particle in a swarm. Hence, the particle-in-cell approach can be used to discuss the behavior and role of every particle in a swarm. The primary objective of the cell model techniques is to consider a single particle from a swarm disassembled in a space. Analyzing fluid flow through a single particle is much easier than a swarm of particles. A condition on the hypothetical cell surface is considered to find the role and contributions of each particle in a swarm, where the hypothetical cell surface is a virtual envelope of the chosen particle. The cell size is assumed so that the particle volume fraction of the membrane should be the ratio of the particle's volume and the volume of a cell. The fluid flow is considered in the separately taken hypothetical cell. In this domain, the primary focus has been on the movement of Newtonian fluid across a membrane. The research predominantly examines particles of a spherical nature, though there is also attention given to those of a cylindrical shape within swarms, encased in a porous coating. Here, the regulation of fluid movement is governed by the Darcy-Brinkman equations.

The thesis aimed to extend the research of this field in terms of geometrical, rheological and thermal aspects of the fluid flow past a membrane composed of swarm of particles. **Chapter 1** provides an introduction to the different aspects of flow past a porous media. It begins with historical developments of fluid flow around a body mentioning some of the important literature in this field followed by the studies considering the flowing medium as a porous material. The next section includes the importance and involvement of membranes in today's lifestyle and provides a classical framework in terms of its types, structures and uses. This section further describes the mathematical modeling of the membrane as a swarm of particles and illustrate the cell model technique in detail with its historical developments including the important literature utilizing this technique to cover different aspects of fluid

flow past a membrane. The role of Heat transfer, Entropy generation and electroosmosis in the membrane is emphasizes using the predominant literature of their respective field. The brief introduction of rheological fluids considered in this thesis in included along with their stress-strain relationship. The governing equations of fluid in different scenarios along with suitable boundary conditions and the methodology are discussed in detail to help readers understand the approach that will be followed. Chapter 1 set the foundation for the research by establishing the need for studying flow past a membrane, identifying research gaps, establishing research objectives, outlining the research methodology, and introducing fundamental concepts critical for understanding the research findings.

Chapter 2 explores the impact of temperature-dependent viscosity on the creeping flow of Jeffrey fluid through a membrane made of porous cylindrical particle aggregates. The flow, moving axially along the cylindrical particles, is analyzed using a cell model approach, leading to governing equations propelled by a constant pressure gradient. The flow is divided into two layers: inside the porous particle (governed by the Brinkman–Forchheimer equation) and outside it (governed by the Stokes equation). Due to the nonlinear nature of the Brinkman–Forchheimer equation, perturbation methods are used for its solution under the assumption of temperature-dependent viscosity. The study derives expressions for velocity, hydrodynamic permeability, and the Kozeny constant, discussing the effects of viscosity, Forchheimer number, permeability, and Jeffrey fluid parameter. The findings align well with existing studies on Newtonian fluids, validating the approach under constant viscosity assumptions in porous media flow.

The aim of the **chapter 3** is to examine the combined effect of electro-hydrodynamic flow and heat transfer on the flow through a membrane made of porous layered cylindrical particles. The study uses steady-state thermal equations to analyze temperature distribution, dominating conduction over convection. Fluid flow is governed by the Brinkman equation in porous region near the particle's solid core and the Stokes equation in non-porous region outside it. The study explores the impact of an “ion drag formulation" utilizing an electric field, represented by the Hartmann electric number, on fluid flow, coupling momentum equations and charge density into a nonlinear differential equation. Analytical solutions for energy equations in both regions are found, further usees in the derivation of velocity expansions derived via perturbation for different nonlinearity parameter values. It assesses how the Hartmann electric number, Grashof number, radiation parameter, viscosity ratio, and porosity affect hydrodynamic permeability, the Kozeny constant of the membrane.

Chapter 4 explores the hydrodynamics and thermodynamics of incompressible Carreau

fluid flow through a membrane composed of uniformly distributed porous cylindrical particles with a solid core, focusing on the non-Newtonian Carreau fluid's impact on the filtration process. It characterizes the flow into two areas: a porous region near the solid core and a non-porous region outside. The Brinkman equation models the porous area, while the Stokes equation describes the non-porous region. By using asymptotic series expansion, the study derives expressions for velocity, hydrodynamic permeability, Kozeny constant, and temperature profile under various conditions. The findings, illustrated through graphs, analyze how factors like the power-law index, viscosity ratio, and Weissenberg number affect these parameters in case of small and large permeabilities of porous layer, comparing them to existing studies on Newtonian fluids to validate the results.

A theoretical attempt has been made in **chapter 5** to explore the behavior of non-Newtonian Carreau-Yasuda fluid flowing through a membrane made of biporous layered cylindrical particles, using a variable permeability model. The study adopts the empirical particle-in-cell method to formulate equations capturing the fluid flow dynamics. It is structured around different regions of flow around the particle: near the solid core, governed by the Brinkman-Forchheimer equation with variable permeability; an intermediate layer by the Brinkman equation; and the outermost layer by the Stokes equation due to its non-porous nature. The complexity arises from nonlinearities and equation coupling, addressed by using empirical regular perturbation for asymptotic solutions under certain conditions, and numerical methods for graphical analysis of flow profiles, examining the effects on membrane permeability, Kozeny constant, and temperature variation across various parameters.

Chapter 6 presents a theoretical framework to analyze entropy production in a creeping flow of a Newtonian fluid through porous layered cylindrical particles, considering their varying permeabilities. It focuses on fully developed, steady, laminar, forced convection within these particles under a constant wall temperature, using Brinkman and Brinkman-Forchheimer models for hyperporous materials. The research highlights the fluid's rheological properties and explores entropy production with an emphasis on heat transfer. The flow past a membrane is modeled using a particle-in-cell approach. Analytical solutions for the Stokes equations are derived, while velocity expressions for the other regions are obtained using perturbation methods. The study examines the effects of various control parameters on hydrodynamic and thermal properties, including membrane permeability, Kozeny constant, temperature, entropy generation number, and Bejan number.

Chapter 7 focuses on the impact of surface roughness on fluid flow in microchannel systems, specifically through membranes composed of porous, corrugated cylindrical particles. With a high surface-to-volume ratio, the roughness of micro objects significantly affects fluid dynamics. The research employs the cell model technique to divide the flow regime

into two: the porous layer governed by the Brinkman equation and the clear fluid region governed by the Stokes equation. A semi-analytical solution for the fluid flow is derived using the regular perturbation technique, with corrugation height as a perturbation parameter. Key findings include the influence of wave number, corrugation height, and porous medium parameters on the fluid velocity and hydrodynamic permeability of the membrane, highlighting that an increase in wave number reduces fluid velocity and affects the membrane's hydrodynamic permeability.

Chapter 8 examines the combined electroosmotic flow (EOF) and pressure-gradient-driven flow of an electrolyte solution through a membrane containing poly-electrolyte coated solid cylindrical particles, under an externally applied electric field. The poly-electrolyte layer, acting as an ion-penetrable porous layer, traps fixed charge ions, forming an electric double layer at the interface with the electrolyte. The flow through the membrane is modeled using a unit cell approach, dividing the flow regime into a poly-electrolyte layer (PEL) governed by the Brinkmann-Forchheimer equation, and a clear fluid region governed by the Stokes equation. Analytical solutions to the governing equations are challenging due to non-linear terms and external forces, thus regular and singular perturbation methods are employed to derive asymptotic analytic expressions for fluid velocity, hydrodynamic permeability, and the Kozeny constant of the membrane.

Chapter 9 is a crucial section of the thesis that summarizes key research findings, highlighting those with significant real-world relevance. It aims to provide a clear and concise overview of the discoveries, emphasizing their reliability and areas for improvement. The chapter also outlines future research directions and potential applications, ensuring the work contributes to further studies and practical use.

Contents

Certificate v

Acknowledgements vii

Abstract ix

Physical Parameters xli

1 Introduction 1

1.1 Flow around a Body . . . 1
1.2 Flow Through a Porous Media . . . 4
1.3 Membranes . . . 7
1.3.1 Flow Through a Swarm of Particles . . . 9
1.3.2 Cell Model Technique . . . 10
1.4 Heat Transfer and Entropy Generation . . . 15
1.4.1 Heat Transfer . . . 15
1.4.2 Entropy Generation . . . 17
1.5 Electroosmosis . . . 18
1.6 Diverse Fluids . . . 20
1.6.1 Newtonian Fluid . . . 20
1.6.2 Jeffrey Fluid . . . 20
1.6.3 Carreau-Yasuda Fluid . . . 21
1.7 Governing Equations . . . 21
1.7.1 Conservation of Mass . . . 22
1.7.2 Conservation of Momentum . . . 22
1.7.3 Convection–Diffusion Equation . . . 22
1.7.4 Momentum Equations in Porous Media . . . 23
1.7.4.1 Brinkmann Equation . . . 23
1.7.4.2 Brinkmann Forchheimer Equation . . . 23
1.8 Boundary Conditions . . . 23

1.9 Mathematical Methods . . . 25
1.9.1 Perturbation Method . . . 26
1.9.1.1 Regular Perturbation . . . 27
1.9.1.2 Singular Perturbation . . . 27
1.9.2 Seperation of Variables . . . 29
1.10 Objectives . . . 29
1.11 Thesis Organization . . . 30

2 Creeping Flow of Jeffrey Fluid through a Swarm of Porous Cylindrical Particles: Brinkman-Forchheimer Model 33
2.1 Introduction . . . 33
2.2 Problem Formulation . . . 37
2.2.1 Statement of the Problem and Model Description . . . 37
2.2.2 Governing Equations . . . 38
2.2.3 Non-Dimensional Parameters and Equations . . . 40
2.2.4 Boundary Conditions . . . 41
2.3 Solution of the Problem . . . 42
2.3.1 Solution of Thermal Equation . . . 42
2.3.2 Solutions of Hydrodynamic Equations . . . 42
2.3.2.1 Asymptotic Solution for the Porous Region . . . 43
2.3.2.2 Analytical Solution for the Clear Fluid Region . . . 48
2.3.3 Hydrodynamical Quantities . . . 48
2.4 Results and Discussion . . . 49
2.4.1 Model Validation . . . 50
2.4.2 Parameter Selection . . . 51
2.4.3 Velocity Profile (w) . . . 51
2.4.4 Hydrodynamic Permeability (L_{11}) . . . 52
2.4.5 Kozeny Constant (K_z) . . . 58
2.5 Summary and Conclusions . . . 59

3 Asymptotic Analysis of Electrohydrodynamic Flow through a Swarm of Porous Layered Cylindrical Particles: A Particle-in-Cell Approach 63
3.1 Introduction . . . 63
3.2 Problem Formulation . . . 66
3.2.1 Statement of the Problem . . . 66
3.2.2 Model Description . . . 67
3.2.3 Governing Equations . . . 69

3.2.3.1 Energy Equations . . . 69
3.2.3.2 Hydrodynamical Equations . . . 70
3.2.3.3 Boundary Conditions . . . 71
3.2.4 Non-Dimesionalization . . . 72
3.2.5 Hydodynamical Quantities . . . 73
3.3 Solution of the Problem . . . 75
3.3.1 Solution of Temperature Equations . . . 75
3.3.2 Solution of Hydrodynamic Equations . . . 76
3.3.2.1 Small Parameter ($\alpha \ll 1$) . . . 76
3.3.3 Large Parameter ($\alpha \gg 1$) . . . 78
3.4 Results and Discussion . . . 80
3.4.1 Parameter Selection . . . 81
3.4.2 Velocity Profile (w) . . . 81
3.4.3 Hydrodynamic Permeability (L_{11}) . . . 84
3.4.4 Kozeny Constant (K_z) . . . 88
3.4.5 Model Validation and Comparative Study . . . 91
3.5 Summary and Conclusion . . . 95

4 Creeping flow of non-Newtonian fluid through membrane of porous cylindrical particles: A particle-in-cell approach 101
4.1 **Introduction** . . . 101
4.2 Mathematical Formulation of the Proposed Work . . . 104
4.2.1 Statement and Assumptions . . . 104
4.2.2 Model Description of the Problem . . . 104
4.2.3 Governing Equations . . . 106
4.2.3.1 Hydrodynamic Equations . . . 106
4.2.4 Non-Dimensional Parameters and Governing Equations . . . 107
4.2.4.1 Hydrodynamic Equations . . . 108
4.2.5 Boundary Conditions . . . 108
4.2.6 Hydrodynamical Quantities and Kozeny Constant . . . 109
4.3 Solution of the Proposed Problem . . . 110
4.3.1 Asymptotic Solution of the Problem . . . 111
4.3.2 Analytical Expression of Fluid Velocity . . . 114
4.3.3 Numerical Solution of the Problem . . . 115
4.4 Temperature Analysis . . . 115
4.4.1 Solution of Temperature Equation . . . 117
4.5 Results and Discussion . . . 118

4.5.1 Parameter Selection . . . 118
4.5.2 Deduction of Special Cases . . . 119
4.5.3 Graphical Analysis . . . 120
4.5.3.1 Asymptotic Analysis . . . 120
4.5.3.2 Numerical Analysis . . . 127
4.6 Summary and Conclusions . . . 134

5 Analytical Study of the Effect of Complex Fluid Rheology and Membrane Parameters on Heat Transfer in Fluid Flow through a Swarm of Cylindrical Particles 137
5.1 Introduction . . . 137
5.2 Problem Formulation . . . 142
5.2.1 Statement of the Problem and Model Assumptions . . . 142
5.2.2 Model Description . . . 144
5.2.3 Governing Equations . . . 144
5.2.4 Boundary Conditions . . . 146
5.2.5 Non-Dimensional Parameters and Governing Equations . . . 147
5.2.6 Boundary Conditions . . . 149
5.2.7 Hydrodynamical Quantities and Kozeny Constant . . . 149
5.3 Asymptotic Solution of the Problem . . . 150
5.3.1 Perturbation Solution for Carreau-Yasuda Fluid . . . 151
5.3.2 Numerical Solution for Small Weissenberg and Permeability $(i.e., S \gg 1)$ 155
5.3.3 Temperature Analysis . . . 156
5.3.4 Solution of Temperature Equations . . . 158
5.3.5 Nusselt Number (Nu) . . . 159
5.4 Results and Discussion . . . 160
5.4.1 Parameter Selection . . . 160
5.4.2 Limiting Cases and Model Validation . . . 161
5.4.3 Velocity Profile (w) . . . 162
5.4.4 Flow Rate (Q_s) . . . 165
5.4.5 Hydrodynamic Permeability (L_{11}) . . . 167
5.4.6 Kozeny Constant (K_z) . . . 174
5.4.7 Temperature Distribution (θ) . . . 176
5.4.8 Nusselt Number (Nu) . . . 179
5.5 Summary and Conclusions . . . 181

6 Analysis of Entropy Generation for a Creeping Flow of Newtonian Fluid through a Swarm of Biporous Layered Cylindrical Particles: Brinkman-Forchheimer Model **185**
6.1 Introduction . . . 185
6.1.1 Entropy Generation . . . 185
6.2 Problem Formulation . . . 188
6.2.1 Statement of the Problem and Model Assumptions . . . 188
6.2.2 Model Description . . . 189
6.2.3 Governing Equations . . . 191
6.2.3.1 Hydrodynamical and Thermal Equations . . . 191
6.2.3.2 Entropy Generation and Bejan Number . . . 193
6.2.3.3 Boundary Conditions . . . 194
6.2.4 Non-Dimensional Parameters and Governing Equations . . . 195
6.2.4.1 Hydrodynamic and Thermal Equations . . . 196
6.2.4.2 Entropy Generation and Bejan Number . . . 197
6.2.4.3 Dimensionless Boundary Conditions . . . 198
6.3 Asymptotic Solution of the Problem . . . 198
6.3.1 Perturbation Solutions for Hydrodynamic Equations . . . 198
6.3.1.1 Solution for Large Permeability $(i.e., S \ll 1)$ . . . 199
6.3.1.2 Solution for Small Permeability $(i.e., S \gg 1)$ . . . 201
6.3.2 Solutions for Thermal Equations . . . 204
6.4 Results and Discussion . . . 205
6.4.1 Model Validation and Limiting Cases . . . 205
6.4.2 Parameter Selection . . . 206
6.4.3 Entropy Generation Number (S) . . . 207
6.4.4 Bejan Number (B_e) . . . 210
6.4.5 Model Validation and Comparative Analysis . . . 212
6.5 Summary and Conclusions . . . 214

7 Effect of Surface Roughness on Flow Past a Membrane composed of Porous Cylindrical Particles **217**
7.1 Introduction . . . 217
7.2 Problem Formulation . . . 219
7.2.1 Statement of the Problem and Model Description . . . 219
7.2.1.1 Hydrodynamic Equations . . . 221
7.2.2 Non-Dimensional Parameters and Governing Equations . . . 222
7.2.2.1 Hydrodynamic Equations . . . 222

7.2.3 Boundary Conditions . . . 222
7.2.4 Hydrodynamical Quantities and Kozeny Constant . . . 223
7.3 Asymptotic Solution of the Problem . . . 224
7.4 Results and Discussion . . . 229
7.4.1 Parameter Selection . . . 230
7.4.2 Velocity Profile . . . 230
7.4.3 Hydrodynamic Permeability . . . 233
7.4.4 Kozeny Constant . . . 237
7.5 Summary and Conclusions . . . 240

8 Electroosmotic Flow past an Array of Poly-Electrolyte Coated Solid Cylindrical Particles: A Particle-in-Cell Approach 243
8.1 **Introduction** . . . 243
8.2 Problem Formulation . . . 245
8.2.1 Statement of the Problem . . . 245
8.2.2 Model Description . . . 245
8.2.3 Governing Equations . . . 246
8.2.3.1 Electric Potential Equation . . . 246
8.2.3.2 Hydrodynamic Equations . . . 249
8.2.4 Non-Dimensional Parameters and Governing Equations . . . 250
8.2.4.1 Poission-Boltzmann Equation . . . 250
8.2.4.2 Hydrodynamic Equations . . . 251
8.2.5 Boundary Conditions . . . 251
8.2.6 Hydrodynamical Quantities and Kozeny Constant . . . 252
8.3 Solution of the Problem . . . 253
8.3.1 Solution of Poisson-Boltzmann equation . . . 253
8.3.2 Solution of Hydrodynamic Equations . . . 254
8.3.3 Large Permeability $(k \gg 1)$ . . . 254
8.3.4 Small Permeability $(k \ll 1)$ . . . 256
8.3.4.1 Solution for the Porous Region . . . 256
8.3.4.2 Solution for the Clear Fluid Region . . . 258
8.4 Results and Discussion . . . 258
8.4.1 Parameter Selection . . . 259
8.4.2 Electric Potential . . . 260
8.4.3 Velocity Profile . . . 261
8.4.4 Hydrodynamic Permeability . . . 266
8.4.5 Kozeny Constant . . . 270

8.4.6 Model Validation and Limiting Cases 272
8.5 Summary and Conclusions 273

9 Conclusions and Research Prospects **277**
9.1 Conclusions 277
9.2 Noteworthy Contributions 278
9.3 Research Prospects 279

List of Publications **301**

Conference/ Workshop Attended **302**

Brief Biography of the Candidate **304**

Brief Biography of the Supervisor **305**

List of Figures

1.1 Electron microscope image of PES 300 membrane 8
1.2 Different type of aggregates with different internal structure.(Lowenfels and Yayne [62]) 10
1.3 Pictorial representation of Uchida's [70] model of swarm of uniformly distributed spherical particles enclosed each in a cubic cell. 12
1.4 Pictorial representation of Happel's [71] model of swarm of uniformly distributed spherical particles enclosed each in a spherical cell. 12
1.5 Physical Model of Veerapanneni for flow through a swarm of spherical particles with radially varying permeability. 14
1.6 Charge distribution in the electrical double layer region near the charged surface. 18

2.1 The physical sketch of a cylindrical particle in cell 38
2.2 the circular cross-section of the cylindrical particle in cell 38
2.3 Variation of velocity profile w with radial distance r for different values of **(2.3a)** viscosity parameter α $(\lambda_1 = F = 1, \beta_S = 0.4)$ and **(2.3b)** Jeffrey fluid parameter λ_1 $(\alpha = 0.1, F = 0, \beta_S = 0.1)$. $(l = \gamma = 0.5, \zeta_h = 5, p_s = 1)$ . . . 52
2.4 Variation of hydrodynamic permeability L_{11} with particle volume fraction γ between present study and Deo *et al.* [3]. $(l = 0.5, \beta_S = 0.1, \zeta_h = 5, \alpha = 0, p_s = 1, F = \lambda_1 = 0)$ 53
2.5 Variation of hydrodynamic permeability L_{11} with particle volume fraction γ for different values of **(a)** viscosity parameter α $(\lambda_1 = 1)$ and **(b)** Jeffrey fluid parameter λ_1 $(\alpha = 0.1)$. $(l = 0.5, \beta_S = 0.1, \zeta_h = 5, p_s = F = 1)$ 54
2.6 Variation of hydrodynamic permeability L_{11} with stress-jump parameter β_S for different values of **(a)** viscosity parameter α $(\lambda_1 = 1)$ and **(b)** Jeffrey fluid parameter λ_1 $(\alpha = 0.1)$. $(l = \gamma = 0.5, \zeta_h = 5, p_s = F = 1)$ 56
2.7 Variation of hydrodynamic permeability L_{11} with particle volume fraction γ between constant and varying viscosity models. $(l \to 0, p_s = 1, \beta_S = 0.1, \zeta_h = 5, k = 0.05, \lambda_1 = F = 0)$ 56

2.8 Variation of hydrodynamic permeability L_{11} with particle volume fraction γ between Newtonian and Jeffrey fluids. ($l \to 0, k \to 0, p_s = 1, \beta_S = 0.1, \zeta_h = 5, \alpha = F = 0$) 57
2.9 Variation of hydrodynamic permeability L_{11} with stress-jump parameter β_S for different values of **(a)** viscosity parameter α ($\lambda_1 = 1$) and **(b)** Jeffrey fluid parameter λ_1 ($\alpha = 0.1$). ($l = \gamma = 0.5, \zeta_h = 5, p_s = F = 1$) 58
2.10 Variation of Kozeny constant K_z with stress-jump parameter β_S for different values of **(a)** viscosity parameter α ($\lambda_1 = 1$) and **(b)** Jeffrey fluid parameter λ_1 ($\alpha = 0.1$). ($l = \varepsilon = 0.5, \zeta_h = 5, p_s = F = 1$) 59

3.1 The physical depiction of an “ion drag" configuration for electrohydrodynamic flow along the axis of an array of porous cylindrical particles 68
3.2 A visual depiction of a circular cross-section revealing a swarm of cylindrical particles with a solid core and porous layer inside a hypothetical cell. . . 69
3.3 Changes in fluid velocity (w) in radial direction(r), with varying Hartmann electric number(H), under high $(k = 100)$ and low $(k = 0.1)$ permeability parameters, (a) large alpha parameter ($\alpha = 4.0$) and (b) small alpha parameter ($\alpha = 0.25$). ($\beta = 0.1, l = 0.5, \gamma = 0.45, Gr = N_1 = 2, \lambda_1 = 1$) 82
3.4 Changes in fluid velocity (w) in radial direction (r), with varying Radiation parameter (N_1), under high $(k = 100)$ and low $(k = 0.1)$ permeability parameters, (a) large alpha parameter ($\alpha = 4.0$) and (b) small alpha parameter ($\alpha = 0.25$). ($\beta = 0.1, H = Gr = 2, l = 0.5, \gamma = 0.45, \lambda_1 = 1$) 82
3.5 Changes in fluid velocity (w) in radial direction (r), with varying viscosity ratio parameter(λ_1), under high $(k = 100)$ and low $(k = 0.1)$ permeability parameters, (a) large alpha parameter ($\alpha = 4.0$) and (b) small alpha parameter ($\alpha = 0.25$). ($\beta = 0.1, l = 0.5, \gamma = 0.45, H = Gr = N_1 = 2$) 83
3.6 Changes in fluid velocity (w) in radial direction (r), with varying Grashof number (Gr), under high $(k = 100)$ and low $(k = 0.1)$ permeability parameters, (a) large alpha parameter ($\alpha = 4.0$) and (b) small alpha parameter ($\alpha = 0.25$). ($\beta = 0.1, \lambda_1 = 1, l = 0.5, \gamma = 0.45, H = N_1 = 2$) 83
3.7 Changes in the hydrodynamic permeability (L_{11}) relying on particle volume fraction (γ) with varying Hartmann electric number (H), under high $(k = 100)$ and low $(k = 0.1)$ permeability parameters. ($\beta = 0.1, \alpha = 4.0, \lambda_1 = 1, l = 0.5, Gr = N_1 = 2.0$) 84
3.8 Changes in L_{11} relying on stress jump parameter β with varying Radiation number(N_1), under high $(k = 100)$ and low $(k = 0.1)$ permeability parameters. ($\alpha = 4.0, \gamma = 0.45, \lambda_1 = 1, l = 0.5, H = 2.0, Gr = 2.0$) 85

3.9 Changes in L_{11} relying on Grashof number Gr with varying viscosity ratio parameter λ_1, under high $(k = 100)$ and low $(k = 0.1)$ permeability parameters. $(\alpha = 4.0, \beta = 0.1, \gamma = 0.45, N_1 = 2.0, l = 0.5, H = 2.0)$ 85
3.10 Changes in L_{11} relying on Hartmann electric number H with varying Grashof number Gr, under high $(k = 100)$ and low $(k = 0.1)$ permeability parameters. $(\alpha = 4.0, \beta = 0.1, \gamma = 0.45, N_1 = 2.0, l = 0.5, \lambda_1 = 1)$ 86
3.11 Changes in L_{11} relying on Hartmann electric number H with varying viscosity ratio parameter λ_1, under high $(k = 100)$ and low $(k = 0.1)$ permeability parameters. $(\alpha = 4.0, \beta = 0.1, \gamma = 0.45, Gr = 2.0, N_1 = 2.0, l = 0.5)$ 86
3.12 Changes in L_{11} relying on Hartmann electric number H with varying stress jump parameter β, under high $(k = 100)$ and low $(k = 0.1)$ permeability parameters. $(\alpha = 4.0, \lambda_1 = 1, \gamma = 0.45, Gr = 2.0, N_1 = 2.0, l = 0.5)$ 87
3.13 Changes in L_{11} relying on Radiation parameter N_1 with varying viscosity ratio parameter λ_1, under high $(k = 100)$ and low $(k = 0.1)$ permeability parameters. $(\alpha = 4.0, \beta = 0.1, \gamma = 0.45, Gr = 2.0, H = 2.0, l = 0.5)$ 87
3.14 Changes in L_{11} relying on Grashof number Gr with varying viscosity ratio parameter λ_1, under high $(k = 100)$ and low $(k = 0.1)$ permeability parameters. $(\alpha = 4.0, \beta = 0.1, \gamma = 0.45, N_1 = 2, H = 2.0, l = 0.5)$ 88
3.15 Changes in L_{11} relying on Hartmann electric number H with varying radiation parameter N_1, under high $(k = 100)$ and low $(k = 0.1)$ permeability parameters. $(\alpha = 0.25, \beta = 0.1, \gamma = 0.45, \lambda_1 = 1, Gr = 2.0, l = 0.5)$ 88
3.16 Changes in L_{11} relying on Hartmann electric number H with varying Grashof number Gr, under high $(k = 100)$ and low $(k = 0.1)$ permeability parameters. $(\alpha = 0.25, \beta = 0.1, \gamma = 0.45, N_1 = 2, \lambda_1 = 1.0, l = 0.5)$ 89
3.17 Changes in L_{11} relying on radiation parameter N_1 with varying stress jump parameter β, under high $(k = 100)$ and low $(k = 0.1)$ permeability parameters. $(\alpha = 0.25, \gamma = 0.45, H = 2, Gr = 2, \lambda_1 = 1.0, l = 0.5)$ 89
3.18 Changes in L_{11} relying on stress jump parameter β with varying Grashof number Gr, under high $(k = 100)$ and low $(k = 0.1)$ permeability parameters. $(\alpha = 0.25, \gamma = 0.45, H = 2, N_1 = 2, \lambda_1 = 1.0, l = 0.5)$ 90
3.19 Changes in L_{11} relying on stress jump parameter β with varying Hartmann electric number H, under high $(k = 100)$ and low $(k = 0.1)$ permeability parameters. $(\alpha = 0.25, \gamma = 0.45, Gr = 2, N_1 = 2, \lambda_1 = 1.0, l = 0.5)$ 90
3.20 Changes in L_{11} relying on stress jump parameter β with varying Hartmann electric number H, under high $(k = 100)$ and low $(k = 0.1)$ permeability parameters. $(\alpha = 4.0, \gamma = 0.6, Gr = 2, N_1 = 2, \varepsilon = l = 0.5, \lambda_1 = 1.0)$ 91

3.21 Changes in Kozeny constant K_z relying on stress jump parameter β with varying Radiation parameter N_1, under high $(k = 100)$ and low $(k = 0.1)$ permeability parameters. $(\alpha = 4.0, \gamma = 0.6, Gr = 2, H = 2, \varepsilon = l = 0.5, \lambda_1 = 1.0)$ 91
3.22 Changes in Kozeny constant K_z relying on Grashof number Gr with varying Hartmann electric number H, under high $(k = 100)$ and low $(k = 0.1)$ permeability parameters. $(\alpha = 4.0, \gamma = 0.6, \beta = 0.1, N_1 = 2, \varepsilon = l = 0.5, \lambda_1 = 1.0)$ 92
3.23 Changes in Kozeny constant K_z relying on Hartmann electric number H with varying Grashof number Gr, under high $(k = 100)$ and low $(k = 0.1)$ permeability parameters. $(\alpha = 4.0, \gamma = 0.6, \beta = 0.1, N_1 = 2, \varepsilon = l = 0.5, \lambda_1 = 1.0)$ 92
3.24 Changes in Kozeny constant K_z relying on Hartmann electric number H with varying viscosity ratio parameter λ_1, under high $(k = 100)$ and low $(k = 0.1)$ permeability parameters. $(\alpha = 4.0, \gamma = 0.6, \beta = 0.1, N_1 = 2, \varepsilon = 0.5, Gr = 2.0, l = 0.5)$ 93
3.25 Changes in Kozeny constant K_z relying on Radiation parameter N_1 with varying viscosity ratio parameter λ_1, under high $(k = 100)$ and low $(k = 0.1)$ permeability parameters. $(\alpha = 4.0, \gamma = 0.6, \beta = 0.1, H = 2.0, Gr = 2.0, \varepsilon = 0.5, , l = 0.5)$ 93
3.26 Changes in Kozeny constant K_z relying on porosity parameter ε with varying Hartmann electric number H under high $(k = 100)$ and low $(k = 0.1)$ permeability parameters. $(\alpha = 4.0, \gamma = 0.6, \beta = 0.1, N_1 = 2, \lambda_1 = 1, Gr = 2.0, l = 0.5)$ 94
3.27 Changes in Kozeny constant K_z relying on stress-jump parameter β with varying Grashof number Gr, under high $(k = 100)$ and low $(k = 0.1)$ permeability parameters. $(\alpha = 0.25, \gamma = 0.0.45, \varepsilon = 0.5, H = 2.0, N_1 = 2, \lambda_1 = 1, l = 0.5)$ 94
3.28 Changes in Kozeny constant K_z relying on Radiation parameter N_1 with varying Hartmann electric number H, under high $(k = 100)$ and low $(k = 0.1)$ permeability parameters. $(\alpha = 0.25, \gamma = 0.45, \varepsilon = 0.5, \beta = 0.1, Gr = 2.0, \lambda_1 = 1, l = 0.5)$ 95
3.29 Changes in Kozeny constant K_z relying on Hartmann electric number H with varying viscosity ratio parameter λ_1, under high $(k = 100)$ and low $(k = 0.1)$ permeability parameters. $(\alpha = 0.25, \gamma = 0.45, \varepsilon = 0.5, \beta = 0.1, Gr = 2.0, N_1 = 2, l = 0.5)$ 95

3.30 Changes in Kozeny constant K_z relying on Hartmann electric number H with varying stress-jump parameter β, under high $(k = 100)$ and low $(k = 0.1)$ permeability parameters. $(\alpha = 0.25, \gamma = 0.45, \varepsilon = 0.5, \lambda_1 = 1.0, Gr = 2.0, N_1 = 2, l = 0.5)$ 96
3.31 Changes in Kozeny constant K_z relying on porosity parameter ε with varying radiation parameter N_1, under high $(k = 100)$ and low $(k = 0.1)$ permeability parameters. $(\alpha = 0.25, \gamma = 0.45, H = 2.0, \lambda_1 = 1.0, Gr = 2.0, \beta = 0.1, l = 0.5)$ 96
3.32 Comparision between radially varying velocities of asymptotic and numerical solutions for the case small non-linearity parameter $\alpha = 0.25$ $(\beta = 0.1, H = 2.0, \lambda_1 = 1, l = 0.5, Gr = 2.0, N_1 = 2, p_z = 1)$ 97
3.33 Variation of the membrane permeability L_{11} with radial distance with asymptotic and numerical variations $(\beta = 0.1, H = 2.0, \alpha = 0.25, \lambda_1 = 1, l = 0.5, Gr = 2.0, N_1 = 2, p_z = 1)$ 97
3.34 Variation of the Kozeny constant K_z with radial distance with asymptotic and numerical variations $(\beta = 0.1, \alpha = 0.25, H = 2.0, \lambda_1 = 1, l = 0.5, Gr = 2.0, N_1 = 2, p_z = 1)$ 98

4.1 The physical depiction of the flow along the axis of an aggregate of porous layered solid cylinders in a membrane 105
4.2 The physical representation of circular cross-sectional view of a swarm consisting of solid cylindrical particle surrounded by a porous layer enclosed in hypothetical cell 105
4.3 The velocity profile w depending upon the radial distance r with varying **(a)** Weissenberg number We $(n = 0.2, \eta = 0.1)$, **(b)** Power-law index n $(\eta = 0.1, \mathrm{We} = 0.3)$. $(\gamma = 0.5, \beta = 0.4, S = 0.1, p_s = 1)$ 120
4.4 The hydrodynamic permeability L_{11} depending upon particle volume fraction γ with varying **(a)** Weissenberg number We $(\beta = 0.1, n = 0.1, \eta = 0.1)$ **(b)** Power-law index n $(\beta = 0.4, \mathrm{We} = 0.3, \eta = 0.1)$, and **(c)** viscosity ratio parameter η $(n = 0.1, \mathrm{We} = 0.3, \beta = 0.1)$. $(S = 0.1, p_s = 1)$ 121
4.5 The hydrodynamic permeability L_{11} depending upon stress-jump parameter β with varying **(a)** Weissenberg number We $(\gamma = 0.5, n = 0.5, \eta = 0.1)$ and **(b)** Power-law index n $(\gamma = 0.5, \mathrm{We} = 0.3, \eta = 0.1)$, and **(c)** viscosity ratio parameter η $(n = 0.5, \mathrm{We} = 0.3, \gamma = 0.5)$. $(S = 0.1, p_s = 1)$ 122
4.6 The hydrodynamic permeability L_{11} depending upon pressure gradient p_s with varying **(a)** Weissenberg number We $(\gamma = 0.5, n = 0.5, \eta = 0.1)$, and **(b)** Power-law index n $(\gamma = 0.5, \mathrm{We} = 0.4, \eta = 0.1)$. $(S = 0.1, \beta = 0.4)$ . . 123

4.7 The Kozeny constant K_z depending upon the porosity ε with varying **(a)** Weissenberg number We $(\gamma = 0.1, n = 0.1, \eta = 0.1)$ and **(b)** Power-law index n $(\gamma = 0.2, \mathrm{We} = 0.3, \eta = 0.1)$, and **(c)** viscosity ratio parameter η $(n = 0.1, \mathrm{We} = 0.5, \beta = 0.1)$. $(S = 0.1, p_s = 1, \beta = 0.1)$ 124
4.8 The Kozeny constant K_z depending upon the stress-jump parameter β with varying **(a)** Weissenberg number We $(n = 0.1, \eta = 0.1)$ and **(b)** Power-law index n $(\mathrm{We} = 0.3, \eta = 0.1)$, and **(c)** viscosity ratio parameter η $(n = 0.1, \mathrm{We} = 0.3)$. $(S = 0.1, p_s = 1, \gamma = 0.5, \varepsilon = 0.5)$ 125
4.9 Variation of temperature θ with radial distance r for different values of **(a)** Nusselt number Nu $(n = \eta = 0.1, \mathrm{We} = 0.4, \beta = 0.1, \gamma = 0.53)$ and **(b)** Power-law index n $(\eta = 0.1, \mathrm{We} = 0.4, \beta = 0.4, \gamma = 0.5, \mathrm{Nu} = 4.0)$. $(S = 0.1, p_s = 1)$ 126
4.10 Variation of temperature θ with radial distance r for different values of **(a)** Weissenberg number We $(n = 0.2, \eta = 0.01)$ and **(b)** viscosity ratio parameter η $(\mathrm{We} = 0.4, n = 0.05)$. $(\gamma = 0.5, S = 0.1, p_s = 1, \mathrm{Nu} = 4, \beta = 0.4)$ . . 126
4.11 Variation of temperature θ with radial distance r for different values of **(a)** Weissenberg number We $(n = 0.2, \eta = 0.01)$ and **(b)** viscosity ratio parameter η $(\mathrm{We} = 0.4, n = 0.05)$. $(\gamma = 0.5, S = 0.1, p_s = 1, \mathrm{Nu} = 4, \beta = 0.4)$ . . 127
4.12 The velocity profile w depending upon the radial distance r with varying **(a)** Weissenberg number We $(n = 2, \eta = 0.1, \beta = 0.4)$ and **(b)** viscosity ratio parameter η $(n = 2, \mathrm{We} = 0.3, \beta = 0.45)$. $(\gamma = 0.5, S = 100, p_s = 1)$ 128
4.13 The hydrodynamic permeability L_{11} depending upon particle volume fraction γ with varying Weissenberg number We $(\beta = 0.1, n = 0.1, \eta = 0.1)$. $(S = 100, p_s = 1)$ 128
4.14 The hydrodynamic permeability L_{11} depending upon stress-jump parameter β with varying Power law index n $(\gamma = 0.8, \mathrm{We} = 0.5, \eta = 0.1)$. $(S = 100, p_s = 1)$ 129
4.15 The Kozeny constant K_z depending upon the porosity ε with varying **(a)** Weissenberg number We $(n = 0.1, \eta = 0.1, \gamma = 0.1)$ and **(b)** Power-law index n $(\mathrm{We} = 0.5, \eta = 0.1, \gamma = 0.2)$, and **(c)** viscosity ratio parameter η $(\mathrm{We} = 0.5, n = 0.1, \gamma = 0.2)$. $(S = 100, p_s = 1, \beta = 0.1)$ 129
4.16 The Kozeny constant K_z depending upon the stress-jump parameter β with varying Power law index n $(\mathrm{We} = 0.5, \eta = 0.1)$. $(S = 100, p_s = 1, \gamma = 0.5, \varepsilon = 0.5)$ 130

4.17 Variation of temperature (θ) with radial distance (r) for different values of **(a)** Nusselt number Nu ($n = 0.1, \eta = 0.1, \beta = 0.1, \text{We} = 0.5$) and **(b)** Weissenberg number We ($\eta = 0.1, n = 2, \beta = 0.4, \text{Nu} = 4.0$). ($\gamma = 0.444, S = 100, p_s = 1$) 132
4.18 Variation of temperature θ with radial distance r for different values of **(a)** viscosity ratio parameter η ($\text{We} = 0.5, n = 2, \beta = 0.4$) and **(b)** Stress-jump parameter β. ($\text{We} = 0.5, \text{Nu} = 4.0, n = 0.05, \eta = 0.01, \gamma = 0.444, p_s = 1$) . 132
4.19 **(a)** The hydrodynamic permeability L_{11} depending on particle volume fraction γ for the case of fully solid cylindrical particle, and **(b)** Validation of hydrodynamic permeability L_{11} of currunt work with the work of Deo *et al.* [3]. 133
4.20 **(a)** The hydrodynamic permeability L_{11} depending on particle volume fraction γ for the case of fully solid cylindrical particle, and **(b)** Validation of hydrodynamic permeability L_{11} of currunt work with the work of Deo *et al.* [3]. 134

5.1 **(a)** The portrayal of the movement along the central axis of a collection of biporous layered solid cylinders within a membrane and **(b)** the circular cross-sectional perspective depicts a swarm composed of a solid cylindrical particle enveloped by biporous layers contained within a hypothetical cell . 143
5.2 The solid core of a cylindrical particle, coated with a swarm and situated within biporous layers, is depicted in the cross-sectional view with nomenclature 144
5.3 Dimensionless velocity w with radial distance r for various values of transition parameter a_1 ($a_1 = 1, 2, 3, 4$) under (**(5.3a)**) large Darcy number ($k = 10, n = 0.1, \varepsilon_f = \varepsilon_b = 0.5$) and **(5.3b)** small Darcy number ($k = 0.1, n = 2.0, \varepsilon_f = \varepsilon_b = 0.2$). ($a = 0.4, b = 0.7, \gamma = 0.445, \beta = 0.5, We = 0.2, \eta = 0.1, F = 1$) 163
5.4 Dimensionless velocity w with radial distance r for various thicknesses of Forchheimer layer b ($b = 0.55, 0.7, 0.85$) under **(5.4a)** large Darcy number ($k = 10, n = 0.1, \varepsilon_f = \varepsilon_b = 0.5$) and **(5.4b)** small Darcy number ($k = 0.1, n = 2, \varepsilon_f = \varepsilon_b = 0.1$). ($a = 0.4, \gamma = 0.445, \beta = 0.5, We = 0.2, a_1 = 3, \eta = 0.1, F = 1$) 163

5.5 Dimensionless velocity w with radial distance r for various values of permeability parameters $(\varepsilon_f, \varepsilon_b)$ under **(5.5a)** large Darcy number $(k = 10, n = 0.1, \varepsilon_f = \varepsilon_b = 0.1, 0.5, 0.9)$ and **(5.5b)** small Darcy number $(k = 0.1, n = 2, \varepsilon_f = \varepsilon_b = 0.1, 0.2, 0.3)$. $(a = 0.4, b = 0.7, \gamma = 0.445, \beta = 0.5, We = 0.2, a_1 = 3, \eta = 0.1, F = 1)$ 164

5.6 Dimensionless velocity w with radial distance r for comparative values of permeability parameters $(\varepsilon_f, \varepsilon_b)$ under **(5.6a)** large Darcy number $(k = 10, n = 0.1)$ and **(5.6b)** small Darcy number $(k = 0.1, n = 2)$. $(a = 0.4, b = 0.7, \gamma = 0.445, \beta = 0.5, We = 0.2, a_1 = 3, \eta = 0.1, F = 1)$ 165

5.7 Changes in flow rate Q_s with Forchheimer number F for various values of the Weissenberg number We $(We = 0.1, 0.3, 0.5)$ under **(5.7a)** large Darcy number $(k = 10, n = 0.1, \varepsilon_f = \varepsilon_b = 0.5, \eta = 0.1)$ and **(5.7b)** small Darcy number $(k = 0.1, n = 2, \varepsilon_f = \varepsilon_b = 0.2, \eta = 0.4)$. $(a = 0.4, b = 0.7, \gamma = 0.444, a_1 = 3, \beta = 0.5)$ 166

5.8 Changes in flow rate Q_s with thickness of Forchheimer layer b for various values of the viscosity ratio parameter η $(\eta = 0.01, 0.2, 0.3)$ under **(5.8a)** large Darcy number $(k = 10, n = 0.1, We = 0.5, \varepsilon_f = \varepsilon_b = 0.5)$ and **(5.8b)** small Darcy number $(k = 0.1, n = 2, We = 0.2, \varepsilon_f = \varepsilon_b = 0.2)$. $(a = 0.4, b = 0.7, \gamma = 0.444, a_1 = 3, \beta = 0.5, F = 1)$ 166

5.9 Changes in flow rate Q_s with particle volume fraction γ for various values of the transition parameter a_1 $(a_1 = 1, 2, 3, 4)$ under **(5.9a)** large Darcy number $(k = 10, n = 0.1, \varepsilon_f = \varepsilon_b = 0.5)$ and **(5.9b)** small Darcy number $(k = 0.1, n = 2, \varepsilon_f = \varepsilon_b = 0.2)$. $(a = 0.4, b = 0.7, F = 1, \beta = 0.5, We = 0.2, \eta = 0.1)$ . . 167

5.10 Dimensionless hydrodynamic permeability L_{11} with particle volume fraction γ for different thicknesses of Forchheimer layer b $(b = 0.55, 0.7, 0.85)$ under **(5.10a)** large Darcy number $(k = 10, n = 0.1, \varepsilon_f = \varepsilon_b = 0.5)$ and **(5.10b)** small Darcy number $(k = 0.12, n = 2, \varepsilon_f = \varepsilon_b = 0.1)$. $(a = 0.4, \beta = 0.5, We = 0.2, a_1 = 3, \eta = 0.1, F = 1)$ 167

5.11 Dimensionless hydrodynamic permeability L_{11} with particle volume fraction γ for various values of permeability parameters $(\varepsilon_f, \varepsilon_b)$ under **(5.11a)** large Darcy number $(k = 10, n = 0.1, \varepsilon_f = \varepsilon_b = 0.1, 0.5, 0.9)$ and **(5.11b)** small Darcy number $(k = 0.12, n = 2, \varepsilon_f = \varepsilon_b = 0.1, 0.2, 0.3)$. $(a = 0.4, b = 0.7, \beta = 0.5, We = 0.2, a_1 = 3, \eta = 0.1, F = 1)$ 168

5.12 Dimensionless hydrodynamic permeability L_{11} with particle volume fraction γ for comparative values of permeability parameters $(\varepsilon_f, \varepsilon_b)$ under **(5.12a)** large Darcy number $(k = 10, n = 0.1)$ and **(5.12b)** small Darcy number $(k = 0.12, n = 2)$. $(a = 0.4, b = 0.7, \beta = 0.5, We = 0.2, a_1 = 3, \eta = 0.1, F = 1)$ 169
5.13 Dimensionless hydrodynamic permeability L_{11} with particle volume fraction γ for various values of transition parameter a_1 $(a_1 = 1, 2, 3, 4)$ under small Darcy number $(k = 0.1, n = 2.0, \varepsilon_f = \varepsilon_b = 0.1, a = 0.4, b = 0.7, \beta = 0.5, We = 0.2, \eta = 0.1, F = 1)$ 169
5.14 Dimensionless hydrodynamic permeability L_{11} with Brinkman permeability parameter ε_b for different thicknesses of Forchheimer layer b under small Darcy number $(k = 0.1, n = 2, \varepsilon_f = 0.1, a_1 = 3, a = 0.4, \gamma = 0.2, \beta = 0.5, We = 0.2, \eta = 0.1, F = 1)$ 170
5.15 Dimensionless hydrodynamic permeability L_{11} with Brinkman permeability parameter ε_b for various values of Forchheimer permeability parameter ε_f under small Darcy number $(k = 0.1, n = 2, a_1 = 3, a = 0.4, b = 0.7, \gamma = 0.2, \beta = 0.5, We = 0.2, \eta = 0.1, F = 1)$ 170
5.16 Dimensionless hydrodynamic permeability L_{11} with thickness of Forchheimer layer b for various values of transition parameter a_1 under small Darcy number $(k = 0.2, n = 2, \varepsilon_f = \varepsilon_b = 0.1, a = 0.4, \gamma = 0.2, \beta = 0.5, We = 0.2, \eta = 0.1, F = 1)$ 171
5.17 Dimensionless hydrodynamic permeability L_{11} with thickness of Forchheimer layer b for various values of Brinkman permeability parameter ε_b under small Darcy number $(k = 0.2, n = 2, \varepsilon_f = 0.1, a_1 = 3, a = 0.4, \gamma = 0.2, \beta = 0.5, We = 0.2, \eta = 0.1, F = 1)$ 172
5.18 Dimensionless hydrodynamic permeability L_{11} with thickness of Forchheimer layer b for various values of Forchheimer permeability parameter ε_f under small Darcy number $(k = 0.15, n = 2, \varepsilon_b = 0.1, a_1 = 3, a = 0.4, \gamma = 0.2, \beta = 0.5, We = 0.2, \eta = 0.1, F = 1)$ 172
5.19 Dimensionless hydrodynamic permeability L_{11} with the Weissenberg number We for various values of transition parameter a_1 $(a_1 = 1, 2, 3, 4)$ under small Darcy number $(k = 0.2, n = 2, \varepsilon_f = \varepsilon_b = 0.1, a = 0.4, b = 0.7, \gamma = 0.445, \beta = 0.5, \eta = 0.1, F = 1)$ 173
5.20 Dimensionless hydrodynamic permeability L_{11} with the Weissenberg number We for comparative values of permeability parameters $(\varepsilon_f, \varepsilon_b)$ under small Darcy number $(k = 0.2, n = 2, a_1 = 3, a = 0.4, b = 0.7, \gamma = 0.445, \beta = 0.5, \eta = 0.1, F = 1)$ 173

5.21 Kozeny constant K_z with stress-jump parameter β for various values of the Forchheimer number F under large Darcy number $(k = 10, n = 0.1, \varepsilon_f = \varepsilon_b = \varepsilon = 0.5, a_1 = 3, a = 0.4, b = 0.7, \gamma = 0.2, We = 0.2, \eta = 0.1)$ 175
5.22 Kozeny constant K_z with porosity parameter ε for various values of permeability parameters, $(\varepsilon_f, \varepsilon_b)$ under **(5.22a)** large Darcy number $(k = 10, n = 0.1)$ and **(5.22b)** small Darcy number $(k = 0.2, n = 2)$. $(a = 0.4, b = 0.7, \gamma = 0.2, \beta = 0.5, a_1 = 3, We = 0.2, \eta = 0.1, F = 1)$ 175
5.23 Kozeny constant K_z with porosity parameter ε for different thicknesses of Forchheimer layer b under large Darcy number $(k = 10, \varepsilon_f = \varepsilon_b = 0.5, a_1 = 3, a = 0.4, b = 0.7, \gamma = 0.2, \beta = 0.5, We = 0.2, \eta = 0.1, F = 1)$ 175
5.24 Kozeny constant K_z with particle volume fraction γ for various values of permeability parameters $(\varepsilon_f, \varepsilon_b)$ under **(5.24a)** large Darcy number $(k = 10, n = 0.1)$ and **(5.24b)** small Darcy number $(k = 0.2, n = 2.0)$. $(a = 0.4, b = 0.7, \beta = 0.5, a_1 = 3, We = 0.2, \eta = 0.1, F = 1, \varepsilon = 0.5)$ 176
5.25 Dimensionless temperature θ with radial direction r for various values of transition parameter a_1 under **(5.25a)** large Darcy number $(k = 10, n = 0.1, \varepsilon_f = \varepsilon_b = 0.5)$ and **(5.25b)** small Darcy number $(k = 0.1, n = 2, \varepsilon_f = \varepsilon_b = 0.2)$. $(a = 0.4, b = 0.7, \gamma = 0.445, \beta = 0.5, We = 0.2, \eta = 0.1, F = 1)$ 177
5.26 Dimensionless temperature θ with radial direction r for different thicknesses of Forchheimer layer b under **(5.26a)** large Darcy number $(k = 10, n = 0.1, \varepsilon_f = \varepsilon_b = 0.5)$ and **(5.26b)** small Darcy number $(k = 0.1, n = 2.0, \varepsilon_f = \varepsilon_b = 0.2)$. $(a = 0.4, \gamma = 0.445, \beta = 0.5, We = 0.2, a_1 = 3.0, \eta = 0.1, F = 1)$ 177
5.27 Dimensionless temperature θ with radial direction r for various values of permeability parameters $(\varepsilon_f, \varepsilon_b)$ under **(5.27a)** large Darcy number $(k = 10, n = 0.1, \varepsilon_f = \varepsilon_b = 0.1, 0.5, 0.9)$ and **(5.27b)** small Darcy number $(k = 0.2, n = 2, \varepsilon_f = \varepsilon_b = 0.1, 0.2, 0.3)$. $(a = 0.4, b = 0.7, \gamma = 0.445, \beta = 0.5, We = 0.2, a_1 = 3, \eta = 0.1, F = 1)$ 178
5.28 Dimensionless temperature θ with radial direction r for various values of the Forchheimer number F $(F = 1, 2, 3)$ under small Darcy number $(k = 0.1, n = 2, \varepsilon_f = \varepsilon_b = 0.1, a = 0.4, b = 0.7, \gamma = 0.445, \beta = 0.5, We = 0.2, a_1 = 3, \eta = 0.1, Br = 1)$ 178
5.29 Dimensionless temperature θ with radial direction r for various values of Brinkman numbers Br $(Br = 0, 1, 2, 3)$ under **(5.29a)** large Darcy number $(k = 10, n = 0.1, \varepsilon_f = \varepsilon_b = 0.5)$ and **(5.29b)** small Darcy number $(k = 0.1, n = 2, \varepsilon_f = \varepsilon_b = 0.2)$. $(a = 0.4, b = 0.7, \gamma = 0.445, \beta = 0.5, We = 0.2, a_1 = 3, \eta = 0.1, F = 1)$ 179

5.30 Changes in Nusselt number Nu with Brinkman number Br for various values of **(5.30a)** varying permeabilities $\varepsilon_f, \varepsilon_b$ $(F = 1)$ and **(5.30b)** Forchheimer number F $(\varepsilon_f = \varepsilon_b = 0.1)$. $(a = 0.4, b = 0.7, \gamma = 0.445, \beta = 0.5, We = 0.2, a_1 = 3, \eta = 0.1)$ 180
5.31 Changes in Nusselt number Nu with particle volume fraction γ for various values of **(5.31a)** Weissenberg number We $(a_1 = 3)$ and **(5.31b)** transition parameter a_1 $(We = 0.2)$. $(a = 0.4, b = 0.7, \varepsilon_f = \varepsilon_b = 0.1, \beta = 0.5, \eta = 0.1, F = 3, Br = 1)$ 180
5.32 Various reduced cases of the current study for large Darcy number $(k = 100)$ $(\gamma = 0.445, \beta = 0.5, \eta = 0.1)$ 180
5.33 Validation of the current study with the study of Saini *et al.* [199] under large Darcy number $(k = 100, n = 0.2, \varepsilon_f = \varepsilon_b = 0, a = 0.5, b = 1.0, \gamma = 0.5, \beta = 0.5, We = 0.5, a_1 = 2, \eta = 0.1, F = 0)$ 181
5.34 Validation of the current study with the study of Deo *et al.* [3] and Saini *et al.* [199] under large Darcy number $(k \to \infty, \varepsilon_f = \varepsilon_b = 0, a = 0.5, b = 1, \gamma = 0.445, \beta = 0.5, a_1 = 3, \eta = 0.1, F = 0)$ 181

6.1 **(a)** The visual representation of the flow along the axis within a membrane consisting of a collection of bi-porous layered solid cylinders, **(b)** A hypothetical cell encloses a biporous layer surrounding a solid cylindrical particle within a swarm, visually depicted as a circular cross-sectional view. 190
6.2 A hypothetical cell encloses a solid core within biporous layers, which in turn are coated with a cylindrical particle exhibiting a circular cross-section in its physical sketch 191
6.3 Dimensionless entropy S with radial distance r for various values of Brinkmann number Br $(Br = 0.1, 1.0, 2.0)$ under **(a)** large Darcy number $(k = 10, T_0 = 1, Pe = 50)$ and **(b)** small Darcy number $(k = 0.1, T_0 = 10, Pe = 500)$.$(\lambda_1 = 1, b = 0.7, \gamma = 0.444, F = 1, Nu = 4.0)$ 207
6.4 Dimensionless entropy S with radial distance r for various values of Peclet number Pe under **(a)** large Darcy number $(k = 10, T_0 = 1, Nu = 4, Br = 0.8)$ and **(b)** small Darcy number $(k = 0.1, T_0 = 10, Nu = 4, Br = 2.0)$.$(\lambda_1 = 1, b = 0.7, \gamma = 0.444, F = 1)$ 208
6.5 Dimensionless entropy S with radial distance r for various values of permeability parameters $\varepsilon_f, \varepsilon_b$ under **(a)** large Darcy number $(k = 10, T_0 = 1, Pe = 50, Br = 0.8)$ and **(b)** small Darcy number $(k = 0.1, T_0 = 10, Pe = 500, Br = 2.0)$.$(\lambda_1 = 1, b = 0.7, \gamma = 0.444, F = 1, Nu = 4.0)$ 208

6.6 Dimensionless entropy S with radial distance r for different thickness of Forchheimer layer b under **(a)** large Darcy number $(k = 10, T_0 = 1, Br = 0.8)$ and **(b)** small Darcy number $(k = 0.1, T_0 = 10, Br = 2.0).(\lambda_1 = 1, b = 0.7, \gamma = 0.444, F = 1, Nu = 4.0, Pe = 50)$ 209
6.7 Dimensionless entropy, S with radial distance, r for various values of Forchheimer number F under **(a)** large Darcy number $(k = 10, T_0 = 1, Br = 0.8)$ and **(b)** small Darcy number $(k = 0.1, T_0 = 10, Br = 2.0).(\lambda_1 = 1, b = 0.7, \gamma = 0.444, F = 1, Nu = 4.0, Pe = 50, \varepsilon_f = \varepsilon_b = 0.5)$ 209
6.8 Dimensionless entropy, S with radial distance, r for various values of viscosity ratio parameter λ_1 under **(a)** large Darcy number $(k = 10, T_0 = 1, Br = 0.8)$ and **(b)** small Darcy number $(k = 0.1, T_0 = 10, Br = 2.0).(b = 0.7, \gamma = 0.444, F = 1, Nu = 4.0, Pe = 50, \varepsilon_f = \varepsilon_b = 0.5)$ 210
6.9 Bejan number, Be with radial distance, r for various values of viscosity ratio parameter λ_1 under small Darcy number $(k = 0.1, T_0 = 1, \varepsilon_f = \varepsilon_b = 0.1).(b = 0.7, \gamma = 0.444, F = 1, Nu = 4.0, Pe = 100)$ 211
6.10 Bejan number, Be with radial distance, r for various values of Peclet number Pe under small Darcy number $(k = 0.1, T_0 = 1, Br = 2, \varepsilon_f = \varepsilon_b = 0.1).(b = 0.7, \gamma = 0.444, F = 1, Nu = 4.0)$ 211
6.11 Bejan number, Be with radial distance, r for various values of viscous dissipation coefficient $\left(\frac{Br}{T_0}\right)$ under small Darcy number $(k = 0.1, \varepsilon_f = \varepsilon_b = 0.1).(b = 0.7, \gamma = 0.444, F = 1, Nu = 4.0, Pe = 100)$ 212
6.12 Bejan number, Be with radial distance, r for various values of variable permeability parameters $(\varepsilon_f, \varepsilon_b)$ under small Darcy number $(k = 0.1, T_0 = 1, Br = 2, \varepsilon_f = \varepsilon_b = 0.1).(b = 0.7, \gamma = 0.444, F = 1)$ 212
6.13 Comparision of velocity obtain via asymptotic solution and numerical solution of the problem for the large permeability case $(k = 100, \varepsilon_f = \varepsilon_b = 0.5, \gamma = 0.445, \lambda_1 = 1, F = 1)$. 213
6.14 Validation of current study with the study of Deo *et al.* in terms of Hydrodynamic permeability, L_{11} for $k \to \infty, a = b = 1$. 214
6.15 Different reduced cases of current work under large permeability parameter $(k = 100, \varepsilon_f = \varepsilon_b = 0.5, \gamma = 0.445, \lambda_1 = 1, F = 3)$. 214

7.1 The cross-section of an array of uniformly distributed corrugated porous layered cylindrical particles 220
7.2 The circular cross-section of an corrugated cylindrical particle with the hypothetical cell 221

7.3 Contours of velocity profile, $w(r,\phi)$ for different wave number, λ. $(a = 0.5, \gamma = 0.445, pz = 1, k = 3, \delta = 0.1, \beta = 0.4)$ . . . 231
7.4 Contours of velocity profile, $w(r,\phi)$ for different height of corrugation δ. $(a = 0.5, \gamma = 0.445, pz = 1, k = 3, \lambda = 6, \beta = 0.4)$ . . . 232
7.5 Contours of velocity profile, $w(r,\phi)$ for different values of the Darcy number, k. $(a = 0.5, \gamma = 0.445, pz = 1, \delta = 0.1, \lambda = 6, \beta = 0.1)$ . . . 232
7.6 Contours of velocity profile, $w(r,\phi)$ for different values of the stress-jump parameter β, for large $(k = 2)$ and small $(k = 0.1)$ permeability of porous media. $(a = 0.5, \gamma = 0.445, pz = 1, \delta = 0.1, \lambda = 6)$ . . . 233
7.7 The dependence of hydrodynamic permeability L_{11} on the corrugation height δ for different values of wave number λ. $(a = 0.5, \gamma = 0.445, pz = 1, k = 0.5, \beta = 0.1)$ . . . 234
7.8 The dependence of hydrodynamic permeability L_{11} on the corrugation height δ for different values of stress-jump parameter β. $(a = 0.5, \gamma = 0.445, pz = 1, k = 0.5, \lambda = 6)$ . . . 234
7.9 The dependence of hydrodynamic permeability L_{11} on the particle volume fraction γ for different values of corrugation height δ. $(a = 0.5, pz = 1, k = 0.5, \lambda = 6, \beta = 0.1)$ . . . 235
7.10 The dependence of hydrodynamic permeability L_{11} on the particle volume fraction γ for different values of wave number λ. $(a = 0.5, pz = 1, k = 0.5, \delta = 0.1, \beta = 0.1)$ . . . 235
7.11 The dependence of hydrodynamic permeability L_{11} on the Darcy number k for different values of corrugation height δ. $(a = 0.5, pz = 1, k = 0.5, \lambda = 6, \beta = 0.2)$ . . . 236
7.12 The dependence of hydrodynamic permeability L_{11} on the Darcy number k for different values of wave number parameter k. $(a = 0.5, pz = 1, k = 0.5, \delta = 0.1, \beta = 0.1)$ . . . 236
7.13 The dependence of the Kozeny constant K_z on the porosity ε for different values of corrugation height δ. $(a = 0.5, pz = 1, k = 0.5, \lambda = 6, \beta = 0.1)$ . . . 237
7.14 The dependence of the Kozeny constant K_z on the porosity ε for different values of particle volume fraction γ. $(a = 0.5, pz = 1, k = 0.5, \lambda = 6, \delta = 0.1, \beta = 0.1)$ . . . 238
7.15 The dependence of the Kozeny constant K_z on corrugation height δ for different values of stress-jump parameter β. $(a = 0.5, pz = 1, k = 0.5, \lambda = 6, \varepsilon = 0.5)$ . . . 238

7.16 The dependence of the Kozeny constant K_z on corrugation height δ for different values of stress-jump parameter β. $(a = 0.5, pz = 1, \beta = 0.1, \lambda = 6, \varepsilon = 0.5)$ 239
7.17 The dependence of the Kozeny constant K_z on corrugation height δ for different values of the wave number λ. $(a = 0.5, pz = 1, k = 0.5, \beta = 0.1, \varepsilon = 0.5)$ 239

8.1 The physical sketch of cell model considered in a swarm of particles 246
8.2 The cross-sectional view of a cylindrical particle having the solid core, coated with a poly-electrolyte(porous) layer. 247
8.3 The electric potential distribution ψ in radial direction r with varying **(a)** thicknesses of EDL layer λ $(K = 1)$, **(b)** ratio parameter K $(\lambda = 0.1)$. $(a = 0.5, \gamma = 0.445, \zeta = 1)$ 261
8.4 The electric potential distribution ψ in radial direction r with varying zeta potential ζ $(K = 1, \lambda = 0.1)$. $(a = 0.5, \gamma = 0.445)$ 261
8.5 The dependence of velocity profile w on the radial distance r for different values of EDL thicknesses (λ) in case of **(a)** large Darcy number $(k = 200, \zeta = 1, \varepsilon_f = 0.5)$, **(b)** small Darcy number $(k = 0.07, \zeta = 0.8, \varepsilon_f = 0.1)$. $(\gamma = 0.444, K = 1, p_s = 1, \mu_R = 1.0, \beta = 0.4, F = 1)$ 262
8.6 The dependence of velocity profile w on the radial distance r for different values of ratio parameter (K) in case of **(a)** large Darcy number $(k = 200, \zeta = 1, \lambda = 0.1, \varepsilon_f = 0.5)$, **(b)** small Darcy number $(k = 0.07, \zeta = 0.8, \lambda = 0.4, \varepsilon_f = 0.1)$. $(\gamma = 0.444, p_s = 1, \mu_R = 1.0, \beta = 0.4, F = 1)$ 262
8.7 The dependence of velocity profile w on the radial distance r for different values of variable permeability parameter (ε_f) in case of **(a)** large Darcy number $(k = 200, \zeta = 1, \lambda = 0.1)$, **(b)** small Darcy number $(k = 0.07, \zeta = 0.8, \lambda = 0.3)$. $(\gamma = 0.444, p_s = 1, K = 1, \mu_R = 1.0, \beta = 0.4, F = 1)$ 263
8.8 The dependence of velocity profile w on the radial distance r for different values of zeta potential (ζ) in case of **(a)** large Darcy number $(k = 200, \lambda = 0.1, \varepsilon_f = 0.5)$, **(b)** small Darcy number $(k = 0.07, \lambda = 0.3, \varepsilon_f = 0.1)$. $(\gamma = 0.444, p_s = 1, K = 1, \mu_R = 1.0, \beta = 0.4, F = 1)$ 263
8.9 The dependence of velocity profile w on the radial distance r for different values of viscosity ratio parameter (μ_R) in case of **(a)** large Darcy number $(k = 200, \zeta = 0.8, \lambda = 0.1, \varepsilon_f = 0.5)$, **(b)** small Darcy number $(k = 0.07, \zeta = 1, \lambda = 0.3, \varepsilon_f = 0.1)$. $(\gamma = 0.444, p_s = 1, K = 1, \beta = 0.4, F = 1)$ 264

8.10 The dependence of velocity profile w on the radial distance r for different values of stress-jump parameter (β) in case of **(a)** large Darcy number ($k = 200, \zeta = 0.8, \lambda = 0.1, \varepsilon_f = 0.5$), **(b)** small Darcy number ($k = 0.07, \zeta = 1, \lambda = 0.3, \varepsilon_f = 0.1$). ($\gamma = 0.444, p_s = 1, K = 1, \mu_R = 1.0, F = 1$) 265
8.11 The dependence of velocity profile w on the radial distance r for different values of Forchheimer number (F) in case of **(a)** large Darcy number ($k = 200, \zeta = 0.8$), **(b)** small Darcy number ($k = 0.07, \zeta = 1$). ($\gamma = 0.444, p_s = 1, K = 1, \lambda = 0.3, \mu_R = 1.0, \varepsilon_f = 0.1, \beta = 0.4$) 265
8.12 The dependence of hydrodynamic permeability L_{11} on the particle volume fraction γ for different EDL thicknesses (λ) in case of **(a)** large Darcy number ($k = 200$), **(b)** small Darcy number ($k = 0.01$). ($p_s = K = \zeta = F = \mu_R = 1.0, \varepsilon_f = 0.1, \beta = 0.4$) 266
8.13 The dependence of hydrodynamic permeability L_{11} on the particle volume fraction γ for different ratio parameter (K) in case of **(a)** large Darcy number ($k = 200$), **(b)** small Darcy number ($k = 0.01$). ($p_s = \zeta = F = \mu_R = 1.0, \lambda = 0.1, \varepsilon_f = 0.1, \beta = 0.4$) 267
8.14 The dependence of hydrodynamic permeability (L_{11}) on the particle volume fraction (γ) for different zeta potential (ζ) in case of **(a)** large Darcy number ($k = 200$), **(b)** small Darcy number ($k = 0.01$). ($p_s = K = F = \mu_R = 1.0, \lambda = 0.3, \varepsilon_f = 0.1, \beta = 0.4$) 268
8.15 The dependence of hydrodynamic permeability (L_{11}) on variable permeability (ε_f) for different ratio parameter (K) in case of **(a)** large Darcy number ($k = 200, \gamma = 0.2$), **(b)** small Darcy number ($k = 0.01, \gamma = 0.44$). ($p_s = \zeta = F = \mu_R = 1.0, \lambda = 0.1, \varepsilon_f = 0.1, \beta = 0.4$) 268
8.16 The dependence of hydrodynamic permeability (L_{11}) on stress-jump parameter (β) for different particle volume fraction (γ) in case of **(a)** large Darcy number ($k = 200$), **(b)** small Darcy number ($k = 0.01$). ($p_s = \zeta = F = K = \mu_R = 1.0, \lambda = 0.3, \varepsilon_f = 0.1$) 269
8.17 The dependence of hydrodynamic permeability (L_{11}) on ratio parameter (K) for different viscosity ratio parameter (μ_R) in case of **(a)** large Darcy number ($k = 200, \gamma = 0.2, \lambda = 0.14$), **(b)** small Darcy number ($k = 0.01, \gamma = 0.444, \lambda = 0.1$). ($p_s = \zeta = F = 1.0, \varepsilon_f = 0.1, \beta = 0.4$) 269
8.18 The dependence of hydrodynamic permeability (L_{11}) on EDL thickness (λ) for different viscosity ratio parameter (μ_R) in case of **(a)** large Darcy number ($k = 200, \gamma = 0.2$), **(b)** small Darcy number ($k = 0.01, \gamma = 0.444$). ($p_s = \zeta = F = K = 1.0, \varepsilon_f = 0.1, \beta = 0.4$) 270

8.19 The dependence of Kozeny constant (K_z) on porosity of the medium(ε) for different ratio parameter (K) in case of **(a)** large Darcy number ($k = 200, \gamma = 0.6$), **(b)** small Darcy number ($k = 0.01, \gamma = 0.444$). ($p_s = \zeta = F = \mu_R = 1, \lambda = 0.1, \varepsilon_f = 0.1, \beta = 0.4$) 271
8.20 The dependence of Kozeny constant (K_z) on porosity of the medium(ε) for different zeta potential (ζ) in case of **(a)** large Darcy number ($k = 200, \gamma = 0.6$), **(b)** small Darcy number ($k = 0.01, \gamma = 0.444$). ($p_s = K = F = \mu_R = 1, \lambda = 0.4, \varepsilon_f = 0.1, \beta = 0.4$) 271
8.21 The dependence of Kozeny constant (K_z) on EDL thickness (λ) for different stress-jump parameter (β) in case of **(a)** large Darcy number ($k = 200, \gamma = 0.6$), **(b)** small Darcy number ($k = 0.01, \gamma = 0.444$). ($p_s = K = \zeta = F = \mu_R = 1, \lambda = 0.4, \varepsilon_f = 0.1$) 272
8.22 The dependence of Kozeny constant (K_z) on ratio parameter(K) for different Forchheimer number (F) in case of **(a)** large Darcy number ($k = 200$), **(b)** small Darcy number ($k = 0.01$). ($p_s = \zeta = \mu_R = 1, \gamma = 0.444, \lambda = 0.1, \varepsilon_f = 0.1, \beta = 0.4$) 272
8.23 **(a)** Comparision among special cases of the current model ($k = 200$), **(b)** Validation of the asymptotic solution of current model with numerical solution (200). 273

List of Tables

1 Range of values for the existing parameters with their resources xli

2.1 Range of values for the existing parameters with their resources 51
2.2 Variation of hydrodynamic permeability of membrane L_{11} for **(a)** small permeability $(k = 0.05)$ and **(b)** large permeability $(k = 100)$ of the porous medium, under different values of viscosity parameter α, Forchheimer number F and Jeffrey fluid parameter λ_1. $(l = \gamma = 0.5, \zeta_h = 5, p_s = 1, \beta_S = 0.1)$ 55
2.3 Variation of hydrodynamic permeability of membrane L_{11} for different values of viscosity parameter α, Forchheimer number F and Jeffrey fluid parameter λ_1. $(l \to 0, \gamma = 0.5, \zeta_h = 5, p_s = 1, k = 0.05, \beta_S = 0.1)$ 57

3.1 Domain of interest for the ongoing parameters with their references 81
3.2 Validation of current work with the study of Deo *et al.* [3] using variations in hydrodynamic permeability L_{11} with particle volume fraction γ. $(\alpha = 0.1)$. 99
3.3 Validation of current work with the study of McKee *et al.* [14] using variations in velocity w in radial direction r for different values electric Hartmann number, H $(H^2 = 1, 10, 100)$. 99

4.1 Domain of interest for the ongoing parameters with their references 119
4.2 Variation of Permeability k on **(a)** the membrane permeability L_{11} and **(b)** Kozeny constant K_z of the porous medium under different values of Weissenberg number We, and Power-law index n. $(l = \varepsilon = 0.5, \gamma = 0.5, p_s = 1, \beta = 0.1, \eta = 0.1)$ 131

5.1 Range of parameters with their references 161
5.2 Validation of current work with the experimental data of Filippov *et al.* [201] using variations in hydrodynamic permeability, L_{11} with porosity, ε. $(a = b = 1, We = 0, \beta = 0, n = \eta = 0, \varepsilon_f = \varepsilon_b = 0, F = 0)$. 174

6.1 Domain of interest for the ongoing parameters with their references 206

7.1 Ranges for the ongoing parameters with their references 230

8.1 Ranges for the ongoing parameters with their references 260

List of Symbols

$\sim$	Represents dimensional quantities
r	Radial (transverse) distance
z	Axial (longitudinal) distance
w_f, w_b, w_s	Axial velocities in Forchheimer, Brinkman and Stokes regions, respectively
w_p, w_c	Axial velocities in Porous and clear fluid regions, respectively
C	Drag coefficient
C_F	Inertial coefficient
C_F	Forchheimer number
p	Pressure
$\mathbf{q}$	Darcian velocity vector
$\mathbf{J}$	Current density
n	Power law index
η	Viscosity ratio parameter
p_s	Pressure gradient in steady flow state
Q_s	Volumetric flow rate for steady flow
k	Permeability in porous medium
w_0	Characteristic (Average) velocity
g	Gravitational acceleration
T	Temperature
Q	Heat absorption coefficient
K	Thermal conductivity
Gr	Grashof number
J_0, Y_0	Bessel functions of first and second kind of order zero, respectively
I_0, K_0	Modified Bessel functions of first and second kind of order zero, respectively
Pe	Peclet number

Greeks letters

ϕ	Azimuthal angle

ρ	Density
θ	Dimensionless temperature
ζ_h	Constant heat absorption parameter
ζ	Wall potential
α	Viscosity parameter
$\alpha_p = 1/\lambda_1^2$	Porosity parameter
τ	Shear stress of fluid
γ	Particle volume fraction
μ	Viscosity of Newtonian fluid
μ_0	Constant viscosity coefficient
μ_e	Effective viscosity coefficient of porous medium
λ_1	Viscosity ratio parameter in Brinkman region
λ_J	Jeffrey fluid parameter
β_S	Stress-jump parameter

Physical Parameters

Values of parameters		
Parameters	Values	Resources
Heat absorption parameter ζ	0-9	[1]
Permeability k	$(0,\infty)$	[2], [3]
Steady pressure gradient p_s	1-10	[4], [5]
Stess-jump parameter β_S	$-1<\beta_S<1$	[3], [5]
Viscosity parameter α	0.0-0.5	[1], [6]
Forchheimer number F	0.0-2.0	[7], [8]
Jeffrey fluid parameter λ_1	0.0-2.0	[9], [10]
Particle volume fraction γ	0.1-1.0	[3], [11]
Radiation parameter N_1	2-15	[12], [13]
Grashof number Gr	0.5-17.0	[13]
Hartmann electric number H	0.1-4.0	[14]
Viscosity ratio parameter λ_1	1.0-1.6	[15], [5]
Weissenberg number We	0-0.8	[6]
Power-law index n	0.1-2.0	[16], [17]
Nusselt number Nu	2.0-8.0	[7]
Viscosity ratio parameter η	0.1-0.4	[18]
Transition parameter a_1	1.0-4.0	[18]
Brinkman number Br	0-10	[19], [20]
Peclet number Pe	1-100	[20]
Porosity parameter ε	0.3-1.0	[3]
Dimensionless temperature constant T_0	1.0	[19]
Corrugation height δ	0-0.1	[21]
Wave number λ	1-7	[21]
EDL thickness λ	(0,0.5)	[22], [23]
Equivalent EDL thickness λ_f	(0,0.5)	[22]
zeta potential ζ	(0.8,1.0)	[22]
Variable permeability parameter ε_f	0.0-0.9	[24]

Table 1: Range of values for the existing parameters with their resources

Chapter 1

Introduction

Fluids are substances that owns the remarkable ability to deform under any externally imposed forces and adapt to the shape of their receptacle, regardless of its size or complexity, setting them apart from solid materials, which maintain their shape and volume under normal circumstances. This inherent characteristic of fluids enables them to appear countless times in our everyday experiences, making them one of the most intriguing subjects for exploring their behavior under various circumstances, particularly for researchers and scientists in the field of fluid dynamics. Researchers and scientists are interested in exploring flow dynamics as it passes around objects and their interaction with different materials, driven by its practical relevance in aerospace engineering, environmental science, and biomedical technology.

1.1 Flow around a Body

If we refer to the history of the study of the flow around a body, one of the most deeply studied problems in viscous hydrodynamics deals with the steady-state flow past a sphere placed in an uniform stream. Although the geometric aspects of this problem may seem straightforward but achieving an exact closed-form solution seems to be permanently out of reach. In 1851, an Irish physicist and mathematician, Sir George Gabriel Stokes [25] gave an asymptotic solution of this problem for small values of Reynolds number, where he approached the challenge by employing the equations governing creeping viscous flow and neglected the inertia terms altogether from the Navier Stokes equation. These approximate solutions are called *Stokes' solutions* and approximation involved in these solutions is often termed as *Stokes' approximation*. In absence of the body forces, the Stokes equation for steady flow of an incompressible fluid, is given by, (1.1)

$$\mu \nabla^2 \mathbf{u} = \nabla p, \tag{1.1}$$

where $\mathbf{u}, p,$ and μ are fluid velocity, pressure and viscosity, respectively. This led to the formulation of the renowned *Stokes' law*, which states that a force of $6\mu\pi U_0 a$ is necessary to sustain a constant velocity U_0 for a sphere with radius a moving through a liquid with a viscosity coefficient of μ. Following Stokes' initial investigations, some conceptual issues emerged with the theory of creeping flow past a body. The later research on this topic is centered around these difficulties. When Stokes endeavored to explore the steady creeping flow around an infinitely long cylinder using the two-dimensional Stokes equations, he encountered challenges in deriving a solution that adequately satisfies both near-field and far-field boundary conditions. As a result, he concluded that an exact solution to this problem does not exist. This absence of such a solution is recognized as *Stokes' paradox*. The paradox draws attention to one of the Stokes equations' shortcomings. They are only valid at very low Reynolds numbers (velocities). The fluid's inertia becomes significant at larger distances from the object, even in slowly-moving fluids, and this effect was not captured by the Stokes equations. In 1910, Carl Wilhelm Oseen [26] introduced the Oseen equations as a solution to this limitation. Oseen noted that the ratio of the inertia term to the viscous term, given by $Re \times \frac{r}{L}$ at a distance r, is insignificant only when both the Reynolds number (Re) and $\frac{r}{L}$ are small. He argued that Stokes' equations failed to satisfy boundary conditions at far distances because Stokes neglected the inertia term entirely. However, Oseen highlighted that at sufficiently large distances, regardless of how small the Reynolds number might be, the ratio of the inertia term to the viscous term becomes non-negligible, leading to comparable magnitudes of inertia and viscous forces. Therefore, the Stokes' approximation becomes ineffective in the far field. Consequently, if one aims to apply Stokes' equations in regions far from the body, the inertia terms must also be considered. However, incorporating these terms introduces non-linearity into the governing equations, rendering the solution of these equations intractable. In response to this challenge, Oseen introduced the modified Stokes equations that take into account the convective acceleration term partly, which is important at larger distances, and provide a more accurate description of the flow in such scenarios. In absence of body forces, the Oseen's equation for steady flow of an incompressible fluid, is given by,

$$\begin{aligned} \rho(\mathbf{U_0}\cdot\nabla)\mathbf{u}' &= -\nabla p + \mu\nabla^2\mathbf{u}', \\ \nabla\cdot\mathbf{u}' &= 0, \end{aligned} \tag{1.2}$$

where $\mathbf{U_0} = (U_0, 0, 0)$ is the constant velocity, and $\mathbf{u}' = (u', v', w')$ is the perturbation term which is small with respect to U_0. The Oseen equation received significant attention due to its analytical tractability, as its solutions provided critical quantitative understandings of characteristics such as drag in low Reynolds number flows around bluff bodies. These

insights were especially useful before the introduction of computational fluid dynamics (CFD). Lamb [27] [28] discussed the limitations of the accepted solutions for the motion of a sphere and circular cylinder through a viscous fluid and presented Oseen's results in a simpler form using a different method, but still subject to the same limitation. Goldstein [29], in 1929, made the initial attempt to solve Oseen's linearized equation of motion analytically, where he focused on examining the steady flow of an incompressible viscous fluid around a sphere and derived an exact expression for the total drag exerted on the sphere. Similarly, Faxen(1927) [30] derived the exact analytical solution for the same problem concerning a circular cylindrical body. Imai [31] made an attempt to solve Oseen's linearized equations for 2D, steady viscous fluid flow past an arbitrary cylindrical body. He developed a new general method based on the fact that the velocity near the cylinder can typically be represented using a pair of analytic functions.

Although Oseen successfully addressed the limitation of the Stokes equation by incorporating the convective acceleration term, which included the effect of inertia far from the body, but his approximation assumed linearization to the free stream velocity, which breaks down on the object's boundary. It is evident that the solution provided by the Stokes equations accurately describes the creeping flow near the body but fails to capture the behavior in the far field. Conversely, the Oseen approximation successfully predicts the flow in the far field, yet encounters limitations near the boundary of the body. In response to this challenge, Proudman and Pearson [32] introduced the technique of matched asymptotic expansion. This approach offers a combined solution that integrates the Stokes flow approximation near the object's's surface with the Oseen flow approximation in regions distant from the object's surface. Kaplun [33] proposed a solution that combines an Oseen and Stokes solution by introducing a third term in the expansion for low Reynolds numbers, while Lamb's solution only includes the first two terms. Several authors [34] [35] [36] also explored the phenomenon of flow past a circular cylinder using experimental methods for low Reynolds numbers and presented different qualitative and quantitative results. Tomotika and Aoi [37] used Goldstein's exact analytical solution of Oseen's linearized equations to explore the flow patterns of viscous fluid around a sphere and a circular cylinder at small Reynolds numbers and derived expressions for the pressure and frictional drag. Furthermore, Tomotika and Aoi [38] developed a power series expansion formula for the drag experienced by a circular cylinder moving through a viscous fluid at low Reynolds numbers, claiming that their expression is a more accurate representation of the drag coefficient because it includes Lamb's well-known formula as its first approximation. Yano and Kieda [39] used a discrete singularity approach with a least squares criterion to solve Oseen's linearized equations for a two-dimensional steady flow of an incompressible viscous fluid past arbitrary cylindrical

bodies while satisfying the no-slip boundary condition.

The analytical results provide a good representation of a flow around simple geometrical bodies, but as geometries become more complex, numerical approaches provide a better foundation for the analysis. Lee and Leal [40] investigated the two-dimensional creeping flow around bodies with arbitrary cross-sectional geometries by employing a numerical implementation of the method of matched asymptotic expansions. Their approach utilized Green's integral representations of velocity to analyze the flow behavior. Chadwick [41] integrated Stokes and Oseen flow in a boundary integral formulation, observing that optimal accuracy is achieved when the matching boundary aligns with the body. He resolved an unexplained aspect of the boundary element technique for Stokes flow by demonstrating that the far-field Green's integral in Stokes flow is zero. This is accomplished by matching it to a far-field Green's integral in Oseen flow.

1.2 Flow Through a Porous Media

Fluid flow through porous media is widespread across diverse scientific and technological fields, including hydrology, soil physics, petroleum engineering, chemical engineering, mining, mineral processing, and oil and gas extraction. This phenomenon finds application in various scenarios such as heat exchangers, packed bed reactors, fluid contacting filtration, and different separation and purification devices, as demonstrated by investigations carried out by researchers such as Sutherland et al. [42], Mandal et al. [43], [44], Harris [45], and Kundu et al. [46]. Porous media include towers filled with pebbles, Berl saddles, Raschig rings, sand beds, granules, or lead shot, porous rocks such as limestone, pumice, or dolomite, fibrous aggregates such as cloth, felt, or filter paper, and catalytic particles with extremely small "micro" pores.

Defining "porous media" as solid bodies with "pores" may appear simple, but determining a precise geometrical definition of a "pore" is complex. While it is intuitive to think of "pores" as void spaces within the material, determining their precise size and distribution requires careful consideration. "Pores" refer to void spaces that are neither extremely small, like 'molecular interstices', nor extremely large, like 'caverns' [47]. Their size falls somewhere between these two extremes, though defining their precise limits remains ambiguous and open to interpretation. Pores in a porous system can be interconnected or disconnected. Interstitial fluid flow occurs only when a portion of the pore space is interconnected, which is known as the porous medium's effective pore space. Two crucial parameters in the analytical treatment of flow through porous media are porosity and permeability. Porosity denotes the ratio of the volume of voids or pores to the total material volume, where each pore can

be interconnected, dead-end, or isolated. Effective porosity specifically refers to the volume fraction of interconnected pores. While it might seem intuitive that a higher number of pores would facilitate easier flow, this is not always the case, as permeability plays a crucial role. Permeability quantifies the inter connectivity of voids in the medium, determining the ease of fluid flow. Porosity and permeability, being macroscopic parameters, are solely dependent on pore structure and are independent of other properties. Permeability, often measured in darcy, is uniquely determined by pore geometry and remains unaffected by fluid properties. For instance, a material is considered to have a permeability of 1 darcy if a pressure difference of 1 atmosphere yields a flow rate of 1 cm³/sec of a fluid with 1 centipoise viscosity through a 1 cm³ cube. Hence,

$$1\ darcy = \frac{1(cm^3/sec)1(cp)}{1(cm^2)1(atm/cm)} = 0.987\mu m^2 \tag{1.3}$$

Due to it's vast domain of applications in geological and industrial problems the fluid flow through porous media has been a topic of immense interest for researchers and has been studied for a long time. In 1856, Henri Darcy [48] conducted research on the flow of water in vertical homogeneous sand filters in Dijon, France, which led to the conclusion that the rate of flow is directly proportional to the pressure drop across a bed of fine particles, establishing a pioneering linear correlation between pressure drop and flow rate in the investigation of fluid flow through packed sand. This relationship, later termed Darcy's law, was subsequently refined to incorporate fluid viscosity, and it can be summarized as follows:

$$\frac{\mu \mathbf{q}}{k} = -\frac{\Delta p}{l} \tag{1.4}$$

where the Darcian velocity or superficial velocity $(\mathbf{q})$ is defined as the volume flow rate divided by the total cross-sectional area of the porous medium. This velocity is influenced by the fluid viscosity (μ), the permeability of the porous media (k), and the pressure gradient $(\Delta p/l)$ over the distance l in the direction of flow. It is evident that in Darcy flow within porous media, the dominant factor controlling the motion is the viscous force. Despite being an empirical law, Darcy's law has shown to be successful in providing strong agreement with experimental data when applied to a variety of biomedical engineering-related problems. Darcy's model was extended by Huyghe and Campen [49] to analyze the mechanics of blood flow through soft tissues, and Vankan et al. [50] compared a hierarchical mixture model of blood-perfused biological tissue, incorporating an extended Darcy equation for blood flow. Both approaches produced good agreement. Along with that, several researchers have confirmed that Darcy's law is applicable only to sufficiently slow and

single-phase fluid flow through porous media [51]. Mokadam [52] developed a comprehensive equation for flow through porous media using irreversible thermodynamics, revealing that Darcy's equation represents a specific scenario. Beyond a critical velocity, nonlinearity emerges in the relationship between pressure drop and velocity, attributed to the growing influence of inertial forces arising from interactions between fluid flow and the solid matrix (Chauveteau & Thirriot [53]). Dupuit [54] and Forchheimer [55] are generally credited with first suggesting a nonlinear relationship between pressure drop and Darcian velocity. They proposed that inertial resistance could be represented by the kinetic energy per unit volume of the fluid, denoted by $\rho \mathbf{q}^2$. As a result, in most engineering applications, the governing law for this fluid flow is a modified form of Darcy's equation, where inertial resistance is combined with viscous resistance.

$$\frac{\mu \mathbf{q}}{k} + \rho C \mathbf{q}^2 = -\frac{\Delta p}{l} \tag{1.5}$$

where k represents permeability in the Darcy regime, ρ stands for fluid density, and C represents the drag coefficient of the medium. The term $\rho C \mathbf{q}^2$ accommodates inertial effects or nonlinear flow resistance within the flow. This equation is commonly referred to as the Forchheimer extended Darcy equation. In a recent development, Joseph et al. [56] adjusted the Forchheimer equation using insights from Ward's [57] research, incorporating an inertial coefficient, C_F, into Equation 1.5, where C_F is defined as the product of C and $k^{1/2}$. Consequently, the equation can be represented as:

$$\frac{\mu \mathbf{q}}{k} + \frac{C_F \rho \mathbf{q}^2}{\sqrt{k}} = -\frac{\Delta p}{l} \tag{1.6}$$

Another limitation of Darcy's law is that it does not accurately describe the behavior of highly permeable porous media. As per equation (1.4), when $k \to \infty$, the pressure difference approaches zero, it suggests increased difficulty in flow within the region, contradicting the definition of permeability. To overcome this limitation, Brinkman introduced an alternative extension of the Darcy equation, known as Brinkman's equation. When inertial terms are disregarded, it adopts the following form:

$$\frac{\mu \mathbf{q}}{k} + \mu_e \nabla^2 \mathbf{q} = -\frac{\Delta p}{l} \tag{1.7}$$

The initial viscous term corresponds to the conventional Darcy term, while the second term resembles the Laplacian term found in the Navier-Stokes equation. The coefficient μ_e represents an effective viscosity of porous medium. Vafai and Tien [58], [59] developed a comprehensive model for fluid transport in porous media, incorporating multiple relevant

factors. The model is represented by the following equation:

$$\frac{\rho_f}{\varepsilon}\left(\frac{\partial\langle\mathbf{u}\rangle}{\partial t}+\langle\langle\mathbf{u}\cdot\nabla\rangle\mathbf{u}\rangle\right)=-\nabla\langle p\rangle^f+\frac{\mu_f}{\varepsilon}\nabla^2\langle\mathbf{u}\rangle-\frac{\mu_f}{k}\langle\mathbf{u}\rangle-\frac{\rho_f F\varepsilon}{\sqrt{k}}(\langle\mathbf{u}\rangle\cdot\langle\mathbf{u}\rangle)\mathbf{J} \tag{1.8}$$

The model includes dimensionless parameters such as F and ρ, representing the inertia term coefficient and fluid density respectively. $\nabla\langle p\rangle^f$ and $\mathbf{J}$ denote the average pressure inside the fluid and a unit vector aligned with the velocity vector $\mathbf{u}$, while $\langle\mathbf{u}\rangle$ and $\langle\langle\mathbf{u}\cdot\nabla\rangle\mathbf{u}\rangle$ represent the local volume averages of $\mathbf{u}$ and $\mathbf{u}\cdot\nabla\mathbf{u}$ associated with the fluid. This generalized model, which also incorporates convective terms, is often referred to as the Brinkman-Forchheimer-Darcy equation, where F is replaced by C_F, a dimensionless Forchheimer coefficient.

1.3 Membranes

A safe and clean drinking water is an essential human need to live a healthy lifestyle. However, due to increased environmental and water contamination issues, the majority of the world's population now lacks access to clean water. A significant way to address this issue is through water purification/filtration, which removes contaminants and other impurities from it, and makes it suitable for everyday use. The increasing worldwide population and urbanization, together with a greater awareness of reducing environmental footprints and stronger government rules governing water treatment, are driving an increase in the use of filtration techniques to fulfill the growing demand for clean water. Apart from this, the food, chemical, pharmaceutical, and other industries including separation or purification applications also depend significantly on filtration technology.[60]

The separation technology industry comprises a wide range of techniques and processes used to extract distinct components from mixtures or solutions. The membrane filtration market is a subset of this industry that uses semi-permeable membranes to extract particles, molecules, and ions from liquids and gases. The membrane filtration market focuses on the production, advancement and implementation of filtration systems using semi-permeable membranes and is a quickly growing market in the world. This market is expected to grow at a compound annual growth rate of 8.33% from USD 18.41 billion in 2023 to USD 32.24 billion by 2030, globally, according to a report added to 360iResearch.com. This growth is attributed to the numerous applications of membrane filters across a range of industries, including food and beverage processing, pharmaceuticals and biotechnology, dairy processing, water and wastewater treatment, and the chemicals industry. Hence, the fluid flow analysis in the membrane filtration process has been a topic of immense interest for researchers

in fluid mechanics who want to gain insight into the flow of a liquid past a membrane.

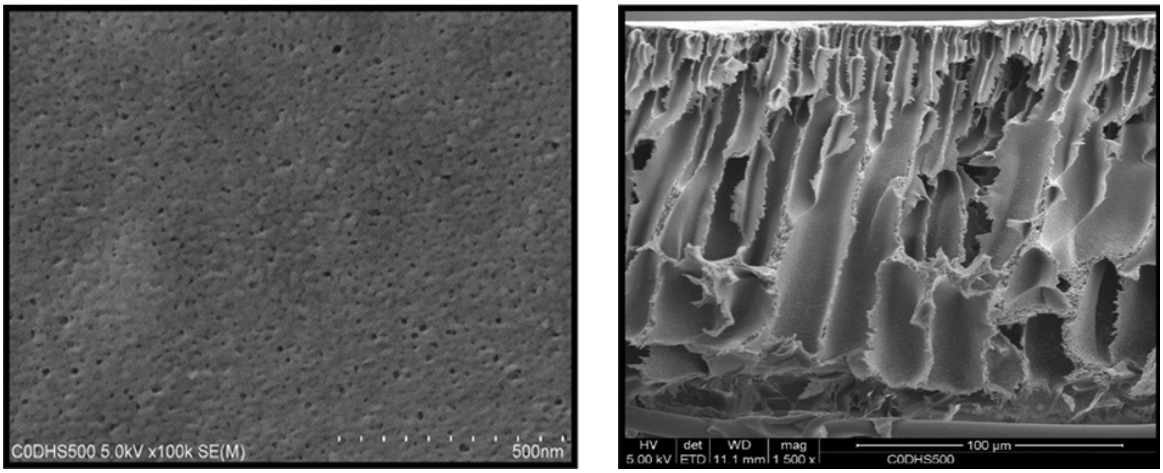

(a) Top View **(b)** X Section

Figure 1.1: Electron microscope image of PES 300 membrane

A membrane is a thin layer of semi-permeable material that is used for solute separation as transmembrane pressure is applied across the membrane. It creates a thin barrier between the macroscopic phases of solute, maintaining a relatively small volume compared to the separated phases. In the early 1700's, membrane separation was first introduced through the word osmosis, which was originally referred to the passage of water through a diaphragm. Following osmosis, the technology advances continuously and used in the membrane distillation, fuel cells, reverse osmosis, gas seperation, electrodialysis and helped to create a plethora of industrial processes, products, and applications.[61]

A membrane has two types: porous and non-porous membrane, and its usefulness often depends upon the degree of selectivity-that is, its capacity to make certain materials easier to transfer between the two bulk phases. Porous membranes are thin, semipermeable membranes that separate solutes when pressure is applied across the membrane. The degree of filtration is largly affected by the charges on the membrane and its porosity. A membrane is having a uniform structure if the pores are symmetric; however non-uniform structured membranes have asymmetric pores have different pore diameters. Porous membranes find primary applications in microfiltration and ultrafiltration processes. These membranes have pores sizes ranging from 0.1 to 10 μm for microfiltration and 0.001 to 0.1 μm for ultrafiltration, which makes particle size-based separation easier. High selectivity requires the pores in the membrane to be smaller than the size of the mixture's particles. Non-porous membranes are primarily employed in gas phase molecular separation, reverse osmosis, and

nanofiltration. These are consist of dense films through which solute diffuses in the presence of pressure, electrical potential, or concentration gradients. The choice of polymeric material significantly influences the membrane's permeability and selectivity. membranes often consist of porous materials with interconnected void spaces

Membranes frequently comprise porous materials, which are structured as particle assemblies or interconnected solid frameworks featuring void spaces either between the particles or within the solid framework itself. Consequently, to investigate fluid flow around a membrane, it becomes necessary to construct a mathematical model focusing on the flow past a particle assembly. This model should account for both the physical and geometrical attributes of the assembly.

1.3.1 Flow Through a Swarm of Particles

Porous materials are typically categorized into two classes: granular media and fibrous media. Granular media comprise compact grains forming a solid matrix with interconnected void spaces characterized by large open pores and narrow constrictions. Examples include rock formations in petroleum reservoirs, catalyst particles, and packed beds in reactors. On the other hand, fibrous media consist of rod-like particles or intricate networks of intertwining fibers. Common examples encompass industrial filters, biological tissues, polymer membranes, and materials in the pulp and paper industry. Fibrous porous media are particularly intriguing due to their properties' close relation to those of fibrous suspensions and entangled polymer networks, emphasizing their multifaceted significance and potential applications in various fields.

Porous structure characteristics are heavily influenced by factors such as particle composition, formation method, and subsequent geological changes, all of which have a significant impact on the media's properties. Clay minerals, for example, tend to form sheet-like structures, whereas granular soils have interlocking Lego block configurations. Figure (1.2) depicts various structures formed by particles of different sizes and shapes.

In this study, our primary focus is on fibrous porous media which is defined as assemblies of fiber like particles (a periodic array of fibers) or interconnected solid frameworks with void spaces between particles or within the solid framework. The void spaces in porous material influence a variety of material properties, including strength, thermal conductivity, and permeability. However, the understanding of the microstructural impact on the permeability of porous materials holds significant relevance across diverse engineering fields. Key research challenges encompass characterizing and quantifying microstructural properties, and integrating these measures effectively into mathematical models that align with physical principles.

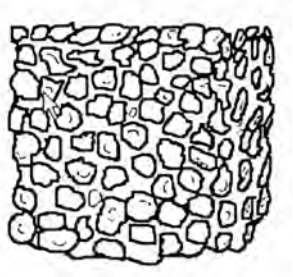

Granular: Similar to cookie crumbs and the size of the particle is usually smaller than 0.6cm.

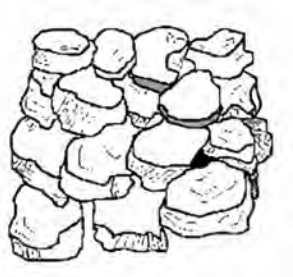

Blocky: Blocks of which the shape is irregular and the diameter ranges from 1.5 to 5.0cm

Prismatic: Vertical columns of soil with length being a number of centimeters long.

Columnar: Vertical columns of soil with a salt “cap"

Platy: Thin, flat plates of soil with horizontal stratification.

Single grained: Soils that have very little or no consistency. The grains do not stick together.

Figure 1.2: Different type of aggregates with different internal structure.(Lowenfels and Yayne [62])

The initial models devised to examine creeping flow within fibrous media were two-dimensional in nature and employed a unit cell comprising either a single fiber or a periodic arrangement of fibers. These models solved the Stokes equations for either parallel flow or transverse flow relative to the fiber axis, from which expressions for hydraulic permeability and/or drag coefficients were deduced. [63, 64, 65, 66, 67, 68] Comprehensive insights into these models can be found in a review article authored by Jackson and James [69].

1.3.2 Cell Model Technique

Most porous structures are inherently complex and it is impossible to precisely describe their solid boundaries, which creates complexities in deriving the solution of the corresponding problem. As a result, it is typically impossible to obtain an accurate mathematical analysis of the fluid flow occurring within porous media. To address this challenge and gain a quantitative understanding, it becomes necessary to adopt a specific model which represent the porous media accurately. The primary objective of a porous media model is to offer a reasonable idealization of the geometrical structure of a specific class of porous media. This idealization allows for the mathematical modeling of a desired fluid transport process. It

is crucial for the model to encompass the most relevant characteristics of the real porous medium while maintaining a manageable level of complexity. From these considerations, it should be clear that the choice of a porous media model depends not only on the porous medium itself but also on the specific process under investigation. Generally, a given porous media model may prove inadequate when applied to studying processes that are more complex or fundamentally different from those for which it was initially formulated.

Recognizing the significance of investigating fluid flow through random arrangements of particles, particularly in groundwater flow modeling, researchers began developing methods to analyze such complex systems. When considering flow through a swarm of particles, the computational burden escalates if the exact positions of all particles within the swarm are accounted for in the flow field solution. To circumvent this complexity, it suffices to derive analytical expressions considering the influence of neighboring particles on the flow field around a single particle within the swarm. Such an approach enables the development of relatively straightforward and dependable models for heat and mass transfer, leading to the emergence of particle-in-cell models.

The central focus throughout this thesis revolves around the utilization of the cell model technique to develop a practical and semi-empirical model that describes the influence of suspended particles on our overall system. This model envisions each particle, referred to as the secondary or suspended phase, positioned at the center of a hypothetical cell containing fluid. Our conceptualization of the two-phase system entails assigning each particle its own distinct cell, characterized by a hypothetical boundary at a uniform radius from the origin of the particle or droplet. This boundary, termed the 'region of influence,' serves as a virtual surface indicating where the properties of the suspension may transition. The fluid enclosed in this region of influence and over the suspended phase is designated as the 'cellular fluid phase,' representing the sole fluid component within the suspending phase affected by the presence of the particle. This approach allows us to discretize the system into three distinct volumes, each of which can be accurately calculated by examining a single cell, owing to the uniformity of our cell structure.

In the beginning, Uchida [70] proposed this model to analyze the creeping flow by assuming fluid to be an infinite cubic assemblage. He considered a hypothetical cubic cell around a randomly chosen particle from swarm. Despite being the space-filling envelope, the undertaken study has a significant drawback of difference in inner and outer geometry which creases mathematical complexities while driving the fluid flow through the swarm.

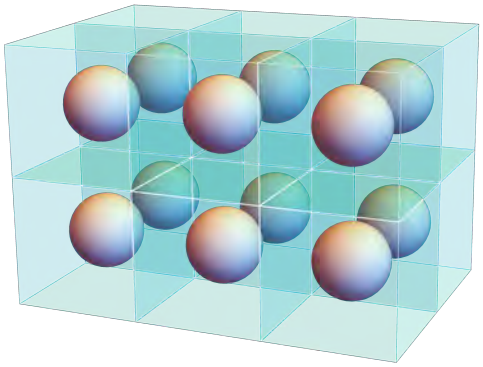

Figure 1.3: Pictorial representation of Uchida's [70] model of swarm of uniformly distributed spherical particles enclosed each in a cubic cell.

Happel ([71], [68]) developed a mathematical treatment based on Uchida's model and removed the limitations by considering both the outer and inner geometry as same. The conditions of uniform velocity with no penetration and no friction at the cell particle's hypothetical surface enable a closed form solution to be acquired, satisfying the Navier-Stokes equation for the flow having low Reynolds number.

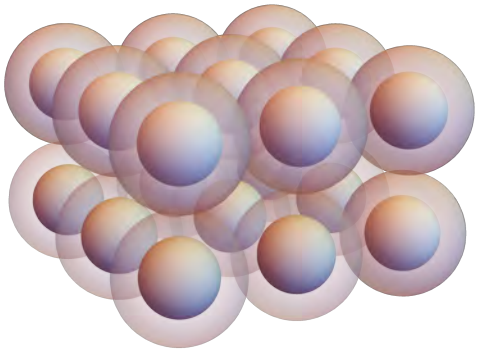

Figure 1.4: Pictorial representation of Happel's [71] model of swarm of uniformly distributed spherical particles enclosed each in a spherical cell.

Kuwabara [67] extended the treatment of regular porous medium to infinitely many circular cylinders or spheres with random and homogeneous distribution in viscous flow. He studied both spherical and cylindrical geometries cases assuming no vorticity on the hypothetical cell surface and derived the expression for velocity and drag force. The Happel formulation is slightly superior to the Kuawbara formulation as each cell exchanges mechanical energy with its surrounding cells in Kuwabara's model. Two other cell models were proposed by Kvashnin [72] and Cunningham [73] (and later by Mehta-Morse [74]) using different boundary conditions on the cell particle's hypothetical surface. In contrast

to the previously proposed models, Kvashnin proposed a variant of the cell model by considering that the tangential component of the velocity attains its minimum value at the free surface concerning radial distance, indicating the symmetry on the cell. Cunningham and Mehta-Morse proposed the boundary condition on the cell surface assuming the tangential velocity is equal to a component of average fluid velocity, signifying the homogeneity of the flow of the cell surface.

With help of the Happel's and Kuwabara's model, Epstein and Masliyah [75] analysed the axisymmetric flow past oblate spheroid, prolate spheroid and elliptical cylinders considering outer envelope same as abovementioned shape and solved the governing equations numerically by finite difference method. Neale and Nadar [76] enhanced Happel's formulation by incorporating the concept of the unit cell being immersed within an infinite, continuous, homogeneous, and isotropic permeable medium. The permeability values derived from this refined model exhibited favorable agreement with existing data. Dassios [77] also studied Happel's and Kuwabara's boundary conditions in the spheroidal particle-in-cell model. Kim and Yuan [78] proposed a new model to evaluate specific hydrodynamic cake resistance by developing a simple hydrodynamic model in which a fractal aggregate is replaced by a solid core particle with a porous shell and located in the center of Happel's hypothetical cell. Bhattacharya [79] and Prakash [80] discussed an arbitrary viscous, incompressible flow past a porous sphere using Brinkmann and Stokes equations for porous and clear fluid regions, respectively, with Ochoa-Tapia and Whitaker [81], [82] boundary condition. With the help of Faxen's law, they have derived the expression for drag, torque and discussed their dependence on the permeability and stress-jump coefficient. Deo [83] also discussed the same case by assuming low Reynolds number flow past a porous approximately spheroid particle for the Kuwabara boundary condition. In order to investigate the flow dynamics within a non-uniform porous medium, Veerapaneni and Wiesner [84] dissected a spherical porous aggregate into numerous spherical layers, each characterized by a distinct permeability value. Their research investigates the dependence of permeability on the radial distance, building upon the foundation laid by earlier studies. Their paper provides a thorough examination of the hydrodynamic properties of fractal aggregates, with a special emphasis on the changes in permeability across different radii. They also compared various models of permeability, pointing out the merits of Happel's model for its combination of simplicity and precision in representing these phenomena. Vasin [85], Deo [3], and Saad [86] did a review by comparing different cell models (Happel's , Kuwabara's, Kvashnin's , and Cunningham's (usually referred to as Mehta–Morse's model)) in a flow past a particle with a porous shell, and investigated the hydrodynamic permeability of the porous medium

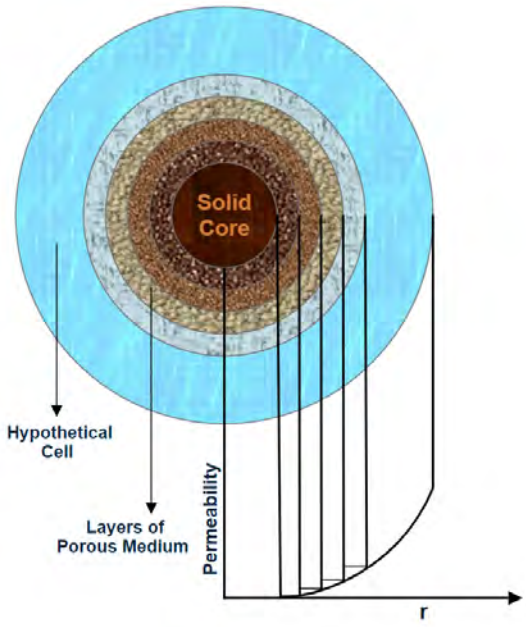

Figure 1.5: Physical Model of Veerapanneni for flow through a swarm of spherical particles with radially varying permeability.

built-up by such particles. Faltas and Saad [87] considered a swarm of slip eccentric spherical particles in Stokes flow, where the center of the solid particle is located away from the center of the hypothetical spherical envelope. Happel and Kuwabara boundary conditions are used to solve the Stokes equation, and the normalized drag force acting on the particle was calculated. Faltas *et al.* [88] considered the flow in corrugated microannuli cylindrical tubes with a slip surface and investigated the effect of the corrugations on the flow rate and pressure gradient. Yadav *et al.* studied a low Reynolds number flow of an incompressible viscous fluid through the membrane composed of non-homogeneous porous cylindrical particles with radially varying permeability. Yadav *et al.* [89] investigated the steady incompressible flow of micropolar fluid sandwiched between two Newtonian fluid layers through a horizontal porous channel under the influence of a magnetic field. In the process of filtration, the construction of membrane can be affected in two ways: (i) dissolution of particles, (ii) adsorption of polymer on the surface of the particles. As a result of these processes, a porous layer is formed on the surface of solid particles, and it affects the drag force exerted by the flow on the particles. Saad [90] investigated the quasi-steady translational and steady rotational motions of a porous spheroid enveloped by a fictitious spheroid in the low Reynolds number flow. The analytical expressions for flow fields were derived by solving Stokes and Brinkman equation. Also they derived the closed form expressions for the hydrodynamic drag force and couple exerted on the porous spheroid in a cell. Yadav *et al.*

[91] emphasized on the hydrodynamic permeability and its controlling parameter by considering unit cell particles to be spheroidal shape covered by a porous layer. Further, they [92] extended this work by analyzing the effect of magnetic fields on hydrodynamic permeability. Tiwari *et al.* [93] considered the assemblage of non-homogeneous porous medium with cylindrical-shaped particle in the stokes flow, and established a comparison of all four cell models (Happel, Kuwabara, Kvashnin and Mehta-Morse/Cunningham). Yadav *et al.* [94] studied a low Reynolds number flow of an incompressible viscous fluid through the membrane composed of non-homogeneous porous cylindrical particles with radially varying permeability. Khanukaeva *et al.* ([95], [96]) considered the flow of micropolar fluid and investigated the flow past an aggregate of solid cylindrical particles with a porous layer in the parallel and perpendicular directions to the cylinder's axis. They solved the governing equations analytically by taking continuity of velocities as well as stresses on porous-liquid surface together with no-couple stress and no-spin condition on the hypothetical cell surface. Kishore *et al.* [97] studied the rate of mass transfer by considering an ensemble of mono sized spherical droplets in a Newtonian fluid with a free surface model and solved the governing equations numerically for moderate Reynolds and Peclet numbers. With the use of power-law fluid at low Reynolds number and Happel's free-surface cell model, Yoshinore and Jaromir [98] obtained an approximate solution for the motion of a swarm of solid spherical particles. Pressure drop, the minimum fluidization velocity, and the rate of mass transfer were also discussed theoretically. Zhu [99] used Happel's free surface cell model to investigate the steady, axisymmetric, and low Reynolds number flow of an incompressible Carreau fluid past aggregates of spherical Newtonian drops and access the effects of viscosity ratios on the drag along with the mass transfer rate. Dang and Steinberg [100] analyzed mass transfer from aggregates of bubbles with chemical reactions between a swarm of bubbles and continuous phase.

1.4 Heat Transfer and Entropy Generation

1.4.1 Heat Transfer

Heat transfer rate in particle-to-fluid interactions at very low Reynolds number is a major topic of research interest, having applications in the combustion of finely dispersed fuel, drying of a gas by a granular absorbent and meteorological studies. It is a crucial phenomenon that occurs in the process of roasting ores, ion exchange, gas chromatography, fibers in adsorbers, electrolyzers, hollow-fiber reactors, and catalytic chemical reactions. In most unit operations or a series of mechanical or chemical operations, one has to face the involvement

of non-uniform temperature and concentration fields, because of which one encounter the heat and mass transfer within the flow domain.

In numerous applications, including chemical reactors and heat transfers arising from particle interactions, heat transfer in a swarm of particles is crucial. The cell model can be used to comprehend liquid flow through a swarm of particles. Further, numerous real-life applications involve a minor increase in temperature or radiation, making the mathematical analysis of its effect on creeping flow an intriguing challenge. Due to increased pollution and significant liquid contaminants, filtering is crucial, and the researchers used mathematical analysis to get further insights into the filtration process.

Over the years, considerable research efforts have been expended in investigating the convection-diffusion equation analytically with the help of appropriate boundary conditions. The cell method in the problems of heat and mass transfer was first studied by Pfeffer and Happel [101]. They solved the energy equation coupled with Happle's free surface model with perturbation technique by expanding the fluid temperature distribution in even powered terms of the spherical angle and obtained a rapidly converging solution. By then, limited work had been done on the analytical approach of investigating heat and mass transfer for creeping flow.

Mandhani *et al.* [102] used the unit cell model technique to investigate the forced convection heat transfer characteristics in a membrane composed of cylindrical bundles. Ferreira and Chhabra [103] applied Happel and Kuwabara cell models and Stokes flow approximation to examine the mass transfer and creeping flow of Power-law fluids over cylinder banks. Narasimha *et al.* [104] explored the role of shear-thinning viscosity on the convective heat transfer in a swarm of particles by solving the governing equation numerically for the free surface cell model. Zhu [105] developed a new cell model for saturated porous medium and determined the effective thermal conductivity based on the developed temperature profile in the cell. Zhu [106] developed a new physical conceptualization of the evolution of water phase saturation using a cell model and estimated the thermal conductivity of unsaturated porous materials. Zhu [107] developed a new approach to separate two mechanisms of conduction and convection explicitly. He considered the flow at low Reynolds number and solved the energy equations by finite difference method for various physical and kinematic conditions. Sharanya *et al.* [108] used the cell model to study the viscous flow of polydisperse spherical drops as a porous media, considering thermocapillary effects, and compared the computed bed permeability with the Carman-Kozeny relation.

1.4.2 Entropy Generation

The suboptimal performance of industrial and engineering flow processes and thermal systems is primarily attributed to the generation of entropy. Identifying the factors responsible for entropy generation is crucial, as minimizing these factors will lead to the optimization of energy resources and the efficiency of the flow system. Entropy analysis is a method used to assess the thermodynamic irreversibility present in fluid flow and heat transfer processes, stemming from the second law of thermodynamics. Entropy generation serves as a metric for quantifying the level of irreversibility inherent in actual processes. Various elements, such as heat transfer across finite temperature gradients, the nature of convective heat transfer, and the influence of viscosity, contribute to the overall entropy generation. The process of entropy generation leads to the dissipation of available energy within a system, resulting in significant additional expenses for any thermal system.

The primary contributors to entropy generation in thermal and engineering processes are the three modes of thermal exchange: conduction, convection, and thermal radiation. Additionally, factors such as fluid friction, the existence of porous media, viscous effects, fluid mixing, buoyancy forces, magnetohydrodynamics, and radiative heat transfer play significant roles in this context. The conversion of energy across various forms like thermal energy, potential energy, and kinetic energy, among others, plays a crucial role in the generation of entropy. These elements contribute to a decrease in the operational efficiency (energy) of diverse thermo-fluid devices. Furthermore, the study of entropy production is a crucial aspect of contemporary engineering thermofluid devices, and it represents one of the most frequently explored areas in research.

Bejan's groundbreaking study ([109], [110], [111], [112], [113]) explores the notion of entropy production across various flow conditions, scenarios, and geometric models. Within the realm of advanced engineering thermodynamics, the scrutiny of entropy production provides invaluable insights for integrating miniature electronic and thermal devices, augmenting the performance of petroleum equipment, and optimizing heat exchangers, among other applications. Relying on information regarding entropy production offers a more dependable approach to designing these devices and amplifying the operational efficiency of thermal technologies. Shit et al. [114] developed a mathematical model to analyze entropy generation in unsteady two-dimensional magnetohydrodynamic flow of nanofluid over an exponentially stretching surface in a porous medium under the influence of thermal radiation. This research was further extended by Shit and Mandal [115], who applied Buongiorno's model to study entropy generation in unsteady magnetohydrodynamic flow of Casson nanofluid over a stretching vertical plate influenced by thermal radiation. Their findings

indicated that the Casson parameter significantly increases entropy generation, while thermal radiation enhances it closer to the plate. Some notable studies pertaining to the entropy generation phenomena are documented in the articles ([116], [117], [118] [119], [120]).

1.5 Electroosmosis

Following Ferdinand Friedrich Reuss's discovery more than two centuries ago that water could flow through a clay plug when an external electric field was applied, a plethora of theoretical and experimental research has been conducted. The most important result of this discovery was the ability to create water flow only by applying an external electric field without any requirement of mechanical component. The concept, subsequently termed as electrokinetic transport, operates through the mechanism where an external electric field interacts with a charged interface. This interaction is balanced by a liquid layer possessing a charge opposite to that of the interface. Electroosmosis within porous materials has gained significance owing to its diverse applications, including soil contaminant removal, dewatering processes, electrochromatography, hot embossing techniques, micropumping mechanisms, and separation procedures. Porous materials often comprise parallel fibers, akin to those found in filters. Prior microscale investigations have focused on theoretical forecasts concerning parallel arrangements of weakly interacting circular cylindrical fibers.

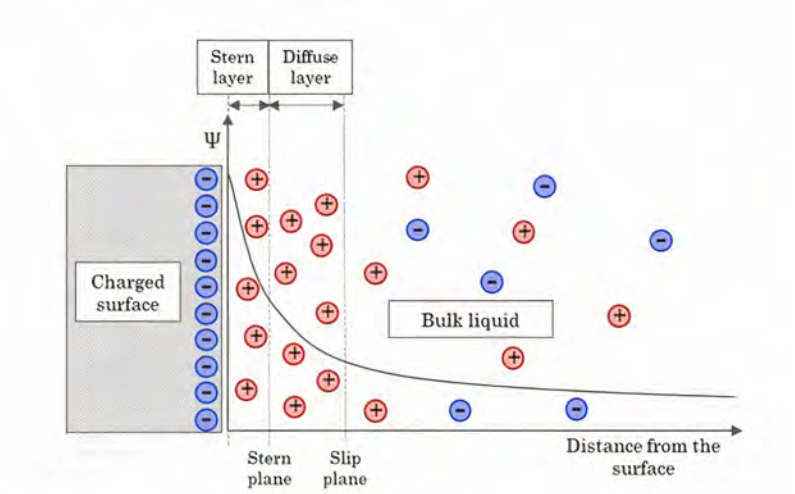

Figure 1.6: Charge distribution in the electrical double layer region near the charged surface.

The electrically charged solid-liquid interface, known as the electrical double layer (EDL), plays a crucial role in the electroosmotic phenomenon. Comprising a charged solid surface and an extremely thin layer of counter-charges in an aqueous solution (typically a

few nanometers thick), the EDL was initially explored in the 19th century [12], and has since been subject to further investigation in the 20th century [13–15] and contemporary research [16–20]. Consequently, deepening our comprehension of the arrangement of water and ionic species in proximity to an electrically charged solid surface holds significant importance.

Levine and Neale [121] noted that in suitable ionizing solvents like water, the particle constitutes a diffuse (double) layer of a significant thickness. So, the results of the Happel [68] and Kuwabara [67] model of uncharged particles should not be applied indiscriminately when dealing with electrolytes. Oshima [122] used the cell model approach to find the mobility expression for a swarm of identical spherical colloidal particles with Kuwabara's [67] boundary condition. Huan and Chen [123] analyzed the body-forced-driven migration in the homogeneous suspension of an electrolyte solution by linearising the governing equation with the assumption that the system is only slightly distorted from equilibrium. Analytical expressions for the settling velocity and the sedimentation potential are derived. Zholkovskij [124] demonstrated several contradictions on imposition of boundary conditions at the outer boundary of the representative spherical cell, and the theory of electrokinetic phenomena in concentrated suspensions was revisited primarily focusing on the boundary conditions at the outer boundary of the spherical cell. Chiang [125] analyzed the transient electrophoresis of a homogeneous suspension of dielectric spherical particles in a step function electric field with the assumption of thin but finite double layers. Cheng and Huan [126] considered a spherical particle in a microtube filled with a gaseous medium and presented a theoretical study to obtain asymptotic analytical results for the thermophoretic mobility of an aerosol sphere. Saad and Faltas [127] derived the expression for electrophoretic apparent velocity slip by considering the time-dependent flow in a charged porous medium under the influence of an electric field. Further, Saad [128] investigated the electrophoretic motion of dielectric cylindrical particle semi analytically in a charged porous medium. Using Happel and Kuwabara's unit cell model, Saad [129] analyzed the starting electrophoresis in a charged porous medium consisting of spherical particles semi-analytically. Theoretical work on the electric conduction of electrolyte solutions in a fibrous porous medium was done by Chen and Huan [130]. They considered parallel charge-regulating cylinders with arbitrary electric double layer thickness and derived the expressions for the electroosmotic mobility and effective electric conductivity by solving the governing electrokinetic equations. Lai and Huan [131] also examined the initiation of electrophoretic motion in a suspension of spherical colloidal charged particles by the unit cell model for hydrodynamic interaction between particles. By extending the case of transient electrophoresis of a dielectric cylindrical particle, Saad [128] presented a semi-analytical study of unsteady electrophoresis of a dielectric

circular cylindrical particle placed in Brinkman medium with a uniform electric field in an arbitrary direction. He [132] extended the above study by considering the time-evolving electrophoresis in the Brinkman medium.

1.6 Diverse Fluids

The world encompasses a multitude of fluid types, each possessing distinct applications across various scientific domains. Examples include modeling groundwater flow, geophysical flows, blood flow through large and small arteries, tidal waves, among others. The present thesis explores several categories of fluids.

1.6.1 Newtonian Fluid

In a Newtonian fluid, the relationship between shear stress and strain rate is characterized by linearity, with the proportionality constant defined as the coefficient of viscosity. This relationship can be expressed mathematically, as

$$\widetilde{\tau} = \widetilde{\mu}\frac{\partial \widetilde{w}}{\partial \widetilde{r}} \tag{1.9}$$

here $\widetilde{\tau}$ is the shear stress, $\widetilde{\mu}$ is the coefficient of viscosity and $\frac{\partial \widetilde{w}}{\partial \widetilde{r}}$ is the rate of strain (velocity gradient).

1.6.2 Jeffrey Fluid

Jeffrey fluid model is a generalization of the Newtonian fluid model having both properties of viscosity and elasticity of the fluid and reduces to the Newtonian fluid model for the specific value of the viscoelastic parameter. The involvement of parameters related to relaxation and retardation time makes the rheology of Jeffery fluid slightly different from the Newtonian fluids without any further complexities. Also, for very low relaxation time, the model reduces to linearized form and hence suitable for an analytical treatment of problems dealing with the flow of Jeffery fluid. Viscoelastic nature of fluid exhibits the shear thinning behavior. The mathematical expression of the extra tensor of Jeffrey fluid is given by

$$\widetilde{\tau}_{\widetilde{r}\widetilde{z}} = \frac{\widetilde{\mu}}{1+\lambda_1}\left(\dot{\gamma}+\lambda_2\ddot{\gamma}\right), \tag{1.10}$$

here, $\widetilde{\tau}_{\widetilde{r}\widetilde{z}}$ denotes the shear stress, $\widetilde{\mu}$ represents the dynamic viscosity of the Jeffrey fluid, $\dot{\gamma}$ stands for the shear rate, and λ_1 and λ_2 refer to the Jeffrey fluid parameters, signifying the

ratio of relaxation to retardation times and retardation times, respectively. The dots signify differentiation with respect to time.

1.6.3 Carreau-Yasuda Fluid

The Carreau-Yasuda fluid model is a non-Newtonian viscoelastic fluid which provides a more generalized description than the Newtonian model. It is more accurate in capturing the variation of viscosity η with shear rate γ than the power law rheological model and has sufficient flexibility to fit a wide variety of experimental $\eta(\dot{\gamma})$ curves; it has proven to be useful for numerical calculations in which one needs an analytical expression for the non-Newtonian viscosity curve. The complexity of parameterization is a key distinction between these formulations. The Carreau-Yasuda equation characterizes fluid rheology with five parameters $(\eta_0, \eta_\infty, \lambda, n, a)$, unlike the power law relation, which has only two parameters (k, n). The stress–strain relation for Carreau-Yasuda fluid is given by [133], [134]

$$\frac{\eta - \eta_\infty}{\eta_0 - \eta_\infty} = \left(1 + (\lambda\dot{\gamma})^a\right)^{\frac{n-1}{a}}, \tag{1.11}$$

where, μ_0 and μ_∞ are the asymptotic viscosities for zero and infinite shear rates, respectively. The parameter λ is a constant possessing units of time, with $\frac{1}{\lambda}$ indicating the critical shear rate at which viscosity starts to decrease. Furthermore, the parameter n serves as the power law index, delineating fluid behavior relative to shear rate: (i) shear-thinning for pseudoplastic fluids when $n < 1$ at high shear rates; (ii) Newtonian behavior when $n = 1$; (iii) shear-thickening for dilatant fluids when $n > 1$ at low shear rates. The nondimensional parameter a represents the width of the transition zone between zero shear rate viscosity and the power law region.

Yasuda [135], [136] later added the transition region parameter, a. For $a = 2$, the equation (1.11), is usually reffered to as the Carreau equation, and given by

$$\frac{\eta - \eta_\infty}{\eta_0 - \eta_\infty} = \left(1 + (\lambda\dot{\gamma})^a\right)^{\frac{n-1}{2}}. \tag{1.12}$$

1.7 Governing Equations

Fluid flow obeys the law of conservation of mass, momentum, and energy. The mathematical expressions for these laws are described as below:

1.7.1 Conservation of Mass

The continuity equation serves as the mathematical representation of the principle of conservation of mass. Assuming a fluid region V devoid of sources or sinks, the conservation of mass dictates that the rate of mass accumulation within V must equate to the cumulative rate of mass inflow into V. For an incompressible fluid flow, the conservation of mass reduces to

$$\nabla \cdot \vec{\mathbf{u}} = 0, \tag{1.13}$$

where $\nabla\cdot$ the divergence operator, and $\vec{\mathbf{u}}$ is the velocity vector of the fluid.

1.7.2 Conservation of Momentum

The law of conservation of momentum states that the rate of change of momentum per unit volume V is caused by pressure, viscous, and gravity forces. Then for incompressible flows

$$\rho \frac{D\vec{\mathbf{u}}}{Dt} = \rho \vec{F} - \nabla p + \mu \nabla^2 \vec{\mathbf{u}}, \tag{1.14}$$

where $\frac{D}{Dt} \equiv \frac{\partial}{\partial t} + (\vec{\mathbf{u}}.\nabla)$ denote the total/material derivative, ∇^2 is the Laplacian operator, $\vec{F}$ is external body force, p is the pressure, $\vec{v}$ is the velocity vector, μ is the viscosity coefficient and ρ is the density of the fluid. The equation (1.14) is also known as Navier-Stokes equation which was given by Navier.

1.7.3 Convection–Diffusion Equation

The convection-diffusion equation can be derived in a straightforward way from the continuity equation, which states that the rate of change for a scalar quantity in a differential control volume is given by flow and diffusion into and out of that part of the system along with any generation or consumption inside the control volume. The vector form of the convection-diffusion equation is given as:

$$\frac{\partial \psi}{\partial t} = \nabla \cdot (D \nabla \psi) - \nabla \cdot (\vec{\mathbf{u}} \psi) + R, \tag{1.15}$$

where ψ is the variable of interest (species concentration for mass transfer, temperature for heat transfer), D is the diffusivity, such as mass diffusivity for particle motion or thermal diffusivity for heat transport, $\vec{\mathbf{u}}$ is the average velocity with which the quantity is moving, R describes "sources" or "sinks" of the quantity ψ.

1.7.4 Momentum Equations in Porous Media

1.7.4.1 Brinkmann Equation

Brinkman [137], [138] proposed a modification to Darcy's law, claiming that the flow rate of a fluid through a porous medium correlates with the pressure gradient within it. He extended Darcy's investigation by taking into account the permeability of the porous zone, specifically micro-sized holes. Unlike Darcy's law, which ignores the effects of fluid viscosity and boundary effects, the Brinkman equation incorporates these factors by adding an effective viscosity and velocity gradient term to Darcy's law. As a result, the equation provides a more comprehensive description of fluid flow in porous media.

$$\rho \frac{\partial \widetilde{\mathbf{u}}}{\partial t} = -\left(\frac{\partial p}{\partial z} + \frac{\mu}{k}\widetilde{\mathbf{u}}\right) + \mu_e \nabla^2(\widetilde{\mathbf{u}}), \tag{1.16}$$

where ρ denotes the fluid density, p denotes the pressure, u is the velocity, μ expresses fluid viscosity, μ_e expresses effective viscosity and k represents the permeability of porous medium.

1.7.4.2 Brinkmann Forchheimer Equation

The Brinkman-Forchheimer equation [55] is an extension of Darcy's law, which provides a comprehensive model for fluid flow through porous media, including scenarios where fluid inertia cannot be ignored. Unlike Darcy's law, which only considers viscous effects, the Brinkman-Forchheimer equation takes into account both viscous and inertial effects. This improved formulation makes it more suitable for accurately modeling flow in porous media, especially under high flow rates. The Brinkman-Forchheimer equation can be written as follows:

$$\rho \frac{\partial \widetilde{\mathbf{u}}}{\partial t} = -\left(\nabla p + \frac{\mu}{k}\widetilde{\mathbf{u}}\right) + \mu_e \nabla^2(\widetilde{\mathbf{u}}) - \frac{C_F}{\sqrt{k}}\rho|\widetilde{\mathbf{u}}|\widetilde{\mathbf{u}}, \tag{1.17}$$

where ρ denotes the fluid density, p denotes the pressure, $\mathbf{u}$ is the velocity, μ expresses viscosity, μ_e expresses effective viscosity, k represents the permeability constant for the porous medium and C_F denotes the inertial coefficient.

1.8 Boundary Conditions

To ensure mathematical consistency in addressing flow problems, it is essential to establish appropriate boundary conditions for evaluating the arbitrary constants involved. Following are some of the useful boundary conditions:

1. Osborne Reynolds [139] introduced the **no-slip condition**, which states that a viscous fluid must reach zero velocity at a solid boundary. Hence the tangential component of velocity vanishes at the solid surface. Reynolds proposed this boundary condition based on findings from his seminal pipe flow experiments. This boundary condition exemplifies a Dirichlet boundary condition.

2. The solid surface to particle is assumed to be held at constant ambient temperature.

3. Velocity profile, shear stress, and temperature profile are assumed to be continuous at the interfaces.

4. Ochoa-Tapia and Whitaker ([81], [82]) proposed a **stress jump boundary condition** for the interface between a fluid and a porous medium, where the porous region is governed by Brinkman's equation. The formulated stress-jump boundary condition is as follows,

$$\tau_{nt}^{(p)} - \tau_{nt}^{(c)} = \frac{\beta\mu}{\sqrt{k}} w_t^{(p)}, \tag{1.18}$$

   In this context, $\tau_{nt}^{(p)}$ and $\tau_{nt}^{(c)}$ represent the tangential stress components within the porous medium and the clear fluid region, respectively. Here, β denotes the stress jump coefficient, μ stands for viscosity, and k represents the permeability of the porous medium.

5. Happel [71] [68] assumed that the outer envelope (or surface) of the cell is frictionless, i.e., the shear stress vanishes at the outer boundary of the cell. The disturbance due to any particle is, therefore, confined within the fluid cell. Thus, Happel boundary condition is

$$\tau_{nt} = 0 \qquad \text{At the cell surface.} \tag{1.19}$$

6. Kuwabara [67] proposed a cell model, similar to the Happel cell model, to explain the forces acting on circular cylinders or spheres randomly distributed in a viscous flow at low Reynolds numbers. In this model, two concentric spheres are used to represent the spherical particle in cell. Instead of requiring no tangential stress on the outer surface, Kuwabara proposed that the vorticity (spin) vanishes on the outer surface. As a result, the Kuwabara boundary condition states that the fluid's spinning motion should come to a halt on the outer surface. Thus, Kuwabara boundary condition is

$$\omega = 0 \qquad \text{At the cell surface.} \tag{1.20}$$

7. Kvashnin [72] introduced a condition stating that the tangential velocity of fluid reaches its lowest point at the surface of the cell when considering its distance from the center. This condition indicates symmetry within the cell. In simpler terms, it means that as you move away from the center of the cell towards its surface, the tangential component of fluid's velocity decreases until it reaches a minimum. In cylindrical coordinates (r, θ) the condition comes out as

$$\frac{\partial v_\theta}{\partial r} = 0 \qquad \text{At the cell surface.} \tag{1.21}$$

8. Mehta-Morse [74] proposed the boundary condition on the cell surface assuming the tangential velocity is equal to a component of average fluid velocity, signifying the homogeneity of the flow of the cell surface. In cylindrical coordinates, this condition is expressed as:

$$v_\theta = 0 \qquad \text{At the cell surface.} \tag{1.22}$$

where v_θ represents the tangential component of velocity. However, Filippov and Vasin [140] demonstrated that this condition is not applicable for analyzing flow through a swarm of particles.

1.9 Mathematical Methods

Fluid flow obeys the law of conservation of mass, momentum, and energy. The mathematical expressions for these laws are described in detail, based on the proposed models. The governing equations corresponding to these conservation laws are set of partial differential equations that are coupled and highly nonlinear so that in most cases, the analytical solutions to these equations are intractable due to the presence of nonlinear inertia term and other body force terms in it. In order to obtain the analytical solution of these equations, researcher often solve the corresponding problem for the special cases where the nonlinear terms are reduced to be zero. However; to overcome from the solution intractability, we may use the semi-analytical/approximate solution methods like the perturbation techniques. Given the representation of swarm of particles as cylindrical shaped particles, mathematical formulations will employ cylindrical coordinate systems (r, ϕ, z), where r and z denote the radial and axial coordinates, respectively, with the origin positioned on the axis of the cylinder. Initially, expressions for the velocity profile across different regions (porous, non-porous/clear fluid) will be determined. Subsequently, these expressions will be utilized to derive analytical expressions for temperature distributions.

1.9.1 Perturbation Method

The perturbation theory emerged as a useful tool for dealing with complex calculations, particularly in the study of fluid motion. In academic contexts, perturbation can be defined as a minor deviation from a predetermined state. A set of analytical techniques contained in perturbation theory helps in deriving the approximate solutions to difficult problems by utilizing the well-known analytical solution of a related but easier problem. The mechanism of perturbation techniques is based on the mechanical transformation's Taylor series expansion with a small dimensionless parameter. In order to clarify this theoretical approach, let us examine real-world phenomena that are subject to a boundary value problem, which can be expressed mathematically as

$$\begin{aligned} &\widetilde{F}[\widetilde{w}(\widetilde{r})] = 0, \\ &\widetilde{B}[\widetilde{w}(\widetilde{r})] = 0 \ \text{ on } \ \partial\widetilde{\delta}. \end{aligned} \tag{1.23}$$

The exact analytical solution of equation (1.23) is often impossible or very difficult to find when the above expression closely resembles real-life phenomena. When dealing with these kinds of situations, it is useful to think about the equation in its non-dimensional form of equation (1.23), with a small parameter, "ε".

$$\begin{aligned} &F[w(r;\varepsilon)] = 0, \\ &B[w(r;\varepsilon)] = 0 \ \text{ on } \ \partial\delta \ (0 < \varepsilon \ll 1). \end{aligned} \tag{1.24}$$

The technique begins with the decomposition of the problem $F[w(r);\varepsilon] = 0$ into two parts as

$$S[w(r)] + P[w(r);\varepsilon] = 0, \tag{1.25}$$

where $S[w(r)]$ represents a closely related, simpler problem, for which an exact analytical solution $w_0(r)$ can be readily obtained, and $P[w(r);\varepsilon]$ denotes a perturbing component of the problem. In perturbation theory, the solution of equation is expressed as a power series in the perturbed parameter, denoted as ε, as follows.

$$w(r) = w_0(r) + \sum_{n=1}^{\infty} \varepsilon^n w_n(r). \tag{1.26}$$

The initial term represents the well-established exact analytical solution to the correlated elementary problem. An approximate perturbation solution of equation (1.24) can be derived by selectively truncating the series expansion (1.27) after a certain number of successive

terms. Typically, the higher-order terms involving greater powers of the dimensionless parameter tend to diminish as more terms are included.

$$w(r) = w_0(r) + \sum_{n=1}^{N} \varepsilon^n w_n(r) + \mathcal{O}(\varepsilon^{N+1}) \tag{1.27}$$

The series (1.14) is recognized as the asymptotic series, and a solution derived from it is termed the asymptotic series solution. Typically, for practical purposes, only the first three terms are retained: the solution to the known problem, and the first and second-order perturbation corrections are included. This can be expressed as:

$$w(r) \approx w_0(r) + \varepsilon w_1(r) + \varepsilon^2 w_2(r) + \mathcal{O}(\varepsilon^3) \tag{1.28}$$

1.9.1.1 Regular Perturbation

A perturbation problem is regular when the perturbed component, characterized by a non-zero small parameter ε, and the unperturbed component both diminish and exhibit significant qualitative resemblance. In such instances, the approximate perturbed solution can be derived by expanding the governing equations as a series in ε, aggregating terms with equivalent powers of ε, and subsequently solving them iteratively to the required degree of accuracy.

1.9.1.2 Singular Perturbation

The singular perturbation problem exhibits qualitative distinctions from its unperturbed problem. Differential equations arising from singular perturbation problems are influenced by varying time scales and length parameters. Generally, singular perturbation problems can be categorized into two main types: boundary layer problems and multiple-scale problems. Boundary layer problems hold particular significance as they are discussed extensively in Chapter 2 and are effectively addressed using the matched asymptotic expansion method. The domain of the singular perturbation problem can be partitioned into two or more regions. Within a predominant primary subdomain, the problem can be treated as a regular perturbation problem, and an approximate solution can be obtained through an asymptotic series (1.28). However, in smaller subdomains termed as boundary layers, the solution cannot be adequately approximated by the asymptotic series (1.28). Boundary layers manifest as narrow regions proximate to the domain boundary. The approximate solution derived from (1.28) for the primary domain remains valid solely outside the boundary layers and therefore known as outer solution and denoted by w^o.

Matched Asymptotic expansion

In continuum mechanics, the need for solutions to classical problems led to the development of matched asymptotic expansions. Boundary layers, being narrow regions, necessitate stretching or magnification to investigate their behavior effectively, thereby enabling the derivation of a uniform solution for singularly perturbed problems. The stretching parameter, introduced as

$$\eta = \frac{r-a}{\varepsilon^{v}}, \tag{1.29}$$

where a is the point where the boundary layer originates and a scale of magnification v. By incorporating the stretching parameter into the boundary value problem (1.24), it is transformed as,

$$\begin{aligned} F[w(\eta);\varepsilon] &= 0, \\ B[w(\eta);\varepsilon] &= 0 \ \text{ on } \ \partial\delta. \end{aligned} \tag{1.30}$$

Subsequently, the approximate solution for (1.30) is obtained through a distinct asymptotic series expansion, denoted as the inner solution and represented by $w^{i}(\eta)$, valid solely within the boundary layer.

In this context, it's worth noting that the primary domain and boundary layers may not be clearly separated and may overlap. As a result, combining the approximate solutions for the primary domain and boundary layers directly is not feasible. Instead, a suitable matching condition is required to generate a composite solution. Prandtl's boundary layer theory, known for its applicability, is commonly used to establish the matching condition, resulting in the derivation of a composite solution for singularly perturbed problems.

Prandtl's Matching Condition

$$w_{\text{overlap}} = (w^{i})^{o} = (w^{o})^{i}. \tag{1.31}$$

Composite Solution

$$w \approx w^{i} + w^{o} + w_{\text{overlap}}. \tag{1.32}$$

In equation (1.32), $(w^{i})^{o}$ represents the limiting value of the inner solution obtained from outside the boundary layer, while $(w^{o})^{i}$ denotes the limiting value of the outer solution derived from outside the primary domain, specifically from within the boundary layers. w_{overlap} refers to the solution within the overlapping region encompassing both the primary domain and boundary layers.

Extensive discussions on the methodology for obtaining solutions to singular perturbation problems employing various matching conditions have been provided by Bush [141] and Nayfeh [142].

1.9.2 Seperation of Variables

The method of separation of variables stands as a prominent technique for solving both ordinary and partial differential equations. This method is suitable for addressing a broad spectrum of problems in mathematical physics, applied mathematics, and engineering science. This method involves algebraic operations to transform an equation such that each of the two variables appear on distinct sides of the equation. The method of separation of variables operates under the assumption that a function can be expressed in the form:

$$u(x,t) = \phi(x)G(t), \tag{1.33}$$

which will constitute a solution to a linear homogeneous partial differential equation in terms of both x and t. Termed as a product solution and provided the boundary conditions are also linear and homogeneous this will also satisfy the boundary conditions.
The separation method offers several advantages, including its simplicity, directness, ease of understanding, and straightforwardness in solving problems. Nonetheless, in complex scenarios such as boundary value problems, the separation of variables method can become intricate and challenging to resolve.

1.10 Objectives

Based on the literature survey and observed gaps in the work done till now, the following objectives have been proposed for the thesis work:

1. To investigate the flow of non-Newtonian fluids through a swarm of particles by using Happel [71], [68], Kuwabara [67], Kvashnin [72], and Cunningham [73] formulations on cell surface.

2. To study the flow through a swarm of porous elliptic cylindrical particles and compare the results with a swarm of rigid circular cylindrical particles.

3. To study the flow through a deformed porous cylindrical particle and swarm of deformed porous cylindrical particles by considering flow across and along the axis.

4. To study the flow of Newtonian and non-Newtonian fluids through a swarm of porous cylindrical/spherical particles by including convective terms in the formulations.

5. To study the flow through a swarm of particles by using Forchheimer formulation for porous medium.

6. To study the mass transfer and heat transfer in fluid flow through a swarm of particles.

7. To study the electrophoresis of a charged particle in cell model.

1.11 Thesis Organization

This thesis contains nine chapters. The first chapter introduces the study of fluid flow past porous media, beginning with historical developments and emphasizing the significance of membranes in modern technology. It explains membrane modeling, including the cell model technique and its development. This chapter also highlights the importance of heat transfer, entropy generation, and electroosmosis in membranes and introduces rheological fluids and their properties. It concludes by setting the research foundation and outlining objectives and methodologies, providing a comprehensive understanding of the research on fluid flow past membranes.

Chapter 2 analyses how temperature-dependent viscosity influences Jeffrey fluid flow through a swarm of porous layered cylindrical particles. It uses the unit cell model to analyze axial flow, dividing it into two layers with Brinkman and stokes equations governing the fluid flow in porous and clear fluid layers, respectively. The study applies perturbation methods to solve the system of equations, deriving key flow characteristics like velocity and permeability. The findings, consistent with existing research on Newtonian fluids, validate the model for porous media flow under constant viscosity conditions.

Chapter 3, we are going to analyze and look at the “ion drag" effect of the electro-hydrodynamic flow and heat transfer-influenced fluid movement through a membrane consisting of porous cylindrical particles. It employs thermal equations to assess temperature effects, primarily conduction and fluid dynamics governed by the Brinkman and Stokes equations in different regions. The study examines the role of an electric field, via the Hartmann electric number, in fluid flow. It also explores the effect of the buoyancy force, effective viscosity, and stress jump of the porous-fluid interface on the membrane’s hydrodynamic permeability and the Kozeny constant.

Chapters 4 and 5 explore the dynamics of non-Newtonian Carreau and Carreau-Yasuda fluid flows through porous membranes, with a focus on understanding the impact of fluid properties on the filtration process. Chapter 4 uses the unit cell model to investigates incompressible Carreau fluid flow through a membrane consisting of uniformly distributed porous cylindrical particles, and utilizing the regular perturbation method to derive semi-analytical expressions for key parameters such as velocity and temperature profile. Building on this,

Chapter 5 delves into Carreau-Yasuda fluid flow through biporous layered cylindrical particles, utilizing a variable permeability model and perturbation method to analyze flow dynamics and its effects on membrane permeability and temperature variation. Both chapters contribute to a deeper understanding of non-Newtonian fluid behavior in filtration processes, highlighting the complex interplay between fluid dynamics and membrane characteristics.
Chapter 6 explores the entropy production in the flow of a Newtonian fluid through biporous layered cylindrical particles with different variable permeabilities. It uses Brinkman and Brinkman-Forchheimer models for analyzing forced convection in hyperporous materials, focusing on heat transfer and the fluid's rheological properties. The study examines the effect of various control parameters on the flow velocity, entropy generation, Bejan number, and other hydrodynamical quantites like hydrodynamic permeability and the Kozeny constant.
Chapter 7 examines the impact of surface roughness on fluid flow in membranescomposed of porous layered corrugated cylindrical particles. It demonstrates how roughness affects fluid dynamics and presents a semi-analytical solution for analyzing fluid flow, highlighting the influence of various parameters on fluid velocity, membrane's hydrodynamic permeability, and the Kozeny constant.
Chapter 8 explores the flow of an electrolyte solution through a membrane with poly-electrolyte coated particles,driven by both electroosmotic force and pressure gradient. The study models the flow, differentiating between the poly-electrolyte layer and the clear fluid region, using specific governing equations to analyze fluid velocity and membrane properties. Regular perturbation method with variation of parameter technique is employed to approximate these characteristics due to the complex nature of the flow.
Chapter 9 provides a summary of the thesis, emphasizing the significant results that have practical importance and potential uses. It contains the main conclusions related to the study throughout the work followed by the recommended directions for future study and ways to strengthen the current work.

Chapter 2

Creeping Flow of Jeffrey Fluid through a Swarm of Porous Cylindrical Particles: Brinkman-Forchheimer Model [1]

2.1 Introduction

The flow of liquids through membrane comprising a swarm of particles has been a topic of immense interest for researchers to get an insight of the flow of fluid through porous media owing to its prominent applications in diverse areas like physical and biological science such as flow through smooth muscle cells [143], petroleum reservoirs and the sand beds. Acknowledging the importance of flow through porous media Kumar *et al.* [144] provided the estimates of poro-mechanical properties of cortical bone surfaces in different anatomical regions. The mathematical conceptualization of the flow of fluid through membrane modeled as a swarm of porous particles is a complex phenomenon in terms of mathematical formulation for flow visualization as it is difficult to simultaneously observe the flow field past several particles as well as its dependence on particle interactions. To address this issue, the cell model technique or particle-in-cell method was introduced. The cell model technique is employed to analyze the flow of fluid a periodic array of particles by considering a particle confined within a hypothetical cell and the appropriate boundary conditions are imposed on the hypothetical cell to formulate the impact of neighboring particles on the particle concerned. The modeling of filtration process through membranes composed of aggregates of particles can be done by applying the traditional particle-in-cell approach to analyze the flow of fluid through a randomly oriented swarm of particles. The advantage of the cell model technique is to select a single particle inside a fluid envelop among large numbers of cells and analyze the behavior of neighboring particles through imposed boundary conditions on the cell surface.

[1] A considerable part of this chapter is published in *International Journal of Multiphase Flow*, 96(12), 125277, 2021.

The stimulation of taking a porous structure on the surface of the rigid cylindrical particle with an impermeable core is due to the dissolution and adsorption of the polymers. The presence of such a layer affects the entire membrane permeability. The slow viscous flow of fluid through membrane composed of a swarm of concentric clusters of porous cylindrical particles has been discussed by Deo *et al.* [145] using Happel's boundary condition and particle-in-cell approach. Deo *et al.* [3] reported the flow of Newtonian fluid parallel and perpendicular to the axis of porous cylindrical particles with impermeable core. Sharif *et al.* [146] and Khanukaeva *et al.* ([95], [96]) discussed the microlevel properties of the fluid flowing through swarm of porous cylindrical particles by taking flows parallel and perpendicular to the axis. Yadav *et al.* [147] reported the impact of magnetic field on the circulation of slow flow through membranes consisting of the aggregates of porous cylindrical particles. Recently, Yadav [148] and Madasu and Bucha [11] investigated the flow of fluid through membrane composed of a porous cylindrical particles having cavity.

Majority of the above works were done for Newtonian fluid flow through the swarm of particles but many researchers used the suitability of creeping flow to model the flow of non-Newtonian fluids through swarm of particles owing to their high viscosity levels ([103], [149], [150]). The introduction of the viscoelastic properties of the fluids in the filtration process that attracted to the researchers and explored their studies to make a better model in the membrane filtration process. Jeffrey fluid model is a generalization of the Newtonian fluid model having the viscoelastic properties of the fluid and reduces to the Newtonian fluid model for the specific value of the viscoelastic parameter. The involvement of parameters related to relaxation and retardation time makes the rheology of Jeffery fluid slightly different from the Newtonian fluids without any further complexities. Also, for very low relaxation time, the model reduces to linearize form and hence suitable for an analytical treatment of problems dealing with the flow of Jeffery fluid. The investigations have been made by Pandey and Tripathi [151], Tripathi *et al.* [10], Ramesh *et al.* [152] and Prakash *et al.* [153] for the flow of viscoelastic fluid through channel/tubes and the closed form of the solutions are presented using long wavelength and small Reynolds numbers approximations. Nallapu and Radhakrishnamacharya [9] used the Jeffrey-Newtonian fluids (two-fluid model of blood) approach to study the blood circulation through arteries, and analyzed the impact of transverse magnetic field on the circulation process.

The above literature emphasized upon the heat transfers through assemblage of particles and their dependence on the flow parameters of fluids flowing through the swarm of particles. It is interesting to observe the effect of heat transfer on fluid flow through a swarm of particles such as drag force, membrane permeability etc. There are several works exploring

many physical processes involving heat transfer under the low Peclet number approximations, leading to negligible convective term effect in the heat transfer. Here, we present a few of the works which have a weak coupling in fluid velocity and temperature. Faltas and Ragab [154] investigated thermophoresis and photophoresis of a spherical aerosol particle in a porous medium and concluded that the thermophoretic velocity of the particle varies with thermal stress slip for small as well as large permeabilities. Another aspect is the thermocapillary effect leading towards motion of a suspended drop in a fluid in the direction of temperature gradient owing to a decay in temperature. The decay was justified due to interfacial tension. Choudhari and Raja Sekhar [155] analyzed the thermocapillary effects on the non-isothermal steady flow of fluid in and around the liquid drop and formulate the governing equations inside and outside of the liquid drop using Stoke's equations consisting the appropriate nonisothermal boundary conditions. Sharanya and Raja Sekhar [156] explored the above study in the unsteady hydrodynamic flow using the Solenoidal decomposition method. Sharanya *et al.* [108] analyzed the impact of permeability of the packed beds of polydisperse droplets under the thermocapillary effects using particle-in-cell approach.

The position or temperature-dependent viscosity plays an important role whenever the physical properties of the fluids may change considerably with the position and temperature. In all the aforementioned works, the authors used the constant viscosity model to analyze the flow of fluid through membranes however, the reduced inner friction due to heat affects the viscosity of the fluids. Therefore, the constant viscosity assumptions is not appropriate everywhere. Also, in the blood flow through small blood vessels, the viscosity of the blood may vary with thickness of the tube. Bali and Awasthi [157] introduced the position-dependent viscosity to analyze the flow of blood through constricted blood vessels. Shit *et al.* [158] examined theoretically the combined aspects of magnetic field and hematocrit-dependent viscosity on the circulation of blood flow through porous blood vessels. Filippov and Koroleva [159] and Koroleva [160] discussed the qualitative properties of the viscous fluid flow through membranes describing a partially filled porous material using varying viscosity approach and deduced the existence and uniqueness of the solutions as well as uniform estimates for boundary value problems. Further, Filippov and Koroleva [161] investigated the dependencies of the hydrodynamical permeability of the membranes on the varying nature of viscosity using the polynomial and exponential viscosity models. Recently, Tiwari and Chauhan ([4], [5], [162], [163]) examined the impact of hematocrit-dependent viscosity on the circulation of blood flow through microvessels and observed that the variable nature of viscosity play an important role to compute the correct measurement of the hemodynamical quantities which is more important for medical treatment. The study

of heat transfer becomes vital in fluid flow problems as fluid viscosity is affected by temperature variation. Nadeem *et al.* [1] formulated the equations governing the peristaltic flow of Newtonian fluid under the long wavelength and temperature-dependent viscosity assumptions and discussed quantitatively the impact of magnetic field and variable viscosity on the behavior of flow quantities like axial velocity, pressure drop and temperature profiles. Mekheimer and Abd Elmaboud [164] discussed the temperature-dependent thermal conductivity and viscosity on the peristaltic flow of Newtonian fluid through asymmetric channel and Akbar *et al.* [6] discussed the impact of temperature-dependent viscosity on the flow of blood through constricted artery with permeable walls.

To best of the author's knowledge and based on the aforementioned literature, the impact of variable viscosity, Jeffrey fluid parameter, and Forchheimer number on the creeping flow of Jeffrey fluid through a swarm of porous cylindrical particles using Brinkman-Forchheimer equation has not earlier been covered. This motivates the authors to explore the impact of temperature dependent viscosity and non-linear inertial resistance of porous medium on flow through a swarm of particles. The slight variation in temperature may affect the viscosity of the fluid and hence affects the flow of fluids through a swarm of porous cylindrical particles. The inclusion of variable viscosity in the flow of Jeffrey fluid may create complexity to resolve the governing equations analytically for flow through porous media. The motivation behind considering the Brinkman-Forchheimer equation to obtain the asymptotic solution using regular and singular perturbation approaches.

The motivation of the present study is to investigate the impact of variable viscosity on the creeping flow of Jeffrey fluid through a swarm of porous cylindrical particles. The flow pattern of the Jeffrey fluid along the axis of the cylindrical particle (tube) is divided into two regions: one is the flow of fluid inside the porous cylindrical particle and the other is the flow of clear fluid outside the porous cylindrical particle. The Brinkman-Forchheimer equation regulates the flow through porous cylindrical particle inside the porous cylindrical particles, however, the Stokes equation regulates the flow of the clear fluid outside the porous cylindrical particles. The analytical technique has been utilized to solve the governing equation outside the porous cylindrical particles, however, a perturbation technique has been used to solve the nonlinear Brinkman-Forchheimer equation using matched asymptotic expansion. The dependencies of hydrodynamic permeability of the membrane and Kozeny constant on the numerous control parameters are analyzed and compared with the previous studies. Some novel results and interesting changes in the flow patterns are reported with stress-jump parameter, particle volume fraction and porosity parameter. The limiting cases of perfectly porous and perfectly solid cylindrical particle in hypothetical cell are also discussed.

The present work is divided into 5 sections. Section 2 deals with mathematical formulation constituting the physical assumptions, model description, governing equations and their non-dimensionalizations. Section 3 introduces the solution strategy and solution expressions of the governing equations followed by the expressions of the hydrodynamical quantities and Kozeny constant. Section 4 reveals the results of the graphical findings with model validation and parameter selections. After completing the results and discussions of the findings, section 5 illustrates the summary of the present study and conclusions followed by references.

2.2 Problem Formulation

2.2.1 Statement of the Problem and Model Description

The horizontal flow is assumed along the axis of the solid cylindrical particle with a porous layer confined within a cell of the same geometry as demonstrated in Figure 2.1 which is an axially symmetric, laminar, incompressible, steady and fully developed flow. The nature of Jeffrey fluid with temperature-dependent viscosity regulates the flow through a swarm of porous cylindrical particles. The flow regime is divided into two regions: Region-I delineates the flow of fluid inside the porous cylindrical particle and Region-II replicates the flow of clear fluid outside the porous cylindrical particle. The Brinkman-Forchheimer equation governs the flow of fluid through porous media inside the porous cylindrical particle, however the Stokes equation governs the flow of clear fluid outside the porous cylindrical particle. The particle geometry is assumed to be right circular cylinder, so we use the cylindrical polar coordinate system $(\widetilde{r}, \phi, \widetilde{z})$ to formulate the equations governing the flow of Jeffrey fluid through cylindrical particle coated over the porous layer confined within the hypothetical cell of same geometry, where $\widetilde{r}$ and $\widetilde{z}$ are the radial and axial coordinates, respectively. The velocity component which regulates the flow of fluid is taken as $(0, 0, \widetilde{w})$, i.e., flow along the axial direction only.

Figure 2.2 delineates the flow of fluid past porous cylindrical particle enclosing a solid core and confined within hypothetical cell. The figure describes a cylindrical particle with solid core of radius $\widetilde{a}$, coaxial interior region of the porous layer with radius $\widetilde{b}$. The radius of the hypothetical cell surface $\widetilde{c}$ is chosen in such a way that the particle volume fraction $\left(\frac{1}{m^2}\right)$ of the impermeable cylinder coated over the porous layer is equal to the volume fraction on the cell.

$$m^2 = \frac{1}{\gamma} = \frac{\pi \widetilde{c}^2}{\pi \widetilde{b}^2}. \tag{2.1}$$

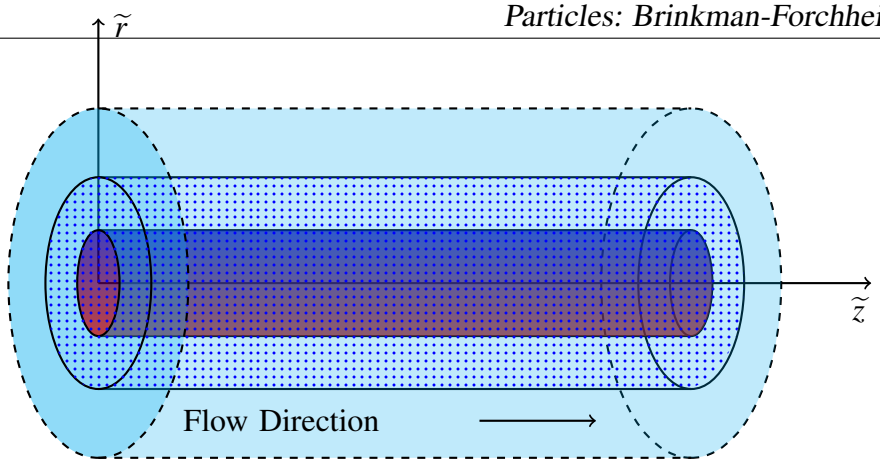

Figure 2.1: The physical sketch of a cylindrical particle in cell

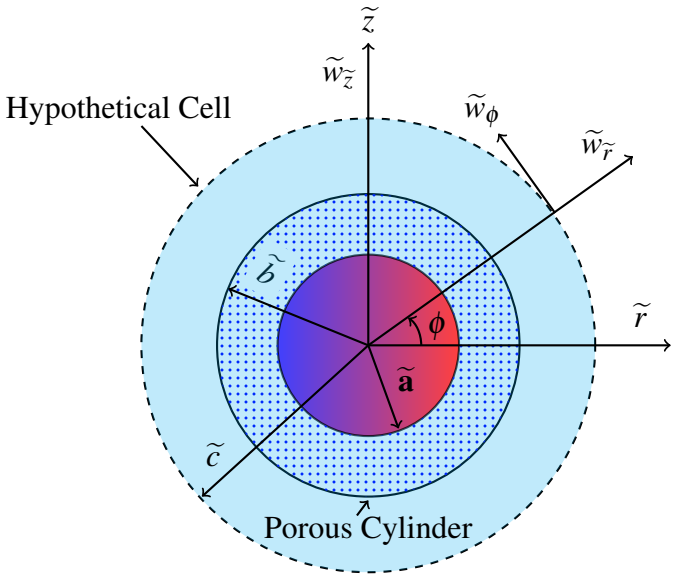

Figure 2.2: the circular cross-section of the cylindrical particle in cell

2.2.2 Governing Equations

In the present section, we present the thermal equation and the momentum equation governing the flow through membranes consisting the aggregates of the porous cylindrical particle.

The flow of Jeffrey fluid is subjected to the thermal effects due to an ambient temperature $\widetilde{T}_0$. The steady state thermal equation in cylindrical coordinate system describing the energy equation by ignoring the convection while considering the heat conduction and heat source is given by

$$\widetilde{K}\left(\frac{\partial^2\widetilde{T}}{\partial\widetilde{r}^2}+\frac{1}{\widetilde{r}}\frac{\partial\widetilde{T}}{\partial\widetilde{r}}\right)+\widetilde{Q}=0, \tag{2.2}$$

where $\widetilde{T}$ is the temperature, $\widetilde{K}$ is the thermal conductivity, and $\widetilde{Q}$ is the heat absorption coefficient, which is taken to be constant.

The thermal boundary conditions on the solid core of the cylindrical particle and surface of the hypothetical cell exhibit the finite temperature at the solid core and constant temperature $(\widetilde{T}_w)$ at the hypothetical cell surface. The respective boundary conditions in dimensional forms are given as

$$\begin{aligned} \frac{\partial \widetilde{T}}{\partial \widetilde{r}} &= 0, \quad \text{at} \quad \widetilde{r} = \widetilde{a}, \\ \widetilde{T} &= \widetilde{T}_w, \quad \text{at} \quad \widetilde{r} = \widetilde{c}, \end{aligned} \tag{2.3}$$

where $\widetilde{T}_w$ is the constant temperature at the surface of the hypothetical cell.

In order to determine the fluid velocity through porous material (medium), Brinkman [137] described the flow of fluid through the porous mass, by modifying the Darcy's law. Permeability of the porous medium depends on the micro-structure of the solid phase involved in the porous material and the properties that affects the permeability of the porous medium are porosity, particle size (solid particles) and the connection of pores with each other. The determination of permeability effects on the flow velocity and membranes permeability are very important for simulating flow in a porous medium. Many authors ([165], [166], [167]) used the Brinkman equation to formulate the governing equation in the flow of fluid through porous materials. In the blood flow through microvessels having an endothelial glycocalyx layer near the tube wall replicating the porous region, Tiwari *et al.* [2] discussed the microlevel properties of the fluid through porous layered tubes and obtained the solutions of the governing equations by imposing suitable boundary conditions along with the stress-jump condition at the fluid-porous interface. Most of the previous works have discussed modeling on the creeping flow of fluid through a swarm of particles adopting Brinkman formulation representing flow through porous media. The Brinkman formulation is valid for small as well large permeability but in the case of a significant fluid inertia such as flow through skeletal tissues, the generalized Brinkman-Forchheimer model is more appropriate for formulating the flow through porous media [168]. Hooman and Gurgency ([7], [8]) adopted the Brinkman-Forchheimer equation to model the forced convection through tubes enclosed with a saturated porous material and employing the asymptotic series expansion method to solve the governing equations for the flow and temperature profiles.

Region- I, i.e., $\widetilde{a} \leq \widetilde{r} \leq \widetilde{b}$

The continuity and Brinkman-Forchheimer equations governing the flow of Jeffrey fluid under temperature-dependent viscosity through porous region (i.e., flow inside the porous

cylindrical particle) are described as

$$\frac{\partial \widetilde{w}_p}{\partial \widetilde{z}} = 0, \tag{2.4a}$$

$$\frac{\partial \widetilde{p}}{\partial \widetilde{z}} = \frac{1}{\widetilde{r}}\frac{\partial}{\partial \widetilde{r}}(\widetilde{r}\widetilde{\tau}_p) - \frac{\widetilde{\mu}(\widetilde{T})\widetilde{w}_p}{\widetilde{k}} - \frac{C_F\widetilde{\rho}\widetilde{w}_p^2}{\sqrt{\widetilde{k}}}, \tag{2.4b}$$

where $\widetilde{\rho}, \widetilde{p}, \widetilde{w}_p, \widetilde{\tau}_p$ are the density, pressure, velocity and shear stress of the fluid in the porous region, respectively; $\widetilde{\mu}(\widetilde{T}) = \widetilde{\mu}_0 e^{-\alpha\left(\frac{\widetilde{T}-\widetilde{T}_0}{\widetilde{T}_w-\widetilde{T}_0}\right)}$ is the temperature-dependent viscosity, $\widetilde{\mu}_0$ is the constant viscosity coefficient of the clear fluid, $\widetilde{T}_0$ is the ambient temperature, $\widetilde{k}$ is the permeability constant of the porous medium and C_F is the inertial coefficient.

The stress-strain relation for Jeffrey fluid under varying viscosity assumption is given by ([9], [1])

$$\widetilde{\tau}_p = \frac{\widetilde{\mu}(\widetilde{T})}{1+\lambda_1}\left(\frac{\partial \widetilde{w}_p}{\partial \widetilde{r}}\right), \tag{2.4c}$$

where λ_1 is the Jeffrey fluid parameter (ratio to relaxation to retardation time).

Region- II, i.e., $\widetilde{b} \leq \widetilde{r} \leq \widetilde{c}$

The continuity and Stokes equations governing the flow of Jeffrey fluid under temperature-dependent viscosity through clear fluid region (i.e., flow outside of the porous cylindrical particle) are given by

$$\frac{\partial \widetilde{w}_c}{\partial \widetilde{z}} = 0, \tag{2.5a}$$

$$\frac{\partial \widetilde{p}}{\partial \widetilde{z}} = \frac{1}{\widetilde{r}}\frac{\partial}{\partial \widetilde{r}}\left(\frac{\widetilde{r}\widetilde{\mu}(\widetilde{T})}{1+\lambda_1}\left(\frac{\partial \widetilde{w}_c}{\partial \widetilde{r}}\right)\right), \tag{2.5b}$$

where $\widetilde{w}_c$ is the axial velocity for the clear fluid.

2.2.3 Non-Dimensional Parameters and Equations

To solve the above system of equations (2.2) – (2.5), the following non-dimensional variables are introduced:

$$\begin{aligned} &p = \frac{\widetilde{p}\widetilde{b}}{\widetilde{w}_0\widetilde{\mu}_0},\ r = \frac{\widetilde{r}}{\widetilde{b}},\ z = \frac{\widetilde{z}}{\widetilde{b}},\ l = \frac{\widetilde{a}}{\widetilde{b}},\ m = \frac{1}{\sqrt{\gamma}} = \frac{\widetilde{c}}{\widetilde{b}},\ S^2 = \frac{1}{k},\ \widetilde{w}_0 = \frac{\widetilde{q}_0\widetilde{b}^2}{\widetilde{\mu}_0},\ \theta = \frac{\widetilde{T}-\widetilde{T}_0}{\widetilde{T}_w-\widetilde{T}_0}, \\ &w_p = \frac{\widetilde{w}_p}{\widetilde{w}_0},\ w_c = \frac{\widetilde{w}_c}{\widetilde{w}_0},\ k = \frac{\widetilde{k}}{\widetilde{b}^2},\ \tau_p = \frac{\widetilde{\tau}_p\widetilde{b}}{\widetilde{w}_0\widetilde{\mu}_0},\ F = \frac{C_F\widetilde{\rho}\widetilde{b}^3\widetilde{q}_0}{\widetilde{\mu}_0^2},\ \zeta_h = \frac{\widetilde{b}^2\widetilde{Q}}{\widetilde{K}(\widetilde{T}_w-\widetilde{T}_0)} \end{aligned} \tag{2.6}$$

where w_0 is the characteristic velocity, F is the Forchheimer number, S is a dimensionless parameter, and $\widetilde{q}_0$ is the characteristic pressure gradient.
The dimensionless form of the energy equation 2.2 is given by

$$\frac{\partial^2\theta}{\partial r^2}+\frac{1}{r}\frac{\partial\theta}{\partial r}+\zeta_h=0, \tag{2.7}$$

where θ is the dimensionless temperature and ζ_h is the constant heat absorption parameter.
The non-dimentional form of the continuity equations (2.4a), (2.5a) and the momentum equations (2.4b), (2.5b) using (2.6) will become
Region- I, i.e., $l \le r \le 1$

$$\frac{\partial w_p}{\partial z}=0, \tag{2.8a}$$

$$\frac{\partial p}{\partial z}=\frac{1}{r}\frac{\partial}{\partial r}\left(\frac{re^{-\alpha\theta(r)}}{1+\lambda_1}\frac{\partial w_p}{\partial r}\right)-\frac{e^{-\alpha\theta(r)}w_p}{k}-\frac{Fw_p^2}{\sqrt{k}}. \tag{2.8b}$$

Region- II, i.e., $1 \le r \le m$

$$\frac{\partial w_c}{\partial z}=0, \tag{2.9a}$$

$$\frac{\partial p}{\partial z}=\frac{1}{r}\frac{\partial}{\partial r}\left(\frac{re^{-\alpha\theta(r)}}{1+\lambda_1}\frac{\partial w_c}{\partial r}\right). \tag{2.9b}$$

2.2.4 Boundary Conditions

The dimensionless boundary conditions are described as

1. No slip condition and zero temperature gradient on the surface of the solid cylinder are considered, i.e.,

$$w_p=0, \text{ and } \frac{d\theta}{dr}=0 \quad \text{at} \quad r=l. \tag{2.10a}$$

2. The continuity of velocities at fluid-porous interface is considered, i.e.,

$$w_p=w_c \quad \text{at} \quad r=1. \tag{2.10b}$$

3. When a fluid flows through two different type of medium there must be a shear stress jump or discontinuity in shear stress. The discontinuity of shear stresses at the fluid-porous interface was proposed by Ochoa-Tapia and Whitaker [81], [82] that demonstrates the momentum transfer between homogeneous porous medium and the clear

fluid, which is commonly known as the stress-jump condition, i.e.,

$$\frac{dw_p}{dr} - \frac{dw_c}{dr} = \frac{\beta_S}{\sqrt{k}} w_p \quad \text{at} \quad r = 1, \tag{2.10c}$$

where β_S is the stress-jump parameter signifying the difference in shear stresses at the fluid-porous interface.

4. The conditions on the hypothetical cell surface are defined for velocity and temperature distributions, i.e.,

$$\frac{dw_c}{dr} = 0, \quad \text{and} \quad \theta(r) = 1 \quad \text{at} \quad r = m. \tag{2.10d}$$

2.3 Solution of the Problem

For the solution of the concerned problem, the fluid flow is driven by the constant pressure gradient, which is same for the porous as well as clear fluid regions, i.e., $\frac{\partial p}{\partial z} = -p_s =$ constant.

2.3.1 Solution of Thermal Equation

The solution of the equation 2.7 describing the thermal equation is obtained analytically

$$\theta(r) = E_1 \log(r) + E_2 - \frac{r^2 \zeta_h}{4}, \tag{2.11}$$

where E_1 and E_2 are constants which are evaluated using the given boundary conditions 2.10a and 2.10d.

2.3.2 Solutions of Hydrodynamic Equations

Due to presence of nonlinear Forchheimer term in the porous region equation, the analytical solution is intractable. In order to overcome this difficulty, we propose here the perturbation approach in case of small and large permeability of the porous medium. First, we are going to tackle the problem for large permeability and later on for small permeability of the porous medium.

2.3.2.1 Asymptotic Solution for the Porous Region

The equation 2.8b may be written in terms of a parameter S

$$\frac{\partial p}{\partial z} = \frac{1}{r}\frac{\partial}{\partial r}\left(\frac{re^{-\alpha\theta(r)}}{1+\lambda_1}\frac{\partial w_p}{\partial r}\right) - S^2 e^{-\alpha\theta(r)} w_p - SFw_p^2, \tag{2.12}$$

where $S^2 = \frac{1}{k}$ is a parameter and k is the permeability of the porous medium. The solution of the above equation 2.12 is difficult to obtain analytically due to presence of nonlinear Forchheimer terms (SFw_p^2) and temperature-dependent viscosity $(e^{-\alpha\theta(r)})$. To overcome these difficulties, we introduce here the perturbation technique for the parameter S which depends on the permeability of the porous medium and the linear approximation of temperature-dependent viscosity (either $e^{-\alpha\theta(r)} = 1-\alpha\theta(r)$ or $e^{\alpha\theta(r)} = 1+\alpha\theta(r)$). Further, the above procedure is used to find the asymptotic expansions of fluid velocity in the porous medium. The solutions of the Eq. 2.12 will be developed for small as well as large values of the parameter S using perturbation approach.

Solution for Large Permeability $(i.e., S \ll 1)$

The asymptotic expansion of the velocity profile w_p of the fluid in the porous region under the assumption of small parameter S can be written as [142]

$$w_p = w_{p0} + Sw_{p1} + S^2 w_{p2} + \ldots, \tag{2.13}$$

where the parameter $S \ll 1$ for the case of large permeability of the porous medium.
Putting the expression of velocity profile w_p of the porous region into the Eq. 2.12 and equating the zeroth, first and second-order coefficients of the parameter S. We have the obtained the zeroth, first and second-order expressions for velocity distribution. The respective expressions for the zeroth, first and second-order expressions for velocity distribution are obtained as

$$\frac{\partial p}{\partial z} = \frac{1}{r}\frac{\partial}{\partial r}\left(\frac{re^{-\alpha\theta(r)}}{1+\lambda_1}\frac{\partial w_{p0}}{\partial r}\right), \tag{2.14a}$$

$$\frac{1}{r}\frac{\partial}{\partial r}\left(\frac{re^{-\alpha\theta(r)}}{1+\lambda_1}\frac{\partial w_{p1}}{\partial r}\right) - Fw_{p0}^2 = 0, \tag{2.14b}$$

$$\frac{1}{r}\frac{\partial}{\partial r}\left(\frac{re^{-\alpha\theta(r)}}{1+\lambda_1}\frac{\partial w_{p2}}{\partial r}\right) - e^{-\alpha\theta(r)} w_{p0} - 2Fw_{p0}w_{p1} = 0. \tag{2.14c}$$

The equations 2.14a-2.14c are solved analytically using MATHEMATICA 10.0 software. The solution expression for the zeroth-order velocity is obtained as

$$\begin{aligned} w_{p0} &= C_1 \int \left(\frac{1+\alpha\theta(r)}{r} \right) dr + C_2 - \frac{p_s Q}{2} \int r(1+\alpha\theta(r))dr \\ &= \frac{C_1}{8} \left(4\log(r)(\alpha E_1 \log(r) + 2\alpha E_2 + 2) - \alpha\zeta_h r^2 \right) + C_2 \\ &+ \frac{p_s Q r^2}{32} \left(4\alpha E_1 - 8\alpha E_1 \log(r) - 8\alpha E_2 + \alpha\zeta_h r^2 - 8 \right). \end{aligned} \tag{2.15a}$$

The solution expression for the first-order velocity is obtained as

$$w_{p1} = C_3 \int \left(\frac{1+\alpha\theta(r)}{r} \right) dr + C_4 + FQ \int \left(\frac{1+\alpha\theta(r)}{r} \left(\int r w_{p0}^2 dr \right) \right) dr \tag{2.15b}$$

$$
\begin{aligned}
&= C_3\left(-\frac{1}{8}\alpha\zeta_h r^2+\frac{1}{2}E_1\alpha\log^2(r)+E_2\alpha\log(r)+\log(r)\right)+C_4\\
&+\frac{FQ}{552960}\left(-\frac{1}{8}9p_s^2Q^2\alpha^3\zeta_h^3r^{12}-\frac{27}{200}p_sQ\alpha^2\zeta_h^2(p_sQ(149E_1\alpha-240(E_2\alpha+1))-100C_1\alpha\zeta_h)r^{10}\right.\\
&-\frac{5}{64}\alpha\zeta_h\left(p_s^2\left(1733E_1^2\alpha^2-5160E_1(E_2\alpha+1)\alpha+4032(E_2\alpha+1)^2\right)Q^2\right.\\
&-8p_s\alpha(C_1(223E_1\alpha-312(E_2\alpha+1))-288C_2)\zeta_hQ+576C_1^2\alpha^2\zeta_h^2\Big)r^8\\
&-\frac{5}{3}\left(8p_s^2\left(13E_1^3\alpha^3-78E_1^2(E_2\alpha+1)\alpha^2+132E_1(E_2\alpha+1)^2\alpha-72(E_2\alpha+1)^3\right)Q^2\right.\\
&+p_s\alpha\left(48C_2(35E_1\alpha-48(E_2\alpha+1))+C_1\left(229E_1^2\alpha^2-564E_1(E_2\alpha+1)\alpha+336(E_2\alpha+1)^2\right)\right)\zeta_hQ\\
&+18C_1\alpha^2(C_1(-5E_1\alpha+12E_2\alpha+12)-48C_2)\zeta_h^2\Big)r^6\\
&-135\left(\alpha\left(87E_1^2\alpha^2-156E_1(E_2\alpha+1)\alpha+80(E_2\alpha+1)^2\right)\zeta_hC_1^2\right.\\
&+\left(p_sQ\left(21E_1^3\alpha^3-84E_1^2(E_2\alpha+1)\alpha^2+128E_1(E_2\alpha+1)^2\alpha-64(E_2\alpha+1)^3\right)\right.\\
&+32C_2\alpha(3E_1\alpha-4E_2\alpha-4)\zeta_h)C_1+8C_2\left(p_sQ\left(5E_1^2\alpha^2-20E_1(E_2\alpha+1)\alpha+16(E_2\alpha+1)^2\right)\right.\\
&\left.+16C_2\alpha\zeta_h)\right)r^4+34560C_1^2E_1^3\alpha^3\log^5(r)r^2\\
&-4320C_1E_1^2\alpha^2\left(2E_1p_sQ\alpha r^2+C_1\left(\alpha\zeta_hr^2+36E_1\alpha-40E_2\alpha-40\right)\right)\log^4(r)r^2\\
&+240E_1\alpha\left(4E_1^2p_s^2Q^2\alpha^2r^4+36C_1^2\left(48E_1^2\alpha^2+E_1\left(\alpha\zeta_hr^2-72E_2\alpha-72\right)\alpha\right.\right.\\
&\left.+2(E_2\alpha+1)\left(-\alpha\zeta_hr^2+16E_2\alpha+16\right)\right)+C_1E_1\alpha\left(p_sQ\left(8\alpha\zeta_hr^2+81E_1\alpha-144E_2\alpha-144\right)r^2\right.\\
&\left.+576C_2)\right)\log^3(r)r^2-5\left(144\left(1008E_1^3\alpha^3-24E_1^2\left(-\alpha\zeta_hr^2+72E_2\alpha+72\right)\alpha^2\right.\right.\\
&+240E_1\alpha\left(4E_1^2p^2Q^2\alpha^2r^4+36C_1^2\left(48E_1^2\alpha^2+E_1\left(\alpha\zeta_hr^2-72E_2\alpha-72\right)\alpha\right.\right.\\
&\left.+2(E_2\alpha+1)\left(-\alpha\zeta_hr^2+16E_2\alpha+16\right)\right)+C_1E_1\alpha\left(p_sQ\left(8\alpha\zeta_hr^2+81E_1\alpha-144E_2\alpha-144\right)r^2\right.\\
&\left.+576C_2)\right)\log^3(r)r^2-5\left(144\left(1008E_1^3\alpha^3-24E_1^2\left(-\alpha\zeta_hr^2+72E_2\alpha+72\right)\alpha^2\right.\right.\\
&+E_1\left(-\alpha^2\zeta_h^2r^4-36\alpha\zeta_hr^2+1056E_2^2\alpha^2+12E_2\alpha\left(176-3r^2\alpha\zeta_h\right)+1056\right)\alpha\\
&-24(E_2\alpha+1)^2\left(-\alpha\zeta_hr^2+8E_2\alpha+8\right)\Big)C_1^2\\
&+2E_1\alpha\left(p_sQ\left(1998E_1^2\alpha^2-4E_1\left(-49\alpha\zeta_hr^2+1458E_2\alpha+1458\right)\alpha\right.\right.\\
&\left.+9\left(\alpha^2\zeta_h^2r^4-64\alpha\zeta_hr^2+480E_2^2\alpha^2-64E_2\alpha\left(r^2\alpha\zeta_h-15\right)+480\right)\right)r^2\\
&\left.+1728C_2\left(\alpha\zeta_hr^2+20E_1\alpha-24E_2\alpha-24\right)\right)C_1\\
&+E_1^2p_sQr^2\alpha^2\left(p_sQ\left(63\alpha\zeta_hr^2+352E_1\alpha-576E_2\alpha-576\right)r^2+3456C_2\right)\Big)\log^2(r)r^2\\
&-8640\left(3\left(15E_1^3\alpha^3-30E_1^2(E_2\alpha+1)\alpha^2+24E_1(E_2\alpha+1)^2\alpha-8(E_2\alpha+1)^3\right)C_1^2\right.\\
&\left.+8C_2\left(3E_1^2\alpha^2-6E_1(E_2\alpha+1)\alpha+4(E_2\alpha+1)^2\right)C_1+8C_2^2(E_1\alpha-2E_2\alpha-2)\right)r^2\\
&+\frac{1}{40}\left(7200\left(4320E_1^3\alpha^3-9E_1^2\left(-13\alpha\zeta_hr^2+896E_2\alpha+896\right)\alpha^2\right.\right.\\
&+2E_1\left(-\alpha^2\zeta_h^2r^4-96\alpha\zeta_hr^2+2880E_2^2\alpha^2-96E_2\alpha\left(r^2\alpha\zeta_h-60\right)+2880\right)\alpha\\
&-8(E_2\alpha+1)\left(-\alpha^2\zeta_h^2r^4-12\alpha\zeta_hr^2+192E_2^2\alpha^2-12E_2\alpha\left(r^2\alpha\zeta_h-32\right)+192\right)\Big)C_1^2\\
&+200\left(3456C_2\left(24E_1^2\alpha^2+E_1\left(\alpha\zeta_hr^2-40E_2\alpha-40\right)\alpha+2(E_2\alpha+1)\left(-\alpha\zeta_hr^2+8E_2\alpha+8\right)\right)\right.\\
&-p_sQr^2\left(-2268E_1^3\alpha^3+4E_1^2\left(-47\alpha\zeta_hr^2+1998E_2\alpha+1998\right)\alpha^2\right.\\
&\left.\left.+E_1\left(39\alpha^2\zeta_h^2r^4+784\alpha\zeta_hr^2-9504E_2^2\alpha^2+16E_2\alpha\left(49r^2\alpha\zeta_h-1188\right)-9504\right)\alpha\right.\right.
\end{aligned}
$$

The solution expression for the second-order velocity is obtained as

$$w_{p2} = C_5 \int \left(\frac{1+\alpha\theta(r)}{r} \right) dr + C_6 + Q \int \left(\frac{1+\alpha\theta(r)}{r} \left(\int (r(1-\alpha\theta(r))w_{p0} + 2Frw_{p0}w_{p1})dr \right) \right) dr, \tag{2.15d}$$

where $Q = 1+\lambda_1$ and due to very large expressions, the complete expression for the second-order velocity of the porous region have not been presented here.

Solution for Small Permeability $(i.e., S \gg 1)$

In the case of small permeability, the parameter S is very large $(S \gg 1)$. Dividing equation 2.12 by S^2 throughout, we obtained

$$\frac{1}{S^2}\left(\frac{\partial p}{\partial z}\right) = \frac{S^{-2}}{r}\frac{\partial}{\partial r}\left(\frac{re^{-\alpha\theta(r)}}{1+\lambda_1}\frac{\partial w_p}{\partial r} \right) - e^{-\alpha\theta(r)}w_p - S^{-1}Fw_p^2, \tag{2.16}$$

where $S^2 = \frac{1}{k}$ is a parameter and in case of small permeability, the parameter S^{-1} is small which is much less than unity.

The above boundary value problem (2.10 and 2.16) is singularly perturbed boundary value problem (SPBVP) in case of very large parameter $(S \gg 1)$ because the limiting case of $S^{-1} \to 0$ reduces the order of the differential Eq. 2.16. At this stage, we can not handle the above equation using regular perturbation approach. To overcome this difficulty, we introduce here the singular perturbation technique with matched asymptotic expansion. Since the difference between the derivative of the term multiplied by the small parameter S^{-1} and the second term free from the small parameter (S^{-1}) is 2. We expect to have two boundary layers, one at each end. Hence the outer expansion is not expected to satisfy one of the boundary conditions [142]. In the above boundary value problem, the boundary layer is located near the fluid-porous interface, i.e., at $r = 1$. The detailed description about the singular perturbation approach are discussed in the work of Nayfeh [120]. Following this approach, we find out the outer solution of the given equation 2.16 far away from the interface by using regular perturbation expansion approach in terms of the small parameter (S^{-1}). By skipping some intermediate terms as mentioned in the above reference book, the

outer solution of the velocity w_p^o is obtained as

$$\begin{aligned} w_p^o = & -\frac{p_s}{64(1+\lambda_1)r^2S^5}\left(4\alpha E_1\log(r)+4\alpha E_2-\alpha\zeta_h r^2+4\right) \\ & \times\left(8S\left(\alpha\left(2\alpha E_1^2-2\alpha E_1\zeta_h r^2+\zeta_h r^2\left(-2\alpha E_2+\alpha\zeta_h r^2+2\right)\right)-2(1+\lambda_1)r^2S^2\right)\right. \\ & +16\alpha^2E_1^2Fp(1+\lambda_1)r^2\log^2(r)-8\alpha E_1r^2\log(r)\left(Fp_s(1+\lambda_1)\right. \\ & \left.\left.\times\left(-4\alpha E_2+\alpha\zeta_h r^2-4\right)+2\alpha\zeta_h S\right)+Fp_s(1+\lambda_1)r^2\left(4\alpha E_2-\alpha\zeta_h r^2+4\right)^2\right), \end{aligned} \tag{2.17}$$

where superscript (o) represents the outer solution and the velocity components are given

$$\begin{aligned} & w_{p0}=w_{p1}=w_{p3}=0, \\ & w_{p2}=p_s(1+\alpha\theta(r))=p_s\left(1+\alpha\left(E_1\log(r)+E_2-\frac{\zeta_h r^2}{4}\right)\right), \\ & w_{p4}=(1+\alpha\theta(r))\left(\frac{1}{r}\frac{d}{dr}\left(\frac{r(1-\alpha\theta(r))}{Q}\frac{dw_{p2}}{dr}\right)\right)=\frac{\alpha p_s}{8(1+\lambda_1)r^2}\times \\ & \quad\left(4\alpha E_1\log(r)+4\alpha E_2-\alpha\zeta_h r^2+4\right)\times \\ & \quad\left(-2\alpha E_1^2+2\alpha E_1\zeta_h r^2+2\alpha E_1\zeta_h r^2\log(r)-\zeta_h r^2\left(-2\alpha E_2+\alpha\zeta_h r^2+2\right)\right), \\ & w_{p5}=-Fw_{p2}^2=-\frac{Fp_s^2}{64}\left(4\alpha E_1\log(r)+4\alpha E_2-\alpha\zeta_h r^2+4\right)^3. \end{aligned} \tag{2.18}$$

We can check the limit of the outer solution in terms of the inner limit

$$(w_p^o)^{in}=\lim_{S\to\infty}w_p^o=0. \tag{2.19}$$

Now, we are going to find out the expression for the inner solution. Firstly, we introduce the stretching variable as below

$$\eta=S(1-r). \tag{2.20}$$

Introducing the parameter η in the equation 2.16 and after neglecting the smaller term $(S^{-1}\to 0)$ to obtain the reduced equation in the following form:

$$\frac{d^2w_p^{in}}{dr^2}-(1+\lambda_1)w_p^{in}=0. \tag{2.21}$$

The solution of the above equation is obtained as the one term solution

$$w_p^{in}=C_7e^{-\eta\sqrt{(1+\lambda_1)}}=C_7e^{-S(1-r)\sqrt{(1+\lambda_1)}}. \tag{2.22}$$

Now, we can check the limit of inner solution in terms of outer limit

$$(w_p^{in})^o = \lim_{\eta\to\infty} w_p^{in} = 0. \tag{2.23}$$

From equations 2.19 and 2.23, we found that the Prandtl's matching condition is satisfied [141]. We have obtained the matching solution from the above equations 2.19 and 2.23

$$w_p^m(r) = 0. \tag{2.24}$$

The composite solution of the above equation 2.16 is obtained below

$$\begin{aligned} w_p &= (w_p)^o + (w_p)^{in} - (w_p)^m, \\ &= C_7 e^{-S(1-r)\sqrt{(1+\lambda_1)}} - \frac{p_s}{64(1+\lambda_1)r^2S^5}\left(4\alpha E_1\log(r) + 4\alpha E_2 - \alpha\zeta_h r^2 + 4\right) \\ &\times \left(8S\left(\alpha\left(2\alpha E_1^2 - 2\alpha E_1\zeta_h r^2 + \zeta_h r^2\left(-2\alpha E_2 + \alpha\zeta_h r^2 + 2\right)\right) - 2(1+\lambda_1)r^2S^2\right)\right. \\ &+ 16\alpha^2 E_1^2 F p(1+\lambda_1)r^2\log^2(r) - 8\alpha E_1 r^2\log(r)\left(F p_s(1+\lambda_1)\right. \\ &\left.\left.\times\left(-4\alpha E_2 + \alpha\zeta_h r^2 - 4\right) + 2\alpha\zeta_h S\right) + F p_s(1+\lambda_1)r^2\left(4\alpha E_2 - \alpha\zeta_h r^2 + 4\right)^2\right). \end{aligned} \tag{2.25}$$

2.3.2.2 Analytical Solution for the Clear Fluid Region

The solution of the equation 2.9b for clear fluid region is obtained analytically

$$\begin{aligned} w_c &= C_8\int\left(\frac{1+\alpha\theta(r)}{r}\right)dr + C_9 - \frac{p_s Q}{2}\int r(1+\alpha\theta(r))dr \\ &= \frac{C_8}{8}\left(4\log(r)(\alpha E_1\log(r) + 2\alpha E_2 + 2) - \alpha\zeta_h r^2\right) + C_9 \\ &+ \frac{p_s Q r^2}{32}\left(4\alpha E_1 - 8\alpha E_1\log(r) - 8\alpha E_2 + \alpha\zeta_h r^2 - 8\right), \end{aligned} \tag{2.26}$$

where C_1 to C_9 are constants appeared in the solution of the given differential equations which can be obtained using the given boundary conditions 2.10.

2.3.3 Hydrodynamical Quantities

The volumetric flow rate Q_s in non-dimensional form is defined as

$$Q_s = 2\pi\int_l^m rw(r)dr = 2\pi\left(\int_l^1 rw_p(r)dr + \int_1^m rw_c(r)dr\right). \tag{2.27}$$

The hydrodynamic permeability L_{11} of the swarm of the porous cylindrical particles is expressed as [96]

$$L_{11} = -\frac{V_f}{\partial p/\partial z}, \tag{2.28}$$

where V_f represent the filtration velocity and is given by $V_f = \frac{Q_s}{\pi m^2}$.
The semi-empirical Kozeny-Karman formula [71] results in the following expression for the permeability of the porous media

$$L_{11} = \frac{\varepsilon \rho_h^2}{K_z \widetilde{b}^2}, \tag{2.29}$$

where ε is the porosity and K_z is the dimensionless Kozeny constant, ρ_h is the hydraulic radius which is equal to the ratio of pore volume to the wetting area.
The Kozeny constant is obtained by the above Eq. 2.29

$$K_z = \frac{\varepsilon \rho_h^2}{\widetilde{b}^2 L_{11}}. \tag{2.30}$$

For the media composed of cylindrical particles, we have

$$\rho_h = \frac{\pi(\widetilde{c}^2 - \widetilde{b}^2)}{2\pi\widetilde{b}} = \frac{\widetilde{b}}{2}\left(\frac{1-\gamma}{\gamma}\right) = \frac{\varepsilon\widetilde{b}}{2(1-\varepsilon)}. \tag{2.31}$$

Substituting the value of ρ_h in the above equation 2.30, we have

$$K_z = \frac{\varepsilon^3}{4(1-\varepsilon)^2 L_{11}}, \tag{2.32}$$

where L_{11} is the hydrodynamic permeability of the membranes.

2.4 Results and Discussion

The present work is a theoretical attempt to analyze the impact of variable viscosity on the flow of Jeffrey fluid through membranes composed of a swarm of porous cylindrical particles with solid core. Before going to discuss the results of present work in detail, an effort has been made to describe the behavior of the Jeffrey fluid. Due to involvement of the viscous and elastic characteristic of the fluid, it is worth acknowledging that Jeffrey fluid

is a realistic in the filtration process of the polymer solutions while modeling the creeping flow of fluid through membranes. The fluid is assumed to be Jeffrey fluid with varying viscosity and the flow is driven by constant pressure gradient. Further, for analytical treatment the relaxation time is assumed to be very small resulting in linear stress-strain relation. The Brinkman-Forchheimer equation regulates the flow through porous media, however the Stokes equation governs the flow outside the porous media. An analytical solution is obtained for flow of clear fluid, however perturbation method is employed to solve the Brinkman-Forchheimer equation for flow through porous media under the small as well as large permeability of the porous medium. The dependency of the hydrodynamic permeability of the membranes and Kozeny constant on the numerous parameters like Forchheimer number, permeability of the porous media, porosity parameter, and Jeffrey fluid parameter are discussed and compared with results of previous studies ([71], [3]).

2.4.1 Model Validation

Our model reduces to following limiting cases:

1. As the Forchheimer number approaches to zero, i.e., ($F \to 0$), the Brinkman-Forchheimer model reduces to the Brinkman model for flow through porous medium.

2. As the Jeffrey fluid parameter ($\lambda_1 = 0$), the present Jeffrey fluid model reduces to the Newtonian fluid model with varying viscosity assumption.

3. As the viscosity parameter approches to zero, i.e.($\alpha \to 0$), the present variable viscosity model reduces to the constant viscosity model.

4. As the radius of the cylindrical tube with solid core approaches to zero, i.e., ($l \to 0$), the present model reduces to porous cylindrical tube without solid core (i.e., fully porous cylindrical particle).

5. As the radius of the cylindrical tube with solid core and the permeability of the porous medium approaches to zero, i.e., ($l \to 0$ and $k \to 0$) or ($l \to 1$), the present model reduces to solid cylindrical particle in cell without porous medium (i.e., fully solid cylindrical particle in cell).

   The expression for the hydrodynamic permeability of the membrane is obtained in the limiting case ($l \to 0$, $k \to 0$, and $F = \lambda_1 = \alpha = 0$) for small permeability formulation, and in the limiting case ($l \to 1$, and $F = \lambda_1 = \alpha = 0$) for large permeability

formulation (Happel's cell model [71]).

$$L_{11} = \frac{-2\ln\gamma - \gamma^2 + 4\gamma - 3}{8\gamma}, \tag{2.33}$$

which is exactly derived in the work of Deo *et al.* [3].

6. As the permeability of the porous medium is very large, i.e., $(k \to \infty)$, the porous medium reduces to the clear fluid.

2.4.2 Parameter Selection

The values of numerous parameters are taken from the various work to perform the graphical analysis of the present work. The range of values of the control parameters with their appropriate resources are given in Table 1.

Values of parameters		
Parameters	Values	Resources
Heat absorption parameter ζ_h	0-9	[1]
Permeability k	$(0,\infty)$	[2], [3]
Steady pressure gradient p_s	1-10	[4], [5]
Stess-jump parameter β_S	$-1 < \beta_S < 1$	[3], [5]
Viscosity parameter α	0.0-0.5	[1], [6]
Forchheimer number F	0.0-2.0	[7], [8]
Jeffrey fluid parameter λ_1	0.0-2.0	[9], [10]
Particle volume fraction γ	0.1-1.0	[3], [11]

Table 2.1: Range of values for the existing parameters with their resources

2.4.3 Velocity Profile (w)

A radially increasing velocity profile is observed with concave for small permeability and convex for large permeability in the porous region but the variation remains the same in the clear fluid region (Fig. 2.3a). A rising viscosity parameter α contributes towards increasing velocity owing to decay in viscosity. Higher viscosity parameter leads to a higher growth rate in the velocity profile for both the formulations (small and large permeability of the porous medium). The effect of the viscosity parameter is more significant for large

permeability. The effect of the Jeffrey fluid parameter λ_1 on the velocity profile for both the formulations (small and large permeability of the porous medium) is delineated in Fig. 2.3b in which the specific case of Newtonian fluid with varying viscosity is represented by $\lambda_1 = 0$. The consistent increase in Jeffrey fluid parameter λ_1 leads to an increase in fluid velocity with a relatively higher growth rate. The effect of the Jeffrey fluid parameter is more significant for the large permeability of the porous medium. A velocity profile is not smooth at the fluid-porous interface owing to the stress-jump boundary condition.

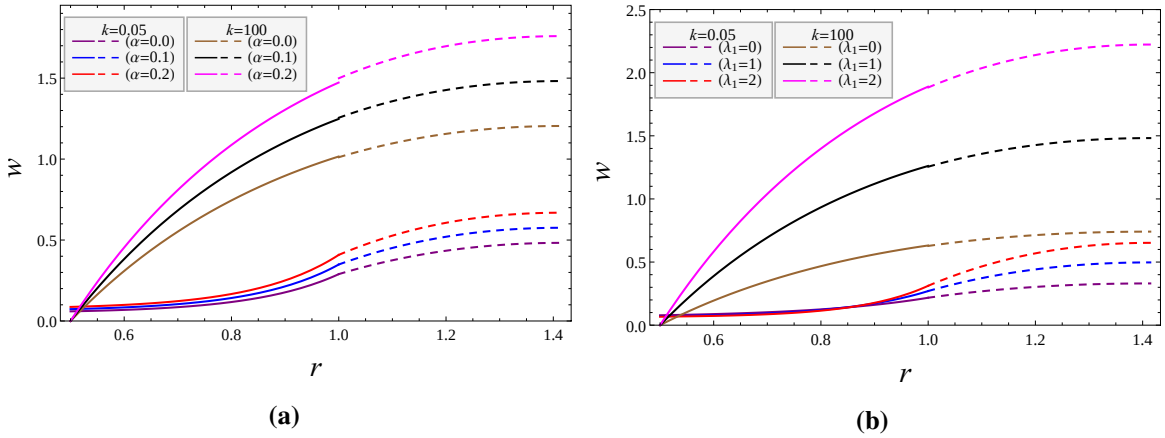

Figure 2.3: Variation of velocity profile w with radial distance r for different values of **(2.3a)** viscosity parameter α $(\lambda_1 = F = 1, \beta_S = 0.4)$ and **(2.3b)** Jeffrey fluid parameter λ_1 $(\alpha = 0.1, F = 0, \beta_S = 0.1)$. $(l = \gamma = 0.5, \zeta_h = 5, p_s = 1)$

2.4.4 Hydrodynamic Permeability (L_{11})

The results of the present study are compared with specific case of Deo *et al.* [3] for viscosity parameter $\alpha \to 0$, Jeffery fluid parameter $\lambda_1 = 0$, and Forchheimer number $F = 0$. Fig. 2.4 illustrates that the limiting case of our solution with Deo *et al.* [3] is in good agreement with the results of Deo *et al.* [3] for the validation of the hydrodynamic permeability with particle volume fraction γ for both the formulations. This further validates the present model.

The flow of Jeffrey fluid with varying viscosity through a porous region with Forchheimer formulation has been discussed and the same has been delineated in Fig. 2.5a. A rising particle volume fraction leads to decay in the hydrodynamic permeability of the swarm of particlees for both the formulations (small and large permeability of the porous medium) owing to the enhanced resistance which can be accredited to the relatively larger space of porous region in comparison to clear fluid region. That is, the envelope occupies lesser region containing clear fluid offering less resistance in comparison to porous region offering more resistance to the fluid flow. It is further observed that the decay rate is relatively higher for higher varying viscosity parameters. Although this difference is relatively lesser

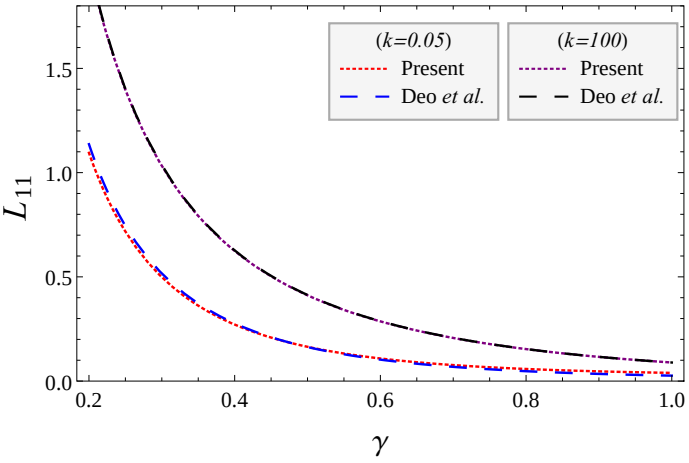

Figure 2.4: Variation of hydrodynamic permeability L_{11} with particle volume fraction γ between present study and Deo *et al.* [3]. $(l = 0.5, \beta_S = 0.1, \zeta_h = 5, \alpha = 0, p_s = 1, F = \lambda_1 = 0)$

for low permeability formulation. The effect of varying viscosity is almost insignificant for higher particle volume fraction. The dependence of the hydrodynamic permeability of the membrane on Jeffrey fluid parameter with particle volume fraction is illustrated in Fig. 2.5b for both the formulations $(k = 0.05$ and $k = 100)$. An increasing Jeffrey fluid parameter contributes towards growth in hydrodynamic permeability. However, the decay rate of hydrodynamic permeability L_{11} with particle volume fraction is relatively higher for higher Jeffrey fluid parameter. It is expected that the hydrodynamic interactions are less prominent if the cylindrical particles are very close to each other. So, at very large particle volume fraction $(\gamma > 0.45)$, it is expected that the variation in the hydrodynamic permeability of the membrane is minimal. The impact of Jeffrey fluid parameter is more significant for large permeability.

The effect of the stress-jump parameter β_S on the membrane permeability reveals a slight growth for large permeability (Fig. 2.6a). However, this variation becomes relatively significant and nonlinear for low permeability owing to a significant contribution of the jump coefficient term in the boundary condition (Eq. 2.10c) for low permeability. The impact of stress-jump parameter β_1 on the hydrodynamic permeability of the membrane is more for Jeffrey fluid and less for Newtonian fluid (Fig. 2.6b).

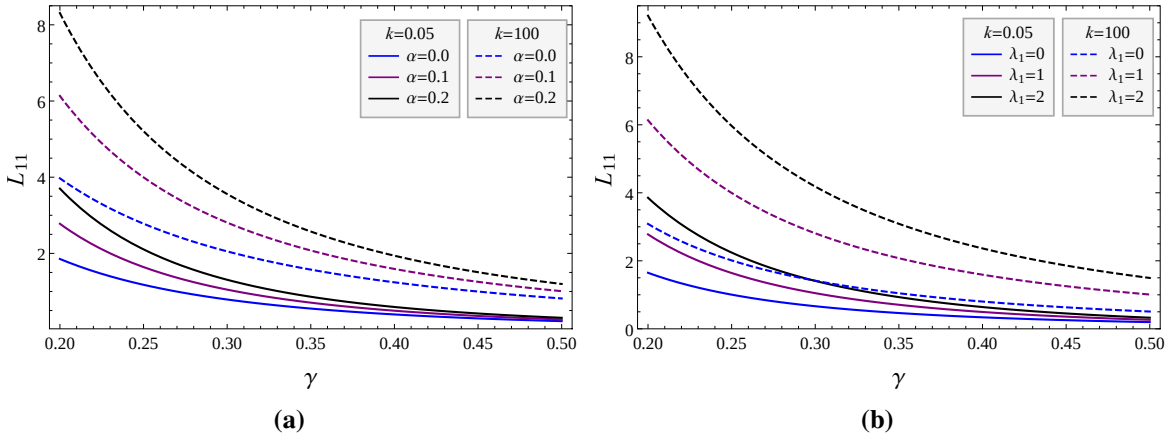

Figure 2.5: Variation of hydrodynamic permeability L_{11} with particle volume fraction γ for different values of **(a)** viscosity parameter α $(\lambda_1 = 1)$ and **(b)** Jeffrey fluid parameter λ_1 $(\alpha = 0.1)$. $(l = 0.5, \beta_S = 0.1, \zeta_h = 5, p_s = F = 1)$

A comparative study of the effect of Forchheimer number F on the hydrodynamic permeability L_{11} of the swarm of particles for the flow of Newtonian and Jeffrey fluids through membrane composed of a swarm of porous cylindrical particles reveals a slight decay in L_{11} with increasing Forchheimer number for low permeability owing to slightly higher resistance (Table 2(a)). However, this decay is relatively more for Jeffrey fluid and varying viscosity. The same observation for high permeability is delineated in Table 2(b). Here also, we observed that the results similar to the low permeability case. The effect of Forchheimer number on hydrodynamic permeability of the membrane for both the fluids (Newtonian and Jeffrey fluids) is analyzed for the limiting case of a perfectly porous particle with low permeability in Table 3. Here, it is evident that the perfectly porous particle (with no solid core) will have a relatively smooth flow as observed in slightly higher values of L_{11}. The rest of the analysis is similar to the observations made in Table 2.

The present model and the approximate solution is being validated through the comparison in the results of limiting cases of the work of Deo *et al.* [3] and $l \to 0, F = \lambda_1 = 0$ in Fig. 2.7. It is observed that the limiting case for the flow of Newtonian fluid with constant viscosity through a swarm of the perfectly porous cylindrical particles $(l \to 0, k \to 0, \alpha \to 0, F = \lambda_1 = 0)$ is in good agreement with the work of Deo *et al.* [3]. The slight difference in L_{11} curve for the two formulations can be accredited to the approximate solution obtained in the present study, yet it also shows the accuracy of the approximate solution. In the same figure, variation of the hydrodynamic permeability of the membrane with particle volume fraction for the limiting case of the flow of Newtonian fluid with varying viscosity through a swarm of perfectly porous cylindrical particles reveals growth in L_{11} with varying viscosity parameter.

$F \downarrow$	Newtonian Fluid ($\lambda_1 = 0$)			Jeffrey Fluid ($\lambda_1 = 1$)		
	$\alpha = 0.0$	$\alpha = 0.1$	$\alpha = 0.2$	$\alpha = 0.0$	$\alpha = 0.1$	$\alpha = 0.2$
$F = 0.0$	0.164388	0.198048	0.232066	0.221629	0.266209	0.310925
$F = 0.5$	0.164123	0.197534	0.231185	0.221371	0.265721	0.310101
$F = 1.0$	0.163857	0.197020	0.230304	0.221113	0.265232	0.309276
$F = 1.5$	0.163592	0.196506	0.229423	0.220855	0.264744	0.308452
$F = 2.0$	0.163327	0.195992	0.228542	0.220597	0.264256	0.307628

(a)

$F \downarrow$	Newtonian Fluid ($\lambda_1 = 0$)			Jeffrey Fluid ($\lambda_1 = 1$)		
	$\alpha = 0.0$	$\alpha = 0.1$	$\alpha = 0.2$	$\alpha = 0.0$	$\alpha = 0.1$	$\alpha = 0.2$
$F = 0.0$	0.411456	0.509371	0.607319	0.822574	1.01834	1.21422
$F = 0.5$	0.411106	0.508696	0.606163	0.819820	1.01307	1.20531
$F = 1.0$	0.410760	0.508032	0.605035	0.817188	1.00817	1.19731
$F = 1.5$	0.410417	0.507379	0.603936	0.814677	1.00364	1.19020
$F = 2.0$	0.410079	0.506738	0.602864	0.812289	0.99947	1.18400

(b)

Table 2.2: Variation of hydrodynamic permeability of membrane L_{11} for **(a)** small permeability ($k = 0.05$) and **(b)** large permeability ($k = 100$) of the porous medium, under different values of viscosity parameter α, Forchheimer number F and Jeffrey fluid parameter λ_1. ($l = \gamma = 0.5, \zeta_h = 5, p_s = 1, \beta_S = 0.1$)

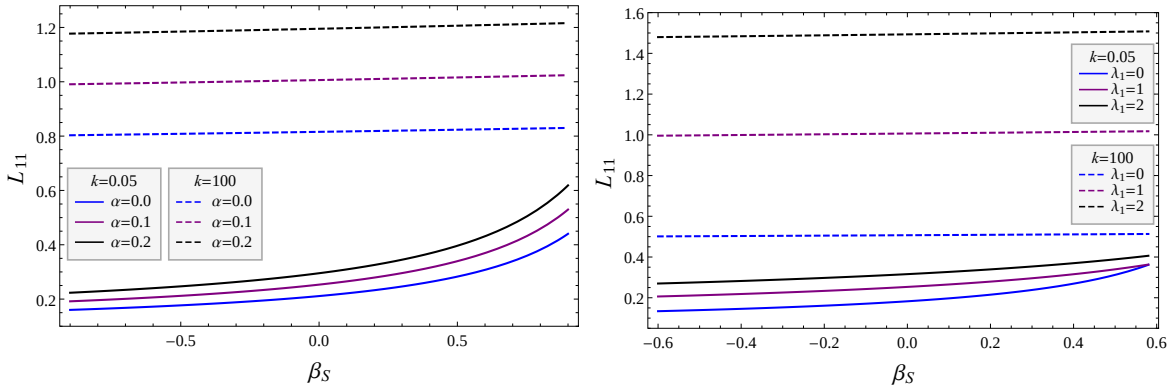

(a) **(b)**

Figure 2.6: Variation of hydrodynamic permeability L_{11} with stress-jump parameter β_S for different values of **(a)** viscosity parameter α $(\lambda_1 = 1)$ and **(b)** Jeffrey fluid parameter λ_1 $(\alpha = 0.1)$. $(l = \gamma = 0.5, \zeta_h = 5, p_s = F = 1)$

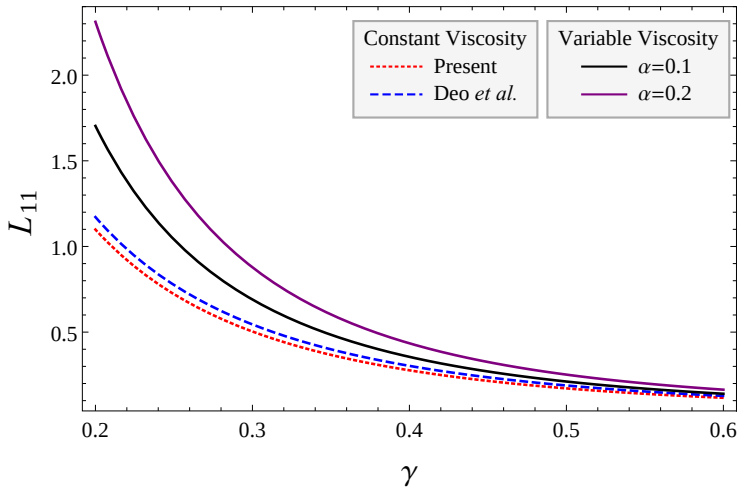

Figure 2.7: Variation of hydrodynamic permeability L_{11} with particle volume fraction γ between constant and varying viscosity models. $(l \to 0, p_s = 1, \beta_S = 0.1, \zeta_h = 5, k = 0.05, \lambda_1 = F = 0)$

$F \downarrow$	Newtonian Fluid ($\lambda_1 = 0$)			Jeffrey Fluid ($\lambda_1 = 1$)		
	$\alpha = 0.0$	$\alpha = 0.1$	$\alpha = 0.2$	$\alpha = 0.0$	$\alpha = 0.1$	$\alpha = 0.2$
$F = 0.0$	0.171569	0.211547	0.251893	0.228285	0.279997	0.331846
$F = 0.5$	0.171269	0.210899	0.250706	0.227992	0.279383	0.330735
$F = 1.0$	0.170969	0.210252	0.249519	0.227699	0.278768	0.329623
$F = 1.5$	0.170668	0.209605	0.248332	0.227406	0.278154	0.328512
$F = 2.0$	0.170368	0.208958	0.247145	0.227113	0.277539	0.327400

Table 2.3: Variation of hydrodynamic permeability of membrane L_{11} for different values of viscosity parameter α, Forchheimer number F and Jeffrey fluid parameter λ_1. ($l \to 0, \gamma = 0.5, \zeta_h = 5, p_s = 1, k = 0.05, \beta_S = 0.1$)

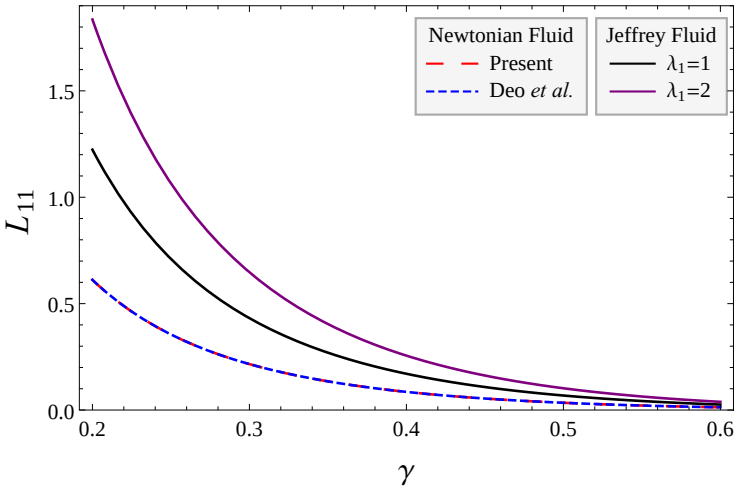

Figure 2.8: Variation of hydrodynamic permeability L_{11} with particle volume fraction γ between Newtonian and Jeffrey fluids. ($l \to 0, k \to 0, p_s = 1, \beta_S = 0.1, \zeta_h = 5, \alpha = F = 0$)

A graphical comparison of the present study with the limiting case of Deo *et al.* [3] is depicted in Fig. 2.8 showing that for the flow of Newtonian fluid with constant viscosity through a swarm of solid cylindrical particles ($l \to 0, k \to 0, \alpha \to 0, F = \lambda_1 = 0$), the limiting case of the present solution exactly matches with the work of Deo *et al.* [3]. The same has already been analytically depicted in equation 2.33. A novel observation is that a rising Jeffrey fluid parameter leads to rise in hydrodynamic permeability of membrane for the flow of Jeffrey fluid with constant viscosity through a swarm of solid cylindrical particles. The effect of particle volume fraction on hydrodynamic permeability of membrane remains same

in this case.

2.4.5 Kozeny Constant (K_z)

The effect of porosity on Kozeny constant K_z for both the formulations (low and high permeability) under varying viscosity assumption reveals that a rising porosity leads to growth in Kozeny constant for high as well as low permeability, which is similar to the observation of Madasu and Buch [11] for the case of Newtonian fluid flow through particles with cavity (Fig. 2.9a). However, the present study reveals that a higher varying viscosity parameter leads to reduced growth rate of Kozeny constant with porosity, illustrating the effect of varying nature of viscosity on Kozeny constant K_z. It is further observed that the higher permeability leads to significantly reduced Kozeny constant K_z. The dependence of Kozeny constant on Jeffrey fluid parameter is illustrated in Fig. 2.9b under varying viscosity and it is noticed that a growth in Kozeny constant with porosity parameter is observed for Newtonian $(\lambda_1 = 0)$ and Jeffrey $(\lambda_1 \neq 0)$ fluids. It is also observed that a rising Jeffrey fluid parameter contributes to decay in growth rate of Kozeny constant with porosity parameter for both the formulations (low as well as high permeability of the porous medium). The impact of Jeffrey fluid parameter on Kozeny constant is more significant in case of low permeability in comparison to high permeability.

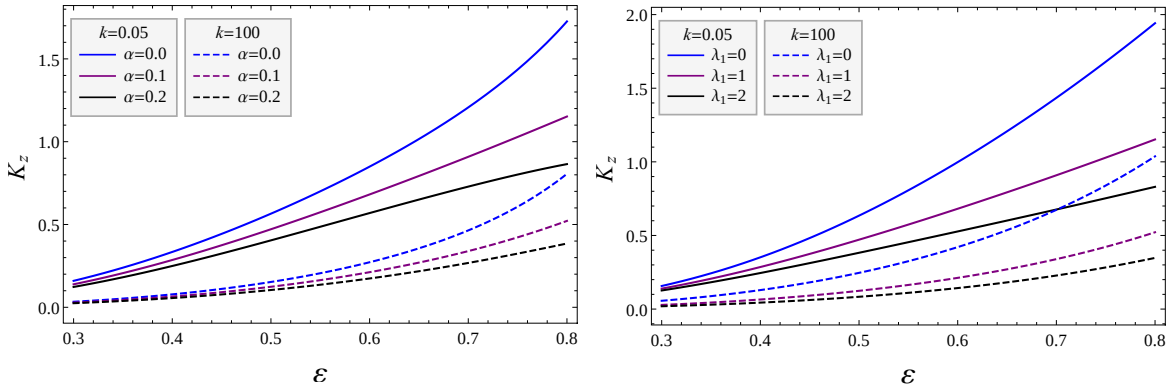

Figure 2.9: Variation of hydrodynamic permeability L_{11} with stress-jump parameter β_S for different values of **(a)** viscosity parameter α $(\lambda_1 = 1)$ and **(b)** Jeffrey fluid parameter λ_1 $(\alpha = 0.1)$. $(l = \gamma = 0.5, \zeta_h = 5, p_s = F = 1)$

A nonlinear decay in Kozeny constant with rising stress-jump parameter β_S for low permeability under varying viscosity assumption is delineated in Fig. 2.10a owing to rise in hydrodynamic permeability of membrane with stress-jump parameter. However, this effect is almost negligible in the case of large permeability owing to an almost negligible presence

of discontinuity in shear stress at the fluid-porous interface for large permeability. The dependence of Kozeny constant on the Jeffrey fluid parameter is demonstrated in Fig. 2.10b for Newtonian ($\lambda_1 = 0$) and Jeffrey ($\lambda_1 \neq 0$) fluids. It is noticed that the fluid with large relaxation time ($\lambda_1 \neq 0$) leads to decay in Kozeny constant however for a larger stress-jump parameter, a reverse trend is observed. The decay rate reduces with increasing Jeffrey fluid parameter in case of low permeability however, a negligible effect of stress-jump parameter on Kozeny constant for high permeability is reported for Newtonian and Jeffrey fluids. It is further noticed that the Kozeny constant is more for Newtonian fluid for both the formulations (low as well as high permeability of the porous medium). It is worth acknowledging that Jeffrey fluid characteristic affects the Kozeny constant more significantly for low permeability in comparison to high permeability.

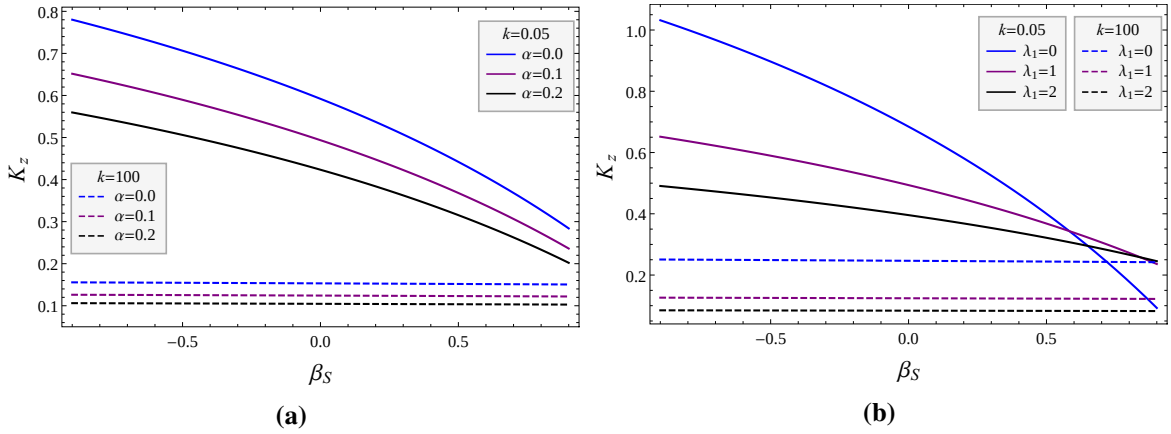

Figure 2.10: Variation of Kozeny constant K_z with stress-jump parameter β_S for different values of **(a)** viscosity parameter α ($\lambda_1 = 1$) and **(b)** Jeffrey fluid parameter λ_1 ($\alpha = 0.1$). ($l = \varepsilon = 0.5, \zeta_h = 5, p_s = F = 1$)

Analogues to Tables 2-3, the similar analysis is being done for Kozeny constant in Tables 4-5. All the three tables shows a rise in Kozeny constant with increasing Forchheimer number F for Newtonian and Jeffrey fluids under constant as well as varying viscosity assumptions.

2.5 Summary and Conclusions

The primary objective of the present study is to evaluate the analytical or asymptotic solution expressions for the velocity profile and hence obtain the expressions for hydrodynamic permeability of the membrane and Kozeny constant. The hydrodynamic equations are coupled with thermal equations via temperature-dependent viscosity. The notable contribution of the present study is to analyze the impact of temperature-dependent viscosity and porous

medium parameters on the flow of Jeffrey fluid through membranes composed of a swarm of porous cylindrical particles with solid core. The Brinkman-Forchheimer and Stoke's equations regulate the flow inside and outside of the porous cylindrical particle, respectively. The regular and singular perturbation techniques with matched asymptotic expansion method have been used to obtain approximate solutions of the Brinkman-Forchheimer equation for low and high permeability of the porous medium, however an analytical solution is being obtained for clear fluid region (outside of the porous cylindrical particle). The dependency of the flow variables, membrane permeability and Kozeny constant on the viscosity and porous layer parameters are discussed comprehensively through graphical and tabular analysis. Some previous results have been deduced as the limiting cases of the present study. From the discussion of the aforementioned results, the main findings are concluded as follows:

1. It is observed that a decay in viscosity leads to growth in velocity profile, and hydrodynamic permeability of the membranes, however a decay in Kozeny constant is observed with increasing viscosity parameter. Further, for large particle volume fraction the impact of viscosity variation and relaxation time on membrane permeability is almost insignificant for the case of low permeability.

2. For low and high permeability, the growth of velocity profile follows different patterns owing to different perturbation approaches (regular and singular perturbation methods).

3. The effect of relaxation time on velocity profile is significantly higher for large permeability whereas the same is almost insignificant for small permeability.

4. For porous cylinder in cell and solid cylinder in cell (both are the limiting cases of our present model), the membrane permeability decays with particle volume fraction but grows with viscosity and Jeffrey fluid parameters.

5. A noteworthy observation is that the rising viscosity parameter and the relaxation time of the Jeffrey fluid ($\lambda_1 \neq 0$) contribute to decay in growth rate of the Kozeny constant with porosity parameter.

6. Due to presence of nonlinear resistance term in the Brinkman-Forchheimer equation, a slight impact of Forchheimer number on the hydrodynamic permeability and Kozeny constant is observed for Newtonian and Jeffrey fluids.

In the present problem, the generalized Brinkman-Forchheimer model has been used to formulate the fluid flow through a swarm of porous particles using cell model technique with

the assumption of temperature-dependent viscosity. It is worth mentioning that the cell model technique gives the good approximation of the computed quantities, so we can conclude that in the processes related to the contaminant clean-up, filtration process, and water purification, the temperature-dependent viscosity and the fluid inertia term in the porous region have significant impact on the membrane permeability and Kozeny constant.

Chapter 3

Asymptotic Analysis of Electrohydrodynamic Flow through a Swarm of Porous Layered Cylindrical Particles: A Particle-in-Cell Approach[1]

3.1 Introduction

The mechanical properties of the fluid flow through tubes or conduits are crucial in the study of diverse areas of research. Several factors enhance or decline the fluid flow through tubes or conduits, and such factors play a pivotal role in studying the physical and biological circumstances [169]. The mechanism of the fluid flow process through a tube or conduit becomes crucial to examine the functioning of the hydrodynamical quantities like velocity, flow rate, and resistance offered against the fluid flow and the relation between prevailing pressure and flow fields. The medium addressed in the fluid's circulation process plays an essential role in understanding the functioning of the fluid flow pattern and the resistance offered against the flow via mediums. In many cases, some obstructions occur in the circulation process of fluid through tubes or conduits, and one of them is the porous material, leading to a reduction in the fluid flow quantity throughout the circulation process. Due to its wide range of applications in science and technology, the fluid flow phenomenon in porous media has been the subject of researchers' ongoing investigation. There are various applications of the fluid flow through porous materials such as pharmaceutical fields, petroleum reservoir rocks, wastewater treatment filtration processes, blood flow via the lungs, and digestive system design [170].

Most works mentioned above delineate the utility of the particle-in-cell approach in the membrane filtration process and discuss the contribution and effect of the numerous control parameters involved in their study on the various hydrodynamic quantities and membrane permeability. Much of the work related to the creeping flow through a swarm of particles

[1] A considerable part of this chapter is published in *Physics of Fluids*, 36(4), 041910, 2024

has been studied by considering fluid flow through the tubes of the circular cross-section. There are various situations in real-life problems where additional body forces like electric fields play an important role in fluid flow past a swarm of particles ([171], [172], [173], [174]). The electrolyte plays a significant role in biology, chemistry, and industrial engineering owing to its ability to conduct electricity when dissolved in a solvent. In the study of the dynamics of electrolyte fluid, electrohydrodynamic flows are encountered in a variety of contexts, making them useful for applications such as EHD drying, MEMS devices, ESPs, heat transfer enhancement, EHD plasma actuators, EHD pumping, and so on. Recently, many researchers have studied the electrohydrodynamic ion drag pumping system, where the electrical precipitation technique is used to control the fluid flow. This technique involves charging particles by ion impact and injecting them into one end of the membrane. During this process, neutral particles were subjected to a corona discharge, which was generated by a high-voltage electrode and led to the establishment of a strong electric field, thereby causing ionization of the surrounding medium. Consequently, the neutral particles obtained charges from the ions present in the medium. The implantation of an external potential difference induces a drag force on these charged particles, prompting them to migrate towards the direction of the opposite electrode. The motion of charged particles within a fluid generates a body force that impacts the fluid's overall mass, hence causing it to flow. The "ion drag" configuration of electrohydrodynamic flow in a circular cylindrical conduit was initially studied by McKee *et al.* [14], where they analyzed the flow velocity in the case of small and large values of the non-linearity parameter α using the perturbation approach. Paullet [14] discussed the qualitative properties (existence and uniqueness) of the solution to the same problem and revealed the bounds and monotonically decreasing behaviour of the approximated solution. He also found an ambiguity in the perturbation solution of McKee for large values of α. In addition, many researchers ([175], [176], [177]) have investigated the "ion drag" configuration of electrohydrodynamic flow employing various approximation approaches and have discussed the convergence of the solution. The EHD thrust arises from the acceleration of ionized fluid within an electric field, resulting from the exchange of momentum between charged particles and neutral molecules has been discussed by Vaddi *et al.* [178]. Based on the preceding conversation and to the best of the authors' understanding, there has been no prior discussion on the inclusion of electrohydrodynamic flow in the context of heat transfer within the membrane filtration process.

The present study aims to discuss the combined effect of electrohydrodynamic flow and heat transfer on fluid flow through a swarm of porous cylindrical particles by adopting the particle-in-cell model approach. The configuration of the flow pattern is divided into two

different regions. The region that is proximate to the solid core is porous. A region surrounded by the porous region free from the porous material is a non-porous region. The nonlinear momentum equation in terms of the Hartmann electric number is introduced to model the EHD effect in the fluid flow through porous and non-porous regions. The solutions of the energy equations for both regions are analytically obtained. In order to solve the momentum equations for both regions, the analytical treatment is challenging due to the presence of nonlinear electric field terms in the momentum equations. The asymptotic series expansions are introduced to solve the nonlinear momentum equations for both regions in terms of small and large values of the parameter α. The expression of velocities and temperature profiles for different regions have been used to derive the expressions of membrane permeability and the Kozeny constant. The efficacy of the numerous control parameters like Hartmann electric number, Grashof number, radiation parameter, viscosity ratio parameter, and porosity of the porous material on the hydrodynamical quantities such as velocity, membrane permeability, and Kozeny constant have been graphically discussed. A comparative graphical analysis of the same with its numerical solution has been done to validate the asymptotic solution.

The framework of the proposed work is split into five sections. Section 1 demonstrates the essential information with applications about the present work. The mathematical formulation with assumptions, model description, the suitable boundary conditions for energy and momentum equations, and the non-dimensionalization are given in section 2. Section 3 reveals the solution methodology for the proposed governing equations. The parameter selection, model validation, results, and graphical analysis for the present work are demonstrated in section- 4. The remarkable contributions of the present work are illustrated in the conclusion (section 5), followed by the author's acknowledgment and references.

3.2 Problem Formulation

3.2.1 Statement of the Problem

The proposed study focuses on the electrohydrodynamic flow of a Newtonian fluid passing through a membrane constructed from a collection of porous cylindrical particles, with an emphasis on incorporating the heat transfer principle. The study employs the particle-in-cell approach to examine the behavior of a swarm of particles, focusing on a porous layered cylindrical particle within the swarm. Additionally, a condition on the hypothetical cell surface is taken into account for further analysis. Examining the impact of electromagnetic forces on hydrodynamic permeability and the Kozeny constant involves incorporating an additional resistance term in the form of an electrical field. Additionally, the membrane filtration process includes the consideration of heat transfer to analyze temperature variations and associated parameters. Throughout filtration procedures, the membrane's composition might experience changes owing to particle dissolution and polymer attachment onto particle surfaces, commonly referred as poisoning. These occurrences result in the formation of a porous shell, like a colloidal or gel layer, encasing solid particles' surfaces, which proves to be notoriously difficult to eradicate. The presence of this porous shell notably impacts the drag force exerted on the particles by the flow. The proposed model's configuration is divided into two clearly defined regions: a porous region near the cylindrical particle's solid core and an outer region devoid of any porous structure, commonly referred as the non-porous (clear fluid) region. The model's structure is designed such that the Brinkman equation governs the porous region proximate to the solid core of the cylindrical particle, while the Stokes equation controls a concentric, non-porous region surrounding the porous region. The equations describing the flow of an electrohydrodynamic Newtonian fluid through a membrane comprising a collection of porous layered cylindrical particles have been derived under the following assumptions:

1. The flow is considered steady, incompressible, demonstrating laminar characteristics, symmetrical within the tube, and fully developed.

2. The Reynolds number is deemed to be extremely low, signifying that viscous forces exert more influence than inertial forces, leading to the convective term being of minimal significance and thus excluded from the present study.

3. To achieve accurate physical representation, the governing equation for a unidirectional flow of Newtonian fluid parallel to the porous layered cylindrical particle is formulated using the cylindrical polar coordinate system $(\widetilde{r}, \theta, \widetilde{z})$.

4. The thermal equations in a steady-state condition are simplified when heat conduction dominates over heat convection, leading to a negligible contribution of the convective term.

5. A uniform electric field E_0 is imposed along the length of cylindrical particles generating using voltage V. The electric field caused by the injected charge is considered to be small in comparison to the applied electric field.

6. The Brinkman and Stokes equations regulate fluid flow through a swarm of porous layered cylindrical particles in porous and non-porous regions, respectively.

3.2.2 Model Description

The physical sketch of the proposed work delineated in Fig. 3.1 represents an electrohydrodynamic (EHD) flow past a membrane composed of a swarm of porous layered cylindrical particles and its cross-sectional view (Fig. 3.2), where the membrane's "ion drag" configuration is set up using the electrical precipitation. During the electrical precipitation process, uncharged particles were exposed to a corona discharge, resulting in their interaction with the ionized medium and subsequent acquisition of ionic charge. When subjected to externally applied potential differences, these charged particles will encounter a drag force that compels them to migrate toward the opposing electrode. The mobile charged particles were exposed to a body force within the bulk fluid, influencing the general mass to flow. The center region of a particle is a solid cylindrical core of radius $\widetilde{a}$ which is surrounded by a porous layer of thickness $(\widetilde{b}-\widetilde{a})$. The cell model has been used to account for the interaction of neighboring particles, according to which the porous layered solid cylindrical particle is assumed to be confined in a hypothetical cell of radius $\widetilde{c}$. The same has been shown in the physical sketch using dashed lines. The two different regions of the present study are considered in such a way that region I is a concentric layer of porous medium adjacent to the solid core of the cylindrical particle. While region II is a non-porous surrounding region I with the thickness of $(\widetilde{c}-\widetilde{b})$. Here $\widetilde{c}$ is the radius of the hypothetical cell, assuming that the particle volume fraction γ, of bulk, is equal to the particle volume fraction inside a unit cell. The relation between the particle volume fraction and the porosity ε, of the membrane can be stated as [3]

$$\gamma = \frac{\pi\widetilde{b}^2}{\pi\widetilde{c}^2} = 1-\varepsilon. \tag{3.1}$$

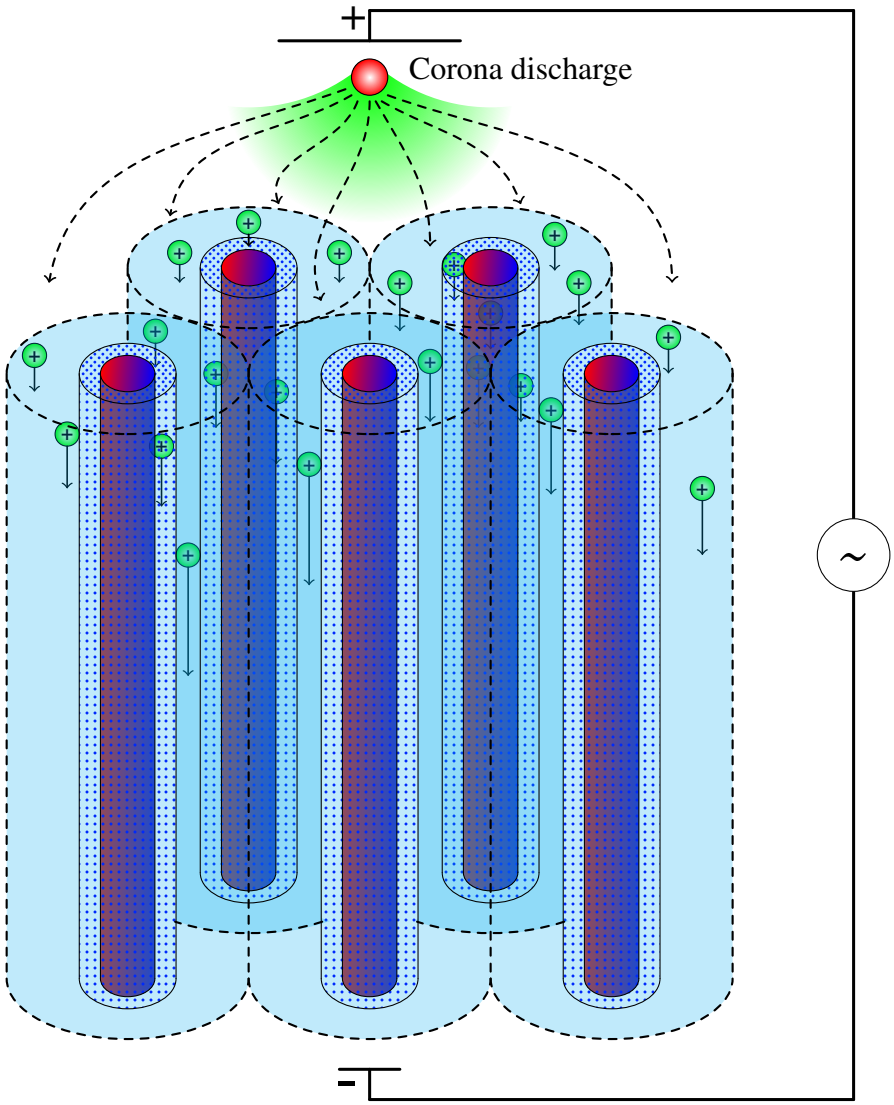

Figure 3.1: The physical depiction of an “ion drag" configuration for electrohydrodynamic flow along the axis of an array of porous cylindrical particles

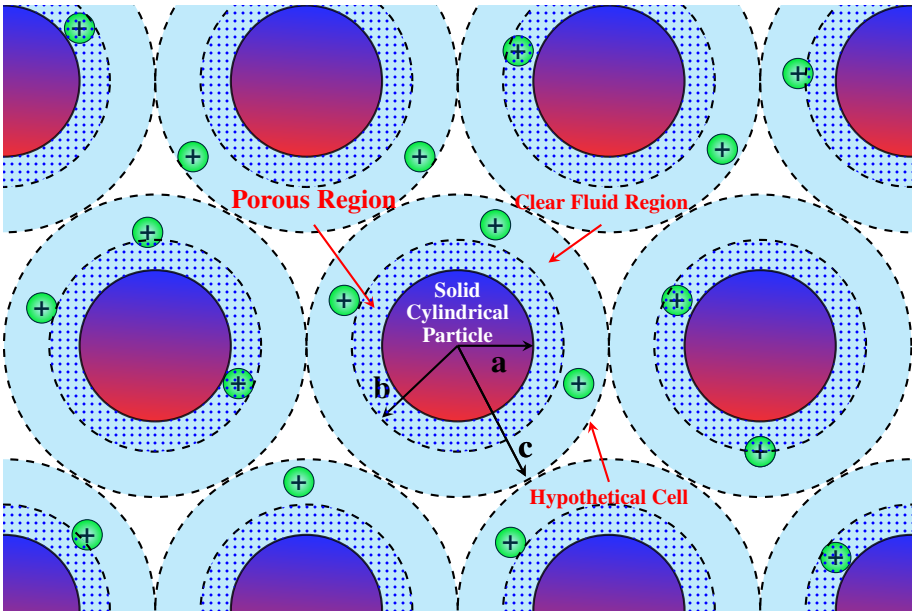

Figure 3.2: A visual depiction of a circular cross-section revealing a swarm of cylindrical particles with a solid core and porous layer inside a hypothetical cell.

3.2.3 Governing Equations

The energy equation regulates the temperature variations in the Newtonian fluid flow through a membrane composed of porous cylindrical particles, which aims to study the temperature variation in the hydrodynamic quantities like velocity, membrane permeability, and Kozeny constant. The continuity and momentum equations with body force (additional electric field) control fluid flow through porous and non-porous media in the membrane filtration process. The Brinkman equation controls the fluid flow through a porous medium. However, the Stokes equation regulates fluid flow through a non-porous region. The mathematical formulation of the temperature equations and flow regimes based on the proposed model is divided into two subsections, as described below:

3.2.3.1 Energy Equations

The energy equation regulates the temperature variation in the porous and non-porous regions of the cylindrical particle is described below ([12], [13])

$$\widetilde{K}\left(\frac{d^2\widetilde{T}}{d\widetilde{r}^2}+\frac{1}{\widetilde{r}}\frac{d\widetilde{T}}{d\widetilde{r}}\right)-\frac{d\widetilde{q}}{d\widetilde{r}}=0, \tag{3.2a}$$

where $\widetilde{K}$ and $\widetilde{T}$ are thermal conductivity and temperature of the fluid, respectively. The radiative heat flux can be expressed as ([12], [13])

$$\frac{d\widetilde{q}}{d\widetilde{r}} = 4\widetilde{\alpha}_r^2(\widetilde{T} - \widetilde{T}_\infty), \tag{3.2b}$$

where $\widetilde{\alpha}_r$ is the mean radiation absorption coefficient for Newtonian fluid and $\widetilde{T}_\infty$ is an ambient (uniform) temperature.

3.2.3.2 Hydrodynamical Equations

After being generated by a corona discharge, the ions are injected at one end of the swarm of parallelly situated cylindrical particles and later collected at the other end by a screen electrode. A voltage V produces an imposed electrical field $\widetilde{E}_0$ across the length of the cylindrical tube ($|\widetilde{E}_0| = \frac{V}{L}$), which is used to pull the ions through the viscous fluid to provide electrohydrodynamic pumping. The total current includes the electric field modified by the charge-space density; however, the electric field caused by fluid charges is small in comparison to the field imposed using voltage, V. The current density $\mathbf{J}$ within the fluid depends upon the ion mobility of the particles, giving

$$\mathbf{J} = q_e(\widetilde{K}\widetilde{E}_0\mathbf{e}_z + \mathbf{v}), \tag{3.3}$$

where q_e is the charge space density of the ion/fluid and $\widetilde{K}$ is the ion mobility [179].
Assumptions for a fully developed flow are as,

$$\mathbf{v} = (0,0,\widetilde{w}), \qquad \mathbf{J} = (0,0,J_z(r)), \qquad q_e = q(r), \qquad \frac{\partial \widetilde{p}}{\partial \widetilde{z}} = \text{const.} \tag{3.4}$$

With $J_z(r) = J_0$ (uniform over the cross-section at the inlet), the charge space density from the z-component of equation (3.3) can be expressed as

$$q_e = \frac{J_0}{\widetilde{K}\widetilde{E}_0 + \widetilde{w}}. \tag{3.5}$$

Since the velocity vector $\mathbf{v}$ and the current density vector, $\mathbf{J}$ are solenoidal, the governing equations for the proposed problem will be as follows ([3], [14], [13]):
Region- I, *i.e.*, $\widetilde{a} \le \widetilde{r} \le \widetilde{b}$

$$\frac{\partial \widetilde{p}}{\partial \widetilde{z}} = \frac{J_0\widetilde{E}_0}{\widetilde{K}\widetilde{E}_0 + \widetilde{w}_p} + \frac{\widetilde{\mu}_e}{\widetilde{r}}\frac{\partial}{\partial \widetilde{r}}\left(\widetilde{r}\frac{\partial \widetilde{w}_p}{\partial \widetilde{r}}\right) - \frac{\widetilde{\mu}_0\widetilde{w}_p}{\widetilde{k}} + \widetilde{g}\widetilde{\rho}\widetilde{\gamma}(\widetilde{T}_p - \widetilde{T}_\infty), \tag{3.6a}$$

where $\widetilde{p}$ represents the pressure, $\widetilde{w}_p$ denotes the velocity in the porous region, $\widetilde{\mu}_e$ signifies the effective viscosity of the fluid, and $\widetilde{k}$ denotes the permeability of the porous medium. Furthermore, the coefficient of fluid's volume expansion in response to changes in temperature, represented by $\widetilde{\gamma}$, and $\widetilde{g}$ is the gravitational acceleration. The interdependence between the fluid flow, temperature, and charged density is characterized by a non-linear coupling, where the body force acting on the fluid is directly proportional to the charge density.
Region- II, *i.e.*, $\widetilde{b} \leq \widetilde{r} \leq \widetilde{c}$

$$\frac{\partial \widetilde{p}}{\partial \widetilde{z}} = \frac{\widetilde{\mu}_0}{\widetilde{r}} \frac{\partial}{\partial \widetilde{r}} \left(\widetilde{r} \frac{\partial \widetilde{w}_c}{\partial \widetilde{r}} \right) + \frac{J_0 \widetilde{E}_0}{\widetilde{K} \widetilde{E}_0 + \widetilde{w}_c} + \widetilde{g} \widetilde{\rho} \widetilde{\gamma} (\widetilde{T}_c - \widetilde{T}_\infty), \tag{3.6b}$$

where $\widetilde{w}_c$ and $\widetilde{\mu}_0$ are the flow parameters describing an axial velocity and viscosity of fluid in clear fluid region, respectively.

3.2.3.3 Boundary Conditions

The incorporation of boundary conditions holds considerable importance in the mathematical modeling of any given process. These conditions can be utilized to solve the governing equations by examining the characteristics of the solutions, taking into account the assumptions made in the physical and biological processes. The current study examines the following boundary conditions applied to the solid surface, fluid-porous interface, and hypothetical cell surface, which aims to understand the behaviour of the neighbouring particles in the filtration process:

1. There is a wall (surface) temperature on the surface of the solid core of the cylindrical particle, and along with that, no slip condition of the surface of the solid cylinder is considered, which states that there is no relative motion between a fluid and a solid boundary, *i.e.*,

$$\widetilde{T} = \widetilde{T}_w, \quad \widetilde{w}_p = 0 \quad \text{at} \quad \widetilde{r} = \widetilde{a}. \tag{3.7a}$$

2. The continuity of velocities at the fluid-porous interface is considered *i.e.*,

$$\widetilde{w}_p = \widetilde{w}_c \quad \text{at} \quad \widetilde{r} = \widetilde{b}. \tag{3.7b}$$

3. The stress-jump condition of tangential stress at the fluid-porous interface is taken into consideration [81], *i.e.*,

$$\frac{1}{\alpha_p}\frac{d\widetilde{w}_p}{d\widetilde{r}} - \frac{d\widetilde{w}_c}{d\widetilde{r}} = \frac{\beta}{\sqrt{\widetilde{k}}}\widetilde{w}_p \quad \text{at} \quad \widetilde{r} = \widetilde{b}, \tag{3.7c}$$

where α_p is the porosity and β is stress-jump parameter.

4. There is zero temperature gradient and zero velocity gradient at the hypothetical cell surface of the cylindrical particle, *i.e.*,

$$\frac{d\widetilde{T}}{d\widetilde{r}} = 0, \quad \frac{d\widetilde{w}_c}{d\widetilde{r}} = 0, \quad \text{at} \quad \widetilde{r} = \widetilde{c}. \tag{3.7d}$$

3.2.4 Non-Dimesionalization

To solve the above system of equations (3.6) along with the boundary conditions (3.7), the following non-dimensional variables are introduced:

$$\begin{aligned}
&p = \frac{\widetilde{p}\widetilde{b}}{\widetilde{w}_0\widetilde{\mu}_0},\ r = \frac{\widetilde{r}}{\widetilde{b}},\ z = \frac{\widetilde{z}}{\widetilde{b}},\ a = \frac{\widetilde{a}}{\widetilde{b}},\ c = \frac{\widetilde{c}}{\widetilde{b}},\ N_1^2 = \frac{4\widetilde{\alpha}^2\widetilde{b}^2}{\widetilde{K}},\ \alpha = \frac{\widetilde{K}}{\widetilde{j}_0}\frac{\partial\widetilde{p}}{\partial\widetilde{z}} - 1,\\
&\theta = \frac{\widetilde{T} - \widetilde{T}_\infty}{\widetilde{T}_w - \widetilde{T}_\infty},\ Gr = \frac{\widetilde{g}\widetilde{\rho}\widetilde{\gamma}\widetilde{b}^2(\widetilde{T}_w - \widetilde{T}_\infty)}{\alpha\widetilde{K}\widetilde{E}_0\widetilde{\mu}_0},\ \widetilde{w}_0 = \frac{\widetilde{q}_0\widetilde{b}^2}{\widetilde{\mu}_0} = -\alpha\widetilde{K}\widetilde{E}_0,\\
&w_p = \frac{\widetilde{w}_p}{-\alpha\widetilde{K}\widetilde{E}_0},\ w_c = \frac{\widetilde{w}_c}{-\alpha\widetilde{K}\widetilde{E}_0},\ k = \frac{\widetilde{k}}{\widetilde{b}^2},\ \lambda_1^2 = \frac{\widetilde{\mu}_e}{\widetilde{\mu}_0}, H = \sqrt{\frac{\widetilde{j}_0\widetilde{b}^2}{\widetilde{K}^2\widetilde{E}_0\widetilde{\mu}_0}},
\end{aligned} \tag{3.8}$$

where $\widetilde{w}_0$ is the average velocity and the Grashof number Gr is a dimensionless parameter that arises in the study of fluid mechanics and heat transfer. It characterizes the relative importance of buoyancy forces to viscous forces in a fluid that is heated from below, causing natural convection. It can be used to predict and control the behavior of charged particles in the fluid under the influence of electric fields, and to optimize the heat transfer in the system. The parameter N_1 is a radiation parameter and it can be used to understand and control the relative importance of radiative and convective heat transfer, and to optimize the temperature distribution and heat transfer performance of the system.
Using the above non-dimensional variables, the non-dimensional form of governing equation (3.2b) regulating the temperature variation in the cylindrical particle is stated as

$$\frac{d^2\theta(r)}{dr^2} + \frac{1}{r}\frac{d\theta(r)}{dr} + N_1^2\theta(r) = 0. \tag{3.9}$$

The hydrodynamic equations (3.6a)-(3.6b) in their non-dimensional form for both porous and non-porous regions are obtained as
Region- I, *i.e.*, $a < r \leq 1$

$$\lambda_1^2 \left(\frac{d^2 w_p}{dr^2} + \frac{1}{r} \frac{dw_p}{dr} \right) - \frac{w_p}{k} + H^2 \left(1 - \frac{w_p}{1 - \alpha w_p} \right) + Gr\theta(r) = 0, \tag{3.10}$$

where the above system of equations has a Hartmann electric number H characterizing the influence of electric forces relative to viscous forces. The fluid in the medium experiences a body force due to the migration of charged particles under the influence of externally applied potential difference. This state is referred to as the “ion drag" configuration. Here, the velocity of the fluid exhibits a nonlinear relationship with the externally applied electric field.
Region- II, *i.e.*, $1 \leq r \leq c$

$$\frac{d^2 w_c}{dr^2} + \frac{1}{r} \frac{dw_c}{dr} + H^2 \left(1 - \frac{w_c}{1 - \alpha w_c} \right) + Gr\theta(r) = 0. \tag{3.11}$$

The non-dimensionless forms of thermal and hydrodynamic boundary conditions are given as follows:

$$w_p = 0, \text{ and } \theta = 1 \quad \text{at} \quad r = a, \tag{3.12a}$$

$$w_p = w_c, \quad \text{at} \quad r = 1, \tag{3.12b}$$

$$\frac{1}{\alpha_p} \frac{dw_p}{dr} - \frac{dw_c}{dr} = \frac{\beta}{\sqrt{k}} w_p \quad \text{at} \quad r = 1, \tag{3.12c}$$

$$\frac{dw_c}{dr} = 0, \text{ and } \frac{d\theta}{dr} = 0 \quad \text{at} \quad r = c. \tag{3.12d}$$

3.2.5 Hydodynamical Quantities

The volumetric flow rate Q_s of a single particle surrounded by the hypothetical cell in its non-dimensional form is stated as [3]

$$Q_s = 2\pi \int_a^c r w(r) dr = 2\pi \left(\int_a^1 r w_p dr + \int_1^c r w_c dr \right). \tag{3.13}$$

The membranes exhibit diverse characteristic features, including their hydrodynamic permeability, referred to as L_{11}. This particular parameter, serving as the primary component of the Onsager kinetic coefficient matrix, signifies the relationship between the flow rate across

the membrane and the imposed pressure gradient. The mechanical characteristics of the membrane material depend on its structural arrangement, composition, and physicochemical traits. Understanding the evolution dynamics during operational use, modifications, and experimental treatments is essential for effectively discerning its functional alterations [180]. Electrohydrodynamic and porous medium parameters notably influence L_{11}, as evident in equations 3.13 and 3.14. The mathematical expression for hydrodynamic permeability of the membrane L_{11} is given by

$$L_{11} = -\frac{V_f}{\partial p/\partial z}, \tag{3.14}$$

where V_f is the filtration velocity of fluid flowing through porous cylindrical particles, relating with the volumetric flow rate stated as $V_f = \frac{Q_s}{\pi c^2}$.
The mathematical expression relating the hydrodynamic permeability of the membrane consisting of a swarm of porous cylindrical particles with porosity ε is given by the classical Kozeny–Karman equation

$$L_{11} = \frac{\varepsilon \rho_h^2}{K_z \widetilde{b^2}}, \tag{3.15}$$

where ρ_h is the hydraulic radius, ε is the porosity of the membrane, and K_z is the dimensionless Kozeny constant, which encapsulates the effect of particle shape, packing arrangement, and tortuosity on the fluid flow through the porous medium. The Kozeny constant is a parameter that describes the flow of fluids through porous media. The physical significance of the Kozeny constant lies in its ability to quantify the resistance to fluid flow in porous media. The Kozeny constant is affected by a variety of factors, including porosity, pore-to-throat size ratio, and the geometry of the porous medium. It provides information about the tortuosity of the flow paths within the porous medium, which influences how easily fluid flows through it. Identifying the Kozeny constant assists researchers and engineers in designing and optimizing processes involving fluid flow through porous materials, such as filtration systems, packed beds, and soil permeability studies [181]. The expression of Kozeny constant from the above relation (3.15) can be derived as

$$K_z = \frac{\varepsilon \rho_h^2}{L_{11} \widetilde{b^2}}. \tag{3.16}$$

The hydraulic radius is derived from the ratio of pore volume to wetting area and can be mathematically expressed as

$$\rho_h = \frac{\pi(\widetilde{c}^2 - \widetilde{b}^2)}{2\pi\widetilde{b}} = \frac{\widetilde{b}}{2}\left(\frac{1-\gamma}{\gamma}\right) = \frac{\varepsilon\widetilde{b}}{2(1-\varepsilon)}, \tag{3.17}$$

using the above expression of hydraulic radius in the equation (3.16), the Kozeny constant in terms of porosity and the hydrodynamic permeability L_{11} is given as

$$K_z = \frac{\varepsilon^3}{4(1-\varepsilon)^2 L_{11}}. \tag{3.18}$$

3.3 Solution of the Problem

The principles of mass, momentum, and energy conservation govern the behaviour of fluid flow. The mathematical formulations of these rules are explained in detail based on their respective proposed models. The governing equations of unidirectional flow (continuity, momentum, and energy equations) of the Newtonian fluid through a membrane composed of porous cylindrical particles are a set of nonlinear coupled ordinary differential equations. Therefore, obtaining analytical solutions to hydrodynamical equations such as the Brinkman and Stokes equations remains challenging due to the presence of a nonlinear electric field term. However, the reduced cases of these equations are analytically solved when the nonlinear electric field term is approximated to zero. Asymptotic or numerical solution techniques may be utilized to derive the velocity expressions for both porous and non-porous regions to determine the solutions of the governing equations. The perturbation solution technique can be utilized in cases where the governing equations feature either a small or large parameter, in accordance with the principle of perturbation techniques, which dictates that the equations must incorporate such a parameter. The proposed model incorporates a nonlinearity parameter, denoted as α, in its governing equations. Consequently, a perturbation technique is employed to convert the nonlinear ODEs into linear ones, facilitating the derivation of asymptotic solutions while the energy equation is solved analytically. The numerical scheme NDSolve within Mathematica software is employed to validate our findings.

3.3.1 Solution of Temperature Equations

The governing equation for temperature (3.9) is the second-order Bessel differential equation that can be solved analytically, and its solution in terms of Bessel functions of the first

and second kind can be written as

$$\theta(r) = C_1 J_0(N_1 r) + C_2 Y_0(N_1 r), \tag{3.19a}$$

where C_1 and C_2 are unknown constants that can be obtained using the temperature boundary conditions mentioned in equation (3.12), and are given as

$$C_1 = \frac{Y_1(cN_1)}{J_0(aN_1)Y_1(cN_1) - Y_0(aN_1)J_1(cN_1)}, \tag{3.20a}$$

$$C_2 = \frac{J_1(cN_1)}{Y_0(aN_1)J_1(cN_1) - J_0(aN_1)Y_1(cN_1)}, \tag{3.20b}$$

where J_0 and J_1 are the Bessel functions of the first kind of orders zero and one, respectively, and Y_0 and Y_1 are the Bessel functions of the second kind of orders zero and one, respectively.

3.3.2 Solution of Hydrodynamic Equations

The hydrodynamic equations governing electrohydrodynamic (EHD) flow in both porous and non-porous regions exhibit nonlinearity, thus rendering the analytical treatment highly intricate. In order to surmount the above challenge, the regular perturbation approach has been employed to find the asymptotic solutions of the equations (3.10), and (3.11) for small and large parameter values α. The solutions of the hydrodynamical equations are divided into two subsections in case of small and large parameters α.

3.3.2.1 Small Parameter ($\alpha \ll 1$)

$$\lambda_1^2 \left(\frac{d^2 w_p}{dr^2} + \frac{1}{r} \frac{dw_p}{dr} \right) - \frac{w_p}{k} + H^2(1 - w_p - \alpha w_p^2 - \alpha^2 w_p^3) - Gr\theta(r) = 0, \tag{3.21}$$

$$\frac{d^2 w_c}{dr^2} + \frac{1}{r}\frac{dw_c}{dr} + H^2(1 - w_c - \alpha w_c^2 - \alpha^2 w_c^3) - Gr\theta(r) = 0. \tag{3.22}$$

An asymptotic series expansion of velocities of porous and non-porous regions in terms of the small perturbation parameter α has been considered of the form [142]

$$w_j(r) = w_j(r;\alpha) = \sum_{n=0}^{m} \alpha^n w_{jn}(r), \quad j = p, c, \tag{3.23}$$

where the subscripts p and c denote the velocities for porous and non-porous regions, respectively.

In order to obtain the first three terms of the velocities in this expansion, introducing (3.23)

into (3.21) and (3.22) and equating the coefficients of $\alpha^0, \alpha^1, \alpha^2$. The zeroth-order approximate velocities for porous and non-porous regions are obtained as

$$\lambda_1^2\left(\frac{d^2w_{p0}}{dr^2}+\frac{1}{r}\frac{dw_{p0}}{dr}\right)-\frac{w_{p0}}{k}-H^2w_{p0}=-H^2+Gr\theta_p(r), \tag{3.24a}$$

$$\frac{d^2w_{c0}}{dr^2}+\frac{1}{r}\frac{dw_{c0}}{dr}-H^2w_{c0}=-H^2+Gr\theta_c(r). \tag{3.24b}$$

The first-order approximate velocities for porous and non-porous regions are obtained as

$$\lambda_1^2\left(\frac{d^2w_{p1}}{dr^2}+\frac{1}{r}\frac{dw_{p1}}{dr}\right)-\frac{w_{p1}}{k}-H^2w_{p1}=H^2w_{p0}^2, \tag{3.24c}$$

$$\frac{d^2w_{c1}}{dr^2}+\frac{1}{r}\frac{dw_{c1}}{dr}-H^2w_{c1}=H^2w_{c0}^2. \tag{3.24d}$$

The second-order approximate velocities for porous and non-porous regions are obtained as

$$\lambda_1^2\left(\frac{d^2w_{p2}}{dr^2}+\frac{1}{r}\frac{dw_{p2}}{dr}\right)-\frac{w_{p2}}{k}-H^2w_{p2}=H^2(2w_{p0}w_{p1}+w_{p0}^3), \tag{3.24e}$$

$$\frac{d^2w_{c2}}{dr^2}+\frac{1}{r}\frac{dw_{c2}}{dr}-H^2w_{c2}=H^2(2w_{c0}w_{c1}+w_{c0}^3). \tag{3.24f}$$

The equations $(3.24a)-(3.24f)$ are non-homogeneous modified Bessel equations. The solution of the homogeneous modified Bessel equation is available in terms of modified Bessel functions I_ν and K_ν, where ν is any positive integer. The solution of the non-homogeneous modified Bessel equation can be obtained using a variation of parameters. Adopting the method of variation of parameters, the solutions of the equations $(3.24a)-(3.24f)$ are given below.

The zeroth-order velocities w_{p0} and w_{c0} for porous and non-porous regions are obtained as

$$w_{p0}=C_3I_0(rS_1)+C_4K_0(rS_1)-\frac{G_1(C_1J_0(N_1r)+C_2Y_0(N_1r))}{N_1^2+S_1^2}+\frac{H_1^2}{S_1^2}, \tag{3.25a}$$

$$w_{c0}=C_5I_0(rH)+C_6K_0(rH)+1+\frac{Gr(C_1J_0(N_1r)+C_2Y_0(N_1r))}{H^2+N_1^2}, \tag{3.25b}$$

where $S_1^2=\frac{1}{\lambda_1^2}\left(\frac{1}{k}+H^2\right)$, $H_1^2=\frac{H^2}{\lambda_1^2}$ and $G_1=\frac{Gr}{\lambda_1^2}$. Here, I_0 and K_0 are the modified Bessel functions of the first and second kinds of order zero, respectively.

The first-order velocities w_{p1} and w_{c1} for porous and non-porous regions are obtained as

$$w_{p1} = \left(C_7 + H_1^2 \left(\int_a^r rK_0(rS_1)(w_{p0})^2 dr \right) \right) I_0(rS_1) + \left(C_8 - H_1^2 \left(\int_a^r rI_0(rS_1)(w_{p0})^2 dr \right) \right) K_0(rS_1), \tag{3.25c}$$

$$w_{c1} = \left(C_9 + H^2 \left(\int_r^c rK_0(rH)(w_{c0})^2 dr \right) \right) I_0(Hr) + \left(C_{10} - H^2 \left(\int_r^c rI_0(rH)(w_{c0})^2 dr \right) \right) K_0(Hr). \tag{3.25d}$$

The second-order velocities w_{p2} and w_{c2} for porous and non-porous regions are obtained as

$$w_{p2} = \left(C_{11} + H_1^2 \left(\int_a^r rK_0(rS_1) \left(2w_{p0}w_{p1} + w_{p0}^3 \right) dr \right) \right) I_0(rS_1) + \left(C_{12} - H_1^2 \left(\int_a^r rI_0(rS_1) \left(2w_{p0}w_{p1} + w_{p0}^3 \right) dr \right) \right) K_0(rS_1), \tag{3.25e}$$

$$w_{c2} = \left(C_{13} + H^2 \left(\int_r^c rK_0(rH) \left(2w_{c0}w_{c1} + w_{c0}^3 \right) dr \right) \right) I_0(Hr) + \left(C_{14} - H^2 \left(\int_r^c rI_0(rH) \left(2w_{c0}w_{c1} + w_{c0}^3 \right) dr \right) \right) K_0(Hr), \tag{3.25f}$$

where $C_3 - C_{14}$ are arbitrary constants that can be determined using the specified boundary conditions. The expressions of the constants $C_3 - C_{14}$ are given in Appendix A. Due to presence of modified Bessel functions in the equations (3.25*a*) and (3.25*b*), the integrals involved in the equations (3.25*c*) – (3.25*f*) have been numerically computed in the Mathematica software 10.3.

3.3.3 Large Parameter $(\alpha \gg 1)$

The above series expansion of the velocity profile mentioned in (3.23) is not a valid series expansion in the case of large parameter α. In order to solve the momentum equations delineating the fluid flow through porous and non-porous media, the equations can be written

in terms of the parameter $\alpha^{-1} = \frac{1}{\alpha} \ll 1$ for a large $\alpha \gg 1$.

$$\lambda_1^2 \left(\frac{d^2 w_p}{dr^2} + \frac{1}{r} \frac{dw_p}{dr} \right) - \frac{w_p}{k} + (1+\alpha^{-1})H^2 - Gr\theta(r) = 0, \tag{3.26a}$$

$$\frac{d^2 w_c}{dr^2} + \frac{1}{r} \frac{dw_c}{dr} + (1+\alpha^{-1})H^2 - Gr\theta(r) = 0. \tag{3.26b}$$

The above equations regulating the fluid flow through porous and non-porous regions can be solved using a perturbation approach in terms of the small parameter α^{-1}. An asymptotic series expansion of the velocities is given below

$$w_j(r) = w_j(r;\alpha) = \sum_{n=0}^{m} \alpha^{-n} w_{jn}(r;\alpha), \quad j = p, c. \tag{3.27}$$

For large values of the parameter $\alpha \gg 1$, the perturbation parameter $\alpha^{-1} \ll 1$ is very small, and hence, the second and higher order velocity components in the above series expansion may have less contributions. Introducing the above series expansions (3.27) into (3.26) and equating the coefficients of $(\alpha^{-1})^0$ and α^{-1}. The zeroth-order velocities w_{p0} and w_{c0} for porous and non-porous regions are obtained as

$$\lambda_1^2 \left(\frac{d^2 w_{p0}}{dr^2} + \frac{1}{r} \frac{dw_{p0}}{dr} \right) - \frac{w_{p0}}{k} + H^2 - Gr\theta(r) = 0, \tag{3.28a}$$

$$\frac{d^2 w_{c0}}{dr^2} + \frac{1}{r} \frac{dw_{c0}}{dr} + H^2 - Gr\theta(r) = 0. \tag{3.28b}$$

The first-order velocities w_{p1} and w_{c1} for porous and non-porous regions are obtained as

$$\lambda_1^2 \left(\frac{d^2 w_{p1}}{dr^2} + \frac{1}{r} \frac{dw_{p1}}{dr} \right) - \frac{w_{p1}}{k} + H^2 = 0, \tag{3.28c}$$

$$\frac{d^2 w_{c1}}{dr^2} + \frac{1}{r} \frac{dw_{c1}}{dr} + H^2 = 0. \tag{3.28d}$$

The equations (3.28a) and (3.28c) are non-homogeneous modified Bessel equations, however, the equations (3.28b) and (3.28d) are non-homogeneous Stokes equations. The analytical solutions of equations (3.28a)-(3.28d) can be obtained using variation of parameters method. The analytical expressions of the zeroth-order velocities for porous and non-porous

regions are obtained as

$$w_{p0} = C_{15} I_0(rS) + C_{16} K_0(rS) + \frac{H_1^2}{S^2} + \frac{G_1(C_1 J_0(N_1 r) + C_2 Y_0(N_1 r))}{N_1^2 + S^2}, \tag{3.29a}$$

$$w_{c0} = C_{17} \log(r) + C_{18} + \frac{Gr(C_1 J_0(N_1 r) + C_2 Y_0(N_1 r))}{N_1^2} - \frac{C_2 Gr}{N_1^2} - \frac{H^2 r^2}{4}. \tag{3.29b}$$

Here, I_0 and K_0 are the modified Bessel functions of the first and second kinds of order zero, respectively.

The analytical expressions of the first-order velocities for porous and non-porous regions are obtained as

$$w_{p1} = C_{19} I_0(rS) + C_{20} K_0(rS) + \frac{H_1^2}{S^2}, \tag{3.29c}$$

$$w_{c1} = C_{21} \log(r) + C_{22} - \frac{H_1^2 r^2}{4}, \tag{3.29d}$$

where $C_{15} - C_{22}$ are the arbitrary constant that can be obtained using the given boundary conditions. The mathematical expressions of the constants $C_{15} - C_{22}$ are given in Appendix B.

3.4 Results and Discussion

The electrohydrodynamic flow of Newtonian fluid through a membrane composed of a swarm of porous cylindrical particles is considered by introducing a heat transfer approach to analyze the combined effect of the Hartmann electric number and temperature variations in the membrane filtration process. The flow regime of the proposed model is segregated into two regions in which region- I is a porous region adjacent to the solid core of the cylindrical particle and regulated by the Brinkman equation. Region- II is a non-porous region surrounding the porous region and regulated by the Stokes equation. The particle-in-cell approach is used to consider the boundary condition on the hypothetical cell surface to demonstrate the effect of neighbouring particles on the concerned particle. The mathematical expressions of the temperature and velocity profiles have been obtained using analytical and asymptotic series expansion techniques, and the same has been used to obtain the hydrodynamical quantities like membrane permeability and Kozeny constant. The graphical analysis of the mathematical expressions of hydrodynamical quantities is presented below, and the contributions of temperature and electric field parameters have been discussed.

3.4.1 Parameter Selection

The measurement of a fluid in motion is a challenge due to the necessity of estimating the mass or volume of the substance as it traverses a pipe or conduit. Difficulties may develop due to the intricate nature of fluid flow dynamics. The quantification of physical factors is typically challenging in the context of flow measurements. The following parameter table 3.1 includes the range of parameter values depending on the applications in various fields. All the critical parameters listed in this table have been thoroughly described in their respective cited literature, which will aid the reader in grasping the concepts involved. The pressure gradient $p_z = 1$ is taken as constant throughout the discussion.

Range of Parameters		
Parameters	Range	Sources
Radiation parameter N_1	2-15	[12], [13]
Grashof number Gr	0.5-17.0	[13]
Steady pressure gradient p_z	1-10	[5], [182]
Permeability k	$(0,\infty)$	[145]
Hartmann electric number H	0.1-4.0	[14]
Stress-jump parameter β	$(-1,1)$	[3], [15], [167]
Viscosity ratio parameter λ_1	1.0-1.6	[15], [5]
Particle volume fraction γ	0.1-1.0	[145], [11]

Table 3.1: Domain of interest for the ongoing parameters with their references

3.4.2 Velocity Profile (w)

Figures 3.3a and 3.3b describe the impact of the Hartmann electric number on the velocity profile for small and large permeabilities and small and large values of the nonlinearity parameter α. In both cases, the graphical analysis reveals that a rising Hartmann electric number leads to growth in velocity, which is relatively more significant for higher permeability. However, this behaviour is reversed for small α and large permeability in the non-porous region. Further, for small permeability, the growth in velocity reduces at higher H in the non-porous region. The effect of the radiation parameter on the velocity profile is depicted in Figure 3.4, signifying the impact of the relative dominance of radiative heat transfer over convective heat transfer on the velocity profile. A rising N_1 leads to a slight delay in fluid

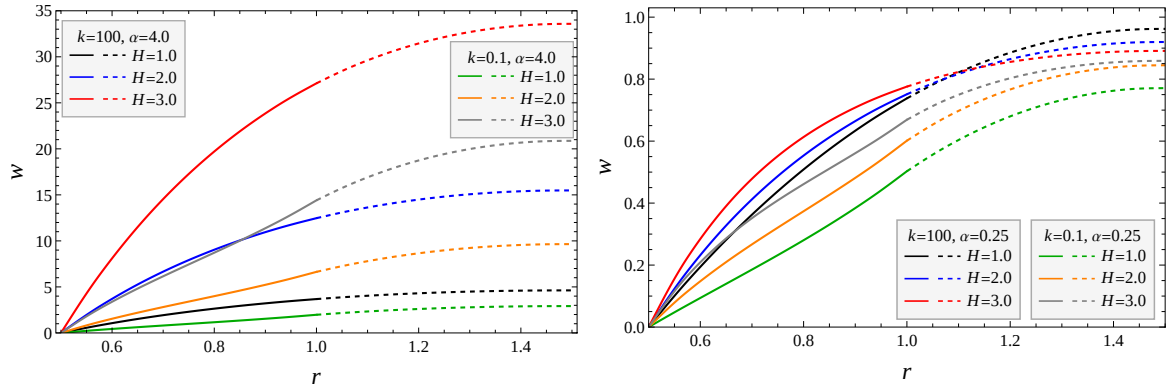

Figure 3.3: Changes in fluid velocity (w) in radial direction(r), with varying Hartmann electric number(H), under high $(k = 100)$ and low $(k = 0.1)$ permeability parameters, (a) large alpha parameter $(\alpha = 4.0)$ and (b) small alpha parameter $(\alpha = 0.25)$. $(\beta = 0.1, l = 0.5, \gamma = 0.45, Gr = N_1 = 2, \lambda_1 = 1)$

velocity in both small and large permeability cases. The same pattern is continued for small nonlinearity parameter α. There is a relatively lesser velocity decay for radiation heat transfer, N_1, varying from 2.3 to 3.0 in comparison to variation from 2.0 to 2.5. This observation is the same for small and large permeability cases. Figure 3.5 delineates the effect of the

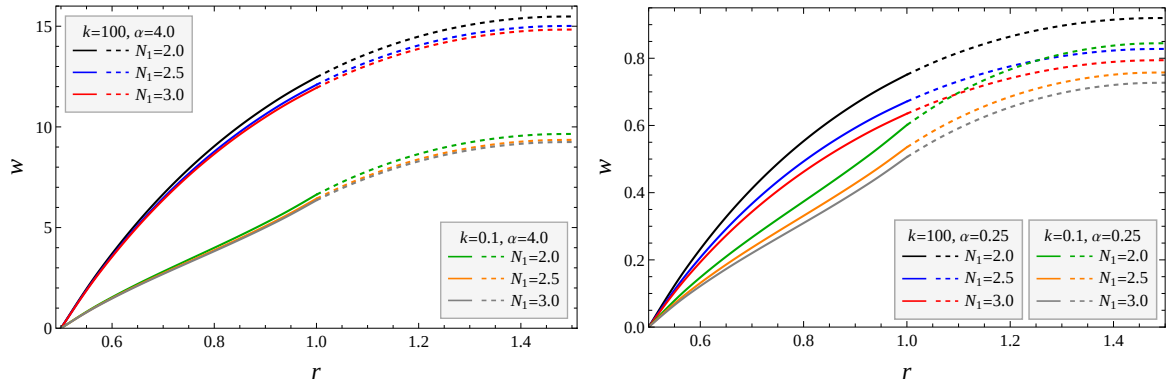

Figure 3.4: Changes in fluid velocity (w) in radial direction (r), with varying Radiation parameter (N_1), under high $(k = 100)$ and low $(k = 0.1)$ permeability parameters, (a) large alpha parameter $(\alpha = 4.0)$ and (b) small alpha parameter $(\alpha = 0.25)$. $(\beta = 0.1, H = Gr = 2, l = 0.5, \gamma = 0.45, \lambda_1 = 1)$

viscosity ratio on the velocity profile for large and small values of α. A rising viscosity ratio leads to relatively higher viscosity in the porous medium, significantly reducing the overall fluid velocity. While this decay is more significant for a large α, it is relatively less for small α. Figures 3.6a and 3.6b depict the relative dominance of buoyancy over viscous forces on fluid velocity for small and large permeability and small and large parameter α,

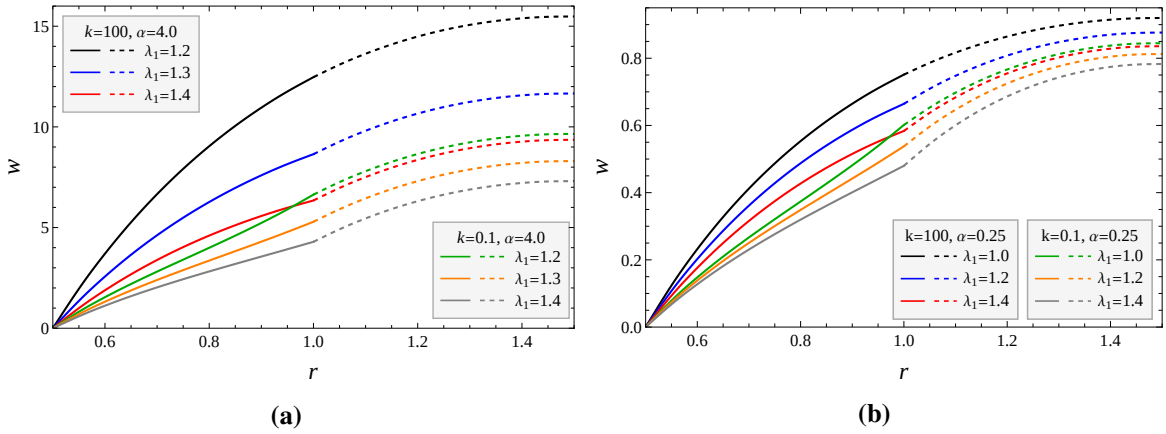

Figure 3.5: Changes in fluid velocity (w) in radial direction (r), with varying viscosity ratio parameter(λ_1), under high $(k = 100)$ and low $(k = 0.1)$ permeability parameters, (a) large alpha parameter $(\alpha = 4.0)$ and (b) small alpha parameter $(\alpha = 0.25)$. $(\beta = 0.1, l = 0.5, \gamma = 0.45, H = Gr = N_1 = 2)$

respectively. It can be interpreted from these figures that, as the buoyant forces dominate the viscous forces, heat transmission in the medium increases, resulting in increased fluid velocity, as illustrated in Figures 3.6a and 3.6b. The growth rate of fluid velocity for large permeability is significantly higher than that for small permeability when α is significant; however, this difference is significantly reduced for a small α. Additionally, the growth rate of velocity increases more significantly with increasing graph of number in case of significant nonlinearity parameter, α.

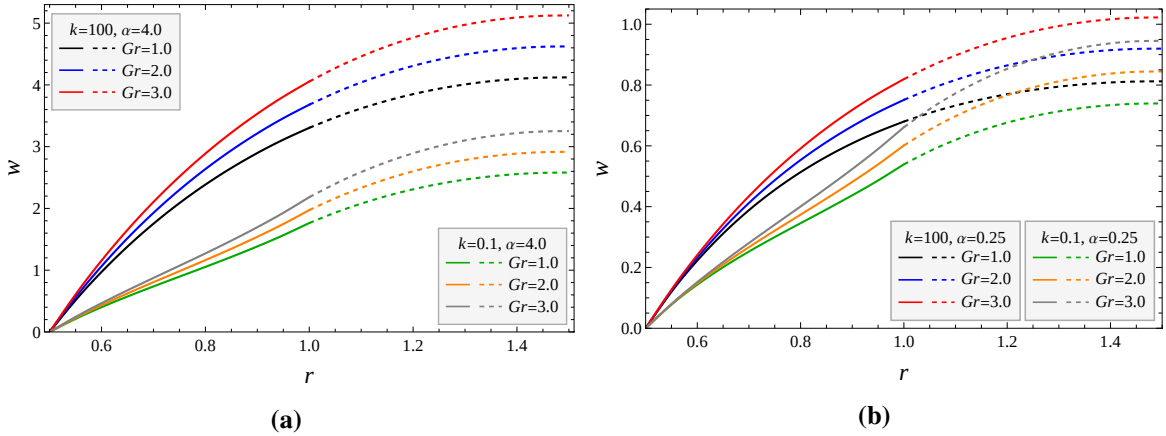

Figure 3.6: Changes in fluid velocity (w) in radial direction (r), with varying Grashof number (Gr), under high $(k = 100)$ and low $(k = 0.1)$ permeability parameters, (a) large alpha parameter $(\alpha = 4.0)$ and (b) small alpha parameter $(\alpha = 0.25)$. $(\beta = 0.1, \lambda_1 = 1, l = 0.5, \gamma = 0.45, H = N_1 = 2)$

3.4.3 Hydrodynamic Permeability (L_{11})

In analyzing flow through a swarm of particles, the hydrodynamic permeability of the swarm of particles plays an important role. Hence, a detailed analysis is presented, revealing the impact of various parameters on the hydrodynamic permeability of the swarm of particles. Here, in Figure 3.7, a decay in the hydrodynamic permeability is observed with the particle volume fraction. This decay rate is relatively higher for the higher Hartmann electric number.

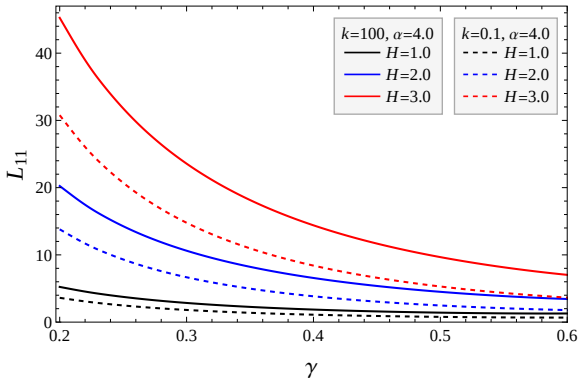

Figure 3.7: Changes in the hydrodynamic permeability (L_{11}) relying on particle volume fraction (γ) with varying Hartmann electric number (H), under high $(k = 100)$ and low $(k = 0.1)$ permeability parameters. $(\beta = 0.1, \alpha = 4.0, \lambda_1 = 1, l = 0.5, Gr = N_1 = 2.0)$

Figure 3.8 depicts an almost negligible impact of β on L_{11}. However, a rising radiation parameter leads to a slight decay in hydrodynamic permeability, which may be attributed to a decay in fluid velocity. Figure 3.9 reveals a slight increase in hydrodynamic permeability with increasing Gr. This can be interpreted as the dominance of buoyancy over viscous forces, leading to a rise in fluid velocity and higher hydrodynamic permeability. Further, it can be seen that a rising viscosity ratio leads to decay in the hydrodynamic permeability owing to a relatively higher fluid viscosity in a porous medium.

Figure 3.10 reveals the growth in hydrodynamic permeability in membranes with increasing Hartmann electric number. While the growth rate is significantly higher for large permeability, it slightly reduces with increasing Grashof number. Figure 3.11 reveals the impact of relatively higher viscosity in the porous medium on the growth rate of L_{11} with increasing H. A relatively higher viscosity in a porous medium is perceived to lead to a decay in the growth rate of hydrodynamic permeability L_{11} with increasing Hartmann electric number H. A similar observation is reported in Figure 3.12, where an increasing stress-jump coefficient for small permeability leads to a higher growth rate of hydrodynamic permeability with increasing Hartmann electric number. However, it is almost negligible for large permeability. This can be interpreted from the fact that a smaller permeability

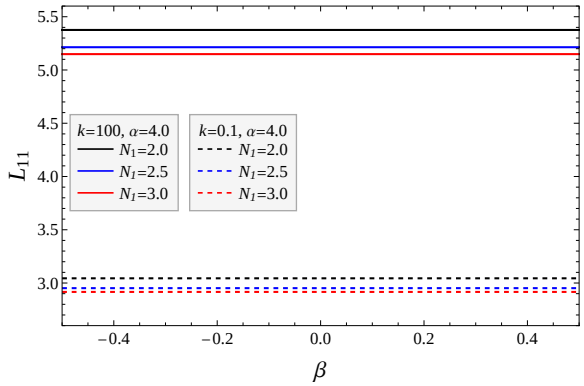

Figure 3.8: Changes in L_{11} relying on stress jump parameter β with varying Radiation number(N_1), under high $(k = 100)$ and low $(k = 0.1)$ permeability parameters. $(\alpha = 4.0, \gamma = 0.45, \lambda_1 = 1, l = 0.5, H = 2.0, Gr = 2.0)$

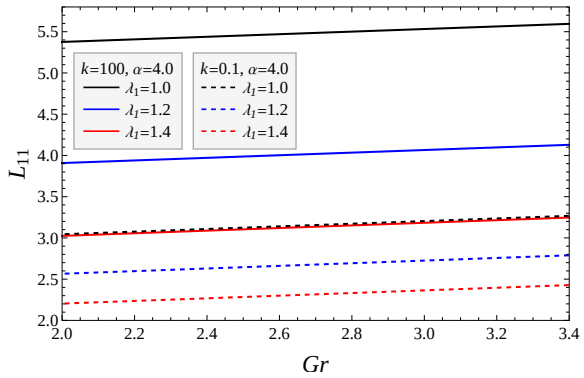

Figure 3.9: Changes in L_{11} relying on Grashof number Gr with varying viscosity ratio parameter λ_1, under high $(k = 100)$ and low $(k = 0.1)$ permeability parameters. $(\alpha = 4.0, \beta = 0.1, \gamma = 0.45, N_1 = 2.0, l = 0.5, H = 2.0)$

makes the difference in shear stress at the fluid-porous interface very significant, leading toward a significant impact of stress-jump parameter β on hydrodynamic permeability. The dominance of radiative heat transfer slightly reduces the hydrodynamic permeability, which becomes almost steady. So, the hydrodynamic permeability remains unaffected for significant dominance of radiative heat transfer (Figure 3.13). All the above observations were made for a significant α parameter; however, it may be interesting to explore the above variations for a small α parameter owing to using a different parameter for the regular perturbation scheme for analytical solutions of governing equations. Figure 3.14 depicts growth in hydrodynamic permeability with increasing Grashof number, signifying that the dominance of thermal buoyancy forces over viscous forces leads to higher membrane permeability. The growth rate of the hydrodynamic permeability is slightly reduced for higher viscosity ratio parameters. Figure 3.15 delineates the growth in hydrodynamic permeability with Hartmann electric number for different radiation parameters. It is perceived that the

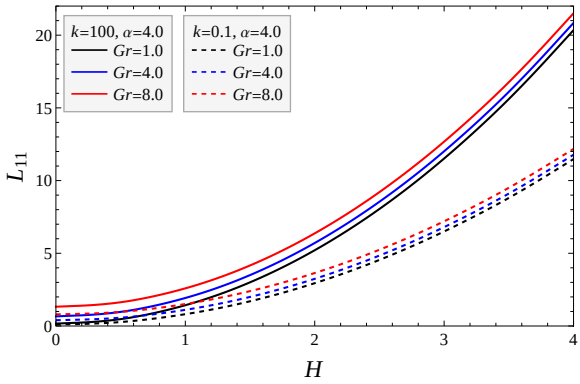

Figure 3.10: Changes in L_{11} relying on Hartmann electric number H with varying Grashof number Gr, under high $(k = 100)$ and low $(k = 0.1)$ permeability parameters. $(\alpha = 4.0, \beta = 0.1, \gamma = 0.45, N_1 = 2.0, l = 0.5, \lambda_1 = 1)$

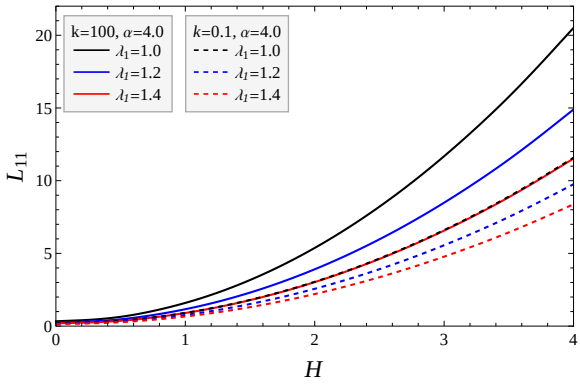

Figure 3.11: Changes in L_{11} relying on Hartmann electric number H with varying viscosity ratio parameter λ_1, under high $(k = 100)$ and low $(k = 0.1)$ permeability parameters. $(\alpha = 4.0, \beta = 0.1, \gamma = 0.45, Gr = 2.0, N_1 = 2.0, l = 0.5)$

dominance of radiative heat transfer over convective heat transfer leads to a higher growth rate for hydrodynamic permeability with the Hartmann electric number. However, in the case of a small non-linearity parameter, the variation of hydrodynamic permeability with the Hartmann electric number will be reversed for a higher Grashof number, like in Figure 3.3b. Figure 3.15 also reveals a decay in hydrodynamic permeability with increasing N_1. The further decay rate is significantly reduced for increasing H. The observation indicates a more significant impact of radiation heat transfer on hydrodynamic permeability for low Hartmann electric numbers. The effect of the Hartmann electric number on hydrodynamic permeability for different Grashof numbers is depicted in Figure 3.16. Unlike the case of significant alpha, here, hydrodynamic permeability shows a decay with increasing Hartmann electric number for the cases where thermal buoyancy forces dominate the viscous forces. However, for small Grashof, the observation is similar to the one discussed for large alpha.

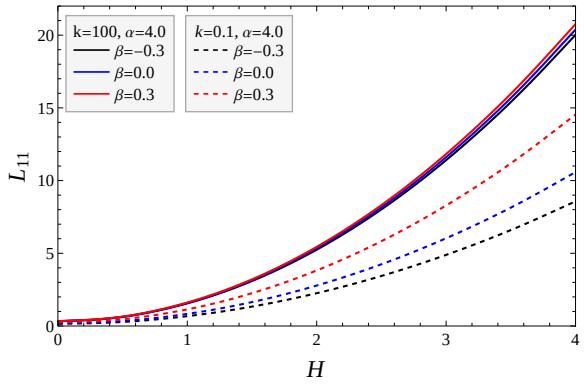

Figure 3.12: Changes in L_{11} relying on Hartmann electric number H with varying stress jump parameter β, under high $(k = 100)$ and low $(k = 0.1)$ permeability parameters. $(\alpha = 4.0, \lambda_1 = 1, \gamma = 0.45, Gr = 2.0, N_1 = 2.0, l = 0.5)$

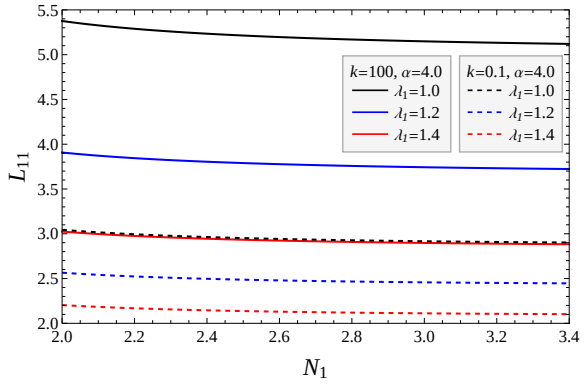

Figure 3.13: Changes in L_{11} relying on Radiation parameter N_1 with varying viscosity ratio parameter λ_1, under high $(k = 100)$ and low $(k = 0.1)$ permeability parameters. $(\alpha = 4.0, \beta = 0.1, \gamma = 0.45, Gr = 2.0, H = 2.0, l = 0.5)$

The decay in the hydrodynamic permeability with radiation parameters for varying beta is depicted in Figure 3.17. It is perceived that an increasing beta leads to a higher decay rate for membrane permeability. This observation can be interpreted as the decay in L_{11} with radiation parameter is more significant when the porous medium has higher shear stress than the non-porous region. Figure 3.18 depicts the impact of the stress-jump parameter on membrane permeability for varying Grashof numbers. While for large permeability, the effect of beta is almost negligible owing to a negligibly slight difference in shear stress at the interface, the variation is significant for low permeability. In the case of low permeability, a rising Grashof number contributes towards a higher growth rate of L_{11} with increasing beta. Figure 3.19 reveals that the growth rate of hydrodynamic permeability with increasing beta reduces for higher Hartmann electric numbers.

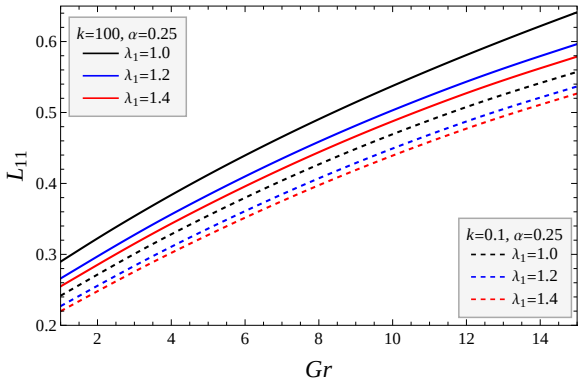

Figure 3.14: Changes in L_{11} relying on Grashof number Gr with varying viscosity ratio parameter λ_1, under high $(k = 100)$ and low $(k = 0.1)$ permeability parameters. $(\alpha = 4.0, \beta = 0.1, \gamma = 0.45, N_1 = 2, H = 2.0, l = 0.5)$

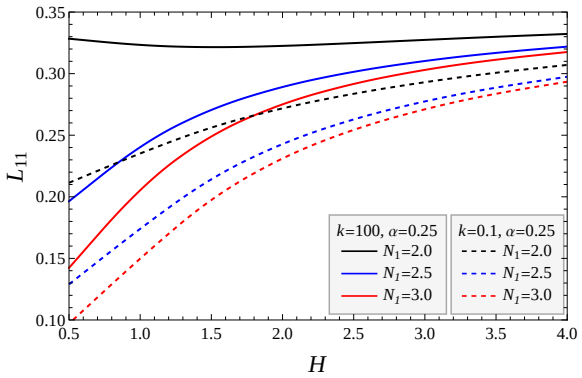

Figure 3.15: Changes in L_{11} relying on Hartmann electric number H with varying radiation parameter N_1, under high $(k = 100)$ and low $(k = 0.1)$ permeability parameters. $(\alpha = 0.25, \beta = 0.1, \gamma = 0.45, \lambda_1 = 1, Gr = 2.0, l = 0.5)$

3.4.4 Kozeny Constant (K_z)

Tortuosity is essential in representing enhanced fluid resistance for flow through porous media in analyzing flow through porous media. The impact of various parameters on the Kozeny constant enhancing the tortuosity is discussed in this section. Figure **??** depicts a decreasing Kozeny constant with increasing β. Further, the decay rate reduces with increasing H, although it is almost negligible for higher permeability. This can be interpreted as, for a low Hartmann electric number, a rise in stress-jump coefficient β more significantly reduces the tortuosity of the porous medium. Figure **??** delineates the same effect under varying radiation parameters. It can be seen that the dominance of radiation heat transfer over convective heat transfer leads to a higher decay rate of the Kozeny constant with β.

The effect of the Grashof number on the Kozeny constant under varying H is similar to

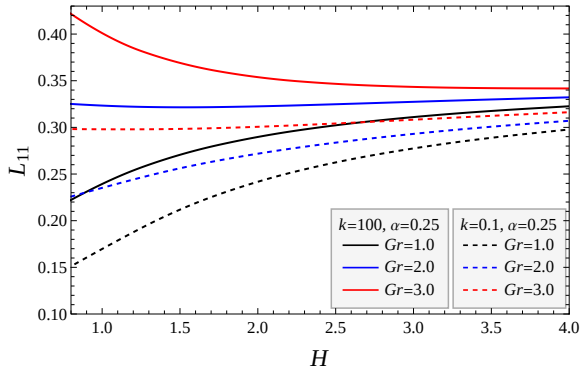

Figure 3.16: Changes in L_{11} relying on Hartmann electric number H with varying Grashof number Gr, under high $(k = 100)$ and low $(k = 0.1)$ permeability parameters. $(\alpha = 0.25, \beta = 0.1, \gamma = 0.45, N_1 = 2, \lambda_1 = 1.0, l = 0.5)$

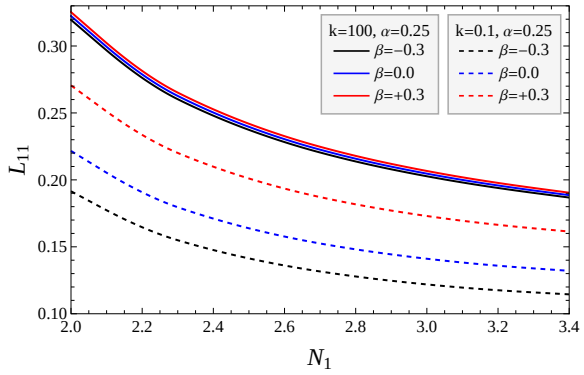

Figure 3.17: Changes in L_{11} relying on radiation parameter N_1 with varying stress jump parameter β, under high $(k = 100)$ and low $(k = 0.1)$ permeability parameters. $(\alpha = 0.25, \gamma = 0.45, H = 2, Gr = 2, \lambda_1 = 1.0, l = 0.5)$

Figure 21, which reveals that the dominance of thermal buoyancy forces over viscous forces reduces the tortuosity of the porous medium, and the decay rate reduces for higher H (Figure 3.22). The Kozeny constant decays with H, and the decay rate significantly reduces with increasing Gr (Figure 3.23). A similar observation is reported in Figure 3.24 for different λ_1, and it can be concluded that a relatively rising viscous effect in porous medium leads to increased tortuosity. A rising radiation parameter leads to a slight increase in the tortuosity, which becomes almost steady, as shown in Figure 3.25.

Figure 3.26 reveals the impact of the porosity of the medium on the Kozeny constant with varying Hartmann electric numbers. Increasing porosity of the porous medium leads to an increase in the Kozeny constant. However, the growth rate decays significantly with the increasing Hartmann electric number. While observing the graphical representations of the Kozeny constant for small values of nonlinearity parameter, Figure 3.27 reveals that in small

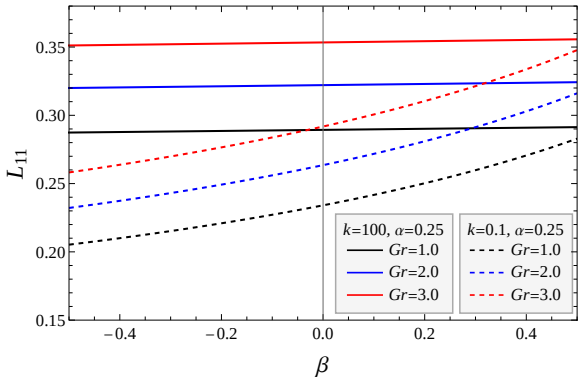

Figure 3.18: Changes in L_{11} relying on stress jump parameter β with varying Grashof number Gr, under high $(k = 100)$ and low $(k = 0.1)$ permeability parameters. $(\alpha = 0.25, \gamma = 0.45, H = 2, N_1 = 2, \lambda_1 = 1.0, l = 0.5)$

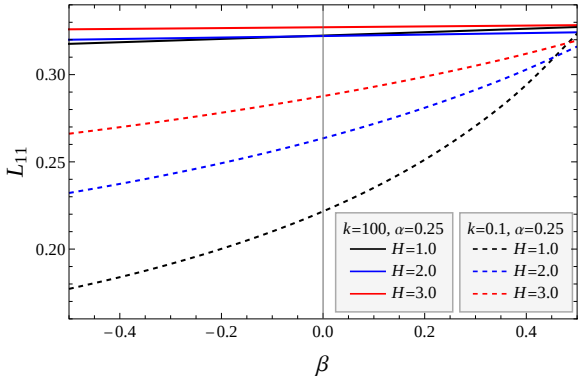

Figure 3.19: Changes in L_{11} relying on stress jump parameter β with varying Hartmann electric number H, under high $(k = 100)$ and low $(k = 0.1)$ permeability parameters. $(\alpha = 0.25, \gamma = 0.45, Gr = 2, N_1 = 2, \lambda_1 = 1.0, l = 0.5)$

permeability, the Kozeny constant decays with the increasing stress difference of porous and non-porous medium at the interface. However, the decay rate reduces with the increasing dominance of thermal buoyancy forces over viscous forces. For highly permeable porous medium, this dependence is almost negligible.

The Kozeny constant shows a higher growth rate with the increasing dominance of radiative heat transfer over convective heat transfer, and this growth rate decreases significantly when the electric Hartman number increases (Figure 3.28). An increasing dominance of the porous medium's viscosity over the clear fluid viscosity (non-porous region's viscosity) leads to an enhancement of the Kozeny constant of the membrane in both cases of permeability (Figure 3.29). The stress jump parameter shows a significant impact on flow behaviour for the case of small permeability owing to the small valued denominator in the RHS of the stress jump boundary condition. The increasing stress jump between porous and

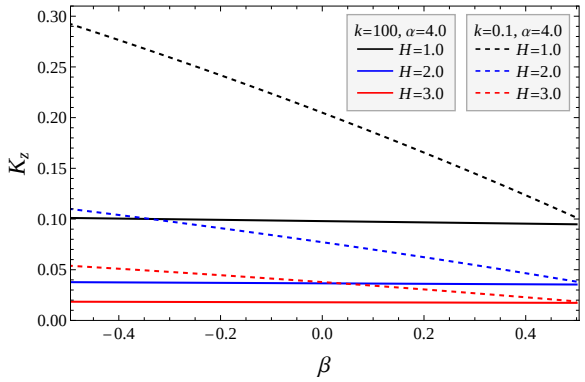

Figure 3.20: Changes in L_{11} relying on stress jump parameter β with varying Hartmann electric number H, under high $(k = 100)$ and low $(k = 0.1)$ permeability parameters. $(\alpha = 4.0, \gamma = 0.6, Gr = 2, N_1 = 2, \varepsilon = l = 0.5, \lambda_1 = 1.0)$

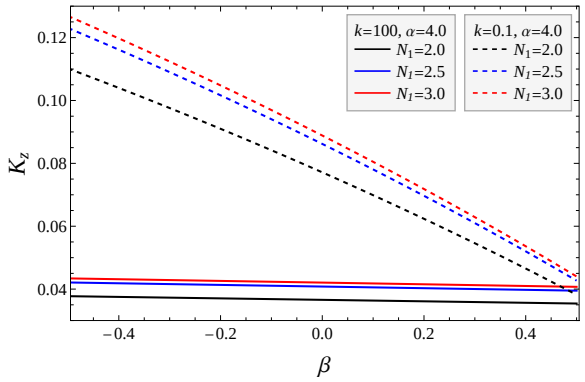

Figure 3.21: Changes in Kozeny constant K_z relying on stress jump parameter β with varying Radiation parameter N_1, under high $(k = 100)$ and low $(k = 0.1)$ permeability parameters. $(\alpha = 4.0, \gamma = 0.6, Gr = 2, H = 2, \varepsilon = l = 0.5, \lambda_1 = 1.0)$

non-porous medium decreases the Kozeny constant and hence enhances the tortuosity of the porous medium (Figure 3.30). The Kozeny constant increases exponentially with the porosity of the medium. Along with that dominance of radiative heat transfer over convective heat transfer leads to enhance value of the Kozeny constant of the membrane, regardless of the permeability cases (Figure 3.31).

3.4.5 Model Validation and Comparative Study

The proposed work is a theoretical attempt to understand the electrohydrodynamic flow (EHD) with heat transfer past a swarm of porous layered cylindrical particles by analyzing the variations of hydro-dynamical quantities like velocity, membrane permeability, and

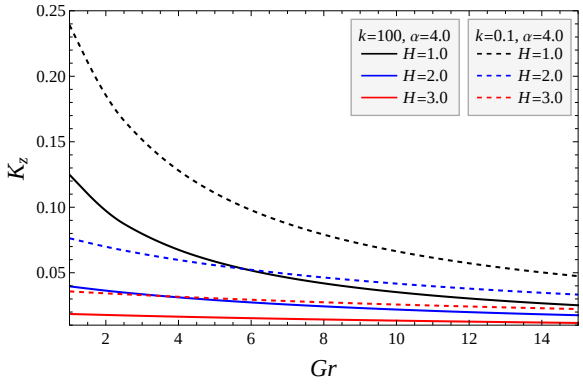

Figure 3.22: Changes in Kozeny constant K_z relying on Grashof number Gr with varying Hartmann electric number H, under high $(k = 100)$ and low $(k = 0.1)$ permeability parameters. $(\alpha = 4.0, \gamma = 0.6, \beta = 0.1, N_1 = 2, \varepsilon = l = 0.5, \lambda_1 = 1.0)$

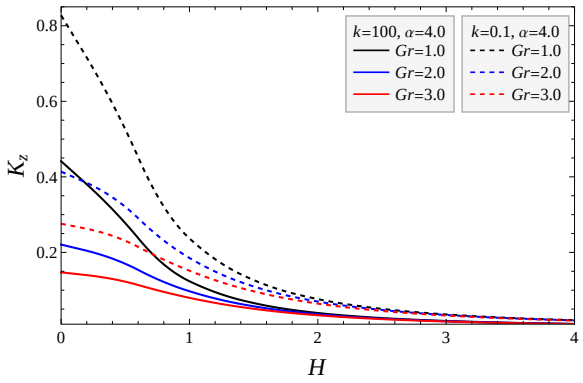

Figure 3.23: Changes in Kozeny constant K_z relying on Hartmann electric number H with varying Grashof number Gr, under high $(k = 100)$ and low $(k = 0.1)$ permeability parameters. $(\alpha = 4.0, \gamma = 0.6, \beta = 0.1, N_1 = 2, \varepsilon = l = 0.5, \lambda_1 = 1.0)$

Kozeny constant with various parameters signifying the effect of the electric field, thermal buoyancy forces, and radiative heat transfer. The comparative graphical analysis of the analytical solution has been made with a numerical solution to validate the approximate solution. The numerical solution is obtained through the NDSolve command in Mathematica 10.3 software. The fluid velocity derived from the two different methods for small nonlinearity parameters is compared in Figure 3.32, where it can be observed that the curve of asymptotic fluid velocity and numerical fluid velocity are in good agreement (a difference of 0.02 can be seen at the fluid-porous interface in the inset). Also, the comparison of both methodologies for the hydrodynamic permeability and the Kozeny constant has been plotted in Figure 3.33 and Figure 3.34, respectively. The numerical solution of the hydrodynamic permeability overlaps with the asymptotic solution from the low Grashof number; however, a slight difference can be seen between these two as the Grashof number goes higher. The

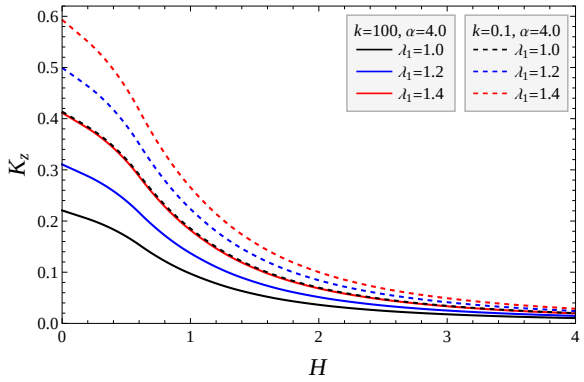

Figure 3.24: Changes in Kozeny constant K_z relying on Hartmann electric number H with varying viscosity ratio parameter λ_1, under high $(k = 100)$ and low $(k = 0.1)$ permeability parameters. $(\alpha = 4.0, \gamma = 0.6, \beta = 0.1, N_1 = 2, \varepsilon = 0.5, Gr = 2.0, l = 0.5)$

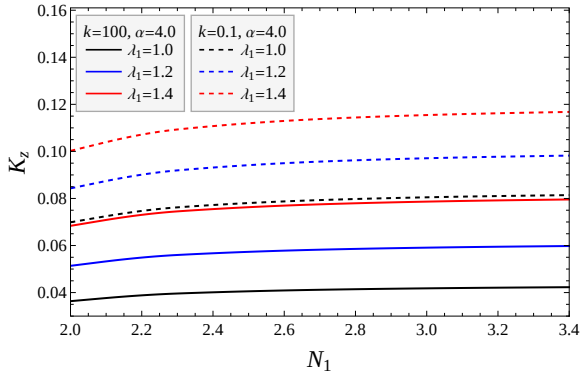

Figure 3.25: Changes in Kozeny constant K_z relying on Radiation parameter N_1 with varying viscosity ratio parameter λ_1, under high $(k = 100)$ and low $(k = 0.1)$ permeability parameters. $(\alpha = 4.0, \gamma = 0.6, \beta = 0.1, H = 2.0, Gr = 2.0, \varepsilon = 0.5, , l = 0.5)$

asymptotic solution of the Kozeny constant with porosity parameter almost coincides with its numerical solution for the case of a small non-linearity parameter.

This subsection also includes the validation of the “ion drag" effect on electrohydrodynamic flow and its dependence on parameters such as electric Hartmann number and non-linearity parameter and is validated from the results of previously published literature. An increasing particle volume fraction leads to a greater occupancy of porous layered particles in the medium and less space for the clear fluid media, which reduces the fluid flow velocity past a membrane. The current study delineates the above-mentioned theory and validates the variation of Hydrodynamic permeability (L_{11}) along particle volume fraction (γ) with the study of Deo *et al.* [3], where L_{11} follows the same behavior with particle volume fraction in both the studies. However, due to the presence of an additional electric field, the decay rate in the present model is slightly less, and the same can be observed in

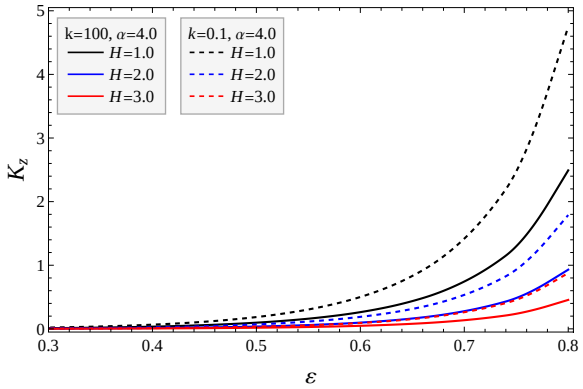

Figure 3.26: Changes in Kozeny constant K_z relying on porosity parameter ε with varying Hartmann electric number H under high $(k = 100)$ and low $(k = 0.1)$ permeability parameters. $(\alpha = 4.0, \gamma = 0.6, \beta = 0.1, N_1 = 2, \lambda_1 = 1, Gr = 2.0, l = 0.5)$

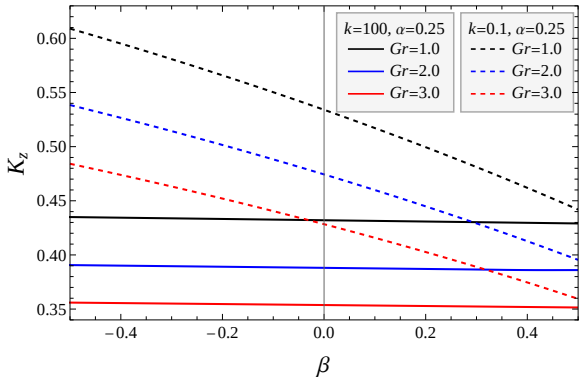

Figure 3.27: Changes in Kozeny constant K_z relying on stress-jump parameter β with varying Grashof number Gr, under high $(k = 100)$ and low $(k = 0.1)$ permeability parameters. $(\alpha = 0.25, \gamma = 0.0.45, \varepsilon = 0.5, H = 2.0, N_1 = 2, \lambda_1 = 1, l = 0.5)$

Table 5.2. The behavior of hydrodynamic permeability in the current work is qualitatively validated. Further, similar behavior has also been observed in various other works involving flows through a swarm of particles such as Vasin *et al.* [85], Prakash *et al.* [183], Yadav *et al.* [92], and Fillipov *et al.* [184]. The findings of the work have also validated the behavior of the electric Hartmann number with the work of McKee *et al.* [14] where velocity is getting higher for the increasing electric Hartmann number in the case of small non-linearity parameter $(\alpha \ll 1)$. The same has been observed in the analysis of the current study and can be verified in Table 3.3.

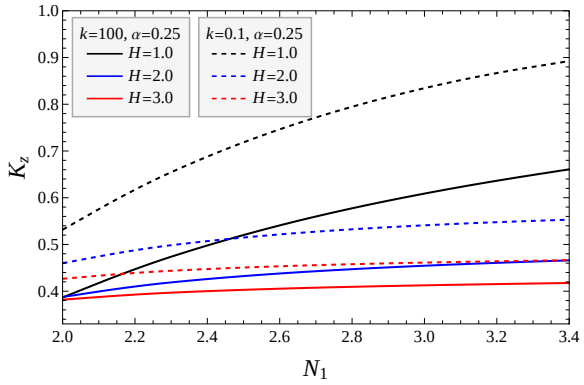

Figure 3.28: Changes in Kozeny constant K_z relying on Radiation parameter N_1 with varying Hartmann electric number H, under high $(k = 100)$ and low $(k = 0.1)$ permeability parameters. $(\alpha = 0.25, \gamma = 0.45, \varepsilon = 0.5, \beta = 0.1, Gr = 2.0, \lambda_1 = 1, l = 0.5)$

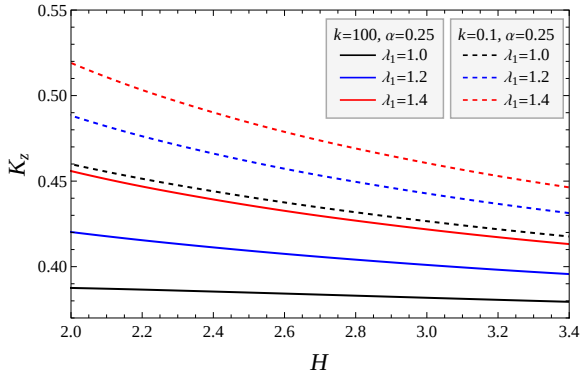

Figure 3.29: Changes in Kozeny constant K_z relying on Hartmann electric number H with varying viscosity ratio parameter λ_1, under high $(k = 100)$ and low $(k = 0.1)$ permeability parameters. $(\alpha = 0.25, \gamma = 0.45, \varepsilon = 0.5, \beta = 0.1, Gr = 2.0, N_1 = 2, l = 0.5)$

3.5 Summary and Conclusion

The consideration of the external electric field and the heat transfer in the flow of Newtonian fluid through membrane aggregates of porous cylindrical particles has been discussed in the present work. The flow regime is separated into two regions in which the fluid flow through the porous medium is considered proximate to the solid core of the cylindrical particle and regulated by the Brinkman equation. However, an envelope enfolded over the porous medium is considered a non-porous region and regulated by the Stokes equation. The analytical solutions of the Brinkman and Stokes equations are difficult to obtain owing to the presence of non-linear body force (external electric field). In order to obtain the solution of the governing equations the regular perturbation method has been employed to solve the governing equations, and the expressions of velocity have been used to obtain the membrane

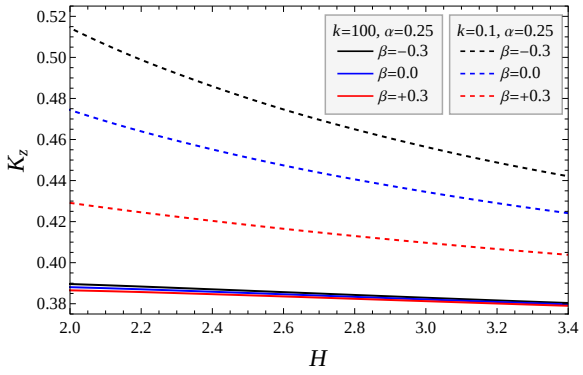

Figure 3.30: Changes in Kozeny constant K_z relying on Hartmann electric number H with varying stress-jump parameter β, under high $(k = 100)$ and low $(k = 0.1)$ permeability parameters. $(\alpha = 0.25, \gamma = 0.45, \varepsilon = 0.5, \lambda_1 = 1.0, Gr = 2.0, N_1 = 2, l = 0.5)$

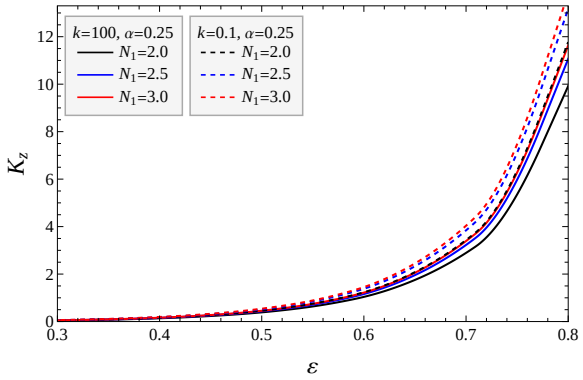

Figure 3.31: Changes in Kozeny constant K_z relying on porosity parameter ε with varying radiation parameter N_1, under high $(k = 100)$ and low $(k = 0.1)$ permeability parameters. $(\alpha = 0.25, \gamma = 0.45, H = 2.0, \lambda_1 = 1.0, Gr = 2.0, \beta = 0.1, l = 0.5)$

permeability and Kozeny constant. The results and discussion section have given a detailed discussion of the graphical analysis. The following novel determinations from the present study are pointed out:

1. The graphical analysis reveals that a rising Hartmann electric number leads to the growth of velocity and membrane permeability, which is relatively more significant for higher permeability. However, the reverse trend is observed in the Kozeny constant with Hartmann electric number, which is relatively less significant for higher permeability.

2. The effect of the radiation parameter on the velocity profile and membrane permeability is discussed, and it is found that a rising radiation parameter leads to a significant

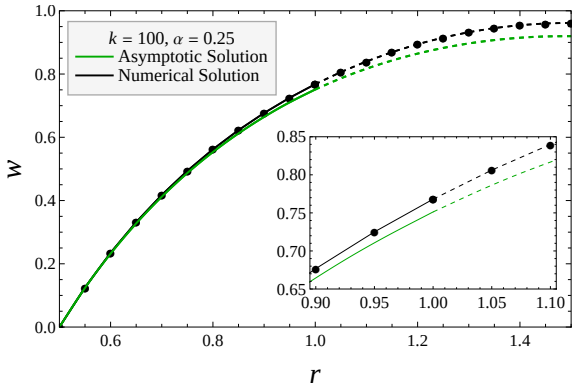

Figure 3.32: Comparision between radially varying velocities of asymptotic and numerical solutions for the case small non-linearity parameter $\alpha = 0.25$ ($\beta = 0.1, H = 2.0, \lambda_1 = 1, l = 0.5, Gr = 2.0, N_1 = 2, p_z = 1$)

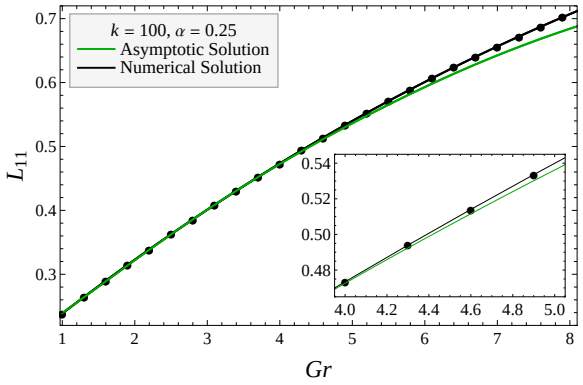

Figure 3.33: Variation of the membrane permeability L_{11} with radial distance with asymptotic and numerical variations ($\beta = 0.1, H = 2.0, \alpha = 0.25, \lambda_1 = 1, l = 0.5, Gr = 2.0, N_1 = 2, p_z = 1$)

decay in fluid velocity and membrane permeability for small α. However, a significant growth in the Kozeny constant is observed with the radiation parameter.

3. The dominance of the thermal buoyancy forces over the viscous forces on the hydrodynamical quantities enhances the velocity and membrane permeability. However, a decline in the Kozeny constant is observed.

4. A significant growth is observed in velocity and membrane permeability for large non-linearity parameters, α in the case of small and large permeability of the porous material. However, a reverse trend is observed in the Kozeny constant for large α.

The suggested explanation has the potential to significantly contribute to the examination of

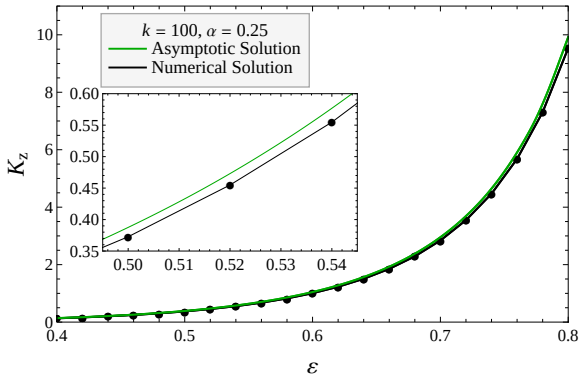

Figure 3.34: Variation of the Kozeny constant K_z with radial distance with asymptotic and numerical variations ($\beta = 0.1, \alpha = 0.25, H = 2.0, \lambda_1 = 1, l = 0.5, Gr = 2.0, N_1 = 2, p_z = 1$)

important physical and biological applications, including petroleum reservoir rocks, wastewater treatment filtration processes, and blood flow through smooth muscle cells. However, empirical validation remains an essential step in establishing the reliability of the proposal. While our research offers valuable insights into electrohydrodynamic flow dynamics and membrane hydrodynamic permeability, it's crucial to recognize certain inherent limitations in our approach. This study modeled the swarm of particles as a uniformly distributed array, though in reality, it may exhibit a randomly oriented distribution. Furthermore, our methodology employs the regular perturbation method to derive asymptotic solutions for governing equations, considering cases of small and large non-linearity parameters ($\alpha \ll 1$ and $\alpha \gg 1$). However, our analysis is constrained by the prescribed parameter domain of α, representing another limitation of our study.

$\gamma \downarrow$	Hydrodynamic Permeability (L_{11})	
	Deo *et al.* [3]	Current Study
$\gamma = 0.25$	0.355044	0.365176
$\gamma = 0.30$	0.215811	0.347859
$\gamma = 0.35$	0.134694	0.331048
$\gamma = 0.40$	0.085182	0.314860
$\gamma = 0.45$	0.054032	0.299385
$\gamma = 0.50$	0.034074	0.284681
$\gamma = 0.55$	0.021176	0.270771
$\gamma = 0.60$	0.012844	0.257654

Table 3.2: Validation of current work with the study of Deo *et al.* [3] using variations in hydrodynamic permeability L_{11} with particle volume fraction γ. $(\alpha = 0.1)$.

$r \downarrow$	McKee *et al.* [14] $(\alpha = 0.1)$			$r \downarrow$	Current Work $(\alpha = 0.1)$		
	$H^2 = 1.0$	$H^2 = 10$	$H^2 = 100$		$H^2 = 1.0$	$H^2 = 10$	$H^2 = 100$
$r = 0.0$	0.209371	0.778501	0.781792	$r = 0.5$	0.0	0.0	0.0
$r = 0.1$	0.206853	0.773975	0.771753	$r = 0.6$	0.053342	0.230540	0.588723
$r = 0.2$	0.202238	0.764922	0.765861	$r = 0.7$	0.094587	0.373586	0.765640
$r = 0.3$	0.192168	0.742291	0.743101	$r = 0.8$	0.130706	0.473453	0.820996
$r = 0.4$	0.178741	0.712871	0.705548	$r = 0.9$	0.166745	0.557559	0.844898
$r = 0.5$	0.160699	0.668741	0.666856	$r = 1.0$	0.206993	0.646145	0.873521
$r = 0.6$	0.140559	0.601980	0.599716	$r = 1.1$	0.244939	0.724957	0.898284
$r = 0.7$	0.110350	0.522772	0.513229	$r = 1.2$	0.272406	0.775292	0.906191
$r = 0.8$	0.078462	0.388119	0.396017	$r = 1.3$	0.290753	0.805741	0.908727
$r = 0.9$	0.043217	0.218388	0.223883	$r = 1.4$	0.300984	0.821604	0.909517
$r = 1.0$	0.0	0.0	0.0	$r = 1.5$	0.303841	0.825889	0.909676

Table 3.3: Validation of current work with the study of McKee *et al.* [14] using variations in velocity w in radial direction r for different values electric Hartmann number, H $(H^2 = 1, 10, 100)$.

Chapter 4

Creeping flow of non-Newtonian fluid through membrane of porous cylindrical particles: A particle-in-cell approach [1]

4.1 Introduction

The fluid flow in a porous medium is an intriguing topic for research in fluid dynamics. This multidisciplinary topic has recently gotten much attention because of its wide range of academic and industrial research applications. It has broad applications in the pharmaceutical field, petroleum reservoir rocks, wastewater treatment filtration processes, blood flow via the lungs, digestive system design, etc. As mentioned above, the flow medium in the applications is a porous material comprising a swarm of particles. Flow throgh such media can be governed by the Darcy [48] and Brinkman equations [137]. Srivastava and Deo [24] considered the Brinkman equation to study the fluid flow in a porous channel. In order to study the flow dynamics in a porous media consisting of an aggregate of particles, one has to derive the hydrodynamic interaction between these swarm particles. It is difficult to study all particles in a multi-particle system at the same time, a new analytical approach is developed in which an arbitrary single particle is taken into consideration, and a hypothetical cell around this particle is chosen in such a way that it incorporates the hydrodynamic interactions of adjacent particles on the particle under consideration.

In the study of fluid filtration processes, the rheological behaviour of fluid can be modelled by a shear-rate-dependent non-Newtonian viscosity and its viscoelasticity. Researchers have identified several rheological fluids that resemble the fluid's non-Newtonian behaviour, and their constitutive relationship may be utilized to imitate a variety of natural occurrences. Researchers have looked at the Carreau fluid model extensively as a generalized Newtonian fluid in the past since it has four parameters that can be used to analyze the fluid's rheology.

[1] A considerable part of this chapter is published in *Physics of Fluids*, 35, 043101, 2023.

This four-parameter model has been beneficial in hemodynamics, and it is flexible enough to accommodate a range of experimental apparent viscosity curves. Carreau fluid acts like Newtonian fluid $(n = 1)$ at low shear rates, whereas it can exhibit both shear-thinning or pseudoplastic $(n < 1)$ and shear thickening or Dilatent $(n > 1)$ behaviour at high shear rates. Rana and Murthy [18] studied the solute dispersion of an unsteady Carreau fluid flow and derived the asymptotic expressions of the effective transport coefficients. Zhu and Satish [185] used the cell method to study the flow of the Carreau fluid slowly moving through a heavily populated array of solid particles. Chaffin and Rees [186] used the Carreau fluid and examined the wall-driven corner flow.

Throughout the studies above, based on the Newtonian, non-Newtonian and polar fluids flowing through membranes consisting of an array of particles using a particle-in-cell model approach, it has been noted that the non-Newtonian fluid flow through membranes has yet to find enough attention from researchers. The non-Newtonian Carreau fluid exhibits the fluid's shear-thinning and thickening behaviour owing to the Power-law index involved in the stress-strain relationship. It has the liquid's elastic nature owing to the Weissenberg number's presence in the governing equation, which is taken as a very small $(\mathrm{We} \ll 1)$ for a more realistic study in the membrane filtration process. The additional benefit of considering the Carreau fluid is that the viscosity ratio parameter η $(0.1 < \eta < 0.4)$ replicates the infinite to zero shear-rate viscosity ratio. The analysis of the supremacy of zero shear-rate viscosity over the infinite shear-rate viscosity or vice-versa may help to understand the behaviour of pseudoplastic fluid flowing through the membrane and hence may be beneficial in the movement of fluid through the porous medium. Temperature variation has a strong effect on the membrane filtering process.

The purpose of this research is to explore the hydrodynamic and thermal aspects of the slow flow of a non-Newtonian Carreau fluid over a membrane comprising a cluster of porous layered solid cylinders owing to its non-Newtonian property of a pseudoplastic fluid. The flow regime in a cross-sectional area of an individual cylinder is separated into two regions, the fluid flow inside the porous annular region proximate to the solid core. At the same time, the other one is the non-porous fluid flow region around the annular layer of porous media. The Brinkman and Stokes equations regulate the Carreau fluid flow in the porous and non-porous (clear fluid) sections, respectively. Due to the existence of a nonlinear velocity gradient term in the stress-strain relationship of Carreau fluid, The exact solutions to the Brinkman and Stokes equations are challenging. An asymptotic (perturbation) series expansion method presuming the small parameters (Weissenberg number $\mathrm{We} \ll 1$ and a dimensionless hydraulic resistivity parameter $S = \frac{1}{\sqrt{k}} \ll 1$) is used to derive the solution expressions for the equation governing fluid flow through the porous region; however, the

perturbation technique based on small Weissenberg number $(\mathrm{We} \ll 1)$ is used to derive the asymptotic solution of flow through the non-porous region. In the low permeability case (*i.e.*, a significant dimensionless parameter $(S \gg 1)$), the equation regulating the flow through porous material is reduced to a non-linear boundary value problem subject to the suitable boundary conditions, which is difficult to solve analytically. Hence the numerical strategy (NDSolve in Mathematica) has been used to demonstrate the results in the graphical form of the present analysis. The expressions of membrane permeability and the Kozeny constant are derived for the large Darcy number case; however, for the small Darcy number, a comparative analysis with the expressions of the large Darcy number is presented in the form of graphical and tabular analysis. The heat flow at the cylinder's wall of the cylinder is maintained constant at the value q'' in the case of forced convection in a porous layered circular cylinder. The steady-state thermal equation is analytically solved without the source of heat, axial conduction, and heat dispersion.

The sketch of the present study is demonstrated in the VI sections. The introduction section (Section- 1) discusses the fundamental knowledge of the work with a preamble, literature survey, gaps in existing research and the objective of the present work. The flow configuration, In Section- 2, the model assumptions, the physical sketch of the work, and the hydrodynamical and thermal equations with the suitable boundary conditions are described, which is followed by the mathematical forms of membrane permeability and Kozeny constant. Section- 3 illustrates the work's solution technique and the associated formulations of the governing equations in small and large Darcy number cases. The temperature equations for porous and non-porous media subject to the appropriate boundary conditions and their solutions are demonstrated in Section- 4. Section- 5 divulges the selection of parameters and their resources for the graphical analysis and model validation in case of asymptotic and numerical solutions of the work. The special cases deduced from the present work and the comprehensive discussion of the present work in the form of graphical and tabular analysis have also been done. A summary and the significant novel contribution of the current research are displayed in the last section (Section- 6), followed by acknowledgement and the references used in the current work.

4.2 Mathematical Formulation of the Proposed Work

4.2.1 Statement and Assumptions

The non-Newtonian Carreau fluid flows through a membrane (porous media) consisting of an array of uniformly distributed porous cylindrical particles with a solid core of radius $\widetilde{a}$, which is surrounded by a porous layer of thickness $\widetilde{b}-\widetilde{a}$, and the flow is considered to be incompressible, steady, and laminar. The fluid flows parallel to the longitudinal centerline of the solid cylindrical-shaped particle. The concept of the particle-in-cell model is used to study the flow through a membrane in which a single porous layered solid cylindrical particle of radius $\widetilde{a}$ is chosen from the swarm. A hypothetical cell of thickness $(\widetilde{c}-\widetilde{b})$ is considered in the vicinity of the porous layer to accommodate the influence of hydrodynamic interactions between neighbouring particles and the particle in consideration. Concerning the geometry of the model, the z-axis is employed such that it corresponds with the central axis of a solid cylinder using the cylindrical polar coordinate system $(\widetilde{r},\phi,\widetilde{z})$, where $\widetilde{r}$ and $\widetilde{z}$ are the radial and axial coordinates, respectively and ϕ is the azimuthal angle. The flow is considered axially symmetric, fully developed flow in the axial direction only, so flow quantities will be independent of the variable ϕ. The velocity component of the fluid is taken as $(0,0,\widetilde{w})$ owing to its unidirectional flow in the axial direction. In the case of low Reynolds number flow, the convective term in the momentum equation has a negligible contribution. So, it can be neglected from the momentum equation. The energy equations regulating the transmission of heat in fluid flow through the membrane are simplified for high Peclet numbers $(Pe \gg 1)$.

4.2.2 Model Description of the Problem

The framework of the proposed model is divided into two regions. The region (Region-I) adjacent to the solid core is a porous region, and an outer region (Region-II) overlying by the porous region, which is free from the porous material, is a non-porous region (or clear fluid region). The Brinkman equation regulates the flow through a porous region; however the Stokes equation regulates the flow through a non-porous region. Figures 4.1 and 4.2 delineate the liquid flow through solid cylindrical particles of the membrane surrounded by the porous layer. The figures describe a solid cylindrical core of radius $\widetilde{a}$ and a coaxial cylindrical layer of the porous medium around the solid core of radius $\widetilde{b}$ with a hypothetical surface layer surrounded over the porous cylindrical cell of radius $\widetilde{c}$. The thickness of the hypothetical cell of a porous cylindrical particle is selected in a manner that the volume

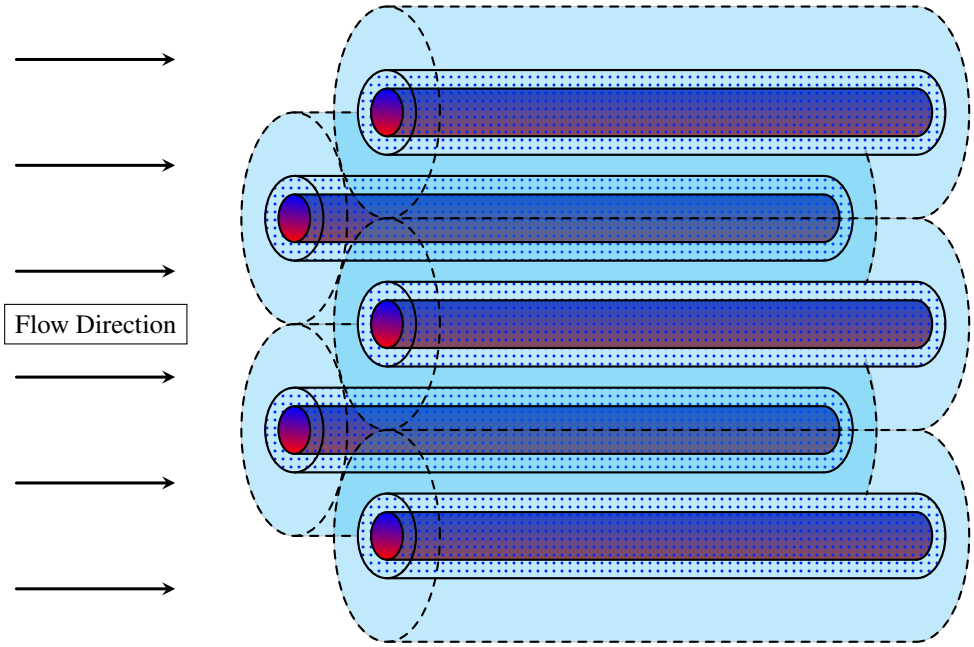

Figure 4.1: The physical depiction of the flow along the axis of an aggregate of porous layered solid cylinders in a membrane

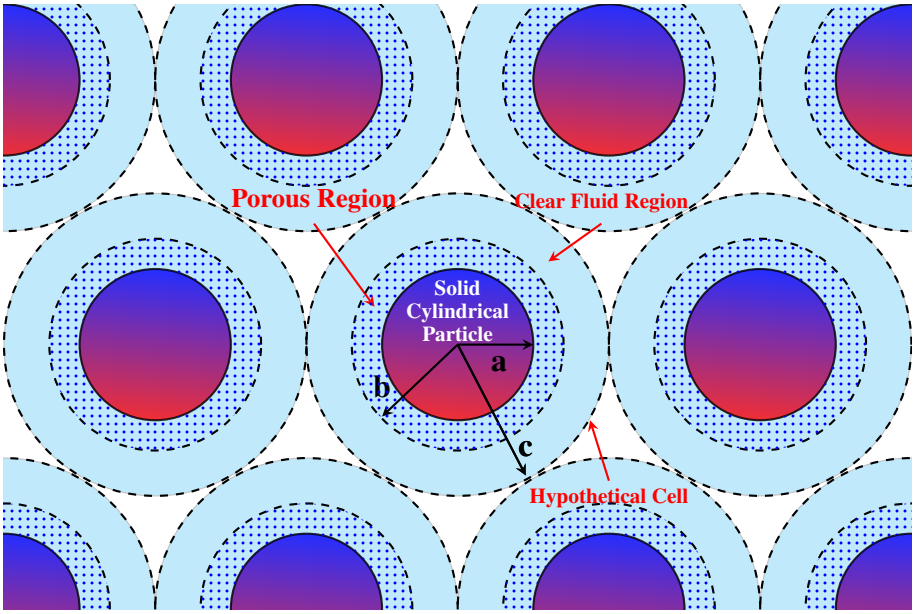

Figure 4.2: The physical representation of circular cross-sectional view of a swarm consisting of solid cylindrical particle surrounded by a porous layer enclosed in hypothetical cell

fraction of the particles in the swarm is equal to the volume fraction of the cell.

$$c^2 = \frac{1}{\gamma} = \frac{\pi\widetilde{c}^2}{\pi\widetilde{b}^2}. \tag{4.1}$$

4.2.3 Governing Equations

4.2.3.1 Hydrodynamic Equations

Following the problem statement and assumptions of the proposed model, the equations governing the flow through the porous ($\widetilde{a} \le \widetilde{r} \le \widetilde{b}$) and non-porous ($\widetilde{b} \le \widetilde{r} \le \widetilde{c}$) cylindrical particle are as follows:
Region- I, *i.e.*, $\widetilde{a} \le \widetilde{r} \le \widetilde{b}$

$$\frac{\partial \widetilde{w}_p}{\partial \widetilde{z}} = 0, \tag{4.2a}$$

$$\frac{\partial \widetilde{p}}{\partial \widetilde{r}} = 0, \tag{4.2b}$$

$$\frac{\partial \widetilde{p}}{\partial \widetilde{z}} = \frac{1}{\widetilde{r}}\frac{\partial}{\partial \widetilde{r}}(\widetilde{r}\widetilde{\tau}_p) - \frac{\widetilde{\mu}_0 \widetilde{w}_p}{\widetilde{k}}, \tag{4.2c}$$

where $\widetilde{p}, \widetilde{w}_p, \widetilde{\tau}_p$ are the pressure, velocity and shear stress of the fluid in the porous region, respectively; $\widetilde{\mu}_0$ is the constant viscosity coefficient of the clear fluid, $\widetilde{k}$ is the permeability constant of the porous medium. The equations (4.2a)-(4.2c) delineate the conservation of mass (*i.e.*, continuity equation), and momentum equations (*i.e.*, conservation of mementum) in radial r and axial z directions, respectively. The momentum equation (4.2c) in the axial direction replicating the Brinkman equation that has an additional resistance term, which is known as the Darcian term.
The stress-strain relation for Carreau fluid in terms of porous medium liquid velocity is given by [18]

$$\widetilde{\tau}_p = \left[\widetilde{\mu}_\infty + (\widetilde{\mu}_0 - \widetilde{\mu}_\infty)\left(1 + \left(\lambda \frac{\partial \widetilde{w}_p}{\partial \widetilde{r}}\right)^2\right)^{\frac{n-1}{2}}\right]\frac{\partial \widetilde{w}_p}{\partial \widetilde{r}}, \tag{4.2d}$$

where $\widetilde{\mu}_0$ and $\widetilde{\mu}_\infty$ are the zero and infinite shear-rate viscosity of Carreau fluid, respectively; n is the Power-law exponent exhibiting the shear-thinning and thickening behavior of the fluid and λ is the time constant.

Region- II, *i.e.*, $\widetilde{b} \leq \widetilde{r} \leq \widetilde{c}$

$$\frac{\partial \widetilde{w}_c}{\partial \widetilde{z}} = 0, \tag{4.3a}$$

$$\frac{\partial \widetilde{p}}{\partial \widetilde{r}} = 0, \tag{4.3b}$$

$$\frac{\partial \widetilde{p}}{\partial \widetilde{z}} = \frac{1}{\widetilde{r}} \frac{\partial}{\partial \widetilde{r}} (\widetilde{r}\widetilde{\tau}_c), \tag{4.3c}$$

where $\widetilde{\tau}_c$ and $\widetilde{w}_c$ are the shear-stress and axial velocity of the the clear fluid (non-porous region liquid). The equations (4.3a)-(4.3c) delineate the conservation of mass (*i.e.*, continuity equation), and momentum equations (*i.e.*, conservation of meomentum) in radial r and axial z directions, respectively. The momentum equation (4.3c) in axial direction replicating the Stokes equation for non-porous (clear fluid) region.

The stress-strain relation for Carreau fluid in terms of clear fluid velocity is given by [18]

$$\widetilde{\tau}_c = \left[\widetilde{\mu}_\infty + (\widetilde{\mu}_0 - \widetilde{\mu}_\infty) \left(1 + \left(\lambda \frac{\partial \widetilde{w}_c}{\partial \widetilde{r}} \right)^2 \right)^{\frac{n-1}{2}} \right] \frac{\partial \widetilde{w}_c}{\partial \widetilde{r}}. \tag{4.3d}$$

4.2.4 Non-Dimensional Parameters and Governing Equations

The non-dimensional variables presented below are used to perform non-dimensionalisation on the aforementioned system of equations: ([3], [18], [7])

$$\begin{aligned} &p = \frac{\widetilde{p}\widetilde{b}}{\widetilde{w}_0 \widetilde{\mu}_0}, \; r = \frac{\widetilde{r}}{\widetilde{b}}, \; z = \frac{\widetilde{z}}{\widetilde{b}}, \; a = \frac{\widetilde{a}}{\widetilde{b}}, \; c = \frac{\widetilde{c}}{\widetilde{b}}, \; S^2 = \frac{1}{k}, \; \widetilde{w}_0 = \frac{\widetilde{q}_0 \widetilde{b}^2}{\widetilde{\mu}_0}, \; \eta = \frac{\widetilde{\mu}_\infty}{\widetilde{\mu}_0}, \\ &w_p = \frac{\widetilde{w}_p}{\widetilde{w}_0}, \; w_c = \frac{\widetilde{w}_c}{\widetilde{w}_0}, \; k = \frac{\widetilde{k}}{\widetilde{b}^2}, \; \tau_p = \frac{\widetilde{\tau}_p \widetilde{b}}{\widetilde{w}_0 \widetilde{\mu}_0}, \; \mathrm{We} = \frac{\lambda \widetilde{w}_0}{\widetilde{b}}, \; \theta = \frac{\widetilde{T} - T_w}{T_m - T_w}, \\ &\mathrm{Nu} = \frac{2q'' \widetilde{b}}{\widetilde{K}(T_w - T_m)}, \end{aligned} \tag{4.4}$$

where $\widetilde{w}_0$ is the average velocity, η is the viscosity ratio parameter, We is the Weissenberg number which is the ratio of elastic forces to the viscous forces (*i.e.* product of the shear rate and characteristic time of the fluid), S is a dimensionless parameter defined in terms of the permeability parameter k, $\widetilde{q}_0$ is the characteristic pressure gradient, Nu is the Nusselt number which is the ratio of convective to conductive heat transfer in a fluid, and θ is the dimentionaless temperature.

4.2.4.1 Hydrodynamic Equations

Using the non-dimensional variables, the governing equations replicating the continuity equation, and momentum equations in radial and axial directions, respetively, for porous ($a \leq r \leq 1$) and non-porous ($1 \leq r \leq c$) fluid flow regions in non-dimensional form are as follows:

Region-I, *i.e.*, $a \leq r \leq 1$

$$\frac{\partial w_p}{\partial z} = 0, \tag{4.5a}$$

$$\frac{\partial p}{\partial r} = 0, \tag{4.5b}$$

$$\frac{\partial p}{\partial z} = \frac{1}{r}\frac{\partial}{\partial r}(r\tau_p) - \frac{w_p}{k}, \tag{4.5c}$$

where the constitutive equation of Carreau fluid in terms of porous medium liquid velocity is given by

$$\tau_p = \left[\eta + (1-\eta)\left(1 + \left(\mathrm{We}\frac{\partial w_p}{\partial r}\right)^2\right)^{\frac{n-1}{2}}\right]\frac{\partial w_p}{\partial r}. \tag{4.5d}$$

Region-II, *i.e.*, $1 \leq r \leq c$

$$\frac{\partial w_c}{\partial z} = 0, \tag{4.6a}$$

$$\frac{\partial p}{\partial r} = 0, \tag{4.6b}$$

$$\frac{\partial p}{\partial z} = \frac{1}{r}\frac{\partial}{\partial r}(r\tau_c), \tag{4.6c}$$

where the constitutive equation of Carreau fluid in terms of clear fluid velocity is given by

$$\tau_c = \left[\eta + (1-\eta)\left(1 + \left(\mathrm{We}\frac{\partial w_c}{\partial r}\right)^2\right)^{\frac{n-1}{2}}\right]\frac{\partial w_c}{\partial r}. \tag{4.6d}$$

4.2.5 Boundary Conditions

In order to obtain the closed form of solutions of the governing equations, the appropriate boundary conditions are required to discuss the fluid flow mechanism through a swarm of porous cylindrical particles. The following dimensionless boundary conditions are considered at the surface of the solid core, fluid-porous interface and hypothetical cell surface:

1. The zero porous layer velocity is considered on the surface of the solid core of the cylinder, *i.e.*,

$$w_p = 0 \quad \text{at} \quad r = a. \tag{4.7a}$$

2. The fluid velocity is assumed to be continuous at the interface of clear fluid (non-porous region fluid) and porous region fluid, *i.e.*,

$$w_p = w_c \quad \text{at} \quad r = 1. \tag{4.7b}$$

3. The usual condition of continuity of shear stress may not be suitable for describing the flow of fluids through the fluid-porous interface. To encounter this inadequacy, Ochoa-Tapia and Whitaker [81] proposed the discontinuous behavior of shear stresses at the interface of clear fluid and porous media, which is referred to as the stress-jump condition along tangential stresses, *i.e.*,

$$\tau_p - \tau_c = \frac{\beta w_p}{\sqrt{k}} \quad \text{at} \quad r = 1, \tag{4.7c}$$

where β is the stress-jump parameter.

4. The Happel, Kuwabara, Kvashnin and Cunningham boundary conditions lead to the following single result [3], *i.e.*,

$$\tau_c = 0 \quad \text{at} \quad r = c. \tag{4.7d}$$

The boundary condition (4.7d) is taken from the work of Deo *et al.* [3], which is Happel's zero stress boundary condition, signifying that the tangential viscous stress vanishes on the cell boundary. The shear stress in the present work is different from Newtonian fluid, but through the perturbation process, it reduces to the zero velocity gradient, *i.e.*, $\frac{dw_c}{dr} = 0$.

4.2.6 Hydrodynamical Quantities and Kozeny Constant

The volumetric flow rate Q_v of fluid flow in non-dimensional form is given by

$$\begin{aligned} Q_v &= 2\pi \int_a^c r w(r) dr, \\ &= 2\pi \left(\int_a^1 r w_p(r) dr + \int_1^c r w_c(r) dr \right). \end{aligned} \tag{4.8}$$

An identical particle from the swarm has been taken into the consideration to analyze the impact of properties of the porous and non-porous material on the membrane permeability. The mathematical expression of the membrane permeability L_{11} is given by [3],

$$L_{11} = -\frac{V_f}{\partial p/\partial z}, \tag{4.9}$$

where V_f denotes the filtration velocity and is reffered by $V_f = \frac{Q_v}{\pi c^2}$.
The classical Kozeny–Karman equation equation that predicts the permeability of a swarm of porous cylinder particles pretty accurately is given as

$$L_{11} = \frac{\varepsilon \rho_h^2}{K_z \tilde{b}^2}, \tag{4.10}$$

where ε is the porosity, K_z is the dimensionless symbolic representation of Kozeny constant, and ρ_h describes the hydraulic radius which is a fractional value of the pore volume and the wetting area.
The Kozeny constant can be written as

$$K_z = \frac{\varepsilon \rho_h^2}{L_{11} \tilde{b}^2}, \tag{4.11}$$

where hydraulic radius for the porous medium composed of porous cylinders is expressed as

$$\rho_h = \frac{\pi(\widetilde{c}^2 - \widetilde{b}^2)}{2\pi\widetilde{b}} = \frac{\widetilde{b}}{2}\left(\frac{1-\gamma}{\gamma}\right) = \frac{\varepsilon\widetilde{b}}{2(1-\varepsilon)}. \tag{4.12}$$

Introducing the expression of hydraulic radius into the expression of the Kozeny constant, the Kozeny constant is obtained as

$$K_z = \frac{\varepsilon^3}{4(1-\varepsilon)^2 L_{11}}, \tag{4.13}$$

where L_{11} is the hydrodynamic permeability of the membrane.

4.3 Solution of the Proposed Problem

The Carreau fluid flow in porous and non-porous regions is governed by the Brinkman and Stokes equations, respectively, which are second-order non-linear equations and is very

difficult to solve analytically. Hence, this work aims to use asymptotic and numerical techniques to solve these governing equations. The double perturbation technique is used to get the asymptotic solution to the problem. The Weissenberg number is used as the first perturbation parameter and is taken to be sufficiently small, while the Darcy number is used as the second perturbation parameter and is held to be sufficiently large to obtain the asymptotic solution to the problem [142]. In MATHEMATICA software 10.3, the NDSolve command is used to solve the governing equations numerically, allowing the darcy number to be as small as possible. The numerical solution of both porous and non-porous regions validates the asymptotic solution ($\mathrm{We} \ll 1, k \gg 1$). A constant pressure gradient continuously propels the fluid in the porous and clear fluid regions, *i.e.*, $\frac{\partial p}{\partial z} = -p_s = \text{constant}$.

4.3.1 Asymptotic Solution of the Problem

In a membrane made up of a swarm of small-radius cylinders at low shear rates, the non-Newtonian characteristics of fluid is quite significant. The stress-strain relation for Carreau fluid with the assumption of low shear rate $\left(\mathrm{We}\frac{\partial w}{\partial r} < 1\right)$ [18] is introduced in the momentum equation for both porous and non-porous region. The expression of the shear stress for porous and non-porous regions can be obtained using the above assumption $\left(\mathrm{We}\frac{\partial w}{\partial r} < 1\right)$ and binomial series expansion upto first order approximation only. The expression of shear stress for Carreau fluid is given by

$$\tau = \left[\eta + (1-\eta)\left(1 + \frac{n-1}{2}\left\{\mathrm{We}\frac{\partial w}{\partial r}\right\}^2\right)\right]\frac{\partial w}{\partial r}.$$

The momentum equations in the axial directions for porous and non-porous liquid regions can be obtained by introducing the expresion of shear stress in the simplified form. The governing equations for the flow of Carreau fluid in porous and clear fluid regions are given by

$$\frac{\partial p}{\partial z} = \frac{1}{r}\frac{\partial}{\partial r}\left(r\left(1 + \frac{(1-\eta)(n-1)\mathrm{We}^2}{2}\left(\frac{\partial w_p}{\partial r}\right)^2\right)\frac{\partial w_p}{\partial r}\right) - \frac{w_p}{k}. \tag{4.14a}$$

$$\frac{\partial p}{\partial z} = \frac{1}{r}\frac{\partial}{\partial r}\left(r\left(1 + \frac{(1-\eta)(n-1)\mathrm{We}^2}{2}\left(\frac{\partial w_c}{\partial r}\right)^2\right)\frac{\partial w_c}{\partial r}\right). \tag{4.14b}$$

The equation (4.14a) and (4.14b) is a second order, non-linear partial differential equation which is complex to solve analytically. So the perturbation method is used to solve these equations analytically. We have to use two level regular perturbation technique in the Weissenberg number and the Darcy number respectively to obtain the series from solution of the

problem. Let us consider a solution of equations (4.14a) and (4.14b) in the series form as [142]

$$w_j(r) = w_j(r;\mathrm{We}) = \sum_{i=0}^{m} \mathrm{We}^{2i} w_{ji}(r), \text{ where } j = p,c. \tag{4.15}$$

Introducing the series form of the porous medium velocity from equation (4.15) into the governing equations (4.14a) and (4.14b), and equating the like powers of the Weissenberg number. The zeroth-order equations are obtained as

$$\frac{\partial p}{\partial z} = \frac{1}{r}\frac{\partial}{\partial r}\left(r\frac{\partial w_{p0}}{\partial r}\right) - \frac{w_{p0}}{k}. \tag{4.16a}$$

$$\frac{\partial p}{\partial z} = \frac{1}{r}\frac{\partial}{\partial r}\left(r\frac{\partial w_{c0}}{\partial r}\right). \tag{4.16b}$$

A series form solution of the equations governing the zeroth order velocity is assumed in the form

$$w_{j0}(r) = w_{j0}(r;S) = \sum_{i=0}^{m} S^i w_{j0i}(r), \text{ where } j = p,c. \tag{4.17}$$

where the non-dimensional parameter $S = \frac{1}{\sqrt{k}}$ in term of the permeability of the porous medium.

Introducing the series form of zeroth order velocities into equations (4.16a) and (4.16b), and equating the like powers of the Darcy number parameter.

$$\frac{\partial p}{\partial z} = \frac{1}{r}\frac{\partial}{\partial r}\left(r\frac{\partial w_{p00}}{\partial r}\right). \tag{4.18a}$$

$$\frac{\partial p}{\partial z} = \frac{1}{r}\frac{\partial}{\partial r}\left(r\frac{\partial w_{c00}}{\partial r}\right). \tag{4.18b}$$

$$\frac{1}{r}\frac{\partial}{\partial r}\left(r\frac{\partial w_{p01}}{\partial r}\right) = 0. \tag{4.18c}$$

$$\frac{1}{r}\frac{\partial}{\partial r}\left(r\frac{\partial w_{c01}}{\partial r}\right) = 0. \tag{4.18d}$$

$$\frac{1}{r}\frac{\partial}{\partial r}\left(r\frac{\partial w_{p02}}{\partial r}\right)-w_{p00}=0. \tag{4.18e}$$

$$\frac{1}{r}\frac{\partial}{\partial r}\left(r\frac{\partial w_{c02}}{\partial r}\right)=0. \tag{4.18f}$$

The equations governing the first order velocities with respect to the Weissenberg number are given as

$$\frac{1}{r}\frac{\partial}{\partial r}\left[r\left(\frac{\partial w_{p1}}{\partial r}+\frac{(n-1)(1-\eta)}{2}\left(-\frac{\partial w_{p0}}{\partial r}\right)^2\frac{\partial w_{p0}}{\partial r}\right)\right]=\frac{w_{p1}}{k}. \tag{4.19}$$

$$\frac{1}{r}\frac{\partial}{\partial r}\left[r\left(\frac{\partial w_{c1}}{\partial r}+\frac{(n-1)(1-\eta)}{2}\left(-\frac{\partial w_{c0}}{\partial r}\right)^2\frac{\partial w_{c0}}{\partial r}\right)\right]=0. \tag{4.20}$$

A series form solution of the equations governing the first order velocities are assumed in the form

$$w_{j1}(r)=w_{j1}(r;S)=\sum_{i=0}^{m}S^i w_{j1i}(r),\ \text{where } j=p,c, \tag{4.21}$$

where $S=\frac{1}{\sqrt{k}}$ is a dimentionless parameter.
Introducing the series form of first order velocity (4.21) into the equations (4.19) and (4.20), and equating the like powers of the Darcy number parameter.

$$\frac{1}{r}\frac{\partial}{\partial r}\left(r\left(\frac{\partial w_{p10}}{\partial r}+\frac{(n-1)(1-\eta)}{2}\left(-\frac{\partial w_{p00}}{\partial r}\right)^2\frac{\partial w_{p00}}{\partial r}\right)\right)=0. \tag{4.22a}$$

$$\frac{1}{r}\frac{\partial}{\partial r}\left(r\left(\frac{\partial w_{c10}}{\partial r}+\frac{(n-1)(1-\eta)}{2}\left(-\frac{\partial w_{c00}}{\partial r}\right)^2\frac{\partial w_{c00}}{\partial r}\right)\right)=0. \tag{4.22b}$$

$$\frac{1}{r}\frac{\partial}{\partial r}\left(r\left(\frac{\partial w_{p11}}{\partial r}+\frac{3(n-1)(1-\eta)}{2}\left(\frac{\partial w_{p00}}{\partial r}\right)^2\frac{\partial w_{p01}}{\partial r}\right)\right)=0. \tag{4.22c}$$

$$\frac{1}{r}\frac{\partial}{\partial r}\left(r\left(\frac{\partial w_{c11}}{\partial r}+\frac{3(n-1)(1-\eta)}{2}\left(\frac{\partial w_{c00}}{\partial r}\right)^2\frac{\partial w_{c01}}{\partial r}\right)\right)=0. \tag{4.22d}$$

$$\frac{1}{r}\frac{\partial}{\partial r}\left(r\left(\frac{\partial w_{p12}}{\partial r}+\frac{3(n-1)(1-\eta)}{2}\left(\frac{\partial w_{p00}}{\partial r}\left(\frac{\partial w_{p01}}{\partial r}\right)^2+\left(\frac{\partial w_{p00}}{\partial r}\right)^2\frac{\partial w_{p02}}{\partial r}\right)\right)\right)-w_{p10}=0. \tag{4.22e}$$

$$\frac{1}{r}\frac{\partial}{\partial r}\left(r\left(\frac{\partial w_{c12}}{\partial r}+\frac{3(n-1)(1-\eta)}{2}\left(\frac{\partial w_{c00}}{\partial r}\left(\frac{\partial w_{c01}}{\partial r}\right)^2+\left(\frac{\partial w_{c00}}{\partial r}\right)^2\frac{\partial w_{c02}}{\partial r}\right)\right)\right)=0. \tag{4.22f}$$

4.3.2 Analytical Expression of Fluid Velocity

The zeroth, first , and second order Darcy number perturbed equations reduced from zeroth order Weissenberg number purturbation can be solved analytically. The general solution of the equations (4.18a)-(4.18f) are obtained as

$$w_{p00}=C_1\log(r)+C_2-\frac{p_s r^2}{4}, \tag{4.23a}$$

$$w_{c00}=C_3\log(r)+C_4-\frac{p_s r^2}{4}, \tag{4.23b}$$

$$w_{p01}=C_5\log(r)+C_6, \tag{4.23c}$$

$$w_{p01}=C_7\log(r)+C_8, \tag{4.23d}$$

$$w_{p02}=\frac{1}{4}r^2(C_2-C_1)+\log(r)\left(\frac{C_1 r^2}{4}+C_9\right)+C_{10}-\frac{p_s r^4}{64}, \tag{4.23e}$$

$$w_{c02}=C_{11}\log(r)+C_{12}, \tag{4.23f}$$

where C_1-C_{12} are arbitrary constants that can be derived from their respective boundary conditions. The exact expressions of these constants are given in the Annexure A.

The zeroth, first, and second order Darcy number perturbed equations reduced from first order Weissenberg number purturbation can be solved analytically. The general solution of

the equations (4.22a)-(4.22f) is given as,

$$w_{p10} = -\frac{(\eta-1)(n-1)\left(16C_1^3 - 12C_1 p_s^2 r^4 + p_s^3 r^6\right)}{64r^2} + C_{13}\log(r) + C_{14}, \tag{4.24a}$$

$$w_{c10} = C_{15}\log(r) + C_{16} - \frac{(\eta-1)(n-1)\left(16C_3^3 - 12C_3 p_s^2 r^4 + p_s^3 r^6\right)}{64r^2}, \tag{4.24b}$$

$$w_{p11} = \frac{3C_5(\eta-1)(n-1)\left(p_s^2 r^4 - 4C_1^2\right)}{16r^2} + C_{17}\log(r) + C_{18}, \tag{4.24c}$$

$$w_{c11} = C_{19}\log(r) + C_{20} + \frac{3C_7(\eta-1)(n-1)\left(p_s^2 r^4 - 4C_3^2\right)}{16r^2}, \tag{4.24d}$$

$$\begin{aligned} w_{p12} = &\frac{1}{64}\log(r)\left(16C_1^3(\eta-1)(n-1)\log(r) + r^2\left(16C_{13} - 3C_1(\eta-1)(n-1)p_s\left(8C_1 - p_s r^2\right)\right)\right. \\ &+64C_{21}) - \frac{(\eta-1)(n-1)}{1152r^2}\left(-54p_s r^4\left(7C_1^2 - 8C_1C_2 + 4C_9 p_s\right) + 864C_1\left(C_1C_9 + C_5^2\right)\right. \\ &\left.\left.-54C_2 p_s^2 r^6 + 5p_s^3 r^8\right) + \frac{1}{4}r^2(C_{14} - C_{13}) + C_{22}, \end{aligned} \tag{4.24e}$$

$$w_{c12} = \frac{3(\eta-1)(n-1)\left(C_{11}p_s^2 r^4 - 4C_3\left(C_{11}C_3 + C_7^2\right)\right)}{16r^2} + C_{23}\log(r) + C_{24}, \tag{4.24f}$$

where $C_{13} - C_{24}$ are arbitrary constants which derived from their respective reduced boundary condition. The exact expressions of these constants are given in the Annexure A.

4.3.3 Numerical Solution of the Problem

The numerical solutions of the governing equations in porous (4.5a)-(4.5d) and non-porous (4.6a)-(4.6d) regions with the appropriate boundary conditions (4.7a)-(4.7d) have been derived using the NDsolve command in MATHEMATICA 10.3. The Darcy number is kept to be small during the analysis and graphical representation.

4.4 Temperature Analysis

In the above section, the velocity of the slow viscous flow of the Carreau fluid through the membrane has been calculated asymptotically and numerically with the appropriate boundary conditions. The velocity will now be used to calculate the radial temperature variation in the porous cylinder with a solid core. The assumptions of homogeneity and local thermal equilibrium are made throughout the analysis. In order to make sure the solution of

the energy equation regulates the heat transfer in porous and non-porous regions, the heat source terms, axial conduction, and thermal dispersion have not been considered [7]. The mathematical expression of the energy equation adopting the above assumptions is given by

$$\widetilde{\rho}\widetilde{c}_p\widetilde{w}\frac{\partial\widetilde{T}}{\partial\widetilde{z}} = \frac{\widetilde{K}}{\widetilde{r}}\frac{\partial}{\partial\widetilde{r}}\left(\widetilde{r}\frac{\partial\widetilde{T}}{\partial\widetilde{r}}\right), \tag{4.25}$$

where $\widetilde{T}$ is the temperature, $\widetilde{\rho}$ is the density of the fluid, $\widetilde{c}_p$ is specific heat at constant pressure, $\widetilde{K}$ is the thermal conductivity, and the temperature gradient in axial direction is taken as

$$\frac{\partial\widetilde{T}}{\partial\widetilde{z}} = \frac{2q''}{\widetilde{\rho}\widetilde{c}_p\widetilde{b}\widetilde{w}_0},$$

where q'' is the wall heat flux.
The bulk mean temperature, denoted by T_m, is determined by the following:

$$T_m = \frac{2}{(\widetilde{c}^2-\widetilde{a}^2)\widetilde{w}_0}\int_{\widetilde{a}}^{\widetilde{c}}\widetilde{w}\widetilde{T}\widetilde{r}d\widetilde{r}.$$

The dimensionless temperature distribution θ, is a function of the radial coordinate $(\widetilde{r})$ solely, as observed by Nield in [187]. However, the local temperature $\widetilde{T}$ varies in axial and radial directions. Although the mean temperature of the bulk is a function of the axial coordinate $(\widetilde{z})$. The transformed energy equation in non-dimensional form is given by

$$\frac{\mathrm{d}^2\theta}{\mathrm{d}r^2} + \frac{1}{r}\frac{\mathrm{d}\theta}{\mathrm{d}r} + w\mathrm{Nu} = 0, \tag{4.26}$$

and the following are the dimensionless boundary conditions:

1. On the outermost layer of the solid core, the temperature is always at the ambient level, *i.e.*,

$$\theta_p = 1 \quad \text{at} \quad r = a. \tag{4.27a}$$

2. The continuity of temperature and temperature gradient are considered at the interface of porous and non-porous regions, *i.e.*,

$$\theta_p = \theta_c \quad \text{at} \quad r = 1, \tag{4.27b}$$

$$\frac{d\theta_p}{dr} = \frac{d\theta_c}{dr} \quad \text{at} \quad r = 1, \tag{4.27c}$$

where the subscriepts p and c repersent the porous and clear fluid (non-porous) regions, respectively.

3. The temperature gradient is taken to be zero on the hypothetical cell, *i.e.*,

$$\frac{d\theta_c}{dr} = 0 \quad \text{at} \quad r = c. \tag{4.27d}$$

4.4.1 Solution of Temperature Equation

The dimensionless temperature equation (4.26) can be solved using their respective velocities for porous and non-porous regions. The exact solutions of temperature in both regions are obtained as

$$\begin{aligned}\theta_p(r) =& \frac{1}{9216}\Big(-288\mathrm{Nu}r^2\left(3C_1^3(\eta-1)(n-1)S^2\mathrm{We}^2 - 8C_1 + 8\left(S(C_{10}S - C_5 + C_6 - C_9S)\right.\right.\\ &+\mathrm{We}^2(-C_{13}+C_{14}+S(-C_{17}+C_{18}-C_{21}S+C_{22}S))+C_2\Big)\Big) - 576C_1(\eta-1)(n-1)\\ &\times\mathrm{NuWe}^2\log^2(r)\left(C_1^2\left(r^2S^2-2\right) - 6C_1S(C_5+C_9S) - 6C_5^2S^2\right) - 12\mathrm{Nu}r^2\log(r)\times\\ &\left(-96C_1^3(\eta-1)(n-1)S^2\mathrm{We}^2 - 18C_1^2(\eta-1)(n-1)p_sr^2S^2\mathrm{We}^2 + C_1\left(r^2S^2\left((\eta-1)\right.\right.\right.\\ &\left.\left.\times(n-1)p_s^2r^2\mathrm{We}^2+12\right)+192\right) + 12\mathrm{We}^2\left(C_{13}\left(r^2S^2+16\right)+16S(C_{17}+C_{21}S)\right)\\ &+192S(C_5+C_9S)) - 9\mathrm{Nu}r^4\left(-8S^2\left(3C_1+\mathrm{We}^2(3C_{13}-2C_{14})-2C_2\right)+p_s\left(3C_1\times\right.\right.\\ &(\eta-1)(n-1)S^2\mathrm{We}^2(11C_1-8C_2)-16\Big) + 12(\eta-1)(n-1)p_s^2\mathrm{We}^2(S(C_5+C_9S)\\ &+C_1)) + 4\mathrm{Nu}p_sr^6\left(S^2\left((\eta-1)(n-1)p_s\mathrm{We}^2(C_1-3C_2)+1\right)+(\eta-1)(n-1)p_s^2\mathrm{We}^2\right)\\ &+\frac{5}{8}(\eta-1)(n-1)\mathrm{Nu}p_s^3r^8S^2\mathrm{We}^2 + 9216T_{12}\log(r)\Big) + T_{11},\end{aligned} \tag{4.28a}$$

$$\begin{aligned}\theta_c(r) =& \frac{\mathrm{Nu}r^2}{2304}\left(576\left(S(C_{11}S-C_{12}S+C_7-C_8)+\mathrm{We}^2(C_{15}-C_{16}+S(C_{19}-C_{20}+C_{23}S-C_{24}S))\right)\right.\\ &-27(\eta-1)(n-1)p_s^2r^2S\mathrm{We}^2(C_{11}S+C_7) + 9C_3\left(3p_s^2r^2\mathrm{We}^2(\eta-\eta n+n-1)+64\right)\\ &-576C_4 + (\eta-1)(n-1)p_s^3r^4\mathrm{We}^2 + 36p_sr^2\Big) + \frac{1}{8}\log(r)\left(-2\mathrm{Nu}r^2\left(S(C_{11}S+C_7)\right.\right.\\ &+\mathrm{We}^2(C_{15}+S(C_{19}+C_{23}S))+C_3\Big) + C_3(\eta-1)(n-1)\mathrm{NuWe}^2\log(r)\left(3C_3S(C_{11}S\right.\\ &\left.\left.+C_7)+C_3^2+3C_7^2S^2\right)+8T_{13}\Big)+T_{14},\end{aligned} \tag{4.28b}$$

where T_{11}, T_{12}, T_{13}, and T_{14} are arbitrary constants which can be obtained from boundary conditions given in equations (4.27a)-(4.27d). The exact expressions of the above constants are given in Annexure B.

4.5 Results and Discussion

The theoretical model of non-Newtonian Carreau fluid flowing through membranes consisting of a swarm of porous cylindrical particles has been investigated in the present work. The configuration of the flow rheology includes a solid cylindrical core enfolded by a porous layer confined in a cylindrical cell. The non-Newtonian characteristic of Carreau fluid, delineating the shear thinning and thickening behaviour of the liquid, is governed by the nonlinear equations regulating the non-Newtonian fluid flow through porous and non-porous regions. The Brinkman equation governs fluid flow in the annular porous cylindrical region, whereas the Stokes equation regulates the flow in the non-porous region. Due to the presence of a nonlinear velocity gradient term in the stress-strain relationship of Carreau fluid, it is challenging to cope with the analytical treatment of governing equations of Carreau fluid through porous and non-porous media. To tide over this complication, the perturbation series expansion approach involving the Wissenberg number $(\mathrm{We} \ll 1)$ and a non-dimensional quantity $(S \ll 1)$ in case of the highly permeable porous medium is utilised to obtain the solution of the Brinkman equation regulating the flow of viscoelastic fluid in the porous region. The Stokes equation governing the non-porous region is solved using the asymptotic series expansion method on the Weissenberg number $(\mathrm{We} \ll 1)$. In order to derive the solution of the Brinkman equation for the case of small permeability of the porous material, the analytical treatment of singularly perturbed Brinkman equation with appropriate boundary conditions is not feasible due to the presence of boundary layer along with a nonlinear stress-strain relationship. The numerical scheme (NDSolve in Mathematica) for the boundary value problems (BVPs) is used to demonstrate the results in the form of graphical analysis and compared with previously published works which is in good agreement with the present study. The impact of numerous parameters like Wissenberg number, particle volume fraction, stress-jump parameter, viscosity ratio parameter, and Power-law index on the membrane permeability, Kozeny constant and temperature profile are discussed in detail. The solution obtained through the asymptotic series expansion for large permeability is validated with the numerical solution obtained through NDSolve in Mathematica.

4.5.1 Parameter Selection

Most of the parameters used in this analysis were taken from previously published works. The numerous parameters used in this study have been presented in the tabular form (4.1) with their respective references to make the results and graphical analysis more visible to the readers.

Range of Parameters		
Parameters	Range	Sources
Weissenberg number We	0-0.8	[6]
Steady pressure gradient p_s	1-10	[5], [4]
Power-law index n	0.1-2.0	[16], [17]
Permeability k	$(0,\infty)$	[2], [3]
Nusselt number Nu	2.0-8.0	[7]
Stess-jump parameter β	$(-1,1)$	[3], [147], [5]
Viscosity ratio parameter η	0.1-0.4	[18]
Particle volume fraction γ	0.1-1.0	[3], [11]

Table 4.1: Domain of interest for the ongoing parameters with their references

4.5.2 Deduction of Special Cases

1. **Carreau Fluid through a Swarm of Fully Solid Cylinders**
   If the permeability of the porous medium (Darcy number) approaches infinity ($k \to \infty$) for a large Darcy number, then the annular porous layer disappears, and the particle reduces to the solid cylinder. The membrane permeability of the Carreau fluid flow through a swarm of solid cylinders is expressed as

$$L_{11} = \frac{1}{\gamma^3}(\gamma(0.0045 - 0.25\gamma)\log(\gamma) - 0.125375\gamma^4 + 0.50225\gamma^3 - 0.38175\gamma^2 + 0.00375\gamma + 0.001125). \tag{4.29}$$

2. **Newtonian Fluid Flow through a Swarm of Fully Solid Cylinders**
   The current study of a flow through a swarm of solid cylinders surrounded by a porous layer of the thickness $(1-l)$ can also be reduced to a fully solid cylinder by approaching the radius of the solid cylinder to fluid-porous interface ($l \to 1$). This can be further reduced to the Newtonian fluid model by approaching either the Power-law index or the viscosity ratio parameter to 1 ($n \to 1, \eta \to 1$) or vanishing the Weissenberg number ($\mathrm{We} \to 0$). The hydrodynamic permeability of the NF flow through a swarm of solid cylinders is expressed as (Happel's cell model) [71]

$$L_{11} = \frac{-0.125\gamma^2 + 0.5\gamma - 0.25\log(\gamma) - 0.375}{\gamma}, \tag{4.30}$$

which is precisely converges to the study of Deo *et al.* [3].

4.5.3 Graphical Analysis

The visual observations of the fluid velocity profile, the hydrodynamic permeability of the membrane, the Kozeny constant, and the temperature have been discussed in terms of asymptotic and numerical analyses using various porous mediums and the Carreau fluid rheological parameters.

4.5.3.1 Asymptotic Analysis

The effect of the Carreau fluid parameters on the radially increasing velocity profile is depicted in Figure 4.3. It is observed from Figure 4.3a that rising Weissenberg number We leads to an enhancement in velocity, which is more significant in the porous region. This can be interpreted as the rising elastic forces compared to viscous forces leading to slightly higher fluid velocity. Figure 4.3b reveals that growth in the Power-law index parameter leads to a decay in the fluid velocity. In other words, as the fluid rheology deviates from shear-thinning to shear-thickening, the fluid velocity decays.

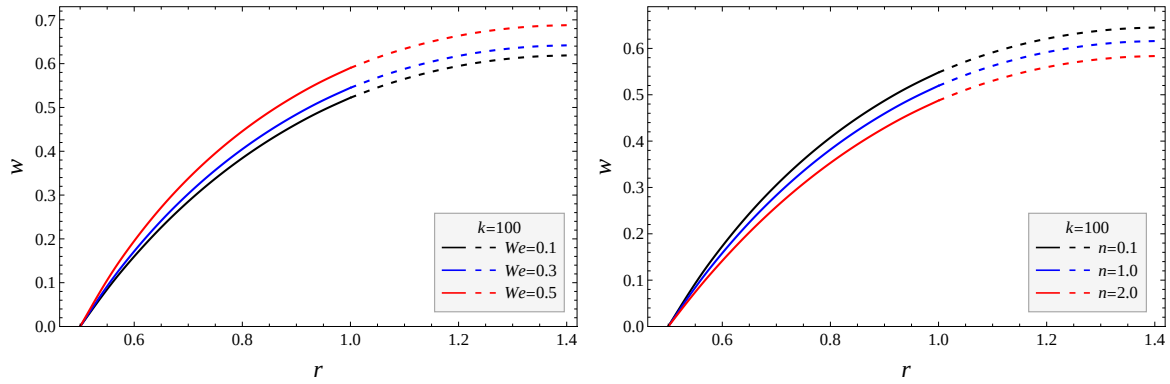

(a) **(b)**

Figure 4.3: The velocity profile w depending upon the radial distance r with varying **(a)** Weissenberg number We $(n = 0.2, \eta = 0.1)$, **(b)** Power-law index n $(\eta = 0.1, \mathrm{We} = 0.3)$. $(\gamma = 0.5, \beta = 0.4, S = 0.1, p_s = 1)$

Figures (4.4-4.6) contain a detailed discussion of the hydrodynamic permeability as it varies with particle volume fraction, stress-jump parameter, and pressure gradient. The viscoelastic effect on the hydrodynamic permeability is almost negligible at higher particle volume fractions γ; however, for low particle volume fractions, this effect is visible, where we can see a relatively significant increase in the membrane's hydrodynamic permeability L_{11} with increasing Weissenberg number We (increasing dominance of elastic forces

over viscous forces) (Figure 4.4a). As the fluid rheology deviates from shear-thinning to shear thickening, the hydrodynamic permeability significantly reduces at low particle volume fraction (Figure 4.4b). This indicates that the fluid rheology significantly affects the swarm's hydrodynamic permeability L_{11}. Figure 4.4c depicts the influence of the viscosity ratio parameter η on hydrodynamic permeability, which states that the lower the decay in the fluid's dynamic viscosity as it deviates from zero shear rates to infinite shear rate, the lower will be the value of L_{11}. Further, it is observed a slightly higher decay rate for the hydrodynamic permeability L_{11} with the particle volume fraction for large viscosity ratio parameter η, which signifies that the particle volume fraction will play a relatively more significant role in exhibiting reduced decay of dynamic viscosity with shear rate.

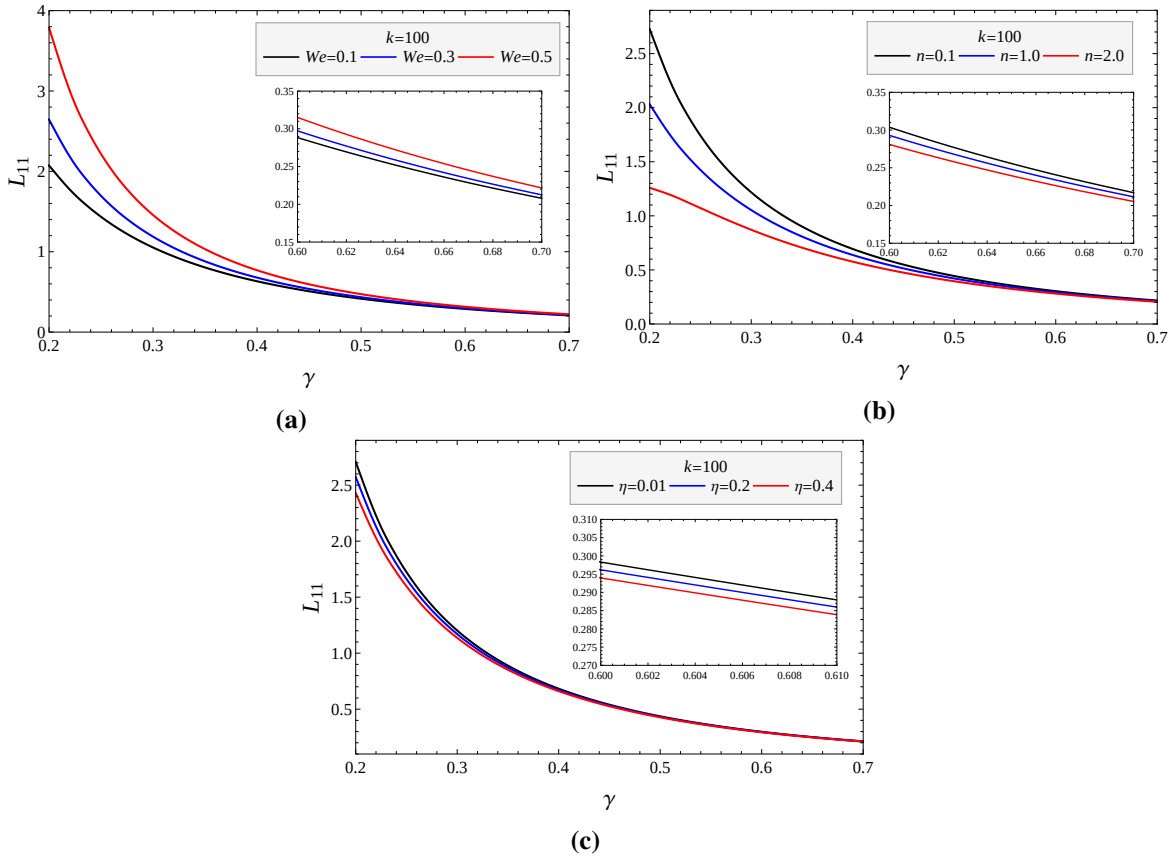

Figure 4.4: The hydrodynamic permeability L_{11} depending upon particle volume fraction γ with varying **(a)** Weissenberg number We $(\beta = 0.1, n = 0.1, \eta = 0.1)$ **(b)** Power-law index n $(\beta = 0.4, \mathrm{We} = 0.3, \eta = 0.1)$, and **(c)** viscosity ratio parameter η $(n = 0.1, \mathrm{We} = 0.3, \beta = 0.1)$. $(S = 0.1, p_s = 1)$

The influence of the parameter β on the membrane permeability L_{11} with varying Carreau fluid parameters is depicted in Figure 4.5. The increasing behaviour of the hydrodynamic permeability with a rising stress-jump coefficient can be seen in Figure 4.5a, where an increment in the L_{11} can be observed with the increasing viscoelasticity of the fluid. In

Figure 4.5b, a decline is observed in the hydrodynamic permeability with increasing Power-law index n, or we can conclude that the hydrodynamic permeability decreases if we deviate the nature of fluid from shear-thinning to shear thickening. A slightly higher growth rate of the hydrodynamic permeability L_{11} with stress-jump parameter β is reported for shear-thinning fluid. A slight decay in the hydrodynamic permeability L_{11} with the increasing viscosity ratio parameter η is reported in Figure 4.5c as the flow is entirely regulated by the pressure, it is interesting to observe that the effect of pressure gradient on the hydrodynamic permeability.

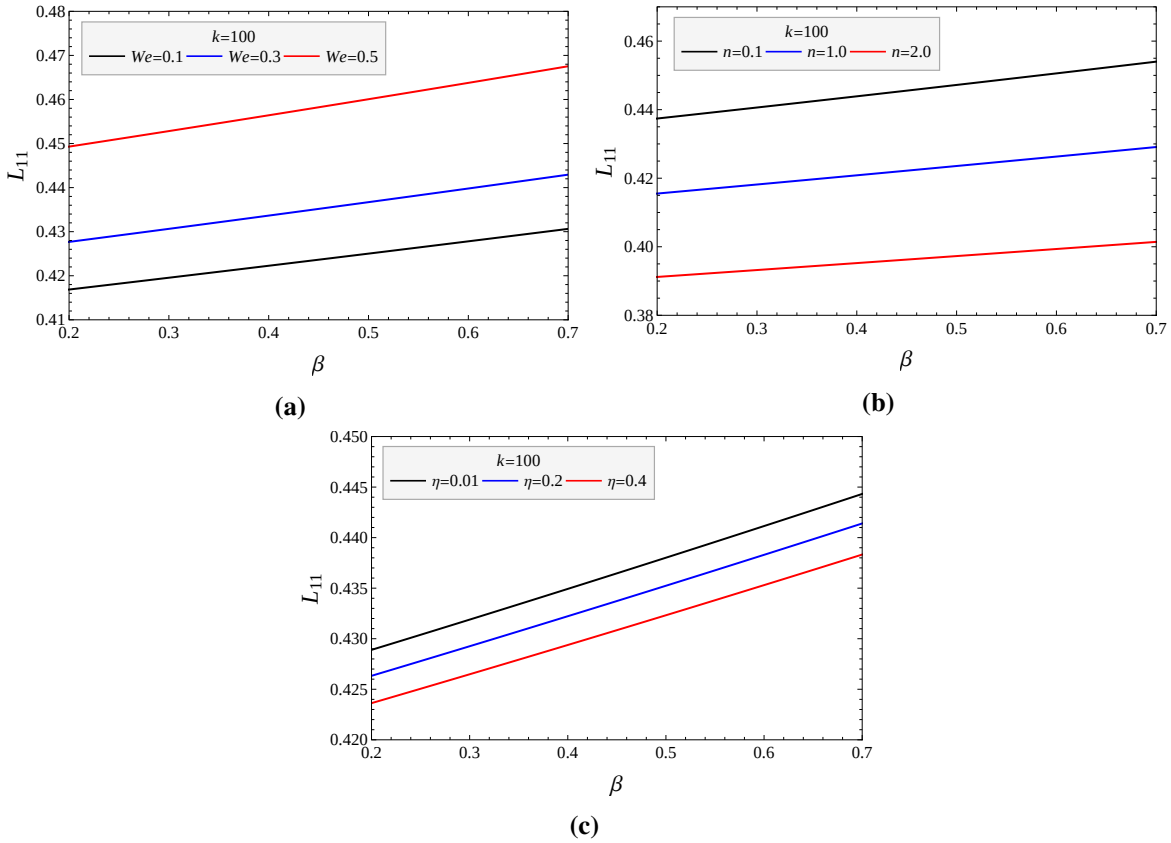

Figure 4.5: The hydrodynamic permeability L_{11} depending upon stress-jump parameter β with varying **(a)** Weissenberg number We $(\gamma = 0.5, n = 0.5, \eta = 0.1)$ and **(b)** Power-law index n $(\gamma = 0.5, \mathrm{We} = 0.3, \eta = 0.1)$, and **(c)** viscosity ratio parameter η $(n = 0.5, \mathrm{We} = 0.3, \gamma = 0.5)$. $(S = 0.1, p_s = 1)$

The increased pressure gradient increases the velocity of the fluid and thus the flow rate, which increases the hydrodynamic permeability, as evident in Figure 4.6a. The dominance of elastic forces leads to a pressure gradient significantly affecting the hydrodynamic permeability of the membrane. The membrane's permeability changes its behaviour and is reduced with increasing pressure gradient when the rheology of fluid shifts from shear thinning to shear thickening (Figure 4.6b).

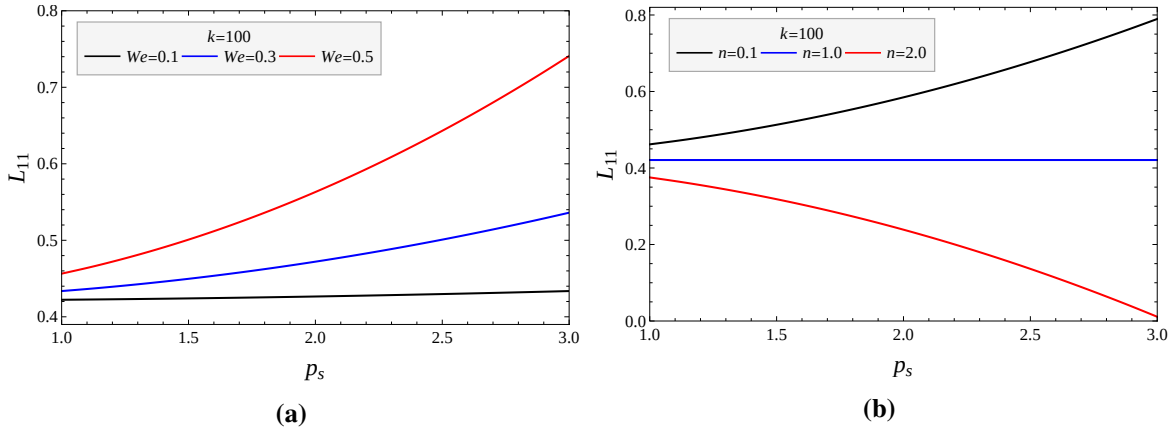

Figure 4.6: The hydrodynamic permeability L_{11} depending upon pressure gradient p_s with varying **(a)** Weissenberg number We $(\gamma = 0.5, n = 0.5, \eta = 0.1)$, and **(b)** Power-law index n $(\gamma = 0.5, \text{We} = 0.4, \eta = 0.1)$. $(S = 0.1, \beta = 0.4)$

The Kozeny constant K_z incorporates the impacts of the flow path (*i.e.*, tortuosity), particle form, and their interactions, and it can be considered directly proportional to tortuosity (Ozgumus *et al.* [181]). So, it will be interesting to see how fluid rheological parameters affect the tortuosity through K_z. Figure 4.7 depicts the behaviour of tortuosity concerning the porosity of the membrane for different parameters. The plot of K_z with the porosity ε of the membrane reveals that increasing porosity contributes to an enhancement in K_z. According to Figure 4.7a, K_z reduces with increasing value of the viscoelastic parameter We, and these variations in the Kozeny constant with the fluid's rheological parameters are more significant for the medium of high porosity. The deviation of fluid's nature from shear thinning to shear thickening or increasing Power-law parameter n enhances the Kozeny constant K_z (Figure 4.7b). The increasing viscosity ratio parameter η causes an increase in the Kozeny constant, indicating an increase in the system's tortuosity for an increasing η (Figure 4.7c).

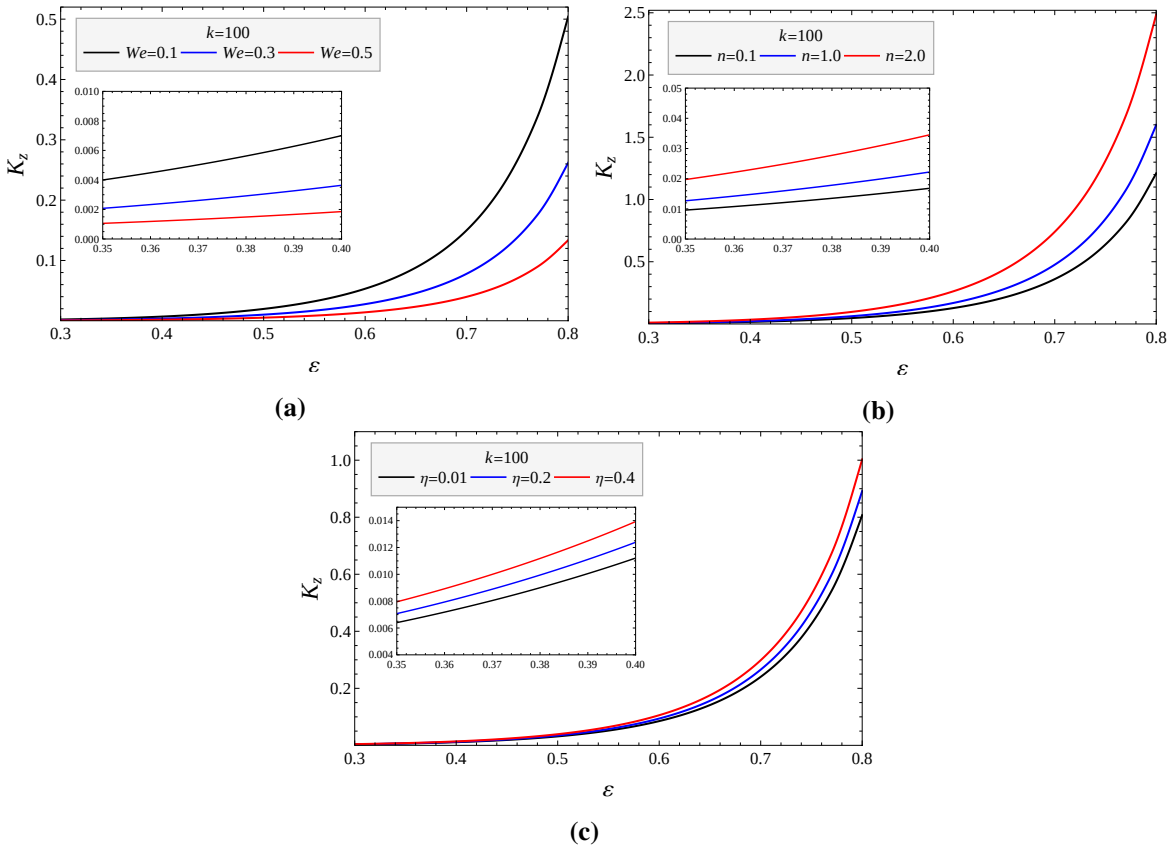

Figure 4.7: The Kozeny constant K_z depending upon the porosity ε with varying **(a)** Weissenberg number We $(\gamma = 0.1, n = 0.1, \eta = 0.1)$ and **(b)** Power-law index n $(\gamma = 0.2, \mathrm{We} = 0.3, \eta = 0.1)$, and **(c)** viscosity ratio parameter η $(n = 0.1, \mathrm{We} = 0.5, \beta = 0.1)$. $(S = 0.1, p_s = 1, \beta = 0.1)$

Figure 4.8 displays the Kozeny constant variation with the stress-jump parameter β, where the increasing stress-jump parameter leads to decay in the Kozeny constant. The Kozeny constant declines as the Carreau fluid's viscoelastic effect grows in terms of the Weissenberg number We (Figure 4.8a). Further, a slightly higher decay rate in K_z with parameter β is observed with increasing the Weissenberg number We. An increase in tortuosity of the porous material is observed in Figure 4.8b as the fluid rheology shift towards the shear-thickening nature. The behaviour of tortuosity for the viscosity ratio parameter is similar to that of the Power-law index. However, it has a lesser effect in this case (Figure 4.8c).

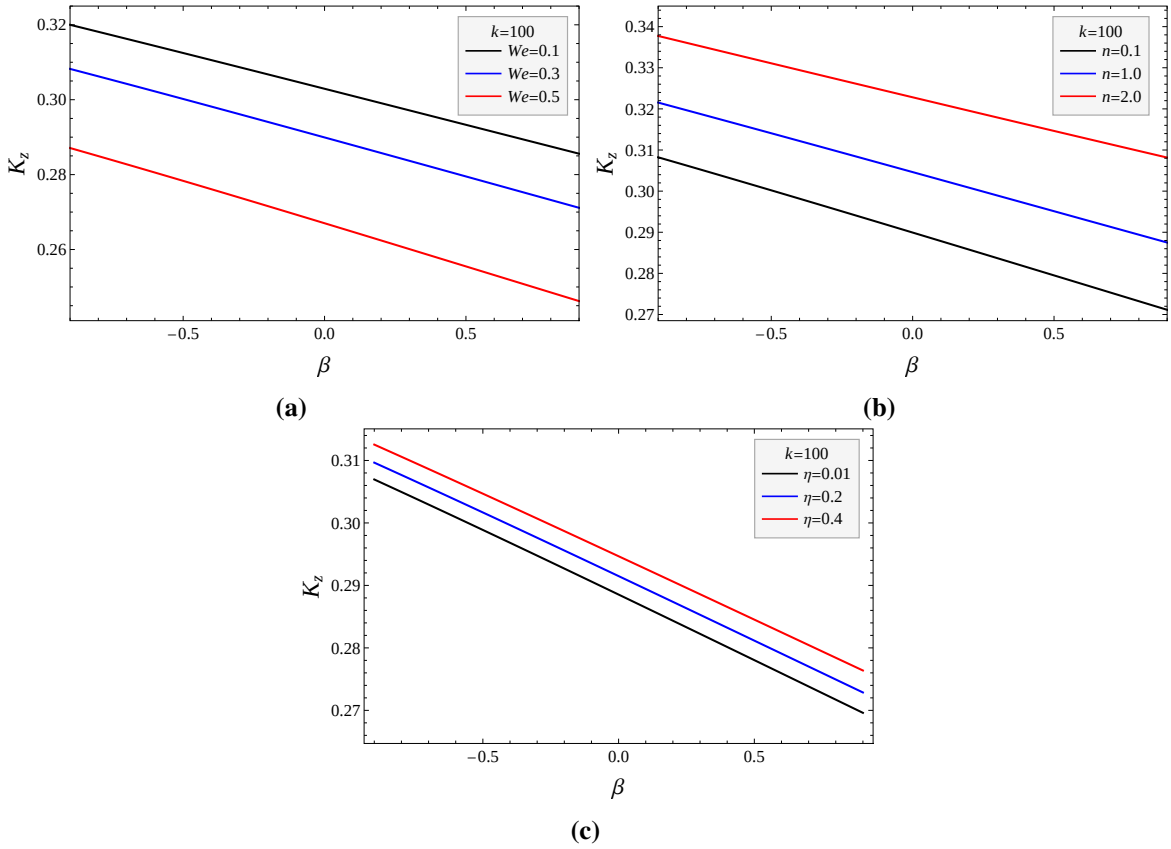

Figure 4.8: The Kozeny constant K_z depending upon the stress-jump parameter β with varying **(a)** Weissenberg number We $(n = 0.1, \eta = 0.1)$ and **(b)** Power-law index n (We $= 0.3, \eta = 0.1$), and **(c)** viscosity ratio parameter η $(n = 0.1, \text{We} = 0.3)$. $(S = 0.1, p_s = 1, \gamma = 0.5, \varepsilon = 0.5)$

Variation of temperature in the porous and non-porous region and its dependence on fluid rheology has been discussed in Figures 4.9, 4.10 , and 4.11. It is observed that the temperature variation follows a parabolic profile and increases along the radial direction as we approach the hypothetical cell. For large permeability rising Nusselt number Nu leads to growth in temperature, signifying that the temperature rises as the flow is dominated by convection (Figure 4.9a). Further, a deviation from shear thinning to shear thickening behaviour (increasing n) of fluid leads to a significant decay in temperature (Figure 4.9b). Figure 4.10a shows that the temperature profile rises as the Weissenberg number rises, implying that the increasing dominance of elastic forces causes an increase in the fluid's temperature, with the effect being more pronounced in the non-porous region. Figure 4.10b interprets the temperature decrease caused by a lesser decline in dynamic viscosity with increasing shear rate (increasing η). The stress-jump parameter involved in the temperature equation through velocity of the Carreau fluid. The effect of stress jump parameter for large permeability of

the porous material on temperature profile through velocity of the Carreau fluid is demonstrated in (Figure 4.11). Although the temperature and its gradient follows continuity at the fluid porous interface, the effect of the stress jump parameter beta on thermal profile comes through the convective term present in the temperature equation (4.25). An increased stress jump at the interface between porous and non-porous regions results in temperature growth.

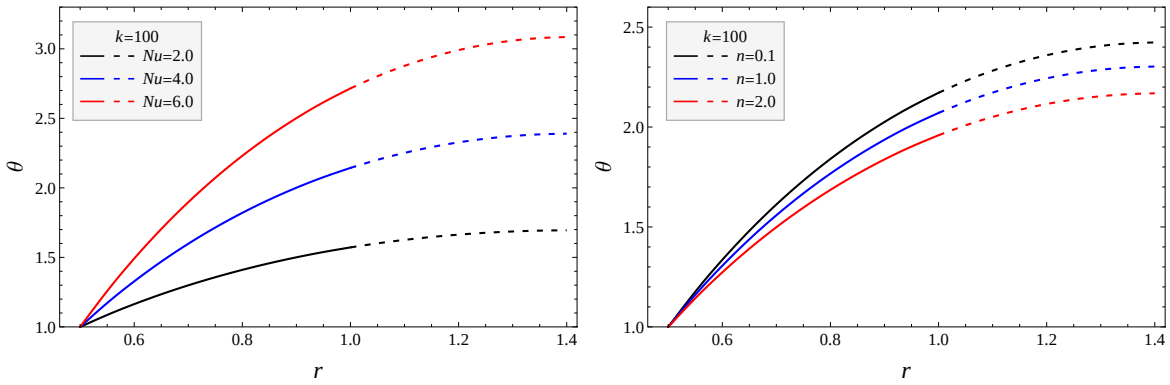

(a) **(b)**

Figure 4.9: Variation of temperature θ with radial distance r for different values of **(a)** Nusselt number Nu $(n=\eta=0.1, \mathrm{We}=0.4, \beta=0.1, \gamma=0.53)$ and **(b)** Power-law index n $(\eta=0.1, \mathrm{We}=0.4, \beta=0.4, \gamma=0.5, \mathrm{Nu}=4.0)$. $(S=0.1, p_s=1)$

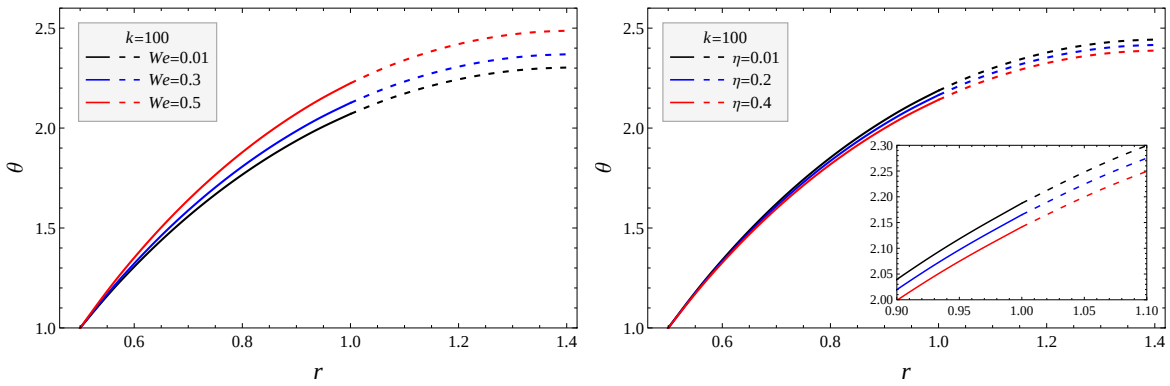

(a) **(b)**

Figure 4.10: Variation of temperature θ with radial distance r for different values of **(a)** Weissenberg number We $(n=0.2, \eta=0.01)$ and **(b)** viscosity ratio parameter η $(\mathrm{We}=0.4, n=0.05)$. $(\gamma=0.5, S=0.1, p_s=1, \mathrm{Nu}=4, \beta=0.4)$

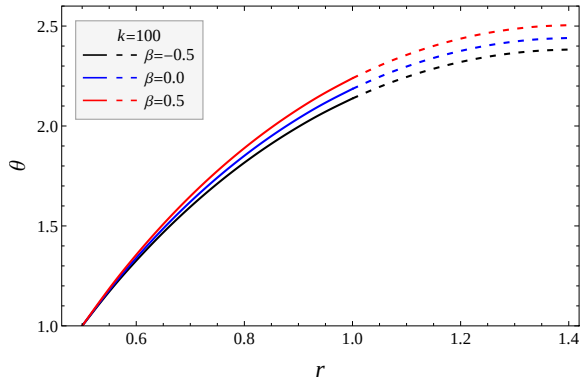

Figure 4.11: Variation of temperature θ with radial distance r for different values of **(a)** Weissenberg number We $(n = 0.2, \eta = 0.01)$ and **(b)** viscosity ratio parameter η $(\text{We} = 0.4, n = 0.05)$. $(\gamma = 0.5, S = 0.1, p_s = 1, \text{Nu} = 4, \beta = 0.4)$

4.5.3.2 Numerical Analysis

In order to discuss the flow of viscoelastic fluid through the membrane for the case of low permeability, the governing equations are solved numerically using the NDSolve in MATHEMATICA software 10.3. The graphical analysis examines the effect of Carreau fluid and porous medium parameters on velocity, hydrodynamic permeability, Kozeny constant and temperature. Figure 4.12 shows that the fluid velocity increases with radial distance in both porous and non-porous regions. At the same time, the non-smoothness at the fluid-porous interface is observed due to the boundary condition of Ochoa-Tapia and Whitaker at the interface. Figure 4.12a shows that for the shear-thickening fluid, a reduction in the fluid velocity is reported with the Weissenberg number, indicating that velocity decreases due to the increasing dominance of elastic forces over inertial forces.For reduced decay of dynamic viscosity with shear rate (η increases), the fluid velocity increases and assumes the most significant value for Newtonian fluid (Figure 4.12b).

Figures 4.13 illustrates the reliance of the hydrodynamic permeability L_{11} on the fluid's rheological parameters and the particle volume fraction γ of the membrane built up by porous cylindrical particles. The value of L_{11} declines as the cylindrical particles of the swarm occupies more space in the system's volume (γ increases). One can observe the gain in hydrodynamic permeability L_{11} as the dominance of elastic forces over the viscous forces increases. This effect is more substantial for lower values of particle volume fraction γ but is almost negligible for more significant particle volume fraction ($\gamma > 0.4$).

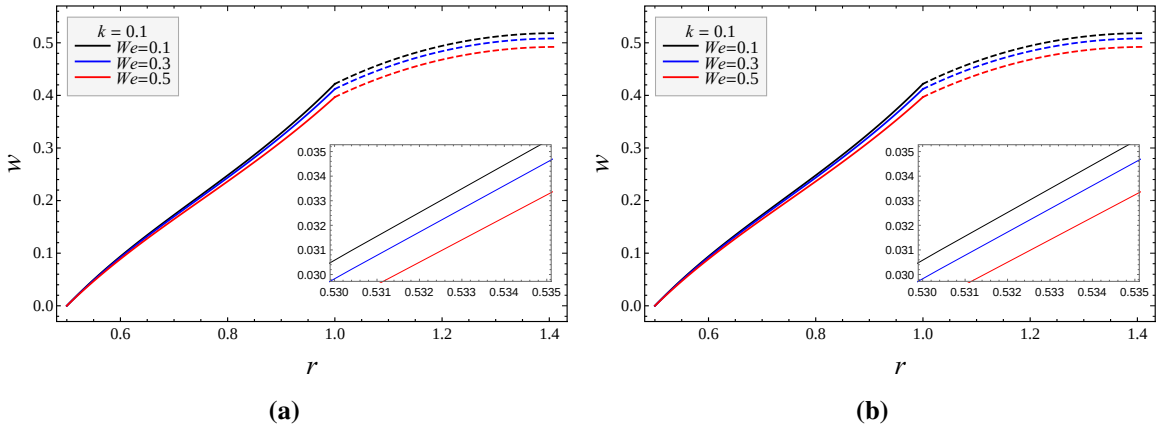

Figure 4.12: The velocity profile w depending upon the radial distance r with varying **(a)** Weissenberg number We $(n=2,\eta=0.1,\beta=0.4)$ and **(b)** viscosity ratio parameter η $(n=2,\text{We}=0.3,\beta=0.45)$. $(\gamma=0.5,S=100,p_s=1)$

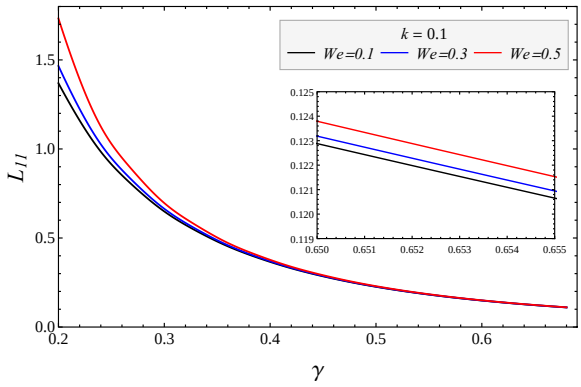

Figure 4.13: The hydrodynamic permeability L_{11} depending upon particle volume fraction γ with varying Weissenberg number We $(\beta=0.1,n=0.1,\eta=0.1)$. $(S=100,p_s=1)$

The hydrodynamic permeability L_{11} increases with the parameter β, and its rate of increase enhances with the stress jump parameter β. (Figure 4.14) reveals a more substantial impact of the stress jump parameter on the hydrodynamic permeability for shear-thinning fluids. Also, like the case of large permeability here, L_{11} increases with β. Figures 4.15 and 4.16 depict the dependence of the Kozeny constant on the porosity and the stress-jump parameter, respectively. It can analyze the impact of these parameters on the tortuosity, particle form, and their interactions.

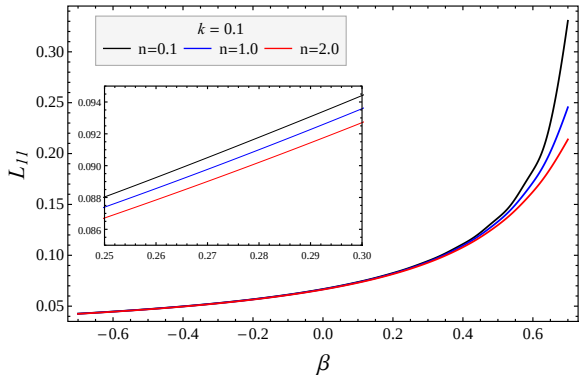

Figure 4.14: The hydrodynamic permeability L_{11} depending upon stress-jump parameter β with varying Power law index n ($\gamma = 0.8, \mathrm{We} = 0.5, \eta = 0.1$). ($S = 100, p_s = 1$)

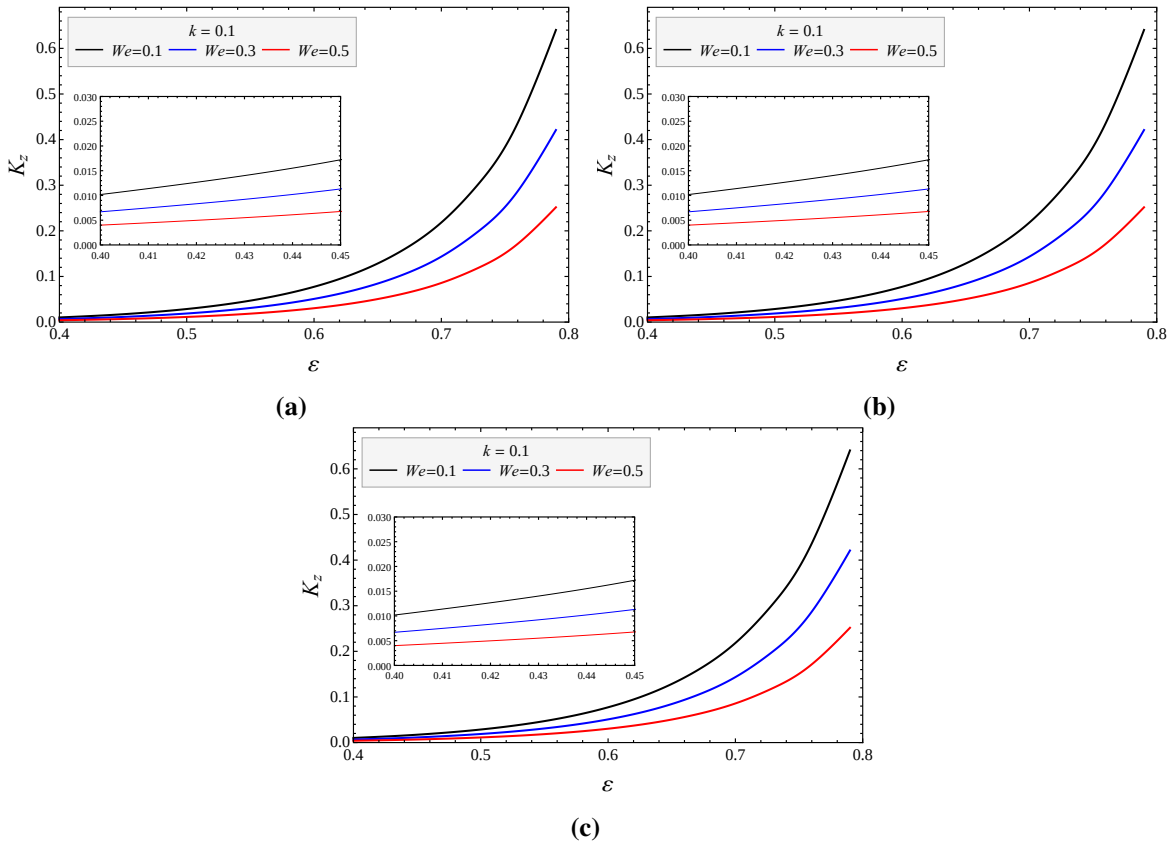

Figure 4.15: The Kozeny constant K_z depending upon the porosity ε with varying **(a)** Weissenberg number We ($n = 0.1, \eta = 0.1, \gamma = 0.1$) and **(b)** Power-law index n ($\mathrm{We} = 0.5, \eta = 0.1, \gamma = 0.2$), and **(c)** viscosity ratio parameter η ($\mathrm{We} = 0.5, n = 0.1, \gamma = 0.2$). ($S = 100, p_s = 1, \beta = 0.1$)

An increase in the membrane's porosity leads to a rise in the Kozeny constant, similar to the case of large permeability. For large porosity, a significant decay in the Kozeny constant can be observed for the increasing visco-elasticity of the fluid (Figures 4.15a). At the same time, it is almost negligible for low porosity (the inset of the cited figure shows

the variation at the third decimal place), which indicates that increasing dominance of the viscoelastic effect leads to decay in the Kozeny constant for flow through a medium with high porosity. Growth in the Kozeny constant can be seen for the increased Power-law index and viscosity ratio parameter in Figures 4.15b and 4.15c, respectively, which defines the tortuosity growth concerning these parameters. A decay in the Kozeny constant with rising stress jump parameter β can be seen in figure 4.16, where the decay rate is dependent on the fluid rheology, making it maximum for shear-thinning fluids.

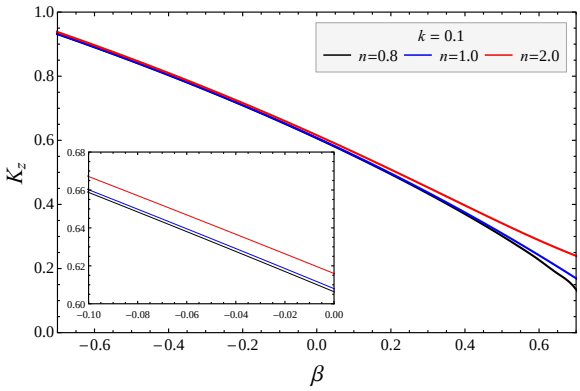

Figure 4.16: The Kozeny constant K_z depending upon the stress-jump parameter β with varying Power law index n (We $= 0.5, \eta = 0.1$). ($S = 100, p_s = 1, \gamma = 0.5, \varepsilon = 0.5$)

The effect of the properties of the porous layer materials and fluid's rheological parameters on the temperature is discussed in figures 4.17 - 4.18. The temperature increases in the flow as we move towards the hypothetical cell, which agrees with the case of large permeability. However, the growth rate in a clear fluid medium is less significant than in the porous layer. The enhancement of heat transfer by convection over conduction (increasing Nu) leads to an increase in the resulting temperature profile (Figure 4.17a). Suppose we enhance the non-Newtonian characteristics of the shear-thinning fluid by increasing the Weissenberg number. In that case, it results in the reduction of the temperature of the fluid (Figure 4.17b). A slight increase in the fluid's temperature profile with the viscosity ratio parameter can be observed in Figure 4.18a. An interesting observation from Figure 4.18b is that the stress jump significantly impacts the temperature profile where the temperature profile's growth rate is higher for positive values of stress jump parameter.

Tables 2a and 2b compare the effect of the permeability k on the Kozeny constant and the hydrodynamic permeability of a membrane composed of a swarm of porous cylindrical particles for different values of Weissenberg number and Power-law index. The hydrodynamic permeability increases with the permeability k, and its variation is more effective for small Darcy numbers than large k. Growth in the hydrodynamic permeability with the increasing viscoelasticity of the Carreau fluid can be seen in Table 2a. Further, L_{11} decays as the

$k \downarrow$	hydrodynamic permeability (L_{11})					
	We $= 0.1$	We $= 0.3$	We $= 0.4$	$n = 0.1$	$n = 1.0$	$n = 2.0$
$k = 0.01$	0.077938	0.078182	0.078399	0.078182	0.077908	0.077612
$k = 0.1$	0.225969	0.227166	0.228217	0.227166	0.225819	0.224368
$k = 1.0$	0.391851	0.406832	0.421302	0.406832	0.390087	0.375446
$k = 2.0$	0.407250	0.425671	0.444007	0.425671	0.405117	0.387867
$k = 3.0$	0.411903	0.431537	0.451297	0.431537	0.409642	0.391525
$k = 4.0$	0.413956	0.434169	0.454623	0.434169	0.411636	0.393116
$k = 5.0$	0.415035	0.435570	0.456416	0.435570	0.412681	0.393940
$k = 7.0$	0.416041	0.436902	0.458151	0.436902	0.413654	0.394694
$k = 10.0$	0.416540	0.437595	0.459085	0.437595	0.414134	0.395050

(a)

$k \downarrow$	Kozeny constant (K_z)					
	We $= 0.1$	We $= 0.3$	We $= 0.5$	$n = 0.1$	$n = 1.0$	$n = 2.0$
$k = 0.01$	1.603850	1.598830	1.588670	1.603850	1.604460	1.605160
$k = 0.1$	0.553174	0.550257	0.544497	0.553174	0.553540	0.553946
$k = 1.0$	0.318998	0.307252	0.282853	0.318998	0.320441	0.322011
$k = 2.0$	0.306937	0.293654	0.265339	0.306937	0.308553	0.310305
$k = 3.0$	0.303470	0.2896630	0.259931	0.303470	0.305144	0.306957
$k = 4.0$	0.301964	0.287906	0.257479	0.301964	0.303666	0.305508
$k = 5.0$	0.301180	0.286980	0.256153	0.301180	0.302897	0.304755
$k = 7.0$	0.300451	0.286105	0.254857	0.300451	0.302185	0.304059
$k = 10.0$	0.300091	0.285653	0.254134	0.300091	0.301834	0.303719

(b)

Table 4.2: Variation of Permeability k on **(a)** the membrane permeability L_{11} and **(b)** Kozeny constant K_z of the porous medium under different values of Weissenberg number We, and Power-law index n. $(l = \varepsilon = 0.5, \gamma = 0.5, p_s = 1, \beta = 0.1, \eta = 0.1)$

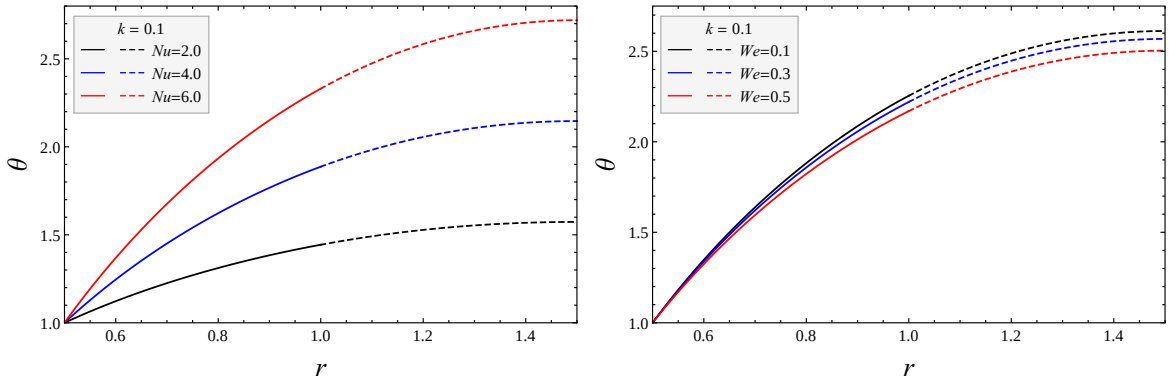

Figure 4.17: Variation of temperature (θ) with radial distance (r) for different values of **(a)** Nusselt number Nu ($n = 0.1, \eta = 0.1, \beta = 0.1, \text{We} = 0.5$) and **(b)** Weissenberg number We ($\eta = 0.1, n = 2, \beta = 0.4, \text{Nu} = 4.0$). ($\gamma = 0.444, S = 100, p_s = 1$)

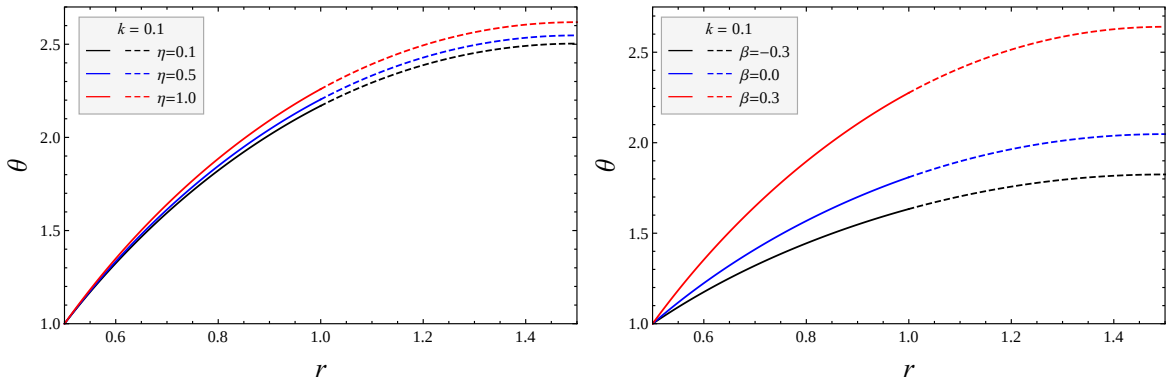

Figure 4.18: Variation of temperature θ with radial distance r for different values of **(a)** viscosity ratio parameter η ($\text{We} = 0.5, n = 2, \beta = 0.4$) and **(b)** Stress-jump parameter β. ($\text{We} = 0.5, \text{Nu} = 4.0, n = 0.05, \eta = 0.01, \gamma = 0.444, p_s = 1$)

fluid rheology shifts from shear thinning to shear thickening. According to the observations in Table 2b, one can conclude that the variation in the Kozeny constant will become less significant for a more permeable porous medium. It decays with the increasing dominance of elastic forces over viscous forces, while growth is observed with the increasing shear-thickening effects of the Carreau fluid.

As a limiting case($a \to 1, k \to \infty$), the current model (solid cylindrical particle surrounded by a porous annular layer of thickness $(1 - l)$) is reduced to a perfectly solid cylinder in a cell. A graphical representation of the hydrodynamic permeability of Carreau fluid passing in an aggregate of perfectly solid cylinders is shown in Figure 4.19a. A novel expression for the same is already mentioned in the equation (4.29). It is depicted in Figure 4.19b that a limiting case of the present model (Newtonian fluid passing in an

aggregate of perfectly solid cylinders) is in perfect agreement with the published work of Deo *et al.*. The equation (4.30) provides an analytical expression of L_{11} for the same. Figure 4.19a will also include a comparison of non-Newtonian characteristics (shear-thinning and shear-thickening) with the above-limiting case of a Newtonian fluid. It can be depicted from Figure 4.19 that the hydrodynamic permeability of the shear-thinning fluid is higher in comparison to the Newtonian fluid, while it is lower in the case of the shear-thickening fluid.

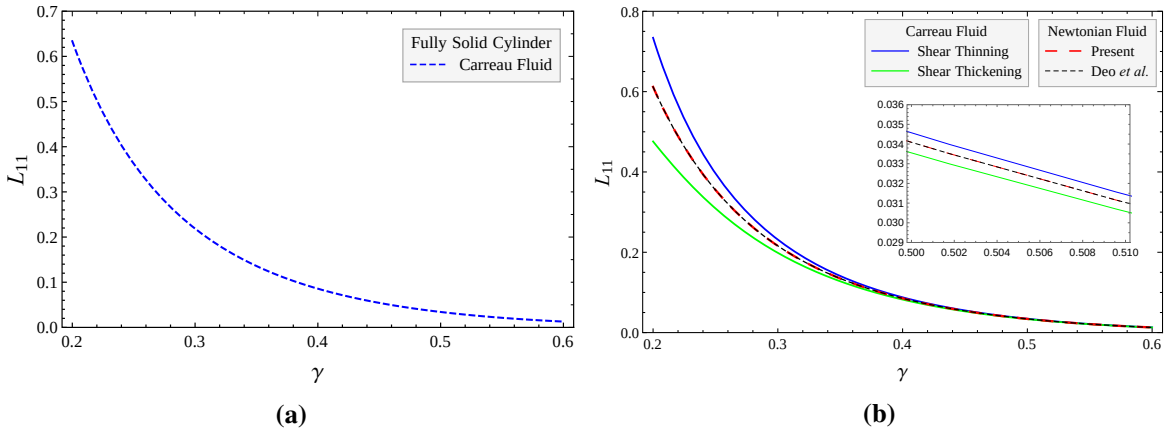

Figure 4.19: **(a)** The hydrodynamic permeability L_{11} depending on particle volume fraction γ for the case of fully solid cylindrical particle, and **(b)** Validation of hydrodynamic permeability L_{11} of currunt work with the work of Deo *et al.* [3].

A graphical comparison of Carreau and Newtonian fluid for both small and large permeability cases are performed in Figure 4.20a. The hydrodynamic permeability of the Carreau fluid is found to be greater in both cases than that of the Newtonian fluid. The difference in the membrane permeability of the shear-thinning Carreau and Newtonian fluid is more significant in the case of large permeability; however, it decreases as we reduce the permeability. It is also observed that the difference in L_{11} for the Carreau fluid and Newtonian fluid diminishes for a higher particle volume fraction. One can conclude that the medium's permeability considerably impacts the flow and its characteristics. The asymptotic solution in the case of large permeability is validated by comparing it with the numerical solution, and Figure 4.20b illustrates the same by graphically comparing the two solutions. It can be observed from Figure 4.20b that the asymptotic solution is in good agreement with the numerical solution. At the same time, the difference can be seen in the inset box, which is up to the third decimal place.

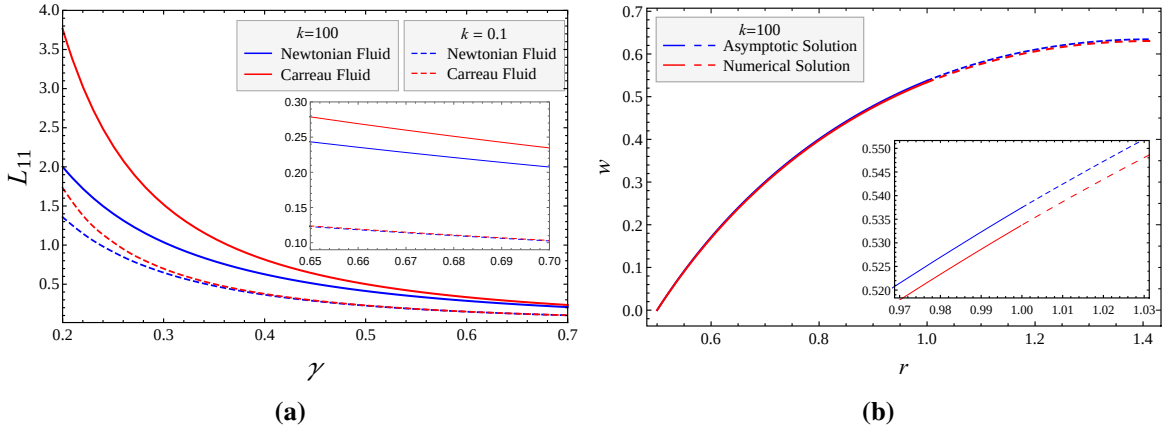

(a) **(b)**

Figure 4.20: (a) The hydrodynamic permeability L_{11} depending on particle volume fraction γ for the case of fully solid cylindrical particle, and **(b)** Validation of hydrodynamic permeability L_{11} of currunt work with the work of Deo *et al.* [3].

4.6 Summary and Conclusions

A study of the non-Newtonian rheology of the Carreau fluid flowing through membranes consisting of a cluster of cylindrical particles with a porous layer has been demonstrated owing to its significant impact on the filtration process of viscoelastic fluids. A particle has been selected from the swarm involving a cluster of identical cylindrical particles to analyse the flow of Carreau fluid through membranes using the particle-in-cell method. The boundary condition has been applied on the cell surface to include the influence of neighbouring particles using the particle-in-cell approach. The layout of the proposed study includes a porous cylindrical layer overlying the solid cylindrical core with a circular cross-section and a non-porous layer enclosing the porous layer. The Brinkman and Stokes equations have been used to formulate the governing equations regulating the flow through porous and non-porous media. The Brinkman and Stokes equations are nonlinear due to the presence of the nonlinear stress-strain relation of the Carreau fluid. This makes analytical solutions of the governing equations difficult to be obtained. Hence, the perturbation series expansion in terms of small parameters (We $\ll 1$ and $S \ll 1$) has been applied to derive the expressions of a velocity profile for different regions, which was then used to obtain the analytical expressions for the hydrodynamical quantities like flow rate, membrane permeability, Kozeny constant and the thermal quantities like temperature profile. The computations reveal that the Carreau fluid and porous layer parameters affect the hydrodynamical quantities and temperature profile. The impact of numerous control parameters on the hydrodynamical quantities and temperature profile are graphically analysed. The results of the limiting cases of the previously published works were deduced to validate the present work. The present study

reveals that the fluid's shear-thining and shear-thickening behaviour significantly influences the medium's membrane permeability and tortuosity.
The following prominent outcomes of the proposed work are pointed out below:

1. The Carreau fluid's rheological parameters significantly impact the hydrodynamic permeability. In a highly permeable porous medium, the hydrodynamic permeability increases with the fluid's viscoelasticity; however, it decreases as the rheology shifts from shear thinning to shear thickening. In the case of small permeability, the impact of viscoelasticity is the same as that of large permeability for shear-thinning; however, it becomes the opposite for shear thickening.

2. For both large and small permeability cases, the Kozeny constant or the tortuosity of the system increases with the medium's porosity. It gets a lesser value for the rising viscoelastic property of Carreau fluid, while it gains as the fluid rheology shifts from shear thinning to shear thickening.

3. The fluid temperature also exhibits different behaviours concerning the Carreau fluid parameters in the cases of small and large permeability. A higher viscoelastic fluid causes a temperature increase in the case of a large permeability, whereas a small permeability has the opposite effect for shear-thickening fluids.

4. For large permeability, the fluid temperature shows decay with rising η, however, for small permeability, an opposite behaviour is observed for shear thickening fluids.

The findings of the present work may be instrumented in analysing various physical and biological processes, including petroleum reservoir rocks, wastewater treatment filtration processes, and blood flow through smooth muscle cells. The following work, however, requires experimental verification.

Chapter 5

Analytical Study of the Effect of Complex Fluid Rheology and Membrane Parameters on Heat Transfer in Fluid Flow through a Swarm of Cylindrical Particles [1]

5.1 Introduction

The membrane filtration processes, or the flow of liquids through a swarm of particles, are emerging subject for researchers owing to the broad engineering and science research domain. The understanding of crucial physical and biological applications, such as filtration processes in wastewater treatment, petroleum reservoir rocks, and the flow of blood through smooth muscle cells, is evident through the noteworthy contributions of these fluid flow processes [143]. The movement of liquids is influenced not only by the pressure and mechanical characteristics of the medium, but also by its mechanical properties. Various factors, including the shape and size of tubes or conduits, as well as the behavior of fluids and mediums, contribute to the fluid circulation process. Studying the flow of fluids within a material composed of pores and solid particles, known as a porous medium, is crucial and serves as a compelling driving force for current research efforts. Fluid flow through porous materials has diverse applications, including but not limited to pharmaceutical fields, petroleum reservoir rocks, filtration processes in wastewater treatment, blood circulation through the lungs, and the design of the digestive system. Tiwari and Deo [2] have focused on examining the movement of Newtonian fluid through porous materials. Their findings indicate that a decrease in pore size leads to a reduction in the permeability of the material, resulting in increased obstruction to the fluid flow process.

[1] A considerable part of this chapter is accepted in *International Communications of Heat and Mass Transfer*, 2024

The preceding research has explored the movement of liquid through a porous tube or conduit. However, emphasizing the movement of fluid through a collection of particles is crucial, given its various applications in processes like membrane filtration, sand bed flow, and petroleum reservoirs. Discussing the theoretical role and contributions of each particle within a swarm poses a challenge. To address this, the particle-in-cell model is utilized to isolate a single particle within the swarm. This enables the examination of the contributions and effects of each particle in the fluid flowing through the swarm. Additionally, a boundary condition on a hypothetical cell surface is applied to illustrate the role of neighboring particles.

The porous configuration on the exterior of the inflexible cylindrical particle, resulting from polymer dissolution and adsorption, initiates stimulation. This stratum carries significance for the membrane's overall permeability. Deo et al. studied a membrane of concentric clusters of porous cylindrical particles [145] for the low Reynolds number and viscous fluid flow using the unit cell model approach by considering Happel's free surface model. Deo at al. [3] analyzed Newtonian fluid past a swarm of cylinders by taking the flow in parallel as well as perpendicular directions. Sharif *et al.* [146] and Khanukaeva *et al.* ([96], [95]) also investigated both parallel and perpendicular flow past through a swarm of cylinders to gain an understanding of the micro-level properties of fluid flow. Sucharitha et al. [188] investigated the peristaltic flow past differently shaped porous channels and analyzed wall flexibility and Joule heating effect on the velocity, concentration, and energy.

The particle-in-cell method was used in all the above described investigations to study the flow of fluids through a group of single-layered porous cylindrical particles. However, Yadav *et al.* [189] and Deo *et al.* [190] investigated the hydrodynamic permeability of a biporous membrane comprising porous cylindrical particles embedded within another porous medium, utilizing cell model methodologies. The governing equations for fluid flow through a biporous layered cylindrical particle are formulated based on the Brinkman equations. They have taken into account constant permeabilities for different porous regions.

The preceding discussion focuses on the analysis of creeping flow passing through a swarm of single or biporous layered cylindrical particles, employing both Newtonian and polar fluids. However, the membrane filtration process relies significantly on the non-Newtonian behavior of the fluid. Bhandari et al. [191] presented a model aimed at examining the pumping and flow attributes arising from wall contraction, encompassing both propagative and non-propagative elements. Furthermore, they examined the impact of the couple stress parameter by employing a fluid model that integrates couple stress effects. Recently,

extensive research has been conducted by employing the Carreau and Carreau–Yasuda models to characterize non-Newtonian fluids. The Carreau fluid model stands out for its straightforward mathematical treatment. A notable advantage of the Carreau–Yasuda fluid model, compared to other non-Newtonian models, is its inclusion of five parameters, enabling a comprehensive interpretation of fluid rheology. This five-parameter model offers ample flexibility to effectively match a diverse range of experimental apparent viscosity curves and has demonstrated its utility in the field of hemodynamics [18]. This model elucidates the variation in fluid viscosity across low to high shear rate ranges and additionally characterizes the fluid's shear-thinning behavior, contributing to its recent surge in popularity. The aim of incorporating the non-Newtonian Carreau-Yasuda fluid into the membrane filtration process is to explore its non-Newtonian rheological effects on various hydrodynamic and thermal quantities such as velocity, membrane permeability, temperature and the Kozeny constant. The discussion of analytical and asymptotic solutions for the flow of Carreau-Yasuda fluid through a porous medium is pending, primarily because of the nonlinear and complex relationship between shear stress and the rate of strain.

When fluid inertia is significant, the form drag exerted by the fluid on the solid object becomes appreciable. Vafai and Tien ([192], [193]) formulated a comprehensive model for the transport of flow in porous media, taking into account various pertinent effects. The extensive model under consideration incorporates convective terms and is widely referred to as the Brinkman–Forchheimer–Darcy equation, whether in its complete formulation or a simplified variant. Research utilizing this model, especially in the realm of biological studies concerning tissue media near the aortas or in high-perfusion skeletal tissues, is limited. The comprehensive examination of the Brinkman-Forchheimer equation, including considerations for heat transfer, can be found in the studies conducted by Khaled and Vafai [168]. Hooman and Gurgency ([7], [8]) chose the Brinkman-Forchheimer model for its broadened application beyond the Darcy model. Chauhan *et al.* [194] discussed the impact of heat transfer and Forchheimer parameters on fluid flow quantities and the Fahraeus effect in physiological fluid flow.

After reviewing through all of the aforementioned works for a constant permeability model, the porous material's permeability might not stay constant because of contaminants and impurities. The radially-varying permeability of a tube filled with Casson fluid was investigated in 1996 by Dash *et al.* [165]. They utilized the Brinkmann model to incorporate the impact of resistance induced by the porous medium. A critical finding from Srivastava and Deo's study [24] is that pollutants and impurities can change a porous material's permeability. Their analysis took into account the permeability's variable nature, which was modeled as a quadratic function of a radial variable. In addition, a thorough stability study

was carried out by Hill and Morad [195] to investigate how mass transport is affected by an anisotropic porous medium when a first-order bulk chemical reaction is present. In order to examine flow in a non-uniform porous media, Veerapaneni and Wiesner [84] divided the spherical porous aggregate into n spherical shells, each of which had a fixed but unique permeability. They looked into permeability's continuous dependence on radial distance in more detail, drawing on several earlier models. According to the aforementioned research, the variable aspect of permeability in membrane filtration has not been addressed, despite its potential significance in determining membrane permeability within the filtration process.

The utilization of the particle-in-cell approach to examine the flow characteristics of Carreau-Yasuda fluid through aggregations of biporous layered cylindrical particles in a membrane has not been previously addressed. Based on the earlier discussions, it is noted that the permeability of the porous medium may vary due to the presence of impurities and contaminants in both the fluid and the medium. However, the discussion has not addressed the influence of variable permeability on the flow of fluid through the membrane. Examining varying permeability across distinct porous regions draws attention to illustrating the prevalence of one porous layer over another and vice versa. An intriguing finding from prior research is that the majority of studies on membrane filtration processes have employed either the Brinkman equation or the Brinkman-Forchheimer equation. Nevertheless, when accounting for fluid inertia, the Brinkman-Forchheimer equation proves to be more suitable for consideration in proximity to the solid core of the cylindrical particle. The fluctuation in temperature within the passage of a non-Newtonian Carreau-Yasuda fluid through a collection of biporous layered cylindrical particles has not been addressed.

This study aims to explore the flow behavior of a non-Newtonian Carreau-Yasuda fluid through a membrane composed of biporous layered cylindrical particles, each with different permeabilities. The widely adopted particle-in-cell approach has been utilized to derive mathematical equations that replicate the continuity, momentum, and temperature equations. The structure of the proposed research is intended to be such that a porous area near the solid core of cylindrical particles follows the Brinkman-Forchheimer equation with varying permeability. Additionally, an intermediate porous region covering the Brinkman-Forchheimer region is controlled by the Brinkman equation with variable permeability. To demonstrates the behaviour of the neighbouring particles, a hypothetical cell surface is considered to mimic the partcles interaction in membrane. The peripheral non-porous region proximate to the hypothetical cell is regulated by Stokes equation. The quadratic polynomial form of different variable permeabilities for different porous mediums are considered to demonstrates the dominance of one porous medium over other and vice versa. The equations regulating the Brinkman-Forchheimer, Brinkman porous regions and a non-porous region adjacent to

the hypothetical cell surface are nonlinear and difficult to obtain the analytical expressions. To deal with this hurdle, the empirical regular perturbation method has been employed to obtain the asymptotic expressions of velocity for large permeability and small Weissenberg number. However, a numerical scheme (NDSolve) in Mathematica is used to illustrates the graphical analysis of the mathematical equations for small permeability and Weissenberg number. The purpose of this research is to explore the membrane filtration processes, taking into account non-Newtonian fluid models, in order to comprehend the various physiological or industrial mechanisms at play.

When adopting the particle-in-cell model approach, the structure of the proposed work is divided into five sections. Section 1 presents fundamental details about the proposed model, including a literature review, identification of gaps in existing research, and the objectives of the current study. In Section 2, the physical mechanism of the proposed work is translated into mathematical equations, utilizing the statements and assumptions outlined in the proposed model. Section 3 outlines the solution techniques for the governing equations, presenting their asymptotic expansions in relation to constants that can be determined through appropriate boundary conditions. Graphical analysis is employed to examine the mathematical equations, and a thorough discussion of the results of the current study is presented in Section 4. The noteworthy results of the current study are discussed in section 5, accompanied by a summary of the proposed work.

5.2 Problem Formulation

5.2.1 Statement of the Problem and Model Assumptions

The present work explores the flow of a Carreau-Yasuda fluid through a collection of biporous layered cylindrical particles under heat transfer approach. The flow of fluid through biporous layered cylindrical particles within the swarm is analysed using the particle-in-cell approach, and an examination of the hypothetical cell surface condition is conducted to investigate the collective behavior of the cylindrical particles in a swarm. The model's structure is designed so that the Brinkman-Forchheimer region near the solid core of the cylindrical particle follows the Brinkman-Forchheimer equation. Simultaneously, an intermediate concentric Brinkman region surrounding the Brinkman-Forchheimer region is governed by the Brinkman equation. The Stokes equation governs a peripheral region encompassing both the Brinkman-Forchheimer and Brinkman regions.

1. The flow is regarded as 1-D steady, incompressible, laminar, symmetrical about the cylindrical tube's axis, and fully developed.

2. To realistically model the unidirectional flow of Carreau-Yasuda fluid through a swarm of biporous layered cylindrical particle, the governing equations are formulated using the cylindrical polar coordinate system $(\widetilde{r}, \phi, \widetilde{z})$. The velocity components in cylindrical polar coordinates according to the proposed model are $(0, 0, \widetilde{w}(\widetilde{r}))$.

3. The Reynolds number is deemed to be quite low, signifying a prevalence of viscous forces over inertial forces. This leads to the convective term making an insignificant contribution, and as such, it is omitted in the present investigation.

4. The stress–strain relationship for Carreau-Yasuda fluid under the assumption of low shear rate $\lambda \left(\frac{\partial \widetilde{w}}{\partial \widetilde{r}}\right) < 1$ is incorporated into the momentum equation for both porous and non-porous regions. By applying this assumption $\lambda \left(\frac{\partial \widetilde{w}}{\partial \widetilde{r}}\right) < 1$ and using a first-order binomial series expansion, the shear stress expressions for both porous and non-porous regions are derived.

5. The permeability in porous regions is modelled as a quadratic polynomial of radial distance to showcase the prevalence of either the Forchheimer porous region or the Brinkman porous region.

6. The thermal equations under steady-state conditions are simplified when heat conduction is the primary mechanism, causing the convective term to be negligible. The

analysis of the temperature profile incorporates the effects of viscoelastic rheology, porous medium, and heat transfer parameters, considering the heat flux and viscous dissipation.

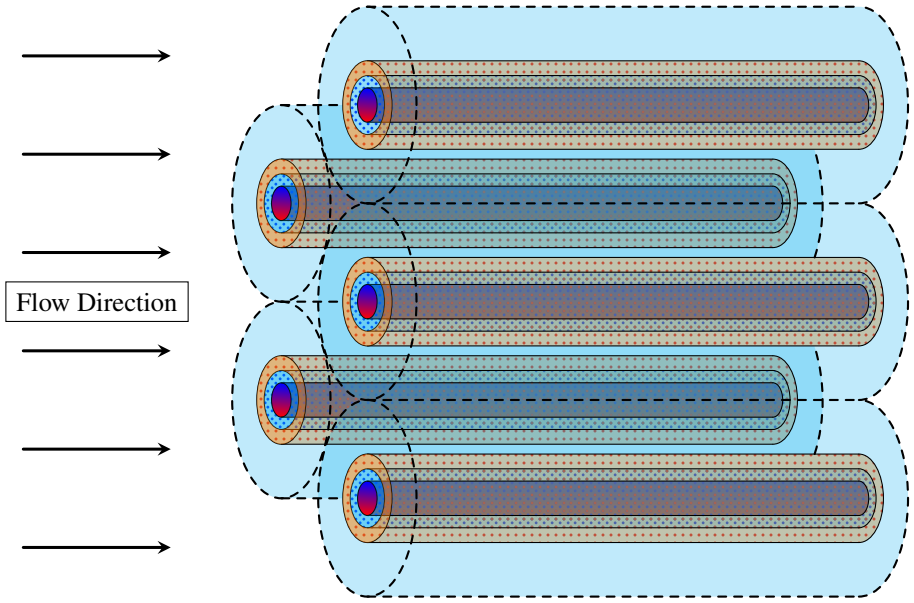

(a)

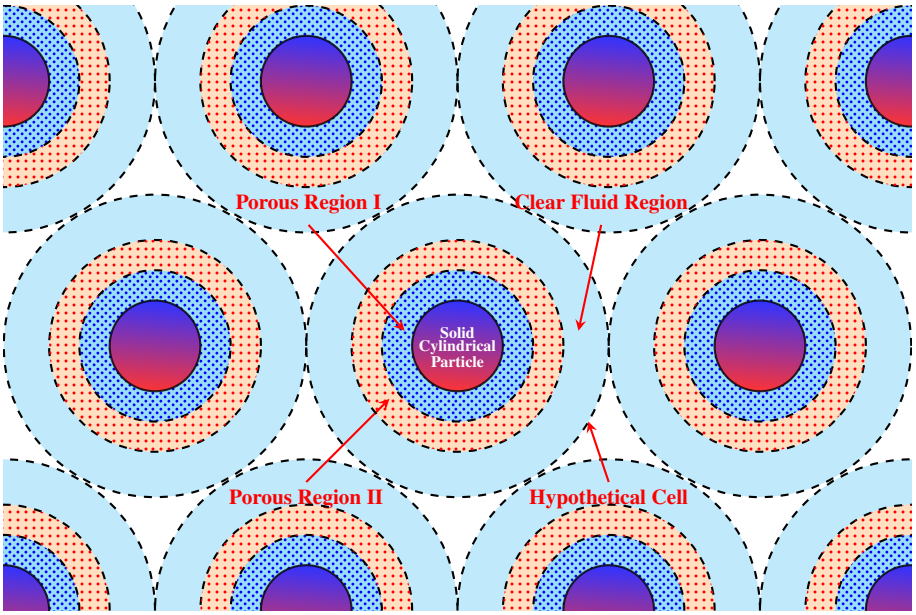

(b)

Figure 5.1: **(a)** The portrayal of the movement along the central axis of a collection of biporous layered solid cylinders within a membrane and **(b)** the circular cross-sectional perspective depicts a swarm composed of a solid cylindrical particle enveloped by biporous layers contained within a hypothetical cell

5.2.2 Model Description

The visual depiction presented in Figure 1 illustrates the conceptual design of the proposed project, showcasing a membrane consisting of a collection of biporous layered cylindrical particles along with its cross-sectional perspective. The three different regions of the present study is taken into consideration in such a procedure that the porous region- I adjacent to the solid core of the cylindrical particle is regulated by Brinkman-Forchheimer equation under the quadratic polynomial form of the variable permeability, and a concentric porous region-II is governed by Brinkman equation under the quadratic polynomial form of the variable permeability. The peripheral non-porous region proximate to the hypothetical cell surface is regulated by the Stokes equation. The selected thickness of the presumed cell within a porous cylindrical particle is adjusted to match the volume fraction of the particles within the assembly to that of the cell, *i.e.*, $d^2 = \frac{1}{\gamma} = \frac{\pi\tilde{d}^2}{\pi\tilde{c}^2}$, where γ is the particle valume fraction.

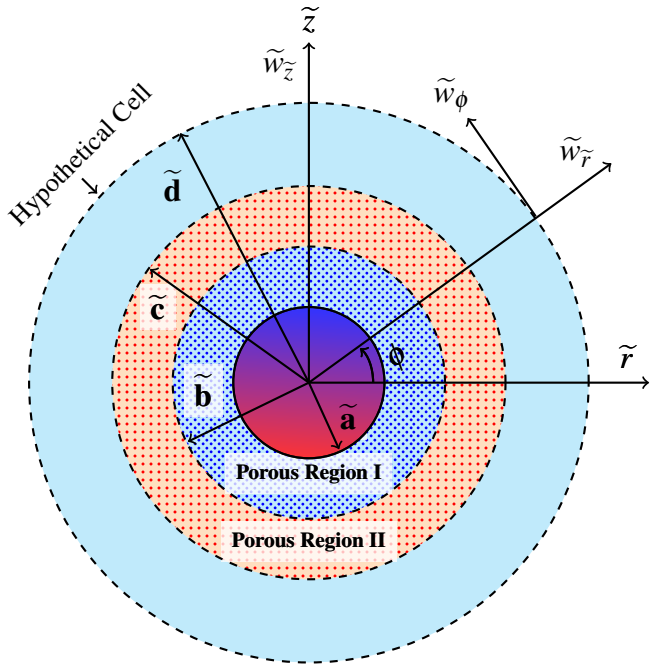

Figure 5.2: The solid core of a cylindrical particle, coated with a swarm and situated within biporous layers, is depicted in the cross-sectional view with nomenclature

5.2.3 Governing Equations

With the aim of formulating the proposed physical model into the mathematical equations, the continuity, momentum and energy equations control the flow of fluid through a swarm of cylindrical particles. As per the intention of particle-in-cell model approach, a biporous layered cylindrical particle from a swarm is considered to analyze the flow of fluid through

a swarm of particle using a boundary condition on the hypotheical cell surface. Following the above hypotheses under variable permeability assumption, the equations govern the flow through the biporous layered cylindrical particle are as follows ([18], [7], [24], [137]):
Porous Region- I, *i.e.*, $\widetilde{a} \leq \widetilde{r} \leq \widetilde{b}$

$$\frac{\partial \widetilde{w}_f}{\partial \widetilde{z}} = 0, \tag{5.1a}$$

$$\frac{\partial \widetilde{p}}{\partial \widetilde{r}} = 0, \tag{5.1b}$$

$$\frac{\partial \widetilde{p}}{\partial \widetilde{z}} = \frac{1}{\widetilde{r}} \frac{\partial}{\partial \widetilde{r}} \left(\widetilde{r} \widetilde{\tau}_f \right) - \frac{\widetilde{\mu}_0 \widetilde{w}_f}{\widetilde{k}_f(r)} - \frac{\widetilde{C}_F \widetilde{\rho} \widetilde{w}_f^2}{\sqrt{\widetilde{k}_f(r)}}, \tag{5.1c}$$

where the parameters $\widetilde{w}_f$ and $\widetilde{\tau}_f$ represent the flow parameters characterizing the axial velocity and shear stress within the fluid region governed by Brinkman-Forchheimer equation, while $\widetilde{p}$, $\widetilde{\rho}$, and $\widetilde{\mu}_0$ correspond to the pressure, density, and zero shear-rate viscosity of the Carreau-Yasuda fluid, respectively, the Brinkman-Forchheimer porous region parameters are $\widetilde{C}_F$ and $\widetilde{k}_f(r) = \widetilde{k}\left(1 - \varepsilon_f \left(\frac{\widetilde{r}}{\widetilde{c}}\right)^2\right)$ delineating the inertial coefficient and the quadratic polynomial form of the variable nature of permeability, respectively, where $\widetilde{k}$ and ε_f are the permeability of the porous medium and variable permeability parameter [24]. The equation (5.1a) represents the continuity equation, while (5.1b) expresses the momentum equation in the radial direction. Additionally, equation (5.1c) pertains to the momentum equation in axial direction within the Brinkman-Forchheimer region, considering variable permeability. The expression describing the relationship between stress and strain for a Carreau-Yasuda fluid, expressed in relation to the velocity within the Forchheimer region, is provided by [18]

$$\widetilde{\tau}_f = \left[\widetilde{\mu}_\infty + (\widetilde{\mu}_0 - \widetilde{\mu}_\infty) \left(1 + \left(\lambda \frac{\partial \widetilde{w}_f}{\partial \widetilde{r}} \right)^{a_1} \right)^{\frac{n-1}{a_1}} \right] \frac{\partial \widetilde{w}_f}{\partial \widetilde{r}}, \tag{5.1d}$$

where the Carreau-Yasuda fluid is distinguished by its parameters $\widetilde{\mu}_\infty, \lambda, n$, and a_1. These parameters respectively represent the infinite shear-rate viscosity, a time constant, the Power-law exponent indicating shear-thinning and thickening tendencies of the fluid, and the Yasuda parameter signifying the transition between the zero shear rate region and the Power-law region.
Porous Region- II, *i.e.*, $\widetilde{b} \leq \widetilde{r} \leq \widetilde{c}$

$$\frac{\partial \widetilde{w}_b}{\partial \widetilde{z}} = 0, \tag{5.2a}$$

$$\frac{\partial \widetilde{p}}{\partial \widetilde{r}} = 0, \tag{5.2b}$$

$$\frac{\partial \widetilde{p}}{\partial \widetilde{z}} = \frac{1}{\widetilde{r}}\frac{\partial}{\partial \widetilde{r}}(\widetilde{r}\widetilde{\tau}_b) - \frac{\widetilde{\mu}_0 \widetilde{w}_b}{\widetilde{k}_b(r)}, \tag{5.2c}$$

where $\widetilde{w}_b, \widetilde{\tau}_b$ are the flow parameters delineating the velocity and shear stress of the Carreau-Yasuda fluid in the Brinman porous region, respectively; the variable nautre of permeability for Brinkman region $\widetilde{k}_b(r) = \widetilde{k}\left(1 - \varepsilon_b\left(\frac{\widetilde{r}}{\widetilde{c}}\right)^2\right)$, where $\widetilde{k}$ is the permeability constant of the porous medium and ε_b is the variable permeability parameter for Brinkman porous region [24].

The expression describing the stress-strain relationship of a Carreau-Yasuda fluid with Brinkman region velocity can be expressed as follows [18]:

$$\widetilde{\tau}_b = \left[\widetilde{\mu}_\infty + (\widetilde{\mu}_0 - \widetilde{\mu}_\infty)\left(1 + \left(\lambda \frac{\partial \widetilde{w}_b}{\partial \widetilde{r}}\right)^{a_1}\right)^{\frac{n-1}{a_1}}\right]\frac{\partial \widetilde{w}_b}{\partial \widetilde{r}}. \tag{5.2d}$$

Non-Porous (Clear Fluid) Region, *i.e.*, $\widetilde{c} \leq \widetilde{r} \leq \widetilde{d}$

$$\frac{\partial \widetilde{w}_s}{\partial \widetilde{z}} = 0, \tag{5.3a}$$

$$\frac{\partial \widetilde{p}}{\partial \widetilde{r}} = 0, \tag{5.3b}$$

$$\frac{\partial \widetilde{p}}{\partial \widetilde{z}} = \frac{1}{\widetilde{r}}\frac{\partial}{\partial \widetilde{r}}(\widetilde{r}\widetilde{\tau}_s), \tag{5.3c}$$

where the axial velocity and shear stress for the clear fluid are denoted as $\widetilde{w}_s$ and $\widetilde{\tau}_s$, respectively.

The velocity-dependent stress-strain relationship for a Carreau-Yasuda fluid is expressed in relation to the velocity within the clear fluid region [18]

$$\widetilde{\tau}_s = \left[\widetilde{\mu}_\infty + (\widetilde{\mu}_0 - \widetilde{\mu}_\infty)\left(1 + \left(\lambda \frac{\partial \widetilde{w}_s}{\partial \widetilde{r}}\right)^{a_1}\right)^{\frac{n-1}{a_1}}\right]\frac{\partial \widetilde{w}_s}{\partial \widetilde{r}}. \tag{5.3d}$$

5.2.4 Boundary Conditions

In the pursuit of deriving closed-form solutions for various regions in the Carreau-Yasuda fluid flow, the boundary and interface conditions are crucial for determining the arbitrary constants associated with the nonlinear second-order ordinary differential equations that govern the flow of Carreau-Yasuda fluid through a cluster of particles. The closed form of

the solutions is derived by addressing the following boundary conditions, and a comprehensive description of the dimensional form of these conditions is provided below:

1. A state of zero velocity is regarded at the solid core of the cylindrical particle, *i.e.*,

$$\widetilde{w}_f = 0, \quad \text{at} \quad \widetilde{r} = \widetilde{a}. \tag{5.4a}$$

2. The consistent flow of velocities and shear stresses is taken into account at the interface between porous materials, *i.e.*,

$$\widetilde{w}_f = \widetilde{w}_b, \ \text{ and } \ \widetilde{\tau}_f = \widetilde{\tau}_b, \quad \text{at} \quad \widetilde{r} = \widetilde{b}. \tag{5.4b}$$

3. The fluid-porous interface considers the continuity of velocity and the stress-jump condition proposed by Ochoa-Tapia and Whitaker [81], *i.e.*,

$$\widetilde{w}_b = \widetilde{w}_s, \ \text{ and } \ \widetilde{\tau}_b - \widetilde{\tau}_s = \frac{\beta \widetilde{w}_b}{\sqrt{\widetilde{k}_b(\widetilde{r})}}, \quad \text{at} \quad \widetilde{r} = \widetilde{c}, \tag{5.4c}$$

   where β is the stress-jump parameter.

4. The hypothetical cell surface of the cylindrical particle exhibits a zero shear stress, *i.e.*,

$$\widetilde{\tau}_s = 0, \quad \text{at} \quad \widetilde{r} = \widetilde{d}. \tag{5.4d}$$

5.2.5 Non-Dimensional Parameters and Governing Equations

The dimensionless numbers (or characteristic numbers) are essential in analyzing the behaviour of fluids and their flow with other transport phenomena. To solve the system of equations outlined in (5.1)-(5.3), along with the associated boundary and interface conditions in (5.4), we introduce the following non-dimensional variables:

$$\begin{aligned}
&p = \frac{\widetilde{p}\widetilde{c}}{\widetilde{w}_0\widetilde{\mu}_0}, \ r = \frac{\widetilde{r}}{\widetilde{c}}, \ z = \frac{\widetilde{z}}{\widetilde{c}}, \ a = \frac{\widetilde{a}}{\widetilde{c}}, \ b = \frac{\widetilde{b}}{\widetilde{c}}, \ d = \frac{\widetilde{d}}{\widetilde{c}}, \ S^2 = \frac{1}{k}, \ \widetilde{w}_0 = \frac{\widetilde{q}_0\widetilde{c}^2}{\widetilde{\mu}_0}, , \ Br = \frac{\widetilde{\mu}_0\widetilde{w}_0^2}{\widetilde{K}(\widetilde{T}_w - \widetilde{T}_\infty)}, \\
&w_f = \frac{\widetilde{w}_f}{\widetilde{w}_0}, \ w_b = \frac{\widetilde{w}_b}{\widetilde{w}_0}, \ w_s = \frac{\widetilde{w}_s}{\widetilde{w}_0}, \ k = \frac{\widetilde{k}}{\widetilde{c}^2}, \ \tau_f = \frac{\widetilde{\tau}_f\widetilde{c}}{\widetilde{w}_0\widetilde{\mu}_0}, \ \tau_b = \frac{\widetilde{\tau}_b\widetilde{c}}{\widetilde{w}_0\widetilde{\mu}_0}, \ \tau_s = \frac{\widetilde{\tau}_s\widetilde{c}}{\widetilde{w}_0\widetilde{\mu}_0}, \\
&We = \frac{\lambda\widetilde{w}_0}{\widetilde{c}}, \ \eta = \frac{\widetilde{\mu}_\infty}{\widetilde{\mu}_0}, \ F = \frac{\widetilde{C}_F\widetilde{\rho}\widetilde{c}^3\widetilde{q}_0}{\widetilde{\mu}_0^2}, \ \theta = \frac{\widetilde{T} - \widetilde{T}_\infty}{\widetilde{T}_w - \widetilde{T}_\infty}, \ Nu = \frac{2q''\widetilde{c}}{\widetilde{K}(\widetilde{T}_w - \widetilde{T}_\infty)},
\end{aligned} \tag{5.5}$$

where the average velocity, represented by $\widetilde{w}_0$, is linked to the Weissenberg number We, calculated as the product of the shear rate and the characteristic time of the fluid. The Nusselt number Nu quantifies the relationship between the combined heat transfer (convection and conduction) and the conductive heat transfer across a boundary. The Brinkman number Br, a dimensionless parameter, represents the relationship between heat generated through viscous dissipation and heat transfered via molecular conduction. Essentially, it gauges the ratio of heat generation due to viscosity against external heating. A higher Brinkman number indicates a slower conduction of heat resulting from viscous dissipation, leading to a greater temperature increase. The parameter θ represents the non-dimensional temperature corresponding to the dimensional temperature $\widetilde{T}$. The parameters $\widetilde{T}_w$ and $\widetilde{T}_\infty$ are the wall (surface) and ambient temperatures, respectively. Additionally, F represents the Forchheimer number, S is a dimensionless parameter, η signifies the viscosity ratio parameter, and $\widetilde{q}_0$ denotes the characteristic pressure gradient.

Utilizing the aforementioned non-dimensional variables (5.5), the governing equations (5.1)-(5.3) will transform into their non-dimensional form:

Porous Region- I, *i.e.*, $a \leq r \leq b$

$$\frac{\partial w_f}{\partial z} = 0, \tag{5.6a}$$

$$\frac{\partial p}{\partial r} = 0, \tag{5.6b}$$

$$\frac{\partial p}{\partial z} = \frac{1}{r}\frac{\partial}{\partial r}\left(r\tau_f\right) - \frac{w_f}{k_f(r)} - \frac{F w_f^2}{\sqrt{k_f(r)}}. \tag{5.6c}$$

where $k_f(r) = k(1-\varepsilon_f r)^2$ is the quadratic polynomial form of the permeability with varying permeability parameter ε_f for Brinkman-Forchheimer region and k is the permeability constant.

The equation for the Carreau-Yasuda fluid provides a description of the nonlinear relationship between shear stress and strain [18]

$$\tau_f = \left[1 + \frac{(1-\eta)(n-1)}{a_1}\left(We\frac{\partial w_f}{\partial r}\right)^{a_1}\right]\frac{\partial w_f}{\partial r}. \tag{5.6d}$$

Porous Region- II, *i.e.*, $b \leq r \leq 1$

$$\frac{\partial w_b}{\partial z} = 0, \tag{5.7a}$$

$$\frac{\partial p}{\partial r} = 0, \tag{5.7b}$$

$$\frac{\partial p}{\partial z} = \frac{1}{r}\frac{\partial}{\partial r}(r\tau_b) - \frac{w_b}{k_b(r)}, \tag{5.7c}$$

where $k_b(r) = k(1-\varepsilon_b r)^2$ is the quadratic polynomial form of the permeability with varying permeability parameter ε_b for Brinkman porous region.
The Carreau-Yasuda fluid equation elucidates the nonlinear correlation between shear stress and strain [18]

$$\tau_b = \left[1 + \frac{(1-\eta)(n-1)}{a_1}\left(We\frac{\partial w_b}{\partial r}\right)^{a_1}\right]\frac{\partial w_b}{\partial r}. \tag{5.7d}$$

Non-Porous (Clear Fluid) Region, *i.e.*, $1 \le r \le d$

$$\frac{\partial w_s}{\partial z} = 0, \tag{5.8a}$$

$$\frac{\partial p}{\partial r} = 0, \tag{5.8b}$$

$$\frac{\partial p}{\partial z} = \frac{1}{r}\frac{\partial}{\partial r}(r\tau_s), \tag{5.8c}$$

where the Carreau-Yasuda fluid equation clarifies the non-linear relationship between shear stress and strain [18]

$$\tau_s = \left[1 + \frac{(1-\eta)(n-1)}{a_1}\left(We\frac{\partial w_s}{\partial r}\right)^{a_1}\right]\frac{\partial w_s}{\partial r}. \tag{5.8d}$$

5.2.6 Boundary Conditions

The dimensionless boundary and interface conditions are given as follows:

$$\begin{gathered} w_f = 0, \quad \text{at} \quad r = a, \\ w_f = w_b, \quad \text{and} \quad \tau_f = \tau_b, \quad \text{at} \quad r = b, \\ w_b = w_s, \quad \text{and} \quad \tau_b - \tau_s = \frac{\beta}{\sqrt{k_b(r)}} w_b, \quad \text{at} \quad r = 1, \\ \tau_s = 0, \quad \text{at} \quad r = d. \end{gathered} \tag{5.9}$$

5.2.7 Hydrodynamical Quantities and Kozeny Constant

The non-dimensional expression for the volumetric flow rate Q_s is defined as follows:

$$Q_s = 2\pi\int_a^d rw(r)dr = 2\pi\left(\int_a^b rw_f(r)dr + \int_b^1 rw_b(r)dr + \int_1^d rw_s(r)dr\right). \tag{5.10}$$

The expression for the hydrodynamic permeability L_{11} of the collective of porous cylindrical particles is formulated as follows [96]

$$L_{11} = -\frac{V_f}{\partial p/\partial z}, \tag{5.11}$$

where V_f denotes the filtration velocity and is expressed as $V_f = \frac{Q_s}{\pi d^2}$.
The permeability of porous media is ascertained through the application of the following expression, derived from the semi-empirical Kozeny-Karman formula [71]

$$L_{11} = \frac{\varepsilon \rho_h^2}{K_z \widetilde{c}^2}, \tag{5.12}$$

where ε represents porosity, K_z denotes the dimensionless Kozeny constant, and ρ_h signifies the hydraulic radius, defined as the ratio of pore volume to wetting area.
The Kozeny constant is obtained by the above equation (5.12)

$$K_z = \frac{\varepsilon \rho_h^2}{\widetilde{c}^2 L_{11}}. \tag{5.13}$$

For the media composed of cylindrical particles, we have

$$\rho_h = \frac{\pi(\widetilde{d}^2 - \widetilde{c}^2)}{2\pi\widetilde{c}} = \frac{\widetilde{c}}{2}\left(\frac{1-\gamma}{\gamma}\right) = \frac{\varepsilon\widetilde{c}}{2(1-\varepsilon)}. \tag{5.14}$$

Substituting the value of ρ_h in the above equation (5.13), we have

$$K_z = \frac{\varepsilon^3}{4(1-\varepsilon)^2 L_{11}}, \tag{5.15}$$

where L_{11} is the hydrodynamic permeability of the membrane.

5.3 Asymptotic Solution of the Problem

The objective is to find solutions to the governing equations that regulate the flow of Carreau-Yasuda fluid through a swarm of biporous layered cylindrical particles. This investigation concentrates on fluid motion driven by a constant pressure gradient, which persists throughout both porous and non-porous fluid regions, *i.e.*, $\frac{\partial p}{\partial z} = -p_z$ (constant). The analytical solutions for the governing equations pose a challenge due to the inclusion of the nonlinear Forchheimer term in the Brinkman-Forchheimer equation, the nonlinear correlation between

shear stress and strain in Carreau-Yasuda fluid, and the variable permeabilities across different porous mediums. To address this challenge, the empirical perturbation approach is employed for solving the governing equations, particularly in situations characterized by a small Weissenberg number and large permeability of the porous medium. The governing equations are solved by considering the binomial series expansions of the varying permeability of the porous regions up to the second order approximations, where $\varepsilon_f < 1$ and $\varepsilon_b < 1$ are considered, *i.e.*,

$$\begin{aligned}
(1-\varepsilon_f r)^{-1} &= 1+\varepsilon_f r+\varepsilon_f^2 r^2+O(\varepsilon_f^3),\\
(1-\varepsilon_f r)^{-2} &= 1+2\varepsilon_f r+3\varepsilon_f^2 r^2+O(\varepsilon_f^3),\\
(1-\varepsilon_b r)^{-1} &= 1+\varepsilon_b r+\varepsilon_b^2 r^2+O(\varepsilon_b^3),\\
(1-\varepsilon_b r)^{-2} &= 1+2\varepsilon_b r+3\varepsilon_b^2 r^2+O(\varepsilon_b^3).
\end{aligned}$$

5.3.1 Perturbation Solution for Carreau-Yasuda Fluid

The perturbation series expansions, expressed in the powers of a small Weissenberg number, provide a direct representation for velocities in distinct porous and non-porous regions [141].

$$w_f(r) = w_{f0} + We^{a_1} w_{f1} + O(We^{2a_1}), \tag{5.16a}$$
$$w_b(r) = w_{b0} + We^{a_1} w_{b1} + O(We^{2a_1}), \tag{5.16b}$$
$$w_s(r) = w_{s0} + We^{a_1} w_{s1} + O(We^{2a_1}). \tag{5.16c}$$

Porous Region- I, *i.e.*, $a \le r \le b$
Introducing the equation (5.16a) into equations (5.6c) and (5.6d), the zeroth and first-order equations are obtained as

$$\frac{\partial p}{\partial z} = \frac{1}{r}\frac{\partial}{\partial r}\left(r\frac{\partial w_{f0}}{\partial r}\right) - \frac{w_{f0}}{k(1-\varepsilon_f r)^2} - \frac{F w_{f0}^2}{\sqrt{k}(1-\varepsilon_f r)}, \tag{5.17a}$$

$$\frac{1}{r}\frac{\partial}{\partial r}\left[r\left(\frac{\partial w_{f1}}{\partial r} + \frac{(n-1)(1-\eta)}{a_1}\left(\frac{\partial w_{f0}}{\partial r}\right)^{a_1}\frac{\partial w_{f0}}{\partial r}\right)\right] = \frac{w_{f1}}{k(1-\varepsilon_f r)^2} + \frac{2F w_{f0} w_{f1}}{\sqrt{k}(1-\varepsilon_f r)}. \tag{5.17b}$$

Solving the equations (5.17a)-(5.17b) governing the Carreau-Yasuda fluid flow through the Forchheimer region becomes challenging due to the nonlinearity introduced by the Forchheimer term and the variable permeability. To address the governing equation for the porous medium with high permeability (where $k \gg 1$), the regular perturbation method is employed

by introducing the small parameter $S = \frac{1}{\sqrt{k}}$. The equations (5.17a)-(5.17b) can be expressed in relation to the small parameter $S \ll 1$.

$$\frac{\partial p}{\partial z} = \frac{1}{r}\frac{\partial}{\partial r}\left(r\frac{\partial w_{f0}}{\partial r}\right) - \frac{S^2 w_{f0}}{(1-\varepsilon_f r)^2} - \frac{SFw_{f0}^2}{(1-\varepsilon_f r)}, \tag{5.17c}$$

$$\frac{1}{r}\frac{\partial}{\partial r}\left[r\left(\frac{\partial w_{f1}}{\partial r} + \frac{(n-1)(1-\eta)}{a_1}\left(\frac{\partial w_{f0}}{\partial r}\right)^{a_1}\frac{\partial w_{f0}}{\partial r}\right)\right] = \frac{S^2 w_{f1}}{(1-\varepsilon_f r)^2} + \left(\frac{2SFw_{f0}w_{f1}}{(1-\varepsilon_f r)}\right). \tag{5.17d}$$

The series expansions, formulated in terms of a small parameter S, offer a straightforward representation for velocities at zeroth and first orders [141].

$$w_{f0}(r) = w_{f00}(r) + Sw_{f01}(r) + S^2 w_{f02}(r) + O(S^3), \tag{5.18a}$$

$$w_{f1}(r) = w_{f10}(r) + Sw_{f11}(r) + S^2 w_{f12}(r) + O(S^3). \tag{5.18b}$$

Equating the coefficient of S in equation (5.17c), the zeroth, first and second order equations are obtained as

$$\frac{1}{r}\frac{\partial}{\partial r}\left(r\frac{\partial w_{f00}}{\partial r}\right) = \frac{\partial p}{\partial z}, \tag{5.19a}$$

$$\frac{1}{r}\frac{\partial}{\partial r}\left(r\frac{\partial w_{f01}}{\partial r}\right) - \frac{Fw_{f00}^2}{(1-\varepsilon_f r)} = 0, \tag{5.19b}$$

$$\frac{1}{r}\frac{\partial}{\partial r}\left(r\frac{\partial w_{f02}}{\partial r}\right) - \frac{w_{f00}}{(1-\varepsilon_f r)^2} - \frac{2Fw_{f00}w_{f01}}{(1-\varepsilon_f r)} = 0. \tag{5.19c}$$

The analytical solutions for the governing equations (5.19a)-(5.19b) have been derived, and the velocity expressions are provided in the Appendix.
Equating the coefficient of S in equation (5.17d), the zeroth, first and second order equations are obtained as

$$\frac{1}{r}\frac{\partial}{\partial r}\left[r\left(\frac{\partial w_{f10}}{\partial r} + \frac{(n-1)(1-\eta)}{a_1}\left(\frac{\partial w_{f00}}{\partial r}\right)^{a_1+1}\right)\right] = 0, \tag{5.20a}$$

$$\frac{1}{r}\frac{\partial}{\partial r}\left[r\left(\frac{\partial w_{f11}}{\partial r} + \frac{(a_1+1)(n-1)(1-\eta)}{a_1}\left(\frac{\partial w_{f00}}{\partial r}\right)^{a_1}\frac{\partial w_{f01}}{\partial r}\right)\right] - \frac{2Fw_{f00}w_{f10}}{(1-\varepsilon_f r)} = 0, \tag{5.20b}$$

$$\frac{1}{r}\frac{\partial}{\partial r}\left[r\left(\frac{\partial w_{f12}}{\partial r} + \frac{(a_1+1)(n-1)(1-\eta)}{2a_1}\left(\frac{\partial w_{f00}}{\partial r}\right)^{a_1-1}\left(a_1\left(\frac{\partial w_{f01}}{\partial r}\right)^2 + 2\frac{\partial w_{f00}}{\partial r}\frac{\partial w_{f02}}{\partial r}\right)\right)\right]$$
$$- \frac{w_{f10}}{(1-\varepsilon_f r)^2} - \frac{2F}{(1-\varepsilon_f r)}(w_{f00}w_{f11} + w_{f01}w_{f10}) = 0. \tag{5.20c}$$

The analytical solutions for the aforementioned equations (5.20a)-(5.20b) are determined using zeroth-order velocity expressions. However, the chapter does not include these solutions due to their extensive nature.

Porous Region- II, *i.e.*, $b \leq r \leq 1$

By incorporating the equation (5.16b) into (5.7a)-(5.7b), we derived both the zeroth and first-order equations. The zeroth and first-order equatione are determined as

$$\frac{\partial p}{\partial z} = \frac{1}{r}\frac{\partial}{\partial r}\left(r\frac{\partial w_{b0}}{\partial r}\right) - \frac{w_{b0}}{k(1-\varepsilon_b r)^2}, \tag{5.21a}$$

$$\frac{1}{r}\frac{\partial}{\partial r}\left[r\left(\frac{\partial w_{b1}}{\partial r} + \frac{(n-1)(1-\eta)}{a_1}\left(\frac{\partial w_{b0}}{\partial r}\right)^{a_1}\frac{\partial w_{b0}}{\partial r}\right)\right] = \frac{w_{b1}}{k(1-\varepsilon_b r)^2}. \tag{5.21b}$$

Addressing the challenge of solving the equations that govern the Carreau-Yasuda fluid flow through the Brinkman region becomes complex, primarily because of the variable permeability. To handle the governing equation for the porous medium with high permeability (where $k \gg 1$), the regular perturbation method is utilized by introducing the small parameter $S = \frac{1}{\sqrt{k}}$. Expressing equations (5.21a)-(5.21b) in terms of the small parameter $S \ll 1$ allows for a more manageable analysis.

$$\frac{\partial p}{\partial z} = \frac{1}{r}\frac{\partial}{\partial r}\left(r\frac{\partial w_{b0}}{\partial r}\right) - \frac{S^2 w_{b0}}{(1-\varepsilon_b r)^2}, \tag{5.21c}$$

$$\frac{1}{r}\frac{\partial}{\partial r}\left[r\left(\frac{\partial w_{b1}}{\partial r} + \frac{(n-1)(1-\eta)}{a_1}\left(\frac{\partial w_{b0}}{\partial r}\right)^{a_1}\frac{\partial w_{b0}}{\partial r}\right)\right] = \frac{S^2 w_{b1}}{(1-\varepsilon_b r)^2}. \tag{5.21d}$$

The provided equations for the zeroth and first-order velocities in Brinkman porous region II are expressed through a series-form solution in terms of small parameter S [141].

$$w_{b0}(r) = w_{b00}(r) + S w_{b01}(r) + S^2 w_{b02}(r) + O(S^3), \tag{5.22a}$$

$$w_{b1}(r) = w_{b10}(r) + S w_{b11}(r) + S^2 w_{b12}(r) + O(S^3). \tag{5.22b}$$

By incorporating equation (5.22a) into (5.21c) and matching the coefficients of powers of the parameter S, we find that the zeroth, first, and second order velocities for Brinkman porous media

$$\frac{1}{r}\frac{\partial}{\partial r}\left(r\frac{\partial w_{b00}}{\partial r}\right) = \frac{\partial p}{\partial z}, \tag{5.23a}$$

$$\frac{1}{r}\frac{\partial}{\partial r}\left(r\frac{\partial w_{b01}}{\partial r}\right) = 0, \tag{5.23b}$$

$$\frac{1}{r}\frac{\partial}{\partial r}\left(r\frac{\partial w_{b02}}{\partial r}\right) - \frac{w_{b00}}{(1-\varepsilon_b r)^2} = 0. \tag{5.23c}$$

The analytical solutions for the governing equations (5.23a)-(5.23c) have been derived, and the velocity expressions are provided in the Appendix.

By incorporating equation (5.22b) into (5.21d) and matching the coefficients of powers of the parameter S, we find that the zeroth, first, and second order velocities for Brinkman porous media

$$\frac{1}{r}\frac{\partial}{\partial r}\left[r\left(\frac{\partial w_{b10}}{\partial r}+\frac{(n-1)(1-\eta)}{a_1}\left(\frac{\partial w_{b00}}{\partial r}\right)^{a_1+1}\right)\right]=0, \tag{5.24a}$$

$$\frac{1}{r}\frac{\partial}{\partial r}\left[r\left(\frac{\partial w_{b11}}{\partial r}+\frac{(a_1+1)(n-1)(1-\eta)}{a_1}\left(\frac{\partial w_{b00}}{\partial r}\right)^{a_1}\frac{\partial w_{b01}}{\partial r}\right)\right]=0, \tag{5.24b}$$

$$\frac{1}{r}\frac{\partial}{\partial r}\left[r\left(\frac{\partial w_{b12}}{\partial r}+\frac{(a_1+1)(n-1)(1-\eta)}{2a_1}\left(\frac{\partial w_{b00}}{\partial r}\right)^{a_1-1}\left(a_1\left(\frac{\partial w_{b01}}{\partial r}\right)^2+2\frac{\partial w_{b00}}{\partial r}\frac{\partial w_{b02}}{\partial r}\right)\right)\right]$$
$$-\frac{w_{b10}}{(1-\varepsilon_b r)^2}=0. \tag{5.24c}$$

The analytical solutions for the aforementioned equations (5.24a)-(5.24c) are determined using zeroth-order velocity expressions. However, the chapter does not include these solutions due to their extensive nature.

Non-Porous (Clear Fluid) Region, *i.e.*, $1 \le r \le d$

By incorporating the equation $(5.16c)$ into equations $(5.8c)-(5.8d)$, we derive the zeroth and first-order equations. The resulting zeroth and first-order equations are expressed as

$$\frac{\partial p}{\partial z}=\frac{1}{r}\frac{\partial}{\partial r}\left(r\frac{\partial w_{s0}}{\partial r}\right), \tag{5.25a}$$

$$\frac{1}{r}\frac{\partial}{\partial r}\left[r\left(\frac{\partial w_{s1}}{\partial r}+\frac{(1-\eta)(n-1)}{a_1}\left(\frac{\partial w_{s0}}{\partial r}\right)^{a_1+1}\right)\right]=0. \tag{5.25b}$$

The equations given for the zeroth and first-order velocities in non-porous region are presented as a series-form solution using the small parameter S [141]

$$w_{s0}(r)=w_{s00}(r)+Sw_{s01}(r)+S^2w_{s02}(r)+O(S^3), \tag{5.26a}$$

$$w_{s1}(r)=w_{s10}(r)+Sw_{s11}(r)+S^2w_{s12}(r)+O(S^3). \tag{5.26b}$$

Equating the coefficient of powers of S in equation $(5.25a)$, the zeroth, first and second order equations are obtained as

$$\frac{1}{r}\frac{\partial}{\partial r}\left(r\frac{\partial w_{s00}}{\partial r}\right)=\frac{\partial p}{\partial z}, \tag{5.27a}$$

$$\frac{1}{r}\frac{\partial}{\partial r}\left(r\frac{\partial w_{s01}}{\partial r}\right)=0, \tag{5.27b}$$

$$\frac{1}{r}\frac{\partial}{\partial r}\left(r\frac{\partial w_{s02}}{\partial r}\right)=0. \tag{5.27c}$$

The analytical solutions for the governing equations (5.27*a*) – (5.27*c*) have been obtained, and the velocity expressions are detailed in the Appendix.

By incorporating equation (5.26*b*) into (5.25*b*) and equating the coefficients of powers of the parameter S, the zeroth, first, and second order velocities for non-porous region are obtained as

$$\frac{1}{r}\frac{\partial}{\partial r}\left[r\left(\frac{\partial w_{s10}}{\partial r}+\frac{(1-\eta)(n-1)}{a_1}\left(\frac{\partial w_{s00}}{\partial r}\right)^{a_1+1}\right)\right]=0, \tag{5.28a}$$

$$\frac{1}{r}\frac{\partial}{\partial r}\left[r\left(\frac{\partial w_{s11}}{\partial r}+\frac{(1-\eta)(n-1)(a_1+1)}{a_1}\left(\frac{\partial w_{s00}}{\partial r}\right)^{a_1}\left(\frac{\partial w_{s01}}{\partial r}\right)\right)\right]=0, \tag{5.28b}$$

$$\frac{1}{r}\frac{\partial}{\partial r}\left[r\left(\frac{\partial w_{s12}}{\partial r}+\frac{(1-\eta)(n-1)(a_1+1)}{2a_1}\left(\frac{\partial w_{s00}}{\partial r}\right)^{a_1-1}\left\{a_1\left(\frac{\partial w_{s01}}{\partial r}\right)^2+2\left(\frac{\partial w_{s00}}{\partial r}\frac{\partial w_{s02}}{\partial r}\right)\right\}\right)\right]=0 \tag{5.28c}$$

The solutions to equations (5.28*a*) – (5.28*c*) are found through zeroth-order velocity expressions, but the manuscript omits these solutions because of their extensive nature.

5.3.2 Numerical Solution for Small Weissenberg and Permeability $(i.e., S \gg 1)$

In the previous calculation, the velocity profiles for different regions are determined through the regular perturbation technique, considering small Weissenberg and large Darcy numbers. The singularly perturbed boundary value problems arise in the regulation of Carreau-Yasuda fluid flow within various porous regions when dealing with small Weissenberg and Darcy numbers. The formulations of the boundary value problems for singularly perturbed systems are presented in relation to a small parameter $S^{-1}=\frac{1}{S}=\sqrt{k}$. The equations for the Forchheimer region under a small Weissenberg number are given for both zeroth and first orders

$$S^{-2}\left(\frac{\partial p}{\partial z}\right)=S^{-2}\left[\frac{1}{r}\frac{\partial}{\partial r}\left(r\frac{\partial w_{f0}}{\partial r}\right)\right]-\frac{w_{f0}}{(1-\varepsilon_f r)^2}-S^{-1}\frac{Fw_{f0}^2}{(1-\varepsilon_f r)}, \tag{5.29a}$$

$$S^{-2}\left(\frac{1}{r}\frac{\partial}{\partial r}\left[r\left(\frac{\partial w_{f1}}{\partial r}+\frac{(n-1)(1-\eta)}{a_1}\left(\frac{\partial w_{f0}}{\partial r}\right)^{a_1}\frac{\partial w_{f0}}{\partial r}\right)\right]\right)=\frac{w_{f1}}{(1-\varepsilon_f r)^2}+\frac{2S^{-1}Fw_{f0}w_{f1}}{(1-\varepsilon_f r)}. \tag{5.29b}$$

The equations for the Brinkman region under a small Weissenberg number are given for both zeroth and first orders

$$S^{-2}\left(\frac{\partial p}{\partial z}\right) = S^{-2}\left[\frac{1}{r}\frac{\partial}{\partial r}\left(r\frac{\partial w_{b0}}{\partial r}\right)\right] - \frac{w_{b0}}{(1-\varepsilon_b r)^2}, \tag{5.30a}$$

$$S^{-2}\left(\frac{1}{r}\frac{\partial}{\partial r}\left[r\left(\frac{\partial w_{b1}}{\partial r} + \frac{(n-1)(1-\eta)}{a_1}\left(\frac{\partial w_{b0}}{\partial r}\right)^{a_1}\frac{\partial w_{b0}}{\partial r}\right)\right]\right) = \frac{w_{b1}}{(1-\varepsilon_b r)^2}. \tag{5.30b}$$

Obtaining analytical solutions for the singularly perturbed BVPs mentioned above is challenging. To obtain solutions for the aforementioned BVPs, the governing equations (5.6)-(5.8) are tackled using the numerical scheme NDSolve in Mathematica. The graphical representation and comparison of numerical solutions for the governing equations, considering small Weissenberg and Darcy numbers, are presented and contrasted with asymptotic solutions in situations characterized by small Weissenberg and large Darcy numbers.

5.3.3 Temperature Analysis

The velocity, flow rate, membrane permeability, and Kozeny constant are determined in the preceding subsections for the creeping, viscous flow of a Carreau-Yasuda fluid through a membrane. This is achieved using both asymptotic series expansions and numerical methods, taking into account the pertinent boundary conditions. The influence of viscoelastic rheological and porous layer parameters on temperature can be analyzed by examining the fluid flow velocity in various porous and non-porous regions, according to the proposed objective. Now, we will utilize this flow velocity to examine the radial temperature variation within a porous layered cylinderical particle featuring a solid core. The analysis presumes a uniform material with consistent heat transfer occurring throughout (local thermal equilibrium). To examine heat transfer across various regions, we've streamlined the equation by omitting heat sources, longitudinal heat conduction along the cylinder, and the conduction of heat within the material. The subsequent mathematical equations that govern energy transfer are deduced as follows ([196] [7], [197], [198]):

$$\frac{\widetilde{K}}{\widetilde{r}}\frac{\partial}{\partial\widetilde{r}}\left(\widetilde{r}\frac{\partial\widetilde{T}_f}{\partial\widetilde{r}}\right) + \frac{\widetilde{\mu}_0\widetilde{w}_f^2}{\widetilde{k}_f(\widetilde{r})} + \frac{\widetilde{C}_F\widetilde{\rho}\widetilde{w}_f^3}{\sqrt{\widetilde{k}_f(\widetilde{r})}} + \left[\widetilde{\mu}_\infty + (\widetilde{\mu}_0 - \widetilde{\mu}_\infty)\left\{1 + \frac{n-1}{a_1}\left(\lambda\frac{\partial\widetilde{w}_f}{\partial\widetilde{r}}\right)^{a_1}\right\}\right]\left(\frac{\partial\widetilde{w}_f}{\partial\widetilde{r}}\right)^2 = 0, \tag{5.31a}$$

$$\frac{\widetilde{K}}{\widetilde{r}}\frac{\partial}{\partial\widetilde{r}}\left(\widetilde{r}\frac{\partial\widetilde{T}_b}{\partial\widetilde{r}}\right) + \frac{\widetilde{\mu}_0\widetilde{w}_b^2}{\widetilde{k}_b(\widetilde{r})} + \left[\widetilde{\mu}_\infty + (\widetilde{\mu}_0 - \widetilde{\mu}_\infty)\left\{1 + \frac{n-1}{a_1}\left(\lambda\frac{\partial\widetilde{w}_b}{\partial\widetilde{r}}\right)^{a_1}\right\}\right]\left(\frac{\partial\widetilde{w}_b}{\partial\widetilde{r}}\right)^2 = 0, \tag{5.31b}$$

$$\frac{\widetilde{K}}{\widetilde{r}}\frac{\partial}{\partial\widetilde{r}}\left(\widetilde{r}\frac{\partial\widetilde{T}_s}{\partial\widetilde{r}}\right)+\left[\widetilde{\mu}_\infty+(\widetilde{\mu}_0-\widetilde{\mu}_\infty)\left\{1+\frac{n-1}{a_1}\left(\lambda\frac{\partial\widetilde{w}_s}{\partial\widetilde{r}}\right)^{a_1}\right\}\right]\left(\frac{\partial\widetilde{w}_s}{\partial\widetilde{r}}\right)^2=0, \tag{5.31c}$$

where the variables include $\widetilde{T}$ for temperature, $\widetilde{\rho}$ for fluid density, $\widetilde{c}_p$ for specific heat at constant pressure, and $\widetilde{K}$ for thermal conductivity.

The appropriate interface and boundary conditions for temperature distribution in dimensional form are taken into account as follows:

1. The surface temperature at the outermost layer of the solid core is considered, *i.e.*,

$$\widetilde{T}_f=\widetilde{T}_w,\quad \text{at}\quad \widetilde{r}=\widetilde{a}, \tag{5.32a}$$

   where $\widetilde{T}_w$ is the surface temperature.

2. The temperature and temperature gradient continuity are taken into account at the interface between two porous mediums, *i.e.*,

$$\widetilde{T}_f=\widetilde{T}_b,\quad \text{at}\quad \widetilde{r}=\widetilde{b}, \tag{5.32b}$$

$$\frac{d\widetilde{T}_f}{d\widetilde{r}}=\frac{d\widetilde{T}_b}{d\widetilde{r}},\quad \text{at}\quad \widetilde{r}=\widetilde{b}, \tag{5.32c}$$

   where the subscriepts f and b repersent the Forchheimer and Brinkman porous regions, respectively.

3. The temperature and temperature gradient continuity are taken into account at the interface between Brinkman and Stokes regions, *i.e.*,

$$\widetilde{T}_b=\widetilde{T}_s,\quad \text{at}\quad \widetilde{r}=\widetilde{c}, \tag{5.32d}$$

$$\frac{d\widetilde{T}_b}{d\widetilde{r}}=\frac{d\widetilde{T}_s}{d\widetilde{r}},\quad \text{at}\quad \widetilde{r}=\widetilde{c}, \tag{5.32e}$$

   where the subscriepts s repersents the Stokes flow (non-porous) region.

4. On the virtual cell surface, the temperature gradient is considered to be zero, *i.e.*,

$$\frac{d\widetilde{T}_s}{d\widetilde{r}}=0,\quad \text{at}\quad \widetilde{r}=\widetilde{d}. \tag{5.32f}$$

By employing the non-dimensional parameters defined in equation (5), the non-dimensional form of the energy equations for different porous and non-porous regions are given as follows:

$$\frac{1}{r}\frac{d}{dr}\left(r\frac{d\theta_f}{dr}\right)+Br\Big[\left(\frac{dw_f}{dr}\right)^2+\frac{(n-1)(1-\eta)}{a_1}\left(We\frac{dw_f}{dr}\right)^{a_1}\left(\frac{dw_f}{dr}\right)^2+\frac{w_f^2}{k_f(r)}+\frac{Fw_f^3}{\sqrt{k_f(r)}}\Big]=0, \tag{5.33a}$$

$$\frac{1}{r}\frac{d}{dr}\left(r\frac{d\theta_b}{dr}\right)+Br\Big[\left(\frac{dw_b}{dr}\right)^2+\frac{(n-1)(1-\eta)}{a_1}\left(We\frac{dw_b}{dr}\right)^{a_1}\left(\frac{dw_b}{dr}\right)^2+\frac{w_b^2}{k_b(r)}\Big]=0, \tag{5.33b}$$

$$\frac{1}{r}\frac{d}{dr}\left(r\frac{d\theta_s}{dr}\right)+Br\Big[\left(\frac{dw_s}{dr}\right)^2+\frac{(n-1)(1-\eta)}{a_1}\left(We\frac{dw_s}{dr}\right)^{a_1}\left(\frac{dw_s}{dr}\right)^2\Big]=0. \tag{5.33c}$$

The dimensionless boundary and interface conditions are outlined below:

$$\begin{aligned}
\theta_f &= 1, \quad \text{at} \quad r=a,\\
\theta_f=\theta_b, \quad \text{and} \quad \frac{d\theta_f}{dr}&=\frac{d\theta_b}{dr}, \quad \text{at} \quad r=b,\\
\theta_b=\theta_s, \quad \text{and} \quad \frac{d\theta_b}{dr}&=\frac{d\theta_s}{dr}, \quad \text{at} \quad r=1,\\
\frac{d\theta_s}{dr}&=0, \quad \text{at} \quad r=d.
\end{aligned} \tag{5.34}$$

5.3.4 Solution of Temperature Equations

The equations $(5.33a)-(5.33c)$ depict second-order ordinary differential equations that are both linear and non-homogeneous. They describe the temperature distribution within different porous and non-porous regions, expressed in terms of velocities. The velocity of both porous and non-porous regions have been evaluated numerically and asymptotically in the preceding subsections. The method of variation of parameters is utilized to derive the temperature distribution for both porous and non-porous regions. The mathematical representation of the temperature distribution within the Forchheimer region is obtained as

$$\theta_f = T_{f1}\log(r)+T_{f2}-A_f(r)\log(r)+B_f(r), \tag{5.35a}$$

$$A_f(r)=\int_a^r rN_f(r)dr,$$

$$B_f(r)=\int_a^r r\log(r)N_f(r)dr,$$

$$N_f(r)=Br\Big[\left(\frac{dw_f}{dr}\right)^2+\frac{(n-1)(1-\eta)}{a_1}\left(We\frac{dw_f}{dr}\right)^{a_1}\left(\frac{dw_f}{dr}\right)^2+\frac{w_f^2}{k_f(r)}+\frac{Fw_f^3}{\sqrt{k_f(r)}}\Big].$$

The mathematical representation of the temperature distribution within the Brinkman region is demonstrated as

$$\theta_b = T_{b1}\log(r) + T_{b2} - A_b(r)\log(r) + B_b(r), \tag{5.35b}$$
$$A_b(r) = \int_b^r rN_b(r)dr,$$
$$B_b(r) = \int_b^r r\log(r)N_b(r)dr,$$
$$N_b(r) = Br\Big[\left(\frac{dw_b}{dr}\right)^2 + \frac{(n-1)(1-\eta)}{a_1}\left(We\frac{dw_b}{dr}\right)^{a_1}\left(\frac{dw_b}{dr}\right)^2 + \frac{w_b^2}{k_b(r)}\Big].$$

The mathematical representation of the temperature distribution within the non-porous region is provided as

$$\theta_s = T_{s1}\log(r) + T_{s2} - A_s(r)\log(r) + B_s(r), \tag{5.35c}$$
$$A_s(r) = \int_1^r rN_s(r)dr,$$
$$B_s(r) = \int_1^r r\log(r)N_s(r)dr,$$
$$N_s(r) = Br\Big[\left(\frac{dw_s}{dr}\right)^2 + \frac{(n-1)(1-\eta)}{a_1}\left(We\frac{dw_s}{dr}\right)^{a_1}\left(\frac{dw_s}{dr}\right)^2\Big].$$

The constants $T_{f1}, T_{f2}, T_{b1}, T_{b2}, T_{s1}$, and T_{s2} involved in the equations (5.35*a*) – (5.35*c*) can be determined through the specified boundary conditions (5.34). The integrals required for evaluating the coefficients A_f, B_f, A_b, B_b, A_s, and B_s are computed numerically using Mathematica 10.3 software.

5.3.5 Nusselt Number (Nu)

In thermal fluid dynamics, the Nusselt number signifies the ratio of overall heat transfer to conductive heat transfer at a fluid boundary, combining both conduction and convection, where convection involves fluid motion and conduction diffusion. Typically falling between 1 and 10, the Nusselt number describes either slug flow or laminar flow. A higher Nusselt number suggests that conductive heat transfer dominates total heat transfer (convection + conduction) across a boundary, leading to a more pronounced temperature increase. The heat transfer coefficient on the surface of the solid cylinder is defined by Fourier's heat conduction law

$$\widetilde{q}'' = \widetilde{K}\left(\frac{d\widetilde{T}_f}{d\widetilde{r}}\right), \quad \text{at} \quad \widetilde{r} = \widetilde{a}, \tag{5.36}$$

where $\widetilde{q}''$ represents the constant heat flux.
The non-dimensional form of the above relation (5.36) is provided below

$$Nu = \frac{d\theta_f}{dr}, \quad \text{at} \quad r = a, \tag{5.37}$$

where Nu is the Nusselt number.

5.4 Results and Discussion

The present study explores the impact of variable permeability in a biporous layer structure within the medium, coupled with the viscoelastic properties of the fluid, on the flow of Carreau-Yasuda fluid through a aggregates of biporous layered cylindrical shaped particles. The objective is to investigate how the varying permeability, diverse porous media, and the non-Newtonian Carreau-Yasuda fluid collectively play a crucial role in modeling fluid flow through a membrane. The physical scketch of the proposed work is constructed in a way that the Brinkman-Forchheimer region close to the solid core of the cylindrical particle is governed by Brinkman-Forchhheimer equation under variable permeability, and a concentric Brinkman porous region is regulated by the Brinkman equation under variable permeability of the medium. However, a region free from the porous structure known as a non-porous region, is governed by the Stokes equation. The mathematical equations regulating the flow of Carreau-Yasuda fluid through a membrane constituting a swarm of biporous layered cylindrical particles are nonlinear and coupled in terms of velocity and shear stress of Carreau-Yasuda fluid and it is difficult to obtain the analytical expressions of the hydrodynamic quantities. With the objective of finding the solutions of the governing equations, the regular perturbation method has been used to obtain the asymptotic expansions of the hydrodynamic quantities. The influence of control parameters like porous medium parameters, Carreau-Yasuda parameters and volume fraction on the hydrodynamic permeability of the membrane, Kozeny constant are investigated. The comparison of results with previously published works in case of single porous layered cylindrical particles are established in the present section. The analysis maintains a constant value of the steady-state pressure gradient, denoted as $p_z = 1$.

5.4.1 Parameter Selection

The graphical analysis in the current work involves extracting values for numerous parameters from various sources. Table 1 provides the range of control parameter values along with their corresponding resources.

Range of parameters		
Parameters	Range	References
Forchheimer number F	0.0-2.0	[7], [8]
Particle volume fraction γ	0.1-1.0	[3], [96]
Permeability k	$(0,\infty)$	[2], [3]
Power-law index n	0.1-2.0	[18], [199]
Nusselt number Nu	2.0-8.0	[7], [8]
Steady pressure gradient p_z	1-10	[5], [167]
Transition parameter a_1	1.0-4.0	[18]
Viscosity ratio parameter η	0.1-0.4	[18], [199]
Weissenberg number We	0.0-0.8	[18], [199]
Stress-jump parameter β	$(-1,1)$	[3], [5]

Table 5.1: Range of parameters with their references

5.4.2 Limiting Cases and Model Validation

Taking into account the Brinkman-Forchheimer equation that governs fluid flow near the solid core of a cylindrical particle, the inclusion of an intermediate Brinkman porous region regulated by the Brinkman equation, variable permeability, and an approach to heat transfer enhances the comprehensiveness of the proposed study. The integration of certain parameters serves to alleviate the intricacy of the model and facilitates the ability to draw analogies with prior research. The limiting cases of present model and their comparisons with the previously published works are descibed below:

1. As the transition parameter a_1 is set to the value 2, the present viscoelastic Carreau-Yasuda model reduces to Carreau fluid model.

2. Further, as the Carreau fluid parameters $(We = 0, n = 1)$, the Carreau fluid model simplifies to the Newtonian fluid model.

3. As the permeability parameters $(\varepsilon_f \to 0)$ and $(\varepsilon_b \to 0)$, the proposed variable permeability model simplifies to the model with constant permeability.

4. As the porous-porous interface radius converges towards the clear fluid interface (*i.e.*, as b approaches 1), the current model simplifies to a single-layered porous cylindrical particle with a solid core.

5. When the Forchheimer number vanishes(*i.e.*, $F \to 0$), the Brinkmann-Forchheimer model converges to the Brinkman model.

6. When the permeability of the porous medium is extremely high, denoted as $(k \to \infty)$, the porous medium behaves like a clear fluid.

The results of the present work for the particular values of control parameters validate the previously published works. The following results and their validations are described below:

1. The current work have been validated with the recently published work of Saini *et al.* [199] under the limiting cases of Carreau fluid $(a_1 = 2)$, constant permeability $(\varepsilon_f \to 0, \varepsilon_b \to 0)$ and, single Brinkmann layer $(b \to 1, F = 0)$, which shows a perfect overlapping alignment of the graphs of fluid velocity of both works.

2. The hydrodynamic permeability L_{11} derived from current study shows a perfect overlapping alignment with the study of Deo *et al.* [3] under the limiting cases of Newtonian fluid $(We = 0, n = 1)$, constant permeability $(\varepsilon_f \to 0, \varepsilon_b \to 0)$, and fully solid cylinder without a porous layer $(k \to \infty)$.

5.4.3 Velocity Profile (w)

The rheological parameter known as the transition parameter a_1 in the Carreau-Yasuda fluid model plays a crucial role in determining the extent of the transition state between the zero shear rate and the power-law regions [200]. This parameter has a notable impact on fluid flow velocity when passing through a membrane composed of porous layered cylinderical particles, regardless of whether the permeability is large or small. In the case of a shear thinning fluid flowing in a highly permeable porous media $(k = 10)$, an augmentation in the transition parameter results in diminution of fluid flow velocity in all regions of the biporous layered circular cylinder or in other words the membrane's flow velocity decreases as the width of transition region (the transition state between the zero shear rate and the power-law behavior of Carreau-Yasuda fluid) gets decreases (Figure 5.3a).

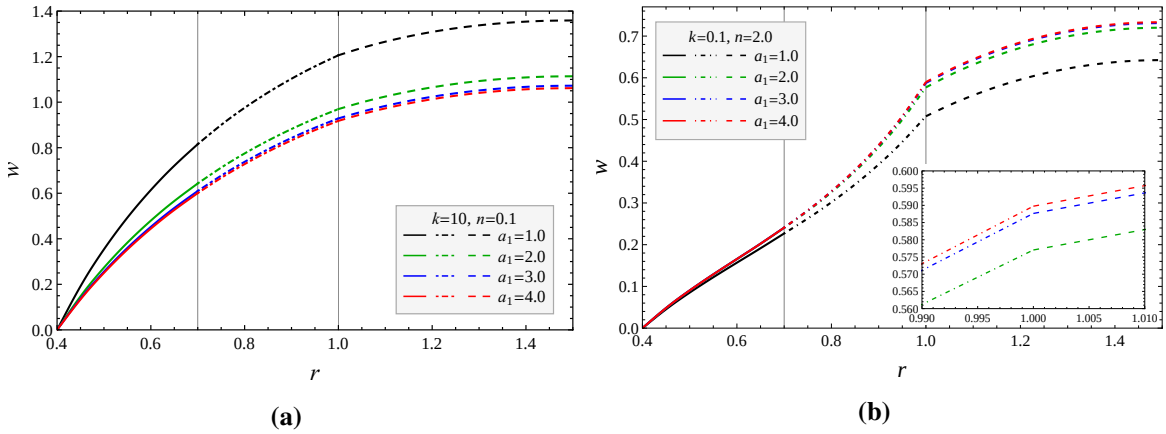

Figure 5.3: Dimensionless velocity w with radial distance r for various values of transition parameter a_1 $(a_1 = 1,2,3,4)$ under ((**5.3a**)) large Darcy number $(k = 10, n = 0.1, \varepsilon_f = \varepsilon_b = 0.5)$ and (**5.3b**) small Darcy number $(k = 0.1, n = 2.0, \varepsilon_f = \varepsilon_b = 0.2)$. $(a = 0.4, b = 0.7, \gamma = 0.445, \beta = 0.5, We = 0.2, \eta = 0.1, F = 1)$

However, this behavior gets reversed for shear thickening Carreau-Yasuda fluid as depicted for low permeability in Figure 5.3b. It will be interesting to observe how the relative thicknesses of the two porous layers in a biporous layered cylindrical particle affect the fluid velocity. As the thickness between the solid surface and the porous-porous interface increases, particularly by expanding the thickness of region I (known as the Forchheimer porous region), the flow velocity decreases in both cases of permeability due to a larger region experiencing inertial resistance. Moreover, an enhanced decay is observed for increased Forchheimer layer thickness (Figure 5.4). Figures 5.5 and 5.6 present the influence

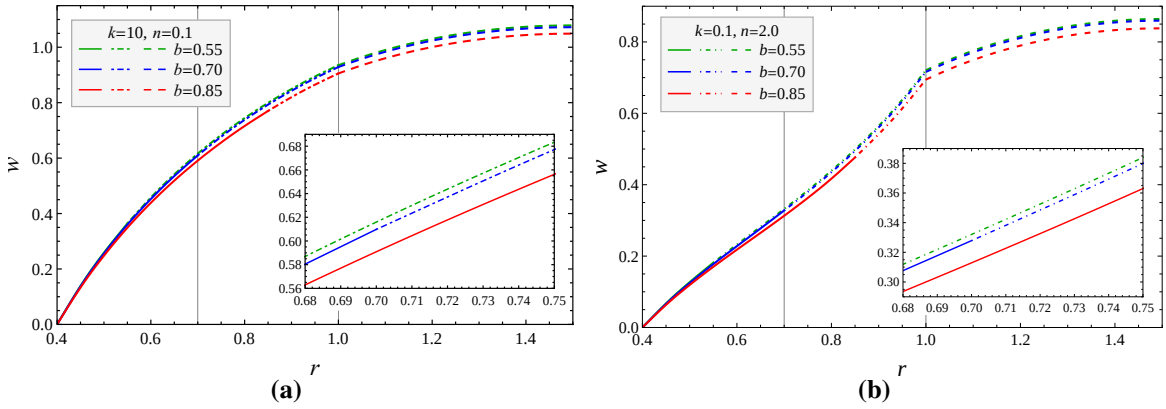

Figure 5.4: Dimensionless velocity w with radial distance r for various thicknesses of Forchheimer layer b $(b = 0.55, 0.7, 0.85)$ under (**5.4a**) large Darcy number $(k = 10, n = 0.1, \varepsilon_f = \varepsilon_b = 0.5)$ and (**5.4b**) small Darcy number $(k = 0.1, n = 2, \varepsilon_f = \varepsilon_b = 0.1)$. $(a = 0.4, \gamma = 0.445, \beta = 0.5, We = 0.2, a_1 = 3, \eta = 0.1, F = 1)$

of radially varying permeability on the flow velocity. Figure 5.5a illustrates a decrease in

fluid velocity that is associated with a consistent increase in the permeability parameters. This occurs while maintaining identical values for both the permeability parameters ε_f and

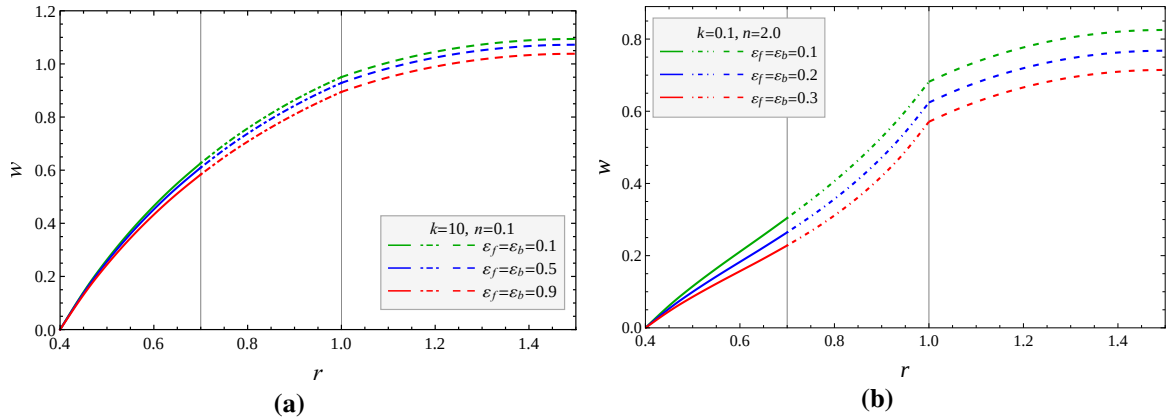

Figure 5.5: Dimensionless velocity w with radial distance r for various values of permeability parameters $(\varepsilon_f, \varepsilon_b)$ under **(5.5a)** large Darcy number $(k = 10, n = 0.1, \varepsilon_f = \varepsilon_b = 0.1, 0.5, 0.9)$ and **(5.5b)** small Darcy number $(k = 0.1, n = 2, \varepsilon_f = \varepsilon_b = 0.1, 0.2, 0.3)$. $(a = 0.4, b = 0.7, \gamma = 0.445, \beta = 0.5, We = 0.2, a_1 = 3, \eta = 0.1, F = 1)$

ε_b in the Forchheimer and Brinkman regions, respectively. This can be interpreted as an increase in the permeability parameter $(\varepsilon_f \backslash \varepsilon_b)$ reduces the overall permeability of the porous region, resulting in a reduction in the flow velocity. The observations are similar for both cases of permeability but the decay rate of flow velocity is more pronounced in the small permeability case owing to the increased contribution of Brinkman and Forchheimer terms in the momentum equation, which are influenced by the small Darcy number Figure 5.5. The analysis of the impact of radially varying permeability on flow velocity, when the permeability of both the layers follows opposite variations, is illustrated in Figures 5.6a and 5.6b. The findings indicate that the velocity increases when the permeability parameter of the Forchheimer layer dominates the permeability parameter of the Brinkman layer, regardless of the medium's permeability being large or small. Alternatively, it can be inferred that the flow velocity in all three regions exhibits an increase when the permeability of the Brinkman region surpasses that of the Brinkman Forchheimer region. This can be attributed to the fact that Brinkamnn region doesn't have an inertial resistance so, an increasing permeability (decreasing ε_b) in Brinkman region dominates the enhanced resistance of Forchheimer region due to increasing ε_b. The same effect with enhanced diffrence can be seen for low permeability as in this case the porous medium resistance and the inertial resistance become more influencial in comparision to large permeability.

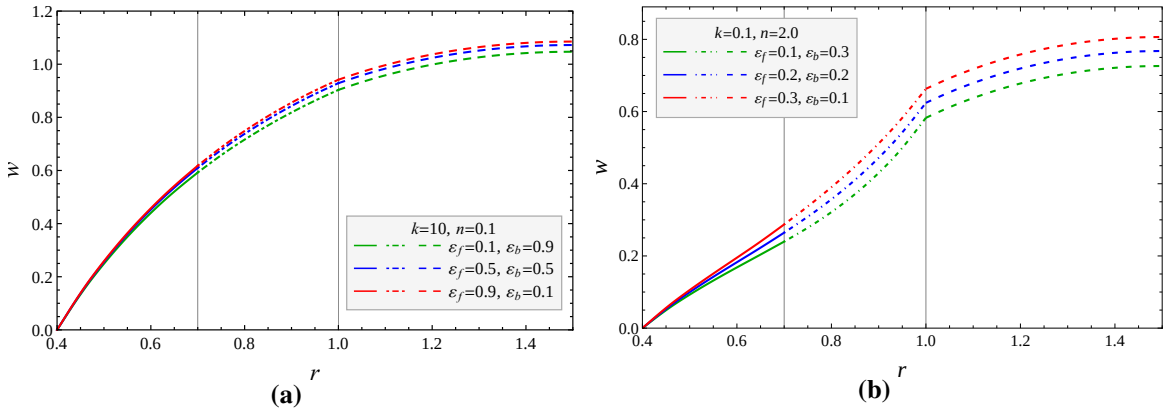

Figure 5.6: Dimensionless velocity w with radial distance r for comparative values of permeability parameters $(\varepsilon_f, \varepsilon_b)$ under **(5.6a)** large Darcy number $(k = 10, n = 0.1)$ and **(5.6b)** small Darcy number $(k = 0.1, n = 2)$. $(a = 0.4, b = 0.7, \gamma = 0.445, \beta = 0.5, We = 0.2, a_1 = 3, \eta = 0.1, F = 1)$

5.4.4 Flow Rate (Q_s)

This subsection examines the impact of various Carreau-Yasuda and porous layer parameters on volumetric flow rate Q_s. Figure 5.7 shows the effect of the Forchheimer number, which incorporates fluid inertia in the Brinkman-Forchheimer equation, on the flow rate across different Weissenberg numbers. The analysis for large permeability pertains to a shear thinning fluid $(n = 0.1)$, while the small permeability case relates to a shear thickening fluid $(n = 2.0)$. The increasing Forchheimer number results in a decreased volumetric flow rate for various Weissenberg numbers due to the growing influence of fluid inertia resistance. The rate of decay in flow rate with Forchheimer number is more pronounced for low permeability compared to high permeability of the porous medium. It is noted that there is a reciprocal relationship between flow rate and Weissenberg number concerning the shear thinning and thickening behavior exhibited by the Carreau-Yasuda fluid. As anticipated, considering the physical significance of porous mediums with varying permeabilities, the flow rate for any Forchheimer number is greater when the permeability of the porous medium is large compared to when it is small.

The analysis of the thickness of Forchheimer porous region, governed by the Brinkman-Forchheimer equation, significantly affects the flow rate of fluid passing through a swarm of porous cylindrical particles. As the thickness of the Forchheimer region increases, the flow rate decreases due to the substantial resistance it imposes on the fluid flow, as shown in Figure 5.8. Additionally, an increase in the viscosity ratio parameter results in a reduction of the flow rate, which is more pronounced in porous media with high permeability compared to those with low permeability. The analysis of the neighboring particles' role and contributions within a swarm is conducted by examining the particle volume fraction on the

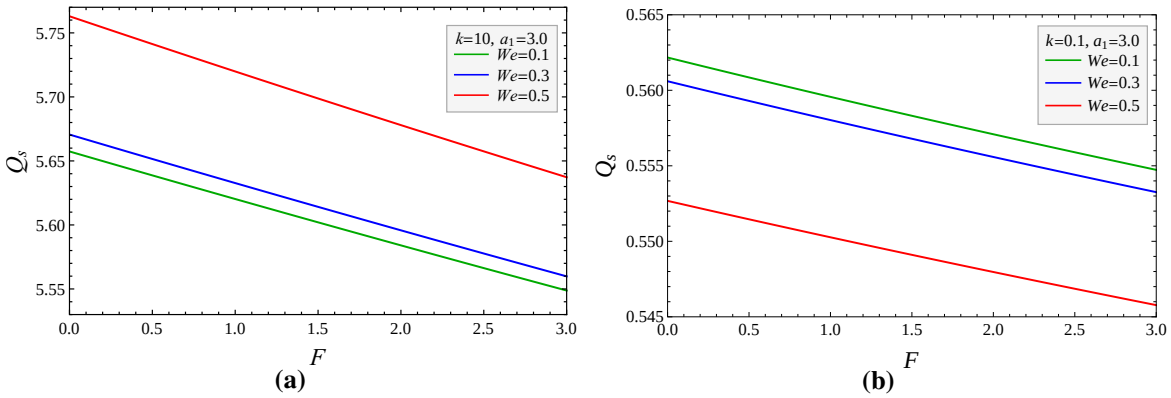

Figure 5.7: Changes in flow rate Q_s with Forchheimer number F for various values of the Weissenberg number We $(We = 0.1, 0.3, 0.5)$ under **(5.7a)** large Darcy number $(k = 10, n = 0.1, \varepsilon_f = \varepsilon_b = 0.5, \eta = 0.1)$ and **(5.7b)** small Darcy number $(k = 0.1, n = 2, \varepsilon_f = \varepsilon_b = 0.2, \eta = 0.4)$. $(a = 0.4, b = 0.7, \gamma = 0.444, a_1 = 3, \beta = 0.5)$

flow rate. The graphical analysis in Figure 5.9 delves into the impact of alterations in parti-

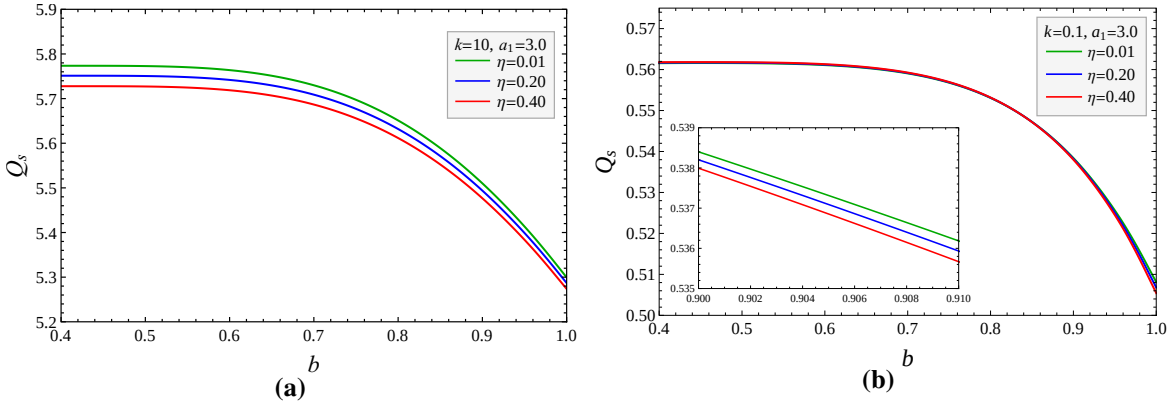

Figure 5.8: Changes in flow rate Q_s with thickness of Forchheimer layer b for various values of the viscosity ratio parameter η $(\eta = 0.01, 0.2, 0.3)$ under **(5.8a)** large Darcy number $(k = 10, n = 0.1, We = 0.5, \varepsilon_f = \varepsilon_b = 0.5)$ and **(5.8b)** small Darcy number $(k = 0.1, n = 2, We = 0.2, \varepsilon_f = \varepsilon_b = 0.2)$. $(a = 0.4, b = 0.7, \gamma = 0.444, a_1 = 3, \beta = 0.5, F = 1)$

cle volume fraction γ on the volumetric flow rate across a range of values for the transition state parameter a_1. As the volume fraction of particles increases, it reduces the clear fluid flow region, consequently leading to a decrease in the volumetric flow rate with increasing particle volume fraction. A reduction in flow rate with an increasing transition parameter a_1 is observed for shear-thinning fluids with high permeability, whereas a slight increase in flow rate with an increasing transition parameter is noted for shear-thickening fluids with low permeability.

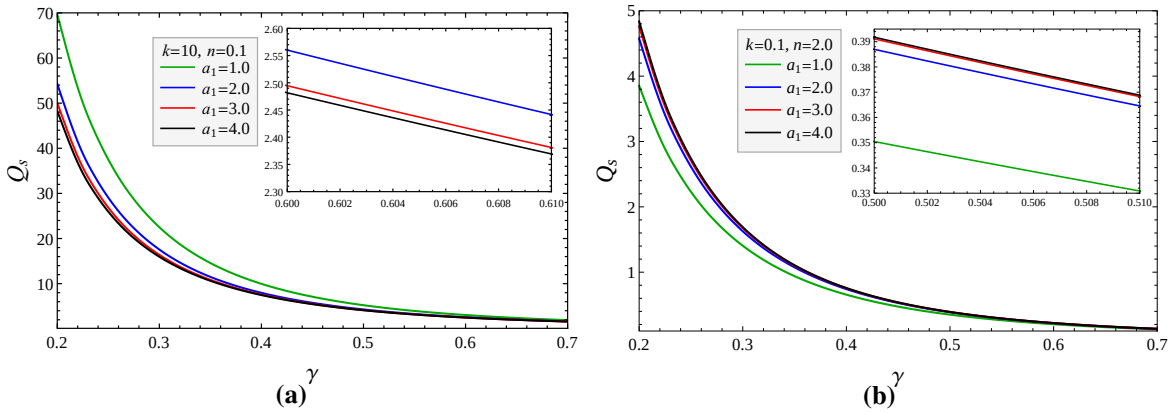

Figure 5.9: Changes in flow rate Q_s with particle volume fraction γ for various values of the transition parameter a_1 $(a_1 = 1,2,3,4)$ under **(5.9a)** large Darcy number $(k = 10, n = 0.1, \varepsilon_f = \varepsilon_b = 0.5)$ and **(5.9b)** small Darcy number $(k = 0.1, n = 2, \varepsilon_f = \varepsilon_b = 0.2)$. $(a = 0.4, b = 0.7, F = 1, \beta = 0.5, We = 0.2, \eta = 0.1)$

5.4.5 Hydrodynamic Permeability (L_{11})

This subsection explores how different Carreau-Yasuda and porous layer parameters influence the hydrodynamic permeability L_{11}. The influence of the porous layer thickness on the membrane's hydrodynamic permeability is shown for large and small permeabilities in Figures 5.10a and 5.10b, respectively. The membrane's hydrodynamic permeability decreases as the thickness of porous-porous interface from the solid surface increases. This can be interpreted as the flow velocity and consequently, the hydrodynamic permeability of the membrane decreases with increasing thickness of Forchheimer layer b owing to a wider region experiencing inertial resistance of porous medium. Figures 5.11a and 5.11b demon-

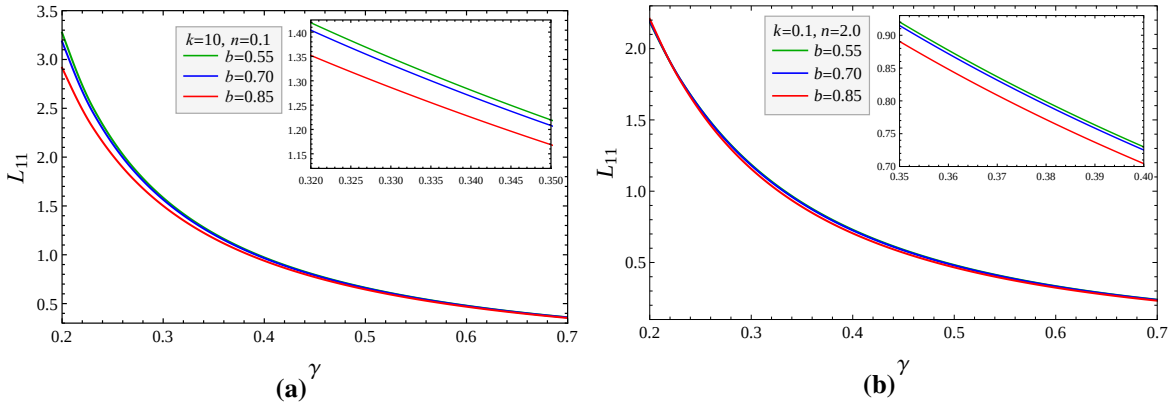

Figure 5.10: Dimensionless hydrodynamic permeability L_{11} with particle volume fraction γ for different thicknesses of Forchheimer layer b $(b = 0.55, 0.7, 0.85)$ under **(5.10a)** large Darcy number $(k = 10, n = 0.1, \varepsilon_f = \varepsilon_b = 0.5)$ and **(5.10b)** small Darcy number $(k = 0.12, n = 2, \varepsilon_f = \varepsilon_b = 0.1)$. $(a = 0.4, \beta = 0.5, We = 0.2, a_1 = 3, \eta = 0.1, F = 1)$

strate a concurrent increase in the permeability parameters of radially varying permeability

inside the porous layers of region I and region II, resulting in a decline in the hydrodynamic permeability of the membrane. Although the observations are same in both cases of permeability but the large permeability analysis corresponds to shear thinning fluid $(n = 0.1)$, whereas the small permeability case corresponds to shear thickening fluid $(n = 2.0)$. Fig-

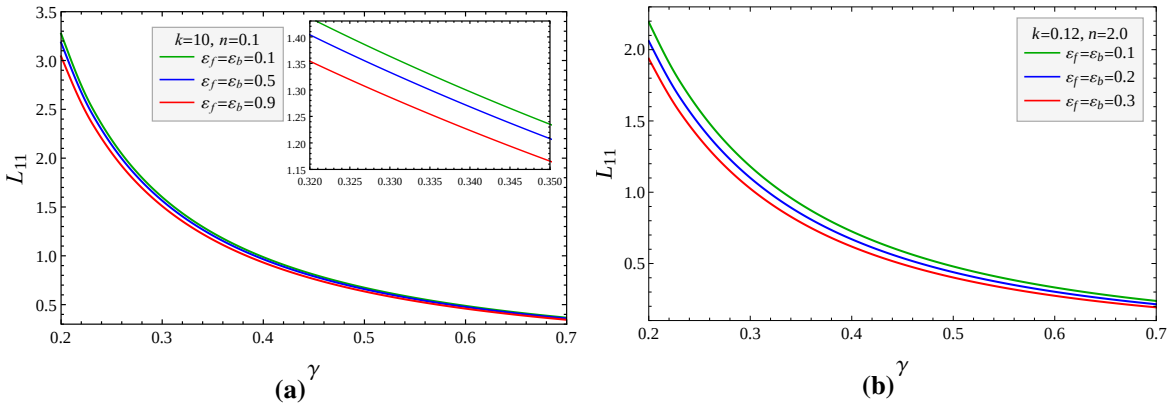

Figure 5.11: Dimensionless hydrodynamic permeability L_{11} with particle volume fraction γ for various values of permeability parameters $(\varepsilon_f, \varepsilon_b)$ under **(5.11a)** large Darcy number $(k = 10, n = 0.1, \varepsilon_f = \varepsilon_b = 0.1, 0.5, 0.9)$ and **(5.11b)** small Darcy number $(k = 0.12, n = 2, \varepsilon_f = \varepsilon_b = 0.1, 0.2, 0.3)$. $(a = 0.4, b = 0.7, \beta = 0.5, We = 0.2, a_1 = 3, \eta = 0.1, F = 1)$

ures 5.12a and 5.12b delineate the comparative impact of variable permeability within two distinct porous layers encompassing a solid cylindrical particle, pertaining to porous media with high and low permeability, respectively. It is evident that a combined effect of the decreasing permeability of the Forchheimer region and an increasing permeability of the Brinkman region leads to an overall growth of the hydrodynamic permeability. This shows the prevailing influence of the Brinkman region over the Forchheimer region. However, the increase in L_{11} is minimal as a reduced permeability of the Forchheimer number suppresses the effect of increasing permeability of the Brinkman region. For porous media characterized by high permeability, a reduction in growth of hydrodynamic permeability becomes apparent as the dominance of permeability within the Brinkman region surpasses that of the Forchheimer region, this can be further justified as the increasing permeability of Brinkman region enhances the flow but the decreasing permeability of Forchheimer region obstructs the flow in Forchheimer region which is further supported by a more influential inertial resistance in this case.

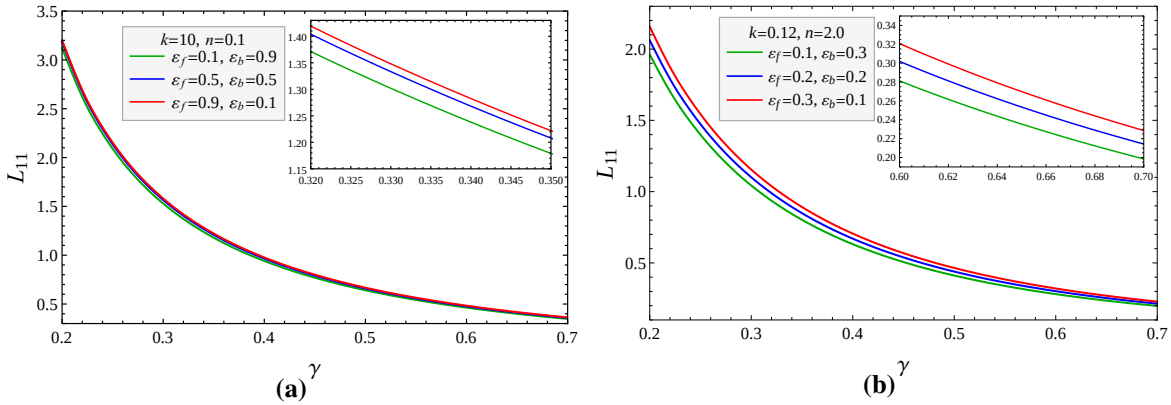

Figure 5.12: Dimensionless hydrodynamic permeability L_{11} with particle volume fraction γ for comparative values of permeability parameters $(\varepsilon_f, \varepsilon_b)$ under **(5.12a)** large Darcy number $(k = 10, n = 0.1)$ and **(5.12b)** small Darcy number $(k = 0.12, n = 2)$. $(a = 0.4, b = 0.7, \beta = 0.5, We = 0.2, a_1 = 3, \eta = 0.1, F = 1)$

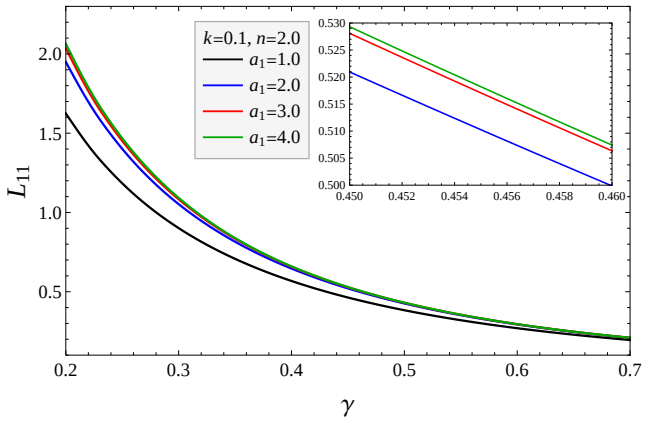

Figure 5.13: Dimensionless hydrodynamic permeability L_{11} with particle volume fraction γ for various values of transition parameter a_1 $(a_1 = 1, 2, 3, 4)$ under small Darcy number $(k = 0.1, n = 2.0, \varepsilon_f = \varepsilon_b = 0.1, a = 0.4, b = 0.7, \beta = 0.5, We = 0.2, \eta = 0.1, F = 1)$

The transition parameter exerts a discernible influence on the fluid dynamics surrounding a membrane. A noticeable ascending trajectory is observed in the hydrodynamic permeability as the transition parameter exhibits an increasing trend. This can be rationalized by a diminished distinction between the zero shear rate state and the power-law state, elucidating the heightened membrane permeability in this context. This diminishing distinction between the two state also increase the decay rate of L_{11} with γ, which can be seen in Figure 5.13.

The interplay between hydrodynamic permeability and the permeability parameter within the Brinkman region, along with a comparison of the thicknesses of the Brinkman and the Forchheimer regions, is graphically presented in Figure 5.14. The figure illustrates a significant reduction in hydrodynamic permeability with an increase in the permeability parameter ε_b, indicating a decline in the overall permeability of the Brinkman region.

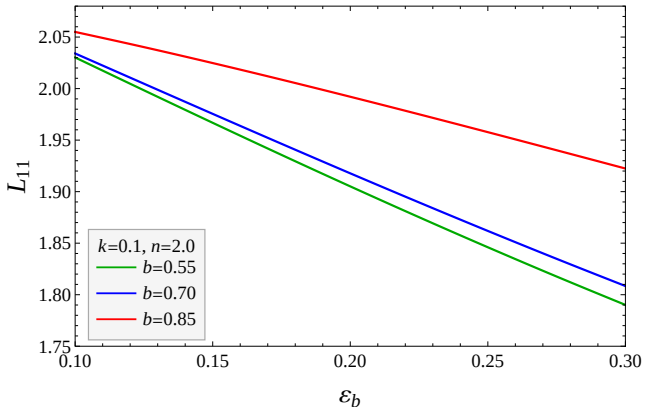

Figure 5.14: Dimensionless hydrodynamic permeability L_{11} with Brinkman permeability parameter ε_b for different thicknesses of Forchheimer layer b under small Darcy number $(k = 0.1, n = 2, \varepsilon_f = 0.1, a_1 = 3, a = 0.4, \gamma = 0.2, \beta = 0.5, We = 0.2, \eta = 0.1, F = 1)$

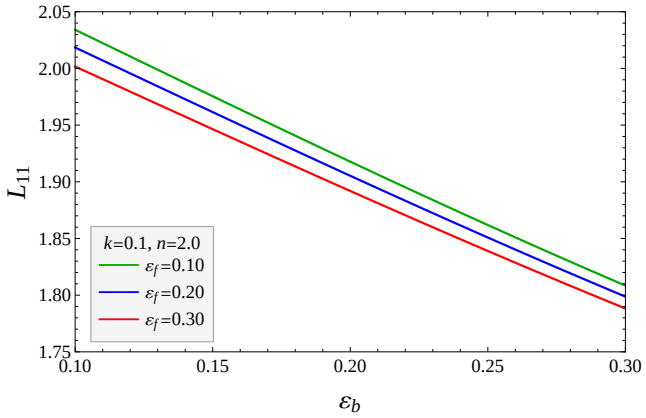

Figure 5.15: Dimensionless hydrodynamic permeability L_{11} with Brinkman permeability parameter ε_b for various values of Forchheimer permeability parameter ε_f under small Darcy number $(k = 0.1, n = 2, a_1 = 3, a = 0.4, b = 0.7, \gamma = 0.2, \beta = 0.5, We = 0.2, \eta = 0.1, F = 1)$

Moreover, a diminished rate of decay in L_{11} is evident under conditions of reduced occupancy of the Brinkman region in comparision to Forchheimer region. Figures 5.15 provide insight into the influence of the permeability parameter of Forchheimer region on the hydrodynamic permeability of a membrane in the context of a slightly permeable porous medium. It can be observed that a reduction in the overall permeability of the Brinkman-Forchheimer region (as ε_f increases) corresponds to a decrease in fluid velocity and hence in overall hydrodynamic permeability. Based on the Figure 5.15, it can be inferred that when dealing with low permeable porous media, the augmentation of viscoelastic properties in the shear thickening Carreau-Yasuda fluid leads to a decrease in the hydrodynamic permeability of

the membrane. The influence of different thicknesses in the porous regions on the hydrodynamic permeability of the membrane is illustrated in Figures 5.16-5.18. These figures specifically examine the impact of the transition parameter, as well as the permeability parameters associated with the Brinkman and Forchheimer regions, respectively. The hydrodynamic permeability of the membrane in a low permeable porous medium is observed to undergo a decay with increased occupancy of Forchheimer region relative to Brinkman region, when subjected to shear thickening fluid. The observed phenomenon of a reduced thickness of transition state between the zero shear state and the power-law state has been found to result in an enhanced hydrodynamic permeability of the membrane (Fig. 5.16). Furthermore, it has been observed that a further reduction in this thickness leads to a reduced growth in L_{11}, as well as decreased decay rate in L_{11} with thickness of Brinkman-Forchheimer region.

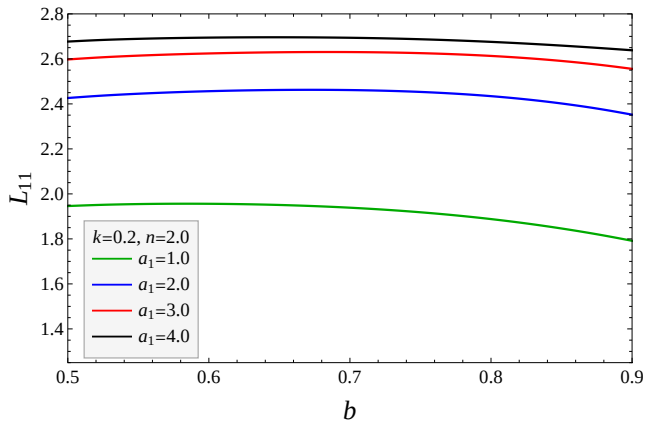

Figure 5.16: Dimensionless hydrodynamic permeability L_{11} with thickness of Forchheimer layer b for various values of transition parameter a_1 under small Darcy number $(k = 0.2, n = 2, \varepsilon_f = \varepsilon_b = 0.1, a = 0.4, \gamma = 0.2, \beta = 0.5, We = 0.2, \eta = 0.1, F = 1)$

An intriguing observation can be made from Figures 5.17-5.18, wherein the permeability parameters of the Brinkman and Brinkman-Forchheimer regions exhibit opposite trends in response to an augmentation in the occupancy of Forchheimer region relative to Brinkman region. The observed phenomenon is a noticeable decrease in the value of L_{11} as the total permeability of the Brinkman region decreases (specifically, as ε_b increases), while the value of ε_f remains constant (Fig. 5.17). Similarly, a significant decrease with an increasing decay rate can be seen in L_{11} with the decay a total permeability of Brinkman-Forchheimer region (specifically, as ε_f increases), while ε_b being constant (Fig. 5.18).

According to the findings presented in Figure 5.19, it can be observed that as the viscoelastic parameter of the shear-thickening fluid increases, there is a corresponding decrease in the hydrodynamic permeability of the membrane. This decrease can be attributed to the

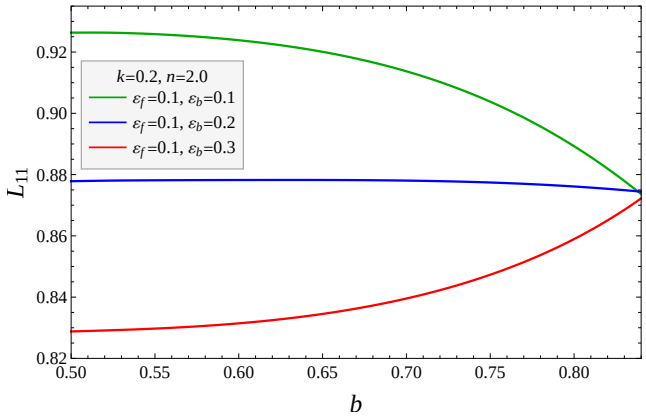

Figure 5.17: Dimensionless hydrodynamic permeability L_{11} with thickness of Forchheimer layer b for various values of Brinkman permeability parameter ε_b under small Darcy number $(k = 0.2, n = 2, \varepsilon_f = 0.1, a_1 = 3, a = 0.4, \gamma = 0.2, \beta = 0.5, We = 0.2, \eta = 0.1, F = 1)$

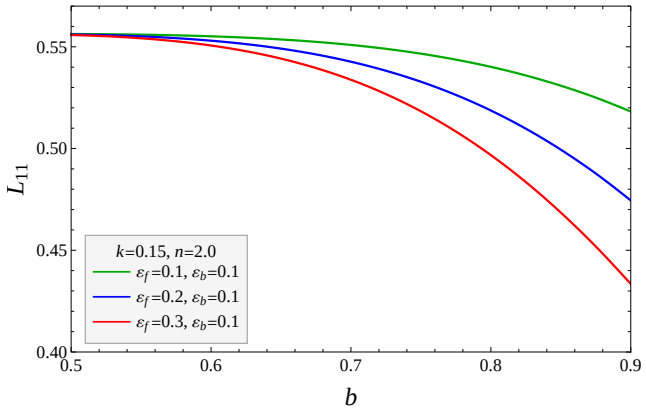

Figure 5.18: Dimensionless hydrodynamic permeability L_{11} with thickness of Forchheimer layer b for various values of Forchheimer permeability parameter ε_f under small Darcy number $(k = 0.15, n = 2, \varepsilon_b = 0.1, a_1 = 3, a = 0.4, \gamma = 0.2, \beta = 0.5, We = 0.2, \eta = 0.1, F = 1)$

growing influence of elastic forces relative to viscous forces. Further, the decay rate significantly reduces with decreasing thickness of transition state between zero shear state and power law state.

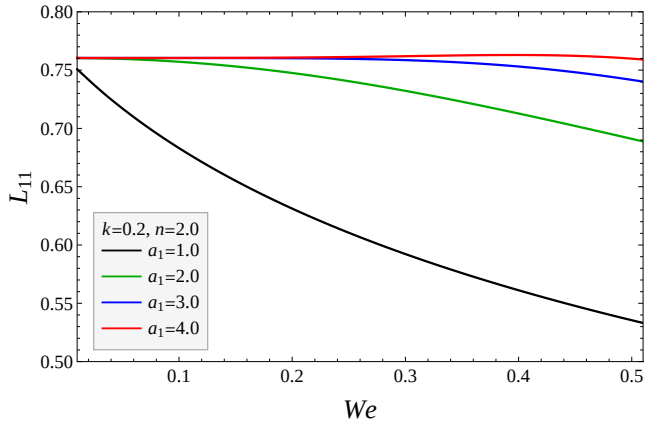

Figure 5.19: Dimensionless hydrodynamic permeability L_{11} with the Weissenberg number We for various values of transition parameter a_1 $(a_1 = 1,2,3,4)$ under small Darcy number $(k = 0.2, n = 2, \varepsilon_f = \varepsilon_b = 0.1, a = 0.4, b = 0.7, \gamma = 0.445, \beta = 0.5, \eta = 0.1, F = 1)$

The findings of the study conducted in Figure 5.20 revealed a noteworthy increase in the hydrodynamic permeability when the permeability parameters of the Brinkman and Brinkman-Forchheimer regions (ε_b and ε_f, respectively) exhibit opposite trends. The observed trend indicates that the growth rate of L_{11} is positively correlated with a decrease in the permeability of the Forchheimer region and, conversely, with an increase in the permeability of the Brinkman region. The growth rate of shear thickening flow past a membrane in slightly permeable porous media becomes increasingly significant a as elastic forces dominates viscous forces. The present study compares its findings with the experimental research on hydrodynamic permeability with porosity conducted by Filippov *et al.* [201], revealing a close correspondence between the results of both studies (Table 5.2).

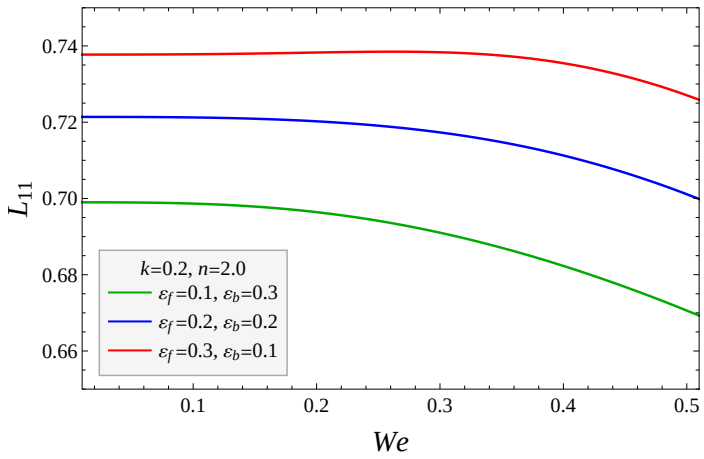

Figure 5.20: Dimensionless hydrodynamic permeability L_{11} with the Weissenberg number We for comparative values of permeability parameters $(\varepsilon_f, \varepsilon_b)$ under small Darcy number $(k = 0.2, n = 2, a_1 = 3, a = 0.4, b = 0.7, \gamma = 0.445, \beta = 0.5, \eta = 0.1, F = 1)$

Porosity(ε) $\downarrow$	Hydrodynamic Permeability (L_{11})	
	Experimental Study (Filippov *et al.*)	Current Study
$\varepsilon = 0.0$	0.0	0.0
$\varepsilon = 0.003742$	0.00001775	4.37×10^{-9}
$\varepsilon = 0.015344$	0.00009467	3.09×10^{-7}
$\varepsilon = 0.018338$	0.00009467	5.07×10^{-7}
$\varepsilon = 0.027320$	0.00019530	1.78×10^{-6}
$\varepsilon = 0.031063$	0.00019530	2.64×10^{-6}
$\varepsilon = 0.075599$	0.00059760	0.0000413
$\varepsilon = 0.086452$	0.00069230	0.0000630
$\varepsilon = 0.094686$	0.00079880	0.0000841
$\varepsilon = 0.108530$	0.00120100	0.0001300
$\varepsilon = 0.123500$	0.00140200	0.0001980
$\varepsilon = 0.136230$	0.00150300	0.0002720
$\varepsilon = 0.209210$	0.00330800	0.0011500
$\varepsilon = 0.240270$	0.00401180	0.0018600
$\varepsilon = 0.224180$	0.00401180	0.0014600

Table 5.2: Validation of current work with the experimental data of Filippov *et al.* [201] using variations in hydrodynamic permeability, L_{11} with porosity, ε. ($a = b = 1, We = 0, \beta = 0, n = \eta = 0, \varepsilon_f = \varepsilon_b = 0, F = 0$).

5.4.6 Kozeny Constant (K_z)

The observed trend in Figure 5.21 indicates a decrease in the Kozeny constant as the stress-jump parameter of the fluid-porous interface increases. This behavior holds true for large permeability of the porous media. The observed phenomenon of an increase in the Kozeny constant in the flow past a membrane can be attributed to the progressive dominance of inertial resistance within the Brinkman-Forchheimer region.

The examination of Figures 5.22-5.23 reveal the relationship between the Kozeny constant and the porosity of the membrane, as well as its dependence on various fluid and porous medium parameters. A notable augmentation in the membrane's tortuosity is seen in correlation with an escalation in the porosity of the membrane. The impact of this augmentation is minimal for materials with low porosity, but it increases significantly when the porosity of the medium is raised. Based on the graphical data presented in Figures 5.22a and 5.22b, it can be inferred that the augmented permeability parameters in both the Brinkman and Brinkman-Forchheimer regions have a favorable influence on the Kozeny constant

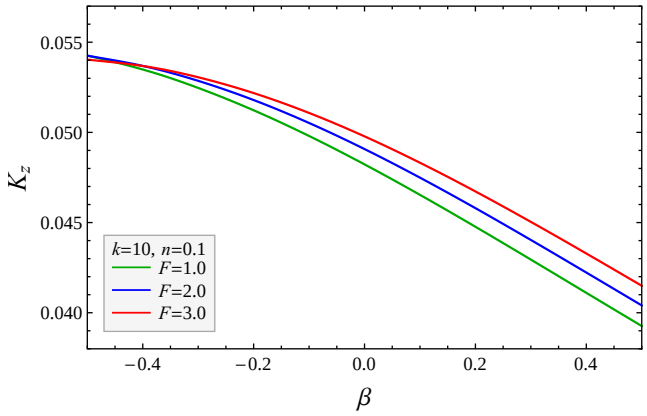

Figure 5.21: Kozeny constant K_z with stress-jump parameter β for various values of the Forchheimer number F under large Darcy number $(k = 10, n = 0.1, \varepsilon_f = \varepsilon_b = \varepsilon = 0.5, a_1 = 3, a = 0.4, b = 0.7, \gamma = 0.2, We = 0.2, \eta = 0.1)$

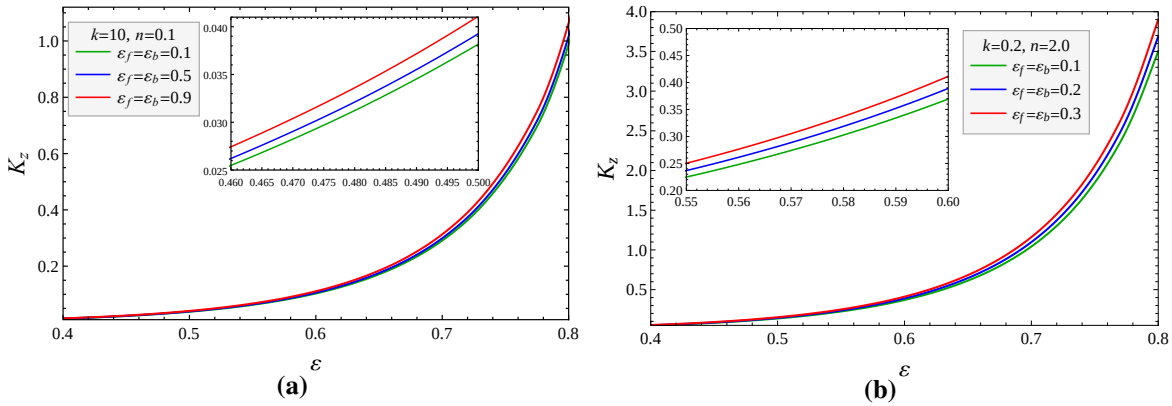

Figure 5.22: Kozeny constant K_z with porosity parameter ε for various values of permeability parameters, $(\varepsilon_f, \varepsilon_b)$ under **(5.22a)** large Darcy number $(k = 10, n = 0.1)$ and **(5.22b)** small Darcy number $(k = 0.2, n = 2)$. $(a = 0.4, b = 0.7, \gamma = 0.2, \beta = 0.5, a_1 = 3, We = 0.2, \eta = 0.1, F = 1)$

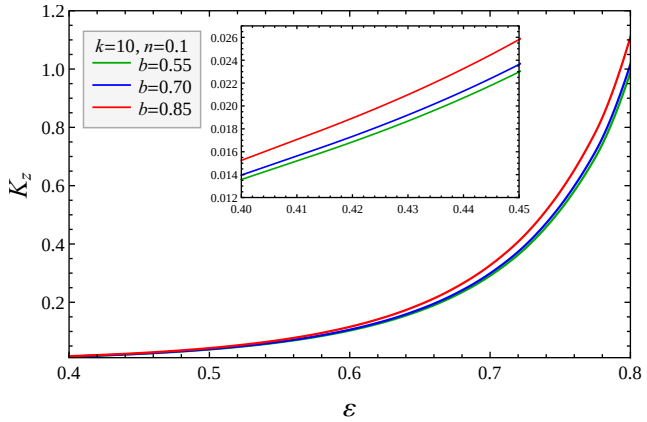

Figure 5.23: Kozeny constant K_z with porosity parameter ε for different thicknesses of Forchheimer layer b under large Darcy number $(k = 10, \varepsilon_f = \varepsilon_b = 0.5, a_1 = 3, a = 0.4, b = 0.7, \gamma = 0.2, \beta = 0.5, We = 0.2, \eta = 0.1, F = 1)$

The dependence of the Kozeny constant on the variable thickness of both porous layers is revealed in Figure 5.23. The dominance of the Brinkman-Forchheimer layer thickness over the Brinkman layer thickness leads to an increase in the Kozeny constant for highly porous media. This can be understood as the heightened impact of inertial resistance, which subsequently decreases the hydrodynamic permeability of membranes, resulting in the amplification of the Kozeny constant. It is also observed that the growth rate of the Kozeny constant is increased with the expansion of the Brinkman-Forchheimer layer within the porous medium encompassing the solid cylindrical particle. The investigation examines the correlation between the Kozeny constant and the particle volume fraction across various permeability parameters of the porous regions. This relationship is visually represented in Figures 5.24a and 5.24b. The observed phenomenon is a notable augmentation in the Kozeny constant as the particle volume fraction of the membrane is increased. The growth rate of this augmentation exhibits a positive correlation with the permeability parameters of both the Brinkman and Brinkman-Forchheimer layers.

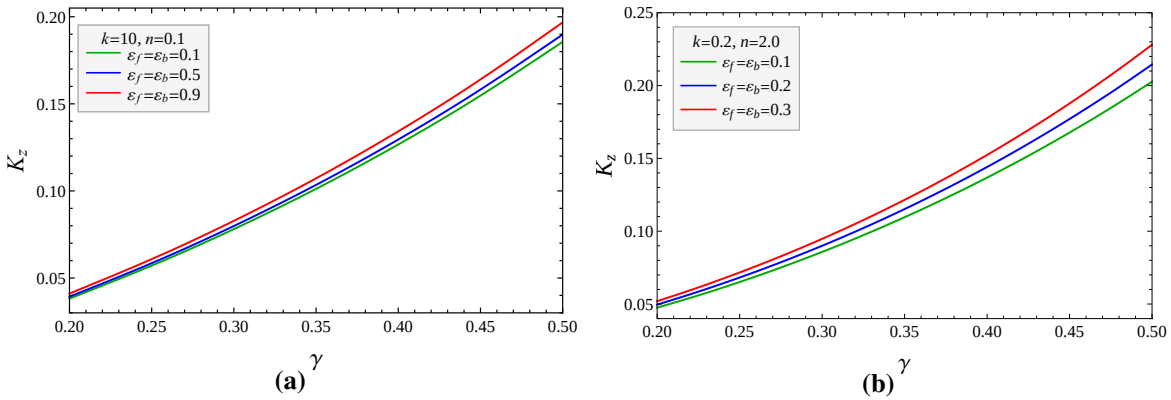

Figure 5.24: Kozeny constant K_z with particle volume fraction γ for various values of permeability parameters $(\varepsilon_f, \varepsilon_b)$ under **(5.24a)** large Darcy number $(k = 10, n = 0.1)$ and **(5.24b)** small Darcy number $(k = 0.2, n = 2.0)$. $(a = 0.4, b = 0.7, \beta = 0.5, a_1 = 3, We = 0.2, \eta = 0.1, F = 1, \varepsilon = 0.5)$

5.4.7 Temperature Distribution (θ)

The notable contribution of this study lies in analyzing the effects of Carreau-Yasuda fluid and porous medium parameters on temperature distribution, considering viscous dissipation. This subsection delves into the significant effects of multiple parameters such as transition parameter, Forchheimer number, thickness of the Forchheimer region, and Brinkman number on temperature distribution, which is contingent upon the radial coordinate. An augmentation in the transition parameter results in an reduction of temperature in all regions of the biporous layered cylinderical particles (Fig. 5.25a). However, this behaviour gets

reversed for shear thickening Carreau-Yasuda fluid as depicted for low permeability in figure (5.25b). Additionally, for large permeability a higher growth rate of temperature with decreasing thickness of transition state is observed.

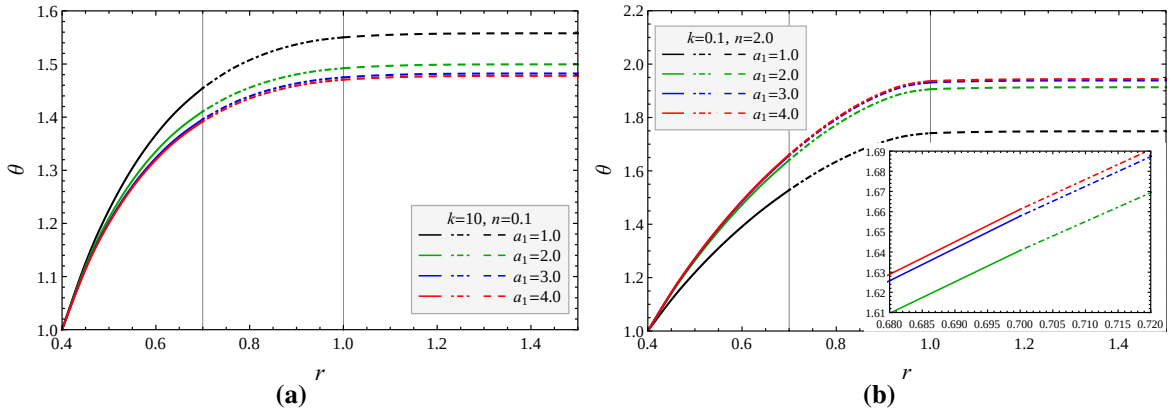

Figure 5.25: Dimensionless temperature θ with radial direction r for various values of transition parameter a_1 under **(5.25a)** large Darcy number $(k = 10, n = 0.1, \varepsilon_f = \varepsilon_b = 0.5)$ and **(5.25b)** small Darcy number $(k = 0.1, n = 2, \varepsilon_f = \varepsilon_b = 0.2)$. $(a = 0.4, b = 0.7, \gamma = 0.445, \beta = 0.5, We = 0.2, \eta = 0.1, F = 1)$

An increasing occupancy of Forchheimer region in the porous layer diminishes the temperature profile in the membrane owing to decreased velocity of the fluid (Figures 5.26a and 5.26b). Figures 5.27a and 5.27bdescribe the variations in the temperature distribution with

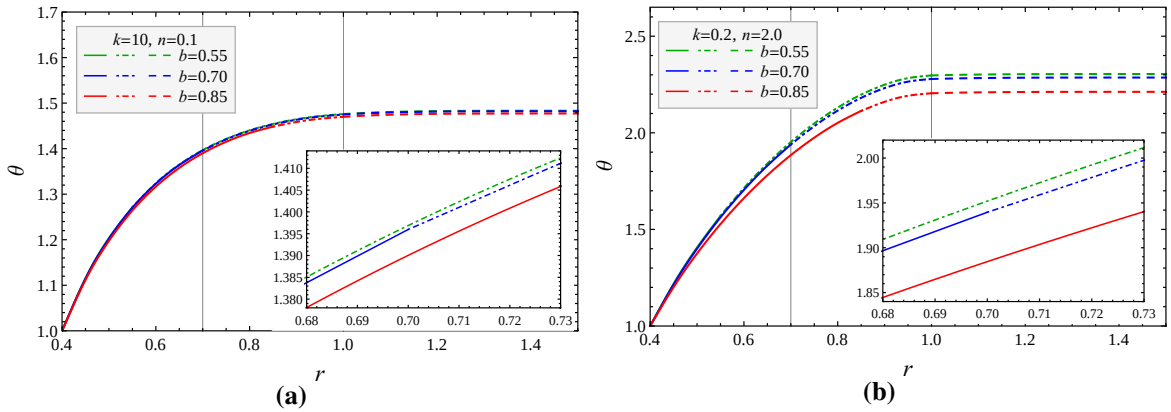

Figure 5.26: Dimensionless temperature θ with radial direction r for different thicknesses of Forchheimer layer b under **(5.26a)** large Darcy number $(k = 10, n = 0.1, \varepsilon_f = \varepsilon_b = 0.5)$ and **(5.26b)** small Darcy number $(k = 0.1, n = 2.0, \varepsilon_f = \varepsilon_b = 0.2)$. $(a = 0.4, \gamma = 0.445, \beta = 0.5, We = 0.2, a_1 = 3.0, \eta = 0.1, F = 1)$

respect to varying permeability. It can be observed from Figures 5.27a and 5.27b, referring for large and small permeability respectively, that the increasing permeability parameters of both Brinkman and Forchheimer layer leads to a decay in the temperature profile in all flow regions owing to decreased permeability of porous layers, signifying the decreasing behavior of velocity in response to the increasing permeability parameters, ε_b, and ε_f. Fig-

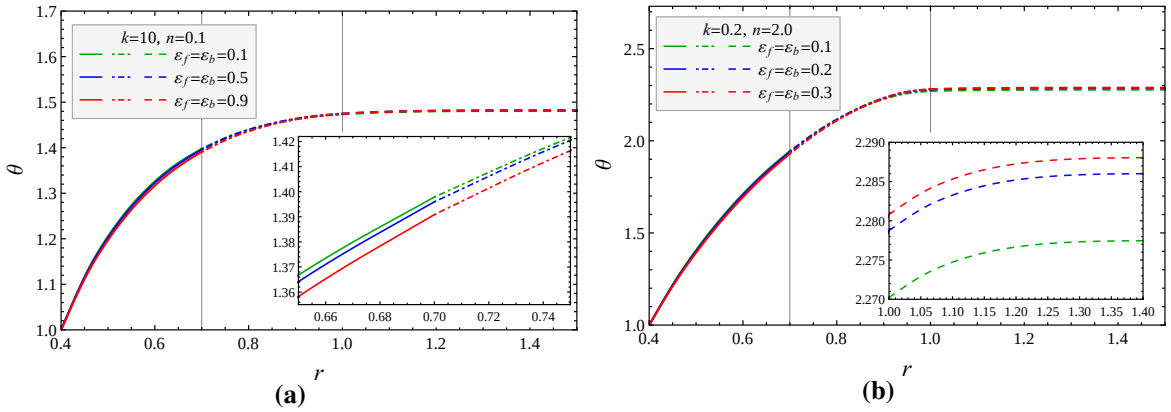

Figure 5.27: Dimensionless temperature θ with radial direction r for various values of permeability parameters $(\varepsilon_f, \varepsilon_b)$ under **(5.27a)** large Darcy number $(k = 10, n = 0.1, \varepsilon_f = \varepsilon_b = 0.1, 0.5, 0.9)$ and **(5.27b)** small Darcy number $(k = 0.2, n = 2, \varepsilon_f = \varepsilon_b = 0.1, 0.2, 0.3)$. $(a = 0.4, b = 0.7, \gamma = 0.445, \beta = 0.5, We = 0.2, a_1 = 3, \eta = 0.1, F = 1)$

ure 5.28, describes that the temperature profile get reduced in response to the increasing Forchheimer number signifying the decreased heat flow due to increasing inertial resistance and manifesting that the fluid velocity and temperature profile are propotional to each other.

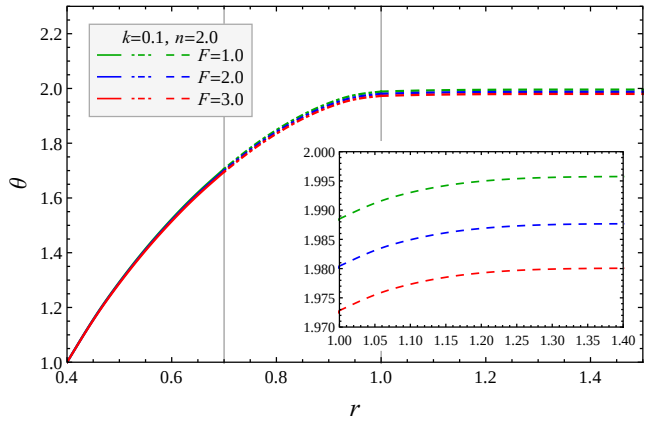

Figure 5.28: Dimensionless temperature θ with radial direction r for various values of the Forchheimer number F $(F = 1, 2, 3)$ under small Darcy number $(k = 0.1, n = 2, \varepsilon_f = \varepsilon_b = 0.1, a = 0.4, b = 0.7, \gamma = 0.445, \beta = 0.5, We = 0.2, a_1 = 3, \eta = 0.1, Br = 1)$

The Brinkman number (Br) is a dimensionless parameter utilized to analyze heat transfer between a wall and a viscous fluid, particularly pertinent in polymer processing. It characterizes the balance between heat produced via viscous dissipation and heat conducted through molecular conduction, effectively comparing internal heat generation to external heating. A higher Brinkman number indicates slower heat conduction due to viscous dissipation, leading to a greater temperature elevation. This significance is apparent in the temperature profiles illustrated in Figure (5.29). The qualitative changes in temperature profiles with the Brinkman number remain consistent irrespective of the permeability of the

porous medium. However, quantitatively, temperature rises more prominently with radial distance for higher permeability, which can be attributed to the porous materials' influence on fluid flow dynamics.

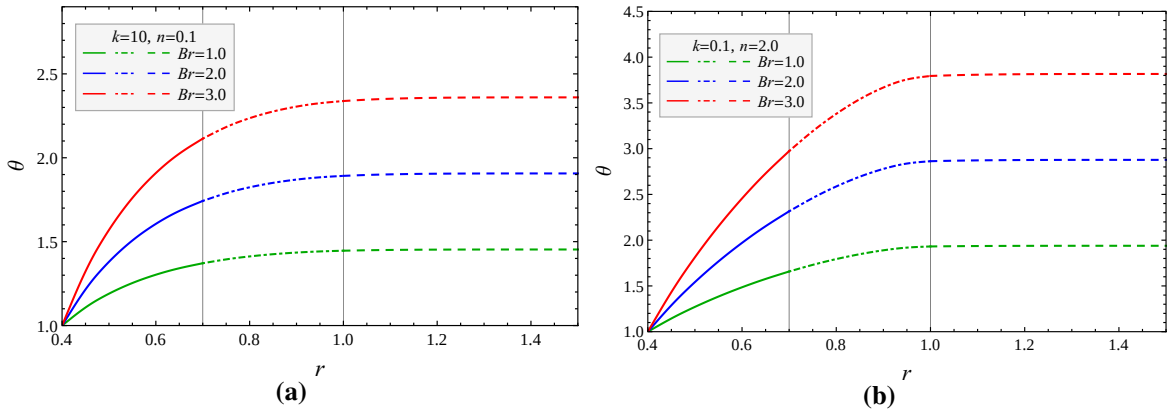

Figure 5.29: Dimensionless temperature θ with radial direction r for various values of Brinkman numbers Br $(Br = 0,1,2,3)$ under **(5.29a)** large Darcy number $(k = 10, n = 0.1, \varepsilon_f = \varepsilon_b = 0.5)$ and **(5.29b)** small Darcy number $(k = 0.1, n = 2, \varepsilon_f = \varepsilon_b = 0.2)$. $(a = 0.4, b = 0.7, \gamma = 0.445, \beta = 0.5, We = 0.2, a_1 = 3, \eta = 0.1, F = 1)$

5.4.8 Nusselt Number (Nu)

Figure 5.30 illustrates how the variation in permeabilities of both the regions impact the Nusselt number Nu due to viscous dissipation through temperature in the flow of Carreau-Yasuda fluid around a cluster of cylindrical particles. The rise in Brinkmann number amplifies the Nusselt number values, a result of heightened membrane temperature caused by greater thermal energy production from viscous dissipation. Moreover, the rising variable permeability parameters within both the Forchheimer and Brinkmann regions as well as Forchheimer number contribute to the decline of fluid velocity and temperature profiles within the flow domain, consequently reducing the Nusselt number profile. The influence of both particle volume fraction and the viscoelastic properties of the fluid on the Nusselt number is depicted in Figure 5.31.The figure suggests that as the hydrodynamic permeability of the membrane decreases (accompanied by a higher particle volume fraction) and the fluid's viscoelasticity improves, the Nusselt number decreases. This phenomenon is likely due to the reduced impact of temperature on the fluid's viscoelastic properties. Furthermore, the gradual reduction in the transition state between the zero shear rate region and the power-law region (indicated by an increasing transition parameter) contributes to an enhanced Nusselt number. This enhancement can be linked to heightened heat transfer within the flow domain for shear-thickening fluids.

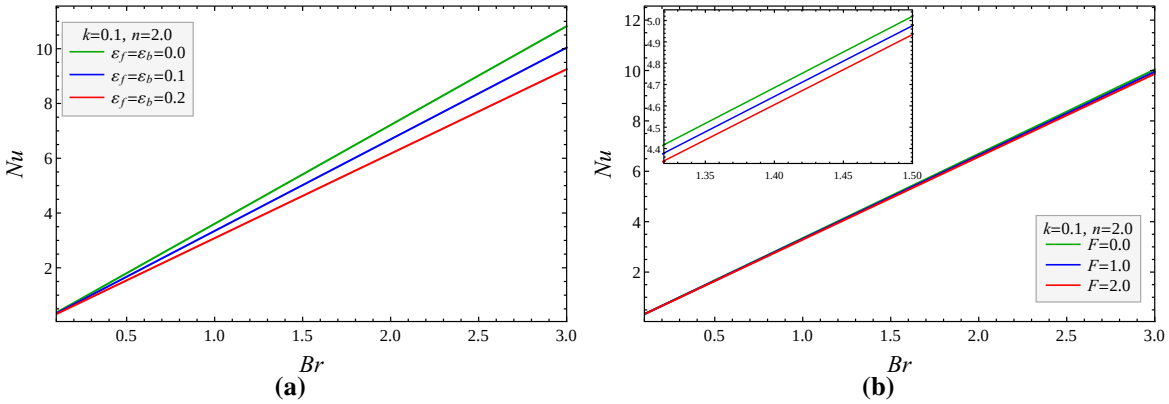

Figure 5.30: Changes in Nusselt number Nu with Brinkman number Br for various values of **(5.30a)** varying permeabilities $\varepsilon_f, \varepsilon_b$ $(F = 1)$ and **(5.30b)** Forchheimer number F $(\varepsilon_f = \varepsilon_b = 0.1)$. $(a = 0.4, b = 0.7, \gamma = 0.445, \beta = 0.5, We = 0.2, a_1 = 3, \eta = 0.1)$

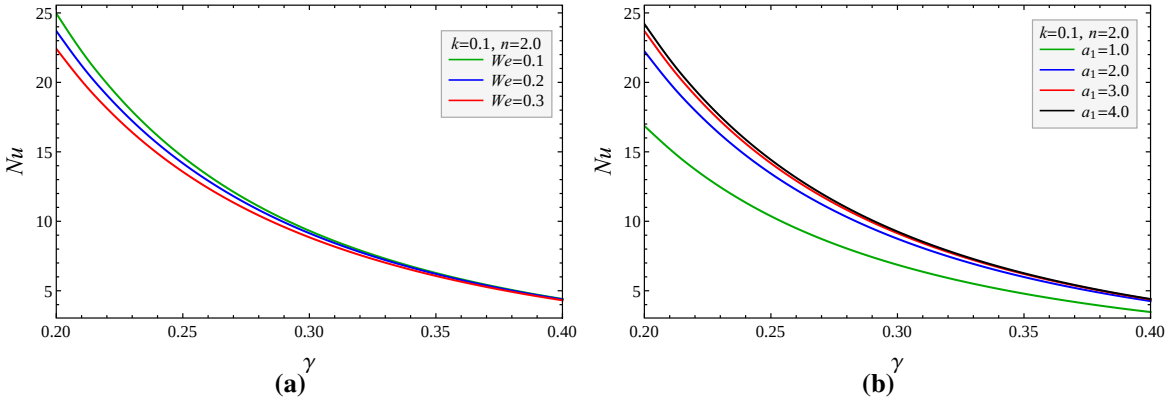

Figure 5.31: Changes in Nusselt number Nu with particle volume fraction γ for various values of **(5.31a)** Weissenberg number We $(a_1 = 3)$ and **(5.31b)** transition parameter a_1 $(We = 0.2)$. $(a = 0.4, b = 0.7, \varepsilon_f = \varepsilon_b = 0.1, \beta = 0.5, \eta = 0.1, F = 3, Br = 1)$

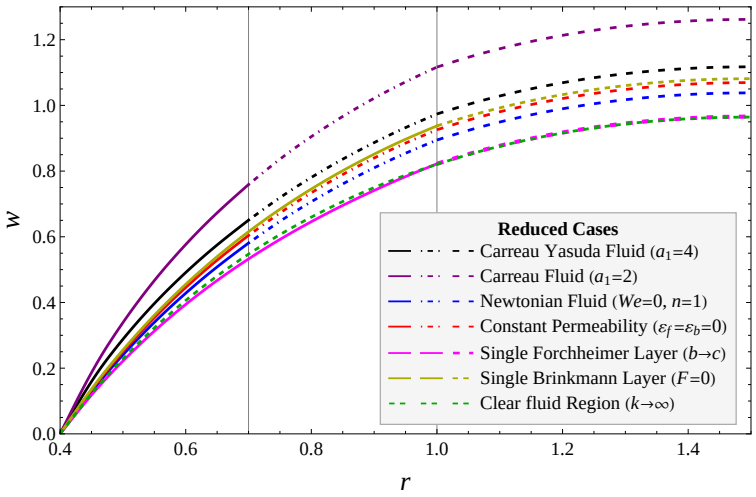

Figure 5.32: Various reduced cases of the current study for large Darcy number $(k = 100)$ $(\gamma = 0.445, \beta = 0.5, \eta = 0.1)$

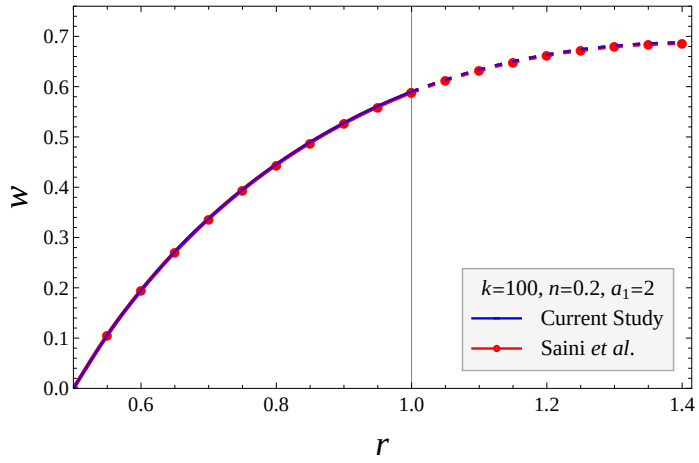

Figure 5.33: Validation of the current study with the study of Saini *et al.* [199] under large Darcy number $(k = 100, n = 0.2, \varepsilon_f = \varepsilon_b = 0, a = 0.5, b = 1.0, \gamma = 0.5, \beta = 0.5, We = 0.5, a_1 = 2, \eta = 0.1, F = 0)$

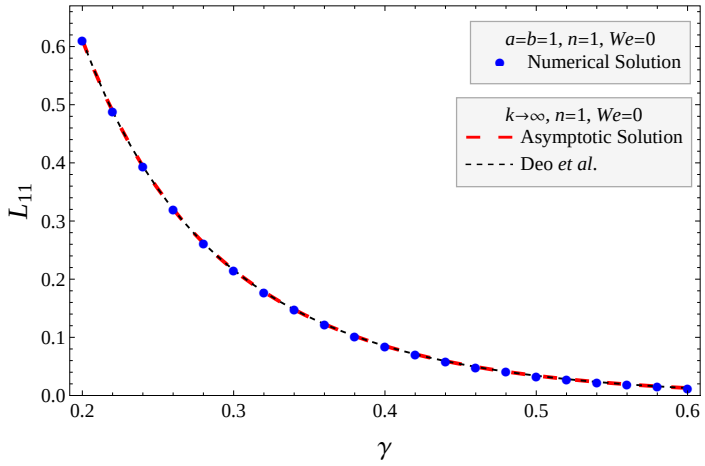

Figure 5.34: Validation of the current study with the study of Deo *et al.* [3] and Saini *et al.* [199] under large Darcy number $(k \to \infty, \varepsilon_f = \varepsilon_b = 0, a = 0.5, b = 1, \gamma = 0.445, \beta = 0.5, a_1 = 3, \eta = 0.1, F = 0)$

5.5 Summary and Conclusions

The creeping flow of non-Newtonian Carreau-Yasuda fluid through an aggregates of bi-porous layered cylindrical particles is investigated using variable permeability, particle-in-cell and heat transfer approaches. The demonstration of the proposed work is designed in such a manner that the Brinkman-Forchheimer region proximate to the solid core of the cylindrical particle is regulated by Brinkman-Forchheimer equation with variable permeability of the porous medium, and an intermediate Brinkman porous region is governed by the Brinkman equation with variable permeability of the porous medium. However, a

peripheral layer of non-porous region is governed by the Stokes equation. The equations governing the flow of Carreau-Yasuda fluid through a membrane composed of a swarm of biporous layered cylindrical particles are nonlinear and coupled in terms of the velocity and stress of the Carreau-Yasuda fluid. To address this complications, the empirical regular perturbation techniques is employed to obtain the asymptotic expansion of the velocities for different (Brinkman-Forchheimer, Brinkman, and non-porous) regions under large permeability and small Weissenberg number. However, a numerical technique (NDSolve) in Mathematica is used to exhibit the graphical analysis for hydrodynamical quantities under the various control parameters like Carreau-Yasuda parameters, porous medium parameters, and Forchheimer number. The equations regulating the temperature distributions for various porous and non-porous regions are solved using the method of variation of parameters. The following remarkable outcomes of the present work is mentioned below:

1. The transition parameter a_1 of the Carreau-Yasuda fluid significantly affects the velocity of fluid flow, permeability of membranes, and temperature as it passes through a membrane made up of porous layered cylinders, irrespective of whether the permeability is high or low.

2. The prevalence of elastic forces over viscous forces (*i.e.*, for increasing Weissenberg number We) results in significantly increased fluid velocity and membrane permeability when dealing with shear-thinning fluid characteristics. However, a reverse behavior is noted with shear thickening fluid.

3. The hydrodynamic permeability of the membrane in a low permeable porous medium is observed to undergo a decay with increased occupancy of Brinkman-Forchheimer region relative to Brinkman region, when subjected to shear thickening fluid.

4. An increase in permeability parameters within both the Brinkman and Brinkman-Forchheimer regions positively impacts the Kozeny constant and leads to an enhancement in the membrane's tortuosity. This enhancement is a result of decreased permeability in the porous areas, which occurs due to the heightened values of the permeability parameters.

5. Emphasizing the growing impact of inertial resistance on hydrodynamic and thermal properties in the flow past a membrane as influenced by the Forchheimer number, a slight decrease in flow velocity, membrane permeability, and temperature distribution is noticeable for both high and low permeability values.

6. The significant discovery in this research lies in the observation that elevating the variable permeability parameters within both the Forchheimer and Brinkmann regions,

alongside the Forchheimer number, results in a decline in fluid velocity and temperature distributions throughout the flow domain, ultimately causing a diminished Nusselt number distribution.

The proposed explanation holds promise for making substantial contributions to the investigation of crucial physical and biological applications, such as the study of petroleum reservoir rocks, wastewater treatment filtration processes, and blood flow through smooth muscle cells. Nevertheless, empirical validation is a necessary step to ensure the credibility of the proposal.

Chapter 6

Analysis of Entropy Generation for a Creeping Flow of Newtonian Fluid through a Swarm of Biporous Layered Cylindrical Particles: Brinkman-Forchheimer Model

6.1 Introduction

The flow of liquids through membranes composed of a cluster of particles has captivated the interest of researchers, providing valuable insights into fluid flow through porous materials. This holds significant applications across a wide array of fields, including physical and biological sciences, such as in the study of flow through smooth muscle cells, petroleum reservoirs, and sand beds.Heat transfer, a classical phenomenon, has been extensively explored by numerous researchers due to its wide-ranging applications in various fields such as chemical engineering, material processing industries, biological systems, polymers, and food processing. The study of heat transfer within a cluster of particles holds significant importance in engineering applications, including chemical reactors and heat exchangers, owing to the interactions among particles.

6.1.1 Entropy Generation

The suboptimal performance of industrial and engineering flow processes and thermal systems is primarily attributed to the generation of entropy. Identifying the factors responsible for entropy generation is crucial, as minimizing these factors will lead to the optimization of energy resources and the efficiency of the flow system. Entropy analysis is a method used to assess the thermodynamic irreversibility present in fluid flow and heat transfer processes, stemming from the second law of thermodynamics. Entropy generation serves as a metric for quantifying the level of irreversibility inherent in actual processes. Various elements,

such as heat transfer across finite temperature gradients, the nature of convective heat transfer, and the influence of viscosity, contribute to the overall entropy generation. The process of entropy generation leads to the dissipation of available energy within a system, resulting in significant additional expenses for any thermal system.

The primary contributors to entropy generation in thermal and engineering processes are the three modes of thermal exchange: conduction, convection, and thermal radiation. Additionally, factors such as fluid friction, the existence of porous media, viscous effects, fluid mixing, buoyancy forces, magnetohydrodynamics, and radiative heat transfer play significant roles in this context. The conversion of energy across various forms like thermal energy, potential energy, and kinetic energy, among others, plays a crucial role in the generation of entropy. These elements contribute to a decrease in the operational efficiency (energy) of diverse thermo-fluidic devices. Furthermore, the study of entropy production is a crucial aspect of contemporary engineering thermo fluidic devices, and it represents one of the most frequently explored areas in research.

Bejan's groundbreaking study ([109], [110]) explored the notion of entropy generation across various flow conditions, scenarios, and geometric models. Within the realm of advanced thermodynamics, the study of entropy generation provides invaluable insights for integrating miniature electronic and thermal devices, augmenting the performance of petroleum equipment, and optimizing heat exchangers, among other applications. Relying on the information regarding entropy generation offers a more dependable approach to designing these devices and amplifying the operational efficiency of thermal technologies.

Murthy *et al.* [202] provided an detailed study of the thermodynamic properties of immiscible Eringen's micropolar fluid within a rectangular pipe. This research holds significant importance in the automobile sector, particularly in the realm of micropolar fluid application as effective lubricants. In another study, Srinivas *et al.* [203] conducted an analysis on entropy generation in the flow of steady, incompressible, immiscible couple stress fluids between two static horizontal isothermal walls, which were filled with porous beds. Furthermore, Srinivas *et al.* [204] investigated the impact of magnetic fields on entropy production in immiscible, steady, and incompressible viscous fluids flowing through an inclined channel model. They utilized the homotopy analysis method to solve nonlinear momentum and thermal energy equations.

This current research seeks to examine entropy generation in the context of the creeping flow of Newtonian fluid through a membrane composed of biporous layered cylindrical particles under different variable permeability assumptions. The flow domain is divided into three distinct layers. The first layer, adjacent to the solid core of the cylindrical particle, is termed the Brinkman-Forchheimer layer and is governed by the Brinkman-Forchheimer

equation, with varying permeability assumption. The second layer, situated between the Brinkman-Forchheimer and peripheral layers, is referred to as the Brinkman porous layer, regulated by the Brinkman equation with varying permeability assumption. Finally, a non-porous liquid layer overlying the porous layers constitutes the non-porous region (clear fluid region), which is governed by the Stokes equation. Attaining analytical solutions for the mathematical equations governing fluid flow through porous media is intricate due to the presence of non-linear inertial terms in the Brinkman-Forchheimer equation, as well as the variability of permeabilities in the Brinkman and Brinkman-Forchheimer equations. To surmount these challenges, regular and singular perturbation methods are applied to derive asymptotic solutions for the equations pertaining to fluid flow through porous media. The resulting asymptotic velocity expressions for three distinct regions are then utilized to derive expressions for membrane permeability, the Kozeny constant, entropy generation number, and Bejan number. The study illustrates and thoroughly discusses the impacts and influences of diverse hydrodynamic, porous medium, and thermal parameters—including variables like permeability, Forchheimer number, particle volume fraction, viscous dissipation and stress-jump parameters on membrane permeability, the Kozeny constant, entropy generation number, and Bejan number. These relationships are visually depicted and comprehensively examined. Furthermore, the research examines limiting cases and the simplified form of the proposed model, comparing it with previously published works that is not consider variable permeability and an additional Brinkman-Forchheimer region near the solid core of the cylindrical particle. The asymptotic analysis has been compared with numerical solutions obtained through Mathematica software to validate our findings.

The framework of the current chapter is structured into five sections. Section 1 provides fundamental information about the research topic, explores its applications across interdisciplinary domains, conducts a literature review covering various aspects, identifies gaps in existing research, and outlines the objectives of the proposed study. In Section 2, the study outlines the statement of the problem, establishes key physical assumptions, provides a detailed model description, presents the governing mathematical equations for fluid flow through a membrane, and introduces their non-dimensional forms. Additionally, asymptotic solutions of the governing equations and their respective expressions are derived using both regular and singular perturbation methods, which are given in Section 3. Section 4 employs the mathematical expressions of velocities for distinct regions to conduct a graphical analysis of diverse hydrodynamical and thermal parameters. This analysis is performed with consideration of various control parameters. Section 5 encapsulates the noteworthy findings from the current research in a summary and conclusion.

6.2 Problem Formulation

6.2.1 Statement of the Problem and Model Assumptions

The present model deals with the generation of entropy in a fully developed creeping flow of a Newtonian fluid passing through a membrane consisting of biporous layered cylindrical particles. To facilitate this, the particle-in-cell approach is employed, focusing on an individual cylindrical particle confined in a cell selected from the swarm and utilizing a condition on the hypothetical cell surface to examine the contributions and effects of each particle within the swarm. Throughout filtration process, modifications can occur within the membrane's composition, triggered by particle dissolution and polymer adherence to particle surfaces, often referred to as poisoning. These alterations result in the development of a porous coating, like a colloidal or gel layer, encasing solid particles, which proves difficult to eradicate. The presence of this porous shell significantly impacts the drag force experienced by particles due to the flow. The model delineates fluid flow through the cylindrical particle across three distinct regions: Brinkman-Forchheimer, Brinkman, and non-porous regions. The analysis of entropy production attributed to heat transfer irreversibility (HTI) and fluid friction irreversibility (FFI) is conducted using the heat transfer approach, assuming local thermal equilibrium and homogeneity. The assumption is made that the flow is fully developed in both hydrodynamic and thermal aspects, with a much greater Peclet number, allowing us to disregard any axial conduction influences. The equations delineating entropy generation within a creeping flow of Newtonian fluid through a membrane composed of biporous layered cylindrical particles have been formulated based on the following assumptions:

1. The flow within the tube is regarded as steady, incompressible, displaying laminar characteristics, and symmetrical about axial direction.

2. The work's formulation involves the Brinkman-Forchheimer equation, which controls the flow of a Newtonian fluid within the Brinkman-Forchheimer (BF) porous region. Meanwhile, the Brinkman equation manages the fluid flow within the Brinkman porous region, while the flow within the non-porous area is regulated by the Stokes equation.

3. The Reynolds number is considered exceedingly low, indicating that viscous forces have a greater impact than inertial forces, resulting in the convective term being of minimal importance and thus omitted from the current study.

4. The formulation of the governing equations for a unidirectional flow of a Newtonian fluid parallel to the biporous layered cylindrical particle is conducted using the cylindrical coordinate system $(\widetilde{r}, \phi, \widetilde{z})$ to ensure precise physical representation.

5. The permeability of the porous material may exhibit variability, and thus, the analysis incorporates this by adopting a quadratic polynomial function of radial distance to account for these variations.

6. When heat conduction prevails over heat convection and a constant heat flux is assumed, the thermal equations in a steady-state condition are simplified, resulting in the convective term making a negligible contribution.

6.2.2 Model Description

Figure 6.1 illustrates the conceptual representation of the proposed model, showcasing a collection of biparous layered cylindrical particles along with their cross-sectional perspectives. For the purpose of examining entropy generation in the flow of a Newtonian fluid through a membrane comprising a swarm of porous cylindrical particles, a porous layered solid cylindrical tube with radius $\widetilde{a}$ is considered. Among the flow three regions, the Brinkman-Forchheimer porous region with thickness $\widetilde{b} - \widetilde{a}$ is regulated by Brinkman-Forchheimer equation, and the Brinkman porous region with thickness $(\widetilde{c} - \widetilde{b})$ Brinkman equation regulated the flow. However, in a non-porous region with thickness $(\widetilde{d} - \widetilde{c})$ overlying the porous regions the flow is is regulated by Stokes equation.

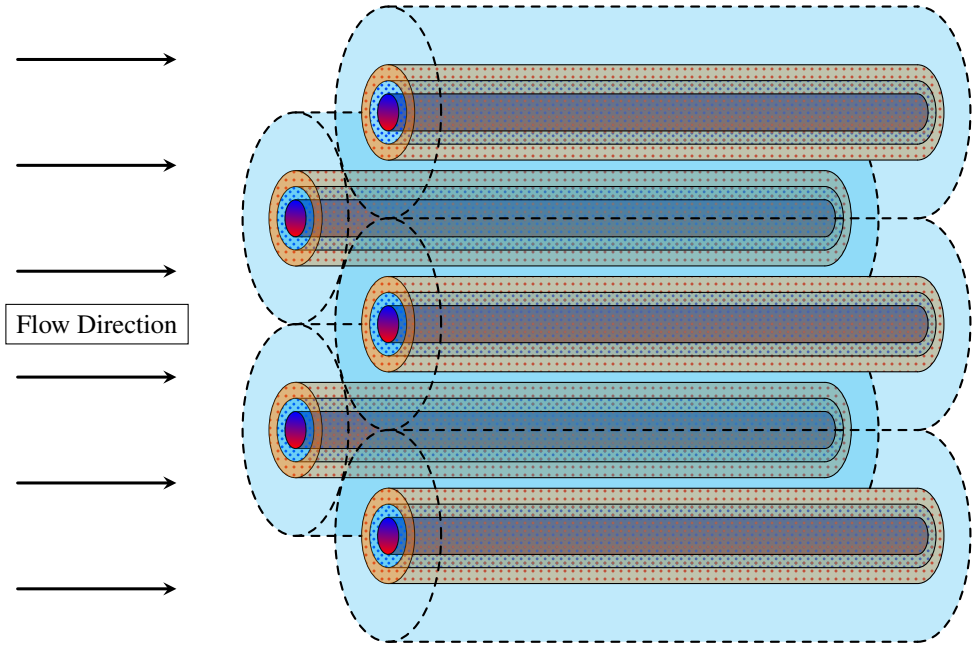

(a)

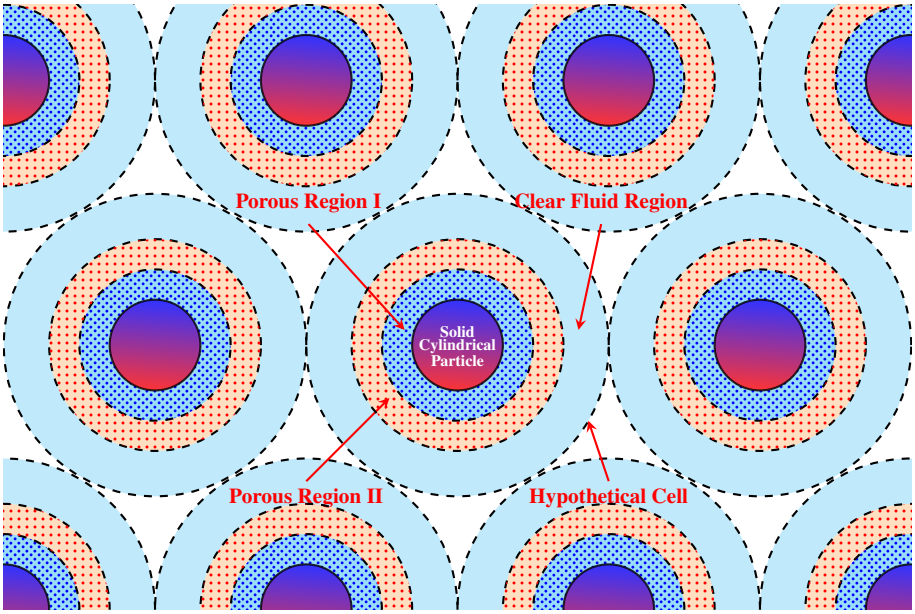

(b)

Figure 6.1: **(a)** The visual representation of the flow along the axis within a membrane consisting of a collection of bi-porous layered solid cylinders, **(b)** A hypothetical cell encloses a biporous layer surrounding a solid cylindrical particle within a swarm, visually depicted as a circular cross-sectional view.

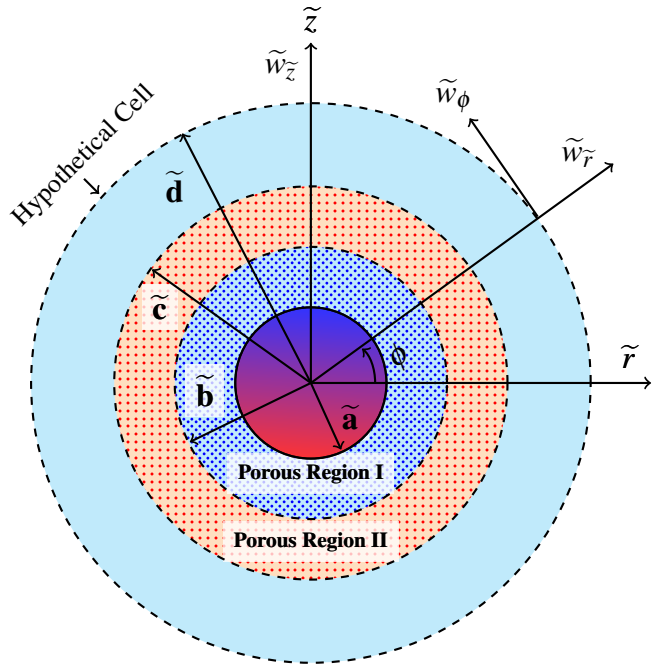

Figure 6.2: A hypothetical cell encloses a solid core within biporous layers, which in turn are coated with a cylindrical particle exhibiting a circular cross-section in its physical sketch

6.2.3 Governing Equations

The principles of mass, momentum, and energy conservation are applied in formulating the equations that govern the flow of fluid through a membrane consisting of a collection of porous cylindrical particles, under the assumptions mentioned earlier. The analysis focuses on pressure-driven flow in the axial direction while maintaining a constant heat flux. According to the construction of the physical model, three distinct areas are taken into account, each with varying thicknesses, *i.e.*, Brinman-Forchheimer region $(\widetilde{a} \leq \widetilde{r} \leq \widetilde{b})$, Brinkman region $(\widetilde{b} \leq \widetilde{r} \leq \widetilde{c})$, and non-porous region $(\widetilde{c} \leq \widetilde{r} \leq \widetilde{d})$.

6.2.3.1 Hydrodynamical and Thermal Equations

Under the assumption of variable permeability as outlined above, the equations that govern the flow through a biporous cylindrical particle are as stated below with their reduced forms: Region- I, *i.e.*, $\widetilde{a} \leq \widetilde{r} \leq \widetilde{b}$

$$\frac{\partial \widetilde{w}_1}{\partial \widetilde{z}} = 0, \tag{6.1a}$$

$$\frac{\partial \widetilde{p}_1}{\partial \widetilde{r}} = 0, \tag{6.1b}$$

$$\frac{\partial \widetilde{p}_1}{\partial \widetilde{z}} = \frac{\widetilde{\mu}_e}{\widetilde{r}}\frac{\partial}{\partial \widetilde{r}}\left(\widetilde{r}\frac{\partial \widetilde{w}_1}{\partial \widetilde{r}}\right) - \frac{\widetilde{\mu}\widetilde{w}_1}{\widetilde{k}_1(\widetilde{r})} - \frac{\widetilde{C}_F\widetilde{\rho}\widetilde{w}_1^2}{\sqrt{\widetilde{k}_1(\widetilde{r})}}, \tag{6.1c}$$

$$\widetilde{\rho}\widetilde{c}_p\widetilde{w}_1\left(\frac{\partial \widetilde{T}_1}{\partial \widetilde{z}}\right) = \frac{\widetilde{K}}{\widetilde{r}}\frac{\partial}{\partial \widetilde{r}}\left(\widetilde{r}\frac{\partial \widetilde{T}_1}{\partial \widetilde{r}}\right) + \frac{\widetilde{\mu}\widetilde{w}_1^2}{\widetilde{k}_1(\widetilde{r})} + \widetilde{\mu}_e\left(\frac{\partial \widetilde{w}_1}{\partial \widetilde{r}}\right)^2 + \frac{\widetilde{C}_F\widetilde{\rho}\widetilde{w}_1^3}{\sqrt{\widetilde{k}_1(\widetilde{r})}}, \tag{6.1d}$$

where the quantities $\widetilde{\rho}$, $\widetilde{p}_1$, and $\widetilde{w}_1$ refer to the density, pressure, and velocity of the fluid within the porous region, respectively. Meanwhile, $\widetilde{\mu}_e$ denotes the effective viscosity coefficient, $\widetilde{\mu}$ represents the constant viscosity coefficient of the Newtonian fluid, and $\widetilde{k}_1(\widetilde{r})$ stands for the variable permeability of the porous medium. Additionally, $\widetilde{T}_1$ signifies the temperature of the Brinkman-Forchheimer region, $\widetilde{K}$ is the thermal conductivity, $\widetilde{c}_p$ denotes the specific heat, and $\widetilde{C}_F$ represents the inertial coefficient. The equation labeled as (6.1*a*) embodies the principle of mass conservation and is commonly referred to as the continuity equation. Equations (6.1*b*) and (6.1*c*) represent the conservation of momentum principle in the radial and axial directions, respectively. Equation (6.1*c*) encompasses the contributions of pressure force, viscous effects, Brinkman resistance in relation to permeability, and a non-linear inertia term. Equation (6.1*d*), which describes the steady-state thermal energy balance in the absence of axial conduction and thermal dispersion, embodies the principle of energy conservation. It is recognized as the thermal equation and encompasses a non-linear convective term.

Region- II, *i.e.*, $\widetilde{b} \le \widetilde{r} \le \widetilde{c}$

$$\frac{\partial \widetilde{w}_2}{\partial \widetilde{z}} = 0, \tag{6.2a}$$

$$\frac{\partial \widetilde{p}_2}{\partial \widetilde{r}} = 0, \tag{6.2b}$$

$$\frac{\partial \widetilde{p}_2}{\partial \widetilde{z}} = \frac{\widetilde{\mu}_e}{\widetilde{r}}\frac{\partial}{\partial \widetilde{r}}\left(\widetilde{r}\frac{\partial \widetilde{w}_2}{\partial \widetilde{r}}\right) - \frac{\widetilde{\mu}\widetilde{w}_2}{\widetilde{k}_2(\widetilde{r})}, \tag{6.2c}$$

$$\widetilde{\rho}\widetilde{c}_p\widetilde{w}_2\left(\frac{\partial \widetilde{T}_2}{\partial \widetilde{z}}\right) = \frac{\widetilde{K}}{\widetilde{r}}\frac{\partial}{\partial \widetilde{r}}\left(\widetilde{r}\frac{\partial \widetilde{T}_2}{\partial \widetilde{r}}\right) + \frac{\widetilde{\mu}\widetilde{w}_2^2}{\widetilde{k}_2(\widetilde{r})} + \widetilde{\mu}_e\left(\frac{\partial \widetilde{w}_2}{\partial \widetilde{r}}\right)^2, \tag{6.2d}$$

where the variables $\widetilde{p}_2$ and $\widetilde{w}_2$ represent the pressure and velocity of the fluid within the Brinkman porous region, respectively. Additionally, $\widetilde{T}_2$ denotes the temperature specific to this region, while $\widetilde{k}_2(\widetilde{r})$ stands for the variable permeability of the porous medium.

Region- III, *i.e.*, $\widetilde{c} \le \widetilde{r} \le \widetilde{d}$

$$\frac{\partial \widetilde{w}_3}{\partial \widetilde{z}} = 0, \tag{6.3a}$$

$$\frac{\partial \widetilde{p}_3}{\partial \widetilde{r}} = 0, \tag{6.3b}$$

$$\frac{\partial \widetilde{p}_3}{\partial \widetilde{z}} = \frac{\widetilde{\mu}}{\widetilde{r}} \frac{\partial}{\partial \widetilde{r}} \left(\widetilde{r} \frac{\partial \widetilde{w}_3}{\partial \widetilde{r}} \right), \tag{6.3c}$$

$$\widetilde{\rho} \widetilde{c}_p \widetilde{w}_3 \left(\frac{\partial \widetilde{T}_3}{\partial \widetilde{z}} \right) = \frac{\widetilde{K}}{\widetilde{r}} \frac{\partial}{\partial \widetilde{r}} \left(\widetilde{r} \frac{\partial \widetilde{T}_3}{\partial \widetilde{r}} \right) + \widetilde{\mu} \left(\frac{\partial \widetilde{w}_3}{\partial \widetilde{r}} \right)^2, \tag{6.3d}$$

where $\widetilde{p}_3, \widetilde{w}_3$ are the pressure, and velocity of the clear fluid region, respectively, $\widetilde{T}_3$ is the temperature of clear fluid region.

6.2.3.2 Entropy Generation and Bejan Number

Entropy generation is a thermodynamic parameter used to quantify the dissipation of useful energy in any irreversible thermodynamic process, such as heat transfer and mass transfer. It is determined by analyzing the velocity and temperature distributions. In tube flow, the convection process naturally leads to irreversibility. This results in entropy generation occurring within the flow field as a consequence of momentum and energy transfer. In the specific scenario under consideration, entropy generation arises from the presence of a porous material, thermal exchange, and fluid friction. Hooman and Ejlali [205] proposed that the rate of volumetric entropy production for a viscous, incompressible Newtonian fluid for Brinkman-Forchheimer region can be described as follows:

$$\widetilde{S}_1 = \frac{\widetilde{K}}{\widetilde{T}_0^2} \left[\left(\frac{\partial \widetilde{T}_1}{\partial \widetilde{r}} \right)^2 + \left(\frac{\partial \widetilde{T}_1}{\partial \widetilde{z}} \right)^2 \right] + \frac{1}{\widetilde{T}_0} \left[\frac{\widetilde{\mu} \widetilde{w}_1^2}{\widetilde{k}_1(\widetilde{r})} + \widetilde{\mu}_e \left(\frac{\partial \widetilde{w}_1}{\partial \widetilde{r}} \right)^2 + \frac{\widetilde{C}_F \widetilde{\rho} \widetilde{w}_1^3}{\sqrt{\widetilde{k}_1(\widetilde{r})}} \right], \tag{6.4a}$$

$$\widetilde{S}_2 = \frac{\widetilde{K}}{\widetilde{T}_0^2} \left[\left(\frac{\partial \widetilde{T}_2}{\partial \widetilde{r}} \right)^2 + \left(\frac{\partial \widetilde{T}_2}{\partial \widetilde{z}} \right)^2 \right] + \frac{1}{\widetilde{T}_0} \left[\frac{\widetilde{\mu} \widetilde{w}_2^2}{\widetilde{k}_2(\widetilde{r})} + \widetilde{\mu}_e \left(\frac{\partial \widetilde{w}_2}{\partial \widetilde{r}} \right)^2 \right], \tag{6.4b}$$

$$\widetilde{S}_3 = \frac{\widetilde{K}}{\widetilde{T}_0^2} \left[\left(\frac{\partial \widetilde{T}_3}{\partial \widetilde{r}} \right)^2 + \left(\frac{\partial \widetilde{T}_3}{\partial \widetilde{z}} \right)^2 \right] + \frac{\widetilde{\mu}}{\widetilde{T}_0} \left(\frac{\partial \widetilde{w}_3}{\partial \widetilde{r}} \right)^2, \tag{6.4c}$$

where $\widetilde{S}_1, \widetilde{S}_2$, and $\widetilde{S}_3$ denote the rate of volumetric entropy generation corresponding to three separate zones: the Brinkman-Forchheimer, Brinkman, and non-porous regions, respectively. The equation (6.4a) comprises five components, with the first two components representing the entropy generation rate due to heat transfer irreversibility. However, the

remaining three components describe the entropy generation arising from viscous dissipation (fluid friction irreversibility) caused by the presence of viscous, Brinkman resistance and fluid inertia terms. The equation (6.4*b*) consists of four components. The first two components correspond to the entropy generation rates arising from radial and axial thermal conduction, respectively. In contrast, the last two components signify the entropy generation resulting from viscous dissipation owing to the presence of viscous and Brinkman resistance term.

The first law of thermodynamics results in

$$\frac{\partial \widetilde{T}_1}{\partial \widetilde{z}} = \frac{\partial \widetilde{T}_2}{\partial \widetilde{z}} = \frac{\partial \widetilde{T}_3}{\partial \widetilde{z}} = \frac{2q''}{\widetilde{\rho}\widetilde{c}_p\widetilde{c}\widetilde{w}_0}. \tag{6.5}$$

The definitions pertain to the mean velocity, U and the bulk mean temperature, T_m

$$U = \frac{2}{(\widetilde{d}^2 - \widetilde{a}^2)} \int_{\widetilde{a}}^{\widetilde{d}} \widetilde{w}\widetilde{r}d\widetilde{r}, \quad T_m = \frac{2}{(\widetilde{d}^2 - \widetilde{a}^2)U} \int_{\widetilde{a}}^{\widetilde{d}} \widetilde{w}\widetilde{T}\widetilde{r}d\widetilde{r}. \tag{6.6}$$

Ultimately, the Nusselt number is characterized as

$$\mathrm{Nu} = \frac{2q''\widetilde{c}}{\widetilde{K}(\widetilde{T}_w - \widetilde{T}_m)}. \tag{6.7}$$

6.2.3.3 Boundary Conditions

In diverse scenarios related to fluid dynamics, there exist exchanges between the fluids and their surroundings at interfaces. These exchanges referred to as boundary conditions, affecting the fluid flow concerning its environment. Derived from the system's properties, these conditions mathematically articulate the physics occurring at these boundaries. When opting for a particular design or flow field, conditions are inherently established. Conversely, if these conditions are readily apparent, it may signal the necessity for a more precise delineation of the system's boundaries, potentially resulting in challenges when tackling problems. Boundary conditions encompass factors like the behaviour of external forces acting on the fluid, mass and momentum exchange rates, values of variables at the boundary, and their interrelationships. When addressing solutions pertaining to the evolution of flow fields over time, both initial and boundary conditions are imperative.

The quantity of conditions necessary is contingent upon the governing equations that depict the behaviour of fluids, as distinct physical phenomena can give rise to various boundary conditions. In essence, there are typically three main classifications of boundary conditions:

1. The state of zero axial velocity at the surface of the solid cylinder is being taken into account and the temperature consistently remains at the ambient level, *i.e.*,

$$\widetilde{w}_1 = 0, \text{ and } \widetilde{T}_1 = \widetilde{T}_\infty, \quad \text{at} \quad \widetilde{r} = \widetilde{a}, \tag{6.8a}$$

2. It is assumed that the fluid's velocity and temperature remain continuous at the interface between the Brinkman-Forchheimer and Brinkman porous regions. Also, it is postulated that the velocity and temperature gradients exhibit continuity at the interface between the Brinkman-Forchheimer and Brinkman porous regions, *i.e.*,

$$\widetilde{w}_1 = \widetilde{w}_2, \text{ and } \widetilde{T}_1 = \widetilde{T}_2, \quad \text{at} \quad \widetilde{r} = \widetilde{b}, \tag{6.8b}$$

$$\frac{d\widetilde{w}_1}{d\widetilde{r}} = \frac{d\widetilde{w}_2}{d\widetilde{r}}, \text{ and } \frac{d\widetilde{T}_1}{d\widetilde{r}} = \frac{d\widetilde{T}_2}{d\widetilde{r}}, \quad \text{at} \quad \widetilde{r} = \widetilde{b}, \tag{6.8c}$$

3. The stress jump boundary along with continuity of temperature gradient is considered at the Brinkman-Stokes interface, *i.e.*,

$$\widetilde{w}_2 = \widetilde{w}_3, \text{ and } \widetilde{T}_2 = \widetilde{T}_3, \quad \text{at} \quad \widetilde{r} = \widetilde{c}, \tag{6.8d}$$

$$\frac{d\widetilde{w}_2}{d\widetilde{r}} - \frac{d\widetilde{w}_3}{d\widetilde{r}} = \frac{\beta \widetilde{w}_2}{\sqrt{\widetilde{k}_2(\widetilde{r})}}, \text{ and } \frac{d\widetilde{T}_2}{d\widetilde{r}} = \frac{d\widetilde{T}_3}{d\widetilde{r}}, \quad \text{at} \quad \widetilde{r} = \widetilde{c}, \tag{6.8e}$$

4. The hypothetical cell surface is assumed to have zero velocity and temperature gradients, *i.e.*,

$$\frac{d\widetilde{w}_3}{d\widetilde{r}} = 0, \text{ and } \frac{d\widetilde{T}_3}{d\widetilde{r}} = 0 \quad \text{at} \quad \widetilde{r} = \widetilde{d}. \tag{6.8f}$$

6.2.4 Non-Dimensional Parameters and Governing Equations

To solve the above system of equations (6.1*a*) – (6.3*d*), the following non-dimensional variables are introduced:

$$\begin{aligned}
&p_i = \frac{\widetilde{p}_i \widetilde{c}}{\widetilde{w}_0 \widetilde{\mu}}, \; r = \frac{\widetilde{r}}{\widetilde{c}}, \; z = \frac{\widetilde{z}}{\widetilde{c}}, \; S^2 = \frac{1}{k}, \; \widetilde{w}_0 = \frac{\widetilde{q}_0 \widetilde{c}^2}{\widetilde{\mu}}, \; Br = \frac{\widetilde{\mu} \widetilde{w}_0^2}{\widetilde{K}(\widetilde{T}_w - \widetilde{T}_\infty)}, \\
&w_i = \frac{\widetilde{w}_i}{\widetilde{w}_0}, \; k = \frac{\widetilde{k}}{\widetilde{c}^2}, \; F = \frac{C_F \widetilde{\rho} \widetilde{c}^3 \widetilde{q}_0}{\widetilde{\mu}_e \widetilde{\mu}}, \; \mathrm{Nu} = \frac{2q'' \widetilde{c}}{\widetilde{K}(\widetilde{T}_w - \widetilde{T}_m)}, \; \lambda_1^2 = \frac{\widetilde{\mu}_e}{\widetilde{\mu}}, \\
&\theta = \frac{\widetilde{T} - \widetilde{T}_w}{\widetilde{T}_m - \widetilde{T}_w}, \; \hat{w} = \frac{\widetilde{w}}{U}
\end{aligned} \tag{6.9}$$

where $\widetilde{w}_0$ represents the average velocity, F denotes the Forchheimer number also referred to as the Forchheimer-Reynolds number, is a dimensionless factor employed to quantify the significance of inertial forces compared to viscous forces in fluid motion. This parameter proves especially valuable when simulating the movement of fluids within permeable substances like soils, rocks, and industrial filters. S stands for a dimensionless parameter and $\widetilde{q}_0$ signifies the characteristic pressure gradient, Nu corresponds to the Nusselt number, Br is therepresents the Brinkman number, and λ_1 is the viscosity ratio parameter. $i = 1,2,3$.

6.2.4.1 Hydrodynamic and Thermal Equations

The provided non-dimensional variables (6.9) lead to the transformation of the governing equations for porous and non-porous regions into their non-dimensional forms as outlined below:

Region- I, *i.e.*, $a \leq r \leq b$

$$\frac{\partial w_1}{\partial z} = 0, \tag{6.10a}$$

$$\frac{\partial p_1}{\partial r} = 0, \tag{6.10b}$$

$$\frac{\partial p_1}{\partial z} = \frac{\lambda_1^2}{r}\frac{\partial}{\partial r}\left(r\frac{\partial w_1}{\partial r}\right) - \frac{w_1}{k_1(r)} - \frac{F\lambda_1^2 w_1^2}{\sqrt{k_1(r)}}, \tag{6.10c}$$

$$\frac{1}{r}\frac{\partial}{\partial r}\left(r\frac{\partial \theta_1}{\partial r}\right) + \mathrm{Nu}w_1 + Br\left[\frac{w_1^2}{k_1(r)} + \lambda_1^2\left(\frac{\partial w_1}{\partial r}\right)^2 + \frac{\lambda_1^2 F w_1^3}{\sqrt{k_1(r)}}\right] = 0. \tag{6.10d}$$

Region- II, *i.e.*, $b \leq r \leq 1$

$$\frac{\partial w_2}{\partial z} = 0, \tag{6.11a}$$

$$\frac{\partial p_2}{\partial r} = 0, \tag{6.11b}$$

$$\frac{\partial p_2}{\partial z} = \frac{\lambda_1^2}{r}\frac{\partial}{\partial r}\left(r\frac{\partial w_2}{\partial r}\right) - \frac{w_2}{k_2(r)}, \tag{6.11c}$$

$$\frac{1}{r}\frac{\partial}{\partial r}\left(r\frac{\partial \theta_2}{\partial r}\right) + \mathrm{Nu}w_2 + Br\left[\frac{w_2^2}{k_2(r)} + \lambda_1^2\left(\frac{\partial w_2}{\partial r}\right)^2\right] = 0. \tag{6.11d}$$

Region- III, *i.e.*, $1 \leq r \leq d$

$$\frac{\partial w_3}{\partial z} = 0, \tag{6.12a}$$

$$\frac{\partial p_3}{\partial r} = 0, \tag{6.12b}$$

$$\frac{\partial p_3}{\partial z} = \frac{1}{r}\frac{\partial}{\partial r}\left(r\frac{\partial w_3}{\partial r}\right), \tag{6.12c}$$

$$\frac{1}{r}\frac{\partial}{\partial r}\left(r\frac{\partial \theta_3}{\partial r}\right) + \mathrm{Nu}w_3 + Br\left(\frac{\partial w_3}{\partial r}\right)^2 = 0. \tag{6.12d}$$

6.2.4.2 Entropy Generation and Bejan Number

The non-dimensional expressions for entropy generation and Bejan number, pertaining to both porous and non-porous regions, are formulated utilizing the non-dimensional parameters outlined in equation (6.9). The mathematical expressions for entropy generation are derived as

$$S_1 = \frac{\widetilde{S}_1}{\widetilde{S}_0} = \left[\left(\frac{d\theta_1}{dr}\right)^2 + \left(\frac{Nu}{Pe}\right)^2\right] + \frac{Br}{T_0}\left[\frac{w_1^2}{k_1(r)} + \lambda_1^2\left(\frac{dw_1}{dr}\right)^2 + \frac{\lambda_1^2 F w_1^3}{\sqrt{k_1(r)}}\right], \tag{6.13a}$$

$$S_2 = \frac{\widetilde{S}_2}{\widetilde{S}_0} = \left[\left(\frac{d\theta_2}{dr}\right)^2 + \left(\frac{Nu}{Pe}\right)^2\right] + \frac{Br}{T_0}\left[\frac{w_2^2}{k_2(r)} + \lambda_1^2\left(\frac{dw_2}{dr}\right)^2\right], \tag{6.13b}$$

$$S_3 = \frac{\widetilde{S}_3}{\widetilde{S}_0} = \left[\left(\frac{d\theta_3}{dr}\right)^2 + \left(\frac{Nu}{Pe}\right)^2\right] + \frac{Br}{T_0}\left(\frac{dw_3}{dr}\right)^2, \tag{6.13c}$$

where S_1, S_2, and S_3 represent the entropy generation associated with three distinct regions: the Brinkman-Forchheimer, Brinkman, and non-porous regions, respectively.
The Bejan number, which quantifies irreversibility resulting from heat transfer, is stipulated as

$$Be_1 = \frac{\left(\frac{d\theta_1}{dr}\right)^2 + \left(\frac{Nu}{Pe}\right)^2}{\left[\left(\frac{d\theta_1}{dr}\right)^2 + \left(\frac{Nu}{Pe}\right)^2\right] + \frac{Br}{T_0}\left[\frac{w_1^2}{k_1(r)} + \lambda_1^2\left(\frac{dw_1}{dr}\right)^2 + \frac{\lambda_1^2 F w_1^3}{\sqrt{k_1(r)}}\right]}, \tag{6.14a}$$

$$Be_2 = \frac{\left(\frac{d\theta_2}{dr}\right)^2 + \left(\frac{Nu}{Pe}\right)^2}{\left[\left(\frac{d\theta_2}{dr}\right)^2 + \left(\frac{Nu}{Pe}\right)^2\right] + \frac{Br}{T_0}\left[\frac{w_2^2}{k_2(r)} + \lambda_1^2\left(\frac{dw_2}{dr}\right)^2\right]}, \tag{6.14b}$$

$$Be_3 = \frac{\left(\frac{d\theta_3}{dr}\right)^2 + \left(\frac{Nu}{Pe}\right)^2}{\left[\left(\frac{d\theta_3}{dr}\right)^2 + \left(\frac{Nu}{Pe}\right)^2\right] + \frac{Br}{T_0}\left(\frac{dw_3}{dr}\right)^2}, \tag{6.14c}$$

where Be_1, Be_2, and Be_3 denote the Bejan numbers corresponding to three separate regions: the Brinkman-Forchheimer, Brinkman, and non-porous regions, respectively.

6.2.4.3 Dimensionless Boundary Conditions

The dimensionless boundary and interface conditions for hydrodynamic and thermal equations are provided as follows:

$$\begin{aligned}
w_1 = 0, \ \text{and} \ \theta_1 = 1, \quad \text{at} \quad r = a. \\
w_1 = w_2, \ \text{and} \ \theta_1 = \theta_2, \quad \text{at} \quad r = b, \\
\frac{dw_1}{dr} = \frac{dw_2}{dr}, \ \text{and} \ \frac{d\theta_1}{dr} = \frac{d\theta_2}{dr}, \quad \text{at} \quad r = b. \\
w_2 = w_3, \ \text{and} \ \theta_2 = \theta_3, \quad \text{at} \quad r = 1, \\
\frac{1}{\alpha_p}\frac{dw_2}{dr} - \frac{dw_3}{dr} = \frac{\beta w_2}{\sqrt{k_2(r)}}, \ \text{and} \ \frac{d\theta_2}{dr} = \frac{d\theta_3}{dr}, \quad \text{at} \quad r = 1. \\
\frac{dw_3}{dr} = 0, \ \text{and} \ \frac{d\theta_3}{dr} = 0, \quad \text{at} \quad r = d.
\end{aligned} \tag{6.15}$$

6.3 Asymptotic Solution of the Problem

In the suggested framework, the governing equations regulating the flow of Newtonian fluid within porous regions become nonlinear second-order ordinary differential equations due to the presence of a nonlinear inertia term in the Brinkman-Forchheimer equation and the variable nature of permeability. The solutions of these nonlinear equations present considerable challenges. To find solutions for these governing equations, either asymptotic or numerical solution techniques may be employed to derive velocity expressions for both the porous regions. The asymptotic expansions of velocities in both the porous regions are determined by considering whether the permeability parameter k is small or large. The numerical scheme NDSolve within Mathematica is utilized to validate our results. For a comprehensive understanding of perturbation techniques, readers are referred to Bush [141] and Nayfeh [142].

6.3.1 Perturbation Solutions for Hydrodynamic Equations

This subsection discusses the asymptotic solutions of the governing equations that analyze entropy generation in a creeping flow of a Newtonian fluid through a swarm of biporous layered cylindrical particles. The solution approach is divided into two subsections: one for low Darcy numbers and the other for large Darcy numbers. A regular perturbation method is employed for large Darcy numbers, while a singular perturbation method, combined with

a matched asymptotic assumption, is used to solve the equations for small Darcy numbers. Below are detailed explanations and derivations for the asymptotic expansions of velocity profiles in porous regions.

6.3.1.1 Solution for Large Permeability $(i.e., S \ll 1)$

$$w_i = w_{i0} + S w_{i1} + S^2 w_{i2} + O(S^3), \tag{6.16a}$$

where $i = 1,2,3$ represent for Forchheimer, Brinkman, and Stokes regions, respectively.

Forchheimer Region $(a \le r \le b)$

The momentum equation along the axial direction governing fluid flow within the Forchheimer region can be expressed using the small parameter $S \ll 1$, particularly applicable for high permeability of the porous medium, as follows:

$$\frac{\partial p_1}{\partial z} = \frac{\lambda_1^2}{r}\frac{\partial}{\partial r}\left(r\frac{\partial w_1}{\partial r}\right) - \frac{S^2 w_1}{(1-\varepsilon_f r)^2} - \frac{SF\lambda_1^2 w_1^2}{1-\varepsilon_f r}, \tag{6.17a}$$

The velocity profiles of zeroth, first, and second order are derived through asymptotic series expansions based on the high permeability of the porous medium. The zeroth, first, and second order velocity profiles are obtained as

$$\frac{\lambda_1^2}{r}\frac{d}{dr}\left(r\frac{dw_{10}}{dr}\right) = -p_s, \tag{6.18a}$$

$$\frac{\lambda_1^2}{r}\frac{d}{dr}\left(r\frac{dw_{11}}{dr}\right) = \frac{F\lambda_1^2 w_{10}^2}{1-\varepsilon_f r}, \tag{6.18b}$$

$$\frac{\lambda_1^2}{r}\frac{d}{dr}\left(r\frac{dw_{12}}{dr}\right) = \frac{w_{10}}{(1-\varepsilon_f r)^2} + \frac{2F\lambda_1^2 w_{10} w_{11}}{1-\varepsilon_f r}, \tag{6.18c}$$

The analytical solutions for the equations governing the velocity profiles of zeroth, first, and second order, denoted as (6.18*a*), (6.18*b*), and (6.18*c*) respectively, are derived as

$$w_{10} = C_1 \log(r) + C_2 - \frac{p_s r^2}{4\lambda_1^2}, \tag{6.19a}$$

$$\begin{aligned} w_{11} = {} & \frac{Fr^2}{3456}\left(C_1^2(\varepsilon_f r(81\varepsilon_f r + 256) + 1296) - 8C_1C_2(\varepsilon_f r(27\varepsilon_f r + 64) + 216) + 24C_2^2(\varepsilon_f r(9\varepsilon_f r + 16) + \right. \\ & + \frac{1}{144}C_1^2 Fr^2(\varepsilon_f r(9\varepsilon_f r + 16) + 36)\log^2(r) \\ & + \frac{F p_s r^4}{216000\lambda_1^2}(C_1(8\varepsilon_f r(125\varepsilon_f r + 216) + 3375) - 30C_2(4\varepsilon_f r(25\varepsilon_f r + 36) + 225)) \end{aligned}$$

$$-\frac{C_1 F r^2 \log(r)}{21600\lambda_1^2}\left(50\lambda_1^2(C_1(\varepsilon_f r(27\varepsilon_f r+64)+216)-6C_2(\varepsilon_f r(9\varepsilon_f r+16)+36))\right.$$
$$\left.+3p_s r^2(4\varepsilon_f r(25\varepsilon_f r+36)+225)\right)+C_3\log(r)+C_4$$
$$+\frac{F p_s^2 r^6(9\varepsilon_f r(49\varepsilon_f r+64)+784)}{451584\lambda_1^4}. \tag{6.19b}$$

Due to very large expressions, the complete expression for the second-order velocity, w_{12}, containing the constants C_5 and C_6 have not been presented here. The constants $C_1 - C_6$ are arbitrary and can be determined by applying boundary conditions (6.15). Due to their lengthy nature, the mathematical expressions for these constants are not included in the chapter.

Brinkman Region ($b \le r \le 1$)

The momentum equation in the axial direction and the thermal equation that governs fluid flow within the Brinkman porous region can be represented using the small parameter $S \ll 1$, which is especially relevant for high permeability of the porous medium, as follows

$$\frac{\partial p_2}{\partial z} = \frac{\lambda_1^2}{r}\frac{\partial}{\partial r}\left(r\frac{\partial w_2}{\partial r}\right) - \frac{S^2 w_2}{(1-\varepsilon_b r)^2}, \tag{6.20a}$$

$$\tag{6.20b}$$

The velocity profiles for zeroth, first, and second orders are obtained by employing asymptotic series expansions, leveraging the high permeability of the porous medium. The velocity profiles for the zeroth, first, and second order are derived as

$$\frac{\lambda_1^2}{r}\frac{\partial}{\partial r}\left(r\frac{\partial w_{20}}{\partial r}\right) = -p_s, \tag{6.21a}$$
$$\frac{\lambda_1^2}{r}\frac{\partial}{\partial r}\left(r\frac{\partial w_{21}}{\partial r}\right) = 0, \tag{6.21b}$$
$$\frac{\lambda_1^2}{r}\frac{\partial}{\partial r}\left(r\frac{\partial w_{22}}{\partial r}\right) = \frac{w_{20}}{(1-\varepsilon_b r)^2}, \tag{6.21c}$$

The analytical solutions for the equations governing the velocity profiles of zeroth, first, and second order, denoted as (6.20*a*), (6.23), and (6.24) respectively, are derived as

$$w_{20} = C_7\log(r) + C_8 - \frac{p_s r^2}{4\lambda_1^2}, \tag{6.22a}$$
$$w_{21} = C_9\log(r) + C_{10}, \tag{6.22b}$$
$$w_{22} = C_{11}\log(r) + C_{12} + \frac{C_7 r^2(\varepsilon_b r(27\varepsilon_b r+32)+36)\log(r)}{144\lambda_1^2}$$

$$-\frac{1}{43200\lambda_1^4}\left[50\lambda_1^2 r^2(C_7(\varepsilon_b r(81\varepsilon_b r+128)+216)-6C_8(\varepsilon_b r(27\varepsilon_b r+32)+36))\right.$$
$$\left.+9p_s r^4(4\varepsilon_b r(25\varepsilon_b r+24)+75)\right], \tag{6.22c}$$

where the constants $C_7 - C_{12}$ are arbitrary and can be established by applying boundary conditions (6.15). Owing to their extensive form, the mathematical expressions for these constants are omitted from the chapter.

Stokes Region $(1 \leq r \leq d)$

The reduced governing equations of velocity profiles for the zeroth, first, and second order are derived as

$$\frac{1}{r}\frac{\partial}{\partial r}\left(r\frac{\partial w_{30}}{\partial r}\right) = -p_s, \tag{6.23}$$
$$\frac{1}{r}\frac{\partial}{\partial r}\left(r\frac{\partial w_{31}}{\partial r}\right) = 0, \tag{6.24}$$
$$\frac{1}{r}\frac{\partial}{\partial r}\left(r\frac{\partial w_{32}}{\partial r}\right) = 0, \tag{6.25}$$

which can be solved exactly, and analytical expression of their solution can be given as,

$$w_{30} = C_{13}\log(r) + C_{14} - \frac{p_s r^2}{4}, \tag{6.26}$$
$$w_{31} = C_{15}\log(r) + C_{16}, \tag{6.27}$$
$$w_{32} = C_{17}\log(r) + C_{18} \tag{6.28}$$

where the constants $C_{13} - C_{18}$ are arbitrary and can be established by applying boundary conditions (6.15).

6.3.1.2 Solution for Small Permeability $(i.e., S \gg 1)$

Taking into account the low permeability of the porous medium $k \ll 1$, the parameter $S \gg 1$ exhibits significant enlargement. The equations governing the flow of a Newtonian fluid through biporous layered cylindrical particles will transform into a singularly perturbed boundary value problem, with the parameter $S^{-1} \ll 1$, where $S = \frac{1}{k}$ and k is the permeability of the porous medium. Finding analytical solutions for these singularly perturbed boundary value problems presents a significant challenge. The equations describing the flow of a Newtonian fluid through porous regions are presented in terms of S^{-1} as follows:

$$S^{-2}\left(\frac{\partial p_1}{\partial z}\right) = \frac{S^{-2}\lambda_1^2}{r}\frac{\partial}{\partial r}\left(r\frac{\partial w_1}{\partial r}\right) - \frac{w_1}{(1-\varepsilon_f r)^2} - \frac{S^{-1}F\lambda_1^2 w_1^2}{1-\varepsilon_f r}, \tag{6.29a}$$

$$S^{-2}\left(\frac{\partial p_2}{\partial z}\right)=\frac{S^{-2}\lambda_1^2}{r}\frac{\partial}{\partial r}\left(r\frac{\partial w_2}{\partial r}\right)-\frac{w_2}{(1-\varepsilon_b r)^2}. \tag{6.29b}$$

The conventional perturbation technique is inadequate for establishing asymptotic solutions to singularly perturbed boundary value problems owing to the presence of the parameter S^{-1} associated with the highest order derivative term.

Outer Solution

$$w_1 = w_{10}+S_1^1 w_{11}+S_1^2 w_{12}+S_1^3 w_{13}+S_1^4 w_{14}+S_1^5 w_{15}+O(S_1^6), \tag{6.30a}$$
$$w_2 = w_{20}+S_1^1 w_{21}+S_1^2 w_{22}+S_1^3 w_{23}+S_1^4 w_{24}+S_1^5 w_{25}+O(S_1^6), \tag{6.30b}$$

The series form of velocities is introduced in the equation 6.29a and 6.29b and equated the like power of the parameter S_1.

$$\begin{aligned} &w_{10}=0,\ w_{11}=0,\ w_{12}=p_z(1-r\varepsilon_f)^2,\ w_{13}=0,\\ &w_{14}=\frac{2\lambda_1^2 p_z\varepsilon_f(r\varepsilon_f-1)^2(2r\varepsilon_f-1)}{r},\ w_{15}=F\lambda_1^2 p_z^2(r\varepsilon_f-1)^5, \end{aligned} \tag{6.31a}$$

$$\begin{aligned} &w_{20}=0,\ w_{21}=0,\ w_{22}=p_z(1-r\varepsilon_b)^2,\ w_{23}=0,\\ &w_{24}=\frac{2\lambda_1^2 p_z\varepsilon_b(r\varepsilon_b-1)^2(2r\varepsilon_b-1)}{r},\ w_{25}=0, \end{aligned} \tag{6.31b}$$

$$\begin{aligned} w_1^o &= w_{10}+S_1 w_{11}+S_1^2 w_{12}+S_1^3 w_{13}+S_1^4 w_{14}+S_1^5 w_{15},\\ &= F\lambda_1^2 p_z^2 S_1^5(r\varepsilon_f-1)^5+\frac{1}{r}2\lambda_1^2 p_z S_1^4\varepsilon_f(2r\varepsilon_f-1)(r\varepsilon_f-1)^2+p_z S_1^2(r\varepsilon_f-1)^2, \end{aligned} \tag{6.32a}$$

$$\begin{aligned} w_2^o &= w_{20}+S_1 w_{21}+S_1^2 w_{22}+S_1^3 w_{23}+S_1^4 w_{24}+S_1^5 w_{25},\\ &= \frac{1}{r}p_z S_1^2(r\varepsilon_b-1)^2\left(4\lambda_1^2 r S_1^2\varepsilon_b^2+r-2\lambda_1^2 S_1^2\varepsilon_b\right), \end{aligned} \tag{6.32b}$$

Inner Solution

To derive the solution for the boundary layer region, a streatching variable (inner variable) will be defined at the left end of each domain, which will be introduced as

$$\eta_1=\frac{r-a}{S_1}, \tag{6.33a}$$
$$\eta_2=\frac{r-b}{S_1}, \tag{6.33b}$$

Introducing these inner variables in the boundary value problem 6.29a, 6.29b and 6.15 and neglecting the smaller terms ($S^{-1} \to 0$).

$$\lambda_1^2 \frac{d^2 w_1}{d\eta_1^2} - (1 + 2\varepsilon_f a + 3\varepsilon_f^2 a^2) w_1 = 0, \tag{6.34a}$$

$$\lambda_1^2 \frac{d^2 w_2}{d\eta_2^2} - (1 + 2\varepsilon_b b + 3\varepsilon_b^2 b^2) w_2 = 0, \tag{6.34b}$$

$$\tag{6.34c}$$

The above set of equations can be solved exactly and their one term bounded solution is represented as

$$w_1^i = c_2 e^{-\frac{\frac{r-a}{S_1}\sqrt{3a^2\varepsilon_f^2 + 2a\varepsilon_f + 1}}{\lambda_1}}, \tag{6.35a}$$

$$w_2^i = c_4 e^{-\frac{\frac{r-b}{S_1}\sqrt{3b^2\varepsilon_b^2 + 2b\varepsilon_b + 1}}{\lambda_1}}, \tag{6.35b}$$

Matching Procedure

The outer solution in terms of inner limit is stated as,

$$(w_1^o)^i = \lim_{S \to +\infty} w_1^o = 0, \tag{6.36a}$$

$$(w_2^o)^i = \lim_{S \to +\infty} w_2^o = 0, \tag{6.36b}$$

The inner solution in terms of outer limit is stated as,

$$(w_1^i)^o = \lim_{\eta_1 \to +\infty} w_1^o = 0, \tag{6.37a}$$

$$(w_2^i)^o = \lim_{\eta_2 \to +\infty} w_2^o = 0, \tag{6.37b}$$

It can be observed from the equations (22) and (23) that the Prandtl's matching condition $(u_k^o)^{in} = (u_k^{in})^o = u_k^m,\ k = 1,2$ is satisfied, where, u_k^m is the match solution of both inner and outer solutions. The matching solution is

$$w_k^m = 0, \quad k = 1,2. \tag{6.38a}$$

By using the inner and outer solution the expression of composite solution of velocities for three different regions is

$$w_k = w_k^o + w_k^i - w_k^m, \quad k = 1,2. \tag{6.39a}$$

Additionally, the analytical expression of velocity for the Stokes region can be derived as

$$w_3 = c_5 \log(r) + c_6 - \frac{p_s r^2}{4} \tag{6.40}$$

Since the boundary layer is assumed on the left side of the Forchheimer and Brinkman region, i.e. $r = a$, and $r = b$, respectively. Therefore, one the condition on the right side of each domain, $r = b$, and $r = c$, respectively, i.e. the conditions of continuity of stresses at the porous-porous interface and fluid-porous interface should be omitted. Hence, the constants c_2, c_4, c_5 and c_6 will be derived using the following set of boundary conditions

$$w_1 = 0 \text{ at } r = a, \tag{6.41a}$$

$$w_1 = w_2 \text{ at } r = b, \tag{6.41b}$$

$$w_2 = w_3 \text{ at } r = 1, \tag{6.41c}$$

$$\frac{dw_3}{dr} = 0 \text{ at } r = d. \tag{6.41d}$$

6.3.2 Solutions for Thermal Equations

The analytical solutions for the equations that control the temperature profiles in the Forchheimer, Brinkman, and Stokes region are obtained using variation of parameter method, and are given as

$$\begin{aligned}\theta_1 =& t_1 \log(r) + t_2 - \log(r) \int_a^b r \left(\mathrm{Nu}\hat{w}_1 + Br \left[\frac{\hat{w}_1^2}{k_1(r)} + \lambda_1^2 \left(\frac{\partial \hat{w}_1}{\partial r} \right)^2 + \frac{\lambda_1^2 F \hat{w}_1^3}{\sqrt{k_1(r)}} \right] \right) dr \\ &+ \int_a^b r \log(r) \left(\mathrm{Nu}\hat{w}_1 + Br \left[\frac{\hat{w}_1^2}{k_1(r)} + \lambda_1^2 \left(\frac{\partial \hat{w}_1}{\partial r} \right)^2 + \frac{\lambda_1^2 F \hat{w}_1^3}{\sqrt{k_1(r)}} \right] \right) dr. \end{aligned} \tag{6.42}$$

$$\begin{aligned}\theta_2 =& t_3 \log(r) + t_4 - \log(r) \int_b^1 r \left(\mathrm{Nu}\hat{w}_2 + Br \left[\frac{\hat{w}_2^2}{k_2(r)} + \lambda_1^2 \left(\frac{\partial \hat{w}_2}{\partial r} \right)^2 \right] \right) dr \\ &+ \int_b^1 r \log(r) \left(\mathrm{Nu}\hat{w}_2 + Br \left[\frac{\hat{w}_2^2}{k_2(r)} + \lambda_1^2 \left(\frac{\partial \hat{w}_2}{\partial r} \right)^2 \right] \right) dr. \end{aligned} \tag{6.43}$$

$$\theta_2 = t_5 \log(r) + t_6 - \log(r) \int_1^d r \left(\mathrm{Nu}\hat{w}_3 + Br \left(\frac{\partial \hat{w}_3}{\partial r} \right)^2 \right) dr$$

$$+\int_1^d r\log(r)\left(\mathrm{Nu}\hat{w}_3+Br\left(\frac{\partial\hat{w}_3}{\partial r}\right)^2\right)dr, \tag{6.44}$$

where the constants t_1-t_6 are arbitrary and can be established by applying boundary conditions (6.15).

6.4 Results and Discussion

The present study delves into the influence of varying permeability and the biporous layer arrangement within the medium, along with the generation of entropy, in the context of the slow, Newtonian flow of fluid through a collection of cylindrical particles with biporous layers. The goal is to shed light on how the changing permeability, diverse porous media, and entropy generation play a crucial role in modeling fluid flow through a membrane. The envisioned work's physical sketch is designed such that the Brinkman-Forchheimer region near the solid core of the cylindrical particle is governed by the Brinkman-Forchheimer equation with variable permeability. Simultaneously, a concentric Brinkman porous region is governed by the Brinkman equation, also under variable permeability of the medium. In contrast, a region without porous region, referred to as the non-porous region, is referred to the Stokes equation. The hydrodynamic quantities in the context of the flow of a Newtonian fluid through a membrane composed of a swarm of biporous layered cylindrical particles are challenging to express analytically due to the nonlinear and coupled nature of the mathematical equations. This complexity arises from the interdependence between velocity and the changing permeability of the porous material. The traditional regular perturbation methods has been employed with the aim of uncovering solutions to the governing equations. This approach has been utilized to derive asymptotic expansions for the hydrodynamic quantities. This enables a thorough examination of the outcomes and their physical implications, including the impact of parameters such as those associated with the porous medium, heat transfer, and volume fraction on the entropy generation.

6.4.1 Model Validation and Limiting Cases

1. When the Forchheimer number tends toward zero, $(F\to 0)$, the Brinkman–Forchheimer model simplifies to the Brinkman model for flow through a porous medium.

2. When the permeability parameters approach zero, denoted as $\varepsilon_f\to 0, \varepsilon_b\to 0$, the current variable permeability model simplifies to the constant permeability model.

3. When both the radius of the solid cylindrical core and radius of the Forchheimer layer tend towards one or the permeability of the porous medium tend towards infinite, denoted as ($a \to 1, b \to 1$ and $k \to \infty$), the current model simplifies to solid cylinder-in-cell.

6.4.2 Parameter Selection

Measuring the movement of a flowing fluid presents a challenge, as it requires estimating the mass or volume of the substance as it moves through a pipe or conduit. Complications may arise due to the complex nature of fluid flow dynamics. Quantifying physical factors is generally difficult in the realm of flow measurements. The table below outlines the range of parameter values, which vary depending on the applications in different fields. All the vital parameters listed in this table have been comprehensively explained in their respective cited sources, giving the reader a better understanding of the underlying concepts.

Range of Parameters		
Parameters	Range	Sources
Brinkman number Br	0-10	[203]
Peclet number Pe	0.001-10	[206]
Steady pressure gradient p_s	1-10	[5], [167]
Permeability k	$(0, \infty)$	[2], [3]
Forchheimer number F	0-2	[7], [8]
Stress-jump parameter β	$(-1, 1)$	[3], [5]
Viscosity ratio parameter λ_1	1.0-1.6	[207], [167]
Particle volume fraction γ	0.1-1.0	[3], [96]
Nusselt number Nu	2-8	[7], [8]
Variable permeability parameters $\varepsilon_f, \varepsilon_b$	0.0-0.9	[24]
Porosity parameter ε	0.3-1.0	[3]
Dimensionless temperature constant T_0	1.0	[203]

Table 6.1: Domain of interest for the ongoing parameters with their references

6.4.3 Entropy Generation Number (S)

This subsection is focused on examining thermodynamic irreversibilities arising from fluid friction, heat conduction, fluid flow through porous mediums with changing permeabilities, and particle interactions within a swarm. Entropy production (or generation) quantifies the amount of entropy generated throughout the process involving heat transfer, serving as a metric for assessing process efficiency.

Figure 6.3 analyzes the relationship between the entropy generation number S and the Brinkman number Br. The graphical analysis reveals that entropy generation number decreases with radial distance for various Brinkman numbers. Elevated Brinkman numbers lead to heightened entropy generation, especially noticeable within porous regions in both formulations (small and large Darcy numbers). A higher Brinkman number Br indicates a reduced rate of heat conduction stemming from viscous dissipation, resulting in greater temperature elevation and hence the entropy generation. The entropy production is comparatively higher when the permeability of the porous medium is small, as it encounters greater resistance from the low permeability medium compared to situations with higher permeability. A higher decay rate is noted as radial distance increases in porous mediums with high permeability, particularly pronounced in Forchheimer region due to the inclusion of the fluid inertia term in the Forchheimer equation.

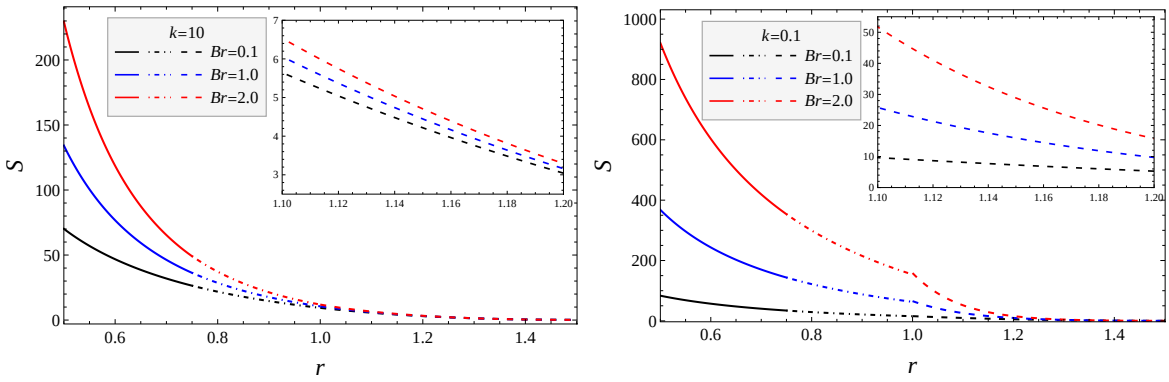

Figure 6.3: Dimensionless entropy S with radial distance r for various values of Brinkmann number Br $(Br = 0.1, 1.0, 2.0)$ under **(a)** large Darcy number $(k = 10, T_0 = 1, Pe = 50)$ and **(b)** small Darcy number $(k = 0.1, T_0 = 10, Pe = 500)$.$(\lambda_1 = 1, b = 0.7, \gamma = 0.444, F = 1, Nu = 4.0)$

The analysis considers the influence of the Peclet number (Pe) on entropy generation (S) across formulations for both small and large Darcy numbers (Fig. 6.4). It is deduced that the prevalence of convective heat transfer over diffusive heat transfer results in an decreased temperature and hence entropy generation. The influence of the Nusselt number Nu is more significant within the Stokes region across both formulations.

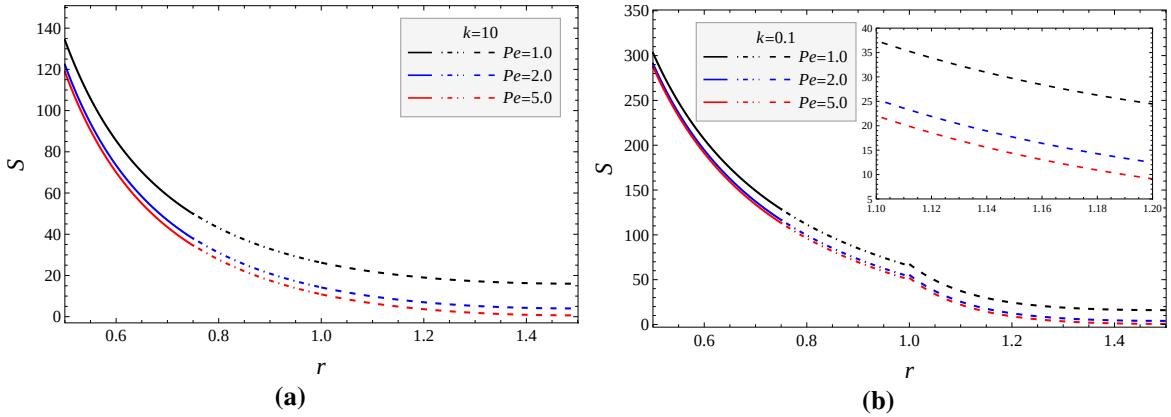

Figure 6.4: Dimensionless entropy S with radial distance r for various values of Peclet number Pe under **(a)** large Darcy number $(k = 10, T_0 = 1, Nu = 4, Br = 0.8)$ and **(b)** small Darcy number $(k = 0.1, T_0 = 10, Nu = 4, Br = 2.0)$.$(\lambda_1 = 1, b = 0.7, \gamma = 0.444, F = 1)$

Figures 6.5a and 6.5b illustrate the alterations in entropy generation across radial distance, corresponding to different permeabilities of porous media. It is apparent from these figures, representing high and low permeabilities respectively, that augmenting the permeability parameter in both the Brinkman and Forchheimer layers leads to increased obstructions in flow to porous media resulting in slight increase in the entropy generation. The impact of varying permeability parameters is more noticeable for low permeability compared to high permeability in the porous medium.

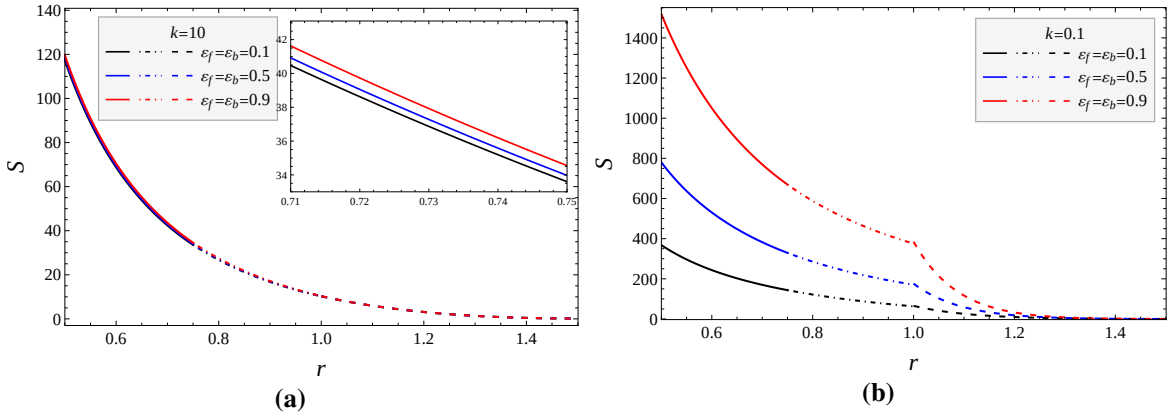

Figure 6.5: Dimensionless entropy S with radial distance r for various values of permeability parameters $\varepsilon_f, \varepsilon_b$ under **(a)** large Darcy number $(k = 10, T_0 = 1, Pe = 50, Br = 0.8)$ and **(b)** small Darcy number $(k = 0.1, T_0 = 10, Pe = 500, Br = 2.0)$.$(\lambda_1 = 1, b = 0.7, \gamma = 0.444, F = 1, Nu = 4.0)$

Figures 6.6a and 6.6b illustrate the radial variation of entropy generation for different thicknesses of the Forchheimer region near the solid cylinder core in both formulations. An increased occupancy of the Forchheimer region within the porous layer leads to a increased

temperature profile in the membrane and consequently enhances entropy generation. Moreover, higher permeability results in a slower decline in entropy generation with expanding Forchheimer region width.

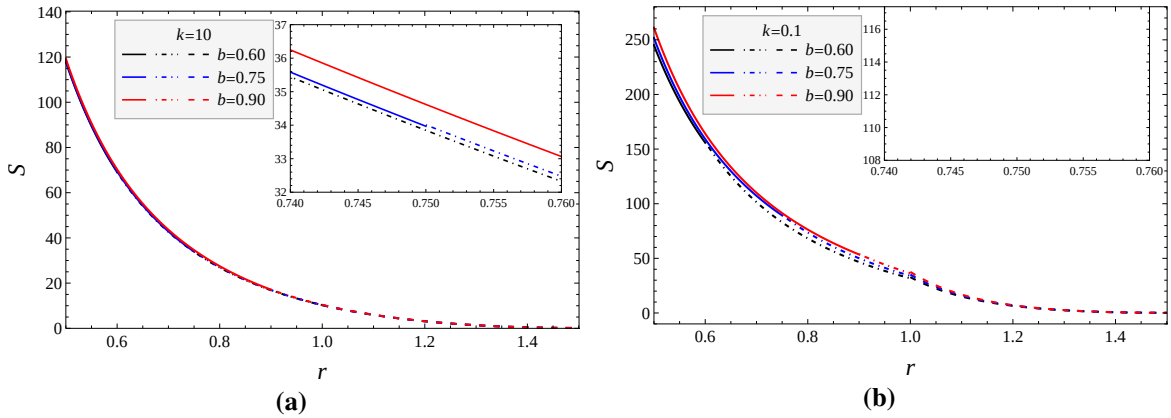

Figure 6.6: Dimensionless entropy S with radial distance r for different thickness of Forchheimer layer b under **(a)** large Darcy number $(k = 10, T_0 = 1, Br = 0.8)$ and **(b)** small Darcy number $(k = 0.1, T_0 = 10, Br = 2.0).(\lambda_1 = 1, b = 0.7, \gamma = 0.444, F = 1, Nu = 4.0, Pe = 50)$

An increase in the Forchheimer number leads to a increase in entropy generation across all areas of the biporous layered cylindrical particles, suggesting a temperature rise due to increased inertial resistance (Fig. 6.7).

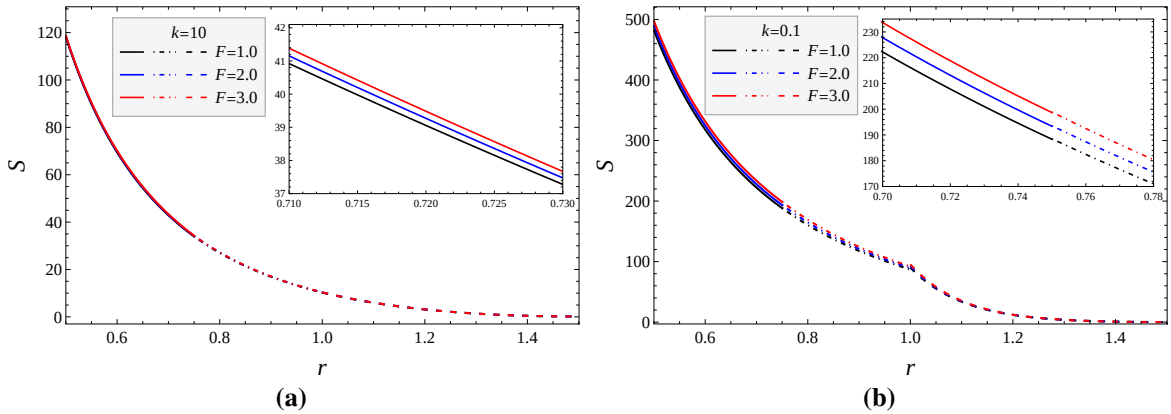

Figure 6.7: Dimensionless entropy, S with radial distance, r for various values of Forchheimer number F under **(a)** large Darcy number $(k = 10, T_0 = 1, Br = 0.8)$ and **(b)** small Darcy number $(k = 0.1, T_0 = 10, Br = 2.0).(\lambda_1 = 1, b = 0.7, \gamma = 0.444, F = 1, Nu = 4.0, Pe = 50, \varepsilon_f = \varepsilon_b = 0.5)$

The impact of the Forchheimer number is more noticeable in low-permeability scenarios compared to high-permeability conditions within the porous medium. Additionally, in low-permeability situations, a gradual increase in entropy generation with rising Forchheimer number is observed.

An increase in the viscosity ratio parameter leads to an enhanced entropy generation throughout all segments of the biporous layered cylindrical particles, as depicted in Figure 6.8. The influence of the viscosity ratio parameter is almost same for both large and small permeability cases. The rising entropy generation can be attributed to enhanced resistance due to increasing viscosity ratio parameter.

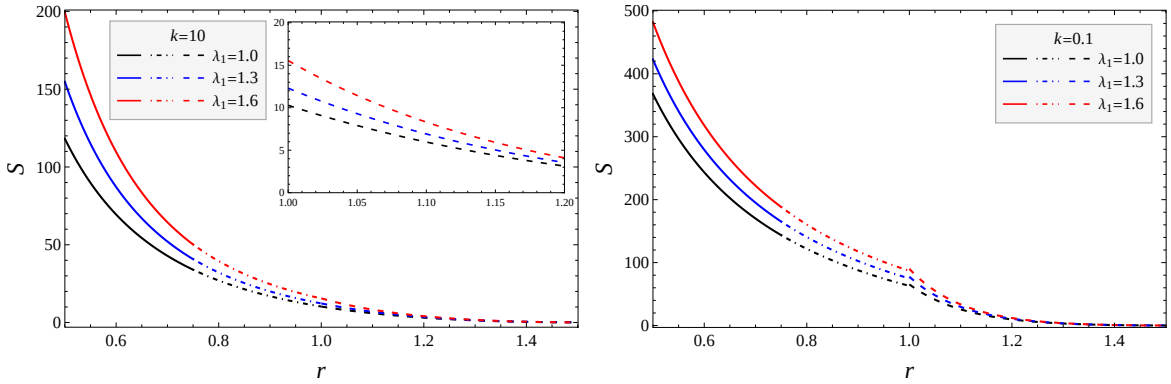

Figure 6.8: Dimensionless entropy, S with radial distance, r for various values of viscosity ratio parameter λ_1 under **(a)** large Darcy number $(k = 10, T_0 = 1, Br = 0.8)$ and **(b)** small Darcy number $(k = 0.1, T_0 = 10, Br = 2.0)$.$(b = 0.7, \gamma = 0.444, F = 1, Nu = 4.0, Pe = 50, \varepsilon_f = \varepsilon_b = 0.5)$

6.4.4 Bejan Number (B_e)

The second law of thermodynamics dictates that minimizing the total entropy generation in any thermofluidic system is crucial for achieving peak efficiency, enabling us to maximize the utilization of usable energy from the system. Following this, our focus shifts to gauging the proportion of entropy generation stemming from heat transport relative to the total entropy within micro confinements. Figure 6.9 illustrates the impact of the viscosity ratio parameter, λ_1 on the Bejan number. The viscosity ratio parameter determines the relative significance of porous medium viscosity compared to clear fluid viscosity. Increasing viscosity ratio parameter contribute towards higher fluid friction, hence leading towards a relatively higher irreversibilities due to viscous dissipation.

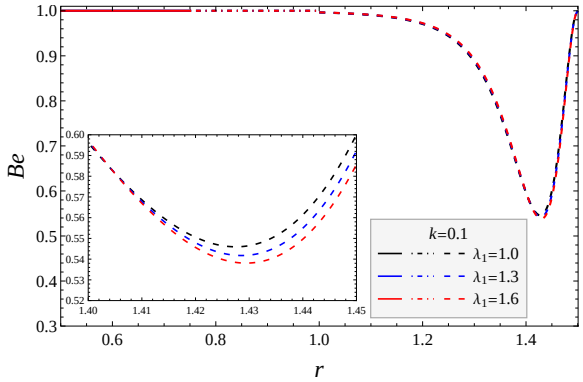

Figure 6.9: Bejan number, Be with radial distance, r for various values of viscosity ratio parameter λ_1 under small Darcy number $(k = 0.1, T_0 = 1, \varepsilon_f = \varepsilon_b = 0.1).(b = 0.7, \gamma = 0.444, F = 1, Nu = 4.0, Pe = 100)$

Figure 6.10 depicts the variation of the Bejan number with the Peclet number across various parameter configurations. The Peclet number signifies the ratio between advection and diffusion rates in a system driven by a temperature gradient. The impact of the Peclet number is notably more significant in clear fluid areas compared to porous regions. It can be understood that a rising Peclet number leads to a reduced thermal irreversiblities whereas the irreversiblities due to viscous dissipation is almost negligible near hypothetical cell owing to Happel boundary condition, which results in reduced Bejan number.

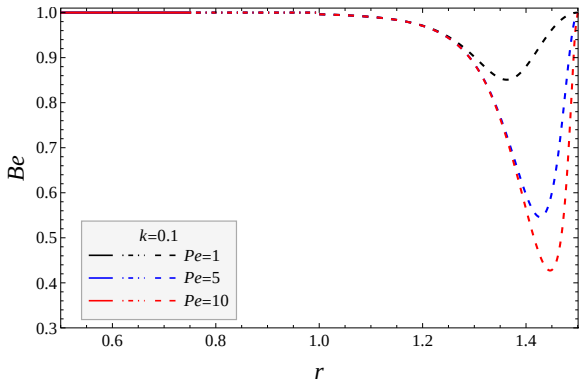

Figure 6.10: Bejan number, Be with radial distance, r for various values of Peclet number Pe under small Darcy number $(k = 0.1, T_0 = 1, Br = 2, \varepsilon_f = \varepsilon_b = 0.1).(b = 0.7, \gamma = 0.444, F = 1, Nu = 4.0)$

The parameter Br/T_0, which represents dissipation, is only present in the temperature equations. A slight increase in Br/T_0 leads to a notable decrease in the Bejan number. Figure 6.11 reveals that near hypothetical cell, the Bejan number reaches its minimum, indicating maximum available energy in the transverse direction. Throughout the porous region and at the hypothetical cell the Bejan number attains its peak value suggesting a dominant fluid friction in those region.

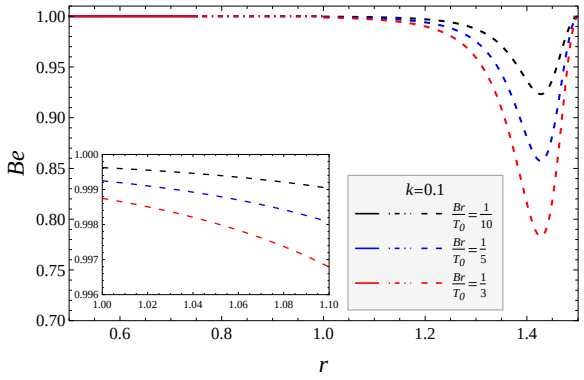

Figure 6.11: Bejan number, Be with radial distance, r for various values of viscous dissipation coefficient $\left(\frac{Br}{T_0}\right)$ under small Darcy number $(k = 0.1, \varepsilon_f = \varepsilon_b = 0.1).(b = 0.7, \gamma = 0.444, F = 1, Nu = 4.0, Pe = 100)$

A varying permeability also has its impact on relative irreversibility due to heat transfer as depicted in figure 6.12. It is evident that a decaying permeability leads to Bejan number attaining its minimum value closer to the hypothetical cell a further reduction in the minimum value. In other words a reduced permeability leads to a reduced irreversibility due to heat transfer near the hypothetical cell.

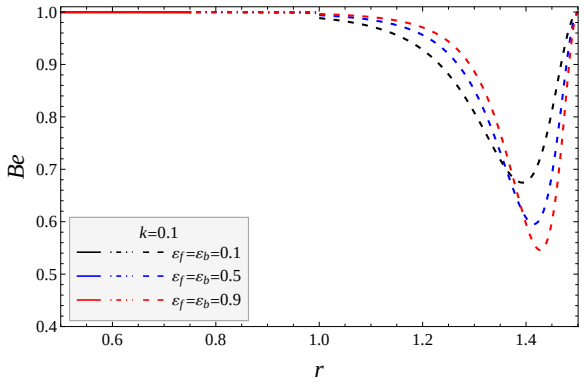

(a)

Figure 6.12: Bejan number, Be with radial distance, r for various values of variable permeability parameters $(\varepsilon_f, \varepsilon_b)$ under small Darcy number $(k = 0.1, T_0 = 1, Br = 2, \varepsilon_f = \varepsilon_b = 0.1).(b = 0.7, \gamma = 0.444, F = 1)$

6.4.5 Model Validation and Comparative Analysis

The graphical analysis described above illustrates the asymptotic behavior of entropy generation in a slow flow of a Newtonian fluid through a membrane composed of biporous layered cylindrical particles, utilizing a particle-in-cell approach. To verify the conclusions drawn from this analysis, it is essential to compare them with existing research in simplified scenarios and validate them through a combination of quantitative and qualitative graphical

analysis, alongside numerical solutions of the governing equations. The Figure (6.13) compares the second order asymptotic solution of the velocity with the numerical solution where both can be seen aligning well with each other, signifying the validation of the asymptotic results. The solution of current study is reduced to the model of flow past a solid cylindrical particles by taking the parameters $(k \to \infty, a = b = 1)$, and the obtained results of the hydrodynamic permeability is compared with the work of Deo *et al.* [3], which shows a perfect alignment of the curves corresponding to both the studies (Figure 6.14). The current model is also reduced to some special cases and represented the results in Figure (6.15), simultaneously. An increased velocity profile for constant permeability model signifies the extra resistance in the fluid flow of variable permeability model. Further increase in fluid velocity for Brinkman model signifies the contribution of extra inertial resistance due to Forchheimer term in the current model. Finally, the flow past a solid cylindrical particles without any coating of porous layer receive a slight enhancement in the fluid velocity of the membrane.

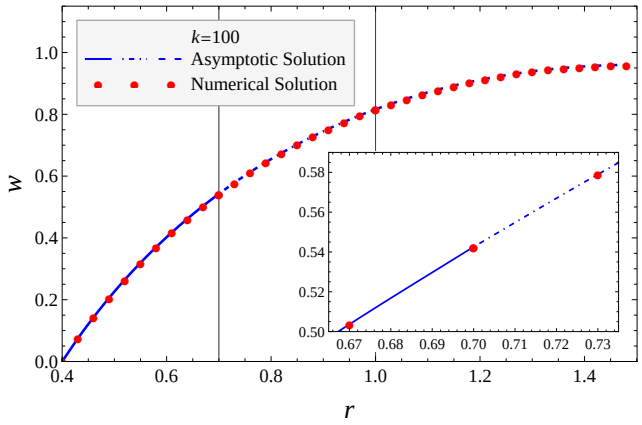

Figure 6.13: Comparision of velocity obtain via asymptotic solution and numerical solution of the problem for the large permeability case $(k = 100, \varepsilon_f = \varepsilon_b = 0.5, \gamma = 0.445, \lambda_1 = 1, F = 1)$.

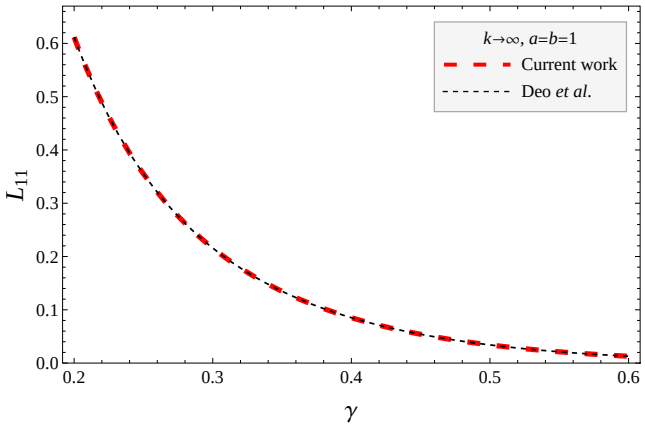

Figure 6.14: Validation of current study with the study of Deo *et al.* in terms of Hydrodynamic permeability, L_{11} for $k \to \infty, a = b = 1$.

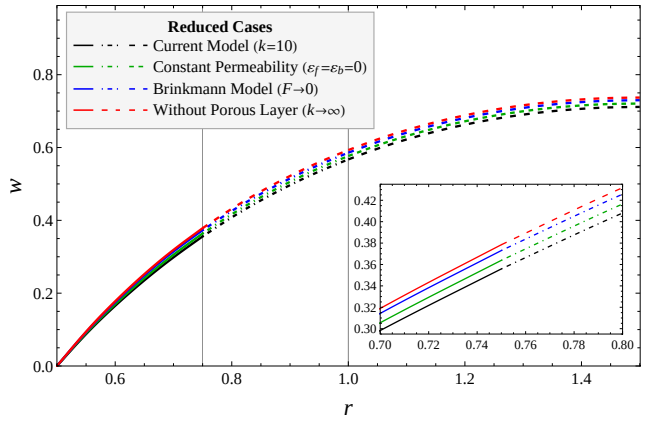

Figure 6.15: Different reduced cases of current work under large permeability parameter $(k = 100, \varepsilon_f = \varepsilon_b = 0.5, \gamma = 0.445, \lambda_1 = 1, F = 3)$.

6.5 Summary and Conclusions

This study undertakes a theoretical effort to examine entropy generation in the context of the slow flow of a Newtonian fluid through aggregated bi-porous layered cylindrical particles within a membrane. This analysis incorporates a variable permeability and heat transfer approach. The proposed work's demonstration is structured to control the Brinkman-Forchheimer region near the solid core of the cylindrical particle using the Brinkman-Forchheimer equation, taking into account the variable permeability of the porous medium. Meanwhile, an intermediate Brinkman porous region is govern by Brinkman equation with variable permeability, also considering the variable permeability of the porous medium. However, a peripheral non-porous layer is governed by the Stokes equation. The equations describing the flow of a Newtonian fluid through a membrane consisting of a collection of bi-porous layered cylindrical particles are complex and interdependent. This complexity

arises from the inclusion of changing permeability and a non-linear fluid inertia term in the governing equations for the porous region. To tackle these complexities, empirical methods involving both regular and singular perturbations are utilized to derive the asymptotic expansion of velocities in various porous regions (such as Brinkman-Forchheimer and Brinkman porous) under conditions of both high and low permeability. To assess the validity of the asymptotic solutions for the governing equations, the NDSolve command of Mathematica software has been employed to graphically analyzed the hydrodynamic variables across a range of control parameters, including parameters related to porous media, heat transfer, and the Forchheimer number. The subsequent noteworthy results of the current study are detailed below:

1. The augmentation in varying permeability parameters of the Brinkman and Forchheimer layers leads to an enhancement in entropy generation owing to reduced fluid velocity.

2. The wider Forchheimer region produces an enhanced inertial resistance to the fluid flow, resulting in a reduced velocity and enhanced temperature profile, which further reduces entropy generation in the membrane.

3. Highlighting the significance of increasing inertial resistance on the hydrodynamic and thermal characteristics in membrane flow, influenced by the Forchheimer number, a subtle reduction in flow velocity and hence an enhancement in temperature distribution and entropy generation becomes apparent across various permeability levels.

4. The increased values of Brinkman number significantly enhances the temperature and entropy of the membrane. The Bejan number shows a decreasing trend for larger Brinkmann number.

The results of the current asymptotic analysis have been confirmed through numerical simulations using the NDSolve command in Mathematica, demonstrating a strong concurrence between our asymptotic analysis and the numerical solutions. To the best of our knowledge, above outcomes are first attempt in flows through swarm of particles and hence can be useful to understand the variations in irreversibility due to variations of different parameters in processes such as filtration processes in wastewater treatment, petroleum reservoir rocks, and the flow of blood within smooth muscle cells.

Chapter 7

Effect of Surface Roughness on Flow Past a Membrane composed of Porous Cylindrical Particles: A Particle-in-Cell Approach

7.1 Introduction

Fluid dynamics within different shaped objects featuring corrugated or irregular boundaries have garnered significant interest among researchers due to their diverse field of applications. Corrugated walls have a rich history of application in improving heat and mass transfer within the fluid flow [208], hence the exploration of fluid flow through objects with irregular surfaces holds immense relevance in fields such as distillation columns and separation processes [209], [210], biological transport phenomena, chemical separation [211], [212], and the determination of pressure drop in micro-channels featuring rough surfaces [213], [214]. Boundary effects in microchannel systems hold a significant importance due to their large surface-to-volume ratio. Therefore, a rough surface of a mirco object has a significant impact on the fluid flow compared to the system's length scale. Hence, the boundary roughness becomes more noticeable in these systems. Consequently, the mathematical treatment of these boundaries is important in the fluid flow problem involving rough surfaces. Many authors attempted to address this problem by considering the roughness as a corrugation of different periodic functions. Phan-Thien [215] initiated the mathematical treatment of flow through objects with corrugated or irregular shaped boundary by studying the flow of Newtonian fluid through a circular cylindrical pipe featuring a sinusoidal corrugated boundary. Apart from this, he [216] also carried out an analytical treatment of the flow problem involving Stokes' flow around a rotating corrugated rod and Stokes' flow within the space between two corrugated cylinders with distinct cross-sectional geometries. Wang [217], [218] studied the stokes flow between two fixed corrugated plates and analyzed the effect of phase difference of the corrugations on the flow rate. He noted that even when

phase difference does not affect the wetted perimeter nor the cross-sectional area, still this has a significant impact on flow depending upon the flow directions. Zhou et al. [219] conducted a study on the the flow of a viscous fluid in a two-dimensional corrugated channel using the perturbation and finite volume approach and compared the result to validate the asymptotic solutions. Additionally they found an explicit relation exists between the critical Reynolds number, at which the wall flow separates, and the dimensionless corrugation height and wavelength of the corrugations. Sherief *et al.* [220] explored the effect of sinusoidal corrugations on the creeping flow of micropolar fluid flowing between two corrugated plates using the perturbation method up to the second order. Ashmawy [21] investigated the effect of both longitudinal and transverse corrugations in the tube flow of a couple stress fluid. He used the sinusoidal corrugations on the surface and utilize the perturbation technique to solve and explore the effect of corrugation control parameter on the flow rate and mean velocity. Many researchers explored the effect of surface roughness in the flow past a porous vessel. Ng and Wang [221] considered a sinusoidal corrugated channel filled with a sparse porous medium and carried out a perturbation analysis of the Newtonian fluid flowing in either parallel or normal to the corrugations. Faltas *et al.* [88] studied the partial slip effect of fluid in the corrugated microannuli cylindrical tubes, where the tube was filled with a porous medium and Brinkman equation regulated the flow. They also emphasize the effect of phase difference in inner and outer wall of the corrugated annular tube.

A prevalent focus in these studies was the examination of geometric influences stemming from wall corrugations on flow resistance or pressure drop within the vessel. This serves as inspiration for our investigation into the influence of surface roughness on flow dynamics within a membrane. The flow past a membrane is a topic which is studied by many researchers from a long time using different models and solving techniques. But as per the authors knowledge, the exploration of the effect of rough surfaces in flow past a membrane is still not studied by anyone. The present study is focused on the influence of surface roughness on the flow past a membrane composed of corrugated porous layered cylindrical particles.

7.2 Problem Formulation

7.2.1 Statement of the Problem and Model Description

The aim of this study is to investigate the steady flow of a Newtonian fluid over a membrane constructed from a concentration suspension of porous layered cylindrical particles featuring sinusoidal grooves which are taken along the transverse direction of the cross-section of the tube as shown in Figure 7.1. The solid particles are coated with a porous layer that replicates the sinusoidal grooves of the solid cylindrical particles, aligning without phase shifting. The sinusoidally corrugated surface of solid cylinder is given by

$$\widetilde{r} = \widetilde{a} + \widetilde{d}\sin(\lambda\phi), \tag{7.1}$$

where $\widetilde{a}$ is the radius of perfectly circular solid cylinder in absence of any corrugations, $\widetilde{d}$ is the height is a corrugation, λ is the wave number that is related with the wave length L by the expression $\lambda = \frac{2\pi}{L}$. The unit cell model technique is utilized to solve the flow around an array of particles. This approach divides the flow domain into two distinct regions. The first region represents the porous layer with a thickness of $(\widetilde{b}-\widetilde{a})$, where $\widetilde{b}$ denotes the outer radius of the porous layer. Fluid flow within this region is regulated by the Brinkmann equation coupled with the continuity equation. The second region encompasses the clear fluid region confined within a hypothetical cell of radius $\widetilde{c}$, enveloping the porous region and intended to take the effect of surrounding particles on the concerned particle. The radius of this hypothetical cell varies based on the concentration or compactness of the particle swarm. In our investigation, we set the thickness of the clear fluid region as $(\widetilde{c}-\widetilde{b})$. Fluid flow within this region is governed by Stokes' law. The z-axis is aligned with the center line of a solid cylinder. The flow is presumed to be fully developed and one dimensional, with velocity components of the fluid being $(0,0,\widetilde{w})$.

The thickness of the concentric cylindrical envelope (hypothetical cell) of the porous cylindrical particle is chosen in such a way that the particle volume fraction of the swarm of porous cylindrical particles is the same as the particle volume fraction of the cell.

$$\gamma = \frac{\int_0^{2\pi}\left(\widetilde{r}+\widetilde{d}\sin(\lambda\phi)\right)\cos(\phi)\frac{\partial}{\partial\phi}\left((\widetilde{r}+\widetilde{d}\sin(\lambda\phi))\sin(\phi)\right)\Big|_{\widetilde{r}=\widetilde{b}}}{\int_0^{2\pi}\left(\widetilde{r}+\widetilde{d}\sin(\lambda\phi)\right)\cos(\phi)\frac{\partial}{\partial\phi}\left((\widetilde{r}+\widetilde{d}\sin(\lambda\phi))\sin(\phi)\right)\Big|_{\widetilde{r}=\widetilde{c}}}. \tag{7.2}$$

The above expression can be used to derive a relation between radius of the hypothetical cell and particle volume fraction of the swarm. The relation is given as,

$$\widetilde{c} = \frac{\sqrt{2G} - 4\delta \sin^2(\pi\lambda)}{4\pi\lambda}, \tag{7.3}$$

where,

$$G = \frac{1}{\gamma}\left(4\pi^2\lambda^2\left(2\widetilde{b}^2 - (\gamma-1)\widetilde{d}^2\right) + \widetilde{d}(-4\cos(2\pi\lambda)(2\pi\widetilde{b}\lambda + \gamma\widetilde{d}) + \pi(\gamma-1)\widetilde{d}\lambda\sin(4\pi\lambda) + \gamma\widetilde{d}\cos(4\pi\lambda)) + 8\pi\widetilde{b}\widetilde{d}\lambda + 3\gamma\widetilde{d}^2\right). \tag{7.4}$$

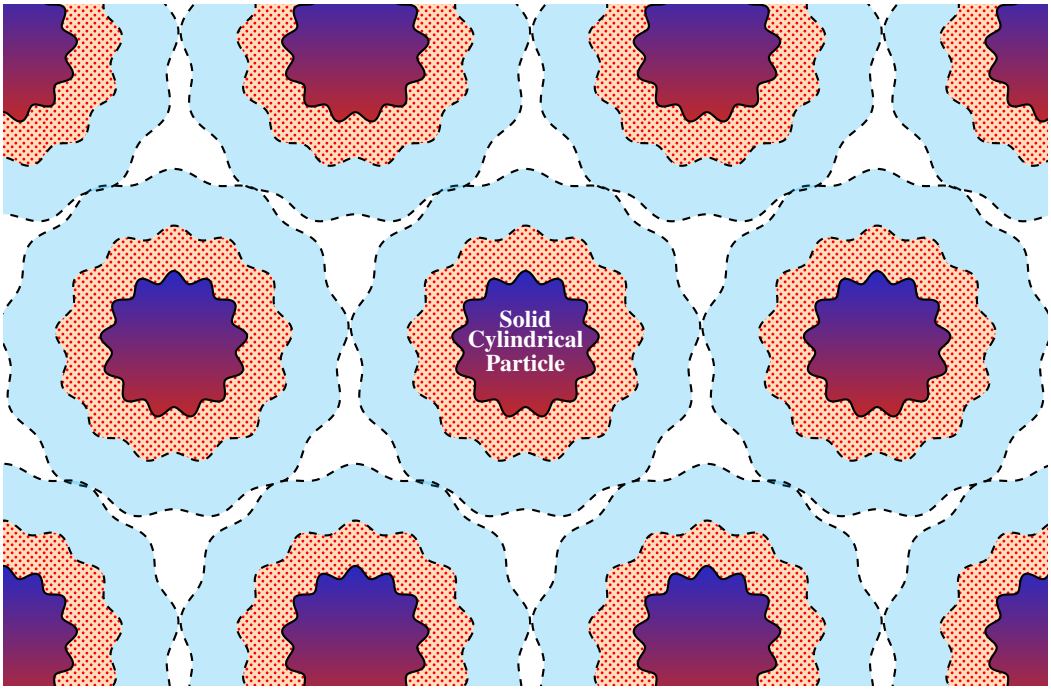

Figure 7.1: The cross-section of an array of uniformly distributed corrugated porous layered cylindrical particles

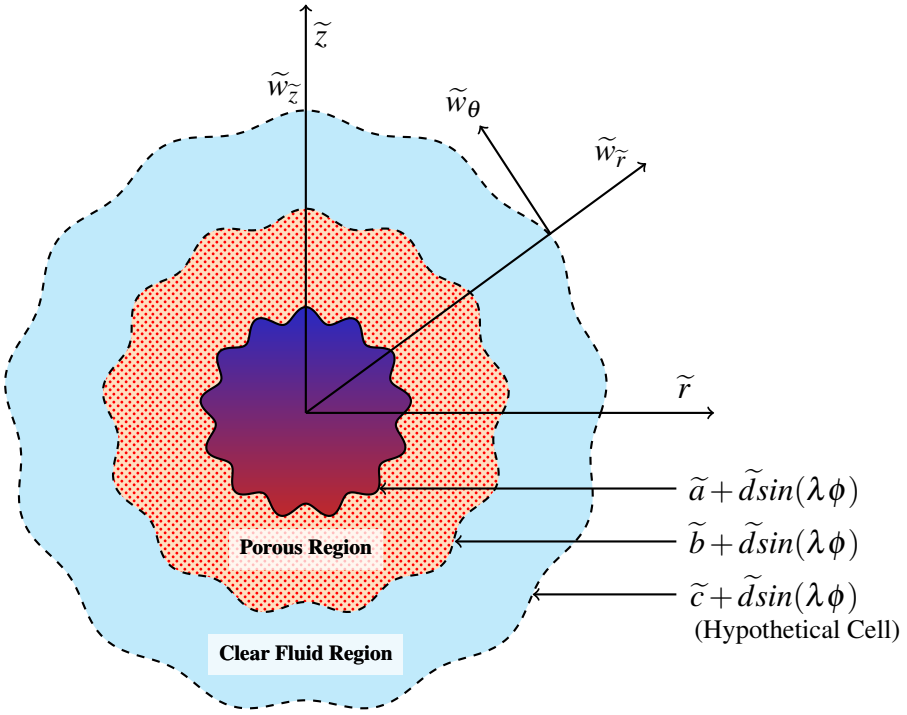

Figure 7.2: The circular cross-section of an corrugated cylindrical particle with the hypothetical cell

7.2.1.1 Hydrodynamic Equations

The hydrodynamic governing equations of a steady, fully developed and unidirectional flow caused by the pressure gradient are given by
Region- I, *i.e.*, $\widetilde{a}+\widetilde{d}\sin(\lambda\phi) \leq \widetilde{r} \leq \widetilde{b}+\widetilde{d}\sin(\lambda\phi)$

$$\frac{\widetilde{\mu}_e}{\widetilde{r}}\frac{\partial}{\partial\widetilde{r}}\left(\widetilde{r}\frac{\partial\widetilde{w}_p}{\partial\widetilde{r}}\right)+\frac{\widetilde{\mu}_e}{\widetilde{r}^2}\frac{\partial^2\widetilde{w}_p}{\partial\phi^2}-\frac{\widetilde{\mu}}{\widetilde{k}}\widetilde{w}_p=\frac{\partial\widetilde{p}}{\partial\widetilde{z}}, \tag{7.5}$$

Region- II, *i.e.*, $\widetilde{b}+\widetilde{d}\sin(\lambda\phi) \leq \widetilde{r} \leq \widetilde{c}+\widetilde{d}\sin(\lambda\phi)$

$$\frac{\widetilde{\mu}}{\widetilde{r}}\frac{\partial}{\partial\widetilde{r}}\left(\widetilde{r}\frac{\partial\widetilde{w}_c}{\partial\widetilde{r}}\right)+\frac{\widetilde{\mu}}{\widetilde{r}^2}\frac{\partial^2\widetilde{w}_c}{\partial\phi^2}=\frac{\partial\widetilde{p}}{\partial\widetilde{z}}, \tag{7.6}$$

where $\widetilde{w}_c$ is the axial velocity for the clear fluid.

7.2.2 Non-Dimensional Parameters and Governing Equations

To solve the above system of equations (7.5,7.6), the following non-dimensional variables are introduced:

$$p=\frac{\widetilde{p}}{\widetilde{p_0}},\ r=\frac{\widetilde{r}}{\widetilde{b}},\ z=\frac{\widetilde{z}}{\widetilde{b}},\ \delta=\frac{\widetilde{d}}{\widetilde{b}},\ S^2=\frac{1}{k},\ \widetilde{w}_0=\frac{\widetilde{p_0}\widetilde{b}^2}{\widetilde{\mu}},\ w_p=\frac{\widetilde{w}_p}{\widetilde{w}_0},$$
$$w_c=\frac{\widetilde{w}_c}{\widetilde{w}_0},\ k=\frac{\widetilde{k}}{\widetilde{a}^2},\widetilde{p}_0=\frac{\widetilde{w}_0\widetilde{\mu}}{\widetilde{b}},\mu_R^2=\frac{\widetilde{\mu}_e}{\widetilde{\mu}} \tag{7.7}$$

where $(\widetilde{\ })$ denotes the quantities with dimensions, w_0 is the average velocity, $\widetilde{p}_0$ is the characteristic pressure, δ is the dimensionless height of a sinusoidal groove, S is a dimensionless parameter, μ_R is the visocity ratio parameter.

7.2.2.1 Hydrodynamic Equations

The non-dimensional variables in equation (7.7) is used to reduce the hydrodynamic equations (7.5),(7.6), in the on-dimensional forms of the same are given as
Region- I, *i.e.*, $a+\delta\sin(\lambda\phi)\le r\le 1+\delta\sin(\lambda\phi)$

$$\frac{\mu_R^2}{r}\frac{\partial}{\partial r}\left(r\frac{\partial w_p}{\partial r}\right)+\frac{\mu_R^2}{r^2}\frac{\partial^2 w_p}{\partial\phi^2}-\frac{w_p}{k}=\frac{\partial p}{\partial z}. \tag{7.8}$$

Region- II, *i.e.*, $1+\delta\sin(\lambda\phi)\le r\le c+\delta\sin(\lambda\phi)$

$$\frac{1}{r}\frac{\partial}{\partial r}\left(r\frac{\partial w_c}{\partial r}\right)+\frac{1}{r^2}\frac{\partial^2 w_c}{\partial\phi^2}=\frac{\partial p}{\partial z}. \tag{7.9}$$

7.2.3 Boundary Conditions

The dimensionless boundary conditions are given as follows:

1. The no slip boundary condition is considered at the corrugated surface of the solid core of the cylinder *i.e.*,

$$w_p=0,\quad \text{at}\quad r=a+\delta\sin(\lambda\phi). \tag{7.10a}$$

2. Continuity of velocity is considered at the fluid-porous interface, *i.e.*,

$$w_p=w_c,\quad \text{at}\quad r=1+\delta\sin(\lambda\phi). \tag{7.10b}$$

3. The stress-jump condition along tangential stresses is also considered at the fluid-porous interface, *i.e.*,

$$\mu_R^2 \frac{dw_p}{dr} - \frac{dw_c}{dr} = \frac{\beta}{\sqrt{k}} w_p, \quad \text{at} \quad r = 1 + \delta \sin(\lambda \phi), \tag{7.10c}$$

where β is the stress-jump parameter.

4. The Happel, Kuwabara, Kvashnin and Cunningham boundary conditions leads to the following single result, *i.e.*,

$$\frac{dw_c}{dr} = 0, \quad \text{at} \quad r = c + \delta \sin(\lambda \phi). \tag{7.10d}$$

7.2.4 Hydrodynamical Quantities and Kozeny Constant

The volumetric flow rate Q_v of fluid flow in non-dimensional form is given by

$$\begin{aligned} Q_v &= 2\pi\lambda \int_0^{\frac{2\pi}{\lambda}} \int_{a+\delta\sin(\lambda\phi)}^{c+\delta\sin(\lambda\phi)} r w(r,\phi) dr d\phi, \\ &= 2\pi\lambda \left(\int_0^{\frac{2\pi}{\lambda}} \int_{a+\delta\sin(\lambda\phi)}^{1+\delta\sin(\lambda\phi)} r w_p(r,\phi) dr d\phi + \int_0^{\frac{2\pi}{\lambda}} \int_{1+\delta\sin(\lambda\phi)}^{c+\delta\sin(\lambda\phi)} r w_c(r,\phi) dr d\phi \right). \end{aligned} \tag{7.11}$$

An identical particle from the swarm has been taken into the consideration to analyze the impact of properties of the porous and non-porous material on the membrane permeability. The mathematical expression of the membrane permeability L_{11} is given by [145],

$$L_{11} = -\frac{V_f}{\partial p / \partial z}, \tag{7.12}$$

where V_f denotes the filtration velocity and is reffered by

$$V_f = \frac{Q_v}{\int_0^{2\pi} \left(\widetilde{r} + \widetilde{d}\sin(\lambda\phi)\right) \cos(\phi) \frac{\partial}{\partial\phi} \left((\widetilde{r} + \widetilde{d}\sin(\lambda\phi)) \sin(\phi) \right) \Big|_{\widetilde{r}=\widetilde{c}} d\phi} \tag{7.13}$$

The classical Kozeny–Karman equation that predicts the permeability of a swarm of porous cylinder particles is given as

$$L_{11} = \frac{\varepsilon \rho_h^2}{K_z \widetilde{b}^2}, \tag{7.14}$$

where ε is the porosity, K_z is the dimensionless of Kozeny constant, and ρ_h describes the hydraulic radius which is a fractional value of the pore volume and the wetting area.
The Kozeny constant can be written as

$$K_z = \frac{\varepsilon \rho_h^2}{L_{11}\widetilde{b^2}}, \tag{7.15}$$

where hydraulic radius for the porous medium composed of porous cylinders is expressed as

$$\rho_h = \frac{A_{\widetilde{c}} - A_{\widetilde{b}}}{P_{\widetilde{b}}} \tag{7.16}$$

$$= \frac{\varepsilon\left(4\pi\lambda\left(2\widetilde{b}^2+\widetilde{d}^2\right)-2\widetilde{d}\cos(2\pi\lambda)(4\widetilde{b}+\widetilde{d}\sin(2\pi\lambda))+8\widetilde{b}\widetilde{d}\right)}{16(1-\varepsilon)\left(\pi\widetilde{b}\lambda+\widetilde{d}\sin^2(\pi\lambda)\right)}. \tag{7.17}$$

Introducing the expression of hydraulic radius into the expression of the Kozeny constant, the Kozeny constant is obtained as

$$K_z = \frac{\varepsilon^3\left(4\pi\left(\delta^2+2\right)\lambda-2\delta\cos(2\pi\lambda)(\delta\sin(2\pi\lambda)+4)+8\delta\right)^2}{256L_{11}(\varepsilon-1)^2\left(\delta\sin^2(\pi\lambda)+\pi\lambda\right)^2}, \tag{7.18}$$

where L_{11} is the hydrodynamic permeability of the membrane.

7.3 Asymptotic Solution of the Problem

The present study addresses the challenge of modeling the fluid flow of a Newtonian fluid past along a uniform array of corrugated cylindrical particles using the cell model approach. Specifically, we employ a system of Brinkman and Stokes equations to describe the steady, unidirectional, fully developed flow within porous and non-porous regions, respectively. Exact analytical solutions to this system of PDEs, particularly in the cylindrical coordinate system with the consideration of the corrugated surface boundary conditions, are mathematically difficult to derive. To address this challenge, we employ the regular perturbation method. This technique requires the assumption of small corrugation height ($\delta \ll 1$) as a perturbation parameter. By expanding the velocity functions in Taylor series expansions along the corrugated boundaries and subsequently employing perturbation series expansions, we systematically derive an asymptotic solution to the problem. A constant pressure gradient continuously propels the fluid in the porous and clear fluid regions, *i.e.*, $\frac{\partial p}{\partial z} = -p_s = \text{constant}$.

The governing equations for both porous and non-porous fluid regions, where the parameter $S = \frac{1}{\sqrt{k}}$, are
Region- I, *i.e.*, $a + \delta \sin(\lambda\phi) \leq r \leq 1 + \delta \sin(\lambda\phi)$

$$\frac{\mu_R^2}{r}\frac{\partial}{\partial r}\left(r\frac{\partial w_p}{\partial r}\right) + \frac{\mu_R^2}{r^2}\frac{\partial^2 w_p}{\partial \phi^2} - S^2 w_p = \frac{\partial p}{\partial z}. \tag{7.19}$$

Region- II, *i.e.*, $1 + \delta \sin(\lambda\phi) \leq r \leq c + \delta \sin(\lambda\phi)$

$$\frac{1}{r}\frac{\partial}{\partial r}\left(r\frac{\partial w_c}{\partial r}\right) + \frac{1}{r^2}\frac{\partial^2 w_c}{\partial \phi^2} = \frac{\partial p}{\partial z}. \tag{7.20}$$

By considering the non-dimensional corrugation height δ as perturbation parameter, the perturbation series expansions of velocity functions are given as

$$w_j(r) = w_j(r;\delta) = \sum_{n=0}^{m} \delta^n w_{jn}(r), \quad j = p, c, \tag{7.21}$$

where the subscripts p and c corresponds to the porous and clear fluid regions respectively. The boundary conditions (7.10*a*-7.10*d*) are expanded using the Taylor series expansion, and using the perturbation series expansion,

1. The no slip condition

$$\begin{aligned} &w_{p0}\big|_{r=a} + \delta\left\{ w_{p1}\big|_{r=a} + \sin(\lambda\phi)\left.\frac{\partial w_{p0}}{\partial r}\right|_{r=a}\right\} \\ &+ \delta^2\left\{ w_{p2}\big|_{r=a} + \sin(\lambda\phi)\left.\frac{\partial w_{p1}}{\partial r}\right|_{r=a} + \frac{\sin^2(\lambda\phi)}{2!}\left.\frac{\partial^2 w_{p0}}{\partial r^2}\right|_{r=a}\right\} + O(\delta^3) = 0. \end{aligned} \tag{7.22}$$

2. The continuity of velocity

$$\begin{aligned} &w_{p0}\big|_{r=1} + \delta\left\{ w_{p1}\big|_{r=1} + \sin(\lambda\phi)\left.\frac{\partial w_{p0}}{\partial r}\right|_{r=1}\right\} + \delta^2\left\{ w_{p2}\big|_{r=b} + \sin(\lambda\phi)\left.\frac{\partial w_{p1}}{\partial r}\right|_{r=1}\right. \\ &\left. + \frac{\sin^2(\lambda\phi)}{2!}\left.\frac{\partial^2 w_{p0}}{\partial r^2}\right|_{r=1}\right\} + O(\delta^3) = w_{c0}|_{r=1} + \delta\left\{ w_{c1}\big|_{r=1} + \sin(\lambda\phi)\left.\frac{\partial w_{c0}}{\partial r}\right|_{r=1}\right\} \\ &+ \delta^2\left\{ w_{c2}|_{r=1} + \sin(\lambda\phi)\left.\frac{\partial w_{c1}}{\partial r}\right|_{r=1} + \frac{\sin^2(\lambda\phi)}{2!}\left.\frac{\partial^2 w_{c0}}{\partial r^2}\right|_{r=1}\right\} + O(\delta^3). \end{aligned} \tag{7.23}$$

3. The stress jump condition

$$\left.\frac{\partial w_{p0}}{\partial r}\right|_{r=1} + \delta\left\{\left.\frac{\partial w_{p1}}{\partial r}\right|_{r=1} + \sin(\lambda\phi)\left.\frac{\partial^2 w_{p0}}{\partial r^2}\right|_{r=1}\right\} + \delta^2\left\{\left.\frac{\partial w_{p2}}{\partial r}\right|_{r=1} + \sin(\lambda\phi)\left.\frac{\partial^2 w_{p1}}{\partial r^2}\right|_{r=1}\right.$$

$$+\frac{\sin^2(\lambda\phi)}{2!}\left.\frac{\partial^3 w_{p0}}{\partial r^3}\right|_{r=1}\Bigg\}+O(\delta^3)=\left.\frac{\partial w_{c0}}{\partial r}\right|_{r=1}+\delta\left\{\left.\frac{\partial w_{c1}}{\partial r}\right|_{r=1}+\sin(\lambda\phi)\left.\frac{\partial^2 w_{c0}}{\partial r^2}\right|_{r=1}\right\}$$
$$+\delta^2\left\{\left.\frac{\partial w_{c2}}{\partial r}\right|_{r=1}+\sin(\lambda\phi)\left.\frac{\partial^2 w_{c1}}{\partial r^2}\right|_{r=1}+\frac{\sin^2(\lambda\phi)}{2!}\left.\frac{\partial^3 w_{c0}}{\partial r^3}\right|_{r=1}\right\}+O(\delta^3)+\frac{\beta}{\sqrt{k}}\left\{w_{p0}\big|_{r=1}\right.$$
$$+\delta\left\{w_{p1}\big|_{r=1}+\sin(\lambda\phi)\left.\frac{\partial w_{p0}}{\partial r}\right|_{r=1}\right\}+\delta^2\left\{w_{p2}\big|_{r=1}+\sin(\lambda\phi)\left.\frac{\partial w_{p1}}{\partial r}\right|_{r=1}+\frac{\sin^2(\lambda\phi)}{2!}\times\right.$$
$$\left.\left.\left.\frac{\partial^2 w_{p0}}{\partial r^2}\right|_{r=1}\right\}\right\}. \tag{7.24}$$

4. The condition of hypothetical cell

$$\left.\frac{\partial w_{c0}}{\partial r}\right|_{r=c}+\delta\left\{\left.\frac{\partial w_{c1}}{\partial r}\right|_{r=c}+\sin(\lambda\phi)\left.\frac{\partial^2 w_{c0}}{\partial r^2}\right|_{r=c}\right\}$$
$$+\delta^2\left\{\left.\frac{\partial w_{c2}}{\partial r}\right|_{r=c}+\sin(\lambda\phi)\left.\frac{\partial^2 w_{c1}}{\partial r^2}\right|_{r=c}+\frac{\sin^2(\lambda\phi)}{2!}\left.\frac{\partial^3 w_{c0}}{\partial r^3}\right|_{r=c}\right\}=0. \tag{7.25}$$

The zeroth order solution, $\mathscr{O}(\delta^0)$

The series expansion (7.21) is introduced in equations (7.19) and (7.20), and equating the like powers of the parameter δ, the zeroth order equations are given as

$$\frac{\mu_R^2}{r}\frac{\partial}{\partial r}\left(r\frac{\partial w_{p0}}{\partial r}\right)-S^2 w_{p0}=\frac{\partial p}{\partial z}, \tag{7.26}$$
$$\frac{1}{r}\frac{\partial}{\partial r}\left(r\frac{\partial w_{c0}}{\partial r}\right)=\frac{\partial p}{\partial z}. \tag{7.27}$$

The corresponding zeroth order boundary condition are

$$\begin{aligned} w_{p0}\big|_{r=a}&=0,\\ w_{p0}\big|_{r=1}&=w_{c0}|_{r=1},\\ \mu_R^2\left.\frac{\partial w_{p0}}{\partial r}\right|_{r=1}&=\left.\frac{\partial w_{c0}}{\partial r}\right|_{r=1}+\beta S\, w_{p0}\big|_{r=1},\\ \left.\frac{\partial w_{c0}}{\partial r}\right|_{r=c}&=0. \end{aligned} \tag{7.28}$$

The general solution of Equations (7.26) and (7.27) are

$$w_{p0}(r)=c_1 I_0(rS)+c_2 K_0(rS)+\frac{p_z}{S^2} \tag{7.29}$$
$$w_{c0}(r)=c_4\log(r)+c_3-\frac{p_z r^2}{4}, \tag{7.30}$$

where,

$$c_1 = \frac{\left(c^2-1\right) S p_z K_0(aS) - 2\mathrm{pz}(-\beta K_0(aS) + \beta K_0(S) + K_1(S))}{2S^2(K_0(aS)(I_1(S) - \beta I_0(S)) + I_0(aS)(\beta K_0(S) + K_1(S)))}, \tag{7.31}$$

$$c_2 = -\frac{I_0(aS)\left(\left(c^2-1\right) S p_z + 2\beta \mathrm{pz}\right) - 2\beta \mathrm{pz} I_0(S) + 2\mathrm{pz} I_1(S)}{2S^2(K_0(aS)(I_1(S) - \beta I_0(S)) + I_0(aS)(\beta K_0(S) + K_1(S)))}, \tag{7.32}$$

$$\begin{aligned} c_3 = &-\frac{1}{4S^3(K_0(aS)(I_1(S) - \beta I_0(S)) + I_0(aS)(\beta K_0(S) + K_1(S)))}\left(-\left(S^2 p_z\left(K_0(aS)\left(I_0(S)\right.\right.\right.\right. \times \\ &\left.\left.\left.\left.\left(2c^2 - \beta S - 2\right) + S I_1(S)\right) + I_0(aS)\left(K_0(S)\left(-2c^2 + \beta S + 2\right) + S K_1(S)\right)\right)\right) \\ &-4p_z(S I_1(S) K_0(aS) + S K_1(S) I_0(aS) - 1)) \end{aligned}$$

$$c_4 = \frac{c^2 p_z}{2} \tag{7.33}$$

The first order solution, $\mathscr{O}(\delta^1)$

By equating the first powers of the parameter δ, the governing equations for first order velocity is reduced in the form

$$\frac{1}{r}\frac{\partial}{\partial r}\left(r\frac{\partial w_{p1}}{\partial r}\right) + \frac{1}{r^2}\frac{\partial^2 w_{p1}}{\partial \phi^2} - S_1^2 w_{p1} = 0, \tag{7.34}$$

$$\frac{1}{r}\frac{\partial}{\partial r}\left(r\frac{\partial w_{c1}}{\partial r}\right) + \frac{1}{r^2}\frac{\partial^2 w_{c1}}{\partial \phi^2} = 0, \tag{7.35}$$

where the parameter, $S_1 = \frac{S}{\mu_R}$.

In the view of first order boundary conditions we can assume solution of first order governing equations in porous and clear fluid regions in the form, $w_{p1}(r,\phi) = f_1(r)\sin(\lambda\phi)$ and $w_{c1}(r,\phi) = g_1(r)\sin(\lambda\phi)$, respectively. The reduced equations independent from coordinate ϕ are

$$\frac{1}{r}\frac{\partial}{\partial r}\left(r\frac{\partial f_1}{\partial r}\right) - \left(\frac{\lambda^2}{r^2} + S_1^2\right) f_1 = 0 \tag{7.36}$$

$$\frac{1}{r}\frac{\partial}{\partial r}\left(r\frac{\partial g_1}{\partial r}\right) - \left(\frac{\lambda^2}{r^2}\right) g_1 = 0 \tag{7.37}$$

The corresponding first order boundary conditions are

$$f_1|_{r=a} + \left.\frac{\partial w_{p0}}{\partial r}\right|_{r=a} = 0$$

$$f_1|_{r=1} + \left.\frac{\partial w_{p0}}{\partial r}\right|_{r=1} - \left\{ g_1|_{r=1} + \left.\frac{\partial w_{c0}}{\partial r}\right|_{r=1}\right\} = 0$$

$$\left.\frac{\partial f_1}{\partial r}\right|_{r=1} + \left.\frac{\partial^2 w_{p0}}{\partial r^2}\right|_{r=1} - \left\{ \left.\frac{\partial g_1}{\partial r}\right|_{r=1} + \left.\frac{\partial^2 w_{c0}}{\partial r^2}\right|_{r=1}\right\} = + \frac{\beta}{\sqrt{k}}\left\{ f_1|_{r=1} + \left.\frac{\partial w_{p0}}{\partial r}\right|_{r=1}\right\}$$

$$\left.\frac{\partial g_1}{\partial r}\right|_{r=c} + \left.\frac{\partial^2 w_{c0}}{\partial r^2}\right|_{r=c} = 0 \tag{7.38}$$

$$w_{p1} = (c_5 I_\lambda(rS) + c_6 K_\lambda(rS))\sin(\lambda\phi) \tag{7.39}$$

$$w_{c1} = (c_7\cosh(\lambda\log(r)) + c_8\sinh(\lambda\log(r)))\sin(\lambda\phi), \tag{7.40}$$

The expression of the constants c_5, c_6, c_7, and c_8 can be derived using the boundary conditions 7.38; however, analytical expressions of these are not mentioned here in this chapter due to their large expressions.

The second order solution, $\mathscr{O}(\delta^2)$

$$\frac{1}{r}\frac{\partial}{\partial r}\left(r\frac{\partial w_{p2}}{\partial r}\right) + \frac{1}{r^2}\frac{\partial^2 w_{p2}}{\partial\phi^2} - S_1^2 w_{p2} = 0 \tag{7.41}$$

$$\frac{1}{r}\frac{\partial}{\partial r}\left(r\frac{\partial w_{c2}}{\partial r}\right) + \frac{1}{r^2}\frac{\partial^2 w_{c2}}{\partial\phi^2} = 0 \tag{7.42}$$

In the view of second order boundary conditions we can assume solution of second order governing equations in porous and clear fluid regions in the form, $w_{p2}(r,\phi) = f_{p2}(r) + g_{p2}(r)\cos(2\lambda\phi)$ and $w_{c2}(r,\phi) = f_{c2}(r) + g_{c2}(r)\cos(2\lambda\phi)$, respectively. The reduced equations independent from coordinate ϕ are

$$\frac{1}{r}\frac{\partial}{\partial r}\left(r\frac{\partial f_{p2}}{\partial r}\right) - S_1^2 f_{p2} = 0, \tag{7.43}$$

$$\frac{1}{r}\frac{\partial}{\partial r}\left(r\frac{\partial g_{p2}}{\partial r}\right) - \left(\frac{4\lambda^2 1}{r^2} + S_1^2\right) g_{p2} = 0, \tag{7.44}$$

$$\frac{1}{r}\frac{\partial}{\partial r}\left(r\frac{\partial f_{c2}}{\partial r}\right) = 0, \tag{7.45}$$

$$\frac{1}{r}\frac{\partial}{\partial r}\left(r\frac{\partial g_{c2}}{\partial r}\right) - \left(\frac{4\lambda^2}{r^2}\right) g_{c2} = 0. \tag{7.46}$$

$$\tag{7.47}$$

The second order boundary conditions corresponding to f_{p2} and f_{c2} are

$$\begin{aligned}
f_{p2}\big|_{r=a} + D_1(r)|_{r=a} &= 0,\\
f_{p2}\big|_{r=1} + D_1(r)|_{r=1} &= f_{c2}|_{r=1} + D_2(r)|_{r=1},\\
\left.\frac{df_{p2}}{dr}\right|_{r=1} + \left.\frac{dD_1(r)}{dr}\right|_{r=1} &= \left.\frac{df_{c2}}{dr}\right|_{r=1} + \left.\frac{dD_2(r)}{dr}\right|_{r=1} + \beta S\left\{ f_{p2}\big|_{r=1} + D_1(r)|_{r=1},\right\}
\end{aligned}$$

$$\left.\frac{df_{c2}}{dr}\right|_{r=c} + \left.\frac{dD_2(r)}{dr}\right|_{r=c} = 0. \tag{7.48}$$

The second order boundary conditions corresponding to g_{p2} and g_{c2} are

$$\begin{aligned}
g_{p2}\big|_{r=a} + D_1(r)|_{r=a} &= 0, \\
g_{p2}\big|_{r=1} + D_1(r)|_{r=1} &= g_{c2}|_{r=1} + D_2(r)|_{r=1}, \\
\left.\frac{dg_{p2}}{dr}\right|_{r=1} + \left.\frac{dD_1(r)}{dr}\right|_{r=1} &= \left.\frac{dg_{c2}}{dr}\right|_{r=1} + \left.\frac{dD_2(r)}{dr}\right|_{r=1} + \beta S\left\{ g_{p2}\big|_{r=1} + D_1(r)|_{r=1}, \right\}
\end{aligned}$$

$$\left.\frac{dg_{c2}}{dr}\right|_{r=c} + \left.\frac{dD_2(r)}{dr}\right|_{r=c} = 0, \tag{7.49}$$

where

$$D_1(r) = \frac{1}{2}\frac{df_1}{dr} + \frac{1}{4}\frac{d^2 w_{p0}}{dr^2}, \tag{7.50}$$

$$D_2(r) = \frac{1}{2}\frac{dg_1}{dr} + \frac{1}{4}\frac{d^2 w_{c0}}{dr^2}. \tag{7.51}$$

$$w_{p2}(r) = c_{10}K_0(rS) + c_9 I_0(rS) - \cos(2\lambda\phi)\left(c_{11}I_{2\lambda}(rS) + c_{12}K_{2\lambda}(rS)\right) \tag{7.52}$$

$$w_{c2}(r) = c_{13}\log(r) + c_{14} - \cos(2\lambda\phi)\left(c_{15}\cosh(2\lambda\log(r)) + c_{16}\sinh(2\lambda\log(r))\right) \tag{7.53}$$

The expression of the constants $c_9 - c_{16}$ can be derived using the boundary conditions (7.48) and (7.49); however, analytical forms of these are not included here in this chapter due to their large expressions.

7.4 Results and Discussion

The present study explores the effect of corrugations on the steady flow of Newtonian fluid past a uniformly distributed array of porous layered cylindrical particles. The aim of this study is to reveal the effect of porous medium and corrugation shape parameters on the flow velocities and hydrodynamic quantities like hydrodynamic permeability and Kozeny constant. The effect of porous medium and corrugated shape of particles lead to generate a set of non-homogeneous partial differential equations which are solved asymptotically using regular perturbation method. The analytical expressions of fluid velocity, hydrodynamic

permeability, and Kozeny constant were then used to analyze the effect of corrugation height (δ), wave number (λ), Darcy number (k), stress jump parameter (β), viscosity ratio parameter (μ_R), particle volume fraction (γ), and porosity (ε) etc.

7.4.1 Parameter Selection

Range of Parameters		
Parameters	Range	Sources
Corrugation height δ	0-0.1	[21]
Wave number λ	1-7	[21]
Steady pressure gradient p_s	1-10	[4], [167]
Permeability k	$(0,\infty)$	[3]
Stress-jump parameter β	$(-1,1)$	[3], [4]
Viscosity ratio parameter μ_R	1.0-1.6	[207], [167]
Particle volume fraction γ	0.1-1.0	[3], [96]
Porosity parameter ε	0.3-1.0	[3]

Table 7.1: Ranges for the ongoing parameters with their references

7.4.2 Velocity Profile

This section includes the contour plots of velocity signifying the effect of different corrugation and porous medium parameters along with the radial as well as azimuthal directions. Figure 7.3 depicts the contours of velocity profile for the cylindrical particles encompassing different wave numbers. The three white closed boundaries represents the three surfaces of on the cross-section of a cylindrical particle where the innermost curve represent the solid surface of particle having zero velocity on it. The middle boundary in white color depicts the interface of porous medium and clear fluid, where the continuity of velocity is applicable which can be verified by checking the continuous curves of velocity contours on this boundary, whereas the outermost boundary in white color depicts the hypothetical cell surface. It can be observed from figure 7.3 that the increasing wave number λ leads to a fading red color, denoting the reduction of velocity in the flow domain. This reduction in fluid velocity with increasing number of corrugation corresponds to the increased wall roughness that leads to enhance the resistance caused to the flow near the boundary, results in decreasing

the velocity profile throughout the flow domain. It can also be observed from the contours that the fluid velocity gets its highest value on the top of a node, however in the saddle part of the domain the fluid velocity is lower a its vicinity.

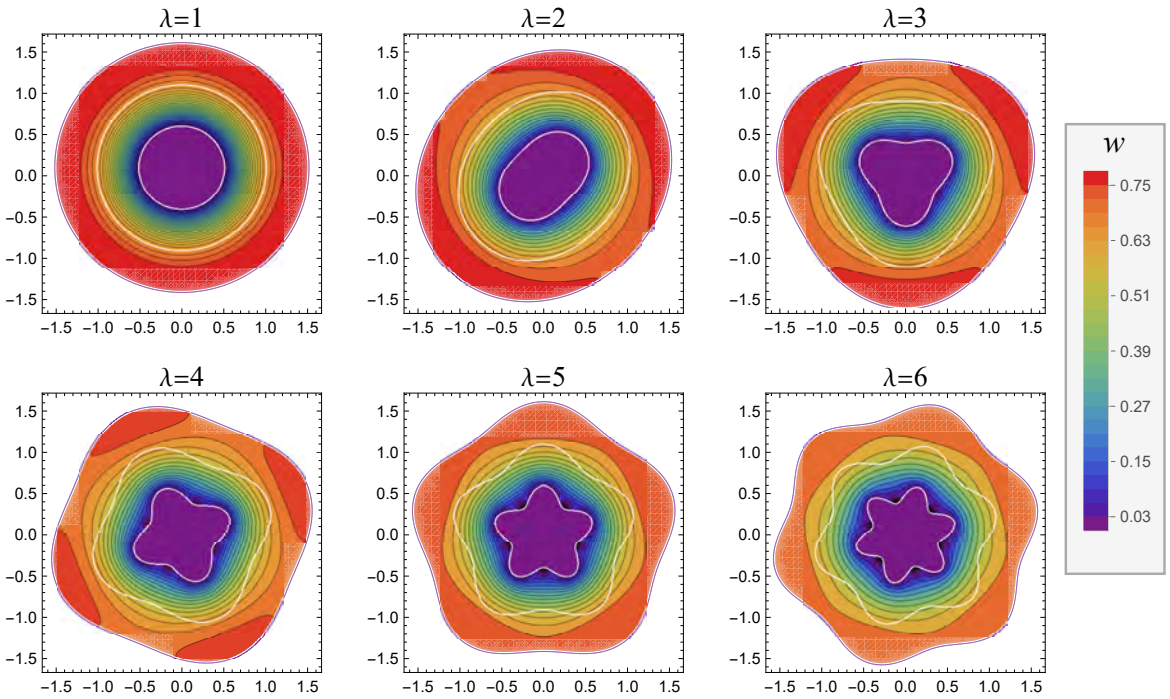

Figure 7.3: Contours of velocity profile, $w(r,\phi)$ for different wave number, λ. $(a = 0.5, \gamma = 0.445, pz = 1, k = 3, \delta = 0.1, \beta = 0.4)$

The figure 7.4 depicts the effect of perturbation parameter ε on the velocity profile of the fluid, where the perturbation parameter corresponds to the height of corrugation. The gradual transition of red color in the hypothetical cell region towards the orange with respect to the increasing parameter δ draws the fact that the increasing height of corrugation leads to a decay in the fluid velocity. This decay can be attributed to the increased wall area of the solid surface within the corrugated cylinder, which leads to heightened flow resistance in the domain, causing a reduction in fluid velocity. According to the findings depicted in Figure 7.5, as the Darcy number k increases, indicating greater permeability of the porous medium, there is a corresponding augmentation in fluid velocity. Figure 7.6 included the velocity contours for different values of stress jump parameters in case of small ($k \ll 1$) as well as ($k \gg 1$) permeability of the porous media. It can be concluded that as the disparity in stresses between the clear fluid and porous regions augmented at the fluid-porous interface, it leads to an escalation in fluid velocity.

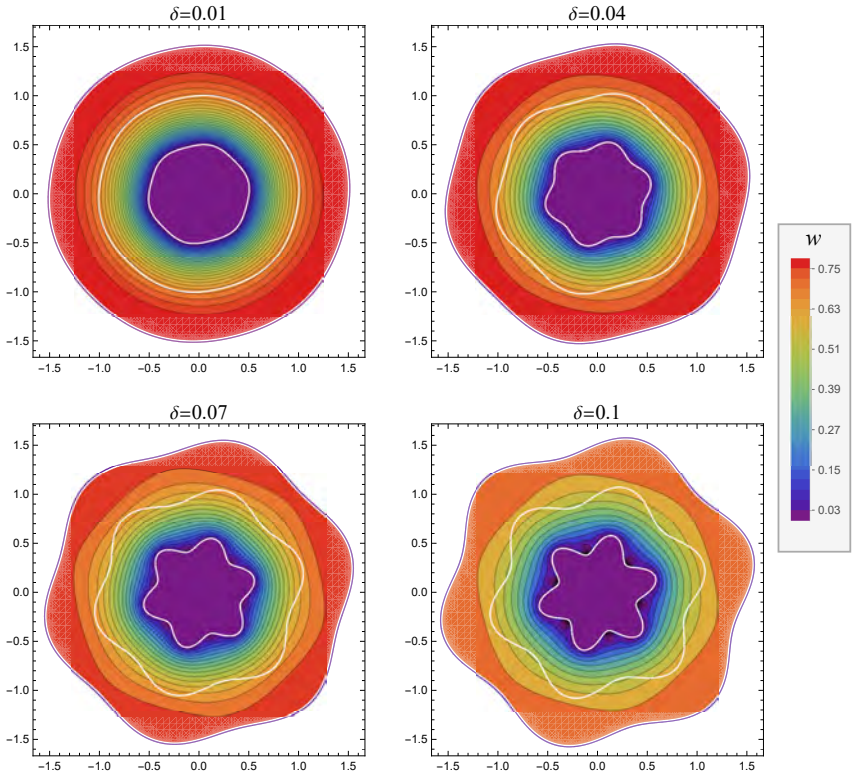

Figure 7.4: Contours of velocity profile, $w(r,\phi)$ for different height of corrugation δ. $(a=0.5, \gamma=0.445, pz=1, k=3, \lambda=6, \beta=0.4)$

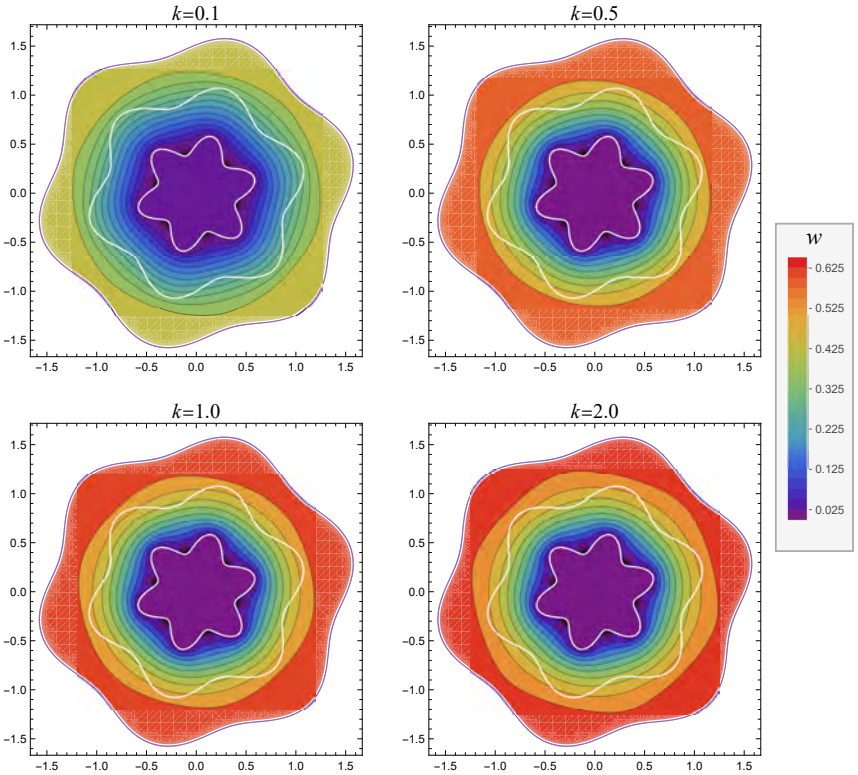

Figure 7.5: Contours of velocity profile, $w(r,\phi)$ for different values of the Darcy number, k. $(a=0.5, \gamma=0.445, pz=1, \delta=0.1, \lambda=6, \beta=0.1)$

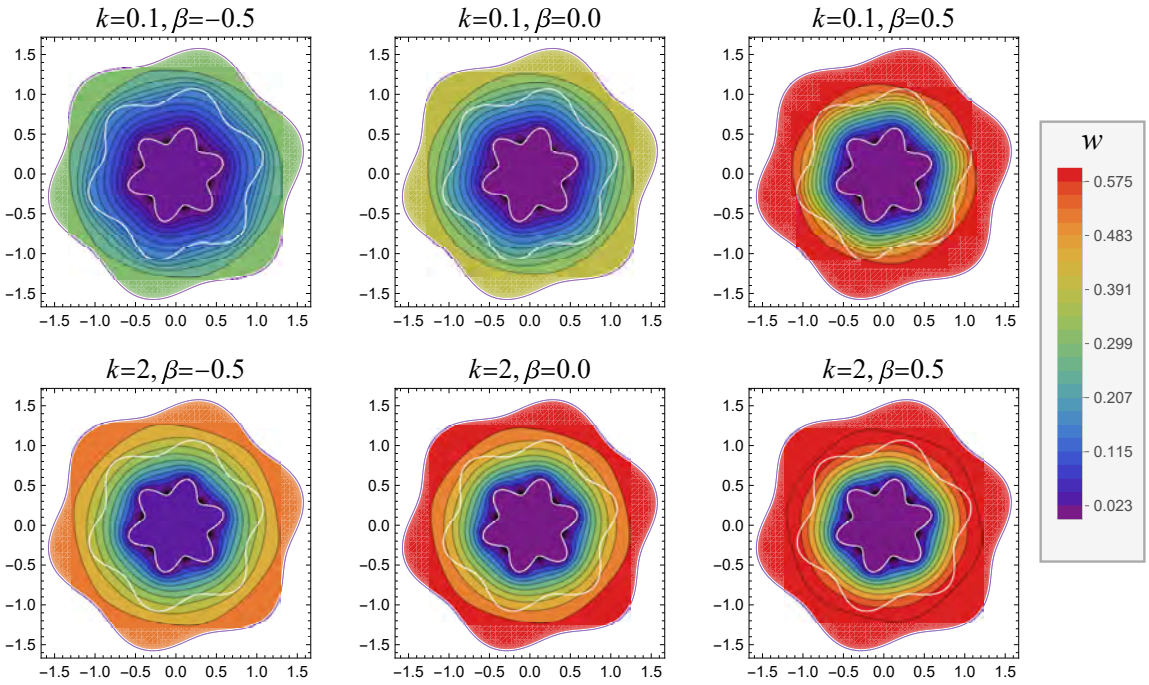

Figure 7.6: Contours of velocity profile, $w(r,\phi)$ for different values of the stress-jump parameter β, for large $(k=2)$ and small $(k=0.1)$ permeability of porous media. $(a=0.5, \gamma=0.445, pz=1, \delta=0.1, \lambda=6)$

7.4.3 Hydrodynamic Permeability

Figures 7.7 and 7.8 depicts the dependence of hydrodynamic permeability of the membrane on the corrugation thickness of cylindrical particles for different wave number and stress-jump coefficient respectively. As the thickness of the corrugations increases, it results in a reduction in the hydrodynamic permeability of the membranes. This can be attributed to an increased wetted area along the surface of the solid cylinder, where the no-slip condition governs. This enlarged wetted area intensifies flow resistance, thereby diminishing the membrane's hydrodynamic permeability. This diminishing effect of hydrodynamic permeability with corrugation height is more significant for the corrugated cylindrical particles with higher wave number. The increasing stress jump parameter enhances the hydrodynamic permeability of the membrane, which corresponds to the previous result of Figure 7.6. Furthermore, observation reveals that the increase in L_{11} is more pronounced for positive values of the stress-jump parameter. This suggests that elevated stress levels within the porous medium, compared to the clear fluid, render the fluid flow more sensitive to variations in the stress-jump parameter. Conversely, higher stress levels in the clear fluid region render it somewhat less responsive to changes in the stress jump.

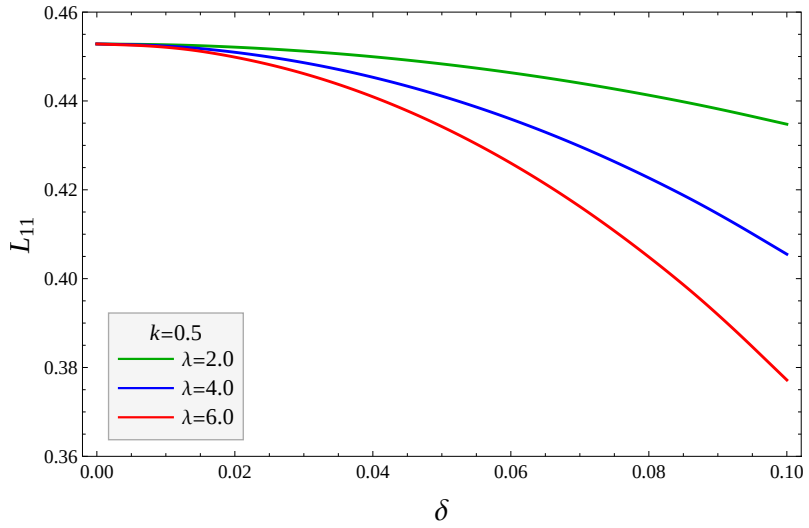

Figure 7.7: The dependence of hydrodynamic permeability L_{11} on the corrugation height δ for different values of wave number λ. $(a = 0.5, \gamma = 0.445, pz = 1, k = 0.5, \beta = 0.1)$

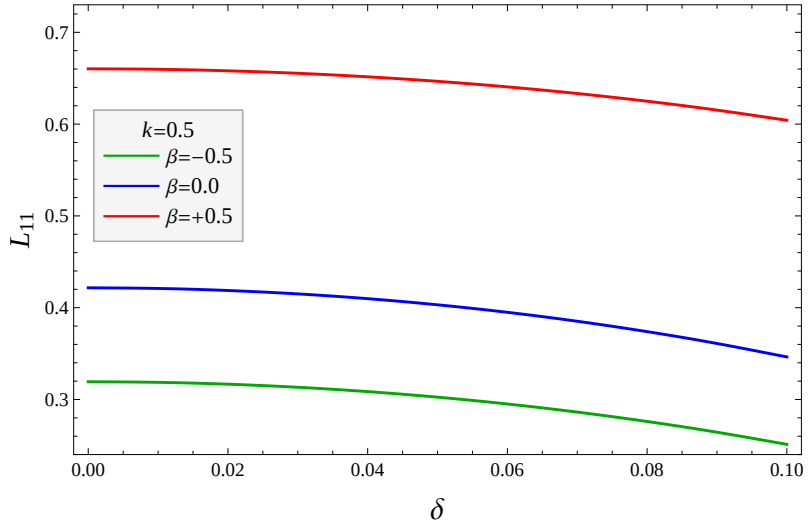

Figure 7.8: The dependence of hydrodynamic permeability L_{11} on the corrugation height δ for different values of stress-jump parameter β. $(a = 0.5, \gamma = 0.445, pz = 1, k = 0.5, \lambda = 6)$

Figure 7.9 illustrates the impact of particle volume fraction on hydrodynamic permeability for various corrugation heights. A notable decreasing trend in L_{11} is evident as the particle volume fraction increases. This decline can be attributed to the cylinders' augmented size, elevating the suspension concentration and consequently diminishing hydrodynamic permeability. Moreover, the influence of corrugation height on the correlation between L_{11} and γ is particularly pronounced for membranes comprising corrugated cylinders with lower particle volume fractions. The wave number of corrugated particles also slightly affect the

dependence of L_{11} on the particle volume fraction, where it leads to decay in hydrodynamic permeability of the membrane (Figure 7.10).

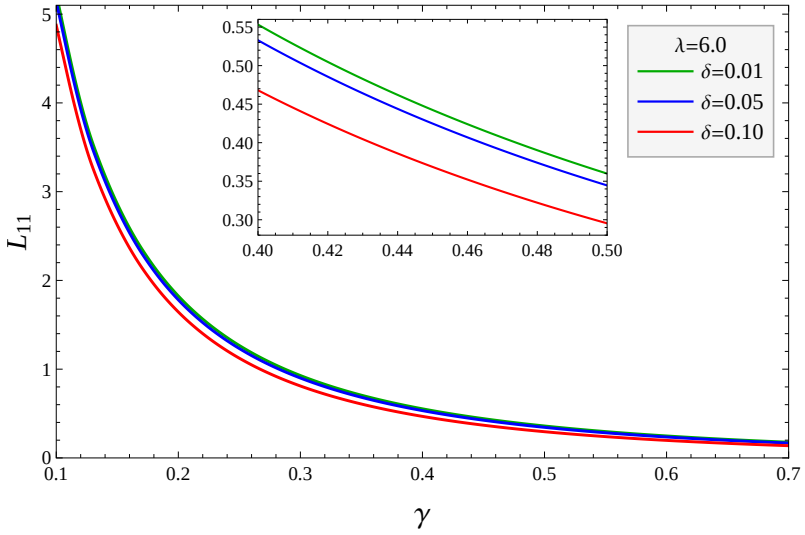

Figure 7.9: The dependence of hydrodynamic permeability L_{11} on the particle volume fraction γ for different values of corrugation height δ. $(a = 0.5, pz = 1, k = 0.5, \lambda = 6, \beta = 0.1)$

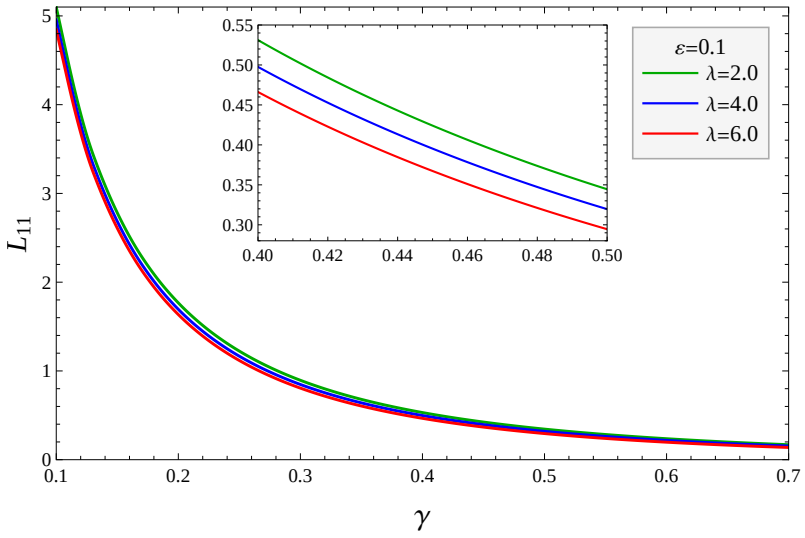

Figure 7.10: The dependence of hydrodynamic permeability L_{11} on the particle volume fraction γ for different values of wave number λ. $(a = 0.5, pz = 1, k = 0.5, \delta = 0.1, \beta = 0.1)$

Figures 7.11 and 7.12 depict the impact of the Darcy number on hydrodynamic permeability across varying corrugation characteristics. It can be concluded from these figures that the increasing Darcy number results in an enhancement of L_{11}. As the Darcy number increases, the L_{11} curve tends towards a plateau, indicating a diminished dependency of

L_{11} on the Darcy number for highly permeable porous media. Specifically, it is discerned that L_{11} exhibits substantial growth for Darcy numbers below unity, while its curve is almost flattened for values exceeding unity. Additionally, an augmentation in the corrugation height leads to reduction in the growth of L_{11} with the Darcy number, representing extra flow resistance due to increased roughness of particles in the flow domain. Following to the observations illustrated in figure 7.12, the hydrodynamic permeability shows a similar behavior of reduced growth rate with the Darcy number for increasing wave number λ.

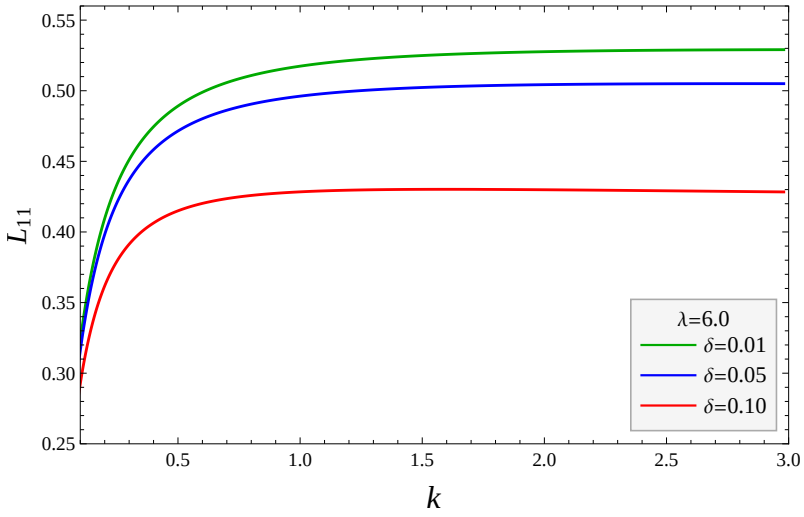

Figure 7.11: The dependence of hydrodynamic permeability L_{11} on the Darcy number k for different values of corrugation height δ. $(a = 0.5, pz = 1, k = 0.5, \lambda = 6, \beta = 0.2)$

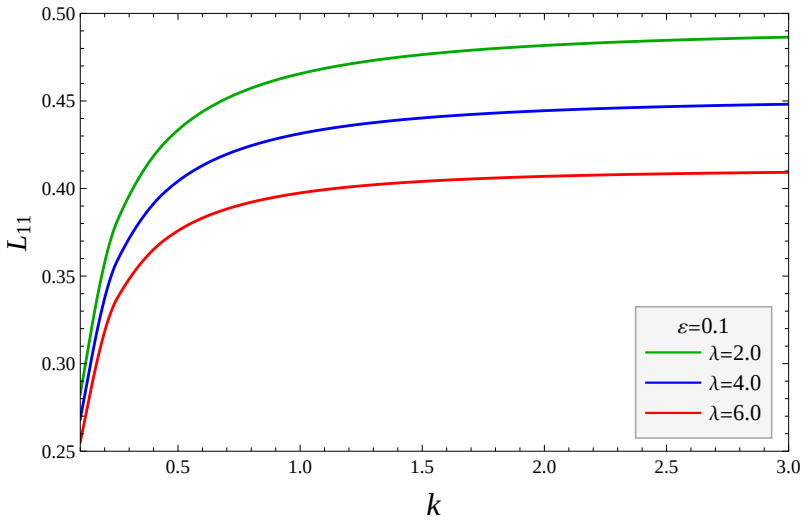

Figure 7.12: The dependence of hydrodynamic permeability L_{11} on the Darcy number k for different values of wave number parameter k. $(a = 0.5, pz = 1, k = 0.5, \delta = 0.1, \beta = 0.1)$

7.4.4 Kozeny Constant

The Kozeny constant, K_z, serves as a comprehensive parameter encompassing the influences of flow path tortuosity, particle shape, and their interplay. Notably, K_z exhibits a direct proportionality to tortuosity, as emphasized by Ozgumus et al. [181]. Thus, it becomes compelling to investigate the impact of corrugation parameters on tortuosity through their influence on K_z. The effect of porosity, ε on the Kozeny constant reveals that the increasing porosity of the porous layer leads to a growth in the Kozeny constant, which is similar to the observation of Madasu and Bucha [11] for the case of Newtonian fluid flow through particles with cavity (Figure 7.13). This growth rate get enhanced for higher values of corrugations height, signifying that the increasing roughness of corrugated particles leads to increase in the tortuosity of the membrane. Figure 7.14 demonstrates that an increasing particle volume fraction significantly enhances the growth rate of K_z with porosity ε. This phenomenon can be accredited to the increasing concentration/compactness of particles within the array leading to a greater tortuosity of the flow path and consequently yielding higher values of K_z.

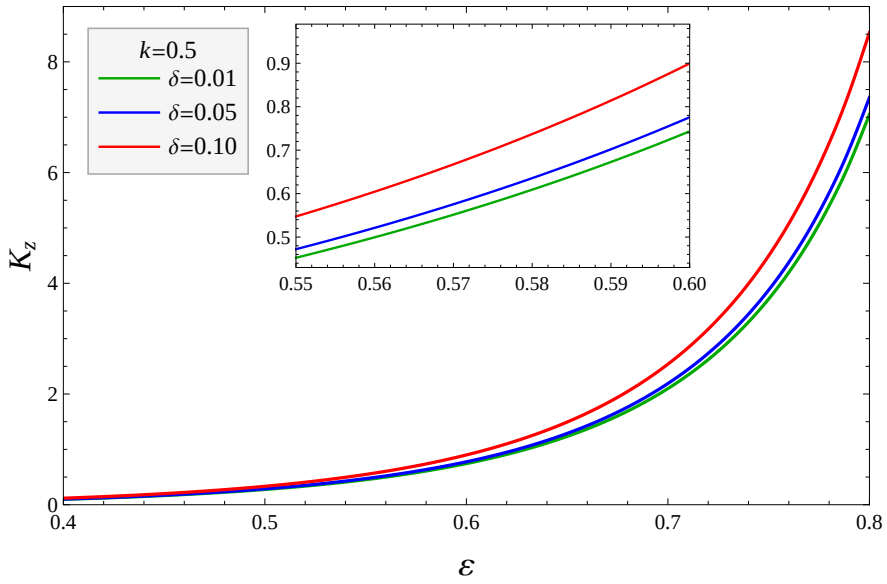

Figure 7.13: The dependence of the Kozeny constant K_z on the porosity ε for different values of corrugation height δ. $(a = 0.5, pz = 1, k = 0.5, \lambda = 6, \beta = 0.1)$

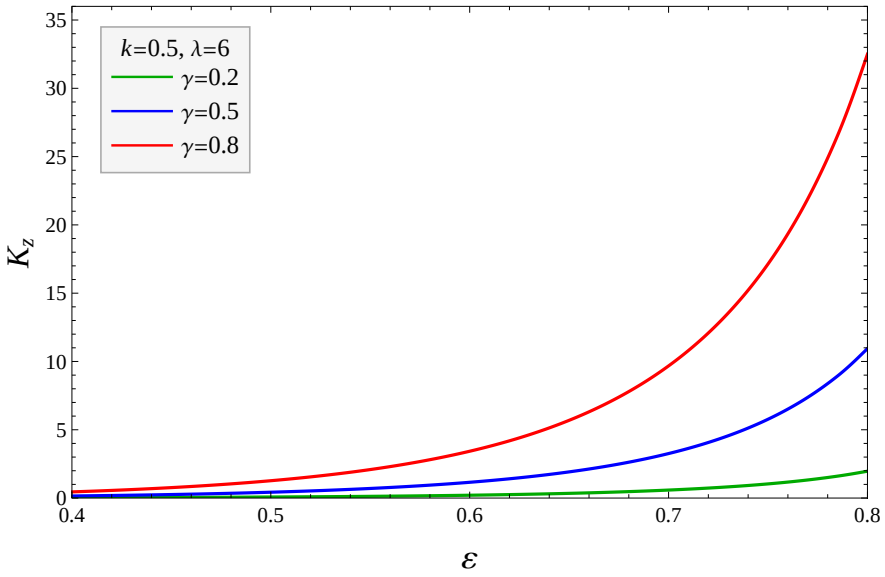

Figure 7.14: The dependence of the Kozeny constant K_z on the porosity ε for different values of particle volume fraction γ. $(a = 0.5, pz = 1, k = 0.5, \lambda = 6, \delta = 0.1, \beta = 0.1)$

Figure 7.15 to 7.17 illustrates the relationship of the Kozeny constant K_z, with the corrugation height δ for different control parameter. The stress-jump parameter reduces the growth rate of the Kozeny constant with roughness of cylindrical particles, which can be validated from the previous result of figure 7.8 describing that the higher stress jump parameter leads to a more permeable membrane, and hence less tortuous flow paths in the membrane (Figure 7.15).

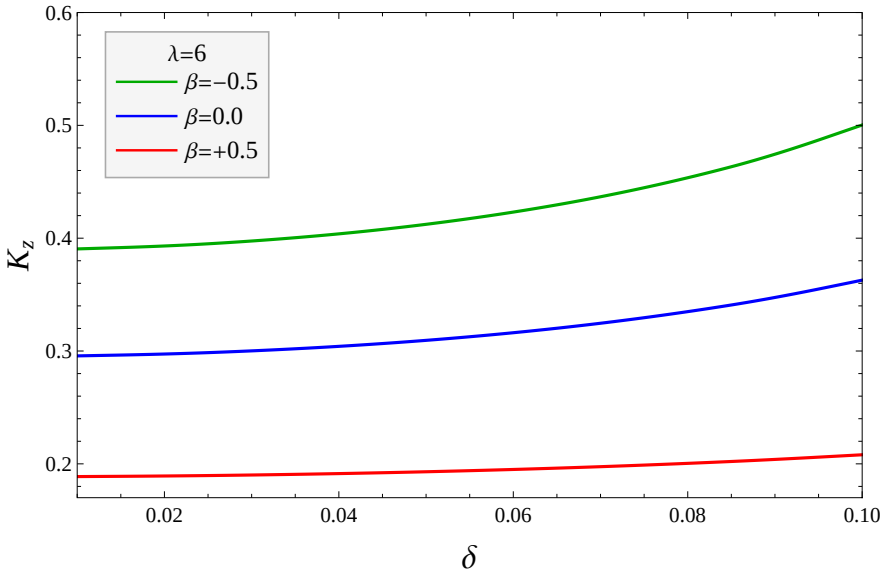

Figure 7.15: The dependence of the Kozeny constant K_z on corrugation height δ for different values of stress-jump parameter β. $(a = 0.5, pz = 1, k = 0.5, \lambda = 6, \varepsilon = 0.5)$

The increasing Darcy number reduces the Kozeny constant K_z, signifying the inversely proportional relation of the Darcy number with tortiosity of the porous medium (Figure 7.16).

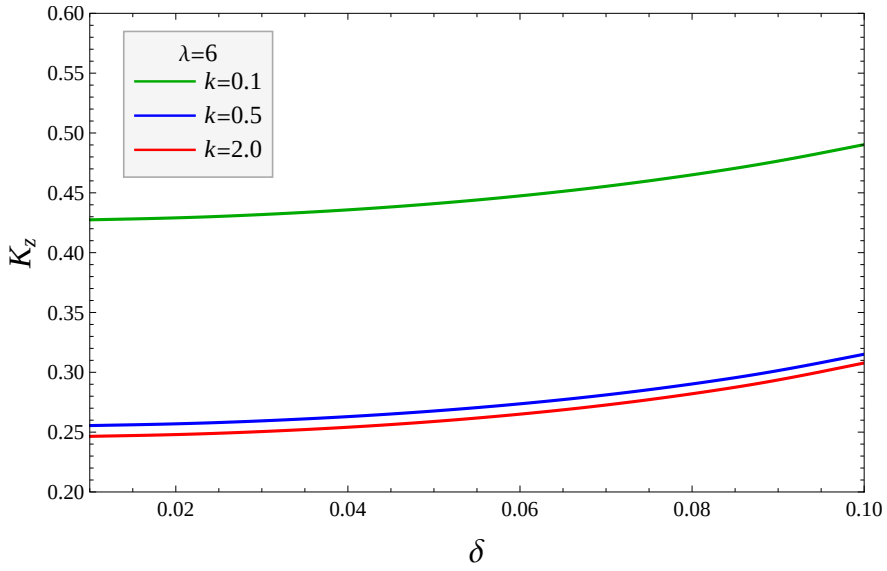

Figure 7.16: The dependence of the Kozeny constant K_z on corrugation height δ for different values of stress-jump parameter β. $(a = 0.5, pz = 1, \beta = 0.1, \lambda = 6, \varepsilon = 0.5)$

It can be observed from Figure 7.17 that the growth rate of the Kozeny constant increases with the particles roughness in terms of corrugations height. However, the wave number contributes in this growth rate and make it more significant for corrugated particles

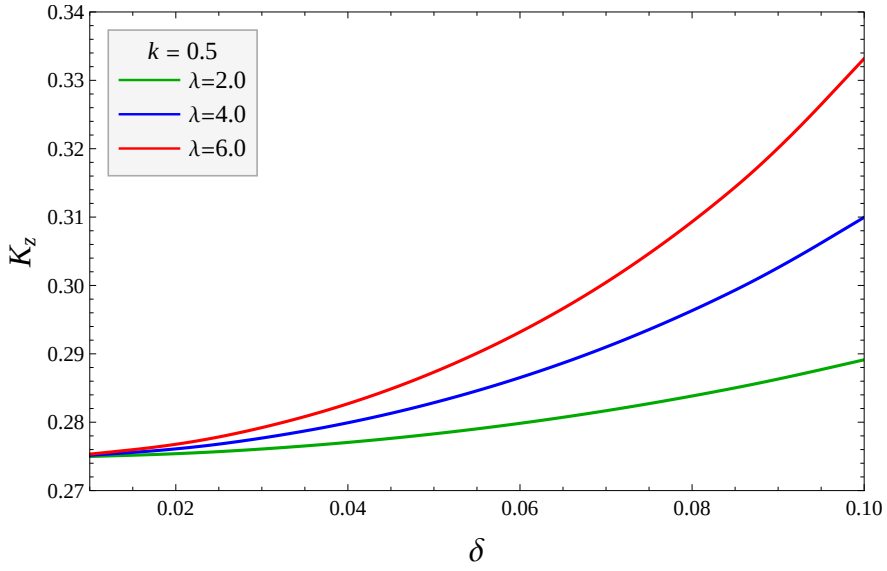

Figure 7.17: The dependence of the Kozeny constant K_z on corrugation height δ for different values of the wave number λ. $(a = 0.5, pz = 1, k = 0.5, \beta = 0.1, \varepsilon = 0.5)$

with higher wave number. This observation signifies that an enhancement in the corrugation height of a groove leads to augmented tortuosity of the medium.

7.5 Summary and Conclusions

In this chapter, the effect of surface corrugations on the flow past a membrane composed of an array of uniformly distributed porous layered cylindrical particles is studied. The sinusoidal transverse corrugation are assumed along the transverse direction of the cross-section of the cylinder. The steady, fully developed, and in-compressible flow of Newtonian fluid is studied using the cell model technique according to which, the flow regime is divided into two segments, one is the porous layer region enveloping the solid corrugated cylindrical particle, in which the fluid flow is governed by the Brinkann equation. Second is the clear fluid region enclosed by a hypothetical cell, where the flow is governed by the Stokes equation. The analytical solution of the system of PDE's governing the fluid flow in corrugated boundaries is difficult to derive. Hence The asymptotic solution were obtained using the regular perturbation technique with the assumption of the corrugation height as a perturbation parameter ($\delta \ll 1$). The hydrodynamic permeability and Kozeny constant of the membrane is analyzed for different corrugation and porous medium control parameters by utilizing the asymptotic expressions of fluid velocity. The results and discussion section have given a detailed discussion of the graphical analysis.
The following novel determinations from the present study have been pointed out:

1. The increasing wave number λ in the corrugated cylindrical particle leads to reduce the fluid velocity. The similar effect of wave number is also seen for hydrodynamic permeability L_{11} of the membrane, owing to enhanced obstruction in fluid flow through membrane.

2. The increasing corrugation height corresponds to increased wall area of the solid surface within the corrugated cylinder, causing a reduction in fluid velocity. An augmented corrugation height leads to reduced hydrodynamic permeability, with increasing decay rate, signifying an enhanced resistance due to increasing δ.

3. The disparity in stresses between the clear fluid and porous regions at the fluid-porous interface, leads to an escalation in fluid velocity. Additionally, the elevated stress levels within the porous medium, compared to the clear fluid, render the fluid flow more sensitive to variations in the stress-jump parameter. Conversely, higher stress levels in the clear fluid render it somewhat less responsive to changes in the stress jump.

4. The growth rate of Kozeny constant with respect to porosity ε get enhanced for higher values of corrugations height, signifying that the increasing roughness of corrugated particles leads to increase the tortuosity of the membrane. The wave number of corrugated particles also affect the K_z in same manner. Additionally, the higher stress jump parameter leads to a more permeable membrane, and hence less tortuous flow paths in the membrane.

These results helps in providing a broader physical insights associated with particle's surface roughness in the flow past a membrane composed of an array of cylindrical particles. The following work, however, requires experimental verification.

Chapter 8

Electroosmotic Flow past an Array of Poly-Electrolyte Coated Solid Cylindrical Particles: A Particle-in-Cell Approach

8.1 Introduction

The electrokinetic transport of electrolytes past charged interfaces is a captivating area of study that has attracted considerable interest among researchers and scientists in both academic and industrial fields. This phenomenon holds significant importance due to its diverse applications across various industries, including but not limited to chemical, pharmaceutical, and life sciences [222, 223, 224, 225, 226, 227, 228]. Several researchers have tried to model the the electrokinetic transport of ionized solution past a soft (poly-electrolyte coated) surfaces due to its wide variety of applications e.g., in energy conversion systems [229], cell membranes [230], bio-sensor [231], drug delivery [232], etc. A soft surface typically consists of an ion-penetrable membrane composed of poly-electrolyte fibers, forming what is known as the Poly-electrolyte Layer (PEL). This layer is situated between a rigid surface and the bulk electrolyte solution. Within the PEL, there exists a density of additional immobile ions that cannot migrate into the bulk electrolyte, thus creating a localized potential known as the Donnan potential. This Donnan potential arises due to the presence of fixed charges within the PEL, resulting in the formation of a layer known as Fixed Charge Layer (FCL). The presence of this FCL and its associated Donnan potential significantly influences the electrostatics of the Electric Double Layer (EDL) across the entire flow domain. Understanding the interplay between the Donnan potential of the FCL and the EDL electrostatics is crucial for studying electrokinetic transport phenomena, particularly when considering flow past soft structures. By explaining these interactions, researchers can gain insights into the complex behavior of soft surfaces in various electrochemical and biophysical applications. Donath and Voigt [233] were the first who studied the electrokinetic transport of

fluid past the soft surfaces, where they have introduced the non-linear Poisson-Boltzmann model to study the potential distribution of fixed charges across the surfaces. Oshima and Kondo [234] extended this study later and done some excellent works in this field of electroosmootic flow near the poly-electrolyte coated soft surfaces [235, 236, 237, 238, 239, 240]. The theory of electrokinetic transport in membrane composed of an array of particles was started in 1974, where Levine and Neale [171] investigated electrokinetic transport of fluid past a concentrated suspensions of spherical colloidal particles, where they solved this problem using the unit cell model approach and considered the effect of neboughring particles using Kuwabara's boundary condition [67]. Kozak and Davis [241] considers the study of elecroosmosis and electrophoresis in a concentrated suspension of particles and extended the work of Levine and Neale by taking the flow past across an array of cylindrical shaped particle system. They derived the expression of electroosmotic velcoity for low zeta potential including the numerical integrations which were later simplified by Oshima [242], where he derived a more accurate electroosmotic velcoity expression without including any numerical integration. Oshima [243] initiated the theory of soft particles (particles coated with poly-electrolyte layer) in the study of EOF flow past a concentrated suspension. He applied the Kuwabara's cell model approach to analyze the flow past an array of soft spherical particles and reduced some special cases for the hard/rigid particles (particles without poly-electrolyte layer). Following to this, he made a significant contribution in the field of electrokinetic transport in concentrated suspension of soft particles, where electrical conductivity, Sedimentation potential, electrophoretic mobility [244, 245, 246].

8.2 Problem Formulation

8.2.1 Statement of the Problem

The proposed study focuses on the electrokinetic transport of electrolyte within a membrane composed of a swarm of uniformly distributed soft cylinderical particles, where is flow is considered along the axis of cylinders. The bulk fluid is considered as an electrolyte which is flowing along the array of cylinders. The uncharged solid cylindrical particles are coated with an ion-penetrable layer of polyelectrolye fibers (referred as PEL), which have their own charge density apart from the mobile ions of the bulk electrolyte. These ions of PEL are immobile/fixed and can not migrate in the bulk electrolyte outside of PEL. Hence the PEL is referred as Fixed Charged Layer or FCL and these ions were called the FCL ions. Following assumptions have been made:

1. The unidirectional flow is considered to be steady, incompressible, axisymmetric around the solid core, and fully developed.

2. The Reynolds number is deemed to be extremely low, signifying that viscous forces exert more influence than inertial forces, leading to the convective term being of minimal significance and thus excluded from the present study.

3. The potential due to the electrical double layer is independent of axial position z in the cylinder (which is valid for long cylinders, neglecting any end effects).

4. the electric potential is assumed to be small as compared to the thermal energy of the ions (Debye-Huckel approximation)

8.2.2 Model Description

The Newtonain electrolyte solution is flowing past a swarm of uniformly distributed solid cylindrical particles of radius $\widetilde{a}$. The surface of solid cylindrical particle is covered by poly-electrolyte materials, also called soft layer or poly-electrolyte layer or PEL, which is considered as a porous layer containing fix charge density of ions. The thickness of PEL is $(\widetilde{b}-\widetilde{a})$. The unidirectional flow of electrolyte is considered to be steady, in-compressible, and flowing along the axis of the solid cylindrical particle. The unit cell model technique is utilized to study the flow past uniformly distributed array of these particles. According to which a virtual envelop or hypothetical cell of radius $\widetilde{c}$ is assumed to incorporate the effect of the particle's surroundings. The flow field around the solid cylindrical particle is divided into two layer of regions. The inner layer region is the PEL region which is a porous region

having permeability k and is governed by the Brinkmann Forchheimer equation; However the outer layer is clear fluid region having free flow and is governed by the Stokes' equation. The geometry of the model is defined by a cylindrical polar coordinate system $(\widetilde{r},\theta,\widetilde{z})$, wherein $\widetilde{r}$ and $\widetilde{z}$ represent the distances in radial and axial directions, respectively. The z-axis is aligned with the center line of a solid cylinder. The flow is presumed to be axially symmetric and fully developed, with velocity components of the fluid being restricted to the axial direction only and given as $(0,0,\widetilde{w})$.

The thickness of the concentric cylindrical envelope (hypothetical cell) of the porous cylindrical particle is chosen in such a way that the particle volume fraction of the swarm of porous cylindrical particles is the same as the particle volume fraction of the cell.

$$c^2 = \frac{1}{\gamma} = \frac{\pi\widetilde{c}^2}{\pi\widetilde{b}^2}. \tag{8.1}$$

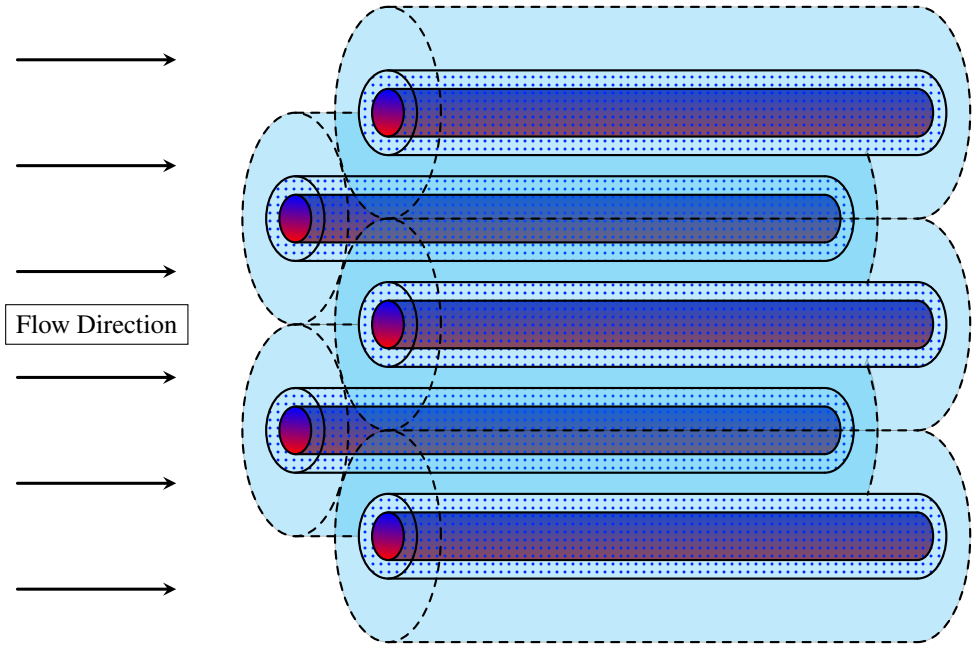

Figure 8.1: The physical sketch of cell model considered in a swarm of particles

8.2.3 Governing Equations

8.2.3.1 Electric Potential Equation

The electric potential in the cylinder is given by $\widetilde{\phi}(\widetilde{r},\widetilde{z})$, which arises due to superposition of the potential difference generated from the charge density of poly electrolyte layer and the

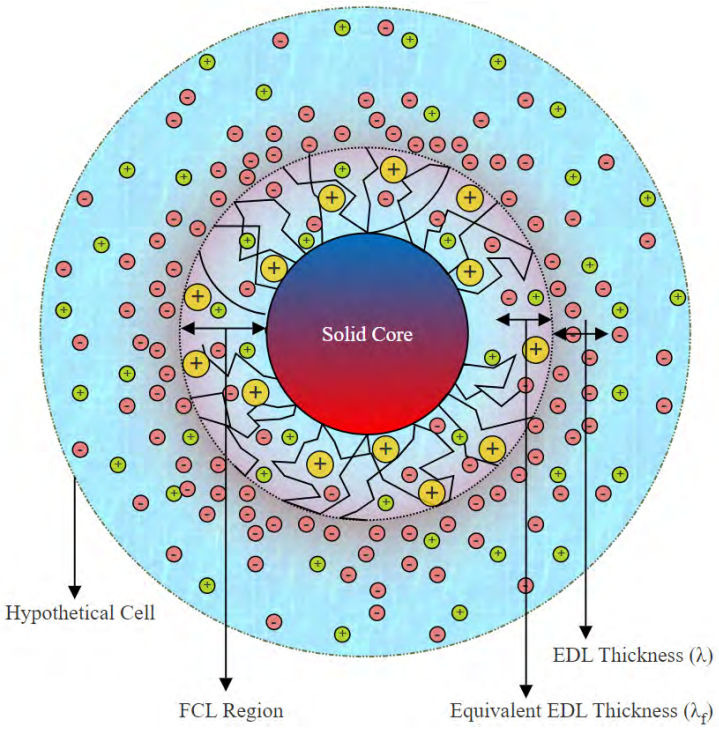

Figure 8.2: The cross-sectional view of a cylindrical particle having the solid core, coated with a poly-electrolyte(porous) layer.

externally applied electric potential.

$$\widetilde{\phi}(\widetilde{r},\widetilde{z}) = \widetilde{\psi}(\widetilde{r}) + (\widetilde{\phi}_0 - \widetilde{z}\widetilde{E}_z), \tag{8.2}$$

where the first term on right hand side, $\widetilde{\psi}(r)$ represents the potential due to EDL at the equilibrium state corresponding to no fluid motion and no applied electric field. The second term on RHS represents the potential at any axial location due to applied electric field strength $\widetilde{E}_z$ in absence of EDL, where $\widetilde{E}_z$ is the electric field strength due to applied potential difference, independent from position and $\widetilde{\phi}_0$ is the value of imposed potential at starting point $\widetilde{z}_0$ of the cylinder.

The equations governing the electric potential in different regions of the poly-electrolyte coated solid cylindrical particles are given by

Region- I, *i.e.*, $\widetilde{a} \leq \widetilde{r} \leq \widetilde{b}$

$$\nabla^2\widetilde{\phi}_p = \frac{1}{\widetilde{r}}\frac{\partial}{\partial\widetilde{r}}\left(\widetilde{r}\frac{\partial\widetilde{\phi}_p}{\partial\widetilde{r}}\right) + \frac{\partial^2\widetilde{\phi}_p}{\partial\widetilde{z}^2} = -\frac{\widetilde{\rho}_e + ZeN}{\varepsilon_0\varepsilon_r}. \tag{8.3}$$

Region- II, *i.e.*, $\widetilde{b} \leq \widetilde{r} \leq \widetilde{c}$

$$\nabla^2 \widetilde{\phi}_c = \frac{1}{\widetilde{r}} \frac{\partial}{\partial \widetilde{r}} \left(\widetilde{r} \frac{\partial \widetilde{\phi}_c}{\partial \widetilde{r}} \right) + \frac{\partial^2 \widetilde{\phi}_c}{\partial \widetilde{z}^2} = -\frac{\widetilde{\rho}_e}{\varepsilon_0 \varepsilon_r}, \tag{8.4}$$

where, the subscripts p and c are for PEL and clear fluid regions, respectively. ε_0 is the permittivity of the free space, ε_r is the relative permittivity of the medium (assumed to be identical in both the FCL and electrolyte), $\widetilde{\rho}_e$ is the free charge density in the electrolyte, e is the fundamental charge of an electron, Z and N are the valence and the ionic number concentration of the FCL ions.

The expression of electric potential from equation (8.2) can be utilized in equations (8.3), and (8.4).

Region- I, *i.e.*, $\widetilde{a} \leq \widetilde{r} \leq \widetilde{b}$

$$\frac{1}{\widetilde{r}} \frac{\partial}{\partial \widetilde{r}} \left(\widetilde{r} \frac{\partial \widetilde{\psi}_p}{\partial \widetilde{r}} \right) = -\frac{\widetilde{\rho}_e + ZeN}{\varepsilon_0 \varepsilon_r}. \tag{8.5}$$

Region- II, *i.e.*, $\widetilde{b} \leq \widetilde{r} \leq \widetilde{c}$

$$\frac{1}{\widetilde{r}} \frac{\partial}{\partial \widetilde{r}} \left(\widetilde{r} \frac{\partial \widetilde{\psi}_c}{\partial \widetilde{r}} \right) = -\frac{\widetilde{\rho}_e}{\varepsilon_0 \varepsilon_r}. \tag{8.6}$$

The free charge density of the electrolyte is given by

$$\widetilde{\rho}_e = e z_e (n_+ - n_-), \tag{8.7}$$

where z_e is the absolute value of the ionic valence, and n_+ and n_- are the ionic number concentrations of the cations and anions in the electrolyte, respectively and satisfies the Boltzmann-distribution given by

$$n_\pm = n_\infty exp \left(\mp \frac{e z_e \widetilde{\psi}}{K_B T} \right), \tag{8.8}$$

where, K_B and T are the Boltzmann constant and absolute temperature, where product of these two represents the thermal energy. n_∞ represents the ionic number concentration at the neutral state where $\widetilde{\psi} = 0$. It should be noted that the equation (8.8) is valid for any values of the EDL thickness; however if the electric potential is assumed to be small as compared to the thermal energy of the ions then,

$$exp \left(\mp \frac{ez\widetilde{\psi}}{K_B T} \right) \approx 1 \mp \frac{ez\widetilde{\psi}}{K_B T}. \tag{8.9}$$

The approximation involved here is called Debye-Hückel linearization or Debye-Hückel approximation, which is used here to analytically solve the governing equations of electric

potential. Now the free charge density can be written as

$$\widetilde{\rho}_e = -\frac{2e^2 z^2 n_\infty \widetilde{\psi}}{K_B T}. \tag{8.10}$$

The Debye-Hückel approximation can be used to linearised the equations (8.5) and (8.6)
Region- I, *i.e.*, $\widetilde{a} \leq \widetilde{r} \leq \widetilde{b}$

$$\frac{1}{\widetilde{r}}\frac{\partial}{\partial \widetilde{r}}\left(\widetilde{r}\frac{\partial \widetilde{\psi}_p}{\partial \widetilde{r}}\right) = \frac{\widetilde{\psi}_p}{\widetilde{\lambda}^2} - \frac{\widetilde{\psi}_s}{\widetilde{\lambda}_f^2}. \tag{8.11}$$

Region- II, *i.e.*, $\widetilde{b} \leq \widetilde{r} \leq \widetilde{c}$

$$\frac{1}{\widetilde{r}}\frac{\partial}{\partial \widetilde{r}}\left(\widetilde{r}\frac{\partial \widetilde{\psi}_c}{\partial \widetilde{r}}\right) = \frac{\widetilde{\psi}_c}{\widetilde{\lambda}^2}, \tag{8.12}$$

where $\widetilde{\lambda} = \left(\frac{\varepsilon_0 \varepsilon_r K_B T}{2n_\infty e^2 z^2}\right)^{\frac{1}{2}}$ represents the thickness of EDL in the clear fluid region and $\widetilde{\lambda}_f = \left(\frac{\varepsilon_0 \varepsilon_r K_B T}{N e^2 Z_z}\right)^{\frac{1}{2}}$ represents the thickness of an equivalent EDL inside the FCL region which corresponds to the distance over which the electric potential (at the interface of FCL and bulk electrolyte) and is formed inside the FCL region.

8.2.3.2 Hydrodynamic Equations

The flow domain is divided into two subdomains, first, the FCL region which is considered as a porous layer with varying permeability, where the flow governed by the Brinkmann-Forchheimer equations, second is the outer layer of clear fluid region which is bounded by a hypothetical cell of redius $\widetilde{c}$, and is governed by the stokes equation. Therefore, the hydrodynamic governing equations of a steady, fully developed and unidirectional flow caused by the combined effect of pressure gradient and electroosmotic body force is given by
Region- I, *i.e.*, $\widetilde{a} \leq \widetilde{r} \leq \widetilde{b}$

$$\frac{\widetilde{\mu}_e}{\widetilde{r}}\frac{\partial}{\partial \widetilde{r}}\left(\widetilde{r}\frac{\partial \widetilde{w}_p}{\partial \widetilde{r}}\right) - \frac{\widetilde{\mu}}{\widetilde{k}(\widetilde{r})}\widetilde{w}_p - \frac{C_F \widetilde{\rho}\widetilde{w}_p^2}{\sqrt{\widetilde{k}(\widetilde{r})}} = \frac{\partial \widetilde{p}}{\partial \widetilde{z}} - \widetilde{\rho}_e \widetilde{E}_z, \tag{8.13}$$

Region- II, *i.e.*, $\widetilde{b} \leq \widetilde{r} \leq \widetilde{c}$

$$\frac{\widetilde{\mu}}{\widetilde{r}}\frac{\partial}{\partial \widetilde{r}}\left(\widetilde{r}\frac{\partial \widetilde{w}_c}{\partial \widetilde{r}}\right) = \frac{\partial \widetilde{p}}{\partial \widetilde{z}} - \widetilde{\rho}_e \widetilde{E}_z, \tag{8.14}$$

where $\widetilde{\rho}, \widetilde{p}$ are the density and pressure, of the electrolyte, respectively. $\widetilde{w}_p$ and $\widetilde{w}_c$ are the velocity of electrolyte in FCL and clear fluid regions, respectively. $\widetilde{\mu}_e$ is the effective viscosity of the electrolyte in FCL region, $\widetilde{\mu}$ is the constant viscosity of electrolyte.

$\widetilde{k}(\widetilde{r}) = \widetilde{k}\left(1-\varepsilon_f\left(\frac{\widetilde{r}}{\widetilde{b}}\right)\right)^2$ is the quadratic form of the variable permeability of the porous medium where $\widetilde{k}$ is the constant permeability coefficient and ε_f $(0 \leq \varepsilon_f < 1)$ is the variable permeability parameter.
where $\widetilde{w}_c$ is the axial velocity for the clear fluid.

8.2.4 Non-Dimensional Parameters and Governing Equations

To solve the above system of equations (8.11)-(8.14), the following non-dimensional variables are introduced:

$$
\begin{aligned}
&p = \frac{\widetilde{p}}{\widetilde{p}_0},\ r = \frac{\widetilde{r}}{\widetilde{b}},\ z = \frac{\widetilde{z}}{\widetilde{b}},\ a = \frac{\widetilde{a}}{\widetilde{b}},\ c = \frac{\widetilde{c}}{\widetilde{b}},\ S^2 = \frac{1}{k},\ \widetilde{w}_0 = -\frac{\varepsilon_0\varepsilon_r\widetilde{\psi}_s\widetilde{E}_x}{\widetilde{\mu}},\ w_p = \frac{\widetilde{w}_p}{\widetilde{w}_0},\\
&w_c = \frac{\widetilde{w}_c}{\widetilde{w}_0},\ k = \frac{\widetilde{k}}{\widetilde{b}^2}, \widetilde{p}_0 = \frac{\widetilde{w}_0\widetilde{\mu}}{\widetilde{b}}, \psi_p = \frac{\widetilde{\psi}_p}{\widetilde{\psi}_s}, \psi_c = \frac{\widetilde{\psi}_c}{\widetilde{\psi}_s},\ \lambda = \frac{\widetilde{\lambda}}{\widetilde{b}},\ \lambda_f = \frac{\widetilde{\lambda}_f}{\widetilde{b}},\ F = \frac{C_F\widetilde{\rho}\widetilde{b}^3\widetilde{p}_0}{\widetilde{\mu}_e\widetilde{\mu}}\\
&\widetilde{\psi}_s = \frac{K_BT}{ez_e}, \zeta = \frac{\widetilde{\zeta}}{\widetilde{\psi}_s},\ \mu_R^2 = \frac{\widetilde{\mu}_e}{\widetilde{\mu}},\ K = \frac{\lambda_f}{\lambda}
\end{aligned}
\tag{8.15}
$$

where $\widetilde{w}_0$ is the characteristic velocity, $\widetilde{p}_0$ is the characteristic pressure, $\widetilde{\psi}_s$ is the characteristic electric potential, $\widetilde{\zeta}$ is the electric potential at $\widetilde{r} = \widetilde{a}$, μ_R is the ratio of effective viscosity of electrolyte in FCL region and constant viscosity of electrolyte, and S is a dimensionless parameter.

8.2.4.1 Poission-Boltzmann Equation

The non-dimentionalised governing equations for electric potential distribution are as follows.
Region- I, *i.e.*, $a \leq r \leq 1$

$$\frac{1}{r}\frac{\partial}{\partial r}\left(r\frac{\partial\psi_p}{\partial r}\right) = \frac{1}{\lambda^2}\left(\psi_p - \frac{1}{K^2}\right). \tag{8.16}$$

Region- II, *i.e.*, $1 \leq r \leq c$

$$\frac{1}{r}\frac{\partial}{\partial r}\left(r\frac{\partial\psi_c}{\partial r}\right) = \frac{\psi_c}{\lambda^2}. \tag{8.17}$$

8.2.4.2 Hydrodynamic Equations

Using the above non-dimensional variables (8.15), the hydrodynamic governing equations in non-dimensional form are given by
Region- I, *i.e.*, $a \leq r \leq 1$

$$\frac{\mu_R^2}{r}\frac{\partial}{\partial r}\left(r\frac{\partial w_p}{\partial r}\right) - \frac{w_p}{k(r)} - \frac{F\mu_R^2 w_p^2}{\sqrt{k(r)}} = \frac{\partial p}{\partial z} - \frac{\psi_p}{\lambda^2}. \tag{8.18}$$

Region- II, *i.e.*, $1 \leq r \leq c$

$$\frac{1}{r}\frac{\partial}{\partial r}\left(r\frac{\partial w_c}{\partial r}\right) = \frac{\partial p}{\partial z} - \frac{\psi_c}{\lambda^2}. \tag{8.19}$$

8.2.5 Boundary Conditions

The dimensionless boundary conditions are given as follows:

1. The no slip boundary condition at the surface of the solid core of the cylinder along with a constant electric potential (zeta potential) at the surface, *i.e.*,

$$w_p = 0, \quad \psi_p = \zeta \quad \text{at} \quad r = a. \tag{8.20a}$$

2. The electrolyte velocity and electric potential are continuous at the FCL and clear fluid interface, *i.e.*,

$$w_p = w_c, \quad \psi_p = \psi_c \quad \text{at} \quad r = 1. \tag{8.20b}$$

3. The stress-jump condition along tangential stresses and continuity of electric potential gradient in radial direction is considered at the FCL and clear fluid interface, *i.e.*,

$$\mu_R^2\frac{\partial w_p}{\partial r} - \frac{\partial w_c}{\partial r} = \frac{\beta}{\sqrt{k}}w_p, \quad \frac{d\psi_p}{dr} = \frac{d\psi_c}{dr} \quad \text{at} \quad r = 1, \tag{8.20c}$$

   where μ_R is the viscosity ratio parameter and β is the stress-jump parameter.

4. The zero potential gradient at the hypothetical cell along with a zero velocity gradient in the redial direction representing the combined result of the Happel, Kuwabara, Kvashnin and Cunningham boundary conditions, is taken *i.e.*,

$$\frac{\partial w_c}{\partial r} = 0, \quad \frac{d\psi_c}{dr} = 0 \quad \text{at} \quad r = c. \tag{8.20d}$$

8.2.6 Hydrodynamical Quantities and Kozeny Constant

The volumetric flow rate Q_s in non-dimensional form is given by

$$\begin{aligned} Q_s &= 2\pi \int_a^c rw(r)dr, \\ &= 2\pi \left(\int_a^1 rw_p(r)dr + \int_1^c rw_c(r)dr \right). \end{aligned} \tag{8.21}$$

The expression for the hydrodynamic permeability L_{11} of the collective of porous cylindrical particles is formulated as follows [95]

$$L_{11} = -\frac{V_f}{\partial p/\partial z}, \tag{8.22}$$

where V_f denotes the filtration velocity and is expressed as $V_f = \frac{Q_s}{\pi c^2}$.
The permeability of porous media can be obtained through the application of the following expression, derived from the semi-empirical Kozeny-Karman formula [71]

$$L_{11} = \frac{\varepsilon \rho_h^2}{K_z \widetilde{b}^2}, \tag{8.23}$$

where ε represents porosity of the medium corresponding to the concentration of particles in the array, K_z denotes the dimensionless Kozeny constant, and ρ_h signifies the hydraulic radius, defined as the ratio of pore volume to wetting area.
The Kozeny constant is obtained by the above equation (12)

$$K_z = \frac{\varepsilon \rho_h^2}{\widetilde{b}^2 L_{11}}. \tag{8.24}$$

For the media composed of cylindrical particles, we have

$$\rho_h = \frac{\pi(\widetilde{c}^2 - \widetilde{b}^2)}{2\pi\widetilde{b}} = \frac{\widetilde{b}}{2}\left(\frac{1-\gamma}{\gamma}\right) = \frac{\varepsilon\widetilde{b}}{2(1-\varepsilon)}. \tag{8.25}$$

Substituting the value of ρ_h in the above equation (8.24), we have

$$K_z = \frac{\varepsilon^3}{4(1-\varepsilon)^2 L_{11}}, \tag{8.26}$$

where L_{11} is the hydrodynamic permeability of the membrane.

8.3 Solution of the Problem

The electroosmotic flow (EOF) of an electrolyte solution past a membrane consisting of poly-electrolyte coated solid cylindrical particles is considered where the separate governing equations are formed for different regions in the flow domain. The fluid flow through membrane is modeled using the unit cell model according to which, the flow regime is divided into two segments, one is the FCL region which is a porous layer of poly-electrolyte fibers, in which the fluid flow is governed using the Brinkann-Forchheimer equation. Second is the clear fluid region enclosed by a hypothetical cell, in which the flow is governed by Stokes equation. The linearized Poisson-Bolzmann equations were solved analytically in cylindrical coordinate system and the respective solution is further used in the electroosmotic body force terms in the hydrodynamic equations. Now, due to the non-linear Forchheimer terms and external body force term (electric force), analytical solution for the system of governing equations is difficult to derive. Hence The the regular and singular perturbation methods were applied to derive the asymptotic analytical expressions of the solution. A constant pressure gradient continuously propels the fluid in the PEL and clear fluid regions, *i.e.*, $\frac{\partial p}{\partial z} = -p_s = \text{constant}$.

8.3.1 Solution of Poisson-Boltzmann equation

The equations 8.16 and 8.17 can be solved analytically and the exact form of their solution is given as

$$\psi_p(r) = \frac{1}{K^2} + p_1 I_0\left(\frac{r}{\lambda}\right) + p_2 K_0\left(\frac{r}{\lambda}\right), \tag{8.27}$$

$$\psi_p(r) = p_3 I_0\left(\frac{r}{\lambda}\right) + p_4 K_0\left(\frac{r}{\lambda}\right), \tag{8.28}$$

where, p_1, p_2, p_3, and p_4 are constants, which will be evaluated using the boundary conditions (8.20a)-(8.20d) and are given as

$$\begin{aligned}
p_1 &= \frac{K_1\left(\frac{c}{\lambda}\right)\left(I_1\left(\frac{1}{\lambda}\right)K_0\left(\frac{a}{\lambda}\right) + \lambda\left(\zeta K^2 - 1\right)\right) - K_1\left(\frac{1}{\lambda}\right)K_0\left(\frac{a}{\lambda}\right)I_1\left(\frac{c}{\lambda}\right)}{K^2\left(\lambda K_0\left(\frac{a}{\lambda}\right)I_1\left(\frac{c}{\lambda}\right) + \lambda I_0\left(\frac{a}{\lambda}\right)K_1\left(\frac{c}{\lambda}\right)\right)}, \\
p_2 &= \frac{I_1\left(\frac{c}{\lambda}\right)\left(K_1\left(\frac{1}{\lambda}\right)I_0\left(\frac{a}{\lambda}\right) + \lambda\left(\zeta K^2 - 1\right)\right) - I_1\left(\frac{1}{\lambda}\right)I_0\left(\frac{a}{\lambda}\right)K_1\left(\frac{c}{\lambda}\right)}{K^2\left(\lambda K_0\left(\frac{a}{\lambda}\right)I_1\left(\frac{c}{\lambda}\right) + \lambda I_0\left(\frac{a}{\lambda}\right)K_1\left(\frac{c}{\lambda}\right)\right)}, \\
p_3 &= \frac{K_1\left(\frac{c}{\lambda}\right)\left(I_1\left(\frac{1}{\lambda}\right)K_0\left(\frac{a}{\lambda}\right) + K_1\left(\frac{1}{\lambda}\right)I_0\left(\frac{a}{\lambda}\right) + \lambda\left(\zeta K^2 - 1\right)\right)}{K^2\left(\lambda K_0\left(\frac{a}{\lambda}\right)I_1\left(\frac{c}{\lambda}\right) + \lambda I_0\left(\frac{a}{\lambda}\right)K_1\left(\frac{c}{\lambda}\right)\right)}, \\
p_4 &= \frac{I_1\left(\frac{c}{\lambda}\right)\left(I_1\left(\frac{1}{\lambda}\right)K_0\left(\frac{a}{\lambda}\right) + K_1\left(\frac{1}{\lambda}\right)I_0\left(\frac{a}{\lambda}\right) + \lambda\left(\zeta K^2 - 1\right)\right)}{K^2\left(\lambda K_0\left(\frac{a}{\lambda}\right)I_1\left(\frac{c}{\lambda}\right) + \lambda I_0\left(\frac{a}{\lambda}\right)K_1\left(\frac{c}{\lambda}\right)\right)}.
\end{aligned} \tag{8.29}$$

8.3.2 Solution of Hydrodynamic Equations

The hydrodynamic equation governing the fluid flow in porous region is a second order non-linear equation with non-homogeneity of body forces as pressure gradient and electroosmotic force, finding the exact analytical solution of this equation is intractable. To overcome this difficulty we have used the regular and singular perturbation technique in the case of large and small Darcy number, respectively.

8.3.3 Large Permeability $(k \gg 1)$

The governing equations for porous or non porous regions in case of the large Darcy number are given as

$$\frac{\mu_R^2}{r}\frac{\partial}{\partial r}\left(r\frac{\partial w_p}{\partial r}\right)-\frac{S^2 w_p}{\left(1-\varepsilon_f r\right)^2}-\frac{SF\mu_R^2 w_p^2}{\left(1-\varepsilon_f r\right)}=\frac{\partial p}{\partial z}-\frac{\psi_p}{\lambda^2}, \tag{8.30}$$

$$\frac{1}{r}\frac{\partial}{\partial r}\left(r\frac{\partial w_c}{\partial r}\right)=\frac{\partial p}{\partial z}-\frac{\psi_c}{\lambda^2}, \tag{8.31}$$

Depending on the position of perturbation parameter in the governing equation, the regular perturbation technique will be used to solve the above-mentioned governing equations. The perturbation series expansions, expressed in the powers of a small Darcy number, provide a direct representation for velocities in distinct porous and non-porous regions

$$w_i(r;S)=w_{io}(r)+Sw_{i1}(r)+S^2w_{i2}(r)+O(S^3), \tag{8.32}$$

where the subscription index $i=p,c$, represents the porous and clear fluid regions, respectively. Equating the coefficient of S in equation (8.30) and (8.31), the zeroth order equations are

$$\frac{\mu_R^2}{r}\frac{\partial}{\partial r}\left(r\frac{\partial w_{p0}}{\partial r}\right)=\frac{\partial p}{\partial z}-\frac{\psi_p}{\lambda^2}, \tag{8.33}$$

$$\frac{1}{r}\frac{\partial}{\partial r}\left(r\frac{\partial w_{c0}}{\partial r}\right)=\frac{\partial p}{\partial z}-\frac{\psi_c}{\lambda^2}, \tag{8.34}$$

Equation (8.33) and (8.34) can be solve analytically using the expressions of electric potential in equations (8.27) and (8.28). Then exact form of solutions are given as

$$w_{p0}(r)=-\frac{r^2\left(\lambda^2K^2p_s+1\right)}{4\lambda^2K^2\mu_R^2}-\frac{p_1\left(I_0\left(\frac{r}{\lambda}\right)-1\right)+p_2K_0\left(\frac{r}{\lambda}\right)}{\mu_R^2}+c_1\log(r)+c_2 \tag{8.35}$$

$$w_{c0}(r)=-\frac{1}{4}r^2p_s-p_3I_0\left(\frac{r}{\lambda}\right)+p_3-p_4K_0\left(\frac{r}{\lambda}\right)+c_3\log(r)+c_4 \tag{8.36}$$

where, c_1, c_2, c_3, and c_4 are constant, which will be evaluated using the boundary conditions (8.20a)-(8.20d) and are given as

$$c_1 = \frac{c^2\lambda^2K^2p_s + 2\lambda K^2\left(cp_3I_1\left(\frac{c}{\lambda}\right) - cp_4K_1\left(\frac{c}{\lambda}\right) + (p_1-p_3)I_1\left(\frac{1}{\lambda}\right) + (p_4-p_2)K_1\left(\frac{1}{\lambda}\right)\right) + 1}{2\lambda^2K^2\mu_R^2},$$

$$\begin{aligned} c_2 = &\frac{1}{4\lambda^2K^2\mu_R^2}\left(a^2\left(\lambda^2K^2p_s+1\right) - 2\log(a)\left(c^2\lambda^2K^2p_s+1\right) + 4\lambda K^2\left(-cp_3\log(a)I_1\left(\frac{c}{\lambda}\right)\right.\right. \\ &+cp_4\log(a)K_1\left(\frac{c}{\lambda}\right) + \lambda p_1I_0\left(\frac{a}{\lambda}\right) + \lambda p_2K_0\left(\frac{a}{\lambda}\right) + (p_3-p_1)\log(a)I_1\left(\frac{1}{\lambda}\right) + (p_2-p_4)\times \\ &\left.\left.\log(a)K_1\left(\frac{1}{\lambda}\right) - \lambda p_1\right)\right), \end{aligned}$$

$$c_3 = \frac{c\left(2p_3I_1\left(\frac{c}{\lambda}\right) - 2p_4K_1\left(\frac{c}{\lambda}\right) + c\lambda p_s\right)}{2\lambda},$$

$$\begin{aligned} c_4 = &\frac{1}{4\lambda^2K^2\mu_R^2}\left(\left(a^2-1\right)\left(\lambda^2K^2p_s+1\right) - 2\log(a)\left(c^2\lambda^2K^2p_s+1\right) + 4\lambda K^2\left(p_3\left(\log(a)\left(I_1\left(\frac{1}{\lambda}\right)\right.\right.\right.\right. \\ &\left.\left.\left.\left.-cI_1\left(\frac{c}{\lambda}\right)\right) + \lambda\mu_R^2\left(I_0\left(\frac{1}{\lambda}\right)-1\right)\right) + p_4\left(c\log(a)K_1\left(\frac{c}{\lambda}\right) - \log(a)K_1\left(\frac{1}{\lambda}\right) + \lambda\mu_R^2K_0\left(\frac{1}{\lambda}\right)\right)\right. \\ &-\left(p_1\left(-\lambda I_0\left(\frac{a}{\lambda}\right) + \log(a)I_1\left(\frac{1}{\lambda}\right) + \lambda I_0\left(\frac{1}{\lambda}\right)\right)\right) + p_2\left(\lambda K_0\left(\frac{a}{\lambda}\right) + \log(a)K_1\left(\frac{1}{\lambda}\right)\right. \\ &\left.\left.\left.-\lambda K_0\left(\frac{1}{\lambda}\right)\right)\right) + \lambda^2K^2\mu_R^2p_s\right). \end{aligned} \tag{8.37}$$

The first order equations are

$$\frac{\mu_R^2}{r}\frac{\partial}{\partial r}\left(r\frac{\partial w_{p1}}{\partial r}\right) - \frac{F\mu_R^2w_{p0}^2}{(1-\varepsilon_f r)} = 0, \tag{8.38}$$

$$\frac{1}{r}\frac{\partial}{\partial r}\left(r\frac{\partial w_{c1}}{\partial r}\right) = 0. \tag{8.39}$$

The solution is given as

$$\begin{aligned} w_{p1}(r) = &c_5\log(r) + c_6 - \log(r)\int_a^r\left(-r\left(F\mu_R^2w_{p0}^2\left(1+\varepsilon_f r+\varepsilon_f^2r^2\right)\right)\right)dr \\ &+\int_a^r\left(-r\log(r)\left(F\mu_R^2w_{p0}^2\left(1+\varepsilon_f r+\varepsilon_f^2r^2\right)\right)\right)dr, \end{aligned} \tag{8.40}$$

$$w_{c1}(r) = c_7\log(r) + c_8. \tag{8.41}$$

The second order equations are

$$\frac{\mu_R^2}{r}\frac{\partial}{\partial r}\left(r\frac{\partial w_{p2}}{\partial r}\right) - \frac{w_{p0}}{(1-\varepsilon_f r)^2} - \frac{F\mu_R^2w_{p0}w_{p1}}{(1-\varepsilon_f r)} = 0, \tag{8.42}$$

$$\frac{1}{r}\frac{\partial}{\partial r}\left(r\frac{\partial w_{c2}}{\partial r}\right)=0. \tag{8.43}$$

The solution is given as

$$\begin{aligned} w_{p1}(r) =& -\log(r)\int_a^r\left(-r\left(w_{p0}(1+2\varepsilon_f r+3\varepsilon_f^2 r^2)+F\mu_R^2 w_{p0}w_{p1}\left(1+\varepsilon_f r+\varepsilon_f^2 r^2\right)\right)\right)dr \\ &+\int_a^r\left(-r\log(r)\left(w_{p0}(1+2\varepsilon_f r+3\varepsilon_f^2 r^2)+F\mu_R^2 w_{p0}w_{p1}\left(1+\varepsilon_f r+\varepsilon_f^2 r^2\right)\right)\right)dr \\ &+c_9\log(r)+c_{10}. \end{aligned} \tag{8.44}$$

$$w_{c1}(r) = c_{11}\log(r)+c_{12}. \tag{8.45}$$

8.3.4 Small Permeability $(k \ll 1)$

8.3.4.1 Solution for the Porous Region

Taking into account the low permeability of the porous medium $k \ll 1$, the parameter $S \gg 1$ exhibits significant enlargement. The equations governing the flow of an electrolyte through a swarm of porous layered cylindrical particles will transform into a singularly perturbed boundary value problem, with the parameter $S^{-1} = S_1 \ll 1$, where $S = \frac{1}{k}$ and k is the permeability of the porous medium. Finding analytical solutions for these singularly perturbed boundary value problems presents a significant challenge. The equation describing the flow of an electrolyte solution through porous region is presented in terms of S^{-1} as follows:

$$\frac{S_1^2\mu_R^2}{r}\frac{\partial}{\partial r}\left(r\frac{\partial w_p}{\partial r}\right)-\frac{w_p}{\left(1-\varepsilon_f r\right)^2}-\frac{S_1 F\mu_R^2 w_p^2}{\left(1-\varepsilon_f r\right)}=S_1^2\frac{\partial p}{\partial z}-S_1^2\frac{\psi_p}{\lambda^2}, \tag{8.46}$$

Outer Solution

$$w_p^o(r;S_1) = w_{p0}+S_1 w_{p1}+S_1^2 w_{p2}+S_1^3 w_{p3}+S_1^4 w_{p4}+S_1^5 w_{p5}+O(S_1^6) \tag{8.47}$$

The series form of velocity is introduced in the equation (8.46) and equated the like power of the parameter S_1.

$$w_{p0}=0,\ w_{p1}=0,\ w_{p2}=(r\varepsilon_f-1)^2\left(\frac{\frac{1}{K^2}+p_1 I_0\left(\frac{r}{\lambda}\right)+p_2 K_0\left(\frac{r}{\lambda}\right)}{\lambda^2}+p_s\right),\ w_{p3}=0,$$

$$\begin{aligned} w_{p4} =& \frac{\mu_R^2(r\varepsilon_f-1)^2}{\lambda^4 K^2 r}\left(K^2\left(p_1\left(I_0\left(\frac{r}{\lambda}\right)\left(2\lambda^2\varepsilon_f(2r\varepsilon_f-1)+r(r\varepsilon_f-1)^2\right)+4\lambda r\varepsilon_f(r\varepsilon_f-1)I_1\left(\frac{r}{\lambda}\right)\right)\right.\right. \\ &\left.\left.+p_2\left(K_0\left(\frac{r}{\lambda}\right)\left(2\lambda^2\varepsilon_f(2r\varepsilon_f-1)+r(r\varepsilon_f-1)^2\right)-4\lambda r\varepsilon_f(r\varepsilon_f-1)K_1\left(\frac{r}{\lambda}\right)\right)\right)+(2r\varepsilon_f-1)\times \end{aligned}$$

$$2\lambda^2\varepsilon_f\left(\lambda^2K^2p_s+1\right)\Big),$$
$$w_{p5}=\frac{F\mu_R^2(r\varepsilon_f-1)^5\left(K^2\left(p_1I_0\left(\frac{r}{\lambda}\right)+p_2K_0\left(\frac{r}{\lambda}\right)\right)+\lambda^2K^2p_s+1\right)^2}{\lambda^4K^4}. \tag{8.48}$$

Inner Solution

To derive the solution for the boundary layer region, a streatching variable (inner variable) will be defined at the right end of porous domian, which will be introduced as

$$\eta=\frac{1-r}{S_1}, \tag{8.49}$$

Introducing these inner variables in the boundary value problem (8.46) and neglecting the smaller terms $(S^{-1}\to 0)$. equation (8.46) is reduced to

$$\mu_R^2\frac{\partial^2 w_p(\eta)}{\partial\eta^2}-\left(1+2\varepsilon_f+3\varepsilon_f^2\right)w_p(\eta)=0 \tag{8.50}$$

The above equation can be solved exactly and their one term bounded solution is represented as

$$w_p^i(r)=c_{13}e^{-\frac{(1-r)\sqrt{1+2\varepsilon_f+3\varepsilon_f^2}}{\mu_RS_1}}+c_{14}e^{\frac{(1-r)\sqrt{1+2\varepsilon_f+3\varepsilon_f^2}}{\mu_RS_1}}. \tag{8.51}$$

Since the boundary layer is assumed on the right side of the porous domain, $(r=1)$, the condition on the left side of the porous domain $(r=a)$ i.e. the no slip boundary condition should be omitted. The constant c_{14} is considered to be vanished due to boundness of the solution under the limit $(\eta\to\infty)$; however, the expression of c_{13} will be derived using the fluid-porous interface boundary condition.

Matching Procedure

The outer solution in terms of inner limit is stated as,

$$(w_p^o)^i=\lim_{S\to+\infty}w_p^o=0, \tag{8.52a}$$

The inner solution in terms of outer limit is stated as,

$$(w_p^i)^o=\lim_{\eta\to+\infty}w_p^o=0, \tag{8.53a}$$

It can be observed from the equations (22) and (23) that the Prandtl's matching condition $(w_p^o)^{in}=(w_p^{in})^o=w_p^m$ is satisfied, where, w_p^m is the matched solution of both inner and outer

solutions. The matching solution is

$$w_p^m = 0. \tag{8.54a}$$

By using the inner and outer solutions the expression of composite solution of velocities for three different regions is

$$w_p = w_p^o + w_p^i - w_p^m. \tag{8.55a}$$

8.3.4.2 Solution for the Clear Fluid Region

The governing equations for clear fluid regions is

$$\frac{1}{r}\frac{\partial}{\partial r}\left(r\frac{\partial w_c}{\partial r}\right) = \frac{\partial p}{\partial z} - \frac{1}{\lambda^2}\left(p_3 I_0\left(\frac{r}{\lambda}\right) + p_4 K_0\left(\frac{r}{\lambda}\right)\right) \tag{8.56}$$

The Solution is given as

$$w_c(r) = -\frac{1}{4}r^2 p_s - p_3 I_0\left(\frac{r}{\lambda}\right) + p_3 - p_4 K_0\left(\frac{r}{\lambda}\right) + c_{15}\log(r) + c_{16} \tag{8.57}$$

The constants $c_{13}, c_{15},$ and c_{16} will be derived using the following set of boundary conditions

$$w_p = w_c \quad \text{at} \quad r = 1 \tag{8.58}$$

$$\mu_R^2 \frac{dw_p}{dr} - \frac{dw_c}{dr} = \frac{\beta}{\sqrt{k}} w_p, \quad \text{at} \quad r = 1, \tag{8.59}$$

$$\frac{dw_c}{dr} = 0, \quad \text{at} \quad r = c. \tag{8.60}$$

8.4 Results and Discussion

The present study explores the effects of the electroosmotic forces in a flow past a membrane composed of swarm of poly electrolyte layered solid cylindrical particles. The aim of this study is to reveal the effect of porous medium parameters such as Darcy number, permeability parameter, Forchheimer number, stress jump coefficient, and electroosmotic parameters such as EDL thickness, zeta potential, fixed charge density in FCL, etc. on the flow velocities and hydrodynamic quantities like hydrodynamic permeability and Kozeny constant. The envisioned work's physical sketch is designed such that the Brinkmann-Forchheimer equation governs the fluid flow in poly-electrolyte layer (porous layer), where the permeability

of the medium is considered in a variable nature with permeability parameter ε_f signifying changes in permeability with radial direction. Along with that the Stokes' equation governs the electroosmotic flow in clear fluid medium (non-porous layer) enclosed by a virtual cell. The effect of porous medium and external body forces (electroosmotic force, pressure gradient, etc.) leads to generate a non homogeneous nonlinear set of governing equations which are handled in an asymptotic manner using regular and singular perturbation techniques. The analytical expressions of fluid velocity, Hydrodynamic permeability, and Kozeny constant were then used to analyze the effect of EDL thickness (λ), fix charge density (λ_f), zeta potential (ζ), stress jump parameter (β), Forchheimer number (F), permeability parameter (ε_f), Darcy number (k), viscosity ratio parameter (μ_R), particle volume fraction (γ), etc. Additionally, a reduction of special cases and validation of current work with previously published works is performed.

8.4.1 Parameter Selection

Measuring the movement of a fluid presents a challenge, as it requires estimating the mass or volume of the substance as it moves through a pipe or conduit. Complications may arise due to the complex nature of fluid flow dynamics. Quantifying physical factors is generally difficult in the realm of flow measurements. The table below outlines the range of parameter values, which vary depending on the applications in different fields. All the vital parameters listed in this table have been comprehensively explained in their respective cited sources, giving the reader a better understanding of the underlying concepts.

Range of Parameters		
Parameters	Range	Sources
EDL thickness λ	(0,0.5)	[22], [23]
Equivalent EDL thickness λ_f	(0,0.5)	[22]
zeta potential ζ	(0.8,1.0)	[22]
Steady pressure gradient p_s	1-10	[5], [167]
Permeability k	$(0,\infty)$	[2], [3]
Forchheimer number F	0.0-3.0	[7], [8]
Stress-jump parameter β	$(-1,1)$	[3], [5]
Viscosity ratio parameter μ_R	1.0-1.6	[207], [167]
Particle volume fraction γ	0.1-1.0	[3], [96]
Variable permeability parameter ε_f	0.0-0.9	[24]
Porosity parameter ε	0.3-1.0	[3]

Table 8.1: Ranges for the ongoing parameters with their references

8.4.2 Electric Potential

The distribution of electric potential depends significantly on electroosmotic parameters and is affected in both the fixed charge layer of poly-electrolytes and the clear fluid region. Increasing the thickness of the Electric Double Layer (EDL) corresponds to a greater movement of ions from the bulk electrolyte to the interface of the Fixed Charge Layer (FCL) and the clear fluid region. This movement enhances the electric potential within the EDL region. Simultaneously, as the EDL layer thickens, a decrease in potential in the FCL region can be observed (as shown in Figure 8.3a). This decrease is attributed to the reduced ionic concentration inside the FCL region. It should be noted that in Figure 8.3a, the parameter K (the ratio of characteristic scale of the mobile charges to the fixed charges within the FCL region) is fixed at a value 1, which ensures a similar enhancement of the equivalent EDL thickness in the FCL region. The relatively larger values of parameter K corresponds to the increasing thickness of equivalent EDL in FCL region, which reduces the number density of the FCL ions, resulting in decrement of the electric potential in both FCL and clear fluid regions (Figure 8.3b). As the zeta potential increases at the solid wall of the cylindrical particle, the rate at which the electric potential decays also increases; however this decay rate is particularly significant in the FCL region. (Figure 8.4)

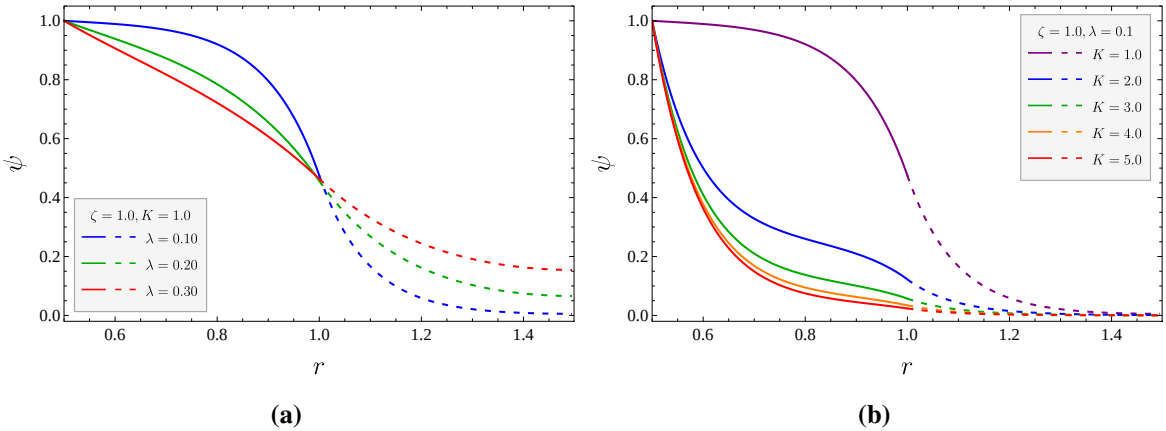

(a) **(b)**

Figure 8.3: The electric potential distribution ψ in radial direction r with varying **(a)** thicknesses of EDL layer λ $(K = 1)$, **(b)** ratio parameter K $(\lambda = 0.1)$. $(a = 0.5, \gamma = 0.445, \zeta = 1)$

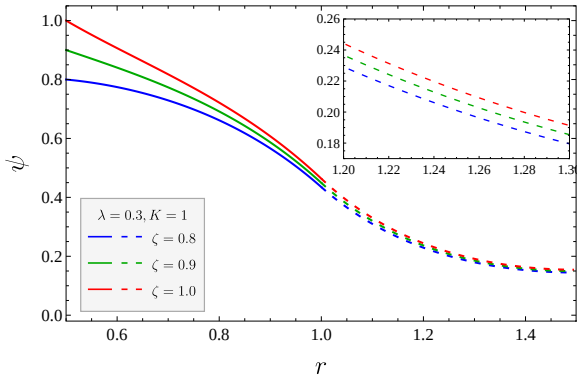

Figure 8.4: The electric potential distribution ψ in radial direction r with varying zeta potential ζ $(K = 1, \lambda = 0.1)$. $(a = 0.5, \gamma = 0.445)$

8.4.3 Velocity Profile

The dimensionless velocity of electrolyte as a function of radial distance r shows variations with respect to electroosmotic and porous medium parameters, which are showed in Figures 8.5 to 8.11. Figure 8.5 illustrates how the thickness of the Electric Double Layer (EDL) affects the flow of electrolyte fluid, considering both high and low permeability cases. As the EDL thickness increases while upholding the ratio of the characteristic scale of the mobile charges to the fixed charges within the FCL region at unity, causes a diminished ion concentration in the FCL region, which will decrease the electric potential and, hence, the electrolyte fluid velocity. This reduction in fluid velocity can be confirmed by equations (8.18) and (8.19). Additionally, the augmentation of Electric Double Layer (EDL) thickness within the clear fluid region leads to an increase in the number of ions having lower mobility compared to the bulk electrolyte in the vicinity of FCL and clear fluid interface. This

occurrence stems from the restricted space and interactions with other ions and the charged surface, which leads to a reduced velocity gradient within the EDL region, contributing to the overall decrease in flow velocity.

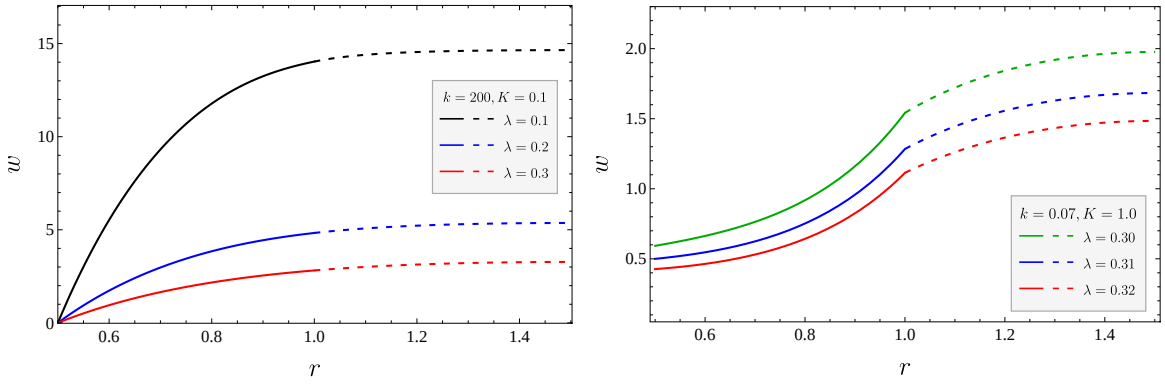

(a) **(b)**

Figure 8.5: The dependence of velocity profile w on the radial distance r for different values of EDL thicknesses (λ) in case of **(a)** large Darcy number ($k = 200, \zeta = 1, \varepsilon_f = 0.5$), **(b)** small Darcy number ($k = 0.07, \zeta = 0.8, \varepsilon_f = 0.1$). ($\gamma = 0.444, K = 1, p_s = 1, \mu_R = 1.0, \beta = 0.4, F = 1$)

In Figures 8.6, the velocity profile decreases for both high and low permeability cases as the ratio parameter K increases. This rise in K corresponds to a decline in electric potential across both the Fixed Charge Layer and the clear fluid region, attributed to the low ionic concentration of fixed charges within the poly-electrolyte layer. Moreover, it is noticeable that the rate of reduction in fluid velocity diminishes as the ratio parameter K attains higher values, particularly evident in the case of high permeability.

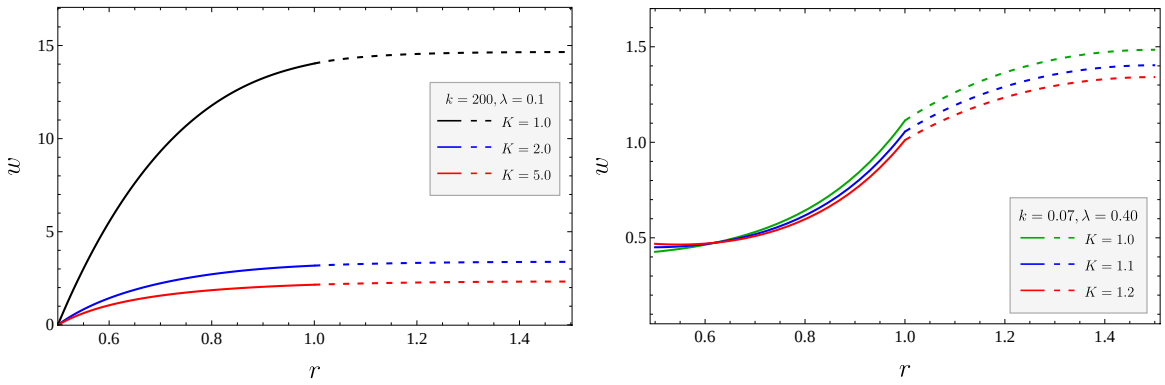

(a) **(b)**

Figure 8.6: The dependence of velocity profile w on the radial distance r for different values of ratio parameter (K) in case of **(a)** large Darcy number ($k = 200, \zeta = 1, \lambda = 0.1, \varepsilon_f = 0.5$), **(b)** small Darcy number ($k = 0.07, \zeta = 0.8, \lambda = 0.4, \varepsilon_f = 0.1$). ($\gamma = 0.444, p_s = 1, \mu_R = 1.0, \beta = 0.4, F = 1$)

Figure 8.7 analyses the influence of the variable permeability of poly-electrolyte layer region on the velocity profile, where the increasing permeability parameter corresponds to a decrease in the overall permeability of PEL region, resulting in an enhanced drag which reduces the flow velocity in both small and large permeability cases.

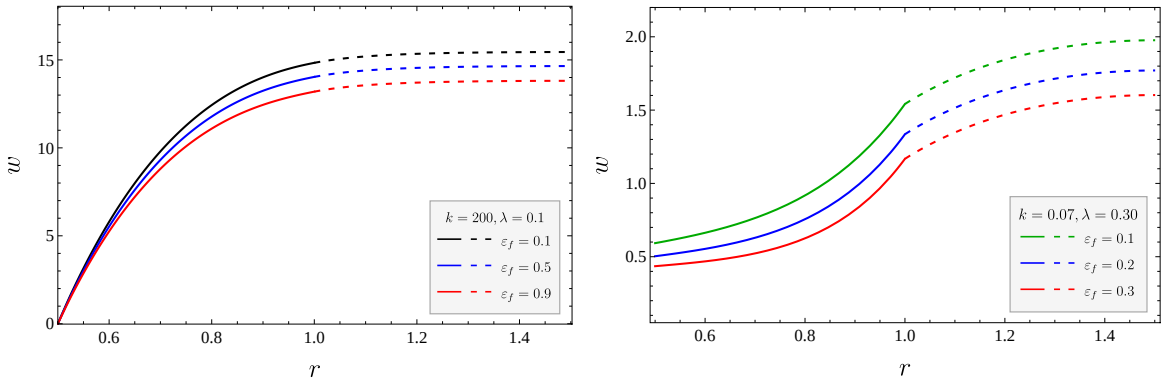

(a) **(b)**

Figure 8.7: The dependence of velocity profile w on the radial distance r for different values of variable permeability parameter (ε_f) in case of **(a)** large Darcy number $(k = 200, \zeta = 1, \lambda = 0.1)$, **(b)** small Darcy number $(k = 0.07, \zeta = 0.8, \lambda = 0.3)$. $(\gamma = 0.444, p_s = 1, K = 1, \mu_R = 1.0, \beta = 0.4, F = 1)$

An augmentation in the fluid's velocity can be seen in response to the increased values of zeta potential in Figure 8.8, which can be interpreted as the increasing zeta potential enhances the overall potential distribution in the flow domain, which enhances the velocity profiles according to equations (8.18) and (8.19) in both small and large permeability cases.

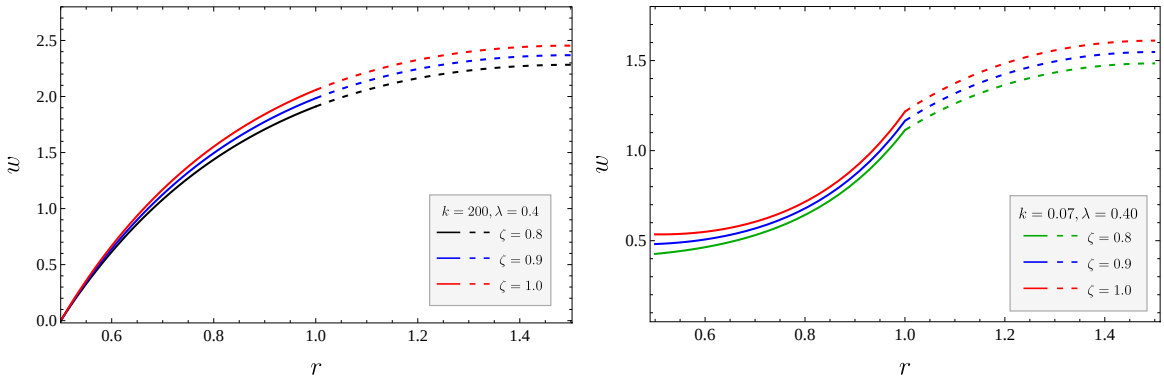

(a) **(b)**

Figure 8.8: The dependence of velocity profile w on the radial distance r for different values of zeta potential (ζ) in case of **(a)** large Darcy number $(k = 200, \lambda = 0.1, \varepsilon_f = 0.5)$, **(b)** small Darcy number $(k = 0.07, \lambda = 0.3, \varepsilon_f = 0.1)$. $(\gamma = 0.444, p_s = 1, K = 1, \mu_R = 1.0, \beta = 0.4, F = 1)$

In Figure 8.9, the correlation between effective viscosity and constant viscosity reveals a notable dependence on fluid flow. As the viscosity ratio parameter rises, the prominence of effective viscosity over constant viscosity becomes apparent. Consequently, this leads to heightened viscous drag in porous layer and a subsequent reduction in fluid velocity. Additionally, in the case of small permeability, the influence of the stress jump parameter vanishes with the growing dominance of effective viscosity over fluid viscosity; However this effect is almost unnoticeable in the case of large permeability owing to large values of the Darcy number.

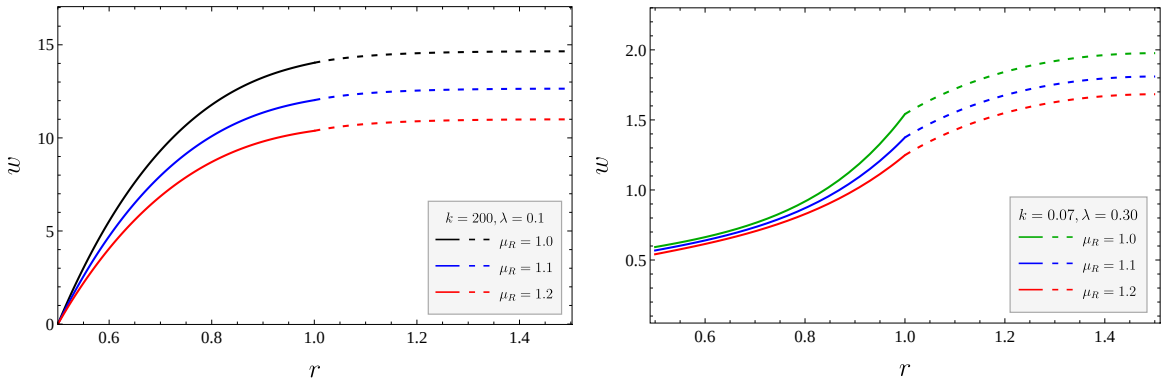

(a) **(b)**

Figure 8.9: The dependence of velocity profile w on the radial distance r for different values of viscosity ratio parameter (μ_R) in case of **(a)** large Darcy number $(k = 200, \zeta = 0.8, \lambda = 0.1, \varepsilon_f = 0.5)$, **(b)** small Darcy number $(k = 0.07, \zeta = 1, \lambda = 0.3, \varepsilon_f = 0.1)$. $(\gamma = 0.444, p_s = 1, K = 1, \beta = 0.4, F = 1)$

Figure 8.10 demonstrates that an increase in the stress jump parameter results in an increased fluid velocity across both large and small permeability cases. This increment in fluid velocity is particularly pronounced in the case of the small Darcy number. This observation can be interpreted from the fact that smaller permeability values magnify the disparity in shear stress at the fluid-porous interface, thereby enhancing the influence of the stress jump parameter.

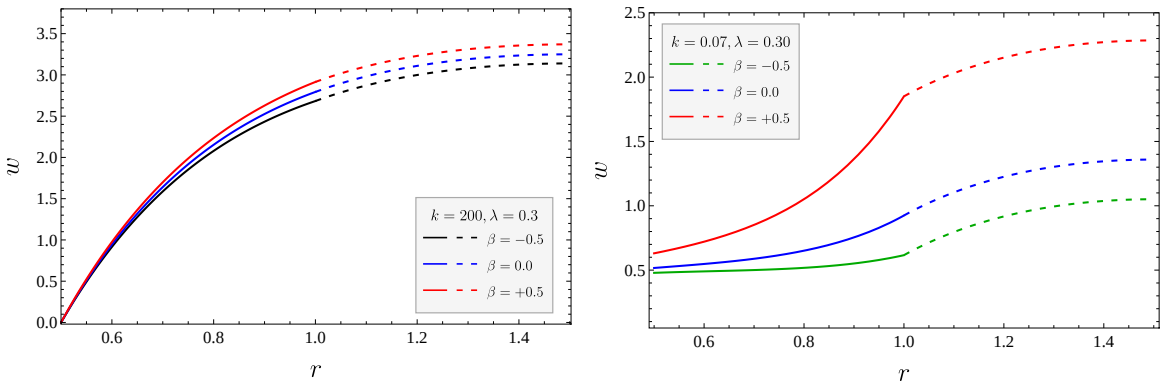

(a) **(b)**

Figure 8.10: The dependence of velocity profile w on the radial distance r for different values of stress-jump parameter (β) in case of **(a)** large Darcy number $(k = 200, \zeta = 0.8, \lambda = 0.1, \varepsilon_f = 0.5)$, **(b)** small Darcy number $(k = 0.07, \zeta = 1, \lambda = 0.3, \varepsilon_f = 0.1)$. $(\gamma = 0.444, p_s = 1, K = 1, \mu_R = 1.0, F = 1)$

The Forchheimer number parameter F signifies the impact of inertial resistance within the porous medium, where higher values result in a decrease in fluid velocity across both high and low permeability cases. However, the effect of inertial resistance is more pronounced in small permeability cases (Figure 8.11). This difference can be attributed to the smaller values of the Darcy number, which amplify the magnitude of the non-linear Forchheimer term in equation (8.18).

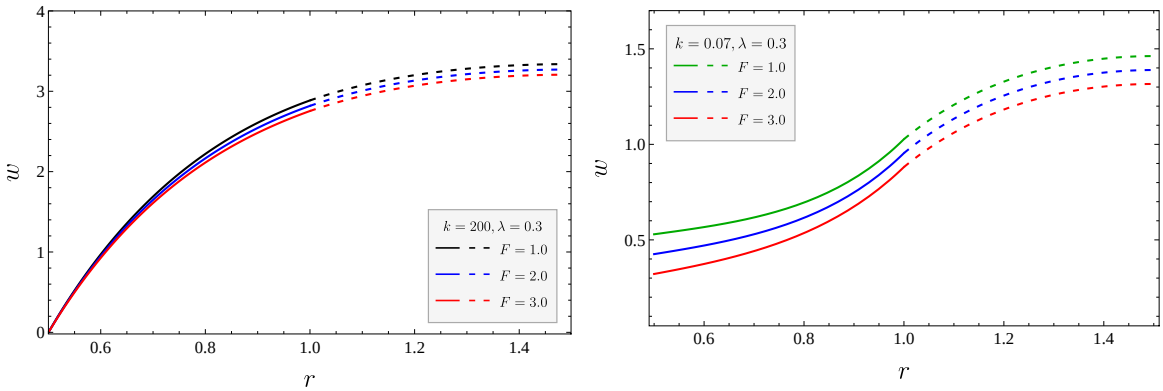

(a) **(b)**

Figure 8.11: The dependence of velocity profile w on the radial distance r for different values of Forchheimer number (F) in case of **(a)** large Darcy number $(k = 200, \zeta = 0.8)$, **(b)** small Darcy number $(k = 0.07, \zeta = 1)$. $(\gamma = 0.444, p_s = 1, K = 1, \lambda = 0.3, \mu_R = 1.0, \varepsilon_f = 0.1, \beta = 0.4)$

8.4.4 Hydrodynamic Permeability

This subsection investigates the impact of various electroosmotic parameters—such as EDL thickness λ, equivalent EDL thickness in the Fixed Charge Layer region λ_f, and zeta potential ζ, as well as porous parameters—including the Forchheimer number F, Darcy number k, variable permeability parameter ε_f, stress-jump parameter β, and viscosity ratio parameter μ_R—along with the particle volume fraction γ of the membrane on the hydrodynamic permeability denoted as L_{11}. Figure 8.12 depicts the relation of hydrodynamic permeability with particle volume fraction for different thickness of EDL region. The hydrodynamic permeability of membrane shows a decaying behavior with increasing particle volume fraction, which can be attributed to the increased occupancy of poly-electrolyte grafted solid cylindrical particles in the bulk electrolyte fluid region, reducing the size of clear fluid region and hence the hydrodynamic permeability of the membrane. Moreover, the increasing thickness of EDL in the clear fluid region leads to a diminished hydrodynamic permeability for both large and small permeability cases, which can be physically justified with the argument that the expansion of the EDL region is associated with an augmentation of the ionic density inside this layer, leading to high resistance against the axial velocity resulting in a decay be in the dimensionless velocity, consequently, a decay in the hydrodynamic permeability. It can also depicted from figure 8.12 that an increasing thickness of EDL region slightly reduces the dependency of particle volume fraction on hydrodynamic permeability of the membrane.

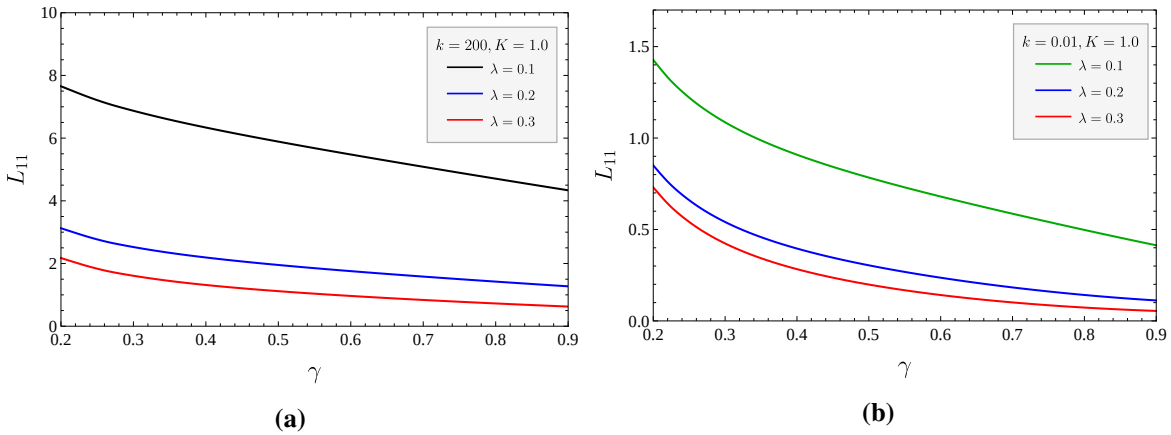

Figure 8.12: The dependence of hydrodynamic permeability L_{11} on the particle volume fraction γ for different EDL thicknesses (λ) in case of **(a)** large Darcy number $(k = 200)$, **(b)** small Darcy number $(k = 0.01)$. $(p_s = K = \zeta = F = \mu_R = 1.0, \varepsilon_f = 0.1, \beta = 0.4)$

Figure 8.13 illustrates the impact of the thickness of the equivalent EDL in the FCL region, denoted as λ_f, on the hydrodynamic permeability of membranes. A noticeable decline

in hydrodynamic permeability is evident with the increasing ratio parameter K, directly proportional to λ_f. Referring back to equation (8.18), it becomes apparent that an increase in λ_f (while keeping other parameters constant) leads to a decrease in the electric potential within the domain. Consequently, this diminishes the driving force exerted by the external electric field, thereby reducing the dimensionless velocity. Furthermore, this analysis can be elucidated by noting that the increasing λ_f corresponds to a decrease in ionic concentration within the poly-electrolyte layer. This decrease in concentration lowers the driving force induced by the external electric field, resulting in reduced velocity and consequently diminishing the hydrodynamic permeability.

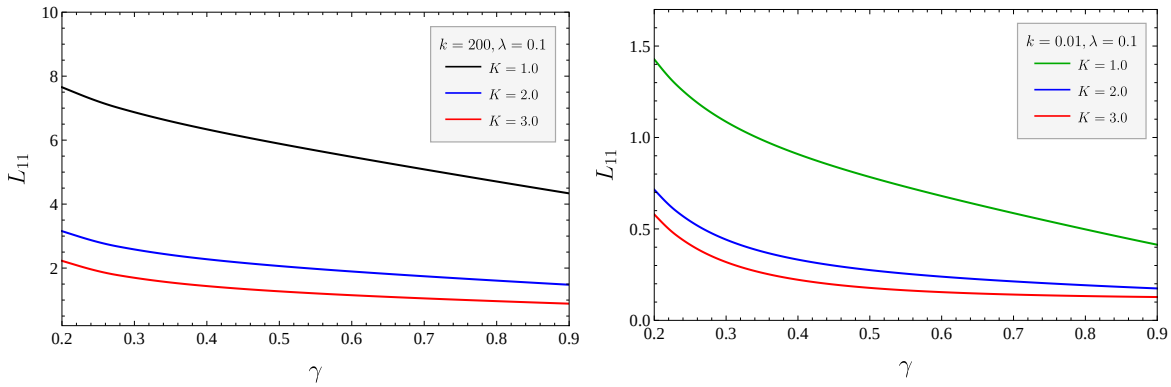

(a) **(b)**

Figure 8.13: The dependence of hydrodynamic permeability L_{11} on the particle volume fraction γ for different ratio parameter (K) in case of **(a)** large Darcy number ($k = 200$), **(b)** small Darcy number ($k = 0.01$). ($p_s = \zeta = F = \mu_R = 1.0, \lambda = 0.1, \varepsilon_f = 0.1, \beta = 0.4$)

In the case of large permeability of PEL region a slight augmentation in the hydrodynamic permeability can be observed in response to the increased zeta potential at the solid surface of the particle; However this effect is almost neglisible for slightly permeable poly-electrolyte layer. The graphical representation of the same can be observed from Figure 8.14b and the behavior can be accessed from equation (8.18) and (8.19).

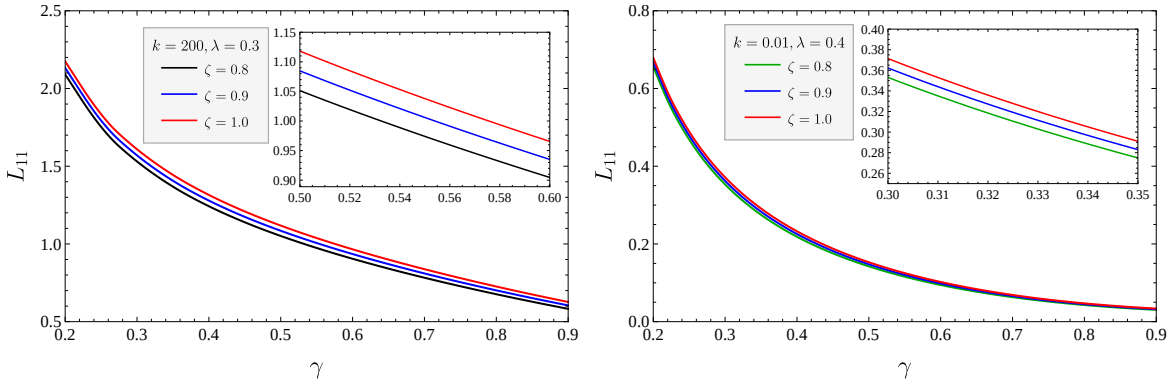

Figure 8.14: The dependence of hydrodynamic permeability (L_{11}) on the particle volume fraction (γ) for different zeta potential (ζ) in case of **(a)** large Darcy number ($k = 200$), **(b)** small Darcy number ($k = 0.01$). ($p_s = K = F = \mu_R = 1.0, \lambda = 0.3, \varepsilon_f = 0.1, \beta = 0.4$)

Figure 8.15 illustrates that an increase in the permeability parameter ε_f, leading to a decrease in the overall permeability of the PEL region, resulting in a reduction of the hydrodynamic permeability of the membrane. This effect of variable permeability on the hydrodynamic permeability is particularly pronounced in the case of the small Darcy number. This prominence can be attributed to the smaller values of the Darcy number, which amplify the drag effect associated with the second and third terms in equation (8.18). Further, a diminished decay rate of L_{11} with respect to ε_f is observed in response to a higher ratio parameter K.

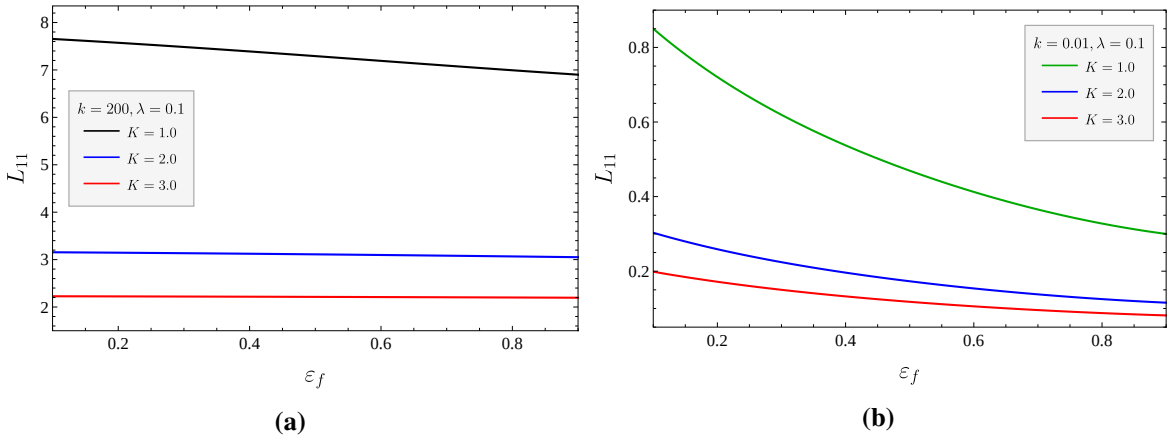

Figure 8.15: The dependence of hydrodynamic permeability (L_{11}) on variable permeability (ε_f) for different ratio parameter (K) in case of **(a)** large Darcy number ($k = 200, \gamma = 0.2$), **(b)** small Darcy number ($k = 0.01, \gamma = 0.44$). ($p_s = \zeta = F = \mu_R = 1.0, \lambda = 0.1, \varepsilon_f = 0.1, \beta = 0.4$)

An augmentation in the stress jump parameter leads to a growth in hydrodynamic permeability for both high and low permeability cases; However this growth rate is higher for

the case of low permeable porous medium owing to a significant contribution of the stress jump coefficient term in the boundary condition 58 for small Darcy number. (Figure 8.16)

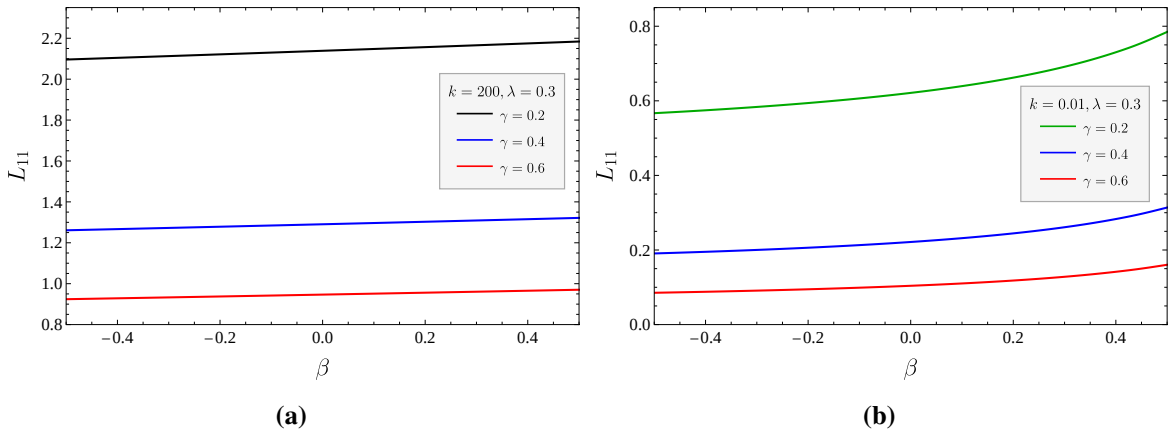

(a) **(b)**

Figure 8.16: The dependence of hydrodynamic permeability (L_{11}) on stress-jump parameter (β) for different particle volume fraction (γ) in case of **(a)** large Darcy number ($k = 200$), **(b)** small Darcy number ($k = 0.01$). ($p_s = \zeta = F = K = \mu_R = 1.0, \lambda = 0.3, \varepsilon_f = 0.1$)

It can be depicted from Figure 8.17 that the decay rate of L_{11} with respect to K is higher, when the values of ratio parameters are in the vicinity of 1, i.e. the EDL thicknesses of FCL and clear fluid regions are of same order; however as the thickness of equivalent EDL in FCL region gets larger relative to EDL in clear fluid region (increasing K), the decay rate of L_{11} gets reduced.

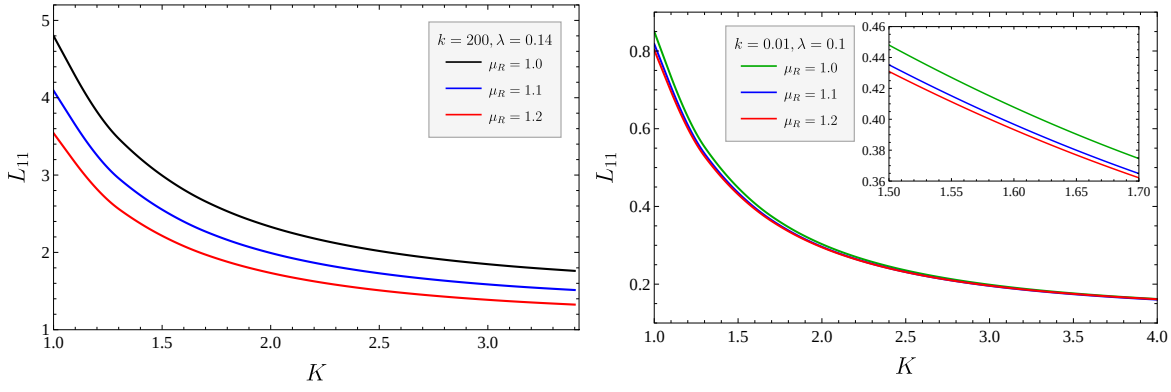

(a) **(b)**

Figure 8.17: The dependence of hydrodynamic permeability (L_{11}) on ratio parameter (K) for different viscosity ratio parameter (μ_R) in case of **(a)** large Darcy number ($k = 200, \gamma = 0.2, \lambda = 0.14$), **(b)** small Darcy number ($k = 0.01, \gamma = 0.444, \lambda = 0.1$). ($p_s = \zeta = F = 1.0, \varepsilon_f = 0.1, \beta = 0.4$)

An augmentation in effective viscosity in comparison to the constant viscosity corresponds to enhancing the viscous drag in the fluid, leads to a decreased permeability of the

membrane. It can be observed from figure 8.18 that the decay rate of hydrodynamic permeability get reduced as the thickness of EDL layer gets enhanced in both cases of permeability.

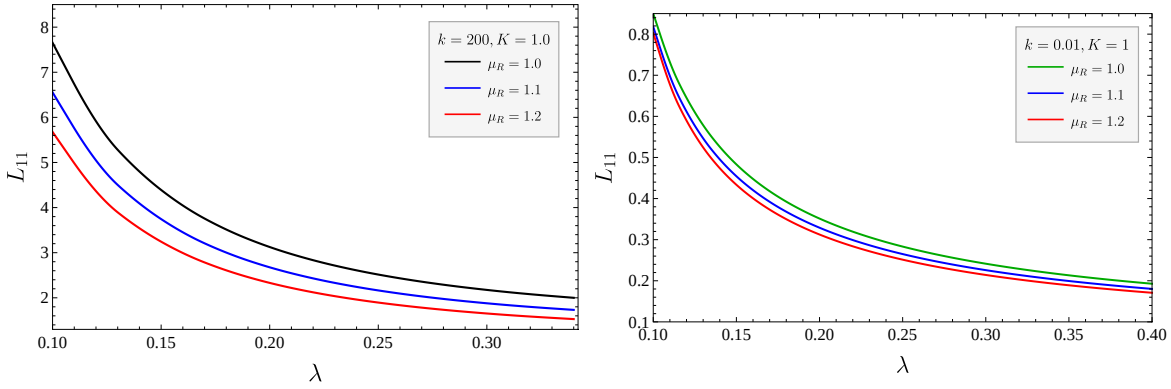

(a) **(b)**

Figure 8.18: The dependence of hydrodynamic permeability (L_{11}) on EDL thickness (λ) for different viscosity ratio parameter (μ_R) in case of **(a)** large Darcy number ($k = 200, \gamma = 0.2$), **(b)** small Darcy number ($k = 0.01, \gamma = 0.444$). ($p_s = \zeta = F = K = 1.0, \varepsilon_f = 0.1, \beta = 0.4$)

8.4.5 Kozeny Constant

The Kozeny constant K_z encapsulates the effects of flow path (tortuosity), particle shape, and their interactions. It can be regarded as directly proportional to tortuosity (Ozgumus et al. [181]). Thus, it is intriguing to examine how electroosmotic parameters influence tortuosity via K_z. The effect of porosity ε on the Kozeny constant for both cases of large and small permeability reveals that the increasing porosity of the poly-electrolyte layer leads to a growth in the Kozeny constant, which is similar to the observation of Madasu and Bucha [11] for the case of Newtonian fluid flow through particles with cavity (Figure 8.19). Additionally, this growth rate get enhanced for larger values of ratio parameter K, signifying the enhanced resistance in the flow domain, which can be attributed to the decreased electric potential in the flow domain due to lower ionic concentration in the FCL region.

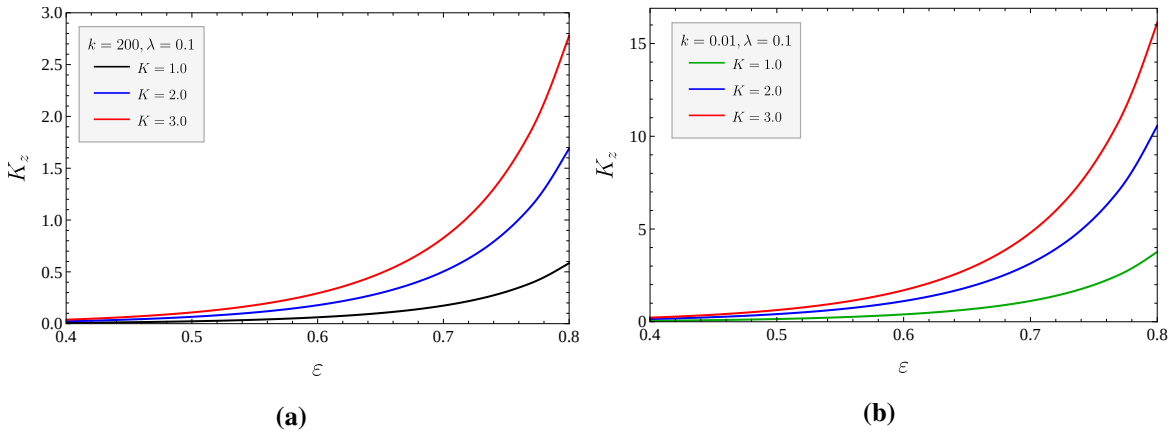

(a) **(b)**

Figure 8.19: The dependence of Kozeny constant (K_z) on porosity of the medium(ε) for different ratio parameter (K) in case of **(a)** large Darcy number ($k = 200, \gamma = 0.6$), **(b)** small Darcy number ($k = 0.01, \gamma = 0.444$). ($p_s = \zeta = F = \mu_R = 1, \lambda = 0.1, \varepsilon_f = 0.1, \beta = 0.4$)

The outcomes of figure 8.20 can be understood with the discussion of figure 8.19. Here, the increased zeta potential enhances the overall electric potential distribution in the flow domain, which will reflect in the enhanced flow velocity, results in acting as the reduced resistance in the overall flow domain, consequently the tortuosity of medium. (Figure 8.20)

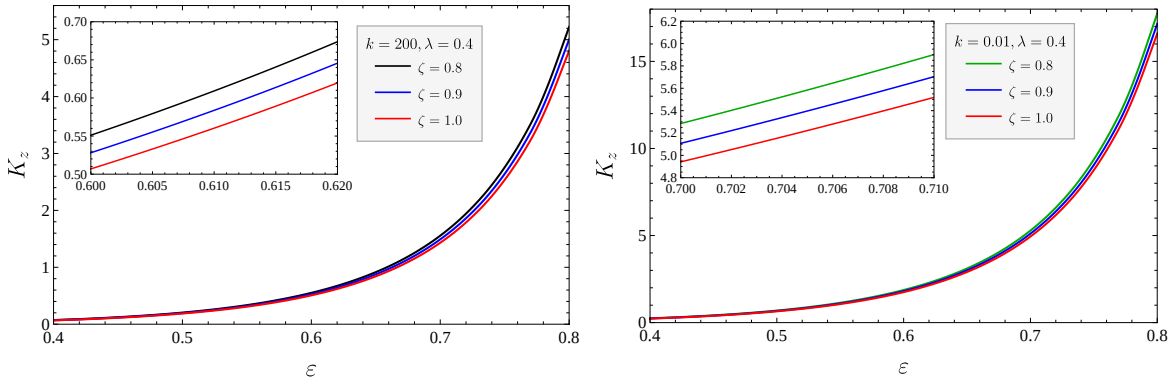

(a) **(b)**

Figure 8.20: The dependence of Kozeny constant (K_z) on porosity of the medium(ε) for different zeta potential (ζ) in case of **(a)** large Darcy number ($k = 200, \gamma = 0.6$), **(b)** small Darcy number ($k = 0.01, \gamma = 0.444$). ($p_s = K = F = \mu_R = 1, \lambda = 0.4, \varepsilon_f = 0.1, \beta = 0.4$)

It can be concluded from figure 8.21 that the increasing thickness of EDL layer leads to increase the tortuosity of the poly-electrolyte layer, which can be supported with the argument that the increasing thickness of EDL layer corresponds to the higher density of ions inside the layer, which create a high resistance against the axial velocity resulting in the increase in the tortuosity of the medium and consequently the Kozeny constant.

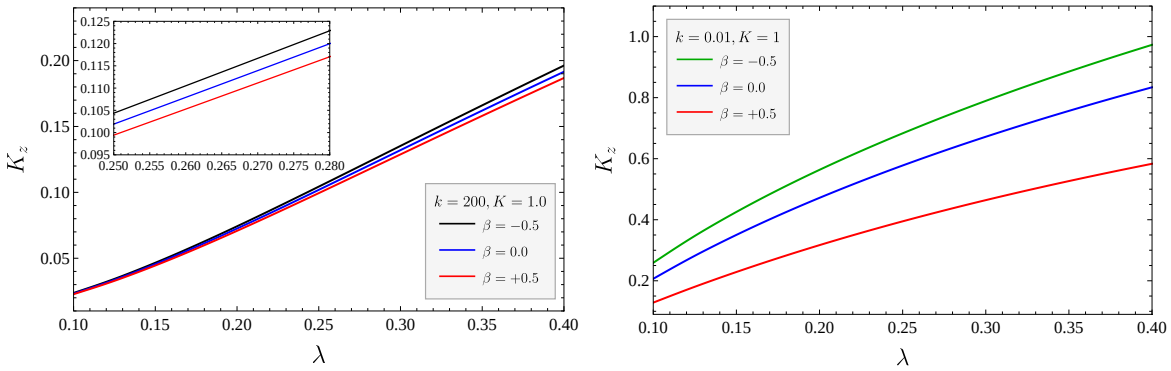

(a) **(b)**

Figure 8.21: The dependence of Kozeny constant (K_z) on EDL thickness (λ) for different stress-jump parameter (β) in case of **(a)** large Darcy number ($k = 200, \gamma = 0.6$), **(b)** small Darcy number ($k = 0.01, \gamma = 0.444$). ($p_s = K = \zeta = F = \mu_R = 1, \lambda = 0.4, \varepsilon_f = 0.1$)

An augmentation in the stress jump parameter results in a decay of Kozeny constant, which is more pronounced in the case of small permeability owing to an enhanced magnitude of stress jump term for small permeability case. The increasing Forchheimer number corresponds to the higher inertial resistance in the fluid flow, which leads to decay in flow velocity and hydrodynamic permeability of the membrane and consequently enhances the value of the Kozeny constant and tortuosity of the medium.

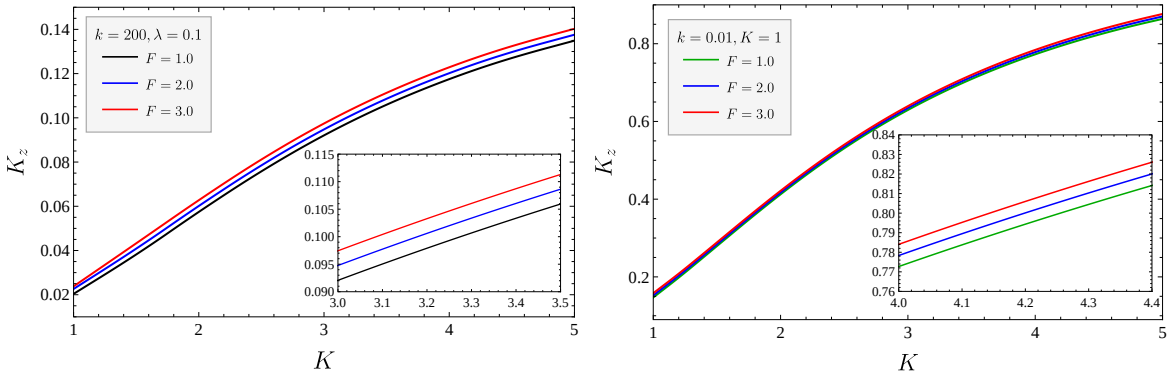

(a) **(b)**

Figure 8.22: The dependence of Kozeny constant (K_z) on ratio parameter(K) for different Forchheimer number (F) in case of **(a)** large Darcy number ($k = 200$), **(b)** small Darcy number ($k = 0.01$). ($p_s = \zeta = \mu_R = 1, \gamma = 0.444, \lambda = 0.1, \varepsilon_f = 0.1, \beta = 0.4$)

8.4.6 Model Validation and Limiting Cases

The limiting cases of the current model are discussed in Figure 8.23a for the large permeability case, which includes the constant permeability model under the limit ($\varepsilon_f \to 0$)

showing the enhanced fluid velocity in comparison to the current model signifying the reduced permeability in the porous medium for non-zero variable permeability parameter ε_f. Further limiting case of Brinkman model under the limit ($F \to 0$) signifying the effect of inertial resistance in the model. The zero stress jump corresponds to the continuity of stress at the fluid porous interface, which results in a reduction of fluid velocity. Further the limit ($k \to \infty$) corresponds to vanishing the PEL layer or a flow of electrolyte fluid past an array of rigid particles. The negligible variation in this case can be attributed to the already highly permeable PEL region ($k = 200$). In Figure 8.23b, The asymptotic solution of current study

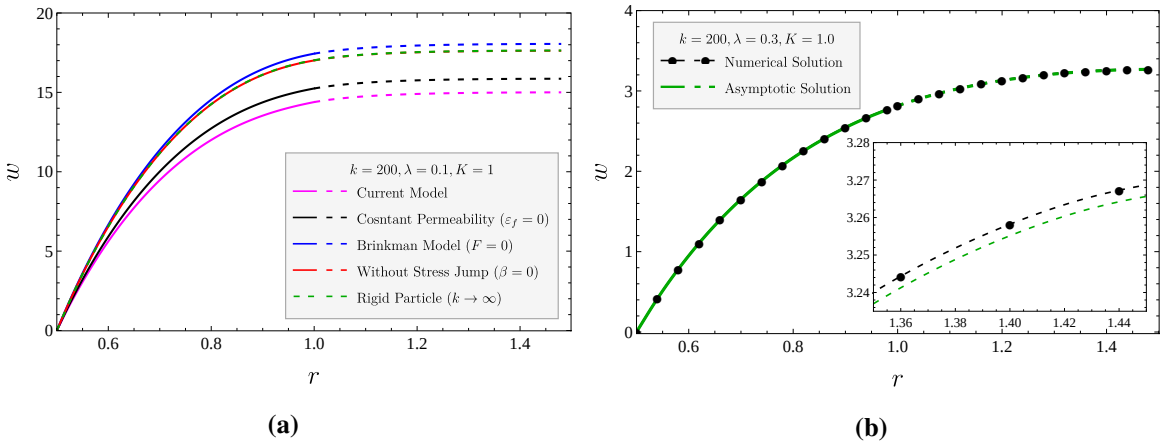

(a) **(b)**

Figure 8.23: **(a)** Comparision among special cases of the current model $(k = 200)$, **(b)** Validation of the asymptotic solution of current model with numerical solution (200).

is compared to the numerical solution computed using NDSolve command in MATHEMATICA 14.0 Software. It can be observe that the asymptotic solution of the current study is in good agreement with the numerical solution, signifying the validation of the second order perturbed solution of fluid velocity.

8.5 Summary and Conclusions

In this chapter, the electroosmotic flow (EOF) along with a constant pressure gradient driven flow of an electrolyte solution past a membrane consisting of poly-electrolyte coated solid cylindrical particles under the effect of an externally applied electric field is analyzed. The poly-electrolyte layer is considered as an ion penetrable porous layer enveloped around the solid cylindrical particles entraps a particular types of ion (different from electrolyte ions) called fixed charge ions. Hence the poly-electrolyte layer (PEL) is also referred as fixed charge layer (FCL). The mobile ions of bulk electrolyte accumulates near the interface of FCL and clear fluid region, which results in the formation of electric double layer. The fluid flow through membrane is modeled using the unit cell model according to which, the

flow regime is divided into two segments, one is the FCL region which is a porous layer of poly-electrolyte fibers, in which the fluid flow is governed using the Brinkann-Forchheimer equation. Second is the clear fluid region enclosed by a hypothetical cell, in which the flow is governed by Stokes equation. Due to the non-linear Forchheimer terms and external body force term (electric force), analytical solution for the system of governing equations is difficult to derive. Hence The the regular and singular perturbation methods were applied to derive the asymptotic analytical expressions of the solution. The hydrodynamic permeability and Kozeny constant of the membrane is analyzed by using the expressions of fluid velocity. The results and discussion section have given a detailed discussion of the graphical analysis.
The following novel determinations from the present study are pointed out:

1. The increasing thickness of the EDL in clear fluid region λ diminishes the flow profile of electrolyte, regardless of the high and low permeability cases. This decay with λ is also seen in the hydrodynamic permeability of the membrane for both cases of permeability. A significant increase is also observed in the Kozeny constant with increasing λ_f.

2. A noticeable decline in hydrodynamic permeability is evident with the increasing ratio parameter K, directly proportional to the equivalent EDL thickness in FCL region λ_f. This qualitative behavior of λ_f is transmitted in the hydrodynamic permeability of the membrane and observed the decay of L_{11} with increasing λ_f; however the Kozeny constant shows an increasing trend with a higher equivalent EDL thickness in FCL region λ_f.

3. An augmentation in the fluid's velocity can be seen in response to the increased values of zeta potential for both cases of permeability. A discernible increment in the hydrodynamic permeability can be observed in response to the increased zeta potential at the solid surface of the particle (for $k \gg 1$); However this effect is almost negligible for slightly permeable poly-electrolyte layer. Additionally, an increasing zeta potential leads to decay the Kozeny constant of the membrane.

4. An increasing values of permeability parameter corresponds to a decrease in the overall permeability of PEL region, resulting in an enhanced drag which reduces the flow velocity in both small and large permeability cases. Consequently, this increasing permeability parameter reduces the hydrodynamic permeability of the membrane.

These results helps in providing a broader physical insights associated with the combined electroosmotic and pressure driven flow of an electrolyte solution past a membrane consisting of poly-electrolyte coated solid cylindrical particles. The following work, however, requires experimental verification.

Chapter 9

Conclusions and Research Prospects

9.1 Conclusions

The aim of this thesis is to use the cell model approach to investigate the flow past a membrane for different physical and rheological scenarios. In particular, we have assumed the membrane is composed of a swarm of uniformly distributed cylindrical-shaped particles. The particles of swarm are modeled as porous cylindrical particles having an impermeable core along the axis, signifying the dissolution and adsorption of the polymers. The effect of inertial resistance is incorporated for the fluid flow within the polymer layer called the porous layer, using a non-linear body force term called the Forchheimer term. The variable nature of permeability within the porous layer is considered to incorporate the effect of non-uniform permeability in the porous layer of a swarm of particles. The flow behavior of different rheological fluids has been analyzed by considering the different Newtonian and non-Newtonian fluid models such as Jeffreys fluid, Carreau fluid, Carreau-Yasuda fluid. Throughout the whole discussion, the main findings are determined as

1. An observable effect of variable viscosity has been seen on the velocity profile and hydrodynamic quantities of the membranes. It is also observed that for the case of slightly permeable porous layer, this effect of variable viscosity is significant only for membranes of low particle volume fraction.

2. The Carreau-Yasuda model is first time applied for flow of non-Newtonian fluid through a membrane composed of an aggregate of porous layered cylindrical particles and the effect of fluid parameters signifying the rheological behavior of fluid on the hydrodynamic quantities of membrane such as hydrodynamic permeability, and Kozeny constant is found to be significant.

3. The surface roughness of cylindrical particles of swarm, depending on the parameters wave number, corrugation height etc., affect the membrane filtration process

significantly, and founded a significant impact on the hydrodynamic permeability and tortuosity of the membrane.

9.2 Noteworthy Contributions

This thesis contributes towards different mathematical models of fluid flow through uniform array of particles under the influence of the varying nature of viscosity and permeability. Effect of different body forces like electro-hydrodynamic force, electroosmotic force, buoyancy force has been analysed on the hydrodynamic and thermal characteristics of the membrane. Throughout the whole study, the main findings as specific contributions are as follows:

1. A decay in variable viscosity leads to growth in velocity profile, and hydrodynamic permeability of the membranes, however a decay in Kozeny constant is observed with increasing viscosity parameter. Further, for large particle volume fraction the impact of viscosity variation and relaxation time on membrane permeability is almost insignificant for the case of low permeability.

2. The visco-elasticity of the Carreau and Carreau-Yasuda fluid significantly affect the flow process within the membrane. In a highly permeable porous medium, the hydrodynamic permeability increases with the fluid's viscoelasticity; however, it decreases as the rheology shifts from shear thinning to shear thickening. In the case of small permeability, the impact of viscoelasticity becomes opposite for shear thickening fluids owing to larger-than-unit values of the power law parameter.

3. The theoretical analysis of electro-hydrodynamic flow reveals that a rising Hartmann electric number leads to the growth of velocity and membrane permeability, which is relatively more significant for higher permeability. However, the reverse trend is observed in the tortuosity of the membrane with Hartmann electric number.

4. The augmentation in varying permeability parameters of the Brinkman and Forchheimer layers leads to an enhancement in entropy generation owing to reduced fluid velocity. Additionally, an enhanced inertial resistance in the fluid flow, results in a enhancement of entropy generation within the membrane.

5. The increasing thickness of the EDL in clear fluid region λ, equivalent EDL thickness in PEL region λ_f, diminishes the flow profile of electrolyte fluid, regardless of the high and low permeability cases. This decay with increasing λ and λ_f is also seen in the hydrodynamic permeability of the membrane for both cases of permeability;

however the tortuosity of the membrane increases significantly with the increment of these thicknesses.

6. The increasing surface roughness of particles of the membrane leads to a significant reduction in the flow past a membrane, and hence it can be concluded that the surface roughness had a significant impact on the hydrodynamic quantities of the membrane.

9.3 Research Prospects

The simplicity of the model lends itself to further applications, both from an academic and industrial point of view; its highly flexible nature allows for a variety of different possibilities. Based on the current study, the following research prospects arises,

1. The membrane filtration process shows significant dependence upon the geometrical perturbations in the shape of the particles of a swarm. The cylindrical shape with sinusoidal corrugation has been analyzed but it can be further extended to arbitrary corrugations, which will surely provide more impactful insights about the flow.

2. The circular cylindrical shape of current study can be further extended to elliptic cylindrical shape or deformed cylindrical shape to analyse the effect of particle shape on the fluid flow past a membrane.

3. The current study is focused on the flow past along the axis of cylindrical particles; however it will be interesting to study to flow across the swarm of cylindrical particles and observe the effect of different Cell model on the hypothetical cell surface.

4. Apart from the already studied fluid models, the behavior of other Non-newtonian fluid models can be analysed to explore the effect of different rheological properties of fluid on the flow past a membrane.

5. The effect of electroosmotic flow on the soft cylindrical particle has been explored in the current study. However, the study of electrophoretic and diffusiophoretic flows in the membrane is a topic of future research.

Bibliography

1. Nadeem, S, Akbar, N. S. & Hameed, M. Peristaltic transport and heat transfer of a MHD Newtonian fluid with variable viscosity. *International journal for numerical methods in fluids* **63,** 1375–1393 (2010).
2. Tiwari, A. & Deo, S. Pulsatile flow in a cylindrical tube with porous walls: applications to blood flow. *Journal of Porous Media* **16** (2013).
3. Deo, S., Filippov, A., Tiwari, A., Vasin, S. & Starov, V. Hydrodynamic permeability of aggregates of porous particles with an impermeable core. *Advances in colloid and interface science* **164,** 21–37 (2011).
4. Tiwari, A. & Chauhan, S. S. Effect of varying viscosity on two-fluid model of blood flow through constricted blood vessels: a comparative study. *Cardiovascular Engineering and Technology* **10,** 155–172 (2019).
5. Tiwari, A. & Chauhan, S. S. Effect of varying viscosity on a two-layer model of the blood flow through porous blood vessels. *The European Physical Journal Plus* **134,** 41 (2019).
6. Akbar, N. S., Tripathi, D. & Bég, O. A. Variable-viscosity thermal hemodynamic slip flow conveying nanoparticles through a permeable-walled composite stenosed artery. *The European Physical Journal Plus* **132,** 1–11 (2017).
7. Hooman, K & Gurgenci, H. A theoretical analysis of forced convection in a porous-saturated circular tube: Brinkman–Forchheimer model. *Transport in porous media* **69,** 289–300 (2007).
8. Hooman, K. A perturbation solution for forced convection in a porous-saturated duct. *Journal of computational and applied mathematics* **211,** 57–66 (2008).
9. Nallapu, S. & Radhakrishnamacharya, G. Jeffrey fluid flow through a narrow tubes in the presence of a magnetic field. *Procedia Engineering* **127,** 185–192 (2015).
10. Tripathi, D, Ali, N, Hayat, T, Chaube, M. & Hendi, A. A. Peristaltic flow of MHD Jeffrey fluid through finite length cylindrical tube. *Applied Mathematics and Mechanics* **32,** 1231–1244 (2011).

11. Madasu, K. P. & Bucha, T. Impact of magnetic field on flow past cylindrical shell using cell model. *Journal of the Brazilian Society of Mechanical Sciences and Engineering* **41,** 320 (2019).

12. Ogulu, A & Abbey, T. M. Simulation of heat transfer on an oscillatory blood flow in an indented porous artery. *International communications in heat and mass transfer* **32,** 983–989 (2005).

13. Ponalagusamy, R & Tamil Selvi, R. Influence of magnetic field and heat transfer on two-phase fluid model for oscillatory blood flow in an arterial stenosis. *Meccanica* **50,** 927–943 (2015).

14. McKee, S, Watson, R, Cuminato, J. A., Caldwell, J & Chen, M. Calculation of electrohydrodynamic flow in a circular cylindrical conduit. *ZAMM-Journal of Applied Mathematics and Mechanics/Zeitschrift für Angewandte Mathematik und Mechanik* **77,** 457–465 (1997).

15. Jaiswal, S. & Yadav, P. K. A micropolar-Newtonian blood flow model through a porous layered artery in the presence of a magnetic field. *Physics of Fluids* **31** (2019).

16. Sankar, D., Lee, U., Nagar, A. K. & Morsidi, M. *Mathematical analysis of Carreau fluid model for blood flow in tapered constricted arteries* in *AIP Conference Proceedings* **2016** (2018).

17. Nadeem, S. & Akbar, N. S. Effects of heat and mass transfer on peristaltic flow of Carreau fluid in a vertical annulus. *Zeitschrift für Naturforschung A* **65,** 781–792 (2010).

18. Rana, J. & Murthy, P. Unsteady solute dispersion in non-Newtonian fluid flow in a tube with wall absorption. *Proceedings of the Royal Society A: Mathematical, Physical and Engineering Sciences* **472,** 20160294 (2016).

19. Yadav, P. K. & Kumar, A. An inclined magnetic field effect on entropy production of non-miscible Newtonian and micropolar fluid in a rectangular conduit. *International Communications in Heat and Mass Transfer* **124,** 105266 (2021).

20. Kumar, D. *et al.* Magnetohydrodynamic flow in horizontal concentric cylinders. *International Journal of Industrial Mathematics* **11,** 89–98 (2019).

21. Ashmawy, E. Effects of surface roughness on a couple stress fluid flow through corrugated tube. *European Journal of Mechanics-B/Fluids* **76,** 365–374 (2019).

22. Li, F., Jian, Y., Chang, L., Zhao, G. & Yang, L. Alternating current electroosmotic flow in polyelectrolyte-grafted nanochannel. *Colloids and Surfaces B: Biointerfaces* **147,** 234–241 (2016).

23. Chanda, S., Sinha, S. & Das, S. Streaming potential and electroviscous effects in soft nanochannels: towards designing more efficient nanofluidic electrochemomechanical energy converters. *Soft Matter* **10,** 7558–7568 (2014).

24. Srivastava, B. G. & Deo, S. Effect of magnetic field on the viscous fluid flow in a channel filled with porous medium of variable permeability. *Applied Mathematics and Computation* **219,** 8959–8964 (2013).

25. Stokes, G. G. *et al.* On the effect of the internal friction of fluids on the motion of pendulums (1851).

26. Oseen, C. W. Uber die Stokes' sche Formel und Uber eine verwandte Aufgabe in der Hydrodynamik. *Arkiv Mat., Astron. och Fysik* **6,** 1 (1910).

27. Lamb, H. XV. On the uniform motion of a sphere through a viscous fluid. *The London, Edinburgh, and Dublin Philosophical Magazine and Journal of Science* **21,** 112–121 (1911).

28. Lamb, H. *Hydrodynamics* (6th edition, Cambridge University Press, 1932).

29. Goldstein, S. & Jeffreys, H. The steady flow of viscous fluid past a fixed spherical obstacle at small reynolds numbers. *Proceedings of the Royal Society of London. Series A, Containing Papers of a Mathematical and Physical Character* **123,** 225–235 (1929).

30. Faxén, H. *Exakte Lösung der Oseenschen Differenzialgleichungen einer zähen Flüssigkeit für den Fall der Translationsbewegung eines Zylinders* (Almqvist & Wiksell, 1927).

31. Imai, I. A new method of solving Oseen's equations and its application to the flow past an inclined elliptic cylinder. *Proceedings of the Royal Society of London. Series A. Mathematical and Physical Sciences* **224,** 141–160 (1954).

32. Proudman, I. & Pearson, J. R. A. Expansions at small Reynolds numbers for the flow past a sphere and a circular cylinder. *Journal of Fluid Mechanics* **2,** 237–262 (1957).

33. Kaplun, S. Low Reynolds number flow past a circular cylinder. *Journal of Mathematics and Mechanics,* 595–603 (1957).

34. Tritton, D. J. Experiments on the flow past a circular cylinder at low Reynolds numbers. *Journal of Fluid Mechanics* **6,** 547–567 (1959).

35. Nisi, H. & Porter, A. W. LXXXVI. On eddies in air. *The London, Edinburgh, and Dublin Philosophical Magazine and Journal of Science* **46,** 754–768 (1923).

36. Taneda, S. Experimental Investigation of the Wakes behind Cylinders and Plates at Low Reynolds Numbers. *Journal of the Physical Society of Japan* **11,** 302–307 (Mar. 1956).

37. Tomotika, S. & Aoi, T. The steady flow of viscous fluid past a sphere and circular cylinder at small reynolds numbers. *The Quarterly Journal of Mechanics and Applied Mathematics* **3,** 141–161 (Jan. 1950).

38. Tomotika, S. & Aoi, T. An expansion formula for the drag on a circular cylinder moving through a viscous fluid at small reynolds numbers. *The Quarterly Journal of Mechanics and Applied Mathematics* **4,** 401–406 (Jan. 1951).

39. Yano, H. & Kieda, A. An approximate method for solving two-dimensional low-Reynolds-number flow past arbitrary cylindrical bodies. *Journal of Fluid Mechanics* **97,** 157–179 (1980).

40. Lee, S. H. & Leal, L. G. Low-Reynolds-number flow past cylindrical bodies of arbitrary cross-sectional shape. *Journal of Fluid Mechanics* **164,** 401–427 (1986).

41. Chadwick, E. The Far-field Green's Integral in Stokes Flow from the Boundary Integral Formulation. *Computer Modeling in Engineering & Sciences* **96,** 177–184 (2013).

42. Sutherland, J. P., Vassilatos, G., Kubota, H. & Osberg, G. L. The effect of packing on a fluidized bed. *AIChE Journal* **9,** 437–441 (1963).

43. Mandal, D., Vinjamur, M. & Sathiyamoorthy, D. Hydrodynamics of beds of small particles in the voids of coarse particles. *Powder Technology* **235,** 256–262. ISSN: 0032-5910 (2013).

44. Mandal, D. Hydrodynamics of particles in liquid–solid packed fluidized bed. *Powder Technology* **276,** 18–25 (2015).

45. Harris, C. Flow through porous media. Examination of the immobile fluid model. *Powder Technology* **17,** 235–252. ISSN: 0032-5910 (1977).

46. Kundu, P., Kumar, V. & Mishra, I. Numerical modeling of turbulent flow through isotropic porous media. *International Journal of Heat and Mass Transfer* **75,** 40–57 (2014).

47. SCHEIDEGGER, A. E. *The Physics of Flow Through Porous Media (3rd Edition)* (2024) (University of Toronto Press, 1974).

48. Darcy, H. Les fontaines publique de la ville de dijon. *Dalmont, Paris* **647** (1856).

49. Huyghe, J. M. & Van Campen, D. H. Finite deformation theory of hierarchically arranged porous solids—I. Balance of mass and momentum. *International journal of engineering science* **33,** 1861–1871 (1995).
50. Vankan, W. J., Huyghe, J. M., Drost, M. R., Janssen, J. D. & Huson, A. A finite element mixture model for hierarchical porous media. *International Journal for Numerical Methods in Engineering* **40,** 193–210 (1997).
51. Lu, X. *Fluid Flow and Heat Transfer in Porous Media Manufactured by a Space Holder Method* (The University of Liverpool (United Kingdom), 2020).
52. Mokadam, R. G. Thermodynamic Analysis of the Darcy Law. *Journal of Applied Mechanics* **28,** 208–212 (1961).
53. Chauveteau, G. & Thirriot, C. Régimes d'écoulement en milieu poreux et limite de la loi de Darcy. *La Houille Blanche* **53,** 141–148 (1967).
54. Dupuit, J. *Études théoriques et pratiques sur le mouvement des eaux dans les canaux découverts et à travers les terrains perméabls: avec des considérations relatives au régime des grandes eaux, au débouché à leur donner, et à la marche des alluvions dans les rivières à fond mobile* (Dunod, 1863).
55. P. Forchheimer. Wasserbewegung durch boden. *Zeitschrift des Vereines Deutscher Ingenieure* **45,** 1782–1788 (1901).
56. Joseph, D. D., Nield, D. A. & Papanicolaou, G. Nonlinear equation governing flow in a saturated porous medium. *Water Resources Research* **18,** 1049–1052 (1982).
57. Ward, J. C. Turbulent Flow in Porous Media. *Journal of the Hydraulics Division* **90,** 1–12 (1964).
58. Vafai, K. & Tien, C. L. Boundary and inertia effects on flow and heat transfer in porous media. *International Journal of Heat and Mass Transfer* **24,** 195–203 (1981).
59. Vafai, K. & Tien, C. Boundary and inertia effects on convective mass transfer in porous media. *International Journal of Heat and Mass Transfer* **25,** 1183–1190 (1982).
60. Rohom, K. *Membrane Filtration Market worth $ 32.24 billion by 2030, growing at a CAGR of 8.33%* https://www.openpr.com/news/3398862/membrane-filtration-market-worth-32-24-billion-by-2030. Feb. 2024.
61. Jankhah, S. *Technology trends in membrane filtration use* https://www.filtsep.com/content/features/technology-trends-in-membrane-filtration-use/. 2018.
62. Lowenfels, J. & Lewis, W. *Teaming with Microbes: A Gardener's Guide to the Soil Food Web* ISBN: 9780881927771 (Timber Press, 2006).

63. Hasimoto, H. On the periodic fundamental solutions of the Stokes equations and their application to viscous flow past a cubic array of spheres. *Journal of Fluid Mechanics* **5,** 317–328 (1959).

64. Drummond, J. & Tahir, M. Laminar viscous flow through regular arrays of parallel solid cylinders. *International Journal of Multiphase Flow* **10,** 515–540 (1984).

65. Sangani, A. & Acrivos, A. Slow flow past periodic arrays of cylinders with application to heat transfer. *International Journal of Multiphase Flow* **8,** 193–206 (1982).

66. Sparrow, E. M. & Loeffler JR., A. L. Longitudinal laminar flow between cylinders arranged in regular array. *AIChE Journal* **5,** 325–330 (1959).

67. Kuwabara, S. The Forces experienced by Randomly Distributed Parallel Circular Cylinders or Spheres in a Viscous Flow at Small Reynolds Numbers. *Journal of the Physical Society of Japan* **14,** 527–532 (1959).

68. Happel, J. Viscous flow relative to arrays of cylinders. *AIChE Journal* **5,** 174–177.

69. Jackson, G. W. & James, D. F. The permeability of fibrous porous media. *The Canadian Journal of Chemical Engineering* **64,** 364–374 (1986).

70. Happel J., M. T. & S., U. Viscous flow in multiparticle systems: slow viscous flow through a mass of particles. *Int. Sci. Technol. Univ. Tokyo (in Japanese)* **3,** 97 (1954).

71. Happel, J. Viscous flow in multiparticle systems: Slow motion of fluids relative to beds of spherical particles. *AIChE Journal* **4,** 197–201 (1958).

72. Kvashnin, A. G. Cell model of suspension of spherical particles. *Fluid Dynamics* **14,** 598–602 (1979).

73. Cunningham, E. & Larmor, J. On the velocity of steady fall of spherical particles through fluid medium. *Proceedings of the Royal Society of London. Series A, Containing Papers of a Mathematical and Physical Character* **83,** 357–365 (1910).

74. Mehta, G. D. & Morse, T. F. Flow through charged membranes. *The Journal of Chemical Physics* **63,** 1878–1889 (1975).

75. Epstein, N. & Masliyah, J. H. Creeping flow through clusters of spheroids and elliptical cylinders. *The Chemical Engineering Journal* **3,** 169–175 (1972).

76. Neale, G., Epstein, N. & Nader, W. Creeping flow relative to permeable spheres. *Chemical Engineering Science* **28,** 1865–1874 (1973).

77. Dassios, G., Hadjinicolaou, M., Coutelieris, F. & Payatakes, A. Stokes flow in spheroidal particle-in-cell models with rappel and kuwabara boundary conditions. *International Journal of Engineering Science* **33,** 1465–1490 (1995).

78. Kim, A. S. & Yuan, R. A new model for calculating specific resistance of aggregated colloidal cake layers in membrane filtration processes. *Journal of Membrane Science* **249,** 89–101 (2005).

79. Bhattacharyya, A. & Raja Sekhar, G. Viscous flow past a porous sphere with an impermeable core : effect of stress jump condition. *Chemical Engineering Science* **59,** 4481–4492 (2004).

80. Prakash, J. & Raja Sekhar, G. P. Arbitrary oscillatory Stokes flow past a porous sphere using Brinkman model. *Meccanica* **47,** 1079–1095 (2012).

81. Ochoa-Tapia, J. A. & Whitaker, S. Momentum transfer at the boundary between a porous medium and a homogeneous fluid—I. Theoretical development. *International Journal of Heat and Mass Transfer* **38,** 2635–2646 (1995).

82. Ochoa-Tapia, J. A. & Whitaker, S. Momentum transfer at the boundary between a porous medium and a homogeneous fluid—II. Comparison with experiment. *International Journal of Heat and Mass Transfer* **38,** 2647–2655 (1995).

83. Deo, S. & Gupta, B. R. Stokes flow past a swarm of porous approximately spheroidal particles with Kuwabara boundary condition. *Acta mechanica* **203,** 241–254 (2009).

84. Veerapaneni, S. & Wiesner, M. R. Hydrodynamics of fractal aggregates with radially varying permeability. *Journal of colloid and interface science* **177,** 45–57 (1996).

85. Vasin, S., Filippov, A. N. & Starov, V. M. Hydrodynamic permeability of membranes built up by particles covered by porous shells: Cell models. *Advances in colloid and interface science* **139,** 83–96 (2008).

86. Saad, E. Stokes flow past an assemblage of axisymmetric porous spherical shell-in-cell models: effect of stress jump condition. *Meccanica* **48,** 1747–1759 (2013).

87. Faltas, M. & Saad, E. Stokes flow past an assemblage of slip eccentric spherical particle-in-cell models. *Mathematical methods in the applied sciences* **34,** 1594–1605 (2011).

88. Faltas, M., Saad, E. & El-Sapa, S. Slip–Brinkman flow through corrugated microannulus with stationary random roughness. *Transport in Porous Media* **116,** 533–566 (2017).

89. Kumar Yadav, P., Jaiswal, S., Asim, T. & Mishra, R. Influence of a magnetic field on the flow of a micropolar fluid sandwiched between two Newtonian fluid layers through a porous medium. *The European Physical Journal Plus* **133,** 1–13 (2018).

90. Saad, E. Translation and rotation of a porous spheroid in a spheroidal container. *Canadian Journal of Physics* **88,** 689–700 (2010).

91. Yadav, P. K., Tiwari, A. & Singh, P. Hydrodynamic permeability of a membrane built up by spheroidal particles covered by porous layer. *Acta Mechanica* **229,** 1869–1892 (2018).

92. Yadav, P. K., Deo, S., Singh, S. P. & Filippov, A. Effect of magnetic field on the hydrodynamic permeability of a membrane built up by porous spherical particles. *Colloid Journal* **79,** 160–171 (2017).

93. Tiwari, A., Yadav, P. K. & Singh, P. Stokes flow through assemblage of non-homogeneous porous cylindrical particles using cell model technique. *National Academy science letters* **41,** 53–57 (2018).

94. Yadav, P. K., Singh, P, Tiwari, A. & Deo, S. Stokes flow through a membrane built up by nonhomogeneous porous cylindrical particles. *Journal of Applied Mechanics and Technical Physics* **60,** 816–826 (2019).

95. Khanukaeva, D. Y., Filippov, A., Yadav, P. & Tiwari, A. Creeping flow of micropolar fluid parallel to the axis of cylindrical cells with porous layer. *European Journal of Mechanics-B/Fluids* **76,** 73–80 (2019).

96. Khanukaeva, D. Y., Filippov, A., Yadav, P. & Tiwari, A. Creeping flow of micropolar fluid through a swarm of cylindrical cells with porous layer (membrane). *Journal of Molecular Liquids* **294,** 111558 (2019).

97. Kishore, N, Chhabra, R. & Eswaran, V. Mass transfer from ensembles of Newtonian fluid spheres at moderate Reynolds and Peclet numbers. *Chemical Engineering Research and Design* **85,** 1203–1214 (2007).

98. Kawase, Y. & Ulbrecht, J. J. Drag and mass transfer in non-Newtonian flows through multi-particle systems at low Reynolds numbers. *Chem. Eng. Sci. (United Kingdom)* **36** (1981).

99. Zhu, J. Drag and mass transfer for flow of a Carreau fluid past a swarm of Newtonian drops. *International journal of multiphase flow* **21,** 935–940 (1995).

100. Dang, V.-D. & Steinberg, M. Mass transfer from swarms of bubbles or drops with chemical reactions in continuous phase. *AIChE Journal* **22,** 925–927 (1976).

101. Pfeffer, R. & Happel, J. An analytical study of heat and mass transfer in multiparticle systems at low Reynolds numbers. *AIChE Journal* **10,** 605–611 (1964).

102. Mandhani, V., Chhabra, R. & Eswaran, V. Forced convection heat transfer in tube banks in cross flow. *Chemical Engineering Science* **57,** 379–391 (2002).

103. Ferreira, J. M. & Chhabra, R. P. Analytical study of drag and mass transfer in creeping power law flow across tube banks. *Industrial & engineering chemistry research* **43,** 3439–3450 (2004).

104. Mangadoddy, N., Prakash, R., Chhabra, R. & Eswaran, V. Forced convection in cross flow of power law fluids over a tube bank. *Chemical engineering science* **59,** 2213–2222 (2004).

105. Zhu, J. A cell model of effective thermal conductivity for saturated porous media. *International Journal of Heat and Mass Transfer* **138,** 1054–1060 (2019).

106. Zhu, J. Unsaturated cell model of effective thermal conductivity of soils. *SN Applied Sciences* **2,** 1395 (2020).

107. Zhu, J. Convective and conductive heat transfer of creeping flow in a multi-particle system. *International Journal of Thermal Sciences* **159,** 106573 (2021).

108. Sharanya, V, Raja Sekhar, G. & Rohde, C. Bed of polydisperse viscous spherical drops under thermocapillary effects. *Zeitschrift für angewandte Mathematik und Physik* **67,** 1–17 (2016).

109. Bejan, A. Second law analysis in heat transfer. *Energy* **5.** Second law analysis of energy devices and processes, 720–732 (1980).

110. Bejan, A. & Kestin, J. Entropy generation through heat and fluid flow (1982).

111. Bejan, A., Tsatsaronis, G. & Moran, M. *Thermal Design and Optimization* (Wiley, 1995).

112. Bejan, A. Method of entropy generation minimization, or modeling and optimization based on combined heat transfer and thermodynamics. *Revue Générale de Thermique* **35,** 637–646 (1996).

113. Bejan, A. *Advanced Engineering Thermodynamics* ISBN: 9781119281047 (Wiley, 2016).

114. Shit, G., Haldar, R. & Mandal, S. Entropy generation on MHD flow and convective heat transfer in a porous medium of exponentially stretching surface saturated by nanofluids. *Advanced Powder Technology* **28,** 1519–1530 (2017).

115. Shit, G. C. & Mandal, S. Entropy Analysis on Unsteady MHD Flow of Casson Nanofluid over a Stretching Vertical Plate with Thermal Radiation Effect. *International Journal of Applied and Computational Mathematics* **6** (2019).

116. Bhatti, M., Sheikholeslami, M, Shahid, A, Hassan, M & Abbas, T. Entropy generation on the interaction of nanoparticles over a stretched surface with thermal radiation. *Colloids and Surfaces A: Physicochemical and Engineering Aspects* **570,** 368–376 (2019).

117. Kumar, A., Tripathi, R. & Singh, R. Entropy generation and regression analysis on stagnation point flow of Casson nanofluid with Arrhenius activation energy. *Journal of the Brazilian Society of Mechanical Sciences and Engineering* **41,** 306 (2019).

118. Sultan, F *et al.* Importance of entropy generation and infinite shear rate viscosity for non-Newtonian nanofluid. *Journal of the Brazilian Society of Mechanical Sciences and Engineering* **41,** 1–13 (2019).

119. Khan, N. *et al.* Aspects of chemical entropy generation in flow of Casson nanofluid between radiative stretching disks. *Entropy* **22,** 495 (2020).

120. Nayak, M. *et al.* Entropy optimized MHD 3D nanomaterial of non-Newtonian fluid: a combined approach to good absorber of solar energy and intensification of heat transport. *Computer methods and programs in biomedicine* **186,** 105131 (2020).

121. Levine, S., Neale, G. & Epstein, N. The prediction of electrokinetic phenomena within multiparticle systems: II. Sedimentation potential. *Journal of Colloid and Interface Science* **57,** 424–437 (1976).

122. Ohshima, H. Electrophoretic mobility of spherical colloidal particles in concentrated suspensions. *Journal of colloid and interface science* **188,** 481–485 (1997).

123. Keh, H. J. & Chen, W. C. Sedimentation velocity and potential in concentrated suspensions of charged porous spheres. *Journal of colloid and interface science* **296,** 710–720 (2006).

124. Zholkovskij, E. K., Masliyah, J. H., Shilov, V. N. & Bhattacharjee, S. Electrokinetic phenomena in concentrated disperse systems: general problem formulation and spherical cell approach. *Advances in colloid and interface science* **134,** 279–321 (2007).

125. Chiang, C. C. & Keh, H. J. Startup of electrophoresis in a suspension of colloidal spheres. *Electrophoresis* **36,** 3002–3008 (2015).

126. Li, C. Y. & Keh, H. J. Thermophoresis of a spherical particle in a microtube. *Journal of Aerosol Science* **113,** 71–84 (2017).

127. Saad, E. & Faltas, M. Time-dependent electrophoresis of a dielectric spherical particle embedded in Brinkman medium. *Zeitschrift für angewandte Mathematik und Physik* **69,** 1–18 (2018).

128. Saad, E. Unsteady electrophoresis of a dielectric cylindrical particle suspended in porous medium. *Journal of Molecular Liquids* **289,** 111050 (2019).

129. Saad, E. Start-up Brinkman electrophoresis of a dielectric sphere for Happel and Kuwabara models. *Mathematical Methods in the Applied Sciences* **41,** 9578–9591 (2018).

130. Chen, W. L. & Keh, H. J. Electroosmosis and Electric Conduction of Electrolyte Solutions in Charge-Regulating Fibrous Media. *Colloids and Interfaces* **5,** 19 (2021).

131. Lai, Y. C. & Keh, H. J. Transient electrophoresis in a suspension of charged particles with arbitrary electric double layers. *Electrophoresis* **42,** 2126–2133 (2021).

132. Saad, E. Time-varying Brinkman electrophoresis of a charged cylinder-in-cell model. *European Journal of Mechanics-B Fluids* **79,** 357–366 (2020).

133. Carreau, P. J. Rheological equations from molecular network theories (Ph.D. thesis). *Transactions of the Society of Rheology* **16,** 99–127 (1972).

134. Carreau, P. J. Rheological Equations from Molecular Network Theories. *Transactions of The Society of Rheology* **16,** 99–127 (1972).

135. Yasuda, K. Investigation of the analogies between viscometric and linear viscoelastic properties of polystyrene fluids (Ph.D. thesis) (Aug. 1979).

136. Yasuda, K, Armstrong, R. C. & Cohen, R. E. Shear flow properties of concentrated solutions of linear and star branched polystyrenes. *Rheologica Acta* **20,** 163–178 (1981).

137. Brinkman, H. C. A calculation of the viscous force exerted by a flowing fluid on a dense swarm of particles. *Flow, Turbulence and Combustion* **1,** 27–34 (1949).

138. Brinkman, H. C. On the permeability of media consisting of closely packed porous particles. *Flow, Turbulence and Combustion* **1,** 81–86 (1949).

139. Reynolds, O. & Stewart, B. I. On the force caused by the communication of heat between a surface and a gas, and on a new photometer. *Proceedings of the Royal Society of London* **24,** 387–391 (1876).

140. Vasin, S. & Filippov, A. Permeability of Complex Porous Media. *Colloid Journal* **71,** 31–45 (Feb. 2009).

141. Bush, A. *Perturbation Methods for Engineers and Scientists (1st ed.)* (Routledge, New York, 1992).

142. Nayfeh, A. *Perturbation Methods* (Wiley, 2008).

143. Wang, D. M. & Tarbell, J. M. Modeling Interstitial Flow in an Artery Wall Allows Estimation of Wall Shear Stress on Smooth Muscle Cells. *Journal of Biomechanical Engineering* **117,** 358–363 (1995).

144. Kumar, R. *et al.* Anatomical variations in cortical bone surface permeability: tibia versus femur. *Journal of the Mechanical Behavior of Biomedical Materials* **113,** 104122 (2021).

145. Deo, S., Yadav, P. K. & Tiwari, A. Slow viscous flow through a membrane built up from porous cylindrical particles with an impermeable core. *Applied mathematical modelling* **34,** 1329–1343 (2010).

146. Sherief, H., Faltas, M., Ashmawy, E. & Abdel-Hameid, A. Parallel and perpendicular flows of a micropolar fluid between slip cylinder and coaxial fictitious cylindrical shell in cell models. *The European Physical Journal Plus* **129,** 1–16 (2014).

147. Yadav, P. K., Jaiswal, S. & Puchakatla, J. Y. Micropolar fluid flow through the membrane composed of impermeable cylindrical particles coated by porous layer under the effect of magnetic field. *Mathematical Methods in the Applied Sciences* **43,** 1925–1937 (2020).

148. Yadav, P. K. Slow motion of a porous cylindrical shell in a concentric cylindrical cavity. *Meccanica* **48,** 1607–1622 (2013).

149. Tripathi, A. & Chhabra, R. P. Slow power law fluid flow relative to an array of infinite cylinders. *Industrial & engineering chemistry research* **31,** 2754–2759 (1992).

150. Tripathi, A & Chhabra, R. Transverse laminar flow of non-Newtonian fluids over a bank of long cylinders. *Chemical Engineering Communications* **147,** 197–212 (1996).

151. Pandey, S. & Tripathi, D. Unsteady model of transportation of Jeffrey-fluid by peristalsis. *International Journal of Biomathematics* **3,** 473–491 (2010).

152. Ramesh, K, Tripathi, D, Bég, O. A. & Kadir, A. Slip and hall current effects on Jeffrey fluid suspension flow in a peristaltic hydromagnetic blood micropump. *Iranian Journal of Science and Technology, Transactions of Mechanical Engineering* **43,** 675–692 (2019).

153. Prakash, J, Ansu, A. K. & Tripathi, D. Alterations in peristaltic pumping of Jeffery nanoliquids with electric and magnetic fields. *Meccanica* **53,** 3719–3738 (2018).

154. Faltas, M. & Ragab, K. E. Thermophoretic and photophoretic velocities and forces of a spherical particle embedded in Brinkman medium. *The European Physical Journal Plus* **134,** 475 (2019).

155. Choudhuri, D & Raja Sekhar, G. Thermocapillary drift on a spherical drop in a viscous fluid. *Physics of Fluids* **25** (2013).

156. Sharanya, V & Raja Sekhar, G. Thermocapillary migration of a spherical drop in an arbitrary transient Stokes flow. *Physics of Fluids* **27** (2015).

157. Bali, R. & Awasthi, U. Effect of a magnetic field on the resistance to blood flow through stenotic artery. *Applied Mathematics and Computation* **188,** 1635–1641 (2007).

158. Shit, G., Roy, M & Sinha, A. Mathematical modelling of blood flow through a tapered overlapping stenosed artery with variable viscosity. *Applied Bionics and Biomechanics* **11,** 185–195 (2014).

159. Filippov, A. & Koroleva, Y. Viscous flow through a porous medium filled by liquid with varying viscosity. *Buletinul Academiei de Ştiinţe a Moldovei. Matematica* **85,** 74–87 (2017).

160. Koroleva, Y. O. Qualitative properties of the Solution to Brinkman-Stokes system modelling a filtration process. *Mathematics and Statistics* **4,** 143 (2017).

161. Filippov, A. & Koroleva, Y. On a hydrodynamic permeability of a system of coaxial partly porous cylinders with superhydrophobic surfaces. *Applied Mathematics and Computation* **338,** 363–375 (2018).

162. Tiwari, A. & Chauhan, S. S. Effect of varying viscosity on two-fluid model of pulsatile blood flow through porous blood vessels: A comparative study. *Microvascular research* **123,** 99–110 (2019).

163. Tiwari, A. & Chauhan, S. S. Effect of varying viscosity on two-layer model of pulsatile flow through blood vessels with porous region near walls. *Transport in Porous Media* **129,** 721–741 (2019).

164. Mekheimer, K. S. & Abd Elmaboud, Y. Simultaneous effects of variable viscosity and thermal conductivity on peristaltic flow in a vertical asymmetric channel. *Canadian Journal of Physics* **92,** 1541–1555 (2014).

165. Dash, R., Mehta, K. & Jayaraman, G. Casson fluid flow in a pipe filled with a homogeneous porous medium. *International Journal of Engineering Science* **34,** 1145–1156 (1996).

166. Tiwari, A., Shah, P. D. & Chauhan, S. S. Solute dispersion in two-fluid flowing through tubes with a porous layer near the absorbing wall: Model for dispersion phenomenon in microvessels. *International Journal of Multiphase Flow* **131,** 103380 (2020).

167. Tiwari, A., Shah, P. D. & Chauhan, S. S. Analytical study of micropolar fluid flow through porous layered microvessels with heat transfer approach. *The European Physical Journal Plus* **135,** 1–32 (2020).

168. Khaled, A.-R. & Vafai, K. The role of porous media in modeling flow and heat transfer in biological tissues. *International Journal of Heat and Mass Transfer* **46,** 4989–5003 (2003).

169. Galdi, G. P., Rannacher, R., Robertson, A. M. & Turek, S. Hemodynamical flows. *Delhi Book Store,* 8–10 (2008).

170. Greenkorn, R. A. Flow phenomena in porous media: fundamentals and applications in petroleum, water and food production (1983).

171. Levine, S & Neale, G. H. The prediction of electrokinetic phenomena within multiparticle systems. I. Electrophoresis and electroosmosis. *Journal of Colloid and Interface Science* **47,** 520–529 (1974).

172. Ohshima, H. Electrokinetic phenomena in a dilute suspension of spherical solid colloidal particles with a hydrodynamically slipping surface in an aqueous electrolyte solution. *Advances in colloid and Interface Science* **272,** 101996 (2019).

173. Ohshima, H. Electroosmotic velocity in an array of parallel cylindrical fibers with a slip surface. *Colloid and Polymer Science* **299,** 937–941 (2021).

174. Keh, H. J. & Wei, Y. K. Diffusioosmosis and electroosmosis of electrolyte solutions in fibrous porous media. *Journal of colloid and interface science* **252,** 354–364 (2002).

175. Roul, P. & Madduri, H. A new approximate method and its convergence for a strongly nonlinear problem governing electrohydrodynamic flow of a fluid in a circular cylindrical conduit. *Applied Mathematics and Computation* **341,** 335–347 (2019).

176. Alomari, A., Erturk, V. S., Momani, S. & Alsaedi, A. An approximate solution method for the fractional version of a singular BVP occurring in the electrohydrodynamic flow in a circular cylindrical conduit. *The European Physical Journal Plus* **134,** 1–11 (2019).

177. Wang, A., Xu, H. & Yu, Q. Homotopy Coiflets wavelet solution of electrohydrodynamic flows in a circular cylindrical conduit. *Applied Mathematics and Mechanics* **41,** 681–698 (2020).

178. Vaddi, R. S., Guan, Y., Mamishev, A. & Novosselov, I. Analytical model for electrohydrodynamic thrust. *Proceedings of the Royal Society A* **476,** 20200220 (2020).

179. Eringen, A. C. & Maugin, G. A. *Electrodynamics of continua II: fluids and complex media* (Springer Science & Business Media, 2012).

180. Khanukaeva, D. Y. Approximation of the hydrodynamic permeability for globular-structured membranes. *Mechanics of Materials* **148,** 103528 (2020).

181. Ozgumus, T., Mobedi, M. & Ozkol, U. Determination of Kozeny constant based on porosity and pore to throat size ratio in porous medium with rectangular rods. *Engineering Applications of Computational Fluid Mechanics* **8,** 308–318 (2014).

182. Sankar, D. & Hemalatha, K. A non-Newtonian fluid flow model for blood flow through a catheterized artery—steady flow. *Applied mathematical modelling* **31,** 1847–1864 (2007).

183. Prakash, J., Raja Sekhar, G. & Kohr, M. Stokes flow of an assemblage of porous particles: stress jump condition. *Zeitschrift für angewandte Mathematik und Physik* **62,** 1027–1046 (2011).

184. Filippov, A., Koroleva, Y. O. & Verma, A. Cell Model of a Fibrous Medium (Membrane). Comparison between Two Different Approaches to Varying Liquid Viscosity. *Membranes and Membrane Technologies* **2,** 230–243 (2020).

185. Zhu, J & Satish, M. Non-Newtonian effects on the drag of creeping flow through packed beds. *International journal of multiphase flow* **18,** 765–777 (1992).

186. Chaffin, S. & Rees, J. Carreau fluid in a wall driven corner flow. *Journal of Non-Newtonian Fluid Mechanics* **253,** 16–26 (2018).

187. Nield, D. A note on a Brinkman–Brinkman forced convection problem. *Transport in porous media* **64,** 185–188 (2006).

188. Sucharitha, G, Lakshminarayana, P & Sandeep, N. Joule heating and wall flexibility effects on the peristaltic flow of magnetohydrodynamic nanofluid. *International Journal of Mechanical Sciences* **131,** 52–62 (2017).

189. Yadav, P. K. *et al.* Hydrodynamic permeability of biporous membrane. *Colloid Journal* **75,** 473–482 (2013).

190. Deo, S., Maurya, D. K. & Filippov, A. Effect of magnetic field on hydrodynamic permeability of biporous membrane relative to micropolar liquid flow. *Colloid Journal* **83,** 662–675 (2021).

191. Bhandari, D., Tripathi, D. & Narla, V. Pumping flow model for couple stress fluids with a propagative membrane contraction. *International Journal of Mechanical Sciences* **188,** 105949 (2020).

192. Vafai, K. & Tien, C. L. Boundary and inertia effects on flow and heat transfer in porous media. *International Journal of Heat and Mass Transfer* **24,** 195–203 (1981).

193. Vafai, K. & Tien, C. Boundary and inertia effects on convective mass transfer in porous media. *International Journal of Heat and Mass Transfer* **25,** 1183–1190 (1982).

194. Chauhan, S. S., Shah, P. D. & Tiwari, A. Analytical study of the effect of variable viscosity and heat transfer on two-fluid flowing through porous layered tubes. *Transport in Porous Media* **142,** 641–668 (2022).

195. Hill, A. A. & Morad, M. Convective stability of carbon sequestration in anisotropic porous media. *Proceedings of the Royal Society A: Mathematical, Physical and Engineering Sciences* **470,** 20140373 (2014).

196. Vaidya, H. *et al.* Scrutiny of MHD impact on Carreau Yasuda (CY) fluid flow over a heated wall of the uniform micro-channel. *Chinese Journal of Physics* **87,** 766–781 (2024).

197. Jangili, S., Adesanya, S., Falade, J. & Gajjela, N. Entropy generation analysis for a radiative micropolar fluid flow through a vertical channel saturated with non-Darcian porous medium. *International Journal of Applied and Computational Mathematics* **3,** 3759–3782 (2017).

198. Khan, M. I. & Alzahrani, F. Entropy-optimized dissipative flow of Carreau–Yasuda fluid with radiative heat flux and chemical reaction. *The European Physical Journal Plus* **135,** 1–16 (2020).

199. Saini, A. K., Chauhan, S. S. & Tiwari, A. Creeping flow of non-Newtonian fluid through membrane of porous cylindrical particles: A particle-in-cell approach. *Physics of Fluids* **35** (2023).

200. Liu, H. C., Zhang, B. B., Schneider, V., Venner, C. & Poll, G. Two-dimensional generalized non-Newtonian EHL lubrication: Shear rate-based solution versus shear stress-based solution. *Proceedings of the Institution of Mechanical Engineers, Part J: Journal of Engineering Tribology* **235,** 2626–2639 (2021).

201. Filippov, A. *et al.* Simulation of the onset of flow through a PTMSP-based polymer membrane during nanofiltration of water-methanol mixture. *Petroleum Chemistry* **55,** 347–362 (2015).

202. Murthy, J. R. & Srinivas, J. Second law analysis for Poiseuille flow of immiscible micropolar fluids in a channel. *International Journal of Heat and Mass Transfer* **65,** 254–264 (2013).

203. Srinivas, J, Murthy, J. R. & Bég, O. A. Entropy generation analysis of radiative heat transfer effects on channel flow of two immiscible couple stress fluids. *Journal of the Brazilian Society of Mechanical Sciences and Engineering* **39,** 2191–2202 (2017).

204. Srinivas, J, Murthy, J. R. & Chamkha, A. J. Analysis of entropy generation in an inclined channel flow containing two immiscible micropolar fluids using HAM. *International Journal of Numerical Methods for Heat & Fluid Flow* **26,** 1027–1049 (2016).

205. Hooman, K & Ejlali, A. Entropy generation for forced convection in a porous saturated circular tube with uniform wall temperature. *International communications in heat and mass transfer* **34,** 408–419 (2007).

206. Pabi, S., Mehta, S. K. & Pati, S. Analysis of thermal transport and entropy generation characteristics for electroosmotic flow through a hydrophobic microchannel considering viscoelectric effect. *International Communications in Heat and Mass Transfer* **127,** 105519 (2021).

207. Srivastava, A. & Srivastava, N. Flow past a porous sphere at small Reynolds number. *Zeitschrift für angewandte Mathematik und Physik ZAMP* **56,** 821–835 (2005).

208. Bergles, A. E. Some Perspectives on Enhanced Heat Transfer—Second-Generation Heat Transfer Technology. *Journal of Heat Transfer* **110,** 1082–1096 (1988).

209. Hufton, J. R., Bravo, J. L. & Fair, J. R. Scale-up of laboratory data for distillation columns containing corrugated metal-type structured packing. *Industrial & engineering chemistry research* **27,** 2096–2100 (1988).

210. Olujiæ, B. K., Jansen, H, Rietfort, T, Zich, E & Frey, G. Distillation column internals/configurations for process intensification. *Chem. Biochem. Eng* **7,** 301–309 (2003).

211. Young, D. F. Effect of a Time-Dependent Stenosis on Flow Through a Tube. *Journal of Engineering for Industry* **90,** 248–254 (1968).

212. Rodbard, S. Dynamics of blood flow in stenotic vascular lesions. *American heart journal* **72,** 698–704 (1966).

213. Qu, W., Mala, G. M. & Li, D. Pressure-driven water flows in trapezoidal silicon microchannels. *International Journal of Heat and Mass Transfer* **43,** 353–364 (2000).

214. Bahrami, M., Yovanovich, M. M. & Culham, J. R. Pressure Drop of Fully Developed, Laminar Flow in Rough Microtubes. *Journal of Fluids Engineering* **128,** 632–637 (2005).

215. Phan-Thien, N. On the Stokes Flow of Viscous Fluids Through Corrugated Pipes. *Journal of Applied Mechanics* **47,** 961–963 (1980).

216. Phan-Thien, N. Couette flow between corrugated cylinders. *Zeitschrift für angewandte Mathematik und Physik ZAMP* **43,** 207–215 (1992).

217. Wang, C.-Y. Parallel flow between corrugated plates. *Journal of the Engineering Mechanics Division* **102,** 1088–1090 (1976).

218. Wang, C.-Y. On Stokes Flow Between Corrugated Plates. *Journal of Applied Mechanics* **46,** 462–464 (1979).

219. Zhou, H., Khayat, R., Martinuzzi, R. & Straatman, A. On the validity of the perturbation approach for the flow inside weakly modulated channels. *International Journal for Numerical Methods in Fluids* **39,** 1139 – 1159 (2002).

220. Sherief, H., Faltas, M., Ashmawy, E. & Abdel-Hameid, A. Creeping motion of a micropolar fluid between two sinusoidal corrugated plates. *European Journal of Mechanics-B/Fluids* **59,** 186–196 (2016).

221. Ng, C.-O. & Wang, C. Darcy–Brinkman flow through a corrugated channel. *Transport in porous media* **85,** 605–618 (2010).

222. Hunter, R. *Foundations of Colloid Science* (Oxford University Press, 2001).

223. Masliyah, J. H. & Bhattacharjee, S. *Electrokinetic and colloid transport phenomena* (John Wiley & Sons, 2006).

224. Ghosal, S. Lubrication theory for electro-osmotic flow in a microfluidic channel of slowly varying cross-section and wall charge. *Journal of Fluid Mechanics* **459,** 103–128 (2002).

225. Bhattacharyya, S, Zheng, Z & Conlisk, A. Electro-osmotic flow in two-dimensional charged micro-and nanochannels. *Journal of Fluid Mechanics* **540,** 247–267 (2005).

226. Ohno, K.-i., Tachikawa, K. & Manz, A. Microfluidics: applications for analytical purposes in chemistry and biochemistry. *Electrophoresis* **29,** 4443–4453 (2008).

227. Friebe, A. & Ulbricht, M. Cylindrical pores responding to two different stimuli via surface-initiated atom transfer radical polymerization for synthesis of grafted diblock copolymers. *Macromolecules* **42,** 1838–1848 (2009).

228. Swaminathan, V. V. *et al.* Ionic transport in nanocapillary membrane systems. *Nanotechnology for Sustainable Development,* 17–31 (2014).

229. Lee, J., Panzer, M. J., He, Y., Lodge, T. P. & Frisbie, C. D. Ion gel gated polymer thin-film transistors. *Journal of the American Chemical Society* **129,** 4532–4533 (2007).

230. Zhang, H., Tian, Y. & Jiang, L. From symmetric to asymmetric design of bio-inspired smart single nanochannels. *Chemical communications* **49,** 10048–10063 (2013).

231. Ding, Z., Fong, R. B., Long, C. J., Stayton, P. S. & Hoffman, A. S. Size-dependent control of the binding of biotinylated proteins to streptavidin using a polymer shield. *Nature* **411,** 59–62 (2001).

232. Schmaljohann, D. Thermo-and pH-responsive polymers in drug delivery. *Advanced drug delivery reviews* **58,** 1655–1670 (2006).

233. Donath, E & Voigt, A. Streaming current and streaming potential on structured surfaces. *Journal of colloid and interface science* **109,** 122–139 (1986).

234. Ohshima, H. & Kondo, T. Electrokinetic flow between two parallel plates with surface charge layers: Electro-osmosis and streaming potential. *Journal of colloid and interface science* **135,** 443–448 (1990).

235. Ohshima, H. Electrophoretic mobility of soft particles. *Journal of colloid and interface science* **163,** 474–483 (1994).

236. Ohshima, H. Electrophoresis of soft particles. *Advances in colloid and interface science* **62,** 189–235 (1995).

237. Ohshima, H. Electrophoretic mobility of soft particles. *Colloids and Surfaces A: Physicochemical and Engineering Aspects* **103,** 249–255 (1995).

238. Ohshima, H. & Furusawa, K. *Electrical phenomena at interfaces: fundamentals: measurements, and applications* (CRC Press, 1998).

239. Ohshima, H. On the general expression for the electrophoretic mobility of a soft particle. *Journal of colloid and interface science* **228,** 190–193 (2000).

240. Ohshima, H. Electrophoretic mobility of a highly charged soft particle: relaxation effect. *Colloids and Surfaces A: Physicochemical and Engineering Aspects* **376,** 72–75 (2011).

241. Kozak, M. W. & Davis, E. J. Electrokinetic phenomena in fibrous porous media. *Journal of colloid and interface science* **112,** 403–411 (1986).

242. Ohshima, H. Electroosmotic velocity in fibrous porous media. *Journal of colloid and interface science* **210,** 397–399 (1999).

243. Ohshima, H. Electrophoretic mobility of soft particles in concentrated suspensions. *Journal of colloid and interface science* **225,** 233–242 (2000).

244. Ohshima, H. Electrical conductivity of a concentrated suspension of soft particles. *Journal of colloid and interface science* **229,** 307–309 (2000).

245. Ohshima, H. Sedimentation potential and velocity in a concentrated suspension of soft particles. *Journal of colloid and interface science* **229,** 140–147 (2000).

246. Ohshima, H. Cell model calculation for electrokinetic phenomena in concentrated suspensions: an Onsager relation between sedimentation potential and electrophoretic mobility. *Advances in Colloid and Interface Science* **88,** 1–18 (2000).

List of Publications

The following works included in this thesis in chapter form have been published/ communicated in the following journals:

1. **A. K. Saini**, S. S. Chauhan, A. Tiwari, Creeping flow of Jeffrey fluid through a swarm of porous cylindrical particles: Brinkman–Forchheimer model, *International Journal of Multiphase Flow* 145 (2021) 103803. **(SCI, IF-3.6, Q1)** (https://doi.org/10.1016/j.ijmultiphaseflow.2021.103803)

2. **A. K. Saini**, S. S. Chauhan, A. Tiwari, Creeping flow of non-Newtonian fluid through membrane of porous cylindrical particles: A particle-in-cell approach, *Physics of Fluids* 35(4) 043101 (2023). **(SCI, IF-4.1, Q1)** (https://doi.org/10.1063/5.0143317)

3. **A. K. Saini**, S. S. Chauhan, A. Tiwari, Asymptotic analysis of Jeffreys–Newtonian fluids flowing through a composite vertical porous layered channel: Brinkman–Forchheimer model, *Physics of Fluids* 35 (2023) 123118. **(SCI, IF-4.1, Q1)** (https://doi.org/10.1063/5.0175488)

4. **A. K. Saini**, S. S. Chauhan, A. Tiwari, Asymptotic analysis of electrohydrodynamic flow through a swarm of porous cylindrical particles, *Physics of Fluids* 36(4) (2024) 041910. **(SCI, IF-4.1, Q1)** (https://doi.org/10.1063/5.0203073)

5. **A. K. Saini**, S. S. Chauhan, A. Tiwari, Analytical Study of the Effect of Complex Fluid Rheology and Membrane Parameters on Heat Transfer in Fluid Flow through a Swarm of Cylindrical Particles, *International Communications in Heat and Mass Transfer* 158 (2024) 107791. **(SCI, IF-6.4, Q1)** (https://doi.org/10.1016/j.icheatmasstransfer.2024.107791)

6. **A. K. Saini**, A. Tiwari, Electroosmotic Flow past an Array of Poly-Electrolyte Coated Solid Cylindrical Particles: A Particle-in-Cell Approach. **(Under-review)**

7. N. Ghiya, **A. K. Saini**, A. Tiwari, Electrohydrodynamic Flow of Viscoelastic non-Newtonian Fluid through a Porous Cylindrical Tube. **(Communicated)**

8. S. S. Chauhan, **A. K. Saini**, A. Tiwari, Analysis of Entropy Generation for a Creeping Flow of Newtonian Fluid through a Swarm of Biporous Layered Cylindrical Particles: Brinkman-Forchheimer Model. **(To be communicated)**

Conferences/ Workshop Attended

1. Presented a paper titled "Effect of Surface Roughness on Flow Past a Membrane composed of Porous Cylindrical Particles: A Particle-in-Cell Approach" at **the International Conference on Recent Advances in Fluid Mechanics and Nanoelectronics (ICRAFMN-2024)** in July-2024 at Manipal University, Jaipur.

2. Presented a paper titled "Electrohydrodynamic Flow through a Swarm of Porous Cylindrical Particles: A Cell Model Approach" In the International conference named **International Conference on Recent Advances in Fluid Mechanics and Nanoelectronics (ICRAFMN-2023)** in July-2023 at Manipal Institute of Technology Bengaluru in Association with National Institute of Technology, Uttarakhand.

3. Presented a paper titled "Electrohydrodynamic Flow through a Swarm of Porous Cylindrical Particles: A Cell Model Approach" In the International conference named **International Conference on Differential Equations and Control Problems (ICDECP23)** in June–2023 at IIT Mandi North Campus.

4. Presented a paper titled "Creeping Flow of Non-Newtonian Fluid through Membrane of Porous Cylindrical Particles: A Particle-in-Cell Approach" In the International conference named **International Conference on Advances in Mechanics, Modelling, Computing and Statistics (ICAMMCS-22)** in March-2021 at Birla Institute of Technology and Science, Pilani.

5. Attended the International Conference titled **2nd International Conference on Fluid under Confinement - 2022** in July–2019 organized by the School of Energy Science and Engineering & Department of Mechanical Engineering, Indian Institute of Technology Kharagpur, Kharagpur.

6. Participated in a one-week online certificate course on **Computational Mathematical Software (MATHEMATICA, MAXIMA & R)** from 22-28 February 2022 organized by the Department of Mathematics, Atma Ram Sanatan Dharma College, University of Delhi.

7. Participated in a two days' workshop on **Numerical Methods for Differential Equations and Applications** from 27-28 March 2023 organized by the Department of Mathematics, Birla Institute of Technology and Science, Pilani.

8. Attended the **International Symposium of Advances in Mathematical Sciences (ISAMS 2024)** organized by Canadian University Dubai, Dubai, UAE in March 2024.

9. Attended the **Asian and European Schools in Mathematics (AESIM 2023) Mathematics for Health Sciences** CIMPA School at Department of Mathematics, Birla Institute of Technology and Science, Pilani in January 2024.

10. Attended a workshop named **Mathematics Towards Machine Learning: Unveiling the Fundamentals**, by Indian Mathematics Professors Association (IMPA) jointly organized with Infinity Research and Development Institute in August-2024.

11. Attended an **International Workshop on Recent Trends in Mathematics**, organized by the Division of Mathematics, School of Advanced Sciences, Vellore Institute of Technology, Chennai, in April 2023.

12. Attended a **workshop on Navier-Stokes Equations: Theory, Numerics, and Applications**, organized by the Department of Mathematics, Birla Institute of Technology and Science, Pilani in March 2023.

13. Attended a **workshop on Python Programming for Data Science**, Department of Mathematics, School of Basic & Applied Sciences, Harcourt Butler Technical University, Kanpur, in February 2022.

Brief Biography of the Candidate

Mr. Amit Kumar Saini earned his Bachelor's degree in Science from Shri Radheshyam R. Morarka Govt. College, Jhunjhunu (Rajasthan). He then pursued his Master's degree in Mathematics at Government Lohia College, Churu (Rajasthan). He was declared successful in the Joint CSIR-UGC Test for Junior Research Fellowship twice with AIR 149 and 95, Eligible for Lectureship (NET), and qualified for GATE in the subject of Mathematical Sciences. He then decided to pursue his doctoral degree at BITS Pilani, where he is currently a senior research fellow under CSIR, conducting research on the mathematical analysis of fluid flow through a membrane under the guidance of Prof. Ashish Tiwari.

Brief Biography of the Supervisor

Dr. Ashish Tiwari serves as an Associate Professor at the Department of Mathematics, Birla Institute of Technology and Science Pilani, Pilani Campus, located in Pilani, Rajasthan. His academic journey includes obtaining a Master of Science (M. Sc. in Mathematics) degree in 2003 and a Doctor of Philosophy (D. Phil) in 2010 from the University of Allahabad, located in Prayagraj, Uttar Pradesh. Following this, he commenced his tenure as an Assistant Professor in the Department of Mathematics at Birla Institute of Technology and Science Pilani, Pilani Campus, Rajasthan, in December 2011. His research interests are in the area of flow through porous media, creeping flow, membrane filtration process, heat and mass transfer, electroosmotic and electrophoresis phenomena, solute dispersion process, homogenization process, and physiological fluid flow. He has published more than 30 research articles in reputed international journals. He has guided two Ph.D. students, namely Dr. Satyendra Singh Chauhan and Dr. Pallav Dhanendrakumar Shah. He is supervising three Ph.D. students, namely Mr. Amit Kumar Saini, Mr. Yogesh Kuntal, and Ms. Neelima Ghiya, while also providing mentorship to two other Ph.D. students, namely Ms. Komal and Ms. Ansal. He served as the principal investigator for two significant projects: "Modelling of cardiovascular flows and influence of magnetic field on circulation" (SR/FTP/MS-038/2011), and a collaborative Indo-Russian project titled "Flow through a membrane modelled of porous cylindrical particles using particle-in-cell approach" (INT/RUS/RFBR/P-212) funded by DST-RFBR, conducted in partnership with Prof. A.N. Filippov from Gubkin Russian State University, Moscow, Russia. Currently, he is a principal investigator of the ongoing METRICS Scheme project “Title” (MTR/2021/000959), which is funded by DST-SERB.